ARTICLE IN PRESS Available online http://jopr.mpob.gov.my/category/article-in-press/

Journal of Oil Palm Research

Vol. 35 (1) • March 2023

REVIEW ARTICLE

- Impact of *Elaeidobius kamerunicus* (Faust) Introduction on Oil Palm Fruit Formation in Malaysia and Factors Affecting its Pollination Efficiency: A Review





eISSN 2811-4701

MPOB

JOURNAL OF OIL PALM RESEARCH (formerly known as ELAEIS)

JOURNAL OF OIL PALM RESEARCH, an international refereed journal, carries full-length original research papers, short communications and scientific review papers on various aspects of oil palm and palm oil and other palms. JOURNAL OF OIL PALM RESEARCH is published four times per year, *i.e.* March, June, September and December.

© Malaysian Palm Oil Board, 2023

All rights reserved. No part of this publication may be reproduced in any form or by any means without the written permission of the Malaysian Palm Oil Board.

Impact Factor:
1.594
data from *2021 Journal Citation Report*® Science Edition
– A Clarivate Analytics product.

For more information on advertisement for the JOURNAL OF OIL PALM RESEARCH, please write to:

Editor-in-Chief
Journal of Oil Palm Research
Malaysian Palm Oil Board
6 Persiaran Institusi, Bandar Baru Bangi
43000 Kajang, Selangor, Malaysia

Tel: *603-8769 4400*
E-mail: *pub@mpob.gov.my*
Website: *jopr.mpob.gov.my*

DISCLAIMER
Views of writers expressed in this publication are not necessarily endorsed by or represent the views of the Malaysian Palm Oil Board.

Published by the Malaysian Palm Oil Board

JOURNAL OF OIL PALM RESEARCH

Vol. 35 (1) March 2023

CONTENTS

REVIEW ARTICLES

1 Impact of *Elaeidobius kamerunicus* (Faust) Introduction on Oil Palm Fruit Formation in Malaysia and Factors Affecting its Pollination Efficiency: A Review
Saharul Abillah Mohamad; Mohamed Mazmira Mohd Masri; Norman Kamarudin; Mohamad Rosman Sulaiman; Arnaud Costa; Meilina Ong-Abdullah; Hasnol Othman; Siti Nurulhidayah Ahmad; Muhammad Nurul Yaqin Syarif; Zam Abdul Karim; Idris Abdul Ghani; Samsudin Amit; Azlina Zakaria; Su Chong Ming; Siaw Ting Chuan; Johari Jalinas; Yap Yau Koong; Ahmad Anuar Sairi; Syed Mohd Faizal Syed Ali; Mahbob Abdullah; Sivapragasam Annamalai; King Jie Hung; Muhamad Azmi Mohammed; Idris Abu Seman; Ramle Moslim and Ghulam Kadir Ahmad Parveez

RESEARCH ARTICLES

23 Stability and Physical Properties of Dihydroxystearic Acid-based Organogels in Different Types of Vegetable Oil
Norashikin Ahmad and Zafarizal Aldrin Azizul Hasan

33 Assessing Electrical and Physicochemical Performance of Chemically Modified Palm Oil as an Alternative Transformer Liquid
Masra, S M W; Arief, Y Z; Rigit, A R H; Sahari, S K; Rahman, M R; Muhammad, M S and Eteruddin, H

45 Characterisations of Bio-Asphalt Incorporating Palm Bio-oil from Waste Empty Fruit Bunches
Tracy Wong Leh Xin; Mok Tai Han; Guo Tai; Mohd Rosli Mohd Hasan; Mohd Asyraf Kassim and Mohamad Azri Sukiran

58 Spatial Distribution of *Rattus* Species (Rodentia: Muridae) in Oil Palm Plantations of Peninsular Malaysia with Species Verification using Cytochrome Oxidase I (COI) Gene
Mohamad Harris Nasir; Muhamad Shakirin Mispan; Subha Bhassu; Khoo Jing Jing; Sazaly Abubakar; Siti Nurul Izzah Mohd Azami; Siti Nabilah Ishak; Farah Shafawati Mohd-Taib and Hasmahzaiti Omar

75 A Comperative Study of Oil Palm Fronds Torrefaction under Flue Gas and Nitrogen Atmospheres
Premchand; Masaharu Komiyama; Aqsha and Yoshimitsu Uemura

86 Comparison of Artificial Intelligence Models to Predict Oil Palm Biomass Pyrolysis and Kinetics using Thermogravimetric Analysis
Yasmin Mohd Zaifullizan; Lim Mei Kuan; Arshad Adam Salema and Kashif Ishaque

100 Development and Field Evaluation of a Seedling Polybag Soil Filling Machine for Oil Palm Nursery
Haslina Hassan; Azmi Yahya; Darius El Pebrian and Ahmad Suhaizi Mat Su

111 Counting of Oil Palm Fresh Fruit Bunches using Computer Vision
Minarni Shiddiq; Dodi Sofyan Arief; Defrianto; Vicky Vernando Dasta; Deborah Margaretha Panjaitan and Doni Saputra

121 Comparison of Real-time PCR, Conventional PCR and RT-LAMP for the Detection of *Coconut Cadang-Cadang Viriod* Variant in Oil Palm
Nur Diyana Roslan; Ganesan Vadamalai; Abu Seman Idris; Kong Lih Ling and Shamala Sundram

133 Designing gRNSs Targeting Oil Palm Phytoene Desaturase (*Eg*PDS) Gene and Construction of Vectors for Oil Palm CRISPR/CAS9 Study
Norfaezah Jamaludin; Bohari Bahariah; Noor Azmi Shaharuddin; Chai Ling Ho; Omar Abdul Rasid; Ghulam Kadir Ahmad Parveez and Mat Yunus Abdul Masani

147 Improving the Growth Performance of Oil Palm seedlings by Mixtures of Organic and Chemical Fertilisers
Mohd Fahmi Keni; Nurhafizhoh Zainuddin and Mohamed Mazmira Mohd Masri

157 Pathogenesis Related Protein Induction in *Streptomyces* GanoSA1 Treated Oil Palm Seedlings during Early Infection by *Ganoderma boninense*
Shariffah-Muzaimah Syed Aripin; Idris Abu Seman; Mohd Hefni Rusli and Shamala Sundram

168 Transpiration of Oil Palm (*Elaeis guineensis* Jacq.) Based on Sap Flow Measurement: The Relation to Soil and Climate Variables
Iput Pradiko; Suroso Rahutomo; Rana Farrasati; Eko Noviandi Ginting; Fandi Hidayat and Muhdan Syarovy

SHORT COMMUNICATION

185 Culturable Bacterial Population in Different Oil Palm Peat Soil Operational Zones
Mohd Shawal Thakib Maidinl Gogula Selvi Asang; Mohd Fahmi Keni and Mohamed Mazmira Mohd Masri

Cover picture: The efficient pollinator for oil palm, *Elaeidobius kamerunicus.*

EDITORIAL BOARD

(1 January 2022 – 31 December 2023)

Datuk Dr. Ahmad Parveez Ghulam Kadir
Malaysia (Editor-in-Chief)

Dr. Carl Traeholt
Malaysia

Prof. Dr. Matthias Finkbenier
Germany

Dr. Julie Flood
United Kingdom

Prof. Dr. Dirk Prufer
Germany

Prof. Dr. Douglas G Hayes
USA

Prof. Fredolin Tangang
Malaysia

Prof. Dr. Norzulani Khalid
Malaysia

Prof. Dr. Ir. Azmi Yahya
Malaysia

PUBLICATION COMMITTEE

CHAIRPERSON
Datuk Dr. Ahmad Parveez Ghulam Kadir

SECRETARY
Anita Taib

COMMITTEE MEMBERS
Dr. Zainab Idris
Dr. Ramle Moslim
Rosidah Radzian
Dr. Astimar Abdul Aziz
Dr. Mohamad Arif Abd Manaf
Dr. Idris Abu Seman
Dr. Aki @ Zaki Aman
Dr. Zafarizal Aldrin Azizul Hasan
Ruba'ah Masri
Johari Minal
Mohd Saufi Awang
Iptisam Abdul Wahab

Journal of Oil Palm Research Vol. 35 (1) March 2023 p. 1-22
DOI: https://doi.org/10.21894/jopr.2022.0021

IMPACT OF *Elaeidobius kamerunicus* (Faust) INTRODUCTION ON OIL PALM FRUIT FORMATION IN MALAYSIA AND FACTORS AFFECTING ITS POLLINATION EFFICIENCY: A REVIEW

SAHARUL ABILLAH MOHAMAD[1,12]*; MOHAMED MAZMIRA MOHD MASRI[1]; NORMAN KAMARUDIN[1]; MOHAMAD ROSMAN SULAIMAN[1]; ARNAUD COSTA[4]; MEILINA ONG-ABDULLAH[1]; HASNOL OTHMAN[1]; SITI NURULHIDAYAH AHMAD[1]; MUHAMMAD NURUL YAQIN SYARIF[1]; ZAM ABDUL KARIM[5]; IDRIS ABDUL GHANI[6]; SAMSUDIN AMIT[7]; AZLINA ZAKARIA[7]; SU CHONG MING[8]; SIAW TING CHUAN[9]; JOHARI JALINAS[10]; YAP YAU KOONG[3]; AHMAD ANUAR SAIRI[11]; SYED MOHD FAIZAL SYED ALI[11]; MAHBOB ABDULLAH[2]; SIVAPRAGASAM ANNAMALAI[4]; KING JIE HUNG[12,13]; MUHAMAD AZMI MOHAMMED[12]; IDRIS ABU SEMAN[1]; RAMLE MOSLIM[1] and GHULAM KADIR AHMAD PARVEEZ[1]

ABSTRACT

The oil palm pollinating weevil, Elaeidobius kamerunicus*, has become the single most important insect pollinator of the commodity crop in Malaysia and Indonesia, 40 years after its introduction. However, in 2020, the average national oil extraction rate (OER) has decreased from 20.21% to 19.92%. The decline was attributed to the lower oil palm fruit bunch quality. This has raised concerns on the pollination efficiency of the pollinator. As such, the factors affecting the pollination efficiency of* E. kamerunicus *were thoroughly discussed in this review. Eight factors, which were categorised into intrinsic and extrinsic factors, were discussed in detail. Intrinsic factors discussed are the genetic make-up of* E. kamerunicus *and its population level. Meanwhile, factors such as planting materials, soil types, plant physiological condition, volatiles emission, diseases/predators threatening* E. kamerunicus *and climatic factors were discussed in the extrinsic factors. Methods for maintaining a healthy pollinator population were suggested, as well as an emphasis on future studies based on the shortlisted factors.*

Keywords: *Elaeidobius kamerunicus*, *Elaeis guineensis*, pollination efficiency.

Received: 1 September 2021; **Accepted:** 16 February 2022; **Published online:** 21 April 2022.

[1] Malaysian Palm Oil Board,
6 Persiaran Institusi, Bandar Baru Bangi,
43000 Kajang, Selangor, Malaysia.

[2] Malaysian Estate Owners' Association,
Ground Floor, Wisma IJM,
Jalan Yong Shook Lin,
Seksyen 7, 46050 Petaling Jaya,
Selangor, Malaysia.

[3] Malaysian Palm Oil Association, T3-08-09,
UOA Business Park 1,Jalan Pengaturcara U1/51A,
40150 Shah Alam, Selangor, Malaysia.

[4] CABI - Malaysia, PO Box 210,
43400 UPM Serdang, Selangor, Malaysia.

[5] No. 16, Jalan SS7/6A,
Kelana Jaya, Selangor, Malaysia.

[6] No. 16, Jalan 4/7Q, Seksyen 4, Bandar Baru Bangi
43650 Bangi, Selangor, Malaysia.

[7] Sime Darby Plantation Berhad,
Main Block, Level 3, Plantation Tower,
No. 2, Jalan PJU 1A/7. Ara Damansara,
47301 Petaling Jaya, Selangor, Malaysia.

[8] Sarawak Oil Palms Berhad,
No. 124-126, Jalan Bendahara, PO Box 547,
98007 Miri, Sarawak, Malaysia.

[9] Jaya Tiasa Holdings Berhad, No. 1-9, Pusat Suria Permata,
Lorong Upper Lanang 10A, 96000 Sibu, Sarawak, Malaysia.

[10] Department of Biological Sciences and Biotechnology,
Faculty of Science and Technology,
Universiti Kebangsaan Malaysia,
43600 UKM Bangi, Selangor, Malaysia.

[11] TH Plantations Berhad, Level 31-35,
Menara TH Platinum, No. 9, Jalan Persiaran KLCC,
50088 Kuala Lumpur, Malaysia.

[12] Faculty of Agricultural Science and Forestry,
Universiti Putra Malaysia, Bintulu, Sarawak Campus,
PO Box 396, Jalan Nyabau, 97008 Bintulu,
Sarawak, Malaysia.

[13] Institut Ekosains Borneo,
Universiti Putra Malaysia, Bintulu, Sarawak Campus,
PO Box 396, Jalan Nyabau, 97008, Bintulu,
Sarawak, Malaysia.

* *Corresponding author e-mail: saharul.abillah@mpob.gov.my*

INTRODUCTION

Malaysia is one of the prominent major exporters of palm oil, contributing to 34.30% of the total palm oil trade (Parveez *et al*., 2021). In Malaysia, 5.87 million hectares of land are currently under oil palm cultivation (Parveez *et al*., 2021). In 2020, the total Malaysian export revenue increased by 8.40% compared to RM64.84 billion collected in the previous year (Parveez *et al*., 2021). In the 2020 overview, Malaysian Palm Oil Board (MPOB) stated that the worldwide COVID-19 pandemic had disrupted the production of crude palm oil (CPO). However, the tight supply of CPO led to a higher CPO price and more significant export revenue of palm oil products (Parveez *et al*., 2021). It was also reported that in 2020, the oil extraction rate (OER) in the palm oil mills declined from 20.21% to 19.92%, mainly due to the reduced quality of fresh fruit bunches (FFB) supplied to the mills (Parveez *et al*., 2021). The lower quality bunch was usually associated with inadequate pollination, which will also reduce the bunch yield and CPO production (Harun and Noor, 2002; Rao and Law, 1998).

In Malaysia's early phases of oil palm cultivation, the formation of oil palm fruit was unsatisfactory, especially in young palms (Syed, 1979). It was observed that poor fruit set formation was due to insufficient pollination, which largely depended on wind and inefficient locally-available insect pollinators (Hardon, 1973; Lewis, 1973; Pardede, 1990; Syed, 1979; Wood, 1968). In the event where pollination is insufficient, the domestication of insect pollinators has been previously done. For example, the introduction of the European honey bee (*Apis mellifera*) was instrumental in increasing the forage production in Hawaii, United States in 1857 (Messing, 1991; Valenzuela, 2018). Similarly, to increase the pollination of tomatoes in North America, Australasia, Asia, Africa, and South America, the introduction of bumblebee (*Bombus terrestris*) was conducted (Velthius and van Doorn, 2006). Another notable example is the domestication of sting bees in tropical and sub-tropical regions (*Melipona* sp., *Trigona* sp.) to assist in the pollination of crops such as avocado, coconut, coffee, macadamia, and mango (Can-Alonzo *et al*., 2005; Heard, 1999; Slaa *et al*., 2006; Viana *et al*., 2014).

To improve the oil palm fruit formation, Malaysia decided to import insect pollinators from Africa (Kang, 1999). The importation efforts led to the mass-field introduction of *Elaeidobius kamerunicus* on three sites in early 1980 (Kang, 1999; Kang and Zam, 1982; Syed *et al*., 1982). The introduced pollinator has since thrived well in the oil palm plantations throughout Malaysia and positively influenced the palm oil industry in the country (Donough and Law, 1988; Kang and Zam, 1982; Lubis and Dono, 2017; Syed *et al*., 1982; Wahid and Kamarudin, 1997; Yee *et al*., 1985).

Despite the positive impacts of *E. kamerunicus* introduction, there have been increasing reports of parthenocarpic fruits and poor fruit set formation (Kamarudin *et al*., 2018). In the MPOB survey, poor fruit set formation was observed primarily in peat areas in Sarawak, Malaysia (Sulaiman *et al*., 2018). The OER has also stagnated and has yet to achieve the favourable OER of 23% (Parveez *et al*., 2021). In line with the industry's sustainable aspirations, the Malaysian government has mandated a cap on oil palm cultivation area at 6.5 million hectares (The Malaysian Reserve, 2019), which means that the improvements in yield must be made without clearing up additional areas. To address the issues related to poor fruit set formation, a Task Force Committee on Fruit Set and Pollinating Weevil comprising of experts from the MPOB, palm oil industry representatives, and related researchers from local universities was formed.

Given the massive economic importance of the palm oil industry and its reliance on efficient pollination services rendered by *E. kamerunicus*, investigating the factors influencing pollination efficiency and proper management of the pollinator population in the oil palm ecosystem should be imperative. In this article, we present a review that dates to the introduction of *E. kamerunicus* in Malaysia. This review also discusses the impacts of the introduction of *E. kamerunicus* on the Malaysian palm oil industry, the factors influencing its pollination efficiency, and ultimately, the management aspects of maintaining its population in the oil palm environment. We conclude by highlighting gaps in the current understanding of fruit set formation factors and identifying potential areas for further improvement.

The Pollinating Insects of Oil Palm

During the early stages of oil palm production in Malaysia, the lack of insects visiting oil palm flowering inflorescences led to the notion that the crop is anemophilous, or wind-pollinated (Hardon and Turner, 1967; Lepesme, 1947; Wood, 1968). Although many insects visited *Elaeis guineensis* inflorescences, these insects only visited specific sexes of the inflorescences. Derelominae, bees, and tabanids only visited the male inflorescences while female inflorescences were only visited by *Pyroderces* spp. (Lepesme, 1947; Syed, 1979). Hence, it was thought that these insects do not offer any pollination services to the oil palm (*i.e*., no pollen was transferred from male inflorescence to female inflorescence). The onset of rains led to a massive reduction of pollen density in the air (Hardon

and Turner, 1967). Somehow, even during regular rainfall, when the pollen availability in the air was minimal, the natural pollination was sufficient and it was then suggested that the insects are playing a vital role in the pollination of the crop (Syed, 1979).

In Cameroon, Africa, Syed (1979) observed that the pollination was satisfactory, with the annual mean of fruit/bunch ratio of 64.8%. Pollination is considered satisfactory if the fruit weight ratio to total bunch weight exceeds 60.0% (Hardon, 1973). In contrast to what was observed in Malaysia, many insects visited both sexes of oil palm inflorescences during anthesis. It was noted that the most abundant species visiting the inflorescences of oil palm were *Elaeidobius* spp. and *Atheta* spp. Unlike Cameroon, less diverse insect species visited oil palm inflorescences in Malaysia (Syed, 1979). In Peninsular Malaysia, only *Thrips hawaiiensis* was observed inhabiting and moving around the anthesising inflorescences (Syed, 1979). *Thrips hawaiiensis* is reported to be a weak flyer and thus has less tendency to fly into open, windy areas, even when the area is closer to older palms (Lewis, 1973; Syed, 1979). Whereas, in Sabah, Malaysia, besides an unidentified midge, many momphid moths (*Pyroderces* spp.) were observed visiting the oil palm inflorescences (Syed, 1979). In Peninsular Malaysia, pollination on the tall palms was found to be sufficient. However, the same cannot be said for younger palms. In such areas, manual hand-assisted pollination has to be done to improve the fruit set formation.

Appiah (1999) observed several insect species (*Elaeidobius* spp. and *Prosoestus minor*) visiting the oil palm inflorescences in Ghana, where the fruit set formation was adequate and uniform throughout the year. Similarly, Mariau and Genty (1988) observed the activities of *Mystrops costaricensis* and *Elaeidobius subvittatus* on the American oil palm, *Elaeis oleifera*. *Elaeidobius subvittatus* was suggested to be introduced to the region from Africa (Mariau and Genty, 1988), before colonising entire Neotropical America (Appiah and Agyei Dwarko, 2013). However, although the presence of the pollinating insect species was observed, the fruit set formation in the area was still inadequate (Mariau and Genty, 1988).

It was clear that insects play an essential role in the pollination of oil palm. The lack of pollinating insects led to poor fruit set formation in Southeast Asia (Syed, 1979). Comparatively, the pollination in the African region is much more satisfactory than those in America and Southeast Asia, possibly due to the presence of various insect pollinators species in the region, which ensured adequate pollination (Appiah, 1999; Syed, 1979; 1981). To supplement the pollination activity by native insect pollinators and to improve fruit set formation in Malaysia, the importation of insect pollinators from Africa was suggested (Kang, 1999).

Selection of Pollinator to be Introduced into Malaysia

Syed (1979) reported that in Cameroon, where natural pollination is deemed adequate, about a dozen insect species were observed pollinating the oil palm. Therefore, selection for the most suitable pollinator to be introduced in Malaysia had to be conducted. Furthermore, more insects are seen visiting male inflorescences compared to female inflorescences. The most abundant species found on male inflorescences were *E. kamerunicus*, followed by *E. subvittatus*, *E. plagiatus* and *Atheta* spp. (Syed, 1979). In terms of the number of pollen grains transported, males of *E. kamerunicus* and the females of *E. plagiatus* were reported to carry an average of 235 and 203 pollen grains, respectively, more significant than other species (Syed, 1979). This figure did not differ much from a recent study by Kouakou *et al.* (2014). They reported that the adult *E. kamerunicus* was able to carry 317 pollen grains. However, Dhileepan (1992) reported that adult *E. kamerunicus* can carry more pollen, ranging from 610 to 2620 grains. The pollen carrying capacity (PCC) was inversely proportional to the pollinator population per spikelet, which means the low number of adult *E. kamerunicus* visiting the inflorescences meant more pollen was available to be carried by an individual insect pollinator, which is the most probable scenario in India, where the sole insect pollinator of the oil palm is *E. kamerunicus* (Dhileepan, 1994), compared to the relatively higher insect pollinator complex in the African region (Kouakou *et al.* 2014; Syed, 1979). Moreover, the population of the insect pollinator on male inflorescences was comparatively lower in India (18.7 to 99.2 *E. kamerunicus* per spikelet) (Dhileepan, 1992) than in Cameroon (1473 *E. kamerunicus* per spikelet) (Syed, 1979).

The abundance of insects visiting the oil palm inflorescences in Africa was observed in both dry and wet seasons, which indicates that changing weather conditions did not affect the population density of these pollinators (Syed, 1979). Due to their better pollen transport capacity and ability to flourish in wet and dry seasons, *Elaeidobius* spp. were chosen as pollinators (Syed, 1980).

Elaeidobius spp. is a curculionid within a small sub-family of Derelominae. *Elaeidobius kamerunicus*, native to tropical Africa, is now distributed into all tropical regions where *E. guineensis* are planted (Haran *et al*., 2020). Lepesme (1947) reported that the geographical distribution and hosts of the various genera of Derelominae are remarkably restricted (*e.g*., *Derelomus* in the Mediterranean area is found

on *Chamaerops*; *Meredolus* is found on *Cocos* in the Pacific; *Prosoestus* and *Elaeidobius* on *Elaeis* in West Africa). This information indicates this sub-family specialised nature, a handy feature in selecting insects to be introduced into Malaysia.

In Cameroon, six species of *Elaeidobius* spp. were found visiting male and female flowers of the oil palm inflorescence: *E. kamerunicus*, *E. plagiatus*, *E. singularis*, *E. subvittatus*, *E. bilineatus* and *E. spatulifer* (Syed, 1980). Other Derelominae (*i.e.*, *Prosoestus sculptilis* and *P. minor*) were usually found only on female flowers. Out of the six *Elaeidobius* spp., three species were observed to be the most abundant, *viz*., *E. kamerunicus*, *E. plagiatus,* and *E. subvittatus* (Syed, 1980).

The abundance of *Elaeidobius* spp. is influenced by the anthesis stage of the inflorescence. The maximum number of insects were found during the third day of anthesis when most florets have opened. These numbers will drop on the fourth and fifth anthesis (Syed, 1979; 1980). Auffray *et al.* (2017) observed that the peak activity of *E. kamerunicus* was synchronised with the anthesis stage of both male and female inflorescences, which helps to maintain the mutualistic insect-plant relationship. *Elaeidobius kamerunicus* (160 individuals per spikelet) was more abundant than the other species (*E. subvittatus* = 22 adults per spikelet; *E. plagiatus* = 21 adults per spikelet). During the rainy season, high larval mortality in both *E. plagiatus* and *E. subvittatus* result in a significant reduction of the adult population in the field. However, *E. kamerunicus* was less affected (Syed, 1980). A summary of this explanation, as suggested by Syed (1980), is listed in *Table 1.*

Syed (1980) also compared the pollinator population on different palm age profiles. In general, younger fields contain a high inflorescence sex ratio (higher number of oil palm female inflorescences). The ratio will naturally diminish over time, which means that the density of male inflorescences will naturally increase as the planting age (Corley, 1976a; Sparnaaij, 1960). It was observed that *E. plagiatus* and *E. singularis* were more numerous in the field with a high density of male inflorescences and *vice versa*. Meanwhile, the number of *E. kamerunicus* was either similar or proportionately low. This suggested that *E. plagiatus* and *E. singularis* have a weaker searching ability than *E. kamerunicus* (Syed, 1980). In contrast, the abundance of *E. subvittatus* in younger fields and higher ground elevations indicated this species' superior searching ability (Syed, 1980). Further trials indicated that *E. subvittatus* has the strongest searching ability, followed by *E. kamerunicus* and *E. plagiatus*. However, *E. subvittatus* was found to be less selective in choosing their host plants, having been observed to breed well on *E. oleifera* (Syed, 1979; 1980). Other species, on the other hand, appeared to be attracted solely to *E. guineensis* (Syed, 1980).

Based on the series of trials and observations, it was found that the most suitable species for introduction to Malaysia was *E. kamerunicus*. This was because it was the most abundant species under the coastal climatic conditions (Kang and Zam, 1982; Syed, 1980). In addition, it had superior pollen transferring capability, was able to adapt to both dry and wet conditions, possessed the good searching ability, and most importantly, extremely host-specific (Auffray *et al*., 2017; Kang and Zam, 1982; Syed, 1980). The introduction of *E. kamerunicus* in Malaysia was executed by packing the larvae and pupae in July 1980, followed by field release in February 1981 at the Pamol Plantations, Kluang, Johor, Malaysia (Kang, 1999; Syed, 1982).

TABLE 1. EFFECTS OF RAINY SEASON ON THREE DIFFERENT MAIN POLLINATING INSECTS ON MALE INFLORESCENCES OF *Elaeis guineensis*

Species	Risky behavioural pattern during the wet season	Effects of rains
Elaeidobius kamerunicus	Location of egg oviposition: The outer side of the anther tube	Comparatively, the drier outer side of the anther tube is less favourable than the inner side of the anther tube for fungi growth. This minimised the fungi infection on first instar larvae and contamination of larvae food source.
E. plagiatus	Location of egg oviposition: Inside of the anther tube	Indirect - Wet circumstances favour the development of fungus, which destroy male inflorescences. Following that, the development of first instar larvae was disturbed.
E. subvittatus	Location of egg oviposition: Just below the anther tube	Direct - The egg is superficially positioned, making it very vulnerable to the run-off effects of heavy rains. Emerged larvae were likewise eating on the shallow portion of the anther and were similarly exposed to danger.

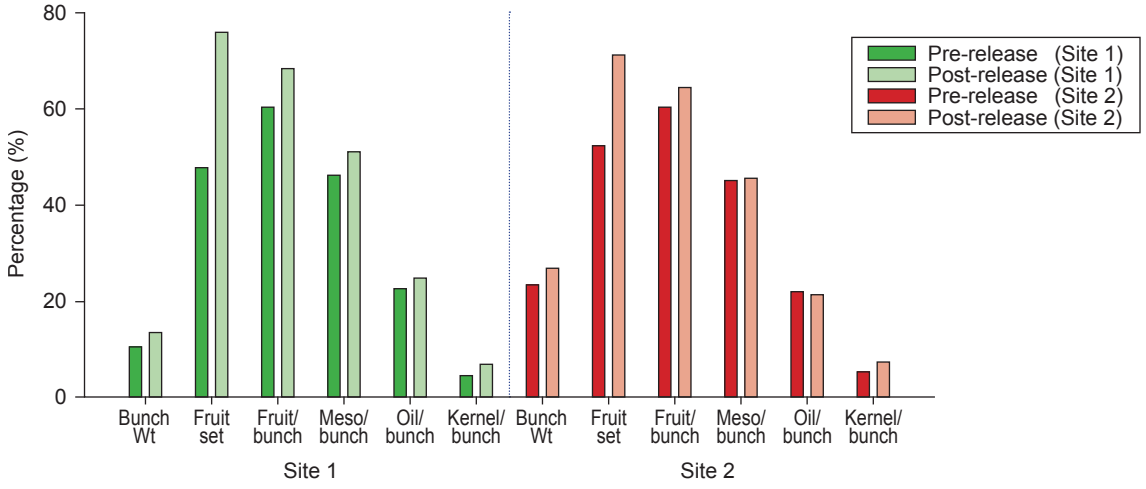
Source: Syed (1980).

Impacts of *E. kamerunicus* Introduction in Oil Palm Plantation

Effects of the introduction of* E. kamerunicus *on the oil palm yield in Malaysia. The impact of the introduction of *E. kamerunicus* to oil palm plantations in Malaysia was immense. The introduction increased the level of pollination (Basri *et al*., 1983; Choong *et al*., 2004; Syed *et al*., 1982). Syed *et al*. (1982) reported that after *E. kamerunicus* introduction, the oil palm yield-related components showed a marked increase. According to Harun and Noor (2002), pollination by the weevils increased fruit set compared to assisted hand pollination by approximately 20%. The enhanced fruit set resulted in an increased bunch weight from a higher fruit-to-bunch ratio (Harun and Noor, 2002). *Figure 1* shows the increments of yield-related components after the introduction in two sites (Site 1 and Site 2) in Johor.

Indirectly, with an increased level of entomophilous pollination with *E. kamerunicus*, the practice of manual pollination was no longer necessary (Kevan *et al*., 1986; Wahid and Kamarudin, 1997). The manual pollination practice was expensive, given the massive number of palms and areas covered in plantation settings (Alvarado *et al*., 2013; Choong *et al*., 2004). Thus, immense savings were made by doing away with the practice. Hussein *et al*. (1991) reported in their study that the introduction of the pollinating weevil allowed the industry to save approximately USD60 million annually. Due to this, the weevil was dubbed as the 'multi-million-dollar weevil' to recognise its massive contribution to the Malaysian palm oil industry (Greathead, 1983; Krantz and Poinar, 2004).

Effects of the introduction to local oil palm pollinating insects in Malaysia. The specific nature of the feeding pattern and habitat preference of *E. kamerunicus* posed minimal risks to other plants in Malaysia (Kang and Zam, 1982; Syed, 1980). However, its introduction had potential effects on the locally available oil palm pollinators (Kang and Zam, 1982). The study on the effects of *E. kamerunicus* introduction on the local pollinators was reported initially by Syed *et al*. (1982) and later by Wahid and Kamarudin (1997) and Anggraeni *et al*. (2013). Interestingly, there was no competition for food sources between *E. kamerunicus* and *T. hawaiiensis*. The latter was observed to feed on pollen grains, while *E. kamerunicus* feeds on anther tubes (Wahid and Kamarudin, 1997). However, weevils occupied the anthesising part of the male inflorescences, which created a disadvantage for the thrips (Syed *et al*., 1982). As a result, the number of thrips on the anthesising male inflorescences was declining. Nevertheless, Wahid and Kamarudin (1997) reported that *E. kamerunicus*, *T. hawaiiensis*, and *Pyroderces* could co-exist. This was attributed to the different habitat requirements for pupation, *i.e*., thrips pupates in the soil while *E. kamerunicus* and *Pyroderces* pupate in spent male inflorescences (Jagoe, 1934; Syed, 1981). In addition, thrips thrive better in dry conditions than weevils (Wahid and Kamarudin, 1997). Additionally, all three species are not active simultaneously, with weevils activity peaking around 1000-1100 hr, while thrips and *Pyroderces* are about 0800-0900 and 1400-1500 hr (Anggraeni *et al*., 2013) and past-sunset (Wahid and Kamarudin, 1997), respectively, thus allowing them to co-exist well.



Source: Syed (1982).

Figure 1. Impacts of the Elaeidobius kamerunicus *introduction on oil palm bunch composition in two sites in Malaysia.*

Factors Influencing the Pollination Efficiency of *E. kamerunicus*

Based on a recent survey conducted by MPOB, the incidence of poor fruit set formation, and stagnating OER was reported on a substantial number of estates, covering an estimated area of more than 88 000 ha, mainly in peat soil areas (Kamarudin *et al*., 2018; Sulaiman *et al*., 2018). In addition to OER, low kernel extraction rate (KER) was also used to indicate the poor fruit set formation (Choong *et al*., 2004). There were inquiries about the need to import new generations or species of pollinators. Intriguingly, poor fruit set formation has also been recorded in Indonesia (Prasetyo and Susanto, 2013; Prasetyo *et al*., 2014). This has prompted research into the factors that may influence *E. kamerunicus* pollination efficiency. After deliberate discussion in the Task Force Committee meeting, predominant factors were shortlisted and discussed in detail in this review. The factors can be divided into two main categories: intrinsic and extrinsic factors (*Figure* 2), as suggested by Costa *et al.* (2018).

(a) Intrinsic factors

***Genetic make-up of* E. kamerunicus.** The initial generation of *E. kamerunicus* introduced to Malaysia in 1981 started from 600 weevil pupae, after having discarded dead, unhealthy, and moribund pupae of the weevil (Syed, 1982). Since then, no further introductions have been made. This led to the belief that pollinating weevils in Malaysia may be suffering from inbreeding depression due to their limited genetic basis, which has negatively influenced pollination efficiency. The detrimental consequences of insect inbreeding have been extensively documented. For example, Fox *et al*. (2007) reported that the inbred larvae of the seed beetle, *Callosobruchus maculatus* (Coleoptera), took a long time to develop to emergence compared to a recent field-collected population. In addition, the larval survival rate is also reduced in the inbred populations. Vitikainen and Sundström (2010) suggested that the genetic stress induced by inbreeding has affected *Formica exsecta* (Hymenoptera) immune defense. Meanwhile, inbreeding depression impacted the lifespan, fecundity, and sex ratio of the parasitoid *Uscana semifumipennis* (Hymenoptera) (Henter, 2003). Similarly, inbreeding in the seed bug, *Oncopeltus fascia* (Hemiptera), resulted in fewer eggs production and a higher progeny mortality rate (Turner, 1960).

Morphological evolution of the domesticated weevil against samples from its region of origin was also used as possible indicators. Muhammad Nasir *et al.* (2020) found a distinct separation in the morphometric characters between the samples in Malaysia and Cameroon. Similarly, Latip *et al.* (2019) concluded that separation existed among the

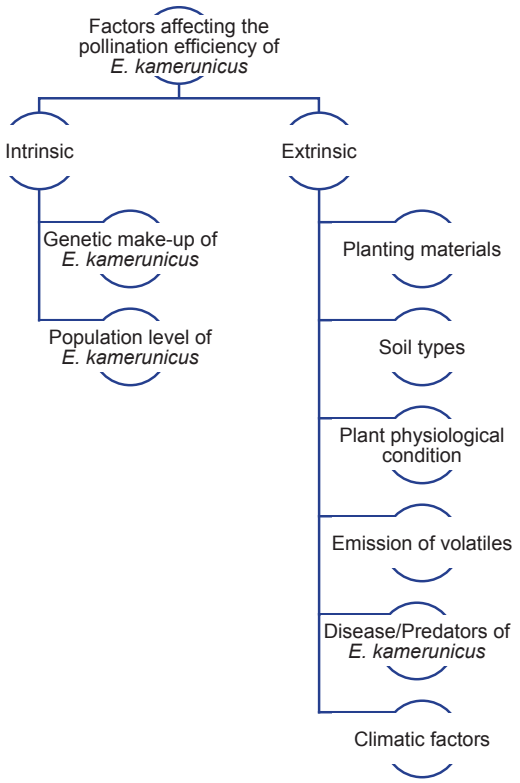


Figure 2. Factors affecting the pollination efficiency of Elaeidobius kamerunicus *discussed in the MPOB-Industry Task Force Committee Meeting on Fruit Set and Pollinating Weevil.*

E. kamerunicus samples from Malaysia, Indonesia, and Liberia. However, they concluded that genetic comparison has to be conducted to validate the results further. Li *et al.* (2019) also suggested that future research should prioritise the study on the effects of homozygosity and inbreeding depression on the introduced oil palm pollinators. Bakara *et al*. (2019) reported that no evidence of inbreeding was found in *E. kamerunicus* populations in Indonesia. In addition, the preliminary data on the genetic study presented to the Task Force Committee suggested similar findings for the adult *E. kamerunicus* sampled from Malaysian, Indonesian, and Papua New Guinea (PNG) oil palm estates. Similar findings were expected as Indonesia sourced the weevils through Malaysia (Hutauruk *et al.*, 1982; Prasetyo and Susanto, 2016). Deleterious recessive alleles that cause inbreeding depression can be 'purged' in both controlled and natural conditions, for example, in *Drosophila melanogaster* (Perez-Pereira *et al*., 2021; Swindell and Bouzat, 2006) and *Harmonia axyridis* (Facon *et al.,* 2011). This possibly explains the lack of inbreeding depression in the introduced *E. kamerunicus* in Southeast Asia (Bakara *et al*., 2019).

In contrast, Haran *et al*. (2020) suggested the introduced *E. kamerunicus* populations in Asia and the South America region may experience a bottleneck. Genetically, the *E. kamerunicus* populations in Asia (*i.e*., Malaysia, Indonesia, Thailand and Myanmar) and South America (*i.e*., Guatemala, Brazil, Colombia, and Ecuador) belong to both Western and Central Africa. They also found a low haplotype number across all Asian populations of *E. kamerunicus*, which suggests that the introductions were made from a limited number of individuals, contributing to a limited genetic base among these populations. Indeed, for the Malaysian population, Syed *et al*. (1982) reported that out of 1200 pupae, only 600 individuals survived upon arrival in Kuala Lumpur, Malaysia from Cameroon. However, Haran *et al*. (2020) agreed that more research is needed to determine how genetic bottlenecking affects the pollination rate. Therefore, studies on the dispersal behaviour and fitness of the current generation of *E. kamerunicus* in Malaysia are needed to enable a better understanding of the genetic patterns observed.

***The population of* E. kamerunicus.** The population level of the pollinating weevil is a crucial factor in ensuring a satisfactory pollination level (Zulkefli *et al*., 2020). The introduction of weevils into Malaysia has positively impacted the oil palm fruit bunch formation (Syed *et al*., 1982). Since then, efforts to monitor its population in the field have been conducted by several researchers *e.g*., Cik Mohd Rizuan *et al.* (2013); Daud and Idris (2016); Mohamad *et al*. (2021b); Wahid *et al.* (1987)]. Various minimum weevil requirements for a satisfactory fruit set formation were suggested. Donough *et al*. (1996) recommended that 20 000 weevils ha^{-1} are required for a fruit set of 55%. Meanwhile, Syed and Salleh (1987) reported that to obtain at least 70% pollination, approximately 3000 weevils per female inflorescence are needed. Meanwhile, Mohamad *et al*. (2021b) suggested that a population of 14 000 individuals ha^{-1} was sufficient to obtain a good fruit set percentage of 65%.

During the first few months after the introduction of *E. kamerunicus*, Syed *et al.* (1982) reported that the introduced population increased rather rapidly. Due to palm height, the density of male inflorescence in the area, wind direction, and human intervention, the dispersal rate on older palms was faster than on the younger ones. During the initial phase of the introduction, the density of *E. kamerunicus* usually remained above 40 individuals per spikelet, reaching as high as more than 200 individuals per spikelet (Syed *et al*., 1982). Several years after, the weevil population in Malaysia has stabilised to between 26 to 29 weevils per spikelet in Peninsular Malaysia and 32 individuals per spikelet in East Malaysia (Wahid *et al*., 1987). Subsequent efforts were regularly conducted in monitoring the pollinating weevil population. Daud and Idris (2016) found that in an estate in West Malaysia, the weevil population ranged from about 14 to 54 individuals per spikelet. Whereas, in Sabah, the mean weevil population was 20 individuals per spikelet (Cik Mohd Rizuan *et al*., 2013). Meanwhile, a smaller population was observed in peat soil regions of Sarawak, where the mean population size of the pollinating weevils was between 16 and 17 individuals per spikelet (Sulaiman *et al*., 2018), a decline compared to the initial studies. However, it should be emphasised that the findings published by Wahid *et al*. (1987) were based on a single estate in Sarawak, and therefore do not necessarily reflect the whole state. Additionally, Mohamad *et al*. (2021a) found that in Sarawak, the average weevil population per spikelet in oil palm estates is located in mineral soil (26 weevils/spikelet) is greater than those in peat soil areas (15-21 weevils/spikelet).

One of the reasons *E. kamerunicus* was selected as the suitable candidate for the importation is its capability to withstand wet seasons, a natural and frequent condition in the tropics (Syed *et al*., 1982). This was substantiated by findings by Daud and Idris (2016); Dhileepan (1994); Latip *et al.* (2018); Wahid *et al.* (1987), that rainfall did not have harmful effects on the weevil population. However, the event of drought (rainfall <100 mm $month^{-1}$) and excessive rainfall (> 370 mm $month^{-1}$) may adversely affect the weevil population level (Wahid *et al*., 1987). However, it was pointed out that the resulting fruit set percentage is in an acceptable range even with the fluctuating

pollinator populations (Mohamad *et al*., 2021b). These findings indicate that other causal factors could influence fruit set formation in addition to the presence of the pollinating weevil.

(b) Extrinsic factors

Planting materials. The crop's limited genetic base, which was derived mainly from direct descendants of seedlings brought to Indonesia in 1848, previously hampered oil palm productivity in Malaysia and exposed the crop to the threats of pests and diseases and productivity stagnancy (Rajanaidu *et al*., 2000). To overcome this problem, MPOB initiated efforts to diversify the genetic profile of the crop via germplasm collection in the early 1970s (Rajanaidu *et al*., 2013). This has enabled MPOB researchers to leverage the diversity of the germplasm in its extensive breeding programme for crop improvements. Disease resistance *e.g*., Hanin *et al*. (2020); Maluin *et al*., 2020, higher nutritional values, and industry-driven desirable traits (*e.g*., short trunk height, short frond length, dwarfness, long-stalk, short rachis length) were given priority in the breeding programme (Idris *et al*., 2004; Kushairi *et al*., 2004; Noh *et al*., 2005; Rajanaidu *et al*., 2000; Teh *et al*., 2020; Zulkifli *et al*., 2017). Propagation of high-yielding materials through tissue culture has increased the yield by 25% (Rohani *et al*., 2000). The most highly productive planting materials selected have a high sex ratio (Rohani *et al*., 2000). A high inflorescence sex ratio tends to reduce the availability of male inflorescences in the field, limiting the food source and the breeding sites of *E. kamerunicus*, subsequently affecting its population (Bulgarelli *et al*., 2002). Furthermore, pollen availability was also affected (Barcelos *et al*., 2015). Some clonal palms, *e.g*., the Federal Land Development Authority (FELDA) Clonal Palm (Latip *et al*., 2018) and DxP Simalungun (Wahyuni *et al*., 2019), were observed to have a higher number of spikelets, which meant more excellent food source and breeding sites available for the weevils. A higher number of spikelets contributed to a significantly greater *E. kamerunicus* population compared to standard planting materials (Latip *et al*., 2018; Wahyuni *et al*., 2019). Some planting materials, *e.g*., DxP Simalungun (Indonesia), produced more pollen grains, due to the 25%-35% increase in the number of spikelets (Wahyuni *et al*., 2019).

Soil types. The level of the productivity of a crop is heavily influenced by soil characteristics (Woittiez *et al*., 2017). In Malaysia, due to the scarcity of suitable land for oil palm cultivation, the crop is planted in peat soils. The development of the peat soils was not ideal due to the issue of carbon emissions and climate changes *e.g*., Murdiyarso *et al*. (2019); Yule (2010). However, many mitigation strategies for reducing carbon dioxide (CO_2) emissions in the oil palm ecosystem have been proposed, including intercropping systems (Kusumawati *et al*., 2021; Li-li *et al*., 2015), soil fauna improvement, and appropriate farming practices (Paterson and Lima, 2018). Woittiez *et al.* (2017) suggested that biochemically constrained soils, such as peat soils, were identified as oil palm yield-limiting factors. Different characteristics of peat (*e.g*., peat composition stage) substantially affected oil palm yield (Veloo *et al*., 2015). Sulaiman *et al.* (2018) also noted that fruit set formation is better in mineral soil regions. Due to the frequent incidence of palm leaning, waterlogging and excessive drying, the crop yields on the peat soil are generally lower than those in mineral soil (Paramananthan, 2013). In addition, Veloo *et al*. (2015) suggested that the oil palm rooting was the main cause of the difference in the oil palm yield. The area with sufficiently decomposed peat (*i.e*., sapric soils) has a better rooting and growth medium than undecomposed peat soil. Still, its level of high porosity means that it does not have good nutrient retention properties. The problem of nutrient leaching in this type of soil is especially severe in the event of heavy precipitation (Veloo *et al*., 2015). The peat soil itself, mainly classified as Tropofibrists and Tropohemists in the United States Department of Agriculture (USDA) soil order of Histosols, has low nutrient content (except for nitrogen) and poor nutrient retention capacity, especially for potassium (Mutert *et al*., 1999). Besides, the peat soil, with its large water holding capacity, posed a risk of water being stagnant during monsoon, and the reduced aeration can negatively affect the roots' formation and functionality. The reduced nutrient supply in the peat soil is usually manifested through shorter frond length (Mutert *et al*., 1999), reduced vegetative growth, and smaller fruit bunch (Ng and Tan, 1974; Ng *et al*., 1990; Turner and Bull, 1967). However, obtaining a high yield comparable to mineral soil is possible with proper planning and management strategies. For example, increasing the soil bulk density will bring subsequent positive impacts on soil capillarity, improved anchorage, and an increase in the supply of nutrients while minimising the risks of subterranean termite infestation (Mutert *et al*., 1999). Furthermore, Zuraidah (2019) reported that the increase in soil bulk density and reduction in total porosity leads to an increase in oil palm yield. It was evident that the soil types on which the crop is cultivated heavily influence the nutrient availability of the crop, potentially altering the physiological development of the palm. This includes the inflorescence development and the volatiles emission, which in turn, affects the population and the behaviour of the pollinating weevil. Zulkefli *et al*. (2020) suggested that further understanding of the relationship between the soil types and their effects on the weevils' behaviour is required.

Plant physiological condition and morphological stress. The availability of male inflorescences affects the food sources and breeding sites for weevil (Eardley *et al*., 2006; Syed *et al*., 1982). The overall field density of the male inflorescences is influenced by various factors, among them are the soil types and the plant stress manifested due to water availability (Bulgarelli *et al*., 2002; Corley, 1976a; Corley and Tinker, 2003). Oil palm has separate male and female flowers on the same plant, embodied in distinct male and female inflorescences (Corley and Tinker, 2003). The sex differentiation of the oil palm inflorescences, which usually occurs 22-24 months before harvesting, is influenced by moisture stress (Corley, 1976b). Prolonged drought will result in the increase of potential evapotranspiration (PET) in mature palms to around 10 mm daily, as opposed to normal PET of 5-5.0 mm daily (Foong, 1999). Whereas, during the wet period, the rate could be as low as 3.0 mm to 3.5 mm daily (Azlan *et al*., 2016). In the period of prolonged drought and water deficit, it was observed that the palms tend to produce more male inflorescences (Adam *et al*., 2011). However, this leads to reduced FFB production and lower yield. Zulkifli *et al*. (2017) highlighted intensive efforts in designing high-yielding palms. These planting materials have more female inflorescences but fewer male ones (Prasetyo *et al*., 2012; Purba *et al*., 2009). Normally, combinations of clonal palm and normal palm planting are recommended (Kushairi *et al*., 2010). In the event of low availability of male inflorescences, Durand-Gasselin *et al*. (1999) suggested that the over-pruning of palm fronds can increase the production of male inflorescences. Increased male inflorescence production has also been reported when high-density planting is implemented *e.g*., 148-86 palms ha^{-1} (Breure *et al*., 1990); 180 and 205 palms ha^{-1} (Bonneau *et al*., 2014). The situation results in decreased frond production, photosynthesis, female inflorescences, and fruit bunches (Bonneau *et al*., 2014; Breure *et al*., 1990). The balance between maintaining a healthy balance between the productions of both sexes of inflorescences is crucial as both are needed to maintain a healthy population of pollinating weevil and obtain satisfactory yield production.

Emission of volatiles. *Elaeidobius kamerunicus* relies on olfactory senses to guide it to oil palm inflorescences. Inflorescences of oil palm emit volatile organic compounds (VOCs), mostly estragole (4-allyl anisole) to attract *E. kamerunicus* (Hussein *et al*., 1991: Lajis *et al*., 1985; Muhamad Fahmi *et al*., 2016). *E. kamerunicus* is primarily attracted to estragole emitted by *E. guineensis* due to the specific arrangement of the methoxy and allyl groups on the aromatic ring (Lajis *et al*., 1985). Male inflorescences produce estragole and 1-dodecyne, for which *E. kamerunicus* has a high affinity, while female inflorescences emit a variety of volatiles, primarily squalene and farnesol (Anggraeni *et al*., 2013). This explains the larger number of *E. kamerunicus* found in male inflorescences (Anggraeni *et al*., 2013; Lajis *et al*., 1985; Syed, 1979). The level of estragole emission in oil palm was different depending on the soil types and planting materials (Idris *et al*., 2018; Muhamad Fahmi *et al*., 2016). In addition to the factors mentioned above, various environmental variables such as temperature, light intensity, and pathogen attacks significantly impacted the VOCs released from plants (Holopainen and Gershenzon, 2010). For example, an increase between 5ºC and 10ºC will cause the release of higher amount of phenethyl acetate in *Trifolium repens* (Jakobsen and Olsen, 1994). In addition to temperature, an increase in light intensity was also found to be inducing the release of a greater amount of VOCs in *Pinus elliotii* (Tingey *et al*., 1980). In other plants, elevated level of VOCs release indicates the presence of pathogen attacks, as observed in legume *Medicago truncantula* (Leitner *et al*., 2008), tobacco plants, *Nicotiana tabacum* (Huang *et al*., 2003) and lima bean, *Phaseolus lunatus* (Yi *et al*., 2009). Herbivory was also proven to induce an increased level of VOCs emission as a plant defensive response (Pare and Tumlinson, 1997; Turlings and Ton, 2006; Turlings and Tumlinson, 1992). In the event of herbivore injured *Zea mays*, an elevated level of terpenoid linalool emission was detected several hours after the damage was inflicted (Ruther and Furstenau, 2005; Turlings and Tumlinson, 1992). Similar observations were also reported in tomato, *Lycopersicon esculentum* (Farag and Pare, 2002), cotton plants, and *Gossypium hirsutum* (Pare and Tumlinson, 1997). Changes in the VOCs emission may alter the plant-insect relationship. In oil palm, Idris *et al*. (2018) suggested that the release of excessive estragole concentrations of 150 ppm and 200 ppm may result in repellent effects on *E. kamerunicus*. Other instances of the changes in the dynamics of plant-insect relationship due to the modification in plant VOCs emission were observed in cabbage, where the changes in the VOCs released by the plants affected the plant-host finding ability of *Plutella xylostella* (Li *et al*., 2016). Similarly, the foraging activity of the herbivore *Rhopalosiphum maidis* was affected in the event of altered VOCs emission in barley (*Hordeum vulgare*) due to elevated atmospheric CO_2 concentration (Chen *et al*., 2019). It was evident that multiple environmental factors can influence the pattern of plant volatiles emission, and modification in the composition and VOC emission level influenced the plant-insect relationship. It is essential to study the factors affecting VOCs emission in oil palm, and the extent of the elevated levels of estragole emissions effects on the density and behaviour of *E. kamerunicus* in the field and the oil palm fruit set formation.

Diseases or Predators of *E. kamerunicus*

Maintaining a sufficient population of *E. kamerunicus* in the field is important to ensure optimal fruit bunch formations. However, the presence of diseases, parasites, and natural enemies of the pollinating weevil may affect their general well-being, jeopardise their pollination efficiency, and threaten their survival if left unchecked. The following section of this review will discuss the types of diseases and predators of *E. kamerunicus* and the extent of their damage to the pollinating weevil.

***Effects of parasitic nematode activities on* E. kamerunicus.** Parasitic nematode *Elaeolenchus parthenonema* was found living inside *E. kamerunicus* body (Poinar *et al*., 2002). It was further revealed that although the nematodes could be present in both genders, the effects can only be seen on heavily infested female weevils, such as reduced egg production, causing them to be sterile, and reducing their size by reducing the fat reserves. The association with this nematode species probably may have a bearing on the weevil's pollination efficiency.

***Microbes found on elytra/ parasitising* E. kamerunicus.** Hussein *et al*. (1991) reported that the bacteria *Serratia marcescens* was isolated from the gut of larvae and pupae from *E. kamerunicus* samples from sites in Peninsular Malaysia. The reported infection rates ranged from 11%-17% (larvae) to 9%-23% (pupae). *Serratia marcescens* is a pathogen of many insects (Aggarwal *et al*., 2015; Flyg and Xanthopoulos, 1983; Kaaya and Darji, 1989; Steinhaus, 1959; Wei *et al*., 2017) and is found to cause mortality in insects, such as *Spodoptera exigua* (Konecka *et al*., 2019) and mosquitoes (Bahia *et al*., 2014). However, the article by Hussein *et al*., (1991) only reported on the presence of the pathogen on *E. kamerunicus* and did not further elaborate on its effects on the pollinating weevil. It will be interesting to assess the current rate of bacterial presence and its effects on *E. kamerunicus*.

***Predator effects on* E. kamerunicus.** The high mortality rate of the immature weevils (*i.e.*, egg, larval, and pupal individuals) due to rat predation was reported previously (Chiu *et al*., 1985). This was mainly observed at post-anthesis male inflorescences, where the immature weevils are abundant (Muhammad Luqman *et al*., 2017; Syed, 1979). Rats start predating the weevils as early as the second day after anthesis (Hussein, 1984). The mortality rate was 82% and 85% on eight-years-old palms and 11-years-old palms, respectively. It was also observed that the damage was more severe in shorter palms, presumably due to easier access of the rats to the crown region of the palm. However, during the study, even with the high rate of rat predation, the healthy weevil populations were sustained, between 54 000-95 000 individuals per hectare (Chiu *et al*., 1985). Kamarudin *et al*. (2018) reported that in peat and mineral soils in Sarawak, Malaysia, the maximum weevil population is less than 50 000 individual ha^{-1}. So, a high rat population may affect the weevil populations in such areas, and proper rat population management procedures should be conducted. In Peninsular Malaysia, the usage of the barn owl (*Tyto alba*) as a biological control agent is common (Wood and Chung, 2003). According to Muhammad Syafiq *et al*. (2016), most of the owl species recorded in Peninsular Malaysia are associated with the oil palm ecosystem. However, the report of comparable practices in other areas of Malaysia was relatively sparse.

Elaeidobius kamerunicus is also preyed upon by reduviid bugs, *Cosmolestes picticeps,* and *Sycanus dichotomus* (Muhammad Luqman *et al*., 2017). Both are prevalent in the oil palm environment and are often used as biological control agents to reduce bagworm populations (*e.g*., *Metisa plana* and *Pteroma pendula*) (Azlina and Tey, 2011; Jamian and Nur Azura, 2018; Jamian *et al*., 2017; Siti Nurulhidayah *et al*., 2020). They were seen preying on mature *E. kamerunicus* on the surface of the male inflorescences. Muhammad Luqman *et al.* (2017) hypothesised that the predation rate on *E. kamerunicus* by both reduviids increased when the level of bagworm populations in the field is low.

Climatic Factors

Crops rely on soil and climate to thrive. While fertilisers can be used to change the chemical composition of soils, other factors such as soil physical features and climate temperature regimes are impossible to be altered in commercial settings. Oil palm is a generally tough crop and able to adapt to suboptimum climatic conditions (Gunawan *et al*., 2020). There are instances in which minimal damages were inflicted on the crops even after an extended dry season (Corley and Tinker, 2003). However, plant-environment interactions are predicted to be impacted by climate change [Intergovernmental Panel on Climate Change (IPCC), 2014]. The expected increase in greenhouse gas (GHG) emissions will elevate the atmospheric CO_2. The influence of elevated atmospheric CO_2 on plant physiology is becoming increasingly well-documented [*e.g*., Kumar *et al*. (2019); Zinta *et al*. (2018)]. In general, the elevated atmospheric CO_2 instigates an increase in the photosynthetic rates, which enables faster crop development (Li *et al*., 2017). Interestingly, the impact of the elevated CO_2 on the development of *E. kamerunicus* was observed to be minimal (Amanina *et al*., 2016). While the

findings from the cited experiment revealed that doubling the concentration of ambient CO_2 to 800 ppm had no significant effect on the emergence of *E. kamerunicus*, long-term effects on its biology and its adaptability to the elevated ambient CO_2 is yet to be fully understood.

Climate warming and changing precipitation patterns are the other aspects of climate change, which may influence the plant-insect relationship. It has been reported that elevated temperature may affect pollination, either on the physiology of the plant itself *e.g.*, sterility in rice (Kobayasi *et al*., 2019), flower and tassel initiation in maize (Adishesha *et al*., 2017), delayed flowering in *Arabidopsis thaliana* (Ward *et al*., 2012) or on the pollinating insects *e.g*., reduced pollinator visitation (Burkle and Runyon, 2016; Glenny *et al*., 2018) and insect coordination and memories (Chen *et al*., 2019; Stec and Kuszewska, 2020). As discussed in the earlier section of this review, increased ambient temperature affects the plant volatiles emission, modifying the composition of the volatiles and the quality of the floral cues (Farré-Armengol *et al*., 2014; Räisänen *et al*., 2008). The signal disruption leads to the breakdown of the recognition process, affecting the pollinator visitation rates (Farré-Armengol *et al*., 2014; Jakobsen and Olsen, 1994).

The rate of rainfall was found to have minimal impacts on the population level of *E. kamerunicus* (Daud and Idris, 2016; Dhileepan, 1994; Latip *et al*., 2018). In fact, the wet season is said to be better for *E. kamerunicus* breeding (Dhileepan, 1994). However, although its population was not affected by rainfall, the pollination efficiency of the pollinating weevil and the pollen viability of the crop was affected by rainfall (Gunawan *et al*., 2020). In the event of rain, the number of pollen grains carried by the weevils was significantly reduced (Appiah and Agyei-Dwarko, 2013; Dhileepan, 1994). In some plant species, high rainfall may reduce the stigma pollen load, affecting the pollen deposition and leading to reduced pollination (Hendrix *et al*., 1999). Hence, obtaining a further understanding of the impact of climate changes on the behaviour and fitness of the pollinating weevil is vital to enable the optimisation of crop pollination in the field.

Managing a Healthy Level of *E. kamerunicus* Population

This review has discussed both intrinsic and extrinsic factors that may have influenced the pollination efficiency of *E. kamerunicus*. Maintaining a sufficient weevil population in the field is critical for satisfactory fruit bunch production. It was also essential to provide enough resources for the weevils while maintaining a profitable fruit bunch production. Plant stress, which can impact physiological characteristics and volatile emissions in the field, can be reduced with the use of good agricultural practices and land preparation. The following section of this article will further elaborate on the strategies to manage the population of *E. kamerunicus* in the field.

Minimising the usage of chemical insecticides. In the oil palm plantation settings, most insects depend on relatively limited resources for food and shelter. Due to this, the management of insect pests also poses risks to beneficial insects, such as *E. kamerunicus*. *Tirathaba mundella* is one of the major insect pests of oil palm in peat areas in Sarawak, Malaysia (Mohamad *et al*., 2017; Ming *et al*., 2016; Sulaiman *et al*., 2021). The moth was observed to be spending most of its initial phase of development in the female inflorescences and spent male inflorescences of oil palm (Mohamad *et al*., 2017; Ming *et al*., 2016; Prasetyo *et al*., 2018; Yaakop and Abdul Manaf, 2015). The larvae of the pest are damaging the oil palm fruit bunch by scrapping the fruitlets and later boring holes in the mesocarp up to the kernel of the palm fruit (Lim, 2012). Prasetyo *et al.* (2018) and Lim (2012) observed that severe infestation of *Tirathaba* adversely affected the fruit set formation. Pest management requires insecticide application on the male inflorescences (Ming and Bong, 2017; Mohamad *et al*., 2017; Prasetyo and Susanto, 2019; Prasetyo *et al*., 2018). Thus, the application of insecticides, especially broad-spectrum chemicals, on the male inflorescences can potentially affect the population of the pollinating weevil (Ming and Bong, 2017; Prasetyo and Susanto, 2019). It was found that the active ingredients of 20% w/w dinotefuran, 80% w/w fipronil, and 5.5% w/w cypermethrin were able to inflict 79.52%, 87.91% and 44.82% mortality on adult *E. kamerunicus* (Ming and Bong, 2017). Some chemical insecticides were reported to have minimal impacts on the mortality of the weevils, such as chlorantraniliprole (Ming and Bong, 2017) and flubendiamide (Asib and Musli, 2020; Prasetyo and Susanto, 2019). Prasetyo and Susanto (2019) reported that the effects of both chlorantraniliprole and flubendiamide on *E. kamerunicus* were comparable to the control samples. Both recorded a mortality rate of 11% and 12% (one-day after treatment), respectively. Meanwhile, *E. kamerunicus* samples treated with water (control) recorded a mortality rate of 9%. Application of biological control agents, such as *Bacillus thuringiensis*, was also reported to reduce the larval population of *Tirathaba* spp. (Mohamad *et al*., 2017; Prasetyo *et al*., 2018). Prasetyo *et al.* (2018) and Ahmad *et al.* (2009) have reported that *B. thuringiensis*, which is mainly applied to control lepidopteran pests (*e.g*., *Pteroma pendula, Metisa plana*, *Tirathaba* spp.), has minimal effect on the mortality of *E. kamerunicus. Bacillus thuringiensis* gave the longest median Lethal Time

(LT_{50}) to induce mortality in *E. kamerunicus* at 137 hr. Comparatively, cypermethrin gave a relatively short LT_{50} of 17 hr (Asib and Musli, 2020). In addition to the application of the insecticides, alternative population control strategies, such as mass-trapping of adult *Tirathaba* moths, were also tested (Sulaiman *et al*., 2021). These studies highlighted the importance of adopting properly-planned pest population controlling strategies while minimising the impacts on the population of beneficial insects in the oil palm ecosystem.

Preservation of biodiversity on pollination levels. Sustainable pest management strategies are vital to minimise the impacts on insect biodiversity and the sustainability of the crop itself. A study by Mayfield (2005) highlights the importance of insect biodiversity on oil palm yield. In the finding, although the areas of palm plantations close to the forest do not have greater floral-visitor diversity per visitation rate, the presence of understory vegetation in oil palm plantations helped increase the number of non-weevils pollinators in the area. Although maintaining understory complexity had no significant effects on fruit set formation, the increased insect biodiversity did not jeopardise the pollination and the population of the pollinator (Harianja *et al.*, 2019). In a biodiversity enrichment trial by Gerard *et al.* (2017), the plot with higher biodiversity had significantly higher yield than the control, even with lower planting density. Stand structural complexity can potentially contribute to establishing a more favourable microclimate (Donfack *et al*., 2021; Tscharntke *et al*., 2011), which also provides the benefits of biological pest control (Tscharntke *et al*., 2011). This study highlights the importance of maintaining a healthy level of biodiversity in the oil palm plantation area by providing complementary pollination services, rendering natural pest population control while maintaining a satisfactory yield and productivity.

Weevil population supplementation. Management factors, effects of the surrounding landscape, and mass-replanting were identified as some of the main factors affecting the pollinating weevil populations and fruit set formations in oil palm plantations (Li *et al*., 2019). In the areas where the mass-replanting of oil palm is conducted, rebuilding the pollinating weevil population usually requires time, resulting in poor fruit formations and a high rate of bunch abortions. In such areas, the practice of re-introduction and supplementing the weevil population is necessary. The weevil hatch and carry system are proven to be successful in improving fruit formation in the field. In Sabah, Malaysia, the application of the system was able to overcome the problem of occasional poor fruit set formation, with the trial field achieving an average fruit set percentage between 58%-59% (Choong *et al*., 2004). Whereas in Indonesia, applying a similar system has resulted in an improvement of fruit set between 15%-21% (Prasetyo *et al*., 2014). The system utilised the spent spikelets of male inflorescences (containing weevil larvae) placed in a wooden shelter in the field. Upon hatching, the new cohorts of weevils will be puffed with viable pollen grains before release (Choong *et al*., 2004; Prasetyo *et al*., 2014). Variation of the hatchery systems is also suggested, and the result is quite promising (Genting Plantations Research Centre, 2018). The system, however, is not without its disadvantages. Some estates are questioning its practicality, citing the additional human resources and time required to source the proper stage of spent male inflorescences, then acquiring sufficient viable pollen grains to be applied on the hatchery, and the general maintenance of the hatchery. Improper application of the practice usually rendered the improvement brought about by the hatchery to be insignificant. Hence, the success of such a system depended on close supervision for precise application and cooperation between the management and field personnel.

Additionally, the introduction of pollinating the weevil population to the newly-opened oil palm plantation has been done previously, consequently improving the estate's yield (Prasetyo and Susanto, 2016). In the event/areas where a constant supply of post-anthesising male inflorescences is complex, supplementation of the weevil population in the field can also be achieved through rearing the weevils on an artificial diet. Studies to develop the artificial diet formulation for the laboratory rearing of the weevils were initiated *e.g*., Zahari *et al*. (2019); Zulkefli *et al*. (2021), and further understanding of the nutritional contents of the natural feed was also reported (Zulkefli *et al*., 2021).

Maintaining a sufficient number of male inflorescences in the field. The food source and breeding site availability for *E. kamerunicus* depends on the density of male inflorescence in the area. With the general aim to maximise yield without further expanding oil palm land use, the emphasis has shifted to developing high-yielding varieties (Kushairi *et al*., 2010; Murphy, 2007; Soh, 2012). However, these varieties typically produce a more significant number of female inflorescences, which will later develop into fruit bunch. This scenario creates an imbalance in the sex ratio of the inflorescences and results in the lack of resources available for the pollinating weevil (Li *et al*., 2019; Rao and Law, 1998). It was recommended that the DxP material be planted in every four rows of clonal material to supply sufficient resources to the pollinating weevil to overcome the imbalance in the inflorescence sex ratio (Kushairi *et al*.,

2010). Furthermore, the inducement of stress and unfavourable conditions are known to be causing the increased production of male inflorescences (Corley, 1976a). Agronomic practices such as over-pruning are shown to artificially induce the production of male inflorescence (Durand-Gasselin *et al*., 1999) and reduce the rate of male inflorescences abortion (Legros *et al*., 2009). As such, prudent management practices are necessary to ensure a sufficient number of male inflorescences are available for *E. kamerunicus* in the field.

What Next: A Way Forward

Several factors have been considered and elaborated on thoroughly in this review to solve the issues and problems regarding pollination efficiency. The committee has agreed that the following factors require further attention to solve the low fruit set problems; 1) Soil types, 2) planting materials, 3) weevil diseases and predators, 4) plant physiological and morphological stress, 5) estragole emission, and 6) sex ratio of the inflorescences. In addition, further understanding of the behaviour of the pollinating weevil is required. This includes the updated information on the fitness levels of *E. kamerunicus*, such as their searching ability and diel activity patterns. Based on the available literature and the research projects undertaken by the committee member, the majority of the committee members opined that for the time being, less priority should be given towards the idea of the importation of a fresh source of *E. kamerunicus* to increase the genetic pool or importation of entirely different pollinating insect species from the African region. Instead, the focus should be directed towards the studies related to the shortlisted factors discussed in this review.

CONCLUSION

Elaeidobius kamerunicus plays a vital role in the pollination of oil palm. Its introduction has brought a significant contribution to improving the oil palm fruit formation. It is difficult to discern a single factor that influences the pollination rate of oil palm. However, the shortlisted factors discussed in this review may be useful to the palm oil industry players and decision-makers in determining their priorities. Preserving healthy population levels of *E. kamerunicus* is essential to maintain the adequate pollination of oil palm. Frequent monitoring and census of the pollinator population have to be done. Practices that may jeopardise the population of pollinators should be avoided. Further understanding of the impacts of climate changes on the population, fitness and the behaviour of *E. kamerunicus* will be crucial.

In addition, a conclusive study on the genetic make-up of the current generation of *E. kamerunicus* in Malaysia is required. Effects of other factors such as VOCs emission (*i.e*., estragole) and nematode parasitisation on weevil certainly require a more thorough understanding. General yield indicators such as bunch count, bunch weight, OER, and KER should be monitored regularly to ensure that fruit formation continues to be satisfactory. Proactive measures can be taken if any irregularities are detected. Some of the factors can be controlled with the provision of good agricultural practices and sound planning during land preparation. This includes the possibility of biodiversity enrichment in the oil palm plantation ecosystem, understory management, and soil management. A thorough understanding of factors affecting the pollination efficiency of *E. kamerunicus* will be instrumental in sustainably improving the productivity of the Malaysian palm oil industry.

ACKNOWLEDGEMENT

The authors would like to extend their gratitude to the Director-General of MPOB for permission to publish this review.

REFERENCES

Adam, H; Collin, M; Ricahud, F; Beule, T; Cros, D; Omore, A; Nodichao, L; Nouy, B and Tregear, J W (2011). Environmental regulation of sex determination in oil palm: Current knowledge and insights from other species. *Ann. Bot.*, *108*: 1529-1537.

Adishesha, K; Janagoudar, B S; Amaregouda, A; Shanawad, U K and Chandranaik, M (2017). Morphological characters of maize (*Zea mays* l.) genotypes to elevated carbon dioxide and temperature regimes. *Int. J. Pure App. Biosci*., *5(5)*: 163-170.

Aggarwal, C; Paul, S; Tripathi, V; Paul, B, and Khan, M A (2015). Chitinolytic activity in *Serratia marcescens* (strain SEN) and potency against different larval instars of *Spodoptera litura* with effect of sublethal doses on insect development. *BioControl*, *60*: 631-640.

Ahmad, M N; Siti Ramlah, A A; Mazmira, M M M and Wahid, M B (2009). Effect of *Bacillus thuringiensis*, Terakil-1 and Teracon-1 against oil palm pollinator, *Elaeidobius kamerunicus* and beneficial insects associated with *Cassia cobanensis*. *J. Oil Palm Res.*, *21*: 667-674.

Alvarado, A; Escobar, R and Henry, J (2013). *El híbrido OxG Amazon: Una alternativa para regiones por pudrición del cogollo en palma de aceite*. *Revista Palmas*, *34*: 305-314.

Amanina, N S; Hasnudin, M Y; Haniff, M H; Roslan, M N; A'fifah, A R and Ramle, M (2016). Effects of high carbon dioxide level on the emergence of oil palm pollinating weevil, *Elaeidobius kamerunicus*. *J. Oil Palm Res.*, *28(2)*: 172-176.

Anggraeni, T; Rahayu, S; Ahmad, I; Esyanti, R R and Putra, R E (2013). Resources partitioning and different foraging behavior is the basis for the coexistence of *Thrips hawaiiensis* (Thysanoptera: Tripidae) and *Elaeidobius kamerunicus* (Coleoptera: Curculionidae) on oil palm (*Elaeis guineensis* Jacq.) flower. *J. Entomol. Nematol.*, *5(5)*: 59-63.

Appiah, S O (1999). Studies into entomophil pollination of oil palm. *J. Ghana Sci. Assoc.*, *1(2)*: 70-77.

Appiah, S O and Agyei Dwarko, D (2013). Studies on entomophil pollination towards sustainable production and increased profitability in the oil palm: A review. *Elixir Agric.*, *55*: 12878-12883.

Auffray, T; Frerot, B; Poveda, R; Louise, C and Beaudoin-Olivier (2017). Diel patterns of activity for insect pollinators of two oil palm species (Arecales: Arecaceae). *J. Insect Sci.*, *17(2)*: 45.

Azlan, A H; Tui, L C; Yaw, S K; Selvaraja, S; Rohan, R; Ariffin, I and Palaniappan, S (2016). Impact of *El Nino* on palm oil production. *Planter*, *92(1088)*: 789-806.

Asib, N and Musli, N N (2020). Effect of six insecticides on oil palm pollinating weevil, *Elaeidobius kamerunicus* (Coleoptera: Curculionidae). *Serangga*, *25(2)*: 1-9.

Azlina, Z and Tey, C C (2011). Killing efficiency of selected insect predator species against bagworm *Metisa plana*. *Proc. of the PIPOC 2011 International Palm Oil Congress*. MPOB, Bangi. p. 1-9.

Bahia, A C; Dong, Y; Blumberg, B J; Mlambo, G; Tripathi, A and Ben Marzouk-Hidalgo, O J (2014). Exploring *Anopheles* gut bacteria for *Plasmodium* blocking activity. *Environ. Microbiol.*, *16*: 2980-2994.

Bakara, R D J; Buchori, D; Kusumah, R Y M; Sahari, B and Apriyanto, A (2019). Genetic diversity of *Elaeidobius kamerunicus* Faust (Coleoptera: Curculionidae) across geographic areas in Indonesia: Implications for oil palm sustainability. *IOP Conf. Ser.: Earth Environ. Sci.*, *325*: 012003. DOI: 10.1088/1755-1315/325/1/012003.

Basri, M W; Halim, A H and Hitam, A H (1983). Current status of *Elaeidobius kamerunicus* Faust and its effects on the oil palm industry in Malaysia. *Occasional Paper, 6*: 39.

Barcelos, E; Rios, S A; Cunha, R N V; Lopes, R; Motoike, S Y; Babiychuk, E; Skirycz, A and Kushnir, S (2015). Oil palm natural diversity and the potential for yield improvement. *Front. Plant Sci.*, *6*: 190.

Bulgarelli, J; Chinchilla, C and Alvarado, A (2002). Vegetative growth curves in a commercial *Deli* x *AVROS* cross. *ASD Oil Palm Papers*, *24*: 30-31.

Burkle, L A and Runyon, J B (2016). Drought and leaf herbivory influence floral volatiles and pollinator attraction. *Glob. Change Biol.*, *22(2016)*: 1644-1654.

Bonneau, X; Vandessel, P; Buabeng, M and Erhahuyi, C (2014). Early impact of oil palm planting density on vegetative and oil yield variables in West Africa. *OCL*, *21(4)*: A401.

Breure, C J; Menendez, T and Powell, M S (1990). The effect of planting density on the yield components of oil palm (*Elaeis guineensis*). *Exp. Agric.*, *26(1)*: 117-124. DOI: 10.1017/S0014479700015453.

Can-Alonzo, C; Quezada-Euan, J J G; Xiu-Ancona, P; Moo-Valle, H; Valdovinos-Nunez, G R and Medina-Peralta, S (2005). Pollination of criollo avocados (*Persea americana*) and the behaviour of associated bees in subtropical Mexico. *J. Apic. Res.*, *44*: 3-8.

Chen, Y; Martin, C; Fingu Mabola, J C; Verheggen, F; Wang, Z; He, K and Francis, F (2019). Effects of host plants reared under elevated CO_2 concentrations on the foraging behavior of different stages of corn leaf aphids *Rhopalosiphum maidis*. *Insects*, *10:* 182. DOI: 10.3390/insects10060182.

Chiu, S B; Khoo, K C and Hussein, M Y (1985). Extent of rat predation on *Elaeidobius kamerunicus* Faust, the pollinating weevil of oil palm. *Planter*, *61*: 101-112.

Choong, F L; Clarence, P J and Mathews, J (2004). Preliminary investigations on supplementing and protecting oil palm pollinating weevils (*Elaeidobius kamerunicus* Faust.) in young matured palms in Sabah. *Int. Conf. on Pest and Diseases of Importance to the Oil Palm Industry*. Kuala Lumpur. p. 388-400.

Cik Mohd Rizuan, Z A; Noor Hisham, H and Samsudin, A (2013). Role of pollinating weevil (*Elaeidobius kamerunicus*), seasonal effect and its relation to fruit set in oil palm area of FELDA. *Proc. of the PIPOC 2013 International Palm Oil Congress. MPOB, Bangi.*

Corley, R H V (1976a). Sex differentiation in oil palm: Effects of growth regulators. *J. Exp. Bot.*, *27*: 553-558.

Corley, R H V (1976b). Inflorescences abortion and sex differentiation. *Oil Palm Res*earch (Corley, R H V; Hardon, J J and Wood, B J eds.). Amsterdam, Elsevier. p. 37-54.

Corley, R H V and Tinker, P B H (2003). *The Oil Palm (World Agriculture Series)*. 4th edition. Blackwell Science, Oxford, UK. 562 pp.

Costa, A; Idris, A G; Edgington, S; Annamalai, S and Flood, J (2018). Research on the oil palm pollinating weevil: The way forward. *6th Steering Committee Meeting on Fruit Set and Pollinating Weevil*. Selangor, Malaysia. 25 September 2018.

Daud, S N S M and Idris, A G (2016). Population density of oil palm pollinator weevil *Elaeidobius kamerunicus* based on seasonal effect and age of oil palm. *AIP Conf. Proc.*, *1784*: 060051. DOI: 10.1063/1.4966889.

Dhileepan, K (1992). Pollen carrying capacity, pollen load and pollen transferring ability of the oil palm pollinating weevil, *Elaeidobius kamerunicus* Faust in India. *Oleagineux*, *47(2)*: 55-61.

Dhileepan, K (1994). Variation in populations of the introduced pollinating weevil (*Elaeidobius kamerunicus*) (Coleoptera: Curculionidae) and its impact on fruitset of oil palm (*Elaeis guineensis*) in India. *Bull. Entomol. Res.*, *84*: 477-485.

Donfack, L S; Röll, A; Ellsäßer, F; Ehbrecht, M; Irawan, B; Hölscher, D; Knohl, A; Kreft, H; Siahaan, E J; Sundawati, L; Stiegler, C and Zemp, D C (2021). Microclimate and land surface temperature in a biodiversity enriched oil palm plantation. *Forest Ecology Manag., 497(2021)*: 119480 DOI: 10.1016/j.foreco.2021.119480.

Donough, C R; Chew, K W and Law, I H (1996). Effect of fruit set on OER and KER: Results from studies at Pamol Estates (Sabah) Sdn. Bhd. *Planter*, *72*: 203-219.

Donough, C R and Law, I H (1988). The effect of weevil pollination on yield and profitability at Pamol Plantations. *Proc. of the 1987 Int. Oil Palm Conf. Progress and Prospects*. PORIM, Bangi. p. 523-527.

Durand-Gasselin, T; Noiret, J M; Kouame, R K; Cochard, B and Adon, B (1999). Availability of quality pollen for improved oil palm (*Elaeis guineensis* Jacq.) seed production. *Plantations, Recherche, Developpement, 6*: 264-276.

Eardley, C; Roth, D; Clarke, J; Buchmann, S and Gemmill, B (2006). Pollinators and pollination: A resource book for policy and practice. The African Pollinator Initiative (API). 77 pp.

Facon, B; Hufbauer, R A; Tayeh, A; Loiseau, A; Lombaert, E; Vitalis, R; Guillemaud, T; Lundgren, J G and Estoup, A (2011). Inbreeding depression is purged in the invasive insect *Harmonia axyridis*. *Current Biology, 21(5)*: 424-427. DOI: 10.1016/j.cub.2011.01.068.

Farag, M A and Pare, P W (2002). C_6-Green leaf volatiles trigger local and systemic VOC emissions in tomato. *Phytochemistry, 61(5)*: 545-554. DOI: 10.1016/s0031-9422(02)00240-6.

Farré-Armengol, G; Filella, I; Llusià, J; Niinemets, Ü and Peñuelas, J (2014). Changes in floral bouquets from compound-specific responses to increasing temperatures. *Glob. Change Biol.*, *20*: 3660-3669. DOI: 10.1111/gcb.12628.

Flyg C, and Xanthopoulos, K G (1983). Insect pathogenic properties of *Serratia marcescens*. Passive and active resistance to insect immunity studied with protease-deficient and phage-resistant mutants. *Microbiology, 129(2)*: 453-464.

Foong, S F (1999). Impact of moisture on potential evapotranspiration, growth and yield of oil palm. *Proc. of the 1999 PORIM Int. Palm Oil Congress.* PORIM, Bangi. p. 64-86.

Genting Plantations Research Centre (2018). Centralized weevils hatch and carry study. Steering Committee Meeting on Pollinating Weevil and Fruit Set. MPOB, Bangi. 6 August 2018.

Gerard, A; Wollni, M; Holscher, D; Irawan, B; Sundawati, L; Teuscher, M and Kreft, H (2017). Oil-palm yields in diversified plantations: Initial results from a biodiversity enrichment experiment in Sumatra, Indonesia. *Agric. Ecosyst. Environ.*, *240*: 253-260.

Glenny, W R; Bunyon, J B and Burkle, L A (2018). Drought and increased CO_2 alter floral visual and olfactory traits with context-dependent effects on pollinator visitation. *New Phytol.*, *220(3)*: 785-798.

Greathead, D J (1983). The multi-million-dollar weevil that pollinates oil palms. *Antenna*, *7*: 105-107.

Gunawan, S; Sri Budiastuti, M T; Sutrisno, J and Wirianata, H (2020). Effects of organic materials and rainfall intensity on the productivity of oil palm grown under sandy soil condition. *Int. J. Adv. Sci. Eng. Inf. Technol.*, *10*: 356-361.

Hanin, A N; Parveez, G K A; Rasid, O A and Abdul Masani, M Y (2020). Biolistic-mediated oil palm transformation with alfalfa glucanase (*AGLU1*) and rice chitinase (*RCH10*) genes for increasing oil palm resistance towards *Ganoderma boninense*. *Ind. Crops Prod.*, *144*: 112008. DOI: 10.1016/j.indcrop.2019.112008.

Haran, J; Abanda, R F X N; Benoit, L; Bakoume, C and Beaudoin-Ollivier, L (2020). Multilocus phylogeography of the world populations of *Elaeidobius kamerunicus* (Coleoptera, Curculionidae), pollinator of the palm *Elaeis guineensis*. *Bull. Entomol. Res.*, *110*: 654-662 DOI: 10.1017/S0007485320000218.

Hardon, J J (1973). Assisted pollination in oil palm: A review. *Advance in Oil Palm Cultivation* (Wastie, R L and Earp, D A eds). Incorporated Kuala Lumpur. p. 184-195.

Hardon, J J and Turner, P D (1967). Observations on natural pollination in commercial plantings of oil palm, *Elaeis guineensis* in Malaya. *Exp. Agric.*, *3*: 105-116.

Harianja, M F; Waters, H S, Setyawan, Y P; Advento, A D, Aryawan, A A K; Naim, M; Caliman, J P and Turner, E C (2019). The impact of understory vegetation complexity on the abundance of *Elaeidobius kamerunicus* weevils in oil palm plantations in Riau, Indonesia. Poster presented at the BES Annual Meeting 2019. Belfast, Ireland. 10-13 December 2019.

Harun, M H and Noor, M R M (2002). Fruit set and oil palm bunch components. *J. Oil Palm Res.*, *14(2)*: 24-33.

Heard, T A (1999). The role of stingless bees in crop pollination. *Annu. Rev. Entomol.*, *44*: 183-206.

Hendrix, S D; Molano-Flores, B and Heard, S B (1999). The effect of population size on stigma pollen load, fruit set and seed set in *Allium stellatum* Ker. (Liliaceae). *Int. J. Plant Sci.*, *160(4)*: 753-757.

Henter, H J (2003). Inbreeding depression and haplodiploidy: Experimental measures in a parasitoid and comparisons across diploid and haplodiploid insect taxa. *Evolution*, *57(8)*: 1793-1803. DOI: 10.1111/j.0014-3820.2003.tb00587.x.

Holopainen, J K and Gershenzon (2010). Multiple stress factors and the emission of plant VOCs. *Trend. Plant. Sci.*, *15(3)*: 176-184.

Huang, J; Cardoza, Y J; Schmelz, E A; Raina, R, Engelberth, J and Tumlinson, J H (2003). Differential volatile emissions and salicylic acid levels from tobacco plants in response to different strains of *Pseudomonas syringae*. *Planta*, *217*: 767-775.

Hussein, M Y (1984). Basic research on the pollinating insect (*Elaeidobius kamerunicus* Fst) of oil palm at Universiti Pertanian Malaysia. Simposium Biologi Kebangsaan 1. 2-4 November 1984. Bangi, Selangor. p. 323-338.

Hussein, M Y; Lajis, N H and Ali, J H (1991). Biological and chemical factors associated with the successful introduction of *Elaeidobius kamerunicus* Faust, the oil palm pollinator in Malaysia. *Acta Hortic.*, *288(1)*: 81-87.

Hutauruk, C H; Sipayung, A and Sudharto, P S (1982). *Elaeidobius kamerunicus* Fst: *Hasil uji kekhususan inang dan peranannya sebagai penyerbuk kelapa sawit*. *Buletin Pusat Penelitian Marihat, 3(2)*: 1-15.

Idris, A B; Latip, N F A; Muhamad Fahmi, M H; Muhamad Luqman, H A; Noor Farehan, I; Dzolkifli, O; Ming, S H; Teo, M T and Abu Hassan, A (2018). Current research on the oil palm pollinating weevil, *Elaeidobius kamerunicus*. *Workshop on Insect Pollination Efficiency in Oil Palm*. 1 March 2018. Selangor, Malaysia.

Idris, A; Kushairi A; Ismail, S and Ariffin, D (2004). Selection for partial resistance in oil palm progenies to *Ganoderma* basal stem rot. *J. Oil Palm Res.*, *16*: 12-18.

Jagoe, R B (1934). Observations and experiments in connection with pollination of oil palm. *Malay. Agric. J.*, *22*: 598-606.

Jakobsen, H B and Olsen, C E (1994). Influence of climatic factors on emission of flower volatiles in situ. *Planta*, *192*: 365-371.

Jamian, S; Norhisham, A; Ghazali, A; Zakaria, A and Azhar, B (2017). Impacts of 2 species of predatory Reduviidae on bagworms in oil palm plantations. *Insect Sci.*, *24(2)*: 285-294. DOI: 10.1111/1744-7917.12309.

Jamian, S and Nur Azura, A (2018). The performance of predatory insect, *Sycanus dichotomus* Stal. (Hemiptera: Reduviidae) on combination of plant host and prey. *Serangga, 23(2)*: 56-64.

Kamarudin, N; Moslim, R; Mohamad, S A and Sulaiman, M R (2018). Fruit set and weevil pollination issues in oil palm. NATSEM Seminar. 16-17 July 2018. Kuala Lumpur, Malaysia. p. 123-135.

Kaaya, G P and Darji, N (1989). Mortality in adult *Glossina morsitans morsitans* caused by entomopathogenic bacteria. *J. Invertebr. Pathol.*, *54*: 32-38.

Kang, S M (1999). The *Elaeidobius kamerunicus* story. *Planter*, *75(876)*: 143-150.

Kang, S M and Zam, A K (1982). Quarantine aspects of the introduction into Malaysia of an oil palm insect pollinator. *Proc. Int. Conf. on Plant Protection in the Tropics*. Kuala Lumpur, Malaysia. p. 1-12.

Kivimäenpää, M; Ghimire, R P and Sutinen, S; Haikio, E; Kasurinen, A; Holopainen, T and Holopainen, J K (2016). Increases in volatile organic compound emissions of Scots pine in response to elevated ozone and warming are modified by herbivory and soil nitrogen availability. *Eur. J. Forest Res.*,*135*: 343-360.

Kobayasi, K; Eydi, M J; Sakai, H; Tokida, T; Nakamura, H; Usui, Y; Yashimoto, M and Hasegawa, T (2019). Effects of free-air CO_2 enrichment on heat-induced sterility and pollination in rice. *Plant Prod. Sci.*, *22(3)*: 374-381.

Kumar, A; Nayak, A K; Das, B S; Panigrahi, N; Dasgupta, P; Mohanty, S; Kumar, U; Panneerselvam, P and Pathak, H (2019). Effects of water deficit stress on agronomic and physiological responses of rice and greenhouse gas emission from rice soil under elevated atmospheric CO_2. *Sci. Total Environ.*, *650(2)*: 2032-2050.

Kusumawati, S A; Yahya, S; Hariyadi; Mulatsih, S and Istina, I N (2021). The dynamic of carbon dioxide (CO_2) emission and land coverage on intercropping system on oil palm replanting area. *J. Oil Palm Res.*, *33(2)*: 267-277.

Kevan, P G; Hussein, M Y; Hussey, N and Wahid, M B (1986). The use of *Elaeidobius kamerunicus* for pollination of oil palm. *Planter*, *62*: 89-99.

Konecka, E; Mokracka, J; Krzyminska, S and Kaznowski, A (2019). Evaluation of the pathogenic potential of insecticidal *Serratia marcescens* strains to humans. *Polish J. Microbiol.*, *68(2)*: 185-191. DOI: 10.33073/pjm-2019-018.

Kouakou, M; Hala, N K; Akpa, A; Akpesse, M; Tuo, Y; Dagnogo, M; Konan, K E and Koua, H K (2014). Comparative efficacy of *Elaeidobius kamerunicus*, *E. plagiatus*, *E. subvittatus* (Coleoptera: Curculionidae) and *Microporum* spp. (Coleoptera: Nitidulidae) in the pollination of oil palm (*Elaeis guineensis*). *J. Exp. Biol. Agric. Sci.*, 2: 538-545.

Krantz, G W and Poinar, Jr, G O (2004). Mites, nematodes and the multimillion dollar weevil. *J. Nat. Hist.*, *38*: 135-141.

Kushairi, A; Rajanaidu, N; Sundram, K and Maizura, I (2004). PS8: Vitamin E breeding population. *MPOB Information Series, No. 222*. MPOB, Bangi.

Kushairi, A; Tarmizi, A H; Zamzuri, I; Ong-Abdullah, M; Samsul Kamal, R; Ooi, S E and Rajanaidu, N (2010). Production, performance and advances in oil palm tissue culture. Paper presented at the International Seminar on Advances in Oil Palm Tissue Culture. Yogyakarta, Indonesia. 29 May 2010.

Lajis, N H; Hussein, M Y and Toia, R F (1985). Extraction and identification of the main compound present in *Elaeis guineensis* flower volatiles. *Pertanika*, *8(1)*: 105-108.

Latip, N F A; Muhamad Fahmi, M H; Luqman, H A; Al-Talafha, H; Noor Nasuha, A A; Cik Mohd Rizuan, Z A and Idris, A B (2018). Effect of oil palm planting materials, rainfall, number of male inflorescence and spikelet on the population abundance of oil palm pollinator, *Elaeidobius kamerunicus* Faust (Coleoptera: Curculionidae). *Serangga*, *23(1)*: 35-45.

Latip, N F A; Idris, A B; Hazmi, I R; Abidin, C M R Z; Sartiami, D; Yacob, S and Muhammad Nasir, D (2019). Morphometric comparison of the oil palm pollinator *Elaeidobus kamerunicus* Faust (Coleoptera: Curculionidae) from Malaysia, Indonesia and Liberia. *Coleop. Bull.*, *73(3)*: 746-756.

Legros, S; Mialet-Serra, I; Calliman, J P; Siregar, F A; Clement-Vidal, A; Fabre, D and Dingkuhn, M (2009). Phenology, growth and physiological adjustments of oil palm (*Elaeis guineensis*) to sink limitation induced by fruit pruning. *Ann. Bot.*, *104*: 1183-1194.

Leitner, M; Kaiser, R; Rasmussen, M O; Driguez, H; Boland, W and Mithofer, A (2008). Microbial oligosaccharides differentially induce volatiles and signaling components in *Medicago truncatula*. *Phytochemistry*, *69(10)*: 2029-2040.

Lepesme, P (1947). *Les Insects des Palmiers*. Paris, Paul Lechavalier. 903 pp.

Lewis, T (1973). *Thrips: Their Biology, Ecology and Economic Importance*. London, Academic Press. 349 pp.

Li, K; Tscharntke, T; Saintes, B; Buchori, D and Grass, I (2019). Critical factors limiting pollination success in oil palm: A systematic review. *Agric., Ecosyst. Environ.*, *280*: 152-160.

Li-li, M; Li-Zhen, Z; Si-ping, Z; Evers, J B; Werf vd, W; Jing-jing, W; Hong-quan, S; Zhi-cheng, S and Spiertz, H (2015). Resource use efficiency, ecological intensification and sustainability of intercropping systems. *J. Integr. Agric.*, *14(8)*: 1542-1550.

Li, P; Li, H; Zong, Y; Li, F Y; Han, Y and Hao, X (2017). Photosynthesis and metabolite responses of *Isatis indigotica* Fortune to elevated CO_2. *Crop J.*, *5(4)*: 345-353.

Li, T; Blande, J and Holopainen, J (2016). Atmospheric transformation of plant volatiles disrupts host plant finding. *Sci. Rep.*, *6*: 33851. DOI: 10.1038/srep33851.

Lim, K H (2012). Integrated pest management of *Tirathaba* bunch moth on oil palm planted on peat. *Planter*, *88(1031)*: 97-104.

Lubis, F I and Dono, D (2017). *Populasi serangga penyerbuk kelapa sawit* Elaeidobius kamerunicus *Faust dan pengaruhnya terhadap nilai fruit set pada tanah berliat, berpasir dan gambut di Kalimantan Tengah, Indonesia*. *J. Agrikultura*, *28*: 39-46.

Maluin, F N; Hussein, M Z and Idris, A S (2020). An overview of the oil palm industry: Challenges and some emerging opportunities for nanotechnology development. *Agronomy*, *10(3)*: 356-376. DOI: 10.3390/agronomy10030356.

Mariau, D and Genty, P (1988). IRHO contribution to the study of oil palm insect pollinators in Africa, South America and Indonesia. *Oléagineux*, *43(6)*: 233-240.

Mayfield, M M (2005). The importance of nearby forest to known and potential pollinators of oil palm (*Elaeis guineensis* Jacq.: Arecaceae) in Southern Costa Rica. *Econ. Bot.*, *59(2)*: 190-196.

Messing, R H (1991). Status of beekeeping in the Hawaiian Islands. *Bee World*, *72(4)*: 147-160. DOI: 10.1080/0005772X.1991.11099098.

Ming, S C and Bong, C F (2017). Effect of different insecticides on the survival of the oil palm pollinator, *Elaeidobius kamerunicus* (Coleoptera: Curculionidae). *Planter*, *93(1100)*: 777-7880.

Ming, S C; Bong, C F and Ahmad, K (2016). Field ablation as cultural control for bunch moth *Tirahaba mundella* infestation in young mature oil palm. *J. Oil Palm Res.*, *28(4)*: 463-470.

Muhamad Fahmi, M H; Ahmad Bukhary, A K; Norma, H and Idris, A B (2016). Analysis of volatile organic compound from *Elaeis guineensis* inflorescences planted on different soil types in Malaysia. *AIP Conf. Proc.*, *1784*: 060020. DOI: 10.1063/1.4966858.

Muhammad Luqman, H A; Dzulhelmi, M N; Idris, A B and Izfa Riza, H (2017). The potential natural predators of *Elaeidobius kamerunicus* Faust, 1878 (Coleoptera: Curculionidae) in Malaysia. *Serangga*, *22(2)*: 239-252.

Muhammad Nasir, D; Mamat, N S; Abdul Muneim, N A; Ong-Abdullah, M; Abd Latip, N F; Su, S and Hazmi, I R (2020). Morphometric analysis of the oil palm pollinating weevil, *Elaeidobius kamerunicus* (Faust, 1878) (Coleoptera: Curculionidae) from oil palm plantations in Malaysia. *J. Entomol. Res. Soc.*, *22(3)*: 275-291.

Muhammad Syafiq, Y; Puan, C L; Badrul, A; Sharifah, N A and Amal, G (2016). Nocturnal bird composition in relation to habitat heterogeneity in small scale oil palm agriculture in Malaysia. *Agric. Ecosyst. Environ.*, *233*: 140-146.

Murphy, D J (2007). Future prospects for oil palm in the 21st century: Biological and related challenges. *Eur. J. Lipid Sci. Technol.*, *109*: 296-306.

Mutert, E; Fairhurst, T H and von Uexküll, H R (1999). Agronomic management of oil palms on deep peat. *Better Crops Int.*, *13(1):* 22-27.

Mohamad, S A; Masijan, Z; Moslim, R; Sulaiman, M R; Ming, S C; Chuan, S T; Kamarudin, N; Ali, S R A and Ahmad, S N (2017). Biological agents and insecticides to control bunch moth, *Tirathaba rufivena* in oil palm estates in Sarawak, Malaysia. *J. Oil Palm Res.*, *29(3)*: 323-332.

Mohamad, S A; Syarif, M N Y; Siti Nurulhidayah, A; Mohd Masri, M M; King, J H and Kamarudin, N (2021a). Population density of *Elaeidobius kamerunicus* Faust in different spikelet position at anthesising male inflorescence of *Elaeis guineensis* Jacq. in Sabah and Sarawak, Malaysia. *J. Oil Palm Res.*, *33(1)*: 21-36. DOI: 10.21894/jopr.2020.0075.

Mohamad, S A; Siti Nurulhidayah, A; Syarif, M N Y; Sulaiman, M R; King, J H; Mohammed, M A and Mohd Masri, M M (2021b). Population abundance of oil palm pollinating weevil, *Elaeidobius kamerunicus* Faust and its relation to fruit set formation in mineral and peat soil areas in Peninsular Malaysia. *Serangga*, *26(2)*: 107-117.

Murdiyarso, D; Lilleskov, E and Kolka, R (2019). Tropical peatlands under siege: The need for evidence-based policies and strategies. *Mitig. Adapt. Strateg. Glob. Change*, *24*: 493-505.

Ng, S K and Tan, Y P (1974). Nutritional complexes of oil palms planted on peat in Malaysia. Foliar symptoms, nutrient composition and yield. *Oléagineux*, *29*: 1-4.

Ng, S K; von Uexküll, H R; Thong, K C and Ooi, S H (1990). Maximum exploitation of genetic yield potentials of some major tropical tree crops in Malaysia. *Proc. Symposium on Maximum Yield Research*. Kyoto, Japan. p. 120-130.

Noh, A; Kushairi, A; Mohd Din, A; Maizura, I; Isa, Z A and Rajanaidu, N (2005). PS10: Breeding population selected for long stalk. *MPOB Information Series No. 263*. MPOB, Bangi.

Paramananthan, S (2013). Managing marginal soils for sustainable growth of oil palms in the tropics. *J. Oil Palm Environ.*, *4*: 1-16.

Pardede, D B (1990). Indigeneous pollinator insects of oil palm at Kertahardja Lebak and Kertajaya estates nucleus estates smallholder project V South Banten. *Bul. Perk.*, *21(1)*: 213-223.

Pare, P W and Tumlinson, J H (1992). De novo biosynthesis of volatiles induced by insect herbivory in cotton plants. *Plant Physiol.*, *114*: 1161-1167.

Parveez, G K A; Ahmad Tarmizi, A H; Sundram, S; Loh, S K; Ong-Abdullah, M; Poo Palam, K D; Mohamed Salleh, K; Mohd Ishak, S and Idris, Z (2021). Oil palm economic performance in Malaysia and R&D progress in 2020. *J. Oil Palm Res.*, *33(2)*: 181-214.

Paterson, R R M and Lima, N (2018). Climate change affecting oil palm agronomy, and oil palm cultivation increasing climate change, requires amelioration. *Ecol. Evol.*, *8(1)*: 452-461. DOI: 10.1002/ece3.3610.

Perez-Pereira, N; Pouso, R; Rus, A; Vilas, A; Lopez-Cortegano, E; Garcia-Dorado, A; Quesada, H and Caballero, A (2021). Long-term exhaustion of the inbreeding load in *Drosophila melanogaster*. *Heredity*, *127*: 373-383.

Poinar, G O; Jackson, T A; Bell, N L and Wahid, M B (2002). Sphaerularioidea: Anandranematidae n. fam.) parasitic in the palm-pollinating weevil *Elaeidobius kamerunicus* Faust, with a phylogenetic synopsis of the Sphaerularioidea Lubbock, 1861. *Syst. Parasitol.*, *52*: 219-225.

Prasetyo, A E; Arif, M and Hidayat, T C (2012). *Buah landak pada tanaman muda kelapa sawit*. *Warta Pusat Penelitian Kelapa Sawit*, *17(1)*: 13-20.

Prasetyo, A E; Lopez, J A; Eldridge, J R; Zommick, D H and Susanto, A (2018). Long-term study of *Bacillus thuringiensis* application to control *Tirathaba rufivena*, along with the impact to *Elaeidobius kamerunicus*, insect biodiversity and oil palm productivity. *J. Oil Palm Res.*, *30(1)*: 71-82.

Prasetyo, A E and Susanto, A (2019). The insecticide effect to the activity and emergence of *Elaeidobius kamerunicus* Faust (Coleoptera: Curclionidae) on oil palm (*Elaeis guineensis* Jacq.) male inflorescence. *J. Penelitian Kelapa Sawit*, *27(1)*: 13-24.

Prasetyo, A E and Susanto, A (2016). *Perkembangan populasi* Elaeidobius kamerunicus *Faust pasca introduksi dan peningkatan fruit set kelapa sawit di Pulau Seram, Maluku, Indonesia*. *J. Penelitian Kelapa Sawit*, *24(1)*: 47-55.

Prasetyo, A E, and Susanto, A (2013). *Peningkatan fruit set kelapa sawit dengan teknik penetasan dan pelepasan* Elaeidobius kamerunicus. *J. Penelitian Kelapa Sawit*, *21(2)*: 82-90.

Prasetyo, A E; Purba, W O and Susanto, A (2014). *Elaeidobius kamerunicus*: Application of hatch and carry technique for increasing oil palm fruit set. *J. Oil Palm Res.*, *26(3)*: 195-202.

Purba, A R; Supriyanto, E; Supena, N and Arif, M (2009). *Peningkatan produktivitas kelapa sawit dengan menggunakan bahan tanaman unggul*. *Prosiding Pertemuan Teknis Kelapa Sawit* (*PTKS*). Jakarta, Indonesia. p 28-29.

Räisänen, T; Ryyppö, A and Kellomäki, S (2008). Effects of elevated CO_2 and temperature on monoterpene emission of Scots pine (Pinus sylvestris L.). *Atmospheric Environment, 42(18)*: 4160-4171.

Rajanaidu, N; Kushairi, A; Rafii, M; Mohd Din, A; Maizura, I and Jalani, B S (2000). Oil palm breeding and genetic resources. *Advances in Oil Palm Research* (Yusof, B; Jalani, B S and Chan, K W eds.). MPOB, Bangi. p. 171-237.

Rajanaidu, N; Ainul, M M; Kushairi, A and Mohd Din, A (2013). Historical review of oil palm breeding for the past 50 years - Malaysia journey. *Proc. Int. Seminar on Oil Palm Breeding – Yesterday, Today and Tomorrow*. Kuala Lumpur, Malaysia. p. 11-28.

Rao, V and Law, I H (1998). The problem of poor fruit set in parts of East Malaysia. *Planter*, *74(870)*: 463-483.

Rohani, O; Sharifah, S A; Mohd Rafii, Y; Ong, M; Tarmizi, A H and Zamzuri, I (2000). Tissue culture of oil palm. *Advances in Oil Palm Research* (Yusof, B;

Jalani, B S and Chan, K W eds.). *Vol. 1*. MPOB, Bangi. p. 238-283.

Ruther, J and Furstenau, B (2005). Emission of herbivore-induced volatiles in absence of a herbivore-response of *Zea mays* to green leaf volatiles and terpenoids. *Z. Naturfosch C J. Biosci. 60(9-10)*: 743-756. DOI: 10.1515/znc-2005-9-1014.

Siti Nurulhidayah, A; Mazmira, M M M and Norman, K (2020). Assessment on voracity and predation by predator, *Sycanus dichotomus* Stal. (Hemiptera: Reduviidae) to oil palm bagworm, *Pteroma pendula. J. Oil Palm Res.*, *32(3)*: 480-487. DOI: 10.21894/jopr.2020.0040.

Slaa, E J; Sánchez, C L A; Malagodi-Braga, K S and Hofstede, F E (2006). Stingless bees in applied pollination: Practice and perspectives. *Apidologie*, *37*: 293-315.

Soh, A C (2012). The future of oil palm clones in Malaysia. *J. Oil Palm Environ.*, *3*: 93-97. DOI: 10.5366/jope.2012.09.

Sparnaaij, L D (1960). The analysis of bunch production in the oil palm. *J. W. Afr. Inst. Oil Palm Res.*, *3*: 109-180.

Stec, D and Kuszewska, K (2020). CO_2 narcosis influences the memory of honey bees. *J. Apic. Res.*, *59(4)*: 663-668.

Steinhaus, E A (1959). *Serratia marcescens* Bizio as an insect pathogen. *Hilgardia*, *28(14)*: 351-380.

Sulaiman, M R; Mohamad, S A; Mohamed Mazmira, M M; Siti Nurulhidayah, A and Kamarudin, N (2021). Preliminary study on efficiency of different time and light source in light traps for capturing population of adult oil palm bunch moth, *Tirathaba mundella* (Lepidoptera: Pyralidae). *J. Oil Palm Res.*, *33(3)*: 413-424.

Sulaiman, M R; Mohamad, S A; Syarif, M N Y; Ahmad, S N; Masri, M M M; Masijan, Z; Moslim, R and Kamarudin, N (2018). Status on oil palm fruit set and pollinating weevil in Malaysia. Workshop on Insect Pollination Efficiency in Oil Palm. 1 March 2018. Selangor, Malaysia.

Swindell, W R and Bouzat, J L (2006). Reduced inbreeding depression due to historial inbreeding in *Drosophila melanogaster*: Evidence for purging. *J. Evol. Biol.*, *19*: 1257-1264.

Syed, R A (1979). Studies on oil palm pollination by insects. *Bull. Entomol. Res.*, *69(1)*: 213-224. DOI: 10.1017/S0007485300017673.

Syed, R A (1980). Pollinating insects of oil palm. Commonwealth Institute of Biological Control (CIBC) Report. p. 39-67.

Syed, R A (1981). Insect pollination of oil palm: Feasibility of introducing Elaeidobius spp. into Malaysia. *Oil Palm News*, *25*: 2-16.

Syed, R A; Law, I H and Corley, R H V (1982). Insect pollination of oil palm: Introduction, establishment and pollinating efficiency of *Elaeidobius kamerunicus* in Malaysia. *Planter*, *58*: 547-561.

Syed, R A and Salleh, A (1987). Population of *Elaeidobius kamerunicus* Fst. in relation to fruit set. *Proc. of the 1987 International Oil Palm/Palm Oil Conferences Progress and Prospects*. Kuala Lumpur, Malaysia.

Teh, C K; Ong, A L; Mayes, S; Massawe, F and Appleton, D R (2020). Major QTLs for trunk height and correlated agronomic traits provide insights into multiple trait integration in oil palm breeding. *Genes*, *11(7)*: 826-841. DOI: 10.3390/genes11070826.

The Malaysian Reserve (2019). Govt. to cap palm plantation at 6.5 m ha until 2023. https://themalaysianreserve.com/2019/03/06/govt-to-cap-palm-plantation-at-6-5m-ha-until-2023/, accessed on 19 February 2020.

Tingey, D T; Manning, M; Grothaus, L C and Burns, W F (1980). Influence of light and temperature on monoterpene emission rates from slash pine. *Plant Physiol.*, *65*: 797-801.

Tscharntke, T; Clough, Y; Bhagwat, S A; Buchori, D; Faust, H; Hertel, D; Hölscher, D; Juhrbandt, J: Kessler, M; Perfecto, I; Scherber, C; Schroth, G; Veldkamp, E and Wanger, T C (2011). Multifunctional shade-tree management in tropical agroforestry landscapes – A review. *J. Appl. Ecol.*, *48*: 619-629. DOI: 10.1111/j.1365-2664.2010.01939.x.

Turlings, T C J and Ton, J (2006). Exploiting scents of distress: The prospect of manipulating herbivore-induced plant odours to enhance the control of agricultural pests. *Curr. Opin. Plant Biol.*, *9*: 421-427.

Turlings, T C J and Tumlinson, J H (1992). Systemic release of chemical signals by herbivore-injured corn. *Proc. Natl. Acad. Sci. USA*, *89*: 8399-8402.

Turner, N (1960). The effect of inbreeding and crossbreeding on number of insects. *Ann. Entomol. Soc. Am.*, *53(5)*: 686-688. DOI: 10.1093/aesa/53.5.686.

Turner, P D and Bull, R A (1967). Diseases and disorders of the oil palm in Malaysia. The Incorporated Society of Planters. Kuala Lumpur. 247 pp.

Valenzuela, H R (2018). Pollinators and sustainable farming in Hawaii. *Bee World*, *95(4)*: 117-121. DOI: 10.1080/0005772X.2018.1507347.

Velthius, H H W and van Doorn, A (2006). A century of advances in bumblebee domestication and the economic and environmental aspects of its commercialization for pollination. *Apidologie*, *37*: 421-451.

Viana, B F; da Encarnacao Coutinho, J G; Garibaldi, L A; Gastagnino, B; Guido, L; Peres Gramacho, K and da Silva, F O (2014). Stingless bees further improve apple pollination and production. *J. Pollinat. Ecol.*, *14*: 261-269.

Wahid, M B B; Hassan, A H B M and Hitam, A B (1983). Current status of *Elaeidobius kamerunicus* Faust and its effects on the oil palm industry in Malaysia. *Occasional Paper*, *Palm Oil Research Institute of Malaysia* (PORIM), *6*: 39.

Wahid, M B; Z; Halim, A H and Mohd Tayeb, D (1987). The population census and the pollination efficiency of the weevil, *Elaeidobius kamerunicus* in Malaysia - A status report, 1983-1986. *Proc. of the 1987 Int. Palm Oil Conf*. Kuala Lumpur. p. 535-549.

Wahid, M B and Kamarudin, N (1997). Role and effectiveness of *Elaeidobius kamerunicus, Thrips hawaiiensis* and *Pyroderces* sp. in pollination of mature oil palm in Peninsular Malaysia. *Elaeis*, *9 (1)*: 1-16.

Wei, G; Lai, Y; Wang, G; Chen, H; Li, F and Wang, S (2017). Insect pathogenic fungus interacts with the gut microbiota to accelerate mosquito mortality. *Proc. of the National Academy of Sciences of the United States of America (PNAS)*, *114(23)*: 5994-5999. DOI: 10.1073/pnas.1703546114.

Wood, B J (1968). Pests of oil palm in Malaysia and their control. Incorporated Society of Planters. Kuala Lumpur. 204 pp.

Wood, B J and Chung, G F (2003). A critical review of the development of rat control in Malaysian agriculture since the 1960's. *Crop Prot.*, *22*: 445-461.

Vitikainen, E and Sundström, L (2010). Inbreeding and caste-specific variation in immune defense in the ant *Formica exsecta*. *Behav. Ecol. Sociobiol.*, *65*: 899-907.

Veloo, R; Ranst, E V and Selliah, P (2015). Peat characteristics and its impact on oil palm yield. *NJAS- Wageningen J. Life Sci.*, *72-73*: 33-40.

Ward, J K; Roy, D S; Chatterjee, I; Bone, C R; Springer, C J; Kelly, J K (2012). Identification of a major QTL that alters flowering time at elevated CO2 in *Arabidopsis thaliana*. *PLoS One, 7(11)*: e49028.

Wahyuni, M; Wagino and Manurung, H (2019). The effect of palm oil planting material characteristics on the population of weevil pollinator (*Elaeidobius kamerunicus*). *J. Phys.: Conf. Ser. 1542(012073)*. 5 pp.

Woittiez, L S; Wijk, M T V; Slingerland, M; Noordwijk, M V and Giller, K E (2017). Yield gaps in oil palm: A quantitative review of contributing factors. *Euro. J. Agronomy*, *83*: 57-77.

Yaakop, S and Abdul Manaf, S M (2015). The bunch moth of the *Tirathaba* species as a hidden pest on the peat soil of oil palm plantations: Implications of biological life cycles, the DNA barcoding approach and infestation detection pattern detection. *3rd Int. Conf. on Chemical, Agricultural and Medical Sciences (CAMS-2015)*. Singapore.

Yee, C B; Lim, K C; Ong, E C and Chan, K W (1985). The effects of *E. kamerunicus* on bunch components of *E. guineensis*. *Proc. Symp. Impact of the pollinating weevil on the Malaysian oil palm industry*. PORIM, Kuala Lumpur. p. 129-139.

Yi, H S; Heil, M; Adame-Alwarez, R M; Ballhorn, D J and Ryu, C M (2009). Airborne induction and priming of plant defenses against a bacterial pathogen. *Plant Physiol.*, *151*: 2152-2161.

Yule, C M (2010). Loss of biodiversity and ecosystem functioning in Indo-Malayan peat swamp forests. *Biodivers. Conserv.*, *19*: 393-409.

Zahari, S N M; Rusli, R; Hussain, M H and Jalinas, J (2019). Survival rate and development of larvae *Elaeidobius kamerunicus* (Coleoptera: Curculionidae) on artificial diets. *Serangga*, *24(1)*: 126-141.

Zinta, G; Abd Elgawad, H; Peshev, D; Weedon, J T; Van den Ende, W; Nijs, I; Janssens, I A; Beemster, G T S and Asard, H (2018). Dynamics of metabolic responses to periods of combined heat and drought in *Arabidopsis thaliana* under ambient and elevated atmospheric CO_2. *J. Exp. Bot.*, *69(8)*: 2159-2170.

Zulkefli, M H H; Jamian, S; Nur Azura, A; Jalinas, J and Mohd Masri, M M (2021). Evaluation of artificial diet on growth development of *Elaeidobius kamerunicus* Faust (Coleoptera: Curculionidae). *Serangga*, *26(2)*: 132-150.

Zulkefli, M H H; Jamian, S; Nur Azura, A; Jalinas, J, Mohamad, S A and Mohd Masri, M M (2020). Beyond four decades of *Elaeidobius kamerunicus* Faust (Coleoptera: Curculionidae) in the Malaysian oil palm industry: A review. *J. Tropical Ecol.*, *36*: 282-292.

Zulkifli, Y; Norziha, A; Naqiuddin, M H; Fadila, A M; Nor Azwani, A B; Suzana, M; Samsul, K R; Ong-Abdullah, M; Singh, R; Parveez, G K A and Kushairi, A (2017). Designing the oil palm of the future. *J. Oil Palm Res.*, *29(4)*: 440-455. DOI: 10.21894/jopr.2017.00015.

Zuraidah, Y (2019). Influence of soil compaction on oil palm yield. *J. Oil Palm Res.*, *31(1)*: 67-72. DOI: 10.21894/jopr.2018.0064.

Journal of Oil Palm Research Vol. 35 (1) March 2023 p. 23-32
DOI: https://doi.org/10.21894/jopr.2022.0022

STABILITY AND PHYSICAL PROPERTIES OF DIHYDROXYSTEARIC ACID BASED ORGANOGELS IN DIFFERENT TYPES OF VEGETABLE OIL

NORASHIKIN AHMAD[1]* and ZAFARIZAL ALDRIN AZIZUL HASAN[1]

ABSTRACT

Dihydroxystearic acid (DHSA) was obtained from epoxidation and hydroxylation of oleic acid from palm oil. Unlike monohydroxystearic acid, only a few publications described DHSA in the gelation of oils. This study aimed to investigate the stability and physical properties of DHSA organogels in different vegetable oils. Five vegetable oils; refined, bleached and deodourised palm olein (RBDPOo); refined, bleached and deodourised super olein (RBDSPOo); refined, bleached and deodourised palm kernel olein (RBDPKOo); medium-chain triglyceride (MCT); and soybean oil (SBO) were used to prepare DHSA organogels. The stability and critical gel concentration (CGC) of organogels were determined at concentrations of DHSA in the range of 0.2%-20.0% (w/w). DHSA organogels were characterised using a polarised light microscope, texture analyser and rheometer. DHSA organogel with RBDSPOo showed a more stable gel with the lowest CGC value at 9.9% than other oils. In microscopic characterisation, DHSA organogel with RBDPOo showed a high density of small needle-like crystals. The hardness and rheological measurements revealed that DHSA organogels with RBDPOo and RBDSPOo showed the highest elasticity, which is more than 10 000 Pa compared to other oils. However, all DHSA organogels were classified as soft gels and have the potential to be used in cosmetic products.

Keywords: dihydroxystearic acid, organogel, vegetable oils.

Received: 12 August 2021; **Accepted:** 2 March 2022; **Published online:** 22 April 2022.

INTRODUCTION

Organogels are defined as semisolid viscoelastic systems having gelator and oil or organic liquid, immobilised within the space of a three-dimensional network structure of gelator molecules. Gelation can be formed with two different interactions, *i.e.*, between organic liquid-gelator and gelator-gelator interactions. Non-covalent interactions within molecular gels include hydrogen bonding, π-π stacking, and van der Waals interactions (Lan and Rogers, 2015; Silva *et al.*, 2021). Gelling ability is related to the balance between soluble and insoluble fractions of gelator in oil. Gelator must be relatively insoluble to self-assemble into anisotropic structures. Instead, it must have a soluble fraction to interact with the oil moieties (Co and Marangoni, 2012). The organogels formulations have several advantages, *i.e.*, long shelf-life and thermo-reversible behaviour. In addition, the preparation of organogels involves a simple process by dissolving a gelator in an organic liquid at sufficiently high temperatures and then cooling down the solution until there is no flow for elongated periods, normally between 24 hr and several days to allow the development of gel (Flöter *et al.*, 2021).

Mineral and vegetable oils are widely used as solvent phases in cosmetic organogels. The low cost and properties of mineral oil, which is transparent, thermostable and safe have made it

[1] Malaysian Palm Oil Board,
6 Persiaran Institusi, Bandar Baru Bangi,
43000 Kajang, Selangor, Malaysia.

* *Corresponding author e-mail: shikin@mpob.gov.my*

a popular solvent used in cosmetics (Martinez *et al.*, 2019). Recently, researchers have shown an increased interest in developing edible organogels in several areas, such as in the pharmaceuticals and cosmetics industries to achieve 'green' claims and eco-friendly alternatives to replace mineral oil. The edible organogel is of interest because it has unique physical and functional properties as well as is safe for human use. In the edible organogel formulations, vegetable oils are used as the organic liquid, and gelators can be chosen from different groups of gelators, *i.e.*, crystalline waxes, low molecular weight gelators (LMWGs), polymeric or inorganic gelators. Generally, vegetable oils are composed of triglycerides containing saturated, monounsaturated, polyunsaturated fatty acids and several minor components. In cosmetics, especially lip care products, edible organogels play an important role in replacing petrolatum. Less purified petrolatum may contain impurities, such as polycyclic aromatic hydrocarbons, which has been reported as a potentially carcinogenic substance (Chen *et al.*, 2020). The safety concern of using petrolatum on human health has driven researchers to explore other renewable alternatives to replace this material (Stortz and Marangoni, 2014).

Several attempts have been made to explore the role of oil and the chemical structure of LMWGs that influences the formation of organogels. One of the best LMWGs that was thoroughly studied for their ability to form organogels is 12-hydroxystearic acid (HSA) (Asaro *et al.*, 2020). The HSA is a fatty acid derivative of castor oil, and it was chosen due to its simple structure, inexpensive and superior gelation capacity. It was reported that the gel formation using HSA involved interactions between carboxylic acid groups and the hydroxyl group, which result in the formation of multiple hydrogen-bond (H-bond) sequences (Zhang and Weiss, 2016).

Another potential LMWG is 9,10-dihydroxystearic acid (DHSA). The presence of carboxyl and hydroxyl groups of the DHSA is similar to HSA except for one additional hydroxyl group adjacent to each other. It is derived by converting the unsaturation of oleic acid to an epoxide ring via peracetic acid or performic acid routes, followed by hydrolysis with hydrogen donours, such as water (Koay *et al.*, 2011). The two hydroxyl groups are located at position-9 and position-10 of an 18-carbon aliphatic chain (*Figure 1*). The *in vitro* and *in vivo* safety evaluation studies revealed that the DHSA is safe to be applied on skin and areas around the eyes. Thus, it can potentially be used as an ingredient in cosmetic formulations. DHSA was reported to be effective in coating pigments for colour cosmetic products. In addition, the use of DHSA has been further studied in sodium soap and transparent soap. The DHSA soap exhibited good corrosion inhibition as well as showed better foamability and detergency than stearic acid soap. Moreover, DHSA incorporated in transparent soap formulation helps to improve the transparency of transparent soap (Ismail *et al.*, 2015). Although extensive research has been carried out on the application of DHSA in cosmetics and personal care products, there has been little discussion about DHSA for the gelation of oils. Zhang and Weiss (2016) reported that DHSA was capable of gelling sunflower and lavender oils but at 2% to 8% concentration.

It is important to notice that there are some challenges of organogels in cosmetics, such as difficulty to predict gelation process between gelator and solvent as well as the stability of the organogel (Martinez *et al.*, 2019). Therefore, this article aimed to study the effect of DHSA on the stability and physical properties of DHSA-based organogels in different vegetable oils, whereby, this basic organogel formulation can be used to formulate lip care products. For this purpose, refined, bleached and deodourised palm olein (RBDPOo); refined, bleached and deodourised super olein (RBDSPOo); refined, bleached and deodourised palm kernel olein (RBDPKOo); medium-chain triglyceride (MCT); and soybean oil (SBO) were chosen due to their differences in the compositions of fatty acids. The stability, critical gel concentration (CGC) and physical properties, such as crystal morphology, hardness, and rheology of DHSA-based organogels were studied.

MATERIALS AND METHODS

Materials

DHSA (appearance: off-white powder, purity: 95%, hydroxyl value: 299 mg KOH g^{-1}, melting point: 91°C and moisture content: 0.6%) and RBDSPOo were obtained from the Malaysian Palm Oil Board.

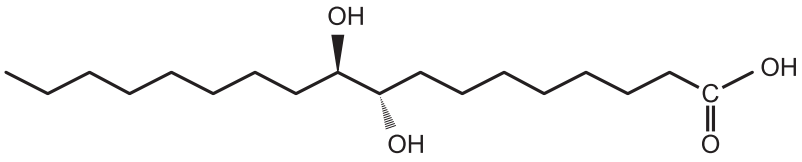


Figure 1. Structural representation of 9,10-dihydroxystearic acid.

RBDPOo and SBO were purchased from Yee Lee Edible Oils Sdn. Bhd., and Kempas Edible Oil Sdn. Bhd., respectively. RBDPKOo was purchased from Southern Edible Oil Industries (M) Sdn. Bhd., Malaysia. MCT or caprylic/capric triglyceride 60/40 was purchased from InterMed Ester Sdn. Bhd., Malaysia. The fatty acid compositions were determined via gas chromatography (GC) analysis.

Determination of Fatty Acid Compositions of Oils

The fatty acid compositions of the oils were determined by GC analysis using Agilent 7890B equipped with a 7693 Series autoinjector from Agilent Technologies, USA. Chromatography separation was achieved with the aid of the HP88 column (60 m x 0.25 mm x 0.20 μm). The GC was operated in the split injection mode using a 100:1 split ratio while maintaining the injector temperature of 250°C. The oil sample was prepared according to a standard method, AOCS Ce 2-66 (AOCS, 2012). Then, 1 μL of the mixture was injected into the GC column with an initial oven temperature of 150°C. The oven temperature was programmed at 3°C min^{-1} until 210°C. The flow rate of the carrier gas helium was 0.8 mL min^{-1}. The temperature of the flame ionisation detector was set at 250°C.

Determination of Viscosity of Oil

The viscosity of oils was measured using a rheometer Physica MCR300 from Anton Paar, Germany. The measurement was performed by a concentric cylinder geometry (CC17) at 25°C. The shear rate was increased step-wise from 1 to 100 s^{-1}.

Preparation of the Organogels

Organogels were prepared in sample tubes (15 cm height x 1.6 cm diameter) with screw caps. The mixtures containing an oil phase (5.00 g), *i.e.*, RBDPOo, RBDSPOo, RBDPKOo, MCT or SBO, respectively. DHSA (0.01-1.25 g) was heated to 95°C ± 2°C and stirred vigorously for 3 min using a vortex. Afterwards, the samples were allowed to cool down to room temperature (25°C) for 24 hr to form gels.

Qualitative Assessment of Gelation Behaviour

The equilibrated organogel in sample tubes were inverted, and the self-standing ability of the samples was assessed visually. The gelation behaviour of organogel samples was monitored up to 12 weeks at 25°C (Burkhardt *et al.*, 2009). The appearance of the samples can be described as two-phase (fluid/gel-like), a mixture of gel and liquid (gel + liquid), and stable gel. Samples that immediately flowed were categorised as a liquid. Samples in which the gel and liquid were clearly separated from the system and slowly flowed were categorised as two-phase. Lastly, samples that did not flow were categorised as a stable gel. However, gels that were unstable upon storage (whereby oil come out from the system) were categorised as gel + liquid. CGC was determined as the lowest concentration of DHSA at which a stable gel was formed at room temperature.

Assessment of Organogel Crystal Morphology with Respect to Different Oils

The crystalline structures of the organogel samples were examined at 25°C under a polarised light microscope via the Olympus System Microscope Model BX53 (Olympus Corporation, Japan). A small sample containing crystals was placed on a glass microscope slide and gently covered with a glass coverslip. Digital images of specimens were acquired using an Olympus microscope digital camera model Olympus DP73 (Olympus Corporation, Japan).

Determination of Organogel Hardness

The hardness of organogel samples was evaluated according to the method described by Onacik Gur *et al.* (2017). The compression measurement was conducted using a texture analyser TA.XT plus (Stable Micro Systems, United Kingdom). A cylindrical probe (P/0.5R) with a diameter of 12.7 mm was used for the measurement. Each organogel sample (approximately 30 mm height) was conditioned in a 20 mL vial. The internal diameter and depth of the vial were 28 mm and 60 mm. The probe was dipped 5 mm into an organogel sample at 1 mm s^{-1}. The test was carried out at room temperature. The measurements were performed in triplicates.

Characterisation of Rheological Property of Organogel

The rheological properties of organogel samples were performed using a rheometer, MCR300 from Anton Paar GmbH, Germany. The measurement was performed using a parallel-plate geometry of 25 mm wide with a 1 mm gap at 25°C. The organogel samples were handled gently to avoid structural damage. The viscoelastic properties of organogel samples were investigated via oscillation tests. First, amplitude sweep was carried out with an increasing strain from 0.01% to 100.00% at a fixed angular frequency of 10 rad s^{-1} to determine the linear viscoelastic region (LVER) of the organogel samples. Then, a frequency sweep was determined from 0.01 to 10.00 Hz at a constant

strain of 0.50%. Storage modulus (G') and loss modulus (G") were evaluated. The flow properties were characterised using the shear rate range of 0.1 to 100.0 s^{-1} to evaluate the thixotropic behaviours of the organogel samples.

Statistical Analysis

The data obtained from the above studies were analysed statistically using the analysis of variance (ANOVA) single factor and the Student's t-Test. The differences were considered significant if the probability was $p<0.05$.

RESULTS AND DISCUSSION

Fatty Acid Compositions of Oils

The compositions of fatty acid and viscosity of the RBDPOo, RBDSPOo, SBO, RBDPKOo and MCT oils, are presented in *Table 1*. It was observed that RBDPOo and RBDSPOo contained an almost equal amount of saturated ($C_{16:0}$) and unsaturated ($C_{18:1}$) fatty acids. SBO contained the highest amount of unsaturated fatty acid ($C_{18:2}$), RBDPKOo contained the highest amount of saturated fatty acid (C_{12}) and MCT contained medium chain fatty acids C_8 and C_{10}. The viscosity of oil was determined at the plateau value from 30 to 100 shear rate (s^{-1}), and the result follows the reducing viscosity order: RBDPOo = RBDSPOo > SBO > RBDPKOo > MCT.

Stability of DHSA Organogels in Various Oils

The relationship between fatty acid compositions and the degree of gelation for DHSA organogels in various oils is depicted in *Figure 2*. Three phases were identified according to the visual appearance of the samples: two-phase, gel + liquid and gel. The gel + liquid was classified as partial syneresis. Syneresis occurred when gels could not hold the oil and resulted in oil flowing out from the system. It is due to the crystal's structure which formed large aggregates and agglomerates into thick bundles (Daman Huri *et al.*, 2013). Our study showed that DHSA could form gels in all studied oils. However, different amounts of DHSA are required to initiate the formation of organogel on different oil. A minimum amount of DHSA to form organogels was observed in RBDSPOo and RBDPOo, followed by SBO, RBDPKOo and MCT. However, syneresis was observed after seven days of storage at 25°C and the lowest CGC of

TABLE 1. FATTY ACID COMPOSITIONS AND VISCOSITY OF OILS

Fatty acids (%)	Oil				
	RBDPOo	RBDSPOo	SBO	RBDPKOo	MCT
$C_{6:0}$	n.d.	n.d.	n.d.	0.2	n.d.
$C_{8:0}$	n.d.	n.d.	n.d.	3.4	54.6
$C_{10:0}$	n.d.	n.d.	n.d.	3.3	45.2
$C_{12:0}$	0.3	0.3	n.d.	42.0	0.2
$C_{14:0}$	0.9	1.0	0.1	13.6	n.d.
$C_{15:0}$	n.d.	n.d.	n.d.	n.d.	n.d.
$C_{16:0}$	38.6	37.6	10.8	9.1	n.d.
$C_{16:1}$	0.2	0.2	0.1	n.d.	n.d.
$C_{17:0}$	0.1	0.1	0.1	n.d.	n.d.
$C_{17:1}$	n.d.	n.d.	0.1	n.d.	n.d.
$C_{18:0}$	4.1	3.9	4.9	2.7	n.d.
$C_{18:1}$	44.2	45.5	24.2	22.0	n.d.
$C_{18:2}$	10.7	10.5	52.3	3.3	n.d.
$C_{18:3}$	0.2	0.2	6.4	n.d.	n.d.
$C_{20:0}$	0.4	0.4	0.4	0.2	n.d.
$C_{20:1}$	0.2	0.2	0.2	0.1	n.d.
$C_{22:0}$	0.1	0.1	0.4	n.d.	n.d.
ΣSAFA	44.6 ± 0.1	43.4 ± 0.1	16.7 ± 0.0	74.4 ± 0.1	100 ± 0.1
ΣMUFA	44.6 ± 0.1	45.9 ± 0.1	24.6 ± 0.1	22.2 ± 0.1	n.d.
ΣPUFA	10.9 ± 0.1	10.7 ± 0.1	58.6 ± 0.1	3.3 ± 0.1	n.d.
Viscosity (mPa.s)	69.0 ± 0.0[a]	69.0 ± 0.0[a]	66.0 ± 0.0[b]	51.0 ± 0.0[c]	23.0 ± 0.0[d]

Note: SAFA - saturated fatty acids; MUFA - monounsaturated fatty acids; PUFA - polyunsaturated fatty acids; n.d. - not detected; means with different letters in the same row are significantly different ($p<0.05$).

DHSA was determined in RBDSPOo followed with RBDPOo, SBO, RBDPKOo and MCT at CGC of 9.90%, 10.70%, 13.00%, 16.00% and 17.40%, respectively. This behaviour could be correlated with the hypothesis that oil polarity and degree of unsaturation provide some effect on its ability to form H-bonds with DHSA molecules (Gravelle *et al.*, 2016). It was found that MUFA helps in stabilising the organogel structure (Rocha-Amador *et al.*, 2014). According to a report by Burkhardt *et al.* (2009), HSA formed gel in MCT at CGC of 0.75%. Thus, HSA is a more efficient gelator than DHSA. The ability of HSA to form self-assembled fibrillar structures occurs most efficiently when the position of the carboxylic headgroup forms cyclic dimers between adjacent HSA molecules and the hydroxyl group at C_{12} interconnected with neighbouring molecules leading to unidirectional hydrogen bonding along the fibre axis (Fameau and Rogers, 2020). In contrast, it was anticipated that DHSA can utilise only one hydroxyl group per molecule to create intermolecular hydroxyl H-bonds per molecule and the other hydroxyl group for intramolecular H-bonding interactions. Due to this interaction, fibrillar structures could not be formed and a higher amount of DHSA is required for the stabilisation of organogel (Zhang *et al.*, 2015). All studied oils contain MUFA except MCT oil. The presence of MUFA in RBDSPOo, RBDPOo, RBDPKOo and SBO helps to stabilise the DHSA based organogel, possibly through the formation of H-bonds between DHSA and MUFA. The RBDSPOo has the highest MUFA, thus, showing a stable gel with the lowest CGC value than the other oils.

Effect of DHSA on Organogel Crystal Morphology

According to a study by Cerqueira *et al.* (2017), there are three steps involved in the process to form an organogel: Crystal nucleation, crystalline branching and crystal growth. Prior to gel formation (at low gelator concentrations), a two-dimensional structure was formed, which led to nucleation and growth of the crystal surface. Then, with increasing gelator concentration, the process continued until a three-dimensional structure was formed, in which the crystal cross-linked or entangled to trap or immobilise the oil molecules. *Figure 3* shows the crystal morphologies of the organogels at 8% (w/w) as well as 16% (w/w) DHSA in RBDSPOo, RBDPOo, SBO, RBDPKOo and MCT, respectively, after 24 hr at room temperature. It was observed that DHSA organogels with RBDSPOo, RBDPOo and SBO have similar crystalline structures, which are in the form of needles. However, DHSA organogels with RBDPKOo and MCT resulted in platelet crystalline structures. This showed that the use of different oils affects the type of crystal formation. Increasing the DHSA concentration, the crystal structure network was more compact, which can entrap more oil and stabilise the organogels.

Effect of DHSA on Hardness of Organogel

The addition of DHSA as a gelator in vegetable oils is to give structure to the gel and immobilise the oils at room temperature. *Figure 4* shows the hardness of organogels at 8% (w/w) and 16% (w/w) DHSA in different oils viscosity, in which the high hardness values indicate a rigid organogel structure. The results showed that the hardness of DHSA organogels was significantly different in the studied oils. It was observed that at 16% (w/w) DHSA could form stable gels with all oils, and its hardness can be determined in all samples. However, 8% (w/w) DHSA formed stable gel in all oils except RBDPKOo and MCT. The maximum hardness achieved for organogel at 16% (w/w) DHSA was more than eight times higher than organogels at 8% (w/w) DHSA. It was observed that increasing SAFA content, especially C_{16} and

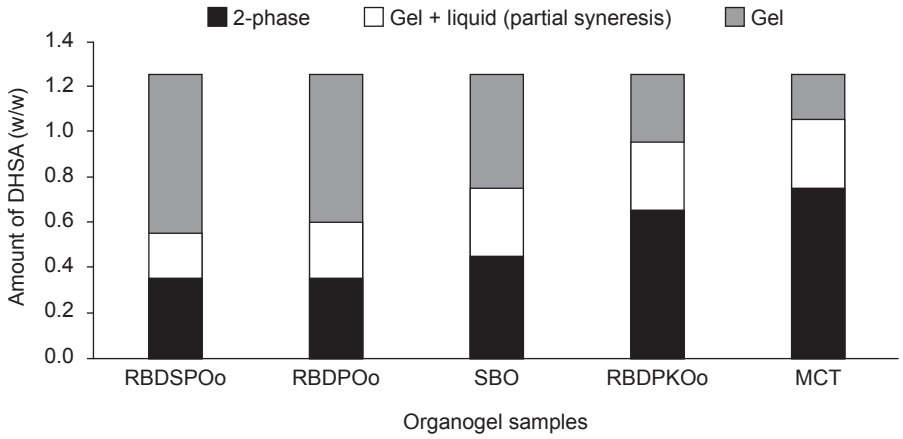


Figure 2. Gelation behaviour of organogels in various oils after 12 weeks at 25°C as a function of added DHSA.

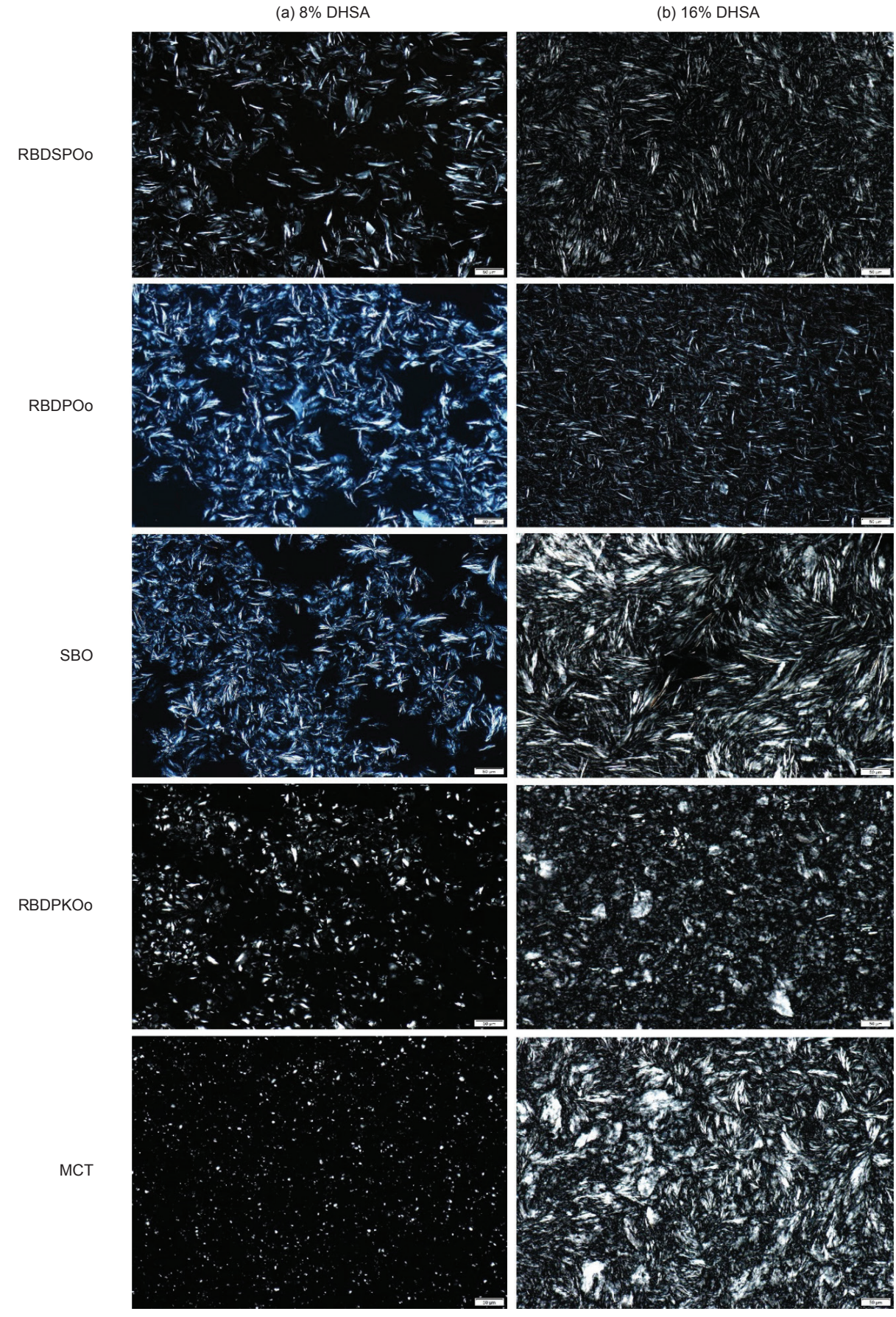


Figure 3. Polarised light microscopy images of organogels at (a) 8% (w/w) DHSA and (b) 16% (w/w) DHSA in oils i.e., *RBDPOo, RBDSPOo, SBO, RBDPKOo and MCT, respectively. The images were analysed at room temperature under objective magnification 20x with a scale bar of 50 µm.*

C_{18} in the oils (RBDPOo, RBDSPOo and SBO) also helped to increase the hardness of organogels. In contrast, the SAFA content in RBDPKOo and MCT did not help to increase the organogel hardness as these two oils had a high content of C_{12} (42.0%) and C_8 (54.6%) with low melting points compared to C_{16} and C_{18}. It was reported by Knothe and Dunn (2009) that melting points of C_{18}, C_{16}, C_{12} and C_8 were 69.29°C, 62.20°C, 43.29°C and 15.41°C, respectively. These findings are in line with Pehlivanoğlu *et al.* (2018) and Dassanayake *et al.* (2012), which reported that vegetable oils with a higher level of saturated fatty acids and high melting fatty acids produced hard organogels. In addition, it was also observed that oils with higher viscosities resulted in higher organogel hardness. These results agree with Valoppi *et al.* (2017) findings, which showed that there is a correlation between hardness and viscosity. Furthermore, the small needle-like crystal with dense distribution observed in DHSA organogel with RBDPOo has also contributed to the highest hardness of the organogel. In addition, the hardness of the organogels could also be affected by several other factors, such as thermal kinetics, the ratio of crystal and oil surfaces, as well as its solubility in oil (Dassanayake *et al.*, 2012; Onacik Gur *et al.*, 2017). Although DHSA organogels in MCT and RBDPKOo have the same crystal platelet structure, the crystalline structures of DHSA organogel in RBDPKOo were less compact, resulting in lower hardness values. Hardness is one of the essential criteria to determine the potential application of organogel in cosmetic products, especially lip products. The hardness for commercial solid lipstick was reported at least 0.29 N (Esposito and Kirilov, 2021) and commercial lip balm was within 0.49-0.64 N (Azmin *et al.*, 2020). Thus, hardness values of all DHSA organogels with the studied oils except for DHSA organogel with SBO were considered acceptable to formulate lip care products.

Rheological Characterisation

The elastic properties such as storage modulus (G′) and loss modulus (G″) of organogels containing 16% (w/w) DHSA in RBDPOo, RBDSPOo, SBO, MCT and RBDPKOo were characterised using oscillating rheological experiments. The viscoelastic behaviour involves structural changes within the organogel, either solid-like (G′) or liquid-like (G″) properties. *Figure 5* shows the frequency sweep of DHSA organogels in various oils at a varied angular frequency and constant strain (0.5%). The results showed that all organogel samples have gel-like behaviour with $G' > G''$ over a broad angular frequency range. DHSA organogel containing RBDPOo and RBDSPOo showed the highest elastic modulus compared to other oils. This showed that DHSA formed a better crystal network and gelation in RBDPOo and RBDSPOo. However, DHSA organogel with RBDPKOo showed G′ and G″ very close to each other at high angular frequency, indicating that this gel has liquid-like behaviour.

In order to determine the gel strength, a graph of tan δ as a function of angular frequency for DHSA organogels in various oils was plotted (*Figure 6*). In general, organogels can be classified into three types, which are strong gels ($G''/G' \leq 0.1$), weak gels ($0.1 \leq G''/G < 1$) and viscous sols ($G''/G' \geq 1$) (Tavernier *et al.*, 2017). All DHSA organogels

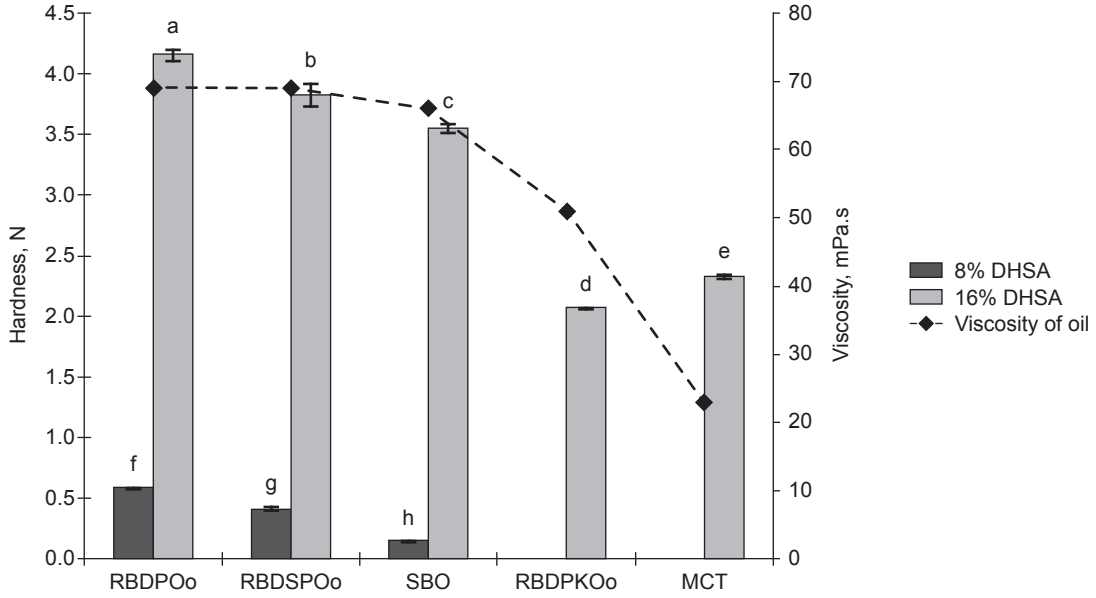


Figure 4. Hardness of organogel samples at 8% (w/w) and 16% (w/w) DHSA in different oils viscosity after seven days of storage at 25°C. Mean values with different letters are significantly different ($p<0.05$).

were classified as weak gels ($0.1 \leq G''/G' < 1$). At high angular frequency, tan δ or G''/G' of DHSA organogel with RBDPKOo is close to unity, which could not be considered as a gel. This is probably due to low oil viscosity. These results agree with Valoppi *et al.* (2017) findings, which showed a correlation between the rheology properties and oil viscosity. However, these correlations are not observed in MCT due to MCT's ability to make the dipole-dipole rotation, which affects the crystallisation behaviour (Cerqueira *et al.*, 2017). MCT containing 100% SAFA can form a more structured crystal than RBDPKOo, which contains mixtures of SAFA, MUFA and PUFA.

CONCLUSION

The main objective of this study was to evaluate the effect of DHSA as a gelling agent for vegetable oils on stability, crystal morphology, hardness and rheological properties. This study has shown that DHSA organogel with RBDSPOo showed a stable gel with the lowest CGC value, followed by RBDPOo, SBO, RBDPKOo and MCT. It was found that a higher percentage of MUFA in the oil contributed to a more stable gel. In addition, needle-shaped crystals and higher DHSA concentrations also help to entrap more oil and thus, improve organogel stability. Regarding texture

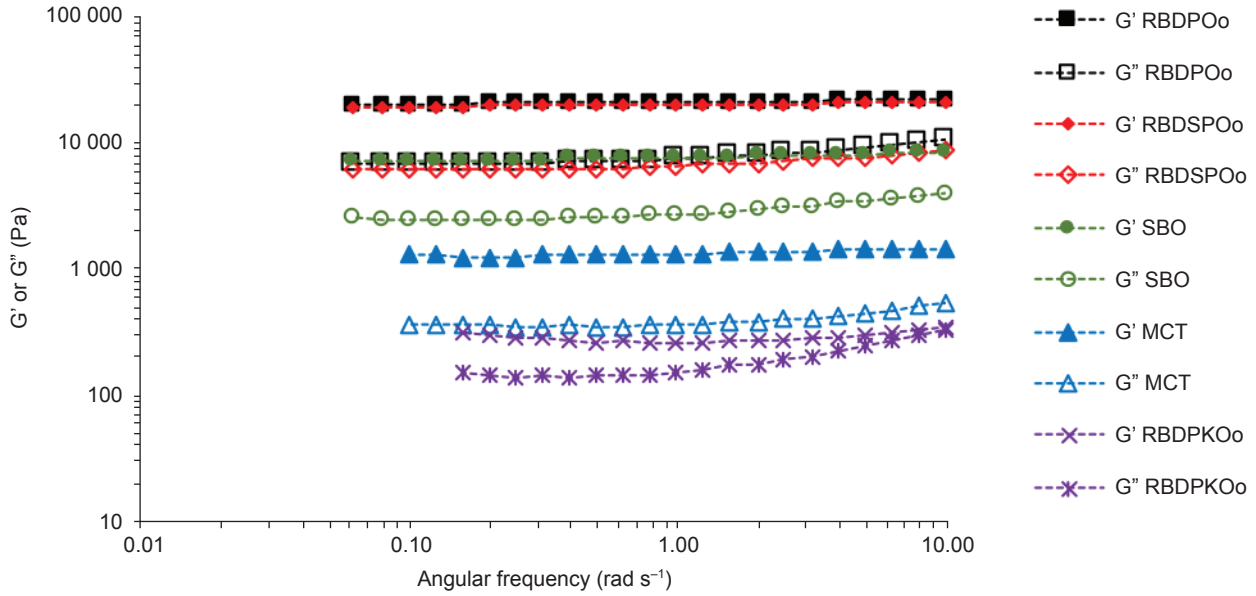


Figure 5. Frequency sweep of DHSA organogel samples as a function of angular frequency at 16% (w/w) DHSA in RBDPOo, RBDSPOo, SBO, MCT and RBDPKOo after seven days of storage at 25°C.

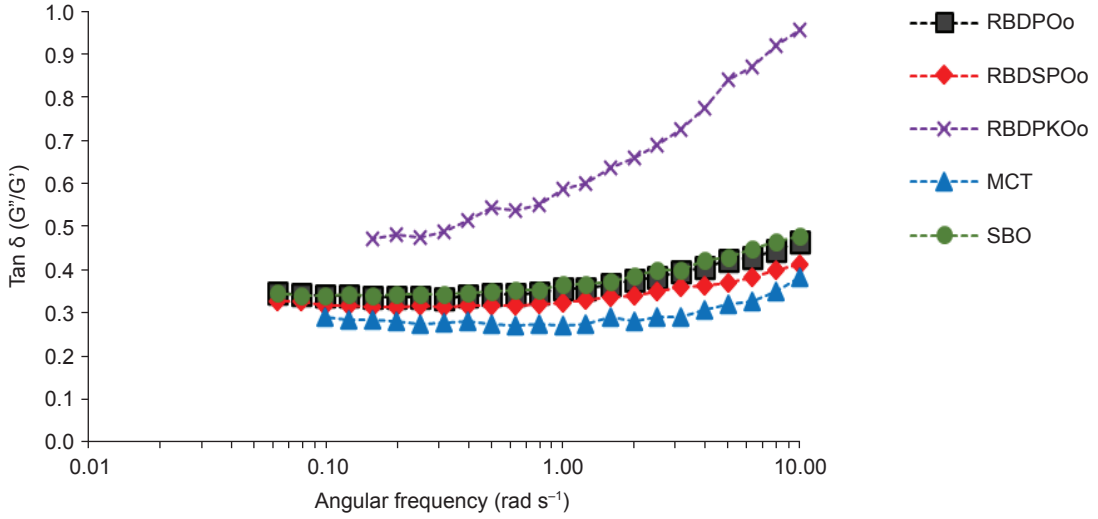


Figure 6. Tan δ value as a function of angular frequency for DHSA organogels at 16% (w/w) DHSA in RBDPOo, RBDSPOo, SBO, MCT and RBDPKOo after seven days of storage at 25°C.

characteristics, the hardness value of the DHSA organogels was improved with the formation of compact crystals and high melting fatty acids of the oil. Finally, it was found that elasticity and strength of the DHSA organogels were correlated with viscosity and degree of unsaturation of the oil as well as crystal network in the DHSA organogel. Considering the hardness value, DHSA organogel has the potential to be formulated in lip care products.

ACKNOWLEDGEMENT

The authors would like to thank the Director-General of MPOB for giving the opportunity to publish this article. Special thanks to Zulina Abd Maurad, Mohd. Nor Mamat @ Jusoh, Siti Hajar Bilal, Rosmah Umam, Puaat Sapar and Bahriah Bilal for their assistance.

REFERENCES

AOCS (2012). Official method Ce 2-66: Preparation of methyl ester of fatty acids. *Official Methods and Recommended Practices of the American Oil Chemists' Society* (Fireston, D ed.). 6th edition. American Oil Chemists' Society. AOCS Press, Urbana, IL, USA. p. 1-2.

Asaro, F; Boga, C; Zorzi, R D; Geremia, S; Gigli, L; Nitti, P and Semeraro, S (2020). (R)-10-hydroxystearic acid: Crystals *vs.* organogel. *Int. J. Mol. Sci.*, *21*: 8124.

Azmin, S N H M; Jaine, N I M and Nor, M S M (2020). Physicochemical and sensory evaluations of moisturising lip balm using natural pigment from *Beta vulgaris*. *Cogent Eng.*, *7(1)*: 1788297.

Burkhardt, M; Kinzel, S and Gradzielski, M (2009). Macroscopic properties and microstructure of HSA based organogels: Sensitivity to polar additives. *J. Colloid Interface Sci.*, *331*: 514-521.

Cerqueira, M A; Fasolin, L H; Picone, C S F; Pastrana, L M; Cunha, R L and Vicente, A A (2017). Structural and mechanical properties of organogels: Role of oil and gelator molecular structure. *Food Res. Int.*, *96*: 161-170.

Chen, X W; Sun, S D; Yang, G L and Ma, C G (2020). Engineering phytosterol-based oleogels for potential application as sustainable petrolatum replacement. *RSC Adv.*, *10(1)*: 244-252.

Co, E D and Marangoni, A G (2012). Organogels: An alternative edible oil-structuring method. *J. Am. Oil Chem. Soc.*, *89*: 749-780.

Daman Huri, M F; Ng, S and Zulfakar, M H (2013). Fish oil-based oleogels: Physicochemicals characterisation and *in vitro* release of betamethasone dipropionate. *Int. J. Pharm. Pharm. Sci.*, *5(3)*: 458-467.

Dassanayake, L S K; Kodali, D R; Ueno, S and Sato, K (2012). Crystallization kinetics of organogels prepared by rice bran wax and vegetable oils. *J. Oleo Sci.*, *61(1)*: 1-9.

Esposito, C L and Kirilov, P (2021). Preparation, characterization and evaluation of organogel-based lipstick formulations: Application in cosmetics. *Gels*, *7(3)*: 97.

Fameau, A L and Rogers, M A (2020). The curious case of 12-hydroxystearic acid - The Dr. Jekyll and Mr. Hyde of molecular gelators. *Curr. Opin. Colloid Interface Sci.*, *45*: 68-82.

Flöter, E; Wettlaufer, T; Conty, V and Scharfe, M (2021). Oleogels-their applicability and methods of characterization. *Molecules*, *26(6)*: 1673 (1-19).

Gravelle, A J; Davidovich-Pinhas, M; Zetzl, A K; Barbut, S and Marangoni, A G (2016). Influence of solvent quality on the mechanical strength of ethylcellulose oleogels. *Carbohydr. Polym.*, *135*: 169-179.

Ismail, R; Awang, R and Hazimah, A H (2015). Palm dihydroxystearic acid (DHSA): A multifunctional ingredient for various applications. *J. Oil Palm Res.*, *27(3)*: 195-211.

Koay, G F; Chuah, T G; Zainal-Abidin, S; Ahmad, S and Choong, T S (2011). Development, characterization and commercial application of palm based dihydroxystearic acid and its derivatives: An overview. *J. Oleo Sci.*, *60(5)*: 237-265.

Knothe, G and Dunn, R O (2009). A comprehensive evaluation of the melting points of fatty acids and esters determined by differential scanning calorimetry. *J. Am. Oil Chem. Soc.*, *86*: 843-856.

Lan, Y and Rogers, M A (2015). 12-hydroxystearic acid SAFiNs in aliphatic diols - A molecular oddity. *CrystEngComm.*, *17*: 8031-8038.

Martinez, R M; Rosado, C; Velasco, M V R; Lannes, S C S and Baby, A R (2019). Main features and applications of organogels in cosmetics. *Int. J. Cosmet. Sci.*, *41(2)*: 109-117.

Onacik Gur, S; Zbikowska, A; Przybysz, M and Kowalska, M (2017). Assessment of physical

properties of structured oils and palm fat. *Mater. Plast*., *54(4)*: 800-805.

Pehlivanoğlu, H; Demirci, M; Toker, O S; Konar, N; Karasu, S and Sagdic, O (2018). Oleogels, a promising structured oil for decreasing saturated fatty acid concentrations: Production and food-based applications. *Crit. Rev. Food Sci. Nutr.*, *58(8)*: 1330-1341.

Rocha-Amador, O G; Gallegos-Infante, J A; Huang, Q; Rocha-Guzman, N E; Moreno-Jimenez, M R and Gonzalez-Laredo, R F (2014). Influence of commercial saturated monoglyceride, mono-/diglycerides mixtures, vegetable oil, stirring speed, and temperature on the physical properties of organogels. *Int. J. Food Sci.*, *2014*: 1-8.

Silva, P M; Martins, A J; Fasolin, L H and Vicente, A A (2021). Modulation and characterization of wax-based olive oil organogels in view of their application in the food industry. *Gels*, *7(1)*: 12 (1-18).

Stortz, T A and Marangoni, A G (2014). The replacement for petrolatum: Thixotropic ethylcellulose oleogels in triglyceride oils. *Green Chem.*, *16*: 3064-3070.

Tavernier, I; Doan C D; Van de Walle, D; Danthine, S; Rimaux, T and Dewettinck, K (2017). Sequential crystallization of high and low melting waxes to improve oil structuring in wax-based oleogels. *RSC Adv.*, *7*: 12113-12125.

Valoppi, F; Calligaris, S; Barba, L; Šegatin, N; Ulrih, N P and Nicoli, M C (2017). Influence of oil type on formation, structure, thermal and physical properties of monoglyceride-based organogel. *Eur. J. Lipid Sci. Technol.*, *119*: 1500549.

Zhang, M; Selvakumar, S; Zhang, X; Sibi, M P and Weiss, R G (2015). Structural and solubility parameter correlations of gelation abilities for dihydroxylated derivatives of long-chain, naturally occurring fatty acids. *Chem. Eur. J.*, *21(23)*: 8530-8543.

Zhang, M and Weiss, R G (2016). Self-assembled networks and molecular gels derived from long-chain, naturally-occurring fatty acids. *J. Braz. Chem. Soc.*, *27(2)*: 239-255.

Journal of Oil Palm Research Vol. 35 (1) March 2023 p. 33-44
DOI: https://doi.org/10.21894/jopr.2022.0042

ASSESSING ELECTRICAL AND PHYSICOCHEMICAL PERFORMANCE OF CHEMICALLY MODIFIED PALM OIL AS AN ALTERNATIVE TRANSFORMER LIQUID

MASRA, S M W[1]*; ARIEF, Y Z[1]; RIGIT, A R H[2]; SAHARI, S K[1]; RAHMAN, M R[3]; MUHAMMAD, M S[1] and ETERUDDIN, H[4]

ABSTRACT

Numerous studies have been conducted on enhancing the dielectric properties of palm oil (PO) with the addition of nanoparticles (NPs). However, insufficient emphasis was given to its physicochemical properties, which are also critical for the function of an insulating liquid. The high viscosity of PO is one of the key factors which deteriorates the usage of natural ester in general, and PO in our case. This study was intended to investigate the performance of chemically modified PO by adopting a sequential transesterification process – NPs addition. The present work explored the transesterified PO blended with insulative (SiO_2) and semiconductive (ZnO) NPs at various concentrations (0.1-0.6 g L^{-1}). The modified oils' dielectric strength and physicochemical properties (density, kinematic viscosity, and water content) were measured using standard testing methods. The results showed that the transesterification process effectively reduced the viscosity of PO, and adding ZnO NPs substantially impacted the PO in terms of AC breakdown voltage, with an optimum performance at 0.2 g L^{-1} concentration of 85% improvement. In contrast, while using SiO_2, its breakdown voltage decreased irrespective of the concentration.

Keywords: chemically modification, nanoparticles, physicochemical properties, transesterification.

Received: 6 January 2022**; Accepted:** 17 June 2022**; Published online:** 27 July 2022.

INTRODUCTION

For decades, petroleum-based mineral oil (MO) has been utilised conventionally as a transformer insulating liquid. However, the usage of MO derived from non-renewable energy resources is affecting the environment due to its non-biodegradable property. As a result, researchers shifted their interest to biodegradable and renewable alternatives. Most research in biodegradable oils for transformer applications has focused on natural ester oils (NEOs) or vegetable oils (VOs). In the late 1990s, ABB developed the first commercial electrical insulating oil, BIOTEMP®, a sunflower oil-based (Boss and Oommen, 1999). In 2000, McShane *et al*. (2000) of Cooper Industries Inc. introduced Envirotemp FR3™ derived from soybean oil, and later, in 2008, Lion Corporation of Japan successfully developed Palm Fatty Acid Ester (PFAE) with the brand name Pastell Neo®, as potential natural ester (NE) insulating liquids for the transformers. VOs are renewable, cost savings, environmentally friendly, biodegradable, and safer alternative insulating oil (Amin *et al*., 2019). Due to the advantages mentioned above, VO is considered a substitute.

[1] Department of Electrical and Electronic Engineering, Faculty of Engineering, Universiti Malaysia Sarawak (UNIMAS), 94300 Kota Samarahan, Sarawak, Malaysia.

[2] Department of Mechanical Engineering, Faculty of Engineering, Universiti Malaysia Sarawak (UNIMAS), 94300 Kota Samarahan, Sarawak, Malaysia.

[3] Department of Chemical Engineering and Energy Sustainability, Faculty of Engineering, Universiti Malaysia Sarawak (UNIMAS), 94300 Kota Samarahan, Sarawak, Malaysia.

[4] Department of Electrical Engineering, Faculty of Engineering, Universitas Lancang Kuning (UNILAK), 28265 Rumbai, Riau Province, Indonesia.

* *Corresponding author e-mail: wmmasnia@unimas.my*

The wealth of literature conducted with the above NEOs has motivated researchers from other countries to begin researching their plant-based insulating liquids that utilise available and accessible renewable and biodegradable energy resources. Several plant oils, such as palm oil, pongamia pinnata oil, olive oil, marula oil, coconut oil, *etc*., have been used as the raw materials. Their potential suitability as transformer oils has been investigated and examined thoroughly by many researchers (Ariffin *et al*., 2017; Baruah *et al*., 2019; Farade *et al*., 2020; Genga Devi *et al*., 2016; Koutras *et al*., 2020a; Oparanti *et al*., 2020; Samikannu *et al*., 2021). Researchers eventually realised that VO-based liquid insulation needed various modifications to overcome its shortcomings and be employed as the insulating liquid in transformers (Moosasait and Maria Siluvairaj, 2021). One of the issues with VOs is their high viscosity, which undoubtedly reduces their efficacy as liquid insulation, making them unsuitable for cooling purposes (Raeisian *et al*., 2019; Yusof *et al*., 2017).

Over the years, researchers have successfully modified VOs for use as transformer liquid (Menkiti *et al*., 2017). Many studies have recognised the chemical modification of NEOs to lower their viscosities and make them comparable to that of MO for transformer application (Baruah *et al*., 2019). These studies have used various methods and base fluids, as summarised in *Table 1*. These methods are direct purification, esterification, transesterification, and epoxidation-esterification methods. Among all, transesterification is one of the options that has gained popularity, similar to the production of biodiesel as performed by various researchers (Ishola *et al*., 2020; Venugopal *et al*., 2021).

In addition, modifications are attempted on the base fluids to achieve superior thermal and dielectric properties by introducing nanoparticles (NPs), resulting in a nanofluid (NF) mixture. The physical, chemical, and thermal characteristics of dispersed NPs, along with the base fluid, as well as their weight or volume concentrations (Pyrgioti *et al*., 2020), have impacted the improvement and performance of NFs (Hussain *et al*., 2020). The influence of conductive (Fe_2O_3, Fe_3O_4), semiconductive (TiO_2, ZnO, CuO) and insulative (SiO_2, Al_2O_3) NPs on the dielectric and physicochemical properties of biodegradable insulating liquids have been extensively studied in the literature. Koutras *et al*. (2020b) reported that the addition of TiO_2 NPs into FR3 enhanced alternating current breakdown voltage (AC BDV) by 22.40% at 0.02 vol% concentration. Oparanti *et al*. (2021) examined the effects of dispersing TiO_2 and Al_2O_3 NPs into palm kernel oil (PKO) on the physicochemical properties, dielectric response, and BDV. The results showed that the dispersion of these two types of NPs enhanced the physicochemical properties of the PKO. In other studies, for instance, Raj *et al*. (2021) reported the excellent performance of marula oil

TABLE 1. SUMMARY OF LITERATURE RELATED TO METHYL ESTER OILS AS ALTERNATIVE TRANSFORMER LIQUID

Modification method	References	Methyl ester oils	Performance	
			Dielectric strength [kV]	Kinematic viscosity (40°C) [$mm^2 s^{-1}$ or cSt]
Direct purification	Menkiti *et al.* (2017)	Modified *Terminalia catappa* kernel oil (MTCKO)	32.88	15.22
Esterification	Sitorus *et al.* (2016)	Jatropha methyl ester oil (JMEO)	87.00	10.45
Transesterification	Maharana *et al.* (2018)	Karanji oil methyl ester (KOME)	85.40	12.00
	Agu *et al.* (2019)	Modified *T. catappa* kernel oil (MTCKO)	48.55	10.29
	Nkouetcha *et al.* (2019)	Castor oil methyl ester (COME)	74.67	18.42
	Ravulapalli *et al.* (2019)	Methyl ester sesbania seeds oil (MESSO)	n/a	0.98×10^{-11}
	Asse *et al.* (2022)	Palm kernel oil methyl ester (PKOME)	32.22	n/a
	Oparanti *et al.* (2022)	Neem oil ester	n/a	5.17
Epoxidation-esterification	Abdelmalik *et al.* (2011)	Palm kernel oil epoxy methyl ester (PKOEME)	45.58	6.14
	Agu *et al.* (2019)	Modified *T. catappa* kernel oil (MTCKO)	50.05	8.56
Blending with fatty acid or fatty esters	Mohd *et al.* (2021)	Blended RBDPO olein	76.80	2.48 – 5.12 (depends on types of fatty acid or fatty esters)

Note: Recommended specification for natural ester (IEEE C57.147:2018) – Dielectric strength ≥35 kV, and kinematic viscosity ≤50 cSt.
n/a – not available.

blended with Al_2O_3 by showing up to 64.00% on its breakdown voltage (BDV) enhancement, and Duzkaya and Beroual (2021) reported the increment of AC BDV of FR3 blended with ZnO at 0.1 to 0.3 g L^{-1} concentrations. On the other hand, some types of NPs do not constantly improve the dielectric strength of NEOs, which others have also reported. For example, dispersion of SiO_2 into commercial NEOs, MIDEL 1204 (Khaled and Beroual, 2019) and FR3 (Charalampakos *et al*., 2017) demonstrated a reduction of their dielectric strengths.

Similarly, some research studies reported the effects of NPs on the dielectric properties of PO, as demonstrated by Makmud *et al*. (2018) and Nor *et al*. (2017). The authors dispersed TiO_2 NPs at various concentrations and reported an apparent enhancement in the dielectric breakdown strength of the NFs. Also, Hussin *et al*. (2021) and Saenkhumwong and Suksri (2017) demonstrated an improvement in PO's BDV using TiO_2 and ZnO. Furthermore, Mohamad *et al*. (2019) compared the effects of Fe_3O_4, CuO, and Al_2O_3 with the presence of surfactant on the dielectric strength of PO. They also reported the enhancement of the BDV at a specific volume concentration. Meanwhile, SiO_2 (Yahya and Amirrazli, 2018), SiC (Yahya and Maliki, 2018), and carbon nanotubes (CNTs) (Suhaimi, 2018) NPs caused the decrement of BDV of PO. From the literature, emphasis has been focused primarily on the dielectric characteristics while ignoring the physiochemical properties of PO. Consequently, in this present study, the authors investigate the chemically modified PO through the sequential transesterification process-NPs addition, for possible use as an alternative transformer liquid. The primary goal of this work is to examine the impact of sequentially optimising the physicochemical properties and addition of NPs on the transesterified refined, bleached, and deodorised palm oil (RBDPO) olein, known as palm oil methyl ester (POME). The characterisation of dielectric strength and physicochemical properties such as density, kinematic viscosity, and water content has been performed to determine the performance of the POME-based NFs.

MATERIALS AND METHODS

Materials

The RBDPO olein used was manufactured by Lam Soon Edible Oils Sdn. Bhd. and purchased from a local grocery store. It was used as received without filtration and purification, and methyl ester was synthesised from it. The SiO_2 and ZnO NPs manufactured by Sigma-Aldrich was used to prepare the NFs. In addition, pure methanol (99.9%) was purchased from Merck. Pure potassium hydroxide (KOH) in the pellet form from the J. T. Baker was used as a catalyst, readily available in the laboratory.

Synthesis of POME by Transesterification Process

The RBDPO olein was transformed into POME via the transesterification process, as shown in *Figure 1*. The RBDPO olein (1000.0 g, 1.182 mol) and methanol (CH_3OH) (227.3 g, 7.094 mol) were placed in separate beakers. In this work, methanol was particularly preferred to produce methyl ester because of its availability, cost, and physical and chemical advantages for quick reaction with triglycerides (Encinar *et al*., 2010; Musa, 2016). Then, KOH as a catalyst was added to the methanol beaker in the pre-determined amounts for the experiment and stirred with the magnetic stirrer until KOH pellets were fully dissolved. The second beaker containing RBDPO olein was heated to 60°C. The methanol and KOH mixture was poured into the RBDPO olein, and both mixtures were heated to 60°C for 60 min. The reaction was conducted using the recommended methanol; oil molar ratio of 6:1 (Baroutian *et al*., 2009; Musa, 2016). The ratio is universally accepted and often used to drive the reaction to the product side, as an incomplete reaction was observed for molar ratios below 6:1, and a higher molar ratios increase the cost to recover the excess alcohol after the completion of the reaction (Encinar *et al*., 2010).

The mixture was allowed to cool to ambient temperature before being transferred to a separatory funnel for separation. Glycerol and methyl ester were split into two layers when the transesterification process was completed. The bottom layer, which is the mixture of crude glycerol and KOH, was drained off. The upper layer, the fatty acid methyl ester (FAME), was then washed with warm distilled water several times to remove excess KOH until it achieved a neutral pH level. It was then heated and stirred at a temperature of 60°C for 30 min to eliminate the remaining water molecules and methanol. POME was used as the base fluid for preparing the NFs.

Preparation of POME-based NF Samples

In this study, the NFs were prepared using the two-step method. The NPs were heated in an oven to remove any moisture from the powder particles. Then, the pre-treated NPs were dispersed into the POME base fluid at different concentrations ranging from 0.1-0.6 g L^{-1} and stirred using a magnetic stirrer for 30 min at 800 rpm. The concentration span provides a range to allow investigation of the optimal dielectric strength and physicochemical properties of the NFs. *Figure 2* is the flow chart of the POME-based NFs preparation in the laboratory.

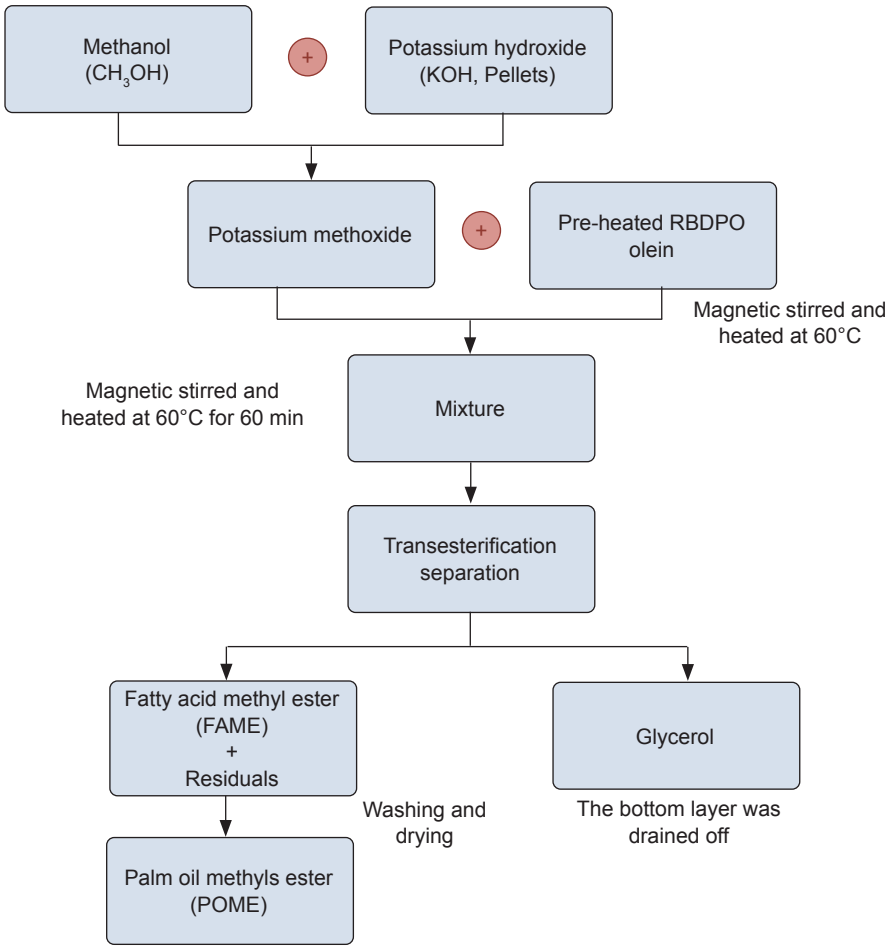


Figure 1. The POME production process in the laboratory.

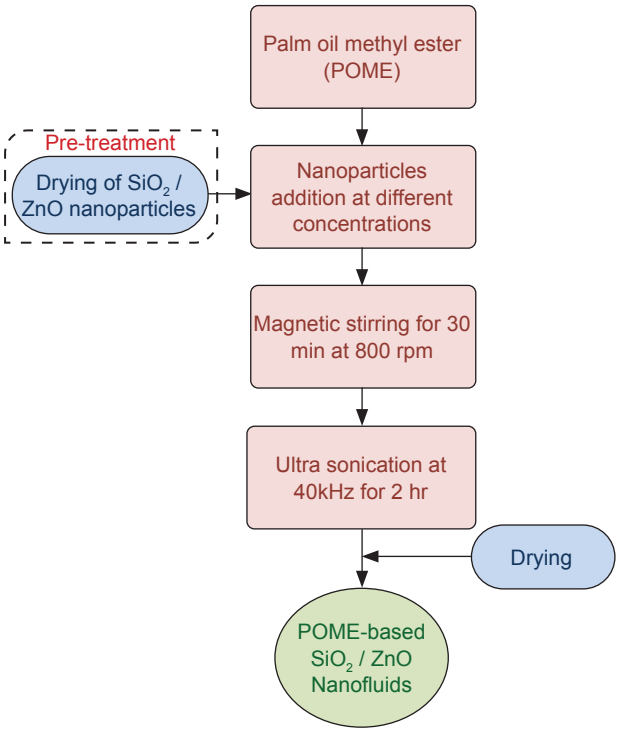


Figure 2. Preparation of POME-based NFs in the laboratory.

Then, the NF samples underwent an ultrasonication for a 2 hr procedure to break up any agglomeration of NPs. This ultrasonic procedure using an ultrasonic cleaner with a heating power of 100 W and a frequency of 40 kHz was applied for 2 hr in intervals of 30 min of agitation with a 10 min waiting period between to avoid overheating of the NFs. The two-step method helped minimise the possibility of agglomeration resulting from the covalent bond between NPs, which induced NPs to be settled. After the drying procedure, a total of six NF oil samples having concentrations of: 0.1 g L^{-1} SiO_2, 0.3 g L^{-1} SiO_2, 0.5 g L^{-1} SiO_2, 0.2 g L^{-1} ZnO, 0.4 g L^{-1} ZnO, and 0.6 g L^{-1} ZnO were prepared for the subsequent experimental tests and analysis.

Scanning Electron Microscopy-Energy Dispersive Spectroscopy (SEM-EDS) and Fourier Transform Infrared-Attenuated Total Reflection (FTIR-ATR) Characterisation

The characterisation of NPs was studied using SEM integrated with EDS analysis, taken with a JEOL JSM - IT500HR Electron Microscope operated

at 20 kV. On the other hand, the characterisation of pure POME and POME-based NFs samples was studied using FTIR-ATR analysis. The observed spectra were the absorbance of the differently prepared oil samples versus the wavenumber range of 4000-400 cm^{-1}.

Electrical and Physicochemical Characterisation

This study investigated the influence of SiO_2 and ZnO NPs, both in various sizes and at varying concentrations on the dielectric strength and physicochemical properties of POME. The physicochemical parameters studied were density, kinematic viscosity, and water content. AC BDV was measured using an insulating oil dielectric strength tester in accordance with IEC 156:1995 (En, 1996). The density at 20°C was measured using DMA 35 basic handheld density meter according to ASTM D7777 (ASTM Standard D7777-13, 2018); kinematic viscosity at 40°C was measured using HK kinematic viscosity apparatus in accordance with ASTM D445 (ASTM D445-06, 2008); and water content by Karl Fischer method in accordance to ASTM D6304 (ASTM Standard D6304-20, 2016). The dielectric strength and physicochemical characterisation of POME were compared to the requirement of IEEE Std C57.147:2018 – IEEE guide for acceptance and maintenance of natural ester insulating liquid in transformers (IEEE 2018). The effect of both NPs used in this study was investigated to understand better the behaviour of POME in the presence of different types of NPs as additives in transformer liquid dielectric.

RESULTS AND DISCUSSION

POME Production

Figure 3 shows the yield of POME from four samples (S1-S4) of RBDPO olein that underwent the transesterification process. From the graph, it can be seen that all the samples achieved more than 90.00% yield. The reaction was the same for all samples; however, a small yield percentage variability could be due to practical losses throughout the procedure. The average POME production yield was 98.43%.

SEM-EDS Analysis

Figures 4a and *4b* show the SEM images of SiO_2 and ZnO NPs with three different magnifications, respectively. Both NPs had a variety of shapes and sizes and a homogeneous distribution with a wide range of dispersion. SiO_2 powder consists of more or less spherical and regular particles (Khaled and Beroual, 2019) with poor agglomeration. The particle size data of both NPs were obtained from measuring 50 particles using ImageJ software. SiO_2 and ZnO have an average size of 28.95 ± 14.9 nm and 40.64 ± 17.4 nm, respectively.

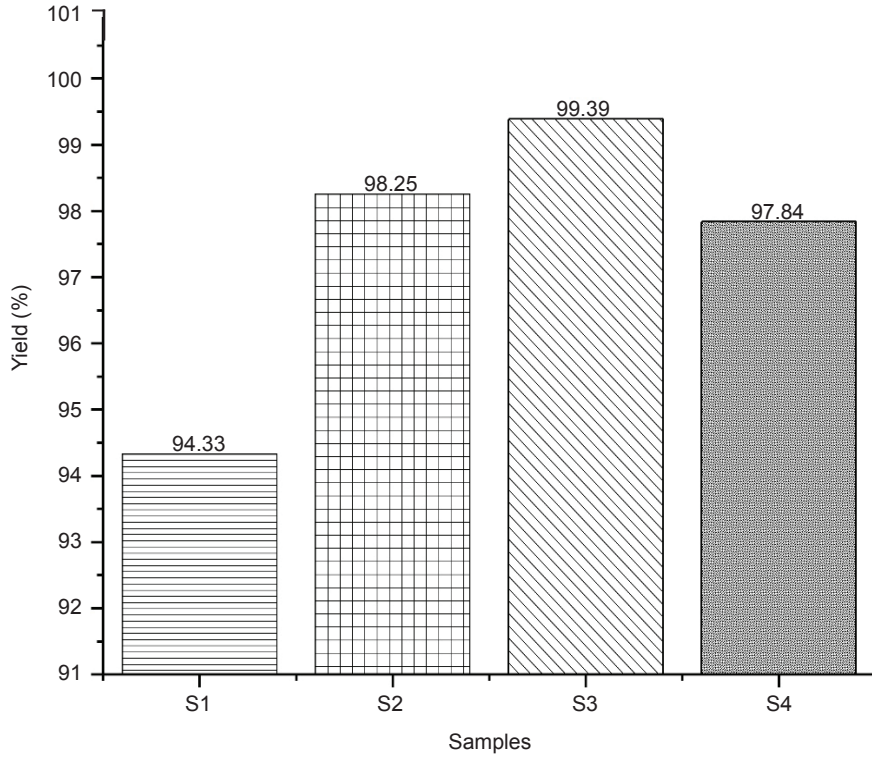


Figure 3. The percentage yield of POME.

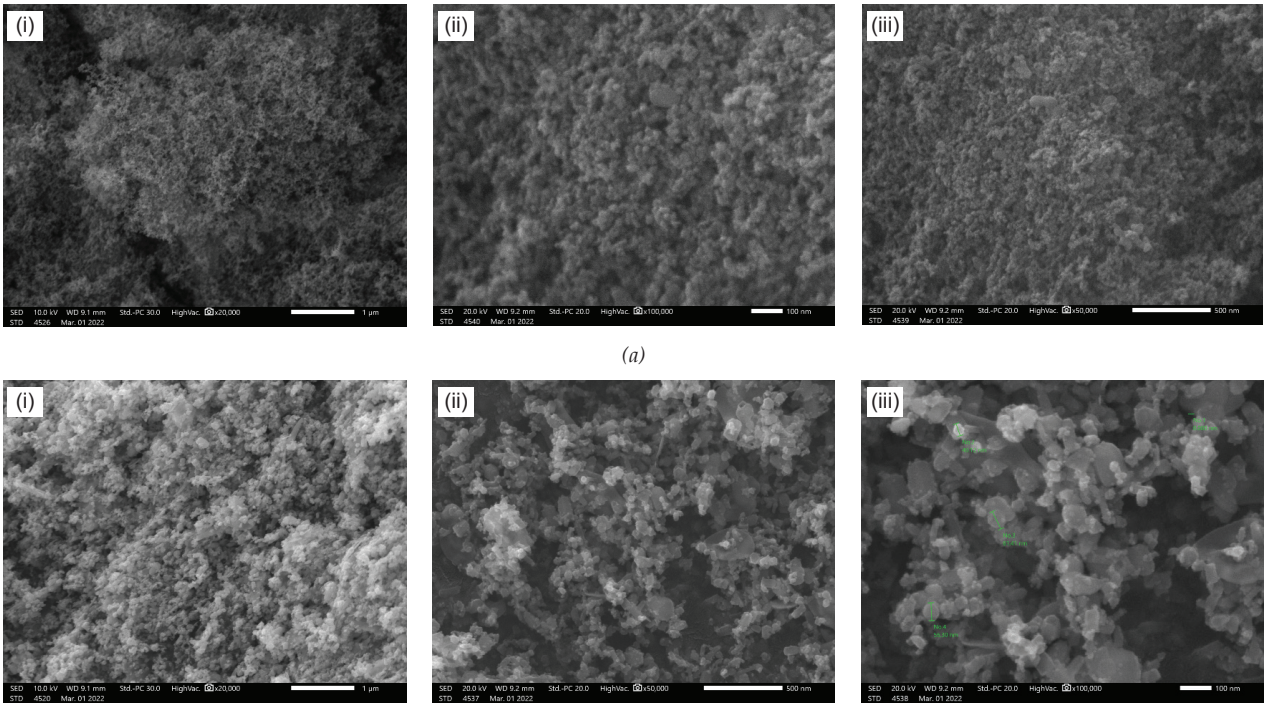


Figure 4. SEM images of (a) SiO_2 and (b) ZnO NPs showing their morphology at three different resolutions at (i) ×20 000, (ii) ×50 000, and (iii) ×100 000 magnification.

Figures 5a and *5b* show the EDS results of SiO_2 and ZnO particles. The spectrum indicates the presence of silicon, zinc particularly, and oxygen, indicating the formation of silica as silicon dioxide and zinc as zinc oxide, respectively.

FTIR-ATR Spectra Analysis

Characterisation of Pure POME, POME-based SiO_2 NFs and POME-based ZnO NFs. Pure POME and all NF samples were characterised using FTIR-ATR spectroscopy studies, as shown in *Figures 6a* and *6b*. In these figures, the x-axis represents the wavenumber (cm^{-1}) and the absorbance in the y-axis. The absorption peaks at 2922.16 cm^{-1} and 2852.72 cm^{-1} represent the asymmetric stretching vibration of C-H of -CH_2 groups and the symmetric stretching vibration of CH_2 groups (Jacob *et al.*, 2020; Jamo *et al.*, 2019; Ramli *et al.*, 2021), respectively. At the absorbance wave number 1741.72 cm^{-1}, a long and narrow, strong peak can be seen for all samples; it represents C=O stretching indicating the formation of ester (Baruah *et al.*, 2020; Jacob *et al.*, 2020; Maharana *et al.*, 2019). The absorbance peaks at a wavenumber of 1168 cm^{-1} and 721.36 cm^{-1} indicated the presence of the C-O band stretching, establishing the existence of an ester (Ravulapalli *et al.*, 2019).

The resemblance in the FTIR-ATR spectra of both POME-based NFs at 2922.16, 2852.72, 1741.72, 1460.11, 1168.86 and 721.38 cm^{-1} is an indication of the presence of a similar chemical group in their compositions (Awogbemi *et al.*, 2019). The introduction of both NPs did not cause any changes in the spectra of investigated POME-based liquids; this infers that varying NPs concentration does not affect the sample's compound structure.

Dielectric Strength Characterisation

AC BDV. The dielectric strength of the pure POME and NFs was studied using the AC BDV test. In this section, the AC BDV of POME-based SiO_2 and ZnO NFs were presented and discussed. *Table 2* tabulates the AC BDV for both investigated NFs and shows the incremental percentage of their breakdown strength with different concentrations of NPs. A significant enhancement of AC BDV for POME-based ZnO NFs was observed compared to POME-based SiO_2 NFs. The results demonstrated that all NFs samples with ZnO addition have higher AC BDV than the pure sample of POME. The optimal concentration for the highest AC BDV was 0.2 g L^{-1}. The BDV increased from 20 kV to 37 kV, equivalent to an 85% increase in magnitude. However, the BDV started to decrease as the concentration of ZnO NPs increased. Similar results were reported by Saenkhumwong and Suksri (2017), where the authors tested the ZnO in palm ester, and the optimal concentration was found to be at 0.2 g L^{-1}.

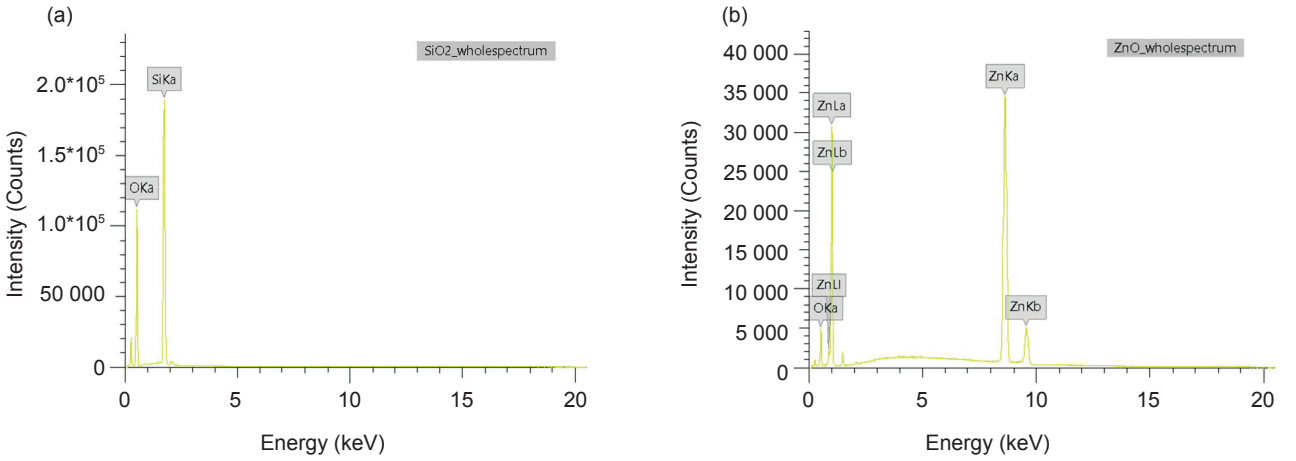


Figure 5. EDS analysis of (a) SiO_2 and (b) ZnO NPs.

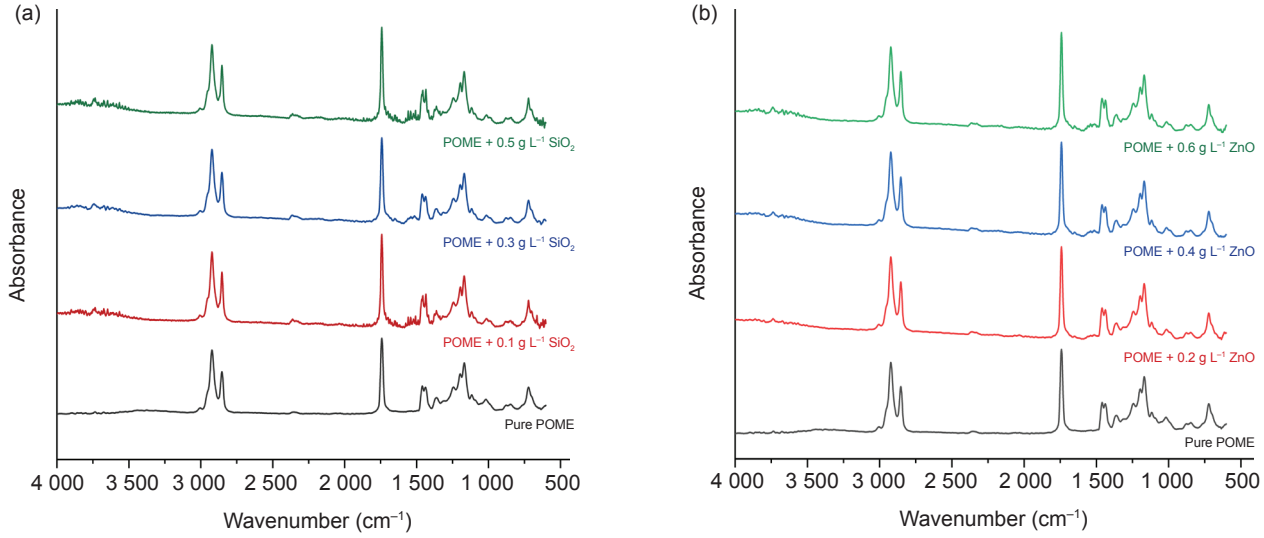


Figure 6. FTIR spectra of POME-based (a) SiO_2 and (b) ZnO NFs.

TABLE 2. INCREMENT PERCENTAGE OF AC BDV

Measurement	Limit IEEE Std C57.147:2018	Pure POME	POME +0.1 g L^{-1} SiO_2	POME +0.3 g L^{-1} SiO_2	POME +0.5 g L^{-1} SiO_2	POME +0.2 g L^{-1} ZnO	POME +0.4 g L^{-1} ZnO	POME +0.6 g L^{-1} ZnO
AC BDV (kV)	≥ 35	20	20	16	19	37	29	28
Increment		-	0	-20%	-5%	85%	45%	40%

In contrast, while using SiO_2, the AC BDV decreased irrespective of the concentration, as shown by the negative incremental percentage in *Table 2*. This observation was similar to Yahya and Amirrazli (2018), who found that SiO_2 NPs did not improve the BDV of PO. Similarly, in other works where the addition of SiO_2 into different types of natural ester, *i.e.*, MIDEL 1204 (Khaled and Beroual, 2019) and FR3 (Charalampakos *et al.*, 2017), they demonstrated a similar reduction of dielectric strength of respective NEOs.

Physicochemical Characterisation

The density of oil samples. In general, the density of the oils varies with each type and temperature, ranging from 0.81 to 0.91 g cm^{-3} (Rotimi, 2016). From the experimental results, compared to non-treated RBDPO olein, whose density was 0.91 g cm^{-3}, POME's density was 0.87 g cm^{-3}, met the IEEE C57.147 standard (≤0.96 g cm^{-3}). An almost similar value was obtained by Jayakar *et al.* (2018), which was 0.873 g cm^{-3}. The value is comparable to MO, which has a density of 0.88 g cm^{-3} (Kanoh *et al.*, 2008).

Kinematic viscosity. The viscosity of PO is 37.300 cSt (Suwarno *et al.*, 2003). After transesterification, the viscosity of the oil was reduced to 4.272 cSt, which implies that the POME complied with the required limit of ≤50 cSt. This study also looked at the effect of insulative NPs on the viscosity of POME. The measured viscosity of POME-based NFs at a temperature of 40°C varied between 4.233 to 4.326 cSt, which also complied with the required limit. This implies that the presence of NPs did not influence the viscosity of POME-based NFs at 40°C. The results demonstrated that the transesterification process had changed the viscosity of POME considerably. The conversion of triglycerides to methyl ester appeared to be the primary cause of the viscosity reduction. Low viscosity transformer oils are preferred because they promote heat transfer and circulation (Mohd *et al.*, 2021; Walvekar *et al.*, 2022).

Water content. According to Toudja *et al*. (2014), water content dissolved in oils is practically inevitable and adversely influences the oil's properties. Consequently, the dielectric strength of the oil degrades. The water content of pure POME, POME-based SiO_2, and POME-based ZnO NFs can be seen in *Figure 7*. It was observed that the pattern in the graph demonstrated that as the amount of SiO_2 NPs employed increased, the water content of their NF decreased. However, when the concentration of ZnO NPs increased, so did the water content in the samples.

Generally, as the water content of the NFs rises, their AC BDV is reduced. As demonstrated by other studies (Ab Ghani *et al.*, 2016; Abdi *et al.*, 2020), the water content is inversely proportional to the AC BDV. However, another factor influencing the mechanism of BDV characteristics of the NFs is the electrical conductivity of NPs (Duzkaya and Beroual, 2021). ZnO is a semiconductive NP that traps high mobility electrons by slowing down the electrons responsible for streamer development with trapping and de-trapping processes (Duzkaya and Beroual, 2021). Approximately 85% of the increment of AC BDV at a concentration of 0.2 g L^{-1} is well explained by this mechanism. Meanwhile, the decreased BDV when NP exceeds a specific concentration may be attributed to the mechanism of bridging or tunnelling, as discussed in the previous study (Duzkaya and Beroual, 2021).

However, water content is still over the threshold under the required standard, which signals that more additional procedures or treatments are needed to lower the water content of POME NFs. These additional treatments include using adsorbents such as silica gel or drying the NFs in an oven at a specific temperature and a particular time to eliminate the existing moisture before conducting further tests.

Comparative Analysis with Previous Studies

Table 3 shows the comparative results obtained by various researchers in assessing the dielectric strength and viscosity properties of the PO. In the current study, the transesterification and addition of NPs methods used to modify the PO demonstrate comparable results to previous studies.

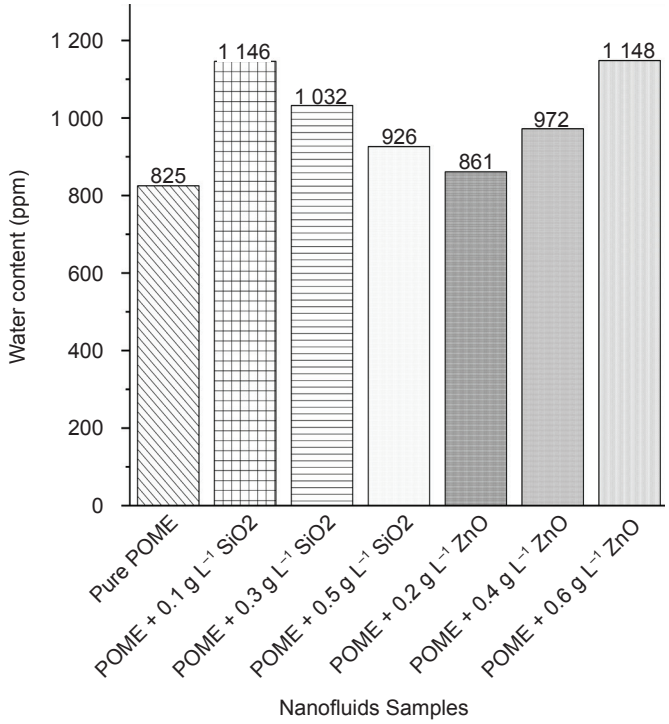


Figure 7. The water content of pure POME, POME-based SiO_2 and ZnO NFs.

TABLE 3. COMPARATIVE ANALYSIS WITH PREVIOUS STUDIES

Modification method	NPs addition / concentration	Breakdown voltage (kV)	Kinematic viscosity (40°C) ($mm^2 s^{-1}$ or cSt)	References
n/a	SiO_2 / 0.100%	25.46	70.000	Yahya and Amirrazli (2018)
n/a	SiC / 0.300%	28.04	140.000	Yahya and Maliki (2018)
n/a	ZnO / 0.005 g L^{-1}	69.28	46.660	Hussin *et al*. (2021)
Transesterification	ZnO / 0.200 g L^{-1}	27.30	0.934	Saenkhumwong and Suksri (2017)
Transesterification	TiO_2 / 0.200 g L^{-1}	29.00	0.925	Saenkhumwong and Suksri (2017)
Transesterification	FeO_3 / 0.100 wt%	32.22	n/a	Asse *et al*. (2022)
Transesterification	ZnO / 0.200 g L^{-1}	37.00	4.326	Current study

Note: n/a - not available.

CONCLUSION

The transesterification process improved the physicochemical property of PO, in particular the viscosity of the oil, allowing it to be used as a potential insulating dielectric liquid for transformers. The addition of NPs to the POME appeared to have a minimal effect on the POME's viscosity and can be considered negligible. POME-based SiO_2 and ZnO NFs complied with the viscosity requirement for their use in transformers. The effects of NPs on AC BDV of POME depend on their types and concentrations. The best increment achieved was 85%; at a concentration of 0.2 g L^{-1} of ZnO NPs. Increasing ZnO concentration beyond this value suggests the implication of the conductivity of the NP, leading to the existence of an optimum concentration that has yet to be established because it is still in the research stage. On the other hand, adding insulative SiO_2 NPs reduced POME's dielectric strength, with SiO_2 at a concentration of 0.3 g L^{-1}, causing a 20% reduction. This work revealed that the developed POME-based ZnO NFs were likely to serve better as an insulating liquid than POME-based SiO_2 NFs.

The study of the impact on chemical modification using the transesterification process and the addition of NPs in PO carried out here is a preliminary study. To ensure the reliability and possibility of POME-based NFs as an insulating liquid in transformers, other physicochemical parameters, including interfacial tension, acidity, pour point, and fire point will be included in future research work.

ACKNOWLEDGEMENT

The authors wish to thank Universiti Malaysia Sarawak (UNIMAS) for supporting this research activity. The authors are also grateful to Mr. Shafri Senawi and Mr. Airul Azhar Jitai for assisting in preparing and measuring the SEM specimens in this study. This study was supported by Universiti Malaysia Sarawak (UNIMAS) under research grants GL/F02/UNILAK/2020, GL/F02/UNILA/2021, and F02/SGS/1784/2018.

REFERENCES

Ab Ghani, S; Muhamad, N A; Chairul, I S and Jamri, N (2016). A study of moisture effects on the breakdown voltage and spectral characteristics of mineral and palm oil-based insulation oils. *ARPN J. Eng. Appl. Sci.*, *11(8)*: 5012-5020.

Abdelmalik, A A; Fothergill, J C and Dodd, S J (2011). Electrical breakdown strength characteristics of palm kernel oil ester-based dielectric fluids. *Annual Report - Conference on Electrical Insulation and Dielectric Phenomena, CEIDP*. p. 183-186.

Abdi, S; Safiddine, L; Boubakeur, A and Haddad, A (2020). The effect of water content on the electrical properties of transformer oil. *Lect. Notes Electr. Eng.*, *599(November)*: 518-527.

Agu, C M; Menkiti, M C; Nwabanne, J T and Onukwuli, O D (2019). Comparative assessment of chemically modified *Terminalia catappa* L. kernel oil samples - A promising ecofriendly transformer fluid. *Ind. Crops Prod.*, *140(August)*: 111727.

Amin, D; Walvekar, R; Khalid, M; Vaka, M; Mujawar, N M and Gupta, T C S M (2019). Recent progress and challenges in transformer oil nanofluid development: A review on thermal and electrical properties. *IEEE Access*, *7*: 151422-151438.

Ariffin, M M; Ishak, M T; Hamid, M H A; Katim, N I A; Ishak, A and Azis, N (2017). Ageing effect of vegetable oils impregnated paper in transformer application. *International Conference on High Voltage Engineering and Power Systems, ICHVEPS 2017* -

Proceeding. Institute of Electrical and Electronics Engineers Inc., New Jersey. p. 183-187.

Asse, J B; Mengounou, G M and Imano, A M (2022). Impact of FeO_3 on the AC breakdown voltage and acidity index of a palm kernel oil methyl ester based nanofluid. *Energy Rep.*, *8*: 275-280.

ASTM D445-06 (2008). Standard test method for kinematic viscosity of transparent and opaque liquids (and calculation of dynamic viscosity). *Man. Hydrocarb.*

ASTM Standard D6304-20 (2016). Standard test method for determination of water in petroleum products, lubricating oils, and additives by coulometric Karl Fischer titration.

ASTM Standard D7777-13 (2018). Standard test method for density, relative density, or API gravity of liquid petroleum by portable digital density meter.

Awogbemi, O; Onuh, E I and Komolafe, C A (2019). Thermal degradation and spectroscopic study of neat palm oil, waste palm oil, and waste palm oil methyl ester. *IOP Conf. Ser. Earth Environ. Sci.*, *331(1)*.

Baroutian, S; Aroua, M K; Raman, A A and Sulaiman, N M (2009). RBD palm olein-based methyl/ethyl esters. *J. Oil Palm Res.*, *21*: 659-666.

Baruah, N; Maharana, M and Nayak, S K (2019). Performance analysis of vegetable oil-based nanofluids used in transformers. *IET Sci. Meas. Technol.*, *13(7)*: 995-1002.

Baruah, N; Dey, S S and Nayak, S K (2020). Evaluation of dissolved gas analysis and long-term performance of non-edible natural ester. *IEEE Trans. Dielectr. Electr. Insul.*, *27(5)*: 1561-1569.

Boss, P and Oommen, T V (1999). New insulating fluids for transformers based on biodegradable high oleic vegetable oil and ester fluid. *IEE Colloq.*, *(119)*: 39-48.

Charalampakos, V P; Bakandritsos, A; Peppas, G D; Pyrgioti, E C and Gonos, I F (2017). A comparative study of natural ester based nanofluids with Fe_2O_3 and SiO_2 nanoparticles. *IEEE Int. Conf. Dielectr. Liq.* p. 1-4.

IEEE (2018). IEEE guide for acceptance and maintenance of natural ester unsulating liquid in transformer. IEEE Std. C57. 145-2018 (Revision IEEE Std. C57. 147-2008). p. 1-47.

Duzkaya, H and Beroual, A (2021). Statistical Analysis of AC dielectric strength of natural ester-based ZnO nanofluids. *Energies*, *14(1)*: 99.

En, B S (1996). Insulating liquids: Determination of the breakdown voltage at power frequency - Test method. 41 pp.

Encinar, J M; González, J F; Pardal, A and Martínez, G (2010). Transesterification of rapeseed oil with methanol in the presence of various co-solvents. *Third Int. Symp. Energy from Biomass Waste*, *November 2(November 2010)*: 1-17.

Farade, R A; Wahab, N I B A; Mansour, Di E A; Azis, N B; Jasni, J; Banapurmath, N R and Soudagar, M E M (2020). Investigation of the dielectric and thermal properties of non-edible cottonseed oil by infusing h-BN nanoparticles. *IEEE Access*, *8*: 76204-76217.

Genga Devi, K; Ravindran, M and Senthil Kumar, S (2016). Analysis of critical parameters of vegetable oil as an alternate dielectric fluid to mineral oil. *Proc. 10th Int. Conf. Intell. Syst. Control. ISCO 2016*.

Hussain, M R; Khan, Q; Khan, A A; Refaat, S S and Abu-Rub, H (2020). Dielectric performance of magneto-nanofluids for advancing oil-immersed power transformer. *IEEE Access*, *8*: 163316-163328.

Hussin, N; Subri, N A; Azizie, N A; Khalil, A N M; Jamil, M K M; Abd-Rahman, R and Arshad, S N M (2021). Low concentration vegetable oil based nanofluid: Dielectric properties, AC breakdown voltage and kinematic viscosity. *J. Phys. Conf. Ser.*, *1878(1)*.

Ishola, F; Adelekan, D; Mamudu, A; Abodunrin, T; Aworinde, A; Olatunji, O and Akinlabi, S (2020). Biodiesel production from palm olein: A sustainable bioresource for Nigeria. *Heliyon*, *6(4)*: e03725.

Jacob, J; Preetha, P and Sindhu, T K (2020). Stability analysis and characterization of natural ester nanofluids for transformers. *IEEE Trans. Dielectr. Electr. Insul.*, *27(5)*: 1715-1723.

Jamo, H U; Umar, I D; Yusuf, B and Auwalu, I A (2019). Enhancement of physical properties of biodesel extracted from palm oil by the addition MgO nanoparticles. *J. Homepage Http//Ijmr. Net. in*, *6(05)*, *(Query date: 2022-01-18 09:19:59)*.

Jayakar, J; Elumalai; Annamalai; Mailainathan, M; Dhinesh, B and Harikrishnan, G (2018). Macroscopic characteristics of palm oil and palm

oil methyl ester using dimensionless analysis. *J. Oil Palm Res.*, *30(4)*: 666-673.

Kanoh, T; Iwabuchi, H; Hoshida, Y; Yamada, J; Hikosaka, T; Yamazaki, A; Hatta, Y and Koide, H (2008). Analyses of electro-chemical characteristics of palm fatty acid esters as insulating oil. *IEEE Int. Conf. Dielectr. Liq*, *(1)*: 28-31.

Khaled, U and Beroual, A (2019). Statistical investigation of AC dielectric strength of natural ester oil-based Fe_3O_4, Al_2O_3, and SiO_2 nano-fluids. *IEEE Access*, *7*: 60594-60601.

Koutras, K; Pyrgioti, E; Naxakis, I; Peppas, G; Charalampakos, V and Gonos, I (2020a). A comparative study on dielectric properties of untreated and surface-modified natural ester based nanofluids. *7th IEEE Int. Conf. High Volt. Eng. Appl. ICHVE 2020 - Proc.*, 4-7.

Koutras, K; Pyrgioti, E; Naxakis, I; Charalampakos, V and Peppas, G (2020b). AC breakdown performance of $a1_2o_3$ and sic natural ester based nanofluids. *Proc. - 2020 IEEE Int. Conf. Environ. Electr. Eng. 2020 IEEE Ind. Commer. Power Syst. Eur. EEEIC/CPS Eur. 2020*, *(2)*: 1-5.

Maharana, M; Nayak, S K and Sahoo, N (2018). Karanji oil as a potential dielectrics liquid for transformer. *IEEE Trans. Dielectr. Electr. Insul.*, *25(5)*: 1871-1879.

Maharana, M; Baruah, N; Nayak, S K S K; Meher, N and Iyer, P K P K (2019). Condition assessment of aged ester-based nanofluid through physicochemical and spectroscopic measurement. *IEEE Trans. Instrum. Meas.*, *68(12)*: 4853-4863.

Makmud, M Z H; Illias, H A; Chee, C Y and Sarjadi, M S (2018). Influence of conductive and semi-conductive nanoparticles on the dielectric response of natural ester-based nanofluid insulation. *Energies*, *11(2)*.

McShane, C P; Corkran, J L; Harthun, R A; Gauger G A; Rapp, K J and Howells, E (2001). Vegetable oil based dielectric coolant. *IEEE Industry Application Magazine, 8(3)*: 34-41.

Menkiti, M C; Agu, C M; Ejikeme, P M and Onyelucheya, O E (2017). Chemically improved *Terminalia catappa* L. oil: A possible renewable substitute for conventional mineral transformer oil. *J. Environ. Chem. Eng.*, *5(1)*: 1107-1118.

Mohamad, N A; Azis, N and Jasni, J (2019). Impact of Fe_3O_4, CuO and Al_2O_3 on the AC breakdown voltage of palm oil and coconut oil in the presence of CTAB. *Energies*, *12*.

Mohd, N K; Wen-Huei, L; Abu Hassan, N A S. and Shoot-Kian, Y (2021). Potential application of palm oil products as electrical insulating medium in oil-immersed transformers. *Environ. Prog. Sustain. Energy*, *40(6)*.

Moosasait, B and Maria Siluvairaj, W I (2021). Impact of ultrasonic treatment process on pour point of vegetable oils based liquid insulation. *Ultrason. Sonochem.*, *71*: 105380.

Musa, I A (2016). The effects of alcohol to oil molar ratios and the type of alcohol on biodiesel production using transesterification process. *Egypt. J. Pet.*, *25(1)*: 21-31.

Nkouetcha, E T; Mengounou, G M and Imano, A M (2019). Elaboration and performance analysis of a bio-based insulating liquid from castor oil for power transformers. *OALib*, *06(05)*: 1-16.

Nor, S F M; Azis, N; Jasni, J; Ab Kadir, M Z A Z A; Yunus, R and Yaakub, Z (2017). Investigation on the electrical properties of palm oil and coconut oil based TiO_2 nanofluids. *IEEE Trans. Dielectr. Electr. Insul.*, *24(6)*: 3432-3442.

Oparanti, S O; Khaleed, A A; Abdelmalik, A A and Chalashkanov, N M (2020). Dielectric characterization of palm kernel oil ester-based insulating nanofluid. *2020 IEEE Conference on Electrical Insulation and Dielectric Phenomena (CEIDP)*. p. 211-214.

Oparanti, S O; Khaleed, A A and Abdelmalik, A A (2021). Nanofluid from palm kernel oil for high voltage insulation. *Mater. Chem. Phys.*, *259(July 2020)*: 123961.

Oparanti, S O; Abdelmalik, A A; Khaleed, A A; Abifarin, J K; Suleiman, M U and Oteikwu, V E (2022). Synthesis and characterization of cooling biodegradable nanofluids from non-edible oil for high voltage application. *Mater. Chem. Phys.*, *277(November 2021)*: 125485.

Pyrgioti, E C; Koutras, K N; Charalampakos, V P; Peppas, G D; Bakandritsos, A P and Naxakis, I A (2020). An experimental study on the influence of surface modification of TiO_2 nanoparticles on breakdown voltage of natural ester nanofluid. *Lect. Notes Electr. Eng.*, *599*: 279-288.

Raeisian, L; Niazmand, H; Ebrahimnia-Bajestan, E and Werle, P (2019). Feasibility study of waste

vegetable oil as an alternative cooling medium in transformers. *Appl. Therm. Eng.*, *151*: 308-317.

Raj, R A; Samikannu, R; Yahya, A and Mosalaosi, M (2021). Investigation of survival/hazard rate of natural ester treated with Al_2O_3 nanoparticle for power transformer liquid dielectric. *Energies*, *14(5)*.

Ramli, R; Ong, H R; Hong, C S; Khan, M D M R; Yunus, R M; Halim, R M; Aziz, A A; Ibrahim, Z and Islam, M R (2021). Investigation on the effect of monoglyceride concentration on palm oil-based alkyd resin preparation. *J. Oil Palm Res.*, *33(2)*: 299-306.

Ravulapalli, S; Ravindhranath, K and Ramamoorty, M (2019). Preparation, characterization and feasibility analysis of methyl ester of Sesbania seeds oil (MESSO) as alternate liquid dielectrics in distribution transformers. *RSC Adv.*, *9(6)*: 3311-3319.

Rotimi, D (2016). Effect of the temperature on dynamic viscosity, density and flow rate of some vegetable oils. *J. Sci. Res. Eng.Tech.*, *1(1)*: 14-24.

Saenkhumwong, W and Suksri, A (2017). The improved dielectric properties of natural ester oil by using ZnO and TiO_2 nanoparticles. *Eng. Appl. Sci. Res.*, *44(3)*: 148-153.

Samikannu, R; Antony Raj, R; Murugesan, S; Venkatachary, S K and Stonier, A A (2021). Assessing the dielectric performance of *Sclerocarya birrea* (Marula oil) and mineral oil for eco-friendly power transformer applications. *Alexandria Eng. J.*, *61(1)*: 355-366.

Sitorus, H B H; Setiabudy, R; Bismo, S and Beroual, A (2016). *Jatropha curcas* methyl ester oil obtaining as vegetable insulating oil. *IEEE Trans. Dielectr. Electr. Insul.*, *23(4)*: 2021-2028.

Suhaimi, N S (2018). Statistical analysis on AC breakdown voltage of CNT nanofluid with mineral oil and palm oil. *Proc. IEEE 7th Int. Conf. Power Energy*. IEEE., p. 111-116.

Suwarno; Sitinjak, F; Suhariadi, I and Imsak, L (2003). Study on the characteristics of palm oil and it's derivatives as liquid insulating materials. *Proc. IEEE Int. Conf. Prop. Appl. Dielectr. Mater.*, *2*: 495-498.

Toudja, T; Moulai, H; Nacer, A; Beldjilali, A; Khelfane, I and Debche, A (2014). Moisture and electrical discharges effect on naphthenic mineral oil properties. *IET Sci. Meas. Technol.*, *8(6)*: 588-594.

Venugopal, I P; Balasubramanian, D and Rajarajan, A (2021). Potential improvement in conventional diesel combustion mode on a common rail direct injection diesel engine with PODE/WCO blend as a high reactive fuel to achieve effective Soot-NOx trade-off. *J. Clean. Prod.*, *327(October)*: 129495.

Walvekar, R; Zairin, D A; Khalid, M; Mubarak, N M and Tcsm, G (2022). Thermo-physical properties of naphthenic-palm oil methyl ester (POME) blended transformer oil. *J. Therm. Anal. Calorim. 147*. p. 7193-7201.

Yahya, M and Amirrazli, F A (2018). Study of breakdown voltage of vegetables oil with SiO_2 nanoparticle additive. *Indones. J. Electr. Eng. Comput. Sci.*, *12(1)*: 296-302.

Yahya, M B and Maliki, N A N B (2018). Identifying the breakdown voltages of vegetable oils with silicone carbide nanoparticle additive as insulating oil for transformers. *Indones. J. Electr. Eng. Comput. Sci.*, *9(1)*: 170-176.

Yusof, S M; Hussin, N; Isa, M; Jamil, M K M and Azmi, K (2017). Study on palm oil and treated waste vegetable oil impregnated paper. *Key Eng. Mater.*, *744*: 511-515.

Journal of Oil Palm Research Vol. 35 (1) March 2023 p. 45-57
DOI: https://doi.org/10.21894/jopr.2022.0047

CHARACTERISATIONS OF BIO-ASPHALT INCORPORATING PALM BIO-OIL FROM WASTE EMPTY FRUIT BUNCHES

TRACY WONG LEH XIN[1]; MOK TAI HAN[1]; GUO TAI[1]; MOHD ROSLI MOHD HASAN[1]*; MOHD ASYRAF KASSIM[2] and MOHAMAD AZRI SUKIRAN[3]

ABSTRACT

Bio-asphalts feature economic, social, and environmental benefits and may thus be potentially substituted for petroleum-based asphalt in asphaltic concrete mixtures. This article presents the experimental investigation of adding palm bio-oil derived from empty fruit bunches (WBO) into the conventional asphalt binder at 5, 10 and 15 wt%. The physical properties of bio-asphalt were assessed via the penetration, softening point, rotational viscosity, ductility, and mass loss after the rolling thin-film oven (RTFO) tests. Fourier-transform infrared spectroscopy (FTIR) and gas chromatography-mass spectrometry (GC-MS) tests were used to identify the chemical composition and functional groups of the bio-oil and bio-asphalt samples. The binder coatability was assessed by static water immersion and water boiling tests. The addition of bio-oil lowers the softening point and viscosity of the binder while increasing its penetration, ductility and mass loss after RTFO. The main absorption peaks for WBO bio-oil and WBO bio-asphalts were corresponding to C=H stretching of alkanes and aliphatic compounds, respectively. The bio-oil was mostly composed of aromatic and oxygenated compounds, as observed from GC-MS results, which justified the FTIR analysis for WBO bio-oil. The addition of WBO bio-oil improved the bonding characteristics of asphalt-aggregates, indicating that it has a significant potential for use in the production of bio-asphalt.

Keywords: bio-oil, chemical composition, empty fruit bunches, physical properties, renewable resources.

Received: 5 February 2022; **Accepted:** 20 June 2022; **Published online:** 10 August 2022.

INTRODUCTION

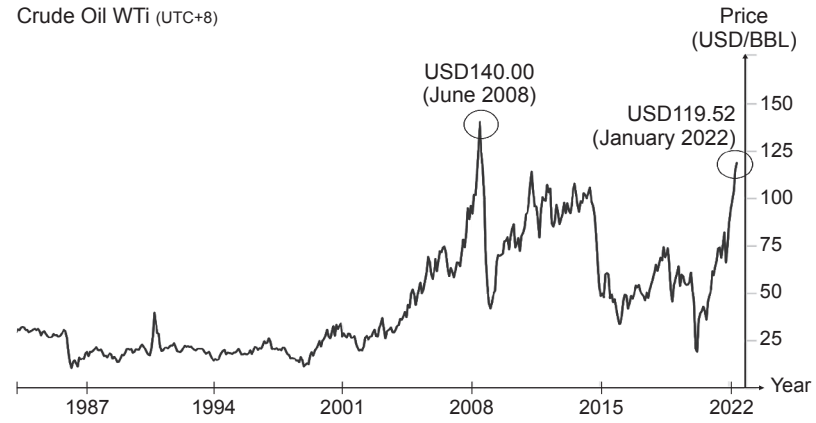
Crude oil is the largest energy resource in the world, including asphalt binder as the main ingredient in road paving material. Several challenges have emerged, such as increasing crude oil consumption, the uncertainty in crude oil prices, and its nature as a non-renewable resource (Lin and Bai, 2021; Maghyereh and Sweidan, 2020; Mensi *et al.*, 2020; Razek and Michieka, 2019). Malaysia is one of the oil producers, Petroliam Nasional Berhad, known as Petronas, produces and handles crude oil production. For the last 25 years, the price of crude oil has been unpredictably fluctuating as shown in *Figure 1*. In particular, the crude oil price was constantly increasing until it reached a peak of USD140.00 per barrel in 2008. The price thereafter began to fluctuate, reaching the second high of USD119.52 per barrel in January 2022 (Trading Economics, 2022). *Figure 2* also indicates that oil consumption has been increasing since 2006, with global demand estimated to reach 104.1 million barrels per day in 2026 (Statista, 2019). To address these challenging problems, industries and researchers have conducted extensive work in search for "green technology" to replace or substitute conventional binders. As a result, there is pressing demand for alternatives to conventional asphalt binders. The utilisation of biomass resources for bio-asphalt production as either a partial or complete substitute for asphalt binder derived from crude oil has been used as an alternate method for producing road paving materials. The substitution may reduce the dependency on the crude oil-based

[1] School of Civil Engineering, Universiti Sains Malaysia (Engineering Campus), 14300 Nibong Tebal, Pulau Pinang, Malaysia.

[2] School of Industrial Technology, Universiti Sains Malaysia, 11850 Minden, Pulau Pinang, Malaysia.

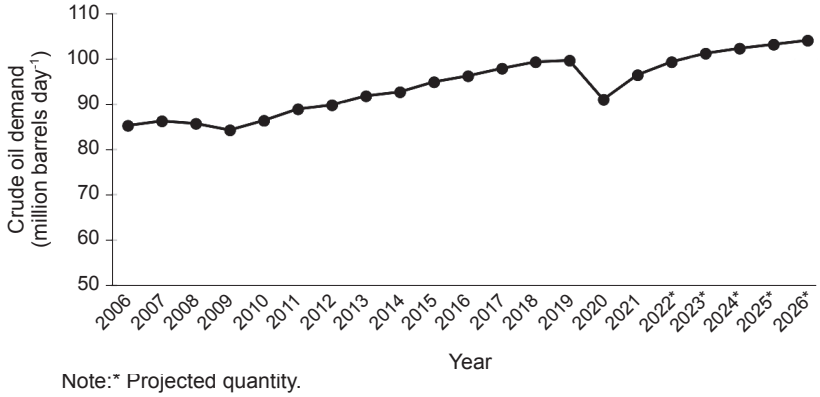
[3] Malaysia Palm Oil Board, 6 Persiaran Institusi, Bandar Baru Bangi, 43000 Kajang, Selangor, Malaysia.

* *Corresponding author e-mail: cerosli@usm.my*



Source: Trading Economics (2022).

Figure 1. The trend of crude oil price for the last 25 years.



Note:* Projected quantity.
Source: Statista (2019).

Figure 2. Global demand for crude oil.

asphalt binder (Sun *et al.*, 2016; Wen *et al.*, 2013; Yang *et al.*, 2013).

Biomass sources have come to the minds of researchers due to their accessibility and environmental friendliness (Wang *et al.*, 2020a). Biomass material is a viable alternative since it may be converted into bio-oil by pyrolysis or hydrothermal liquefaction. It is renewable, eco-friendly and has rheological properties comparable to conventional asphalt. Bio-oil may be derived from a wide range of biomass sources throughout the globe, including algae (Abdul Latif *et al.*, 2019), switchgrass (Yue *et al.*, 2017), corn stover (Yang *et al.*, 2017), swine manure (Fini *et al.*, 2011; Mills-Beale *et al.*, 2014; Wang *et al.*, 2020b), waste wood resources (Gürer *et al.*, 2020; Ingrassia *et al.*, 2020; Yang *et al.*, 2013; 2014) and waste cooking oil (Sun *et al.*, 2016; Wen *et al.*, 2013; Zahoor *et al.*, 2021). Particularly in Malaysia, the extraction of palm oil results in a substantial amount of biomass waste, including mesocarp fruit fibres (MF), palm kernel shells (PKS), palm oil mill effluent (POME), and empty fruit bunches (EFB). These palm oil wastes might serve as biomass feedstock for bio-oil production, especially the EFB (Abdullah *et al.*, 2011; 2017; Chang, 2018; Pogaku *et al.*, 2016; Rosli *et al.*, 2017; Yiin *et al.*, 2016).

Over the years, it has been established that much research has been undertaken in quest of an asphalt binder alternative. However, there is still limited research on EFB-based bio-asphalt. As oil palm plantations in Malaysia have generated a significant amount of biomass waste, it is suggested that EFB might be utilised to produce bio-oil in advance of bio-asphalt. Therefore, in this experimental study, bio-oil produced from EFB (designated as WBO bio-oil) was used to partially replace the asphalt binder at 5, 10 and 15 wt%. This research assessed the physical properties, chemical characteristics, and coatability of bio-asphalts.

MATERIALS AND METHODS

Materials

The Malaysian Palm Oil Board (MPOB), Bangi, Selangor, Malaysia, provided the WBO bio-oil used in this investigation, which was used in the experiment as received. It was derived from the

pyrolysis of EFB at 500°C for a residence time of 30 min. The elemental analysis revealed that carbon was the most prevalent element in the chemical composition of the bio-oil. The chemical formula of bio-oil can be written as $CH_{1.92}O_{0.61}N_{0.03}$, and its characteristics are shown in *Table 1*. In asphalt mixtures, the use of EFB will enhance waste recycling and sustainable material consumption. This will aid in reducing the depletion of non-renewable resources as well as the usage of substantial amounts of energy and greenhouse gas emissions. The higher heating value (HHV) or calorific value of bio-oil is 40% to 50% lower than that of petroleum fuel, indicating that bio-oil releases less energy in its compounded state, making it more stable or less energetic. Besides, conventional 60/70 penetration grade (60/70 PEN) binder and crushed granite aggregates with properties conforming to Malaysian Public Works Department (PWD) or Jabatan Kerja Raya (JKR) standard specifications (JKR, 2008) were adopted in this study. *Table 2* displays the physical parameters of the standard binder.

Preparation of Asphalt Binder Samples

The 60/70 PEN asphalt binder was used as the base binder. The WBO was added to the base binder and mixed using a propeller mixer at 145°C and 1000 revolutions per minute (rpm) for 30 min to prepare bio-asphalt. The pre-heated asphalt binders were blended with WBO bio-oil at 5, 10 and 15 wt%. These products were designated as 5%, 10% and 15% WBO bio-asphalts, and their characteristics and performance were evaluated.

TABLE 1. CHARACTERISTICS OF WBO BIO-OIL DERIVED FROM EFB

Properties		Units	WBO bio-oil
Elemental analysis	C	wt%	49.80
	H		7.98
	N		1.93
	O		40.29
H/C molar ratio			1.92
O/C molar ratio			0.61
Water		wt%	18.74
Calorific value		MJ kg^{-1}	21.41
Molecular formula			$CH_{1.92}O_{0.61}N_{0.03}$

Preparation of Loose Asphalt Mixture Samples

Granite was used as the aggregate in the loose asphalt mixture prepared for the static water immersion and water boiling tests. The asphalt mixture preparation technique followed the standard of AASHTO PP2 (AASHTO, 2001). The asphalt mixture was prepared by mixing the base binder or bio-asphalt with the designated aggregate sizes. The asphalt binder was pre-heated at 160°C for 2 hr before mixing. Meanwhile, aggregates were pre-heated for at least 4 hr at the same temperature. During the mixing process, a designated percentage of binder was added to the aggregate and mixed for approximately 1 min to obtain a well-coated, loose mixture. After mixing, the mixture was placed on a metal tray and conditioned for 2 hr at 150°C in the oven to facilitate the binder absorption of aggregates.

Physicochemical Analysis

Fourier Transform Infrared Spectroscopy (FTIR). FTIR-Attenuated Total Reflectance (ATR) test was conducted using a Bruker Tensor 27 (Shimadzu, model IR Prestige-21). The test was conducted to identify the functional groups present in samples of WBO bio-oil and bio-asphalt. Generally, the FTIR test produced a spectrum with peaks illustrating transmittance against wavenumber. A prominent peak observed at a specific wave number indicated the existence of the specified functional group in the samples that were tested. For this analysis, approximately 0.1 to 0.4 mL of sample was placed over the surface of a diamond, and the analysis was performed approximately three times with 4 cm^{-1} resolutions with a range of 4000 to 600 cm^{-1}. The FTIR graph illustrates transmittance *vs.* wavenumber. The *x*-axis represents wave number ranging from 500 – 4000 cm^{-1}, with >1500 cm^{-1} representing the functional group region and <1500 cm^{-1} representing the fingerprint region. The peak may be classified as strong, moderate, and weak (Hareru and Ghebrab, 2020). In addition, the *y*-axis displays transmittance ranging from 0%-100%. This test is performed according to ASTM D7414 (ASTM, 2009b).

Gas Chromatography-Mass Spectrometry (GC-MS). GC-MS was performed according to ASTM D8276 (ASTM, 2019a) to determine the nature and type of

TABLE 2. PHYSICAL PROPERTIES OF THE CONVENTIONAL BINDER

Properties	Units	Specification range	Results	References
Penetration (at 25°C, 100 g, 10 s)	0.1 mm	60-70	64	ASTM (2013)
Softening point	°C	48-56	49.5	ASTM (2014)
Ductility (at 25°C)	cm	>100	>100	ASTM (2017)
Density	g cm^{-3}	1.01 to 1.06	1.03	ASTM (2009a)

organic compounds in WBO bio-oil and bio-asphalts. This analysis was conducted using Shimadzu GC2010 Plus equipped with a quadrupole detector (GCMS-QP2010) and a BPX5 capillary column (20 m film thickness x 0.25 mm). The temperature of the column oven was maintained at 50°C before being raised by 2°C min^{-1} to 180°C withhold 3 min, then to 280°C at the same rate withhold 5 min, and finally to 300°C by 2°C min^{-1} withhold 7 min. The injector temperature was kept at 290°C. At a constant flow rate of 1 mL min^{-1}, helium was employed as the carrier gas. At the same time, the potential chemical components in WBO bio-oil and bio-asphalts were studied using the Mass Spectrometry (MS) search libraries.

Binder's Physical Test

Penetration test. A penetration test measures consistency by determining the binder's grade via the penetration value. This test was conducted using a penetrometer with the standard loaded needle penetrating vertically in 5 s while the temperature of the asphalt binder sample was maintained at 25°C in accordance with ASTM D5 (ASTM, 2013).

Softening point test. Based on ASTM D36 (ASTM, 2014), the softening point (SP) of asphalt binders was determined through the ring and ball test. Asphalt binder is a viscoelastic material that becomes softer and less viscous as the temperature rises.

Penetration index. The penetration index (PI) is used to measure the temperature susceptibility of a binder based on the linear relationship between log penetration and temperature. Pfeiffer and Van Doormal (1940) have developed an equation to establish the relationship between the asphalt binder consistency and the temperature sensitivity at the temperature of 25°C based on the penetration value and softening point. The equation is shown as Equation (1). All asphalt binder samples exhibit thermoplastic properties, becoming softer when heated and hardening when cooled.

$$PI = \frac{1952 - 500 logPen - 20 Softening\ Point}{50 logPen - Softening\ Point - 120} \quad (1)$$

Rotational viscosity (RV) test. RV test was conducted to determine the viscosity of asphalt binders at high temperatures. The rotational viscometer measured the torque required to maintain the rotating speed of the spindle in the asphalt binder at a constant rate. In this test, four different temperatures (120°C, 140°C, 160°C and 180°C) were used to test the control and bio-asphalt binders. A #27 spindle was used, and a constant rotating speed of 20 rpm was set. The standard procedures were in accordance with ASTM D4402 (ASTM, 2015).

Ductility test. Based on ASTM D113 (ASTM, 2017), the ductility test measures the asphalt binder's ability to stretch. It is measured by the distance, in centimetres, to which a sample will elongate before breaking at a specific temperature and speed. The pulling rate of the ductilometer was maintained at 50 mm min^{-1}, while the water bath temperature was kept around 25°C. Insufficient ductility in the binder will lead to lower resistance to fatigue cracking under repeated traffic loads.

RTFO mass change. Based on ASTM D2872 (ASTM, 2019b), a rolling-thin film oven (RTFO) is conducted to mimic the short-term aging of the asphalt binder. The RTFO test studies the effect of heat and air on a moving film of asphalt binder under rotation. Asphalt binder experiences short-term aging during transportation, mixing, storage, and handling processes. The RTFO provides a quantitative measure of the volatile loss (mass change) during the aging process. The mass change of the asphalt binder can be determined by using Equation (2).

$$Mass\ change = \frac{m_2 - m_1}{m_1 - m_b} \quad (2)$$

where m_1 is the mass of the RTFO bottle with the asphalt sample before aging, and m_2 is the mass of the RTFO bottle with the sample after aging. Then, m_b is the mass of an empty RTFO bottle.

Binder Coatability Tests

Static water immersion test. The static water immersion test was conducted to determine the percentage of asphalt binder that remained coated on aggregate after being immersed in water. Each sample was represented by 100.0 g of oven-dry aggregates, prepared and mixed with 5.5 g of asphalt binder. The loose asphalt-coated aggregates were conditioned for 2 hr in an oven. After conditioning, the sample was transferred to a glass container and immersed in water at 25°C for 16–18 hr. Water infiltration between the thin asphalt binder film and aggregates may occur due to weak adhesion between the asphalt binder and aggregates. It caused the asphalt binder films to strip from the aggregates. A visual evaluation of the asphalt binder's coatability is conducted by observing the remaining covered area. The test was conducted in accordance with AASHTO T182 (AASHTO, 1993).

Water boiling test. Based on ASTM D3625 (ASTM, 2020), a standard protocol was performed to evaluate

the adhesion loss in a loose mix of aggregate coated with asphalt binder due to the boiling water effect. The sample containing 250 g of the uncompacted aggregate-binder mixture was prepared and boiled for about 10 min in a beaker filled with water. Before placing the mixture into the boiling water, the temperature of the mixture was checked to ensure that it was below the boiling point of the water but over 85°C. After 10 min of the boiling process, the excessive asphalt binder floating on the water surface was skimmed off to avoid recoating. The sample was then transferred onto a piece of the white paper sheet and cooled at room temperature. The level of stripping of the sample after cooling was determined using eye inspection.

RESULTS AND DISCUSSION

Physicochemical Analysis

FTIR analysis. *Figure 3* shows the FTIR spectra for WBO bio-oil, control asphalt binder, and bio-asphalts prepared with 5, 10 and 15 wt% WBO incorporation. From the spectra data, the functional groups of WBO bio-oil were mainly phenols, alcohols, ketones, aldehydes, and carboxylic acids (Sukiran *et al.*, 2009). The existence of O-H stretching vibrations at 3400 cm^{-1} implied the presence of alcohols, phenol, polymeric O-H and water. The absorbance peaks between 1812 cm^{-1} and 1650 cm^{-1} represented the C=O stretching vibrations and indicated the presence of ketones, aldehydes, carboxylic acids and their derivatives. Carbonyl components such as phenol and ester were detected by C-O stretching vibrations at 1263 cm^{-1}. The presence of C-H plane bending within 900 cm^{-1} to 700 cm^{-1} indicated the presence of aromatic compounds, which was further verified by C=C stretching vibrations at 1602 cm^{-1}. Additionally, the FTIR spectra analysis results in *Table 3* are consistent with the previous research using the same bio-oil (Sukiran *et al.*, 2009; Sutrisno and Hidayat, 2018). The FTIR study showed that the bio-oil composition was found to include highly oxygenated species, which were contributed by the pyrolysis of cellulose and lignin (Sukiran *et al.*, 2009). However, the FTIR spectra of WBO bio-oil and WBO bio-asphalt were distinct. The main absorption peaks for WBO bio-oil and WBO bio-asphalts were located at 3040 to 2800 cm^{-1} and 1480 to 1300 cm^{-1}, respectively, which correspond to the C=H stretching of alkanes and aliphatic compounds.

The spectra peak of the control binder (CS) was comparable to the WBO bio-asphalt with 5, 10 and 15 wt% WBO. Similar results were obtained with control asphalt, poppy capsule pulp bio-asphalt, and molasses bio-asphalt (Gürer *et al.*, 2020; Hareru and Ghebrab, 2020) due to the low bio-oil incorporation in the asphalt binder. Furthermore, the similar spectra indicated no substantial differences across functional groups, even when the dehydration occurred after bio-oil mixing with the control binder (Hareru and Ghebrab, 2020). After combining the conventional asphalt binder with WBO bio-oil in the current study, the absorbance for the wavenumber ranges of 900 cm^{-1} to 700 cm^{-1} and 1260 cm^{-1} was lowered in all bio-asphalt samples.

GC-MS analysis. The chemical compounds in the asphalt binder, WBO bio-oil and WBO bio-asphalts are listed in *Table 4*. Phenol was the most abundant chemical in the bio-oil, with a percentage area of 20.69%. The majority of the chemicals discovered in bio-oil were determined to be lightweight chemicals. The other chemicals, such as phenol, 2,6-dimethoxy-(CAS)2,6-dimethyl and 1,2-benzenediol, were also detected in the bio-oil with percentage areas of 9.11% and 4.67%, respectively. The bio-oil was mostly

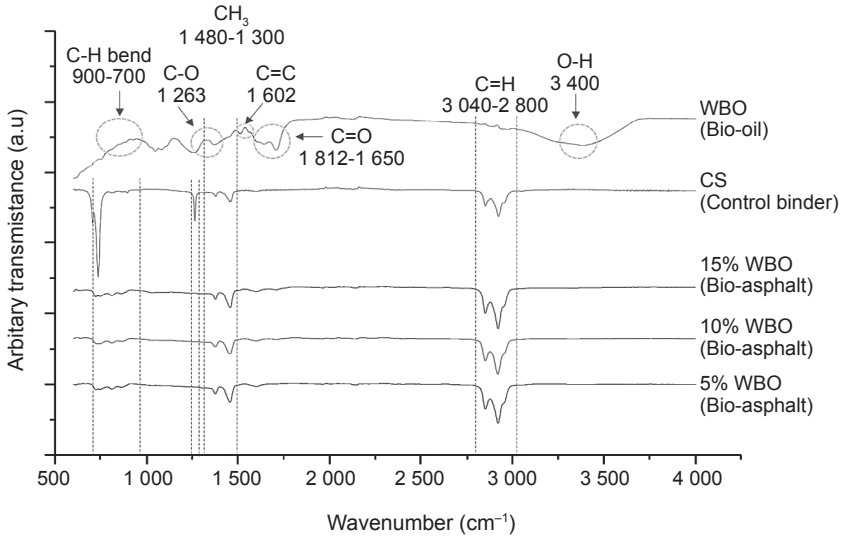


Figure 3. FTIR spectra analysis for bio-oil, asphalt and WBO.

TABLE 3. FTIR FUNCTIONAL GROUPS IDENTIFIED IN TESTED SAMPLES

Wavenumber (cm^{-1})	Functional group	Class of compounds
3 400	O-H stretching	Polymeric O-H, Water
3 040-2 800	C-H stretching	Alkanes
1 812-1 650	C=O stretching	Ketones, Aldehydes, Carboxylic acids
1 602	C=C ring stretch	Aromatic compounds
1 519	-NO_2 stretching	Nitrogenous compounds (usually do not appear in bio-oil spectra)
1 482-1 379	CH_3	Aliphatic compounds
1 263	C-O stretching	Phenol, Ester
1 100-997	S=O stretching	Sulfoxide compounds (usually do not appear in bio-oil spectra)
900-700	C-H plane bending	Aromatic compounds

composed of aromatic and oxygenated compounds, according to the GC-MS data, which supported the FTIR study of WBO bio-oil.

Furthermore, the dominant compounds found in WBO bio-asphalts were dodecenoic acid, 1,2,3-propanetriyl ester, which consisted of 46.87% of the total sample. The other major compounds were Nonadecane (CAS) n-Nonadecane, myristic acid vinyl ester and fumaric acid, 3,3-dimethylbut-2-yl hexyl ester. Based on this analysis, the material characteristics and quality index of the bio-asphalt are dependent on the presence of different chemical compositions. Bio-asphalts that contain high levels of lightweight chemicals increase evaporation rate and mass loss. The lightweight chemical components in the 15% WBO bio-asphalt interact significantly with the stationary phase in the capillary column, leading to a longer retention duration. The substantial mass loss seen with 15% WBO bio-asphalt was proven and validated by the chemical profile from this research, which revealed a large number of lightweight elements.

Binder's Physical Properties

Penetration test results. *Figure 4 shows* the penetration and softening point test results of the asphalt binders. As seen in *Figure 4*, the penetration value for the CS, 5% WBO bio-asphalt, 10% WBO bio-asphalt, and 15% WBO bio-asphalt was recorded as 64, 74, 82 and 90 dmm, respectively. The penetration values of bio-asphalt increased as the WBO content increased, thus indicating that WBO had the potential to reduce the stiffness of the binder.

Softening point test results. As shown in *Figure 4*, the higher bio-oil content has significantly reduced the softening point of the asphalt binder. Raman *et al.* (2015) also recorded a lower softening point after adding WBO as a partially replaced ingredient in a base binder. From the results, 15% WBO bio-asphalt had the lowest softening point (44.3°C), while the control binder had the greatest softening point (49.5°C). An appropriate dosage of WBO bio-oil during the production of bio-asphalt is essential in ensuring the asphalt binder achieves an appropriate characteristic.

The penetration index ranges from -2 for a high-temperature susceptible binder to roughly +2 for a highly blown low-temperature susceptible binder. A binder with a penetration index within the range of -2 to +2 is suitable for use as a conventional paving asphalt binder (Read and Whiteoak, 2003). Theoretically, a lower softening point signifies a low viscosity asphalt binder, resulting in a higher penetration index, which is typically utilised in cold climates. Meanwhile, a binder with a lower penetration index is preferred in countries with warm climates due to its higher stiffness. According to the penetration index analysis findings in *Table 5*, WBO bio-asphalt has the potential to be used as a conventional paving asphalt binder in road construction. However, it would be premature to establish an optimal ratio for road construction at this stage. More research is needed to determine the long-term performance and durability of bio-asphalt mixtures in extreme conditions.

Rotational viscosity test results. *Figure 5* illustrates that the viscosity of the bio-asphalts altered drastically independent of the WBO bio-oil dosages throughout the range of testing temperature. The addition of WBO bio-oil lowered the viscosity of the binder, implying that the bio-asphalt had higher workability than the CS due to its lower viscosity, which would consume less energy during the mixing process and throughout the pavement construction stage. The rotational viscosity value of all the samples was lower than 3 Pa·S at 135°C, which is the maximum permissible rotational viscosity value according to the Superpave standard to avoid excessively high mixing and compaction temperatures (AASHTO, 2016; ASTM, 2018). The laboratory mixing and compaction temperatures of the asphalt binders were determined based on the ideal viscosity ranges of 0.17 ± 0.02 Pa·S (mixing temperature range) and 0.28 ± 0.03 Pa·S, respectively (Asphalt Institute, 1989). *Table 6* shows the optimum mixing and compaction temperatures for all asphalt binders. Theoretically,

TABLE 4. CHEMICAL COMPOUND DISTRIBUTION IN WBO BIO-OIL, CONTROL BINDER AND WBO BIO-ASPHALTS

Compounds	CS	WBO bio-oil	Bio-asphalt		
			5% WBO	10% WBO	15% WBO
1-Hydroxy-2-butanone		√			
2-Cyclopenten-1-one		√	√		
Urea, N-[5-(ethylsulfonyl)-1,3,4-thiadiazol-2-yl		√	√		
1,2-Ethanediol, diacetate (CAS) Ethylene diacetate		√	√		
2(5H)-Furanone		√	√		
Phenol (CAS) Izal		√			
4H-Pyran-4-one		√	√		
2,3-Dimethyl-2-cyclopenten-1-one		√	√		
Cresol <ortho->		√			
Phenol, 4-methyl- (CAS) p-Cresol		√			
Phenol, 2-methoxy-		√			
Cyclohexane-1,2-dione <3-methyl->		√	√		
2-Cyclopenten-1-one, 3-ethyl-2-hydroxy-		√			
Xylenol <2,5->		√	√		
Creosol		√			
Benzoic acid (CAS) Retardex		√	√		
Phenol, 2-methoxy-4-methyl-		√			
1,2-Benzenediol		√	√		
1,4:3,6-Dianhydro-.alpha.-d-glucopyranose		√	√		
1,2-Benzenediol, 3-methoxy-		√	√		
Ethanone, 1-(2,5-dihydroxyphenyl)-		√	√		
1,2-Benzenediol, 4-methyl-		√			
Syringol <4-methyl->		√			
Ethanone, 1-(4-hydroxy-3-methoxyphenyl)- (CAS) Acetovanillone		√	√		
Fumaric acid, cyclopentylmethyl isohexyl ester	√		√	√	
Heptadecane, 8-methyl-	√		√	√	
Dodecanoic acid, ethenyl ester	√		√	√	
Fumaric acid, hexyl 2-methyl allyl ester	√		√	√	
V Dodecanoic acid, 1-(hydroxymethyl)-1,2-ethanediyl ester	√			√	
Dodecanoic acid, ethenyl ester	√			√	
Butane, 1,1'-oxybis[4-iodo]-	√				
Dodecanoic acid, 1,2,3-propanetriyl ester	√		√	√	√
Fumaric acid, 2-ethylhexyl isohexyl ester	√		√	√	
Dodecanoic acid, ethenyl ester (CAS) Vinyl dodecanoate	√				√
Dodecanoic acid, 1,2,3-propanetriyl ester	√				
Dodecanoic acid, ethenyl ester	√				√
Fumaric acid, 2-butyl hexyl ester	√				√
Dodecanoic acid, 1,2,3-propanetriyl ester	√				√
Dodecanoic acid, 1,2,3-propanetriyl ester	√		√	√	
Dichloroacetic acid, undecyl ester					√
Octadecanoic acid					√
Hexadecane					√
Oxalic acid			√	√	√
Eicosanoic acid					√
Aziridine					√
4-Pentylcyclohexanone			√		√
Azacyclohexane			√		√
4-Nitrophenyl laurate	√			√	
Myristic acid vinyl ester	√			√	
Glyceryl tridodecanoate				√	
Glyceryl tri-2,2-dideuterio dodecanoate				√	√
Oxalic acid, octadecyl propyl ester				√	√

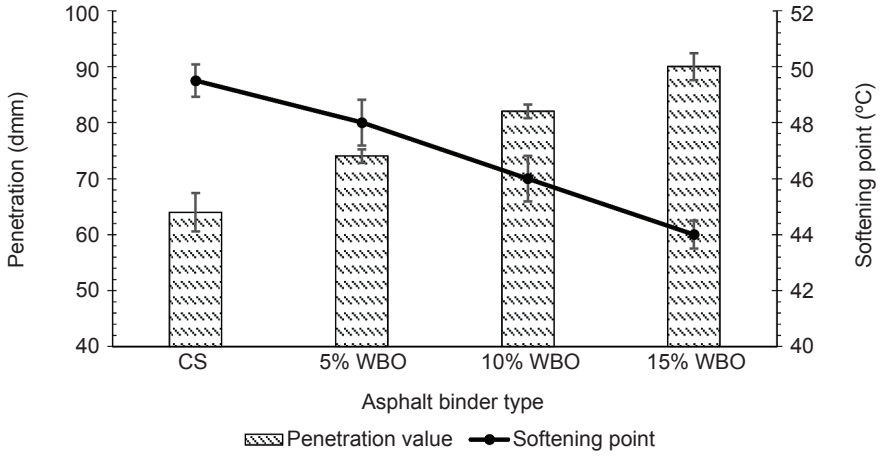


Figure 4. Penetration and softening point test results of asphalt binders.

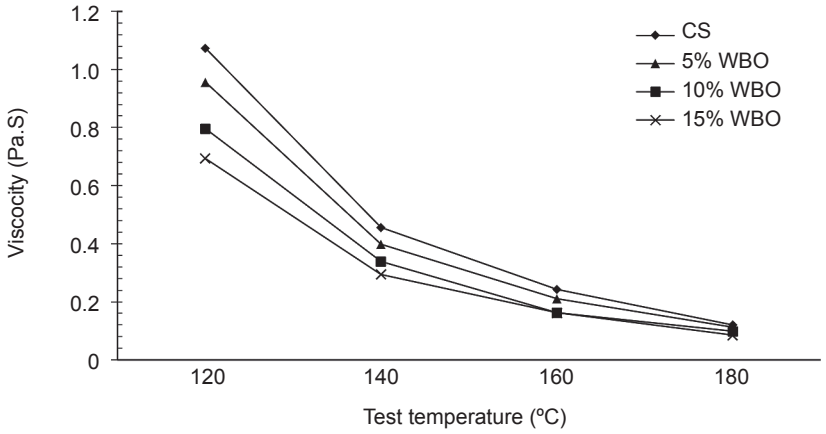


Figure 5. Rotational viscosity test results.

TABLE 5. THE PENETRATION INDICES OF THE CONTROL AND BIO-ASPHALT BINDERS

Designation	Binder type	Penetration index	Best possible use
CS	PEN 60/70	-0.7439	Conventional paving asphalt binder
5% WBO		-0.7699	Conventional paving asphalt binder
10% WBO	Bio-asphalt	-1.0680	Conventional paving asphalt binder
15% WBO		-1.3348	Conventional paving asphalt binder

Note: % is referring to wt%.

TABLE 6. RANGE OF MIXING AND COMPACTION TEMPERATURES FOR EACH SAMPLE

Binder	Temperature (°C)	
	Mixing	Compaction
CS	169-175	153-159
5% WBO	164-172	149-156
10% WBO	157-164	143-150
15% WBO	156-163	139-147

the WBO bio-asphalt has higher workability than the conventional binder, resulting in decreased energy consumption during the mixing and compaction process of the asphalt mixture.

Ductility test results. *Figure 6a* illustrates the ductility test results of the asphalt binders. In comparison to the CS, the use of WBO in partially replacing the asphalt binder significantly improved its ductility regardless of the amount of bio-oil added. The bio-oil significantly lowered the viscosity of the asphalt binder. The CS and bio-asphalts presented adequate ductility by meeting the JKR standard specification. This is essential to reduce the fatigue cracking potential typically induced by the continuous, repetitive traffic loadings.

Mass loss after RTFO. *Figure 6b* presents the mass loss for the control and bio-asphalt samples. From

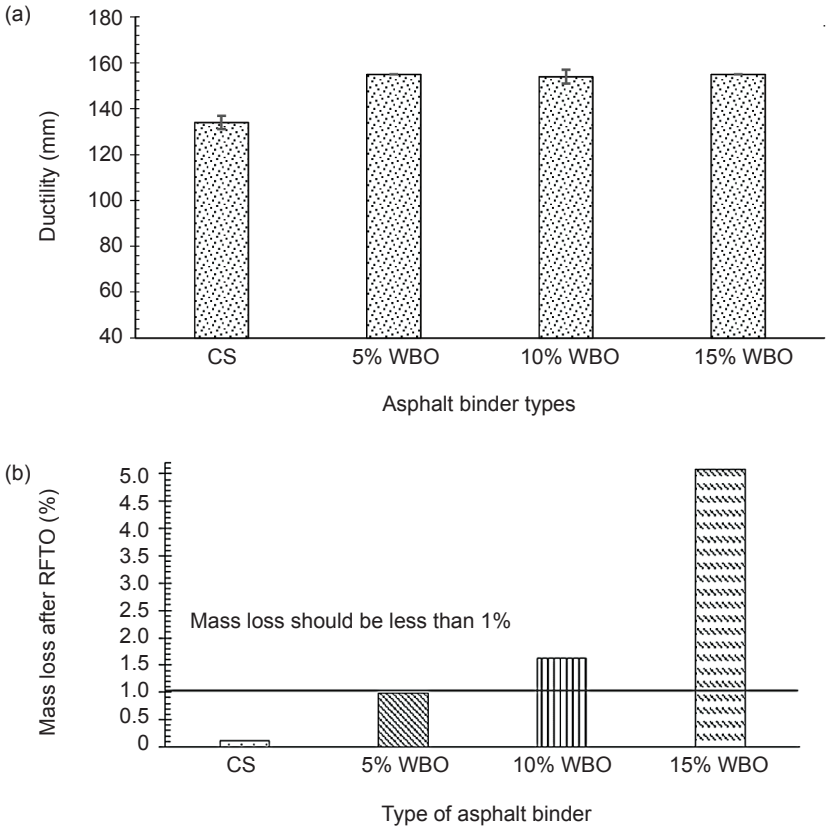


Figure 6. (a) Ductility values for the control and bio-asphalts, (b) RTFO mass loss test results.

the results, the mass loss of CS and 5% WBO bio-asphalt binders conforms to the Superpave requirement of less than 1.00%. In contrast, the 10% WBO and 15% WBO bio-asphalts had surpassed the requirement with mass losses of 1.62% and 5.09%, respectively. The higher the integration of WBO bio-oil, the greater the mass loss of bio-asphalts. The high mass loss is caused by its high water content of 18.74% and the presence of volatile elements, as reported by Sukiran *et al.* (2009). It is suggested that pre-treatment or pre-heating is required to eliminate the excess water content in WBO bio-oil. As a result, the 10% WBO bio-asphalt and 15% WBO bio-asphalt are less recommended for road construction without any pre-requisite treatment owing to their substantial mass loss that exceeds the standard specification.

Binder Coatability Index in Asphalt Mixtures

Static water immersion test. *Table 7* displays the coatability index or the percentage of the coated region that remained after 16 hr in water at 25°C. From observation (*Figure 7)*, all the asphalt binders demonstrated high retained coated aggregate areas of more than 95% after the static water immersion test. This indicated that the WBO bio-asphalts exhibited equivalent adhesion strength to the CS under the static effect of moisture. All binder samples displayed good coatability and low stripping potential.

Water boiling test. *Table 7* summarises the results of the water boiling tests for control and bio-asphalt binders. From visual observation (*Figure 8*), the addition of WBO bio-oil enhanced the coatability of the loose asphalt mixture when compared to CS. Furthermore, the higher bio-oil incorporation increased the aggregate areas that remained coated. Therefore, it is implied that WBO bio-asphalts help to strengthen the bonding between asphalt binder film and aggregates.

CONCLUSION

WBO bio-asphalt is being researched as an alternative resource to replace the conventional asphalt binder, as well as to solve the problem of empty fruit bunch disposal. The physical and chemical parameters of 5, 10 and 15 wt% WBO integrated bio-asphalt were established by laboratory testing and data analysis. WBO bio-oil decreases the softening point and viscosity of the binder while increasing the penetration and mass loss after RTFO when compared to the control binder. The ductility of the WBO bio-asphalt rises regardless of the quantity of WBO bio-oil supplied. According to the mass

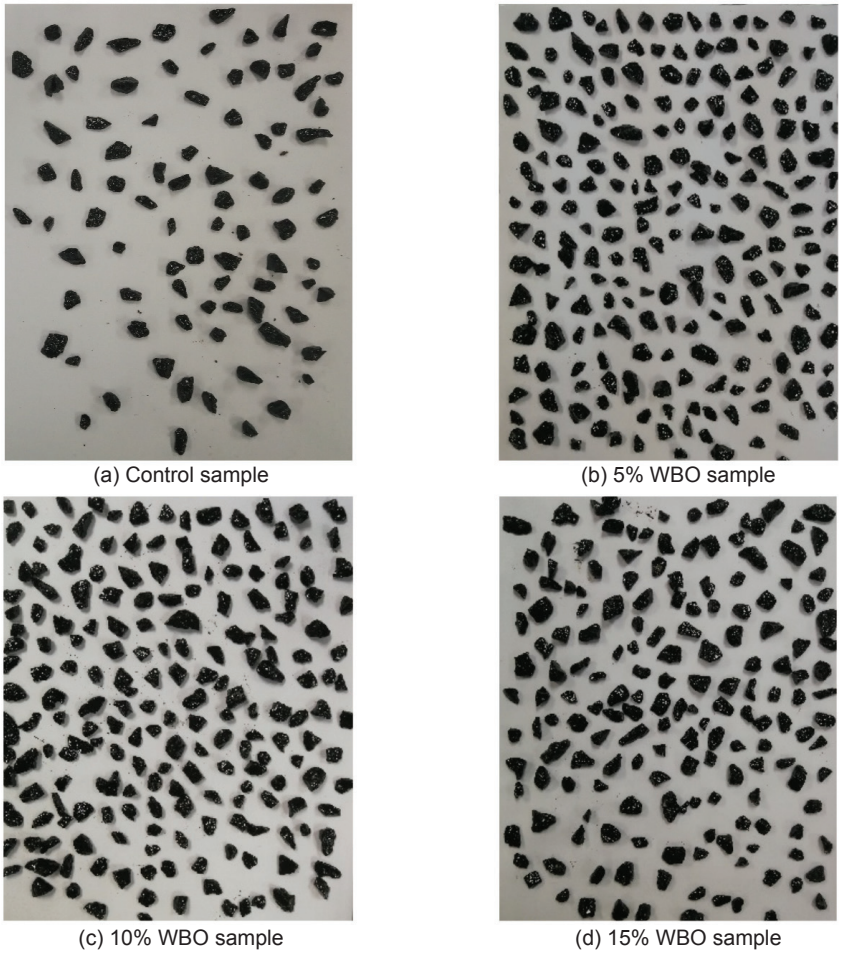


Figure 7. Observation of the aggregate coating in static water immersion test.

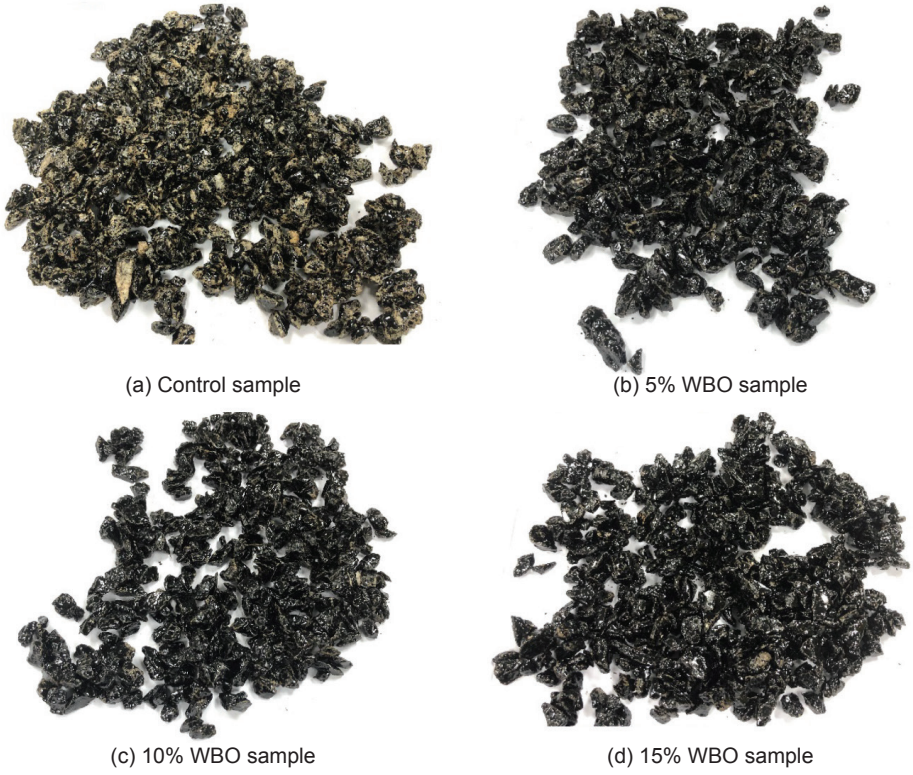


Figure 8. Binder coatability of loose mixes in water boiling test.

TABLE 7. BINDER COATABILITY IN ASPHALT MIXTURES: STATIC WATER IMMERSION TEST AND WATER BOILING TEST

Sample	Static water immersion test	Water boiling test
	Coatability index (%)	
CS	>95	47.5
5% WBO	>95	82.5
10% WBO	>95	90.0
15% WBO	>95	95.0

loss results, only the 5% WBO bio-asphalt achieved a mass loss of less than 1%, as required by the Superpave standard. The substantial mass loss is attributed to the material's high water content and the presence of volatile elements, according to physicochemical analyses. As a consequence, a pre-treatment of the WBO bio-oil to remove excess water should be considered. However, it would be premature to recommend an optimal proportion of bio-oil to be used in the production of bio-asphalt at this moment. More research should be done to assess the long-term performance of bio-asphalt in severe conditions. Besides, WBO bio-oil also contains phenol, alcohols, ketones, aldehydes, aromatic compounds, and carboxylic acids. The GC-MS analysis results showed that phenol and dodecenoic acid, 1,2,3-propanetriyl ester, are dominant in WBO bio-oil and bio-asphalt, respectively. In static water immersion and water boiling tests, all WBO bio-asphalts displayed increased coatability and strengthened adhesion strength between the asphalt binder film and aggregates. As a result, WBO bio-asphalt has a significant potential for application in the development of bio-asphalts as a partially substituted material.

ACKNOWLEDGEMENT

The authors sincerely acknowledge Universiti Sains Malaysia for offering financial support via Research University Individual (RUI) Grant 1001. PAWAM.8014140 to conduct this research work. Special thanks to the Malaysian Palm Oil Board (MPOB) for providing EFB bio-oil. The authors also express their appreciation to the technicians of the Highway Engineering Laboratory at Universiti Sains Malaysia for their continuous assistance.

REFERENCES

AASHTO (1993). AASHTO T 182: Standard Method of Test for Coating and Stripping of Bitumen-Aggregate Mixtures.

AASHTO (2001). AASHTO PP2: Standard Practice for Mixture Conditioning of Hot Mix Asphalt (HMA).

AASHTO (2016). AASHTO M320: Standard specification for performance-graded asphalt binder. Washington, DC.

Abdul Latif, N I S; Ong, M Y and Nomanbhay, S (2019). Hydrothermal liquefaction of Malaysia's algal biomass for high-quality bio-oil production. *Eng. Life Sci., 19(4)*: 246-269. DOI: 10.1002/elsc.201800144.

Abdullah, N; Safana, A A; Sulaiman, F and Abdullahi, I I (2017). A comparative analysis of physical and chemical properties of biochars and bio-oils obtained from pyrolytic process of mesocarp fibre and empty fruit bunch. *Solid State Phenom., 268*: 387-392. DOI: 10.4028/www.scientific.net/SSP.268.387.

Abdullah, N; Sulaiman, F and Gerhauser, H (2011). Characterisation of oil palm empty fruit bunches for fuel application. *J. Phys. Sci., 22(1)*: 1-24.

Asphalt Institute (1989). The Asphalt Handbook, Manual Series No. 4.

ASTM (2009a). ASTM D70 - 09. Standard Test Method for Density of Semi-Solid Bituminous Materials (Pycnometer).

ASTM (2009b). ASTM D7414 - 09. Standard test method for condition monitoring of oxidation in ın-service petroleum and hydrocarbon based lubricants by trend analysis using Fourier transform ınfrared (FT-IR) Spectrometry. ASTM International, West Conshohocken, PA.

ASTM (2013). ASTM D5 / D5M - 13: Standard Test Method for Penetration of Bituminous Materials.

ASTM (2014). ASTM D36 / D36M - 14: Standard Test Method for Softening Point of Bitumen (Ring-and-Ball Apparatus).

ASTM (2015). ASTM D4402 / D4402M - 15: Standard Test Method for Viscosity Determination of Asphalt at Elevated Temperatures Using a Rotational Viscometer.

ASTM (2017). ASTM D113 - 17: Standard Test Method for Ductility of Asphalt Materials.

ASTM (2018). ASTM D3381: Standard specification for viscosity-graded asphalt binder for use in pavement construction. ASTM D3381, West Conshohocken, PA.

ASTM (2019a). ASTM D8276 - 19: Standard Test Method for Hydrocarbon Types in Middle Distillates,

including Biodiesel Blends by Gas Chromatography/Mass Spectrometry.

ASTM (2019b). ASTM D2872 - 19: Standard Test Method for Effect of Heat and Air on a Moving Film of Asphalt (Rolling Thin-Film Oven Test).

ASTM (2020). ASTM D3625 / D3625M - 20: Standard Practice for Effect of Water on Asphalt-Coated Aggregate Using Boiling Water.

Chang, S H (2018). Bio-oil derived from palm empty fruit bunches: Fast pyrolysis, liquefaction and future prospects. *Biomass Bioenergy, 119*: 263-276. DOI: 10.1016/j.biombioe.2018.09.033.

Fini, E H; Kalberer, E W; Shahbazi, A; Basti, M; You, Z; Ozer, H and Aurangzeb, Q (2011). Chemical characterization of biobinder from swine manure: Sustainable modifier for asphalt binder. *J. Mater. Civ. Eng., 23(11)*: 1506-1513. DOI: 10.1061/(asce)mt.1943-5533.0000237.

Gürer, C; Elmacı, A; Alagöz, O and Yılmaz, N (2020). Rheological behavior of bituminous binders replaced by poppy capsule pulp-based bio-oil. *Constr. Build. Mater., 264*. DOI: 10.1016/j.conbuildmat.2020.120631.

Hareru, W and Ghebrab, T (2020). Rheological Properties and application of molasses modified bitumen in hot mix asphalt (HMA). *Appl. Sci., 10(6)*: 1931. DOI: 10.3390/app10061931.

Ingrassia, L P; Lu, X; Ferrotti, G and Canestrari, F (2020). Chemical, morphological and rheological characterization of bitumen partially replaced with wood bio-oil: Towards more sustainable materials in road pavements. *J. Traffic Transp. Eng. (English Edition), 7(2)*: 192-204. DOI: 10.1016/j.jtte.2019.04.003.

Jabatan Kerja Raya, (2008). Standard Specification for Road Works (JKR/SPJ/Rev2008), Malaysia.

Lin, B and Bai, R (2021). Oil prices and economic policy uncertainty: Evidence from global, oil importers, and exporters' perspective. *Res. Int. Bus. Finance, 56(June 2020)*: 101357. DOI: 10.1016/j.ribaf.2020.101357.

Maghyereh, A I and Sweidan, O D (2020). Do structural shocks in the crude oil market affect biofuel prices? *In International Economics 164*. p. 183-193. DOI: 10.1016/j.inteco.2020.09.002.

Mensi, W; Sensoy, A; Vo, X V and Kang, S H (2020). Impact of COVID-19 outbreak on asymmetric multifractality of gold and oil prices. *Resources Policy, 69(July)*: 101829-101829. DOI: 10.1016/j.resourpol.2020.101829.

Mills-Beale, J; You, Z; Fini, E; Zada, B; Lee, C H and Yap, Y K (2014). Aging influence on rheology properties of petroleum-based asphalt modified with biobinder. *J. Mater. Civ. Eng., 26(2)*: 358-366. DOI: 10.1061/(asce)mt.1943-5533.0000712.

Pfeiffer, J P and Van Doormal, P M (1940), The rheological properties of asphaltic bitumens. *J. Phys. Chem., 44 (2)*: 149-165.

Pogaku, R; Hardinge, B S; Vuthaluru, H and Amir, H A (2016). Production of bio-oil from oil palm empty fruit bunch by catalytic fast pyrolysis: A review. *Biofuels, 7(6)*: 647-660. DOI: 10.1080/17597269.2016.1187539.

Raman, N A A; Hainin, M R; Hassan, N A; Ani, F N; Warid, M N M; Idham, M K and Mamat, R (2015). Effect of bio-oil from empty fruit bunch on penetration index of asphalt binder. *J. Teknol., 77(23)*: 13-16. DOI: 10.11113/jt.v77.6680.

Razek, N H A and Michieka, N M (2019). OPEC and non-OPEC production, global demand, and the financialization of oil. Research in International Business and Finance, 50 (October 2018), 201-225. DOI: 10.1016/j.ribaf.2019.05.009.

Read, J and Whiteoak, D (2003). *The Shell Bitumen Handbook*. 5th edition. Thomas Telford Ltd., London. 460 pp.

Rosli, N S; Harum, S; Jahim, J M and Othaman, R (2017). Chemical and physical characterization of oil palm empty. *Malaysian J. Anal. Sci., 21(1)*: 188-196. DOI: 10.17576/mjas-2017-2101-22.

Statista (2019). Daily demand for crude oil worldwide from 2006 to 2020, with a forecast until 2026. https://www.statista.com/statistics/271823/daily-global-crude-oil-demand-since-2006/, accessed on 13 June 2022.

Sukiran, M A; Chin, C M and Bakar, N K A (2009). Bio-oils from pyrolysis of oil palm empty fruit bunches. *Am. J. Appl. Sci., 6(5)*: 869-875. DOI: 10.3844/ajas.2009.869.875.

Sun, Z; Yi, J; Huang, Y; Feng, D and Guo, C (2016). Properties of asphalt binder modified by bio-oil derived from waste cooking oil. *Constr. Build. Mater., 102*: 496-504. DOI: 10.1016/j.conbuildmat.2015.10.173.

Sutrisno, B and Hidayat, A (2018). Pyrolysis of palm empty fruit bunch: Yields and analysis of bio-oil. *In MATEC Web of Conferences*, EDP Sciences, 154. p. 01036. DOI: 10.1051/matecconf/201815401036.

Trading Economics (2022). Crude oil. https://tradingeconomics.com/commodity/crude-oil, accessed on 13 June 2022.

Wang, H; Ma, Z; Chen, X and Hasan, M R M (2020a). Preparation process of bio-oil and bio-asphalt, their performance, and the application of bio-asphalt: A comprehensive review. *J. Traffic Transp. Eng. (English Edition), 7(2)*: 137-151. DOI: 10.1016/j.jtte.2020.03.002.

Wang, H; Wang, L; Zhang, J; Jing, Y and Cao, Y (2020b). Effects of pyrolysis temperature and reaction time on the performance of swine-manure-derived bio-binder. *Trans. Res. D. Trans. Environ., 89*: 102608. DOI: 10.1016/j.trd.2020.102608.

Wen, H; Bhusal, S and Wen, B (2013). Laboratory Evaluation of waste cooking oil-based bioasphalt as an alternative binder for hot mix asphalt. *J. Mater. Civ. Eng., 25(10)*: 1432-1437. DOI: 10.1061/(asce)mt.1943-5533.0000713.

Yang, W; Fu, P and Yi, W M (2017). Catalytic fast pyrolysis of corn stover in a fluidized bed heated by hot flue gas: Physicochemical properties of bio-oil and its application. *Int. J. Agric. Biol. Eng., 10(5)*: 226-233. DOI: 10.25165/j.ijabe.20171005.2473.

Yang, X; You, Z; Dai, Q and Mills-Beale, J (2014). Mechanical performance of asphalt mixtures modified by bio-oils derived from waste wood resources. *Constr. Build. Mater., 51*: 424-431. DOI: 10.1016/j.conbuildmat.2013.11.017.

Yang, X; Yu, Z and Dai, Q (2013). Performance evaluation of asphalt binder modified by bio-oil generated from waste wood resources. *Int. J. Pavement Res. Technol., 6(4)*: 431-439. DOI: 10.6135/ijprt.org.tw/2013.6(4).431.

Yiin, C L; Yusup, S; Mohamed, M; Udomsap, P; Yoosuk, B and Sukkasi, S (2016). Stabilization of empty fruit bunch derived bio-oil using solvents. *J. Sustain. Dev. Energy Water Environ. Syst., 4(1)*: 38-47. DOI: 10.13044/j.sdewes.2016.04.0004.

Yue, Y; Lin, Q; Irfan, M; Chen, Q; Zhao, X and Li, G (2017). Characteristics and potential values of bio-products derived from switchgrass grown in a saline soil using a fixed-bed slow pyrolysis system. *BioResources, 12(3)*: 6529-6544. DOI: 10.15376/biores.12.3.6529-6544.

Zahoor, M; Nizamuddin, S; Madapusi, S and Giustozzi, F (2021). Sustainable asphalt rejuvenation using waste cooking oil: A comprehensive review. *J. Clean. Prod., 278*: 123304. DOI: 10.1016/j.jclepro.2020.123304.

Journal of Oil Palm Research Vol. 35 (1) March 2023 p. 58-74
DOI: https://doi.org/10.21894/jopr.2022.0026

SPATIAL DISTRIBUTION OF *Rattus* SPECIES (RODENTIA: MURIDAE) IN OIL PALM PLANTATIONS OF PENINSULAR MALAYSIA WITH SPECIES VERIFICATION USING CYTOCHROME OXIDASE I (COI) GENE

MOHAMAD HARRIS NASIR[1]; MUHAMAD SHAKIRIN MISPAN[1]; SUBHA BHASSU[1,2]; KHOO JING JING[4]; SAZALY ABUBAKAR[4]; SITI NURUL IZZAH MOHD AZAMI[5]; SITI NABILAH ISHAK[6]; FARAH SHAFAWATI MOHD-TAIB[6] and HASMAHZAITI OMAR[1,2,3]*

ABSTRACT

Rats have caused severe problems in oil palm production in Malaysia. Rattus *species is the majority group of Muridae found in this area, and it is crucial to know about the species distribution in oil palm plantations (OPP) in Peninsular Malaysia. DNA barcoding method using Cytochrome Oxidase I (COI) gene was performed to identify all rat species captured in OPP aside from morphological identification. The data were then used to estimate the species diversity based on palm tree age. A total of 341 rats were captured and identified as* Rattus tiomanicus, R. argentiventer, R. rattus diardii, R. exulans *and* R. tanezumi. *Among these species,* R. tiomanicus *dominated the plantation with the highest diversity index (H'= 1.31), followed by* R. argentiventer *and* R. rattus diardii. *Most species of rats were commonly dispersed in the mature oil palm area. The annual precipitation showed a negative correlation (-0.258,* $p<0.05$*) with the species abundance, indicating that rats were more abundant during the dry season. In conclusion, the identification of rat species using molecular tools conforms to the morphological identification to determine the rats' distribution in the OPP. This can be associated with the oil palm age stage and abiotic factors of seasonal change.*

Keywords: molecular identification, oil palm age, rat pest, species diversity.

Received: 5 April 2021; **Accepted:** 7 March 2022; **Published online:** 20 May 2022.

[1] Institute of Biological Sciences, Faculty of Science, Universiti Malaya, 50603 Kuala Lumpur, Malaysia.

[2] Centre for Biotechnology in Agriculture, Universiti Malaya, 50603 Kuala Lumpur, Malaysia.

[3] Museum of Zoology, (Block J14), Institute of Biological Sciences, Faculty of Science, Universiti Malaya, 50603 Kuala Lumpur, Malaysia.

[4] Tropical Infectious Diseases Research and Education Centre (TIDREC), Universiti Malaya, 50603 Kuala Lumpur, Malaysia.

[5] Tick Cell Biobank Asia Outpost, Tropical Infectious Diseases Research and Education Centre (TIDREC), Universiti Malaya, 50603 Kuala Lumpur, Malaysia.

[6] Department of Biological Sciences and Biotechnology, Universiti Kebangsaan Malaysia, 43600 Bangi, Selangor, Malaysia.

* *Corresponding author e-mail: zaiti_1978@um.edu.my*

INTRODUCTION

The oil palm is one of the most rapidly increasing crops in the tropics (Kushairi *et al.*, 2017; Shevade and Loboda, 2019; Xu *et al.*, 2020). In 2019, Malaysia was the second-biggest share (20.7%) globally, behind Indonesia (33.9%) in producing palm oil and palm kernel oil market (MPOC, 2020). Since 1990, oil palm has remained the largest crop in Malaysia, contributing to Malaysia's third-largest external trade in 2019 (MPOC and MPOB, 2020). More than 5.9 million hectares of land have been converted from other crops such as rubber plants into oil palm plantations (OPP) to meet the market demand in 2019 (MPOC, 2020). However, this establishment has invited rats as notorious pests in the OPP (Hood *et al.*, 2019). Rats can cause damage up to 24% of fresh fruit bunch (FFB) in OPP (Chung, 2012; Rizuan and Noor Hisham, 2015).

Management of rat infestations in OPP has been dealt with using physical, biological and chemical methods. Physical methods such as shooting, dog hunting, and trapping were successful against individual rats but did not guarantee complete control of the rat populations (Lupo, 2011; Saravanan *et al.*, 2020). The barn owl, *Tyto alba javanica* is a classic example of a biological control approach to control rats in oil palm after its discovery in a Johor, Malaysia OPP in the late 1960s (Kamarudin *et al.*, 2019; Labuschagne *et al.*, 2016; Zainal Abidin *et al.*, 2021). On the other hand, the chemical approach is often considered the most favourable, cost-effective, humane, and gives the fastest result (Chia, 2005). Anticoagulant rodenticides (ARs) are chronic rodenticide that is probably the most effective and commonly used to manage rodents (van den Brink *et al.*, 2018). The plantation in Malaysia has started using the ARs by mixing them with a wide range of materials for field acceptability and practicality since the mid-1960s (Wood, 1976; Wood and Fee, 2003).

The genus *Rattus* has been identified as the primary rat pest infesting OPP (Ikhsan *et al.*, 2020), known to be distributed widely in Southeast Asia and comprises 561 species in 126 genera (Musser and Carleton, 2005). Rats are small mammals that quickly adapt in oil palm habitat due to easy access, breed and safety from predators (Puan *et al.*, 2011b; Tri Kwatrina *et al.*, 2018). Three main *Rattus* species were recorded in an oil palm plantation in Malaysia: *R. rattus diardii*, *R. argentiventer* and *R. tiomanicus* (Hafidzi and Saayon, 2001; Puan *et al.*, 2011a; 2011b). *Rattus rattus diardii* and *R. tiomanicus* dominate the matured palm area, while *R. argentiventer* was dominant in younger tree areas (Chia, 2005; Hafidzi and Saayon, 2001). This is because of the large body size of the *R. argentiventer* that limits its ability to climb off the older palm tree, which is high for them (Corley and Tinker, 2003; Liau *et al.*, 1991; Puan *et al.*, 2011a; Wood and Fee, 2003).

Morphological characteristics and skull measurements have been helpful tools in identifying rat species in the field. However, misidentification due to similarities and vast external features can happen during identification. Therefore, the molecular analysis will support the confirmation of rats' identification from the field study. Thus, this study aimed to investigate the rat species present in the OPP using genetic information and determine the species diversity of rats based on the age of the palm trees and seasonal factors.

MATERIALS AND METHODS

Study Site

Rats were collected from five OPP located in three states of Peninsular Malaysia from December 2018 until December 2019. The study sites located in Johor were: 1) Universiti Malaya (UM) Oil Palm Research Plantation at Kota Tinggi (N2.02916, E103.87076), 2) Paya Lang Plantation (N2.61125, E102.69362) and 3) Tambang Plantation (N2.63018, E102.70772) at Segamat, while in Pahang; 4) Pukin Plantation at Rompin, (N2.73600, E103.03200) and in Perak; 5) Tumbuh Hangat Plantation (N4.313903, E100.929009) at Perak Tengah (*Figure 1*). These study sites represent two age stages of OPP. Paya Lang estate and Tambang estate were young oil palm age (3-7 planting years), while UM plantation and Tumbuh Hangat plantation were matured oil palm age (10-15 planting years). Pukin estate contained both types of oil palm growth phase. The monthly rainfall data between December 2018 to December 2019 for each trapping location were provided by the plantation management office.

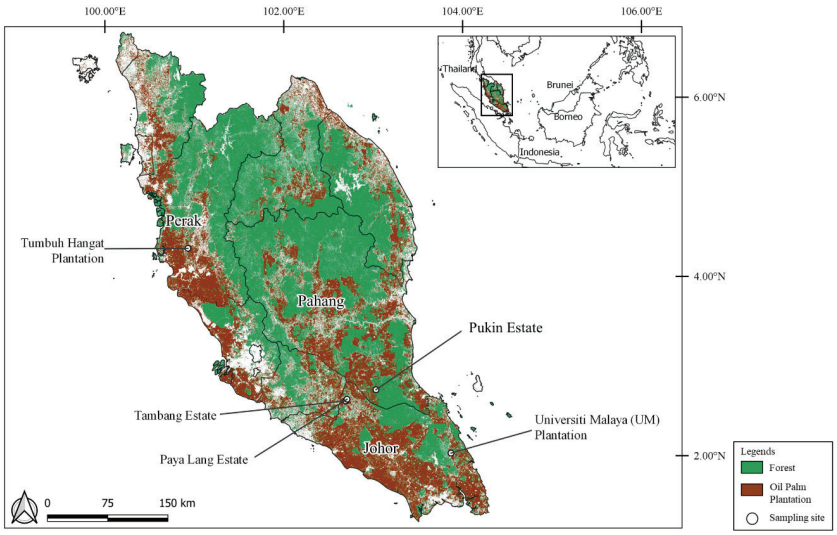


Figure 1. Sampling site selected at oil palm plantation in three states of Peninsular Malaysia.

Sampling Technique

A total of 150 rat trap cages, 28 cm x 15 cm x 12 cm, were placed in every plantation and set up randomly between frond heaps at the inter-planting rows of the selected plots in the plantations. Fresh oil palm fruit, salted fish and fresh corn pieces were used as bait in each trap (Mohd-Taib and Ishak, 2021; Saarani *et al.*, 2021). The traps were checked twice per day, during early morning and late afternoon, for five consecutive days at each plantation.

Rat's Handling and Research Approval

All captured rats were euthanised using Zoletil® through intramuscular injection (>50 mg kg^{-1}) (Ferrari *et al.*, 2005; Mohd-Taib and Ishak, 2021). Liver samples were extracted and stored at -20°C. In contrast, the body and skull of the sample were kept in 70% ethanol as wet specimens (Tingga *et al.*, 2012) and then were deposited at the Museum of Zoology, Universiti Malaya, Malaysia. Five linear measurements were measured: head to body length (HB), tail length (TL), hindfoot length (HF), ear length (E) and weight following Herbreteau *et al.* (2011). This study received approval from the Institutional Animal Care and Use Committee, Universiti Malaya, Malaysia (UM IACUC) (S/18042019/26112018-04/R) and the Department of Wildlife and National Parks [JPHL&TN(IP): 100-34/1.24 Jld. 14(02)].

Species Identification

Morphological and deoxyribonucleic acid (DNA) sequences were used for species identification. Morphological identification was based on five body measurements which include body length (BL), TL, HF, E and weight (Aplin *et al.*, 2003; Francis, 2008). In addition, all individuals were identified based on morphological features such as the colour of the dorsal fur, belly fur, mid-belly line, and tail, the texture of the dorsal fur and guard hairs, the length of the snout, and the number and position of the mammae (Aplin *et al.*, 2003; Lim, 2015; Paramasvaran *et al.*, 2013).

DNA Extraction

A total of 341 samples of genomic DNA of *Rattus* species were extracted from liver tissues using the GF-1 Tissue DNA Extraction kit (Vivantis®) following a protocol provided by the manufacturer. A total of 250 µL of Tissue Lysis Buffer (Buffer TL) was added to the liver tissue together with 20 µL of Proteinase K and 12 µL of Lysis Enhancer solution. The mixture was mixed immediately and incubated in the water bath at 65°C for 1 hr. After that, 560 µL of Tissue Genomic DNA Binding Buffer (Buffer TB) were added and mixed thoroughly by pulsed-vertexing and incubated for 10 min in a 65°C water bath. The column then underwent washing steps where the column was loaded with 650 µL of wash buffer and centrifuged at 5000 x g for 1 min, and the solution that flowed through was discarded, and the same step was repeated. 50 µL of preheated Elution Buffer was added directly onto the column membrane and allowed to stand at room temperature for 2 min. The DNA obtained was stored at -20°C. NanoDrop™ 2000 Spectrophotometer (Thermo Fisher Scientific, USA) was used to quantify the isolated genomic DNA's concentration and purity.

PCR Amplification and DNA Barcoding

Molecular identification was carried out by amplifying a partial mitochondrial cytochrome oxidase I (COI) gene. The polymerase chain reaction (PCR) was employed to amplify the targeted locus using Mastercycler® Nexus (Eppendorf North America, Inc.). PCR was conducted by using the PCR reagent, which were included 12.5 µL of 2X Power Taq MasterMix (BioTeke, Beijing), 0.5 µL of each 10 micromolar (µM) of forward and reverse primer, 1.0 µL of genomic DNA template and 10.5 µL of ultrapure water added to make the final volume of 25 µL, as per suggested by the manufacturer. PCR was performed by using a set of established primer corresponding to the (mtDNA) COI marker, forward Batl. 5310 primer 5 'CCTACTCRGCCATTTTACCTATG' 3 and reverse R6036R primer 5 'ACTTCTGGGTGT CCAAAGAATCA' 3 (Robins *et al.*, 2007). The PCR condition was as follows; initial denaturation for 4 min at 94°C, continued with 35 cycles of denaturation for 30 s at 94°C, annealing for 30 s at 48°C, an extension for 1 min at 72°C and a final extension stage for 10 min at 72°C, before holding-up to 10°C after the reaction was completed (Ikbal *et al.*, 2019a; 2019b).

The amplicons were purified and sent out for sequencing to the third-party company (1st BASE DNA Sequencing Division). Sequencing was done using the Applied Biosystems 3730XL Genetic Analyser via the Sanger Sequencing method. Both aligned forward and reversed sequences were trimmed using Molecular Evolutionary Genetics Analysis Version X (MEGA X) (Kumar *et al.*, 2018). All assembled sequences were searched in the National Centre for Biotechnology Information (NCBI) database using BLAST (http://BLAST.ncbi.nlm.nih.gov/BLAST.cgi) and the MEGA X software for a first sequence quality assessment and preliminary species identification. As standards for successful conspecific identification, we chose the top-matching hit with the greatest (>98%) maximum percent identity score. We

reconstructed the species identification for all of our sequences using phylogenetic tree analysis as was demonstrated in Pulgarín-R *et al.* (2021).

Phylogenetic Analysis

All sequenced DNA was analysed by building phylogenetic trees to visualise the species speciation together with representatives of each *Rattus* species sequence from GenBank; EF186528 *Rattus* sp. ABTC, HM217499 *Rattus* sp. ABTC, HM217498 *Rattus* sp. R3, FR775826 *R. tiomanicus*, JX533999 *R. tanezumi*, KC010285 *Rattus* sp. R3, KC010291 *R. tiomanicus* and KC617850 *R. exulans*. The phylogenetic trees were built using the Neighbour Joining (NJ) by MEGA X software. The Kimura-2-Parameter (K2P) algorithm model was used with a bootstrap value of 1000. JF459655 *Leopoldamys sabanus* (Muridae; Murinae) was included as the outgroup for this analysis.

Data Analyses for Species Diversity

Data assessed for normality by the Shapiro-Wilk test (p=0.581, $p>0.05$) were normally distributed. The Minitab 17 software was fully utilised for the analysis of variance (ANOVA) test for all variables used in this study. The significance of differences between males and females were investigated using a t-test for every external measurement. General trends of the external measurement were studied via principal component analysis (PCA). Collective data of the individuals captured from different localities were used to compute Shannon diversity index (H') by using PAST 3.26 (PAleontological STatistics) computer software (Hammer *et al.*, 2001). Cluster analysis was used to distinguish the species composition's similarity in the five locations, using the Euclidean (Pythagorean) distance measure. The Pc-Ord Version 5 programme (Grandin, 2006) was used for cluster analysis. Regression analysis was used to estimate the relationships between species abundance and annual rainfall using Minitab version 19.0.

To calculate the estimated population of rats in the oil palm plantation, we used the non-removal trapping system using the Zippin method (Zippin, 1958). Estimating the rats' population was based on the first, second and third catches, where the rats trapped would be counted and not rereleased. The total catch (T) was calculated based on the Equation (1);

$$T = \sum_{i=1}^{k} Yi \quad (1)$$

where k is the number repeat of sampling and Yi is caught on the ith captured. The ratio (R) of the total catch was calculated based on the Equation (2);

$$R = \frac{\sum_{i=1}^{k} (i-1)Yi}{T} \quad (2)$$

After the R was determined, the captured individuals' probability was estimated using a ($1\text{-}q^k$) probability graph (*Figure 2*). The estimated population size (N_o) was calculated using the Equation (3);

$$N_o = \frac{T}{(1-q^k)} \quad (3)$$

The standard deviation (SD) of N_o is given by Equation (4);

$$SD(N_o) = \sqrt{\frac{N_o(N_o-T)T}{T^2 - N_o(N_o - T)\left(\frac{k.p^2}{[1-p]}\right)}} \quad (4)$$

RESULTS

Species Identification

A total of 341 rats were collected throughout 9120 trap nights in five locations of OPP in Peninsular Malaysia. A total of five species (*i.e.*, *Rattus tiomanicus*, *Rattus rattus diardii*, *Rattus argentiventer*, *Rattus exulans* and *Rattus tanezumi*) were identified in the field based on morphological characteristics (*Figure 3*). *Rattus tiomanicus* was identified based on pure-white belly fur with dark midline strike, smooth olive-brown dorsal fur and 10 mammary tits. While *R. argentiventer* belly fur appears silvery grey with no midline middle streak, uniformly dark tail and dorsal fur of orange-brown colour intermixed with black. *Rattus rattus diardii* has greyish dorsal fur and whitish or grey-based belly fur with cream to buff tips on a combination of 2 (pectoral pairs) + 3 (inguinal pairs) mammae. The dorsal fur of *R. tanezumi* has a shade of brown, while the belly fur is whitish or grey based fur with pale yellow or orange tips. The only species with eight pairs of mammary tits was identified as *R. exulans*, the smallest rats among the *Rattus* genus with spiny reddish-brown dorsal fur, grey belly fur with a white-tip fur. The characteristics were referred from previous studies and guidebooks (Aplin *et al.*, 2003; Francis, 2008; Lim, 2015; Paramasvaran *et al.*, 2013).

All the COI sequences were aligned with no stop codon, insertion and deletion observed, a total of 708 bp of COI gene were retrieved, including 499 conserved sites, 209 variable sites, 163 Parsimony informative and 46 Singleton. All species except

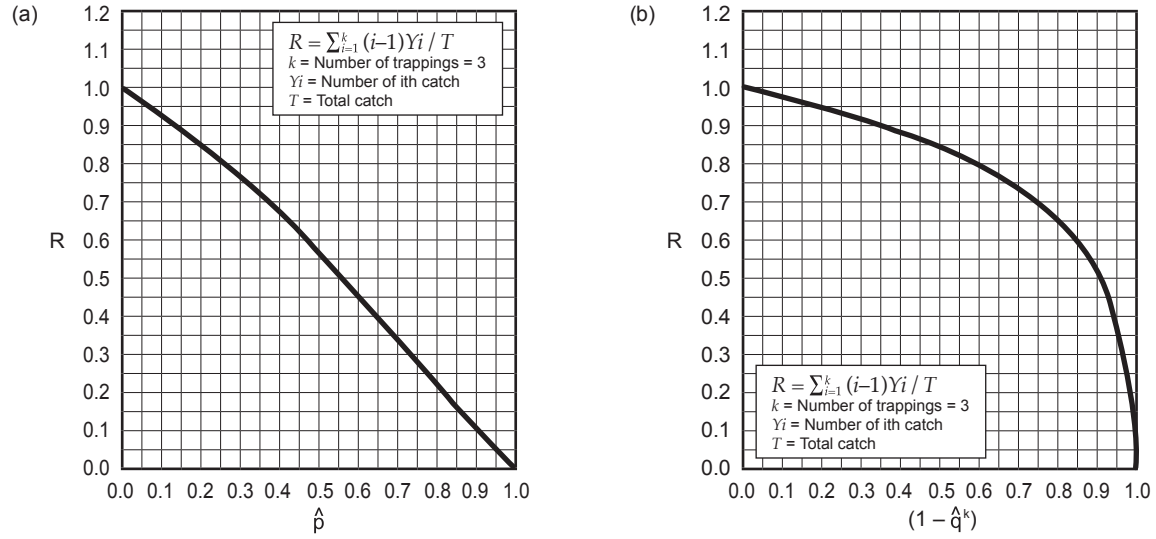


Figure 2. (a) Graphs for estimation from ratio R in removal trapping (b) Graph to estimate the p*-value.*

R. rattus diardii were confirmed by the DNA barcoding method of the COI gene marker with a high (>99%) match score. A total of 117 unclassified *Rattus* species were identified based on COI gene marker, including 88.9% *Rattus* sp. R3 and 11.1% *Rattus* sp. ABTC. In this study, all these unclassified *Rattus* species were referred to as *R. rattus diardii* based on their morphological field identification.

The phylogenetic relationship of the five *Rattus* species recorded in this study was reconstructed in NJ trees prior to the BLAST result (*Figure 4*). The sequences analyses revealed that *Rattus* COI falls into five well-supported clades categorised into *R. rattus diardii*, *R. tiomanicus*, *R. argentiventer*, *R. tanezumi*, and *R. exulans* with high bootstrap value ($96 \leq Bp \leq 100$). *Rattus tanezumi* is clustered with 86% bootstrap values with a clade of *R. rattus* originating (100%) as a sister taxon. Three mitochondrial lineages are associated with the house rat, which is *Rattus* sp. R3, *R. rattus diardii* and *R. rattus* (RrC) lineage IV form a single clade. The *R. rattus diardii* clade represents a cryptic species because molecular data was not accessible in the GenBank database, yet these lineages were clustered together in the same clade. This study included a sequence of *R. norvegicus* to show a special relationship between *R. rattus diardii* and *R. rattus* species.

Principal component (PC) 1 shows 63% of the variation, whereas PC2 shows 27% variation in morphological measurements. The highest PCA loadings from PC1 were total length, followed by HB and weight, indicating a high contribution of these morphological measurements in distinguishing species (*Table 1*). While weight (0.082) has the largest PCA loading in PC2, followed by E, the hindfoot was negatively correlated with the other variables (-0.623). The PCA plots the morphological measurement of all species produced by two contrasting groups (*Figure 5*). The first group comprised of *R. tiomanicus* and *R. argentiventer*, with only a few *R. rattus diardii* individuals spotted. The second group included *R. rattus diardii*, *R. exulans* and *R. tanezumi*. However, some *R. tiomanicus* and *R. argentiventer* overlapped with the other species in group 2. These plots revealed that species from the same group closely resembled each other for specific morphological measurements, as mentioned earlier. One way ANOVA analysis of the morphological measurements between males and females showed no significant difference with a *p*-value of 0.245 ($p>0.05$).

The ANOVA analysis of the *Rattus* species' external measurements showed no significant difference ($p=0.273$, $p>0.05$). However, *post hoc* analysis using Tukey's honestly significant difference test showed that this genus head-to-body measurement could be divided into two groups with a significant difference of $p<0.05$ separated into alphabetical groups in *Table 2*. *Rattus tiomanicus* and *R. exulans* have smaller HB (159-389 mm) and weight (10-200 g). In contrast, *R. argentiventer* and *R. rattus diardii* have a larger body size (176-462 mm) and weight (21-332 g). In this study, the TL appeared shorter than the HB for all species captured. *Rattus tiomanicus* and *R. exulans* BL showed a significant difference between *R. argentiventer* and *R. rattus diardii*. Simultaneously, the mean TL for every species was significantly different from each other, where *R. exulans* has the shortest tail among other *Rattus* species. For hindfoot measurement, only *R. exulans* was significantly different ($p<0.05$) than the other species, with an average of 25.06 ± 1.56 mm. While for E measurement, *R. tiomanicus* was significantly different ($p<0.05$) than the other species with an average length of 28.07 ± 0.54 mm. The number of female rats trapped was higher (51.73%) than male (48.27%) (*Table 2*).

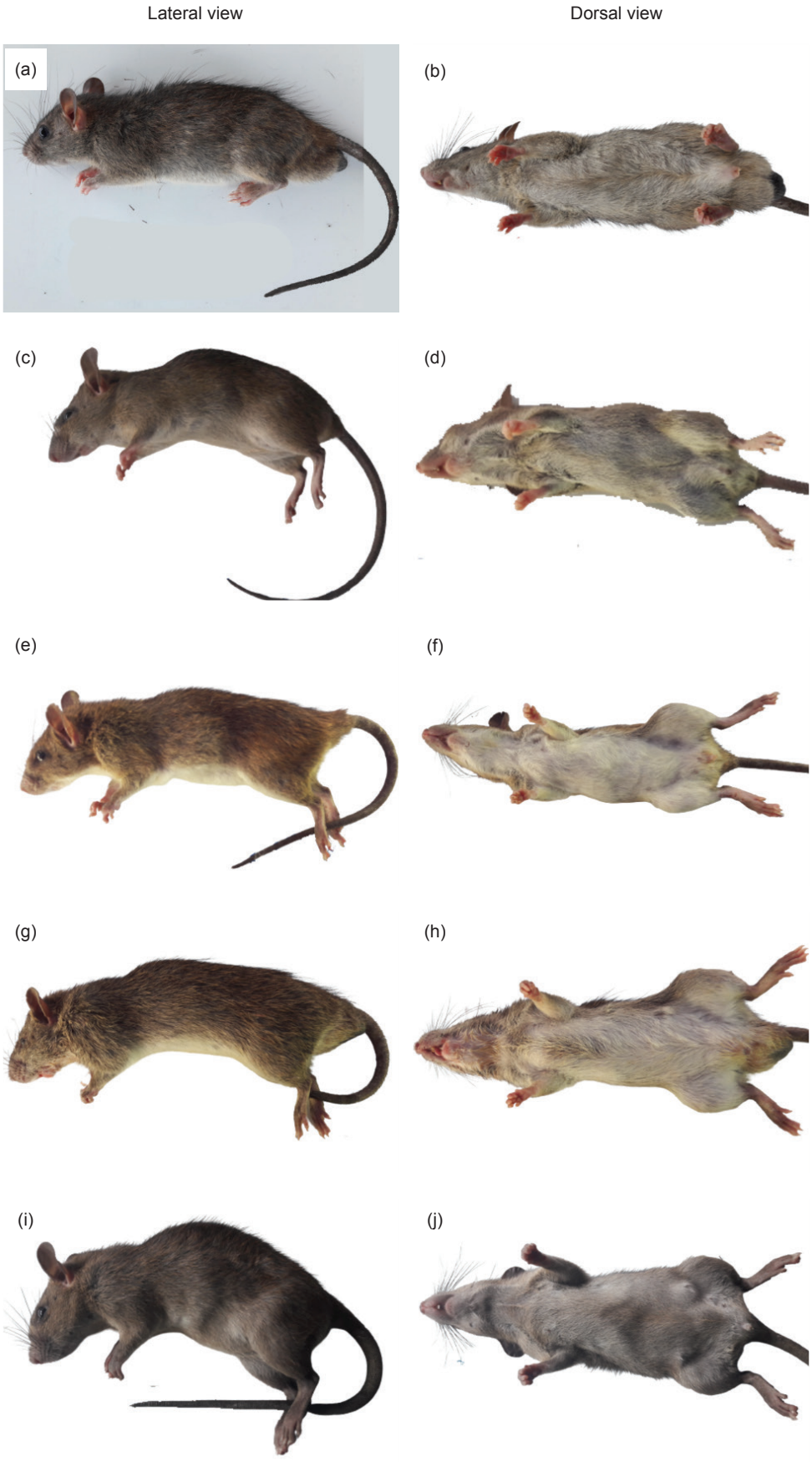


Figure 3. Rattus *species captured in the oil palm plantation. (a-b)* Rattus rattus diardii *(c-d)* Rattus exulans *(e-f)* Rattus tiomanicus *(g-h)* Rattus argentiventer *(i-j)* Rattus tanezumi.

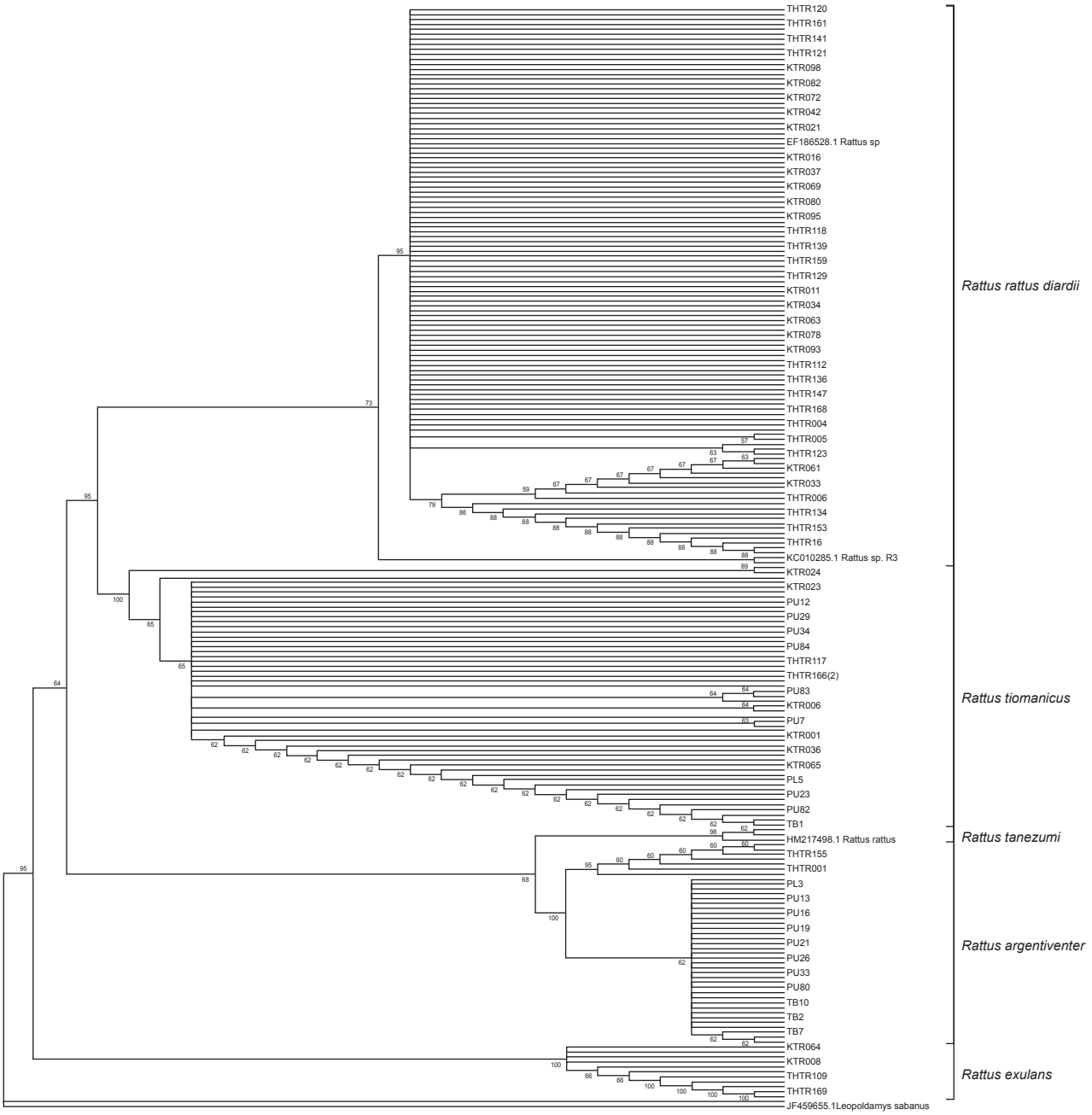


Figure 4. The Neighbour-Joining (NJ) phylogenetic tree (NJ/MP=89/76) illustrates the relationships between the Rattus *species based on the COI genes using the Kimura-2-parameter algorithm and 1000 bootstrap replication. The optimal tree sum of branch = 0.5739 is shown for the NJ tree.*

TABLE 1. FACTOR LOADINGS FOR THE PRINCIPAL COMPONENT ANALYSIS (PCA) BASED ON SIX EXTERNAL CHARACTERISTICS

Variable	PC1	PC2	t-test analysis against gender		
			df	*p*-value	p-variance
Head to body length	0.481	0.047	339	0.0816	0.8756
Tail length	0.455	0.113	339	0.7089	0.3272
Total length	0.505	0.086	339	0.2449	0.7600
Ear	0.029	0.763	339	0.7403	0.2754
Hind foot	0.286	-0.623	339	0.8591	0.8789
Weight	0.473	0.082	339	0.5089	0.7249
Eigenvalue	3.797	1.6357	-	-	-
% total variance	63.1712	27.2895	-	-	-

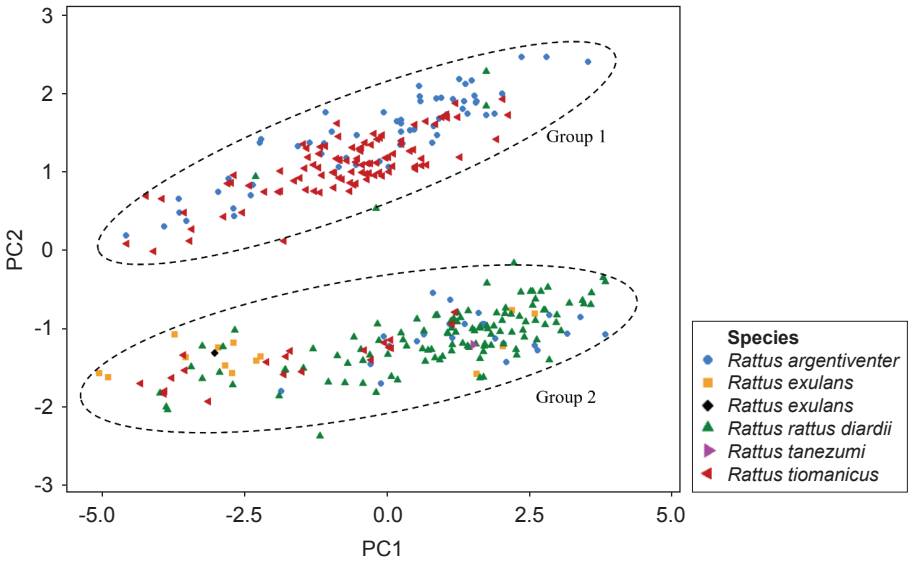


Figure 5. PC1 and PC2 of the PCA for six external measurements of the Rattus *species.*

TABLE 2. LIST OF SPECIES AND MEAN MEASUREMENT ± STANDARD ERROR (maximum and minimum ranges)

Species	Sex		Measurement (mm)				Weight (g)
	M	F	HB	TL	HF	E	
Rattus tiomanicus	66	59	148.00 ± 2.38^{b} (85-200)	141.69 ± 2.49^{c} (90-189)	19.76 ± 0.38^{a} (17-35)	28.07 ± 0.54^{b} (14-37)	88.07 ± 3.42^{b} (19-118)
Rattus argentiventer	34	51	162.60 ± 3.19^{a} (84-260)	156.20 ± 2.45^{b} (92-202)	23.05 ± 0.87^{a} (10-40)	29.63 ± 0.73^{a} (16-40)	129.46 ± 5.95^{a} (30-239)
Rattus rattus diardi	59	56	173.95 ± 2.58^{a} (98-220)	167.75 ± 2.41^{a} (94-220)	32.45 ± 0.44^{a} (16-39)	20.31 ± 0.29^{a} (14-35)	131.61 ± 5.29^{a} (21-332)
Rattus exulans	9	6	129.82 ± 9.17^{b} (80-205)	122.06 ± 7.26^{c} (79-180)	25.06 ± 1.56^{b} (17-39)	16.71 ± 0.72^{a} (12-22)	66.60 ± 15.8^{b} (10-200)
Rattus tanezumi	0	1	184^{ab}	163^{abc}	35^{ab}	20^{ab}	143^{ab}

Note: *Alphabets indicate the significant level (p<0.05).
N - total individuals; HB - head to body length; TL - tail length; HF - hind foot; E - ear.

Diversity and Abundance

The three most abundant species collected in this study were *R. tiomanicus* (36.6%, 125 individuals), *R. rattus diardii* (33.7%, 115 individuals), and *R. argentiventer* (24.93%, 85 individuals) (*Figure 6*). Only 15 individuals of *R. exulans* and one individual *R. tanezumi* were captured throughout this sampling. The value of the H′ strongly supports that the *R. tiomanicus* (H′=1.31, E= 0.77, D_{Mg}= 0.83) was the most dominant rat in OPP (*Figure 7*). *Rattus argentiventer* has the second-highest value of H′ compared to *R. rattus diardi,* although the number of individuals for this species was lower than *R. rattus diardii* with Shannon diversity index (H′= 1.19, E= 0.82, D_{Mg}= 0.68) and (H′= 0.73, E=.70, D_{Mg}=0.42), respectively. The *R. rattus diardi* was only captured in UM plantation and Tumbuh Hangat plantation but not in the other three plantations. Aside from *R. rattus diardii*, *R. exulans* has the lowest diversity index and richness score among the other species, with H′=0.50 and D_{Mg} of 0.37. *Rattus tanezumi* scored 0 for H′ and D_{Mg}, indicating the lowest evenness index between other species with only one individual captured in all OPP sites.

The species composition in all locations showed a significant difference (H′=1.24; df= 6, p<0.05) (*Table 3*). Tumbuh Hangat plantation has the highest diversity of species (N=111; H′=1.18), while Paya Lang has the lowest diversity score (N=47, H′= 0.46). Pukin plantation (N= 97, H′= 0.74) with both young and mature palm trees scored a higher diversity index than UM plantation (N=67, H′=0.64) due to differences in the species number. The estimated population size for each plantation is shown in *Table 3*. In line with the highest rat abundance in Tumbuh Hangat plantation, the estimated population size scored the highest with 314 ± 62 individuals per hectare, followed by

Pukin plantation (124 ± 28/ha) and UM plantation (103 ± 17/ha). The younger palm trees (3-7 planting years) area has a lower recorded population of rats, fewer than 50 individuals per hectare. It showed that the rat abundance was concentrated in the matured palm area (10-15 planting years) than in the young palm.

Rattus species captured in the UM and Tumbuh Hangat plantations showed a 100% similarity index, while Tambang and Paya Lang plantations shared 89% of the clustering analysis (*Figure 8*). Pukin plantation was separated from Paya Lang and Tambang plantations by a similarity index of less than 75%. Based on the clustering analysis, the five *Rattus* species were grouped into three with an overlapping value of >95%. Group 1 consisted of *R. tiomanicus* and *R. argentiventer*, where these species were concentrated in Paya Lang plantation, Tambang plantation, and Pukin plantation with a similarity score of 90%. *Rattus rattus diardii* and *R. exulans* were grouped into group 2 captured from UM and Tumbuh Hangat plantations, while *R. tanezumi* was categorised in Group 3 (100%) alone and can only be found in Tumbuh Hangat plantation.

Association of Rats Species with Rainfall and Oil Palm Age

The monthly data collection of *Rattus* with the mean rainfall dataset of all locations was recorded from December 2018 to December 2019 (*Figure 9a*). Four changes in the mean rainfall have been recorded throughout the sampling periods between four quartiles of the year. The average rainfall data throughout the sampling period in all locations was 192.73 mm. The first drop of the mean rainfall was recorded between December 2018 to February 2019, with an average rainfall of 125.75 mm. During this period, a significantly high number of rats were trapped, with 20 to 63 individuals that included *R. argentiventer, R. tiomanicus*, *R. rattus diardii* and *R. exulans*. The highest captured species were *R. argentiventer* (N=63), while *R. exulans* (N=9) was the lowest. The second quartile of the year recorded an increased rainfall was between April 2019 to June 2019 (189.41 mm). The total trapped individuals reduced when the rainfall increased, especially in May 2018 (N=10, 198.70 mm), and the number increased in June

TABLE 3. SPECIES DIVERSITY OF RATS CAPTURED IN FIVE DIFFERENT OPP

Plantation	Ha	Captured individuals	Shannon diversity index (*H'*)	Estimated population size (N_o/Ha)
Tambang Plantation	134	19	0.68	18 ± 16
Paya Lang Plantation	141	47	0.46	48 ± 13
UM Plantation	136	67	0.64	103 ± 17
Pukin Plantation	142	97	0.74	124 ± 28
Tumbuh Hangat Plantation	142	111	1.18	314 ± 62
Total	695	341	1.24	920 ± 90

Note: H' - shannon diversity index, N_o/Ha - estimated population size.

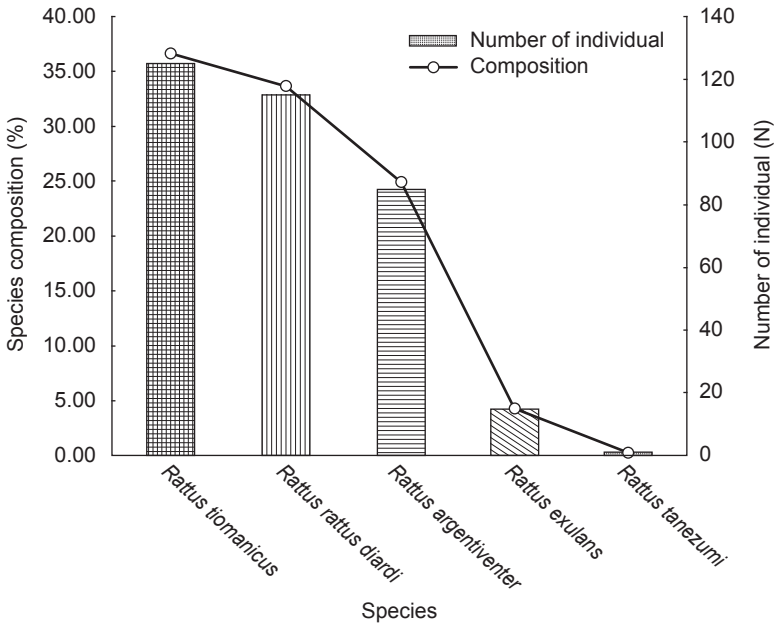


Figure 6. Species composition and the number of individuals captured of the Rattus *species collected in OPP of Peninsular Malaysia.*

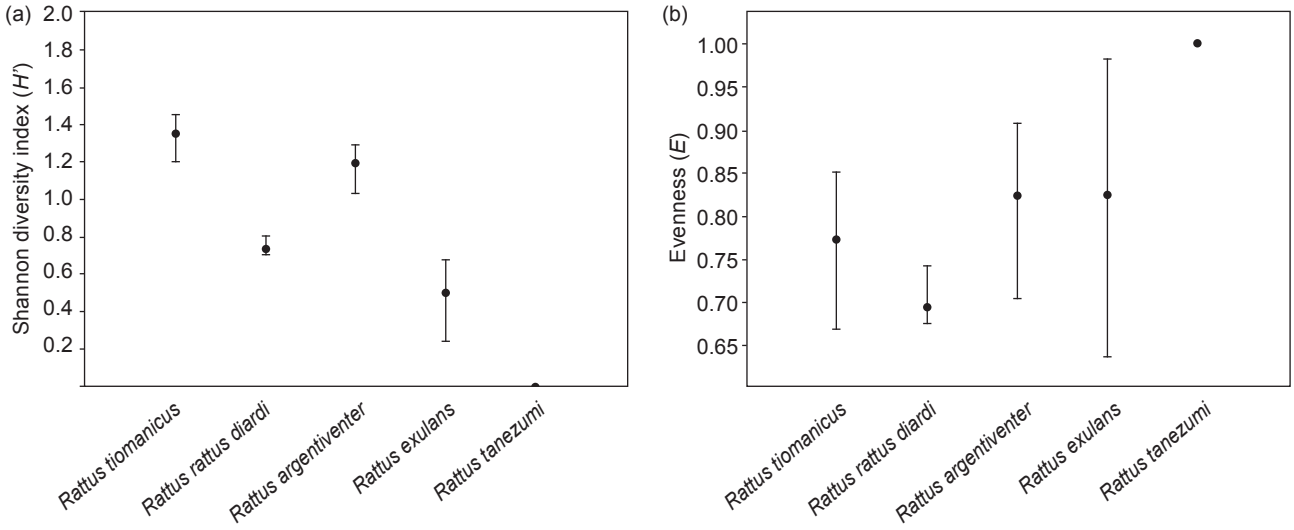


Figure 7. Mean box and whisker plot for each rat species captured with (a) Shannon diversity index (H'), (b) Evenness (E).

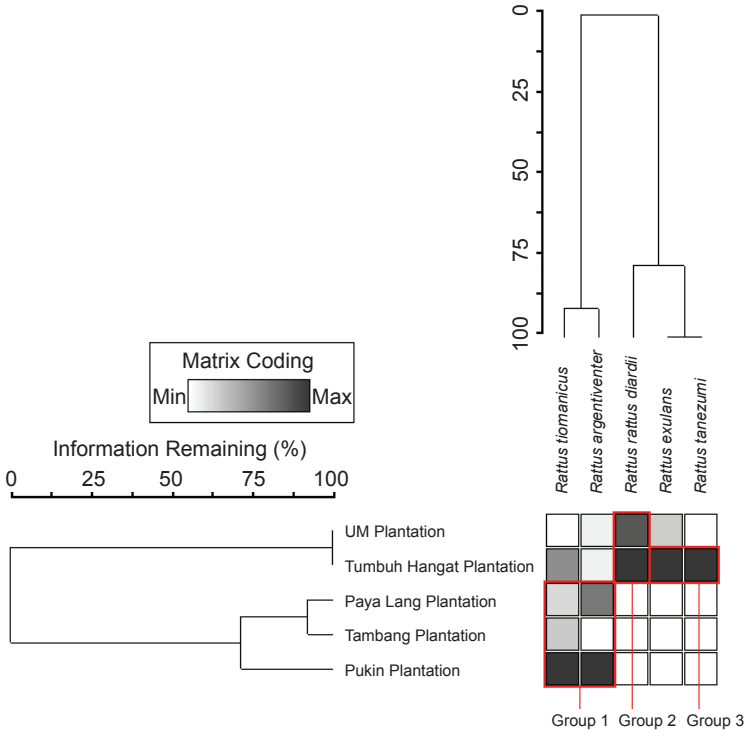


Figure 8. Clustering analysis between the composition of Rattus *species in the OPP.*

2019 (N=51, 173.10 mm) with the decreasing rainfall. With the drop of rainfall in July 2019 (134.10 mm), the number of trapped rats rose to the highest (N=77) compared to the other sampling months. The number of trapped rats dropped from September 2019 to December 2019, when the wet season started with an average rainfall of 286.44 mm. Overall, the trapped rats showed a significant negative correlation (r=-0.258, p=0.038) with the average rainfall. The number of trapped rats decreased with the increase of mean rainfall (*Figure 9b*; R^2=6.68%, F=4.51, DF=64, p<0.05). We observed a non-significant correlation (r=0.305, p=0.618) between the two palm age groups based on the captured rats species in this study (R2=9.28%, F = 0.31, p=0.618).

DISCUSSION

Reference DNA sequences under *R. rattus diardii* (Jentink, 1880) were unavailable in the GenBank, which could explain why our sequences were matched with *Rattus* sp. R3 and *Rattus* sp. ABTC

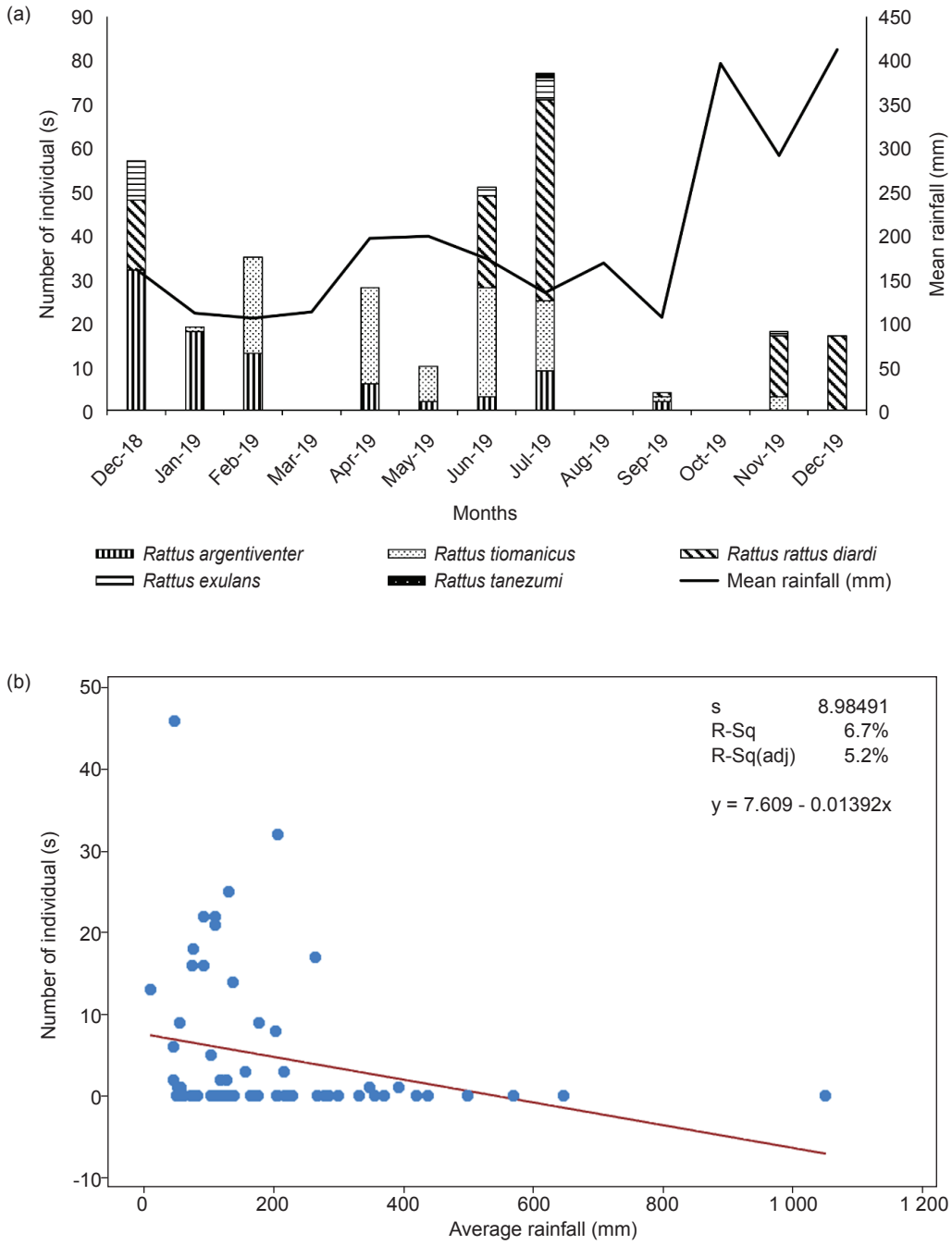


Figure 9. (a) Comparing individuals collected with the mean monthly rainfall data (mm). (b) Species abundance decreases across a regional gradient of mean rainfall (mm).

of unknown *Rattus* species. This was supported by the phylogenetic tree that shows the R3 lineage was grouped with our *R. rattus diardii* sequences. However, based on previous studies of unrecognised sequences of original data, both *Rattus* sp. R3 and *Rattus* sp. ABTC were initially identified as *R. rattus diardii* by field identification based on the physical appearance of this species. However, in another study conducted by Robins *et al.* (2007), sequences of *R. rattus diardii* collected from Kuala Lumpur were deposited as *Rattus* sp. ABTC according to their voucher name instead of the original species name. While the *Rattus* sp. R3 was proposed by Pagès *et al.* (2010) when the author used a DNA sequence of unidentified *Rattus* sp. from Thailand and then later classified them under the R3 lineage based on the phylogenetic analysis. In Indonesia, this species was also referred to as *R. rattus diardii* by local taxonomists as the species responsible for the infestation and damage of the oil palm tree (Andru *et al.*, 2013; Ikhsan *et al.*, 2020).

Rattus rattus diardii clade was well separated from other species in this study, including *R. rattus* and *R. norvegicus* retrieved from GenBank data sources. Thus, this study emphasises a suitable terminology for all individuals in this clade, such as *R. rattus diardii* (Malayan House Rat) (Jentink, 1880). The other *Rattus* species recorded in this study were well separated in their well-supported clade. DNA-based identification has proven to be helpful to distinguish cryptic species with the development of genetic lineage divergence to eliminate the taxonomic uncertainty introduced by morphological identification (Hebert *et al.*, 2004). However, morphology identification is still needed to distinguish rat species better since it does not change as rapidly as the genetic lineage (Hebert *et al.*, 2004; Matisoo-Smith and Robins, 2009; Wada *et al.*, 2003).

Rattus rattus diardii came second as the most abundant species captured in this study but came third in the diversity index score. *Rattus rattus diardii* was a typical household and urban pest (Lim, 2015). In Borneo, Zainal Abidin *et al.* (2021), live trapping revealed that *R. rattus diardii* was the predominant species in the oil palm plantation. The feeding preferences of *R. rattus diardii* are not limited to fruit bunches but also any leftover food present surrounding the worker settlements area within the plantation, as we observed their existence in two plantations (UM and Tumbuh Hangat plantation). In contrast to the other plantation, which was remote from human settlements, the two plantations were surrounded by human settlements, such as the aborigine's village, other crop fields, and the surrounding residential area.

This study observed *R. tiomanicus* as the most dominant species, especially in the matured oil palm plantation. *Rattus tiomanicus* has adapted well to the oil palm plantation due to its agility and arboreal habits that make it difficult to control. Small body size gives this species the advantage of becoming a great climber with their well-developed slight ridges pattern on their broad footpads. Furthermore, a longer tail than the BL gives advantages to the arboreal rats to keep their balance while climbing (Hori *et al.*, 2011). *Rattus tiomanicus* spend most of their time on trees but was often found on the ground (Francis, 2008). Other species such as *R. rattus diardii, R. tanezumi* and *M. hellwaldii* share the same characteristic of having a longer tail than HB, but the climbing ability is not as good as *R. tiomanicus* (Ikhsan *et al.*, 2020). In this study, we have observed that *R. rattus diardii* and *R. exulans* shared the same characteristic of the TL as *R. tiomanicus* to maintain their stability and balance. While in comparison, the tail of the terrestrial rat, such as *R. argentiventer* is usually shorter than the HB (Carrizo *et al.*, 2014).

In Peninsular Malaysia, *R. tiomanicus* was reported as the main rat pest infesting the oil palm plantation along with *R. rattus diardii* and *R. argentiventer* (Hafidzi and Saayon, 2001; Nursyazana *et al.*, 2013; Puan *et al.*, 2011a; 2011b; Rizuan and Noor Hisham, 2015). However, the situation in Borneo OPP was different, where the *R. tiomanicus* was less recorded and predominated with *R. rattus diardii*, *Maxomys whiteheadi*, *R. argentiventer* and *R. exulans* (Abidin *et al.*, 2014; Buckle *et al.*, 1997; Phua *et al.*, 2018; Stryjek *et al.*, 2018). In Indonesia, the population of *R. tiomanicus* was reported growing and expanding after converting the secondary forest to OPP (Nugroho and Santosa, 2018; Santosa and Rejeki, 2019).

The next most dominant rat species in OPP was *R. argentiventer*, and even the abundance was relatively low compared to *R. rattus diardi*. This species was more likely to invade the young palms (Corley and Tinker, 2003; Wood, 1976) as they were terrestrial rats and the limitation to climb as the palm grows higher (Yasuma and Andau, 2000). However, the correlation between the palm age and the abundance of *R. argentiventer* was negative in Puan *et al.* (2011b) studies, where this species was widely found in OPP with matured palms. The same observation was recorded in this study, where many rats were reported in mature palm planting sites such as Tumbuh Hangat plantation and Pukin plantation. There was a possibility that this species has migrated from the surrounding paddy field at Tumbuh Hangat plantation that may have caused the high rate of capture as they were a common species of grassy field and paddy field (Tristiani and Murakami, 2003; Tristiani *et al.*, 2003).

Rattus argentiventer was initially an important small mammal pest of the rice field in Southeast Asia (Buckle *et al.*, 1982; Tristiani *et al.*, 2000). However, an increasing number of these species has been recorded in OPP, leading to a potential threat for this crop. Their presence in OPP has been reported since 1976 (Payne *et al.*, 1985; Wood, 1976), and their growing population has caused great damage to FFB in oil palm (Hafidzi and Saayon, 2001; Zainal Abidin *et al.*, 2021). With an abundance of oil palm fruit available in OPP, this species can survive and adapt to its new environment moving away from its natural habitat in the rice field.

Only a small number of the Polynesian rat, *R. exulans* were captured in this study. This species was concentrated only in the Tumbuh Hangat plantation, surrounded by forest, human settlements, and other agriculture crops. *Rattus exulans*, like *R. rattus diardii,* is a rodent that is commonly found in households and lives in forest and agricultural environments (Paramasvaran *et al.*, 2013). Smaller rats, such as *R. exulans* and *M. whiteheadi* were often recorded in immature palm areas (Rizuan and Noor Hisham, 2015).

However, in Tumbuh Hangat plantation, the oil palm trees were in a mature stage, and there was a possibility that this site was in their foraging pathway during the trapping session.

The connection between the activity of rats and ground materials can be species-specific and can differ depending on the palms' age (Puan *et al.*, 2011c). As indicated in this study, the captured rats' population size has a higher density in the matured planted palm tree area of Pukin plantation, UM plantation and Tumbuh Hangat plantation. The clustering analysis also supports the rat distribution according to the palm planted age where the *R. tiomanicus*, *R. rattus diardii* and *R. exulans* concentrated on the higher and older palms from the five species identified. The older palm areas also have a higher diversity of rats relative to the young palm area. Radio-tagged movements of *R. tiomanicus* in the oil palms in Malaysia have shown a preference for the use of ground vegetation areas, and the frond heaps were another vital habitat structure for rats, especially as shelters (Buckle *et al.*, 1997). It was suggested that frond heaps could benefit rats by improving foraging or hiding spots from predators (Lambert *et al.*, 2008). Denser and grassy crop environment was preferred by *R. argentiventer* for foraging, nesting, and protection (Brown and Singleton, 2001). This species was positively associated with high ground vegetation cover of small shrubs in the plantation with young palm trees.

More female individuals were captured than male rats (*Table 2*). Female rats were easily caught as they foraged their young individually around their nest, while the male rats have a more extended home range but are limited to their territory (Priyambodo, 2003; Takahashi and Miczek, 2013). Although female rats' foraging ranges are different throughout their life expectancy, their nutritional requirement is high, especially during gestation and lactation stages (Sadleir *et al.*, 1973; Tristiani *et al.*, 2003). The home range of rats is dispersed individually between males and females during the pre-mating season. However, their home range completely overlapped before the breeding season, where the males are clustered around the females (Tristiani *et al.*, 2000). In theory, males should be easily captured in the field due to their larger home range than females. However, females were captured more frequently in this study due to the female-biased ratio. Like most mammals, rodents produce roughly equal males and females (Labov *et al.*, 1986; Rosenfeld *et al.*, 2003; Rugh, 1968), but litters with significant sex imbalances can emerge spontaneously. However, due to various external factors, including stress, competition and a shortage of food in nature, the resulting litters are biased toward females (Pratt and Lisk, 1989; Wolff, 2007).

The absence of sexual dimorphism was also obviously recognised. In this study, the sizes of male *Rattus* showed no differences compared to the females. Several studies on the morphometric variation of *R. rattus* using conventional morphometrics confirmed the absence of sexual dimorphism and age variation (Faleh *et al.*, 2012; Ventura and Fuster, 2000). However, *Aethomys ineptus Calomys musculinus*, *Akodon azarae* and *Oxymycterus rufus* population showed a strong sexual dimorphism between males and females (Abdel-Rahman *et al.*, 2009; Martínez *et al.*, 2014). Based on the PCA plots, the PC1 scores were positive, indicating that the first PC score increases with all the external variables. This implies that the high PC1 score is associated with larger measurements of the variables.

The trapped rats' distribution in the oil palm plantation showed a significant difference between the rainy and dry seasons. The strong influence of precipitation on the rat's abundance in the regression analysis could be due to food availability changes with the rainfall pattern (Taylor and Green, 1976). In some studies, high annual rainfall triggered the outbreak of *R. villosissimus* in central Australia because this species is not physiologically well adapted to dry conditions (Greenville *et al.*, 2013). There was an important link between high rainfall (>600 mm) and rodent abundance, especially in tropical and arid zones with annual rainfall patterns to determine the species' abundance (Madsen and Shine, 1999; Singleton, 2008). Seasonal samplings can be continued in the future to confirm the association between precipitation and the distribution and abundance of rats in the study areas.

CONCLUSION

In conclusion, molecular identification using COI gene marker was proven to be helpful to verify the correct ambiguity of the morphological identification of rat pests in OPP. Molecular tools can provide consistent data and reduce the variations for species identification. *R. tiomanicus*, *R. rattus diardii* and *R. argentiventer* are the three dominant pest species observed infesting the oil palm plantation with a significant population coverage per hectare. More data that include biotic and abiotic factors such as intraspecific and interspecific interaction, nutrient flows, or weather should be considered to estimate this pest's population dynamics in the oil palm plantation.

ACKNOWLEDGEMENT

We are grateful to the agronomist at IOI Research Centre, Gemencheh, Negeri Sembilan, Malaysia for their transportation, accommodation, and

information throughout the sampling period. This research is funded in parts through research grant PV037-2018 awarded by Yayasan Tan Sri Lee Shin Chen, the Higher Institution Centre of Excellence (HICoE) program (Project MO002-2019), Ministry of Education, Malaysia for niche area research, and the Institutional Links, ID 332192305, program under the Newton-Ungku Omar Fund partnership. The grant is funded by the UK Department for Business, Energy and Industrial Strategy and Malaysian Industry-Government Group for High Technology (MIGHT) and delivered by the British Council and MIGHT.

REFERENCES

Abdel-Rahman, E H; Taylor, P J; Contrafatto, G; Lamb, J M; Bloomer, P and Chimimba, C T (2009). Geometric craniometric analysis of sexual dimorphism and ontogenetic variation: A case study based on two geographically disparate species, *Aethomys ineptus* from southern Africa and *Arvicanthis niloticus* from Sudan (Rodentia: Muridae). *Mamm. Biol.*, *74*: 361-373.

Abidin, M R Z; Hamid, N H and Noor, H M (2014). Observations of the diet of Blackwinged kite *Elanus caeruleus* in the oil-palm plantations of the Sahabat area, Sabah, Borneo, Malaysia. *BirdingASIA*, *22*: 55-57.

Andru, J; Cosson, J F; Caliman, J P and Benoit, E (2013). Coumatetralyl resistance of *Rattus tanezumi* infesting oil palm plantations in Indonesia. *Ecotoxicology*, *22*: 377-386. DOI: 10.1007/s10646-012-1032-y.

Aplin, K P P; Brown, P R; Jacob, J; Krebs, C J and Singleton, G R (2003). Field methods for rodent studies in Asia and the Indo-Pacific. Monographs, Australian Centre for International Agricultural Research, Number 114053, Canberra, Australia.

Brown, P R and Singleton, G R (2001). Habitat use and movements of the rice-field rat, *Rattus argentiventer*, in West Java, Indonesia. *Mammalia*, *65*: 151-166.

Buckle, A P; Chia, T H; Fenn, M G P and Visvalingam, M (1997). Ranging behaviour and habitat utilisation of the Malayan wood rat (*Rattus tiomanicus*) in an oil palm plantation in Johore, Malaysia. *Crop Prot.*, *16*: 467-473.

Buckle, A P; Rowe, F P and Husin, A R (1982). Laboratory evaluation of the anticoagulants coumatetralyl and brodifacoum against *Rattus argentiventer* in Peninsular Malaysia. *Trop. Pest Manag.*, *28*: 126-130.

Carrizo, L V; Tulli, M J; Dos Santos, D A and Abdala, V (2014). Interplay between postcranial morphology and locomotor types in Neotropical sigmodontine rodents. *J. Anat.*, *224*: 469-481.

Chia, T (2005). Rat control in oil palm plantations: A review. *Planter*, *81*: 15-26.

Chung, G F (2012). *Effect of Pests and Diseases on Oil Palm Yield, Palm Oil* (Lai, O M; Tan, C P and Akoh, C C eds.). AOCS Press. p. 163-210.

Corley, R H V and Tinker, P B H (2003). *The Oil Palm*. 4th edition. Blackwell Science Ltd, Oxford, Great Britain. 592 pp.

Faleh, A Ben; Annabi, A and Said, K (2012). Morphometric variation in black rat *Rattus rattus* (Rodentia: Muridae) from Tunisia. *Acta Zool. Bulg.*, *64*: 381-387.

Ferrari, L; Turrini, G; Rostello, C; Guidi, A; Casartelli, A; Piaia, A and Sartori, M (2005). Evaluation of two combinations of Domitor, Zoletil 100 and Euthatal to obtain long-term nonrecovery anesthesia in Sprague-Dawley rats. *Comp. Med.*, *55*: 256-264.

Francis, C M (2008). *A Field Guide to the Mammals of Southeast Asia*. Asia Books Company, Limited. 416 pp.

Grandin, U (2006). PC-ORD version 5: A user-friendly toolbox for ecologists. *J. Veg. Sci.*, *17*: 843-844.

Greenville, A C; Wardle, G M and Dickman, C R (2013). Extreme rainfall events predict irruptions of rat plagues in central Australia. *Austral Ecol.*, *38*: 754-764.

Hafidzi, M N and Saayon, M K (2001). Status of rat infestation and recent control strategies in oil palm plantations in Peninsular Malaysia. *Pertanika J. Trop. Agric. Sci.*, *24*: 109-114.

Hammer, Ø; Harper, D A T and Ryan, P D (2001). PAST: Paleontological statistics software package for education and data analysis. *Palaeontol. Electron.*, *4*: 9.

Hebert, P D N; Penton, E H; Burns, J M; Janzen, D H and Hallwachs, W (2004). Ten species in one: DNA barcoding reveals cryptic species in the neotropical skipper butterfly *Astraptes fulgerator. Proc. of the National Academy of Sciences of the United States of America*. p. 14812-14817.

Herbreteau, V; Jittapalapong, S and Rerkamnuaychoke, W (2011). Protocols for field and laboratory rodent studies. Kasetsart University.

Hood, A S C; Aryawan, A A K; Advento, A D; Purnomo, D; Wahyuningsih, R; Luke, S H; Sudharto, P S; Snaddon, J L; Foster, W A; Caliman, J P; Turner, E C and Mohammad Naim (2019). Understory vegetation in oil palm plantations promotes leopard cat activity, but does not affect rats or rat damage. *Front. For. Glob. Change*, *2*: 51.

Hori, H; Fukutani, T; Nakane, H; Iino, S and Nojyo, Y (2011). Participation of ventral and dorsal tail muscles in bending movements of rat tail. *Anat. Sci. Int.*, *86*: 194-203.

Ikbal, N H M; Bhassu, S; Simarani, K; Uni, S; Chan, C C and Omar, H (2019a). Prevalence and genetic divergence of *Leptospira interrogans* and *Leptospira borgpetersenii* in house rats (*Rattus rattus*) from Peninsular Malaysia. *Asian Pac. J. Trop. Med.*, *12*: 463.

Ikbal, N H M; Pathmanathan, D and Bhassu, S (2019b). Morphometric analysis of craniodental characters of the house rat, *Rattus rattus* (Rodentia: Muridae) in Peninsular Malaysia. *Sains Malays.*, *48*: 2103-2111.

Ikhsan, M; Priyambodo, S; Nurmansyah, A; Hendarjanti, H and Sahari, B (2020). Species diversity, abundance and damaged caused by rats in oil palm plantation in west and central Sulawesi, Indonesia. *Biodiversitas*, *21*: 5632-5639. DOI: 10.13057/biodiv/d211208.

Jentink, F A (1880). On some hitherto undescribed species of *Mus* in the Leyden Museum. *Notes from Leyden Museum*, *2(11)*: 13-19.

Kamarudin, N; Seman, I A and Masri, M M M (2019). Prospects in sustainable control of oil palm pests and diseases through the enhancement of ecosystem services - The way forward. *J. Oil Palm Res.*, *31*: 381-393. DOI: 10.21894/jopr.2019.0030.

Kumar, S; Stecher, G; Li, M; Knyaz, C and Tamura, K (2018). MEGA X: Molecular evolutionary genetics analysis across computing platforms. *Mol. Biol. Evol.*, *35*: 1547.

Kushairi, A; Singh, R and Ong-Abdullah, M (2017). The oil palm industry in Malaysia: Thriving with transformative technologies. *J. Oil Palm Res.*, *29*: 431-439.

Labov, J B; Huck, U W; Vaswani, P and Lisk, R D (1986). Sex ratio manipulation and decreased growth of male offspring of undernourished golden hamsters (*Mesocricetus auratus*). *Behav. Ecol. Sociobiol.*, *18*: 241-249.

Labuschagne, L; Swanepoel, L H; Taylor, P J; Belmain, S R and Keith, M (2016). Are avian predators effective biological control agents for rodent pest management in agricultural systems? *Biol. Control*, *101*: 94-102. DOI: 10.1016/j.biocontrol.2016.07.003.

Lambert, M S; Quy, R J; Smith, R H and Cowan, D P (2008). The effect of habitat management on home-range size and survival of rural Norway rat populations. *J. Appl. Ecol.*, *45*: 1753-1761. DOI: 10.1111/j.1365-2664.2008.01543.x.

Liau, S; Chung, G and Sim, S (1991). Rat species composition and distribution in West Malaysian plantations (with particular reference to oil palm plantations). *Proc. of the 1991 PORIM International Palm Oil Conference – Progress, Prospects and Challenges Towards the 21st Century, Module I Agriculture*. Kuala Lumpur. p. 9-14.

Lim, B L (2015). The field rats and field mouse in Malaysia and Southeast Asia. *Utar Agric. Sci. J.*, *1*: 35-42.

Lupo, K D (2011). A dog is for hunting. *Ethnozooarchaeology: The Present and Past of Human-Animal Relationships* (Albarella, U and Trentacoste, A eds.). Oxbow Books. p. 208.

Madsen, T and Shine, R (1999). Rainfall and rats: Climatically-driven dynamics of a tropical rodent population. *Aust. J. Ecol.*, *24*: 80-89.

Martínez, J J; Millien, V; Simone, I and Priotto, J W (2014). Ecological preference between generalist and specialist rodents: Spatial and environmental correlates of phenotypic variation. *Biol. J. Linn. Soc.*, *112*: 180-203.

Matisoo-Smith, E and Robins, J (2009). Mitochondrial DNA evidence for the spread of Pacific rats through Oceania. *Biol. Invasions*, *11*: 1521-1527. DOI: 10.1007/s10530-008-9404-1.

Mohd-Taib, F S and Ishak, S N (2021). Bait preferences by different small mammal assemblages for effective cage-trapping. *Malaysian J. Sci.*, *40*: 1-15.

MPOC (2020). Annual Report 2019. Malaysian Palm Oil Council (MPOC). Petaling Jaya, Selangor.

MPOC and MPOB (2020). Malaysian Palm Oil Fact Sheets 2020. 66 pp.

Musser, G and Carleton, M (2005). Family Muridae. *Mammal Species of the World: A Taxonomic and Geographic Reference* (Wilson, D E and Reeder, D M eds.). John Hopkins University Press, Baltimore. p. 894-1531.

Nugroho, S S and Santosa, Y (2018). The estimation loss and gain of mammal species diversity due to oil palm plantations: A case study of BPME Estate, Riau, Indonesia. *E3S Web of Conferences*. *EDP Sciences*. p. 42.

Nursyazana, M T; Mohdzain, S N and Jeffery, J (2013). Biodiversity and macroparasitic distribution of the wild rat population of Carey Island, Klang. *Trop. Biomed.*, *30*: 199-210.

Pagès, M; Chaval, Y; Herbreteau, V; Waengsothorn, S; Cosson, J F; Hugot, J P; Morand, S and Michaux, J (2010). Revisiting the taxonomy of the Rattini tribe: A phylogeny-based delimitation of species boundaries. *BMC Evol. Biol.*, *10*: 1-27. DOI: 10.1186/1471-2148-10-184.

Paramasvaran, S; Sn, M Z; Jeffery, J; Selvanesan, S; Hassan, L; Sani, R A; Santhana, R L; Latifah, I; Rahmat, M S and Amal, N M (2013). Distribution and morphological measurements of wild and urban rodents from four habitats in the states of Selangor and Negeri Sembilan, Malaysia. *Malaysian J. Vet. Res.*, *4*: 1-12.

Payne, J; Francis, C M and Phillipps, K (1985). Field guide to the mammals of Borneo. Sabah Society, Kuala Lumpur.

Phua, M H; Chong, C W; Ahmad, A H and Hafidzi, M N (2018). Understanding rat occurrences in oil palm plantation using high-resolution satellite image and GIS data. *Precision Agric.*, *19*: 42-54. DOI: 10.1007/s11119-016-9496-z.

Pratt, N C and Lisk, R D (1989). Effects of social stress during early pregnancy on litter size and sex ratio in the golden hamster (*Mesocricetus auratus*). *Reproduction*, *87*: 763-769.

Priyambodo, S (2003). Integrated Rat Management: Ecological, Economic and Sociocultural Approaches. Penebar Swadaya, Jakarta, Indonesia.

Puan, C L; Goldizen, A W; Zakaria, M and Baxter, G S (2011a). Understanding of relationships between ground cover and rat abundances: An integrative approach for management of the oil palm agroecosystem. *Crop Prot.*, *30*: 1263-1268.

Puan, C L; Goldizen, A W; Zakaria, M; Hafidzi, M N and Baxter, G S (2011b). Relationships among rat numbers, abundance of oil palm fruit and damage levels to fruit in an oil palm plantation. *Integr. Zool.*, *6*: 130-139.

Puan, C L; Goldizen, A W; Zakaria, M; Hafiz, M N and Baxter, G S (2011c). Absence of differential predation on rats by Malaysian barn owls in oil palm plantations. *J. Raptor Res.*, *45*: 71-78.

Pulgarín-R, P C; Olivera-Angel, M; Ortíz, L; Nanclares, D; Velásquez-Restrepo, S and Díaz-Nieto, J F (2021). DNA barcodes of birds from Northern Colombia. *Biodivers. Data J.*, *9*: e64842.

Rizuan, Z A C M and Noor Hisham, H (2015). Composition and distribution of small rodents in FGV's oil palm regions in Sabah and Sarawak. Paper presented at the PIPOC 2015 International Palm Oil Congress. MPOB, Selangor.

Robins, J J H; Hingston, M; Matisoo-Smith, E and Ross, H A (2007). Identifying *Rattus* species using mitochondrial DNA. *Mol. Ecol. Notes*, *7*: 717-729. DOI: 10.1111/j.1471-8286.2007.01752.x.

Rosenfeld, C S; Grimm, K M; Livingston, K A; Brokman, A M; Lamberson, W E and Roberts, R M (2003). Striking variation in the sex ratio of pups born to mice according to whether maternal diet is high in fat or carbohydrate. *Proc. Natl. Acad. Sci., 100*: 4628-4632.

Rugh, R (1968). The mouse. Its reproduction and development. Burgess Publishing Co., Minneapolis.

Saarani, M A F; Abd Wahab, M F; Nasir, M H; Saad, N M and Omar, H (2021). The non-volant terrestrial small mammals at Ulu Muda Forest Reserve, Kedah, Malaysia. *J. Trop. Biol. Conserv.*, *18*: 173-184.

Sadleir, R M; Casperson, K D and Harling, J (1973). Intake and requirements of energy and protein for the breeding of wild deermice, *Peromyscus maniculatus*. *J. Reprod. Fertil. Suppl.*, *19*: 237-252.

Santosa, Y and Rejeki, S (2019). Impact of oil palm plantation on mammal and herpetofauna species diversity. *IOP Conf. Ser.: Earth Environ. Sci.*, *336*: 12027.

Saravanan, K; Idrus, M A and Prakash, A (2020). Control of rat damage in oil palm plantation using local hunting dogs - IOI Kahang estate experience. *The Planters, 96(1132)*: 479-485.

Shevade, V S and Loboda, T V (2019). Oil palm plantations in Peninsular Malaysia: Determinants and constraints on expansion. *PLoS ONE*, *14*: e0210628.

Singleton, G R (2008). *Philippine Rats: Ecology and Management*. PhilRice, Los Banos (Philippines). 215 pp.

Stryjek, R; Mioduszewska, B; Spaltabaka-Gędek, E and Juszczak, G R (2018). Wild Norway rats do not avoid predator scents when collecting food in a familiar habitat: A field study. *Sci. Rep.*, *8*: 1-11.

Takahashi, A and Miczek, K A (2013). Neurogenetics of aggressive behavior: Studies in rodents. *Neuroscience of Aggression*. *Current Topics in Behavioral Neurosciences, Vol. 17* (Miczek, K and Meyer-Lindenberg, A eds.). Springer, Berlin. p. 3-44.

Taylor, K D and Green, M G (1976). The influence of rainfall on diet and reproduction in four African rodent species. *J. Zool.*, *180*: 367-389.

Tingga, R C T; Anwarali, F A; Ridwan, A R M; Senawi, J and Abdullah, M T (2012). Small mammals from Kuala Atok, Taman Negara Pahang, Malaysia. *Sains Malays.*, *41*: 659-669.

Tri Kwatrina, R; Santosa, Y; Bismark, M and Santoso, N (2018). The impacts of oil palm plantation establishment on the habitat type, species diversity, and feeding guild of mammals and herpetofauna. *Biodiversitas*, *19*: 2085-4722.

Tristiani, H and Murakami, O (2003). Rates of population increase in the ricefield rat (*Rattus argentiventer*) as a function of food supply: An enclosure study in Jatisari, West Java. *J. Zool.*, *259*: 239-244.

Tristiani, H; Murakami, O and Kuno, E (2000). Rice plant damage distribution and home range distribution of the ricefield rat *Rattus argentiventer* (Rodentia: Muridae). *Belgian J. Zool.*, *130*: 83-92.

Tristiani, H; Murakami, O and Watanabe, H (2003). Ranging and nesting behavior of the ricefield rat *Rattus argentiventer* (Rodentia: Muridae) in West Java, Indonesia. *J. Mammal.*, *84*: 1228-1236. DOI: 10.1644/BEM-024.

van den Brink, N W; Elliott, J E; Shore, R F; Rattner, B A; Brink, N W van den; Elliott, J E; Shore, R F and Rattner, B A (2018). Anticoagulant rodenticides and wildlife: Concluding remarks. *Anticoagulant Rodenticides and Wildlife*. Springer. p. 379-386.

Ventura, J and Fuster, M J L (2000). Morphometric analysis of the black rat, *Rattus rattus*, from Congreso Island (Chafarinas Archipielago, Spain). *Orsis N*, *15*: 91-102.

Wada, S; Oishi, M and Yamada, T K (2003). A newly discovered species of living baleen whale. *Nature*, *426*: 278-281.

Wolff, J O (2007). Social biology of rodents. *Integr. Zool.*, *2*: 193-204.

Wood, B J (1976). Vertebrate pests. *Oil Palm Research*. Elsevier Press, Amsterdam. p. 395-418.

Wood, B J and Fee, C G (2003). A critical review of the development of rat control in Malaysian agriculture since the 1960s. *Crop Prot.*, *22*: 445-461.

Xu, Y; Yu, L; Li, W; Ciais, P; Cheng, Y and Gong, P (2020). Annual oil palm plantation maps in Malaysia and Indonesia from 2001 to 2016. *Earth Syst. Sci. Data*, *12*: 847-867.

Yasuma, S and Andau, M (2000). Mammals of Sabah: Field guide and identification. Japan, International Cooperation Agency (JICA), Malaysia, Sabah Wildlife Department.

Zainal Abidin, C M R; Mohd Noor, H; Hamid, N H; Ravindran, S; Puan, C L; Kasim, A and Salim, H (2021). Comparison of effectiveness of introduced barn owls, *Tyto alba javanica*, and rodenticide treatments on rat control in oil palm plantations. *J. Pest Sci.*, *95*: 1009-1022.

Zippin, C (1958). The removal method of population estimation. *J. Wildl. Manage.*, *22*: 82-90.

Journal of Oil Palm Research Vol. 35 (1) March 2023 p. 75-85
DOI: https://doi.org/10.21894/jopr.2022.0027

A COMPARATIVE STUDY OF OIL PALM FRONDS TORREFACTION UNDER FLUE GAS AND NITROGEN ATMOSPHERES

PREMCHAND[1]; MASAHARU KOMIYAMA[1,2,3]*; AQSHA[4] and YOSHIMITSU UEMURA[2]

ABSTRACT

Oil palm fronds' (OPF) leaves and stems were torrefied under flue gas (produced by flameless burning of wood pellets) and under inert gas (N_2) atmospheres using a fixed-bed vertical tubular reactor. The flue gas consisted of N_2 (73.7-80.2 vol%), carbon dioxide (CO_2) (12.6-16.5 vol%), oxygen (O_2) (3.7-4.6 vol%), carbon monoxide (CO) (3.7-6.0 vol%) and trace amounts of hydrogen (H_2) (up to 1.15 vol%). Detailed analyses of feed and torrefied products by proximate and ultimate analyses, thermogravimetry and infrared spectroscopy indicated that in the temperature range between 200°C and 300°C, flue gas torrefaction showed enhanced oxygen removal compared to inert gas torrefaction from both feeds, resulting in solid biomass with lower oxygen content and higher energy density. The enhanced oxygen removal under flue gas atmosphere in this temperature range was prominent for hemicellulose/cellulose components and not for lignin. The effect was attributed to O_2 present in the flue gas, accelerating the decomposition of oxygen-bearing functional groups of hemicellulose/cellulose into water, CO_2 and CO. Flue gas atmosphere did not affect the volatilisation of biomass in the form of larger organic compounds such as acetic acid, furfural and phenol within the temperature range examined here.

Keywords: calorific value ratio, energy yield, flue gas atmosphere, role of lignin, torrefaction.

Received: 1 September 2021; **Accepted:** 22 March 2022; **Published online:** 27 May 2022.

INTRODUCTION

Malaysia produces a huge amount of solid waste biomass from its oil palm industry. Many studies have been conducted on the production of biofuels via thermochemical treatments from oil palm biomasses generated at milling sites, such as empty fruit bunches (EFB), palm kernel shells (PKS) and mesocarp fibres, using torrefaction (Na *et al.*, 2013; Nyakuma *et al.*, 2021; Sabil *et al.*, 2013), pyrolysis (Asadullah *et al.*, 2013; Chantanumat *et al.*, 2022) and gasification (Iovane *et al.*, 2013). However, less consideration has been given to oil palm frond (OPF) generated at plantation sites even though OPF is the main oil palm residue which makes up to 70% of total waste from the oil palm industry (Tan *et al.*, 2016) and is available throughout the year during the pruning and harvesting of the fresh fruit bunches (FFB) (Aljuboori, 2013). Despite the fact that both OPT and OPF make up the majority of the biomass waste, the OPF are either used to feed the livestock or as a mulch, *i.e.*, being left on the plantation field to improve soil properties after the pruning process, while the trunks are usually left to decay in the plantation (Kaniapan *et al.*, 2021;

[1] Chemical Engineering Department, Universiti Teknologi PETRONAS, 32610 Seri Iskandar, Perak, Malaysia.

[2] HICoE-Center for Biofuel and Biochemical Research, Institute of Self-Sustainable Building, Universiti Teknologi PETRONAS, 32610 Seri Iskandar, Perak, Malaysia.

[3] Clean Energy Research Center, University of Yamanashi, 4-3-11 Takeda, Kofu, 400-8511 Japan.

[4] Department of Chemical Engineering, Faculty of Industrial Technology, Institut Teknologi Bandung, Jl. Ganesa No.10, Bandung, Jawa Barat, 40132 Indonesia.

* *Corresponding author e-mail: masaharu.komiyama@utp.edu.my*

Poh *et al.*, 2020). This practice offers limited benefits to the oil palm industry, as OPF is lignocellulosic biomass and has a huge potential to be used as a renewable energy source (Shuit *et al.*, 2009).

To utilise lignocellulosic biomass efficiently for biofuel production, some of its drawbacks including high moisture, high volatile matter and high oxygen contents, low energy density and hydrophilic nature must be addressed (Kanaujia *et al.*, 2014; Tabakaev *et al.*, 2017). A number of thermochemical pre-treatment techniques exist to overcome these limitations and convert raw biomass into denser energy fuels with improved properties (Zhang and Zhang, 2019). Torrefaction, a slow heating process of lignocellulosic biomass at lower temperatures (200°C-300°C) under inert atmosphere, has been presented as a promising technology to upgrade biomass to solid fuel with lower O/C ratio (Brojolall and Surroop, 2022; Prins *et al.*, 2006). Torrefaction reduces the moisture content and lowers organic volatile matters and oxygen contents within the biomass resulting in the increase of carbon content and energy density of the biomass with improved grind ability and hydrophobicity (Agar *et al.*, 2012; Ibrahim *et al.*, 2013). However, the concerns of large-scale use of inert gas in the process have drawn researchers' attention to find an effective substitute. The concept of utilising industrial flue gases as torrefaction atmosphere can be an efficient way to upscale this process. This would not only replace the need of pure nitrogen (N_2) gas in the torrefaction but also would provide thermal energy necessary for torrefaction process. In light of this, several studies have been conducted for torrefaction under non-inert atmospheres [air, oxygen (O_2), carbon dioxide (CO_2) and their mixtures] and the effects of these gases on torrefaction performance have been reported (Eseltine *et al.*, 2013; Li *et al.*, 2016; 2021; Rousset *et al.*, 2012; Tran *et al.*, 2016; Uemura *et al.*, 2013). For instance, the addition of O_2 (3%-15%) in N_2 resulted in the decrease of both mass yield and energy yield (Uemura *et al.*, 2013). Torrefaction of corncob found that pure CO_2 atmosphere gives higher solid yield and better energy yield compared to pure N_2 atmosphere at 260°C (Li *et al.*, 2018).

Along with N_2, CO_2 and O_2, there are some other gases also present in flue gases in minor quantities such as carbon monoxide (CO), hydrogen (H_2) and water vapour and thus, the previous studies about utilisation of a mixture of N_2, O_2 and/or CO_2 from the cylinders may not show the same effect of real flue gas on torrefaction. In the near past, our group carried out torrefaction of EFB and OPF in the atmosphere of real combustion gas generated by burning wood pellets with the findings that flue gases from the industrial boilers can be used in the torrefaction reactor without any significant problem (Premchand *et al.*, 2020; Uemura *et al.*, 2017).

In the present study, torrefaction of OPF has been carried out under flue gas and inert (N_2) gas atmospheres in the temperature range between 200°C and 300°C. Oil palm frond was separated into frond leaves (OPFL) and frond stems (OPFS) to compare the effect of proximate compositional differences. The research gaps present are twofold: 1) torrefaction characteristics of OPF have not been well known, and 2) the mechanism of flue gas torrefaction has not been well understood for any lignocellulosic feed. The present research tried to present data for gap and tried to present new insight into possible flue gas torrefaction mechanism for gap. Findings from this research would aid in utilising a huge amount of OPF waste through the economic flue-gas torrefaction process.

MATERIALS AND METHODS

Sample Preparation

OPF were collected from an oil palm plantation in Bota, Perak, Malaysia. The fronds were washed and separated into two portions; one was the stem part (OPFS) and the other was the leaf part (OPFL). These two portions have widely differed proximate, ultimate and ash compositions to each other as listed in *Table 1*, which are expected to affect their torrefaction behaviour. Respective samples were dried at 105°C before their characterisations and torrefaction experiments.

Torrefaction Process

The reactor setup and the details of torrefaction procedure are found elsewhere (Uemura *et al.*, 2017). Briefly, the torrefaction reactor consisted of two stainless steel vertical chambers: One chamber for wood pellets combustion and the other for conducting torrefaction experiments. Torrefaction chamber was equipped with an electric heater and four thermocouples installed within the reactor at different depths of the biomass bed. Two glass condensers dipped into the ice water chiller were connected in series at the outlet of the torrefaction chamber for collecting condensable liquid products.

For inert gas torrefaction, N_2 gas was directly introduced to the torrefaction reactor from a cylinder. For flue gas torrefaction, first the wood chips placed in the combustion chamber were ignited and burnt until they reached flameless char combustion stage. Then, the flue gas from the combustion chamber was introduced into the torrefaction reactor through an air-cooled stainless-steel pipe. This way it is assured that only non-condensable gases (N_2, O_2, CO_2, CO and H_2) from the combustion chamber would enter the torrefaction chamber. Flue gas compositions at

TABLE 1. PROXIMATE, ULTIMATE, CALORIFIC VALUE, AND ASH COMPOSITIONS OF FEEDSTOCKS

Item	OPFL (wt%)	OPFS (wt%)
Proximate composition		
Moisture (wb)	6.86	5.01
Ash (db)	3.89	2.79
Volatile matter (db)	81.94	85.49
Fixed carbon (db)	14.17	11.72
Hemicellulose/cellulose (Abnisa *et al.*, 2013; Hashim *et al.*, 2011)	55	73
Lignin (Abnisa *et al.*, 2013; Hashim *et al.*, 2011)	26-27	20-22
Ultimate composition (db)		
Total carbon	47.65	44.02
Hydrogen	6.96	5.61
Nitrogen	1.68	0.52
Oxygen	39.82	47.06
Calorific value (MJ/kg)	18.02	17.39
Ash composition (db)		
Calcium	58.3	74.3
Potassium	8.8	8.9
Silicon	22.0	5.2
Magnesium	2.1	4.0
Sulphur	1.8	2.8
Phosphorus	4.1	2.4
Chlorine	0.7	0.9
Iron	0.7	0.5
Manganese	1.0	0.3

Note: wb - wet basis; db - dry basis.

the inlet of the torrefaction chamber are listed in *Table 2*, along with the outlet compositions of non-condensable product gases, for all the torrefaction runs performed here. All values presented in *Table 2* are the average over the 30-min torrefaction period (time-integrated), the procedure of which was justified since the gas compositions during the torrefaction was quite stable. The temperature of the torrefaction chamber was raised from room temperature with a heating rate of 4°C/min up to the desired temperature and kept at the temperature for 30 min. The flow rate of N_2 or flue gas to torrefaction reactor was kept at 4 L/min or 5 L/min by a mass flow controller. The temperatures of

TABLE 2. COMPOSITIONS (VOL %) OF INLET AND OUTLET GASES FROM TORREFACTION OF OPFL AND OPFS

		N_2 atmosphere						Flue gas atmosphere					
		200°C		250°C		300°C		200°C		250°C		300°C	
		Inlet	Outlet	Inlet	Outlet	Inlet	Outlet	Inlet	Outlet	Inlet	Outlet	Inlet	Outlet
OPFL	N_2	100.00	98.32	100.00	93.32	100.00	93.53	75.79	74.48	80.21	77.77	78.97	70.63
	H_2	-	0.00	-	0.00	-	0.28	1.01	0.86	0.32	0.28	1.08	1.78
	O_2	-	0.43	-	0.42	-	0.49	3.18	2.73	4.56	2.51	4.38	0.19
	CO	-	0.00	-	0.00	-	0.67	3.77	4.42	1.69	3.78	2.93	9.23
	CO_2	-	1.25	-	6.26	-	5.02	16.25	17.07	13.21	15.66	12.63	18.18
OPFS	N_2	100.00	96.20	100.00	91.27	100.00	84.53	75.51	74.07	79.18	68.79	78.28	63.56
	H_2	-	0.00	-	0.00	-	0.78	1.15	0.64	0.38	0.31	0.82	0.31
	O_2	-	0.54	-	0.48	-	1.05	2.63	2.09	2.94	0.37	4.62	0.15
	CO	-	0.38	-	0.00	-	3.46	4.22	6.02	2.94	6.50	2.62	7.94
	CO_2	-	2.88	-	8.24	-	10.18	16.49	18.99	14.56	24.03	13.66	28.03

torrefaction chamber were closely monitored using four thermocouples inserted to the various depth of the chamber. While there were certain variations of chamber temperature depending on the position, each thermocouple reading was quite stable during the torrefaction. No signs of hot spot appearance, which would indicate local combustion of samples due to O_2 in the flue gas, were observed.

Product Characterisation and Data Processing

The feed and solid products were characterised by proximate (following respective ASTM procedures), ultimate (Series II CHNS/O Analyser 2400, Perkin Elmer) and calorific value (Bomb Calorimeter Model C200, IKA Werke) analyses. Ash compositions were analysed by using X-ray fluorescence analyser (Model S8 Tiger). Surface functional groups on the feed and torrefied biomass were observed by using an Fourier transform infrared spectroscopy (FT-IR) spectrophotometer (Nicolet iS10). Thermogravimetry was carried out by using a thermogravimetric analyser (TGA) (TGA Q50, TA instruments). The water content in liquid bio-oil collected at the outlet of the torrefaction chamber was determined through a volumetric Karl Fischer titrator (Model V30) and the organic compounds in bio-oil were identified through a gas chromatography-mass spectrometer (Agilent GC-MSodel 7890A) with a column HP 5MS. The compositions of inlet flue gas and non-condensable gases from the torrefaction process were analysed by using a gas chromatography with a thermal conductivity detector (Shimadzu GC-8A) with column packings of MS-5A and Porapak Q. The liquid yield (Y_l), solid yield(Y_m), calorific value ratio (CV_{ratio}), energy yield (Y_E), CO_2 yield (Y_{CO_2}) and CO yield (Y_{CO}) were calculated by using the following Equations:

$$Y_l\,(\text{wt\%}) = \frac{m_l}{m_i} \times 100 \quad (1)$$

$$Y_m\,(\text{wt\%}) = \frac{m_f}{m_i} \times 100 \quad (2)$$

$$CV_{ratio} = \frac{CV_f}{CV_i} \times 100 \quad (3)$$

$$Y_E = Y_m \times CV_{ratio} \quad (4)$$

$$Y_{CO_2} = Y_g \times \textit{mass fraction of } CO_2 \textit{ in the inlet or outlet gas} \quad (5)$$

$$Y_{CO} = Y_g \times \textit{mass fraction of CO in the inlet or outlet gas} \quad (6)$$

where m indicates the mass of biomass and subscripts i and f denote the initial stage (before torrefaction) and the final stage (after torrefaction), respectively.

RESULTS AND DISCUSSION

Effect of Flue Gas on Torrefaction Products

Figure 1 compares the torrefaction product (gas, liquid and solid) yields in weight percentages (wt%). Overall, it shows that flue gas torrefaction (right half of the figure) gives higher amounts of liquid (bio-oil) and gaseous products combined at the cost of solid yields compared to inert-gas torrefaction (left half of the figure) at all the three temperatures examined here. Within each torrefaction atmosphere, higher temperature produces a higher amount of gas and liquid combined at the cost of solid yields. Obviously, higher temperature increases the severity of torrefaction, and the flue gas atmosphere enhances the severity as compared to the N_2 atmosphere. This trend is consistent with the previously reported observations (Onsree *et al.*, 2019; Uemura *et al.*, 2017).

First, the details of solid product which is the main objective of biomass torrefaction are examined. The effect of torrefaction atmosphere and temperature on energy yield and calorific value ratio (CV_{ratio}, a ratio of CV of each solid product to the CV of respective biomass feed, used here only for solid product) from torrefaction of OPFL and OPFS are shown in *Figure 2*. Calorific value ratio (CV_{ratio}) increases as temperature rises from 200°C to 300°C for both the biomass feed and for both the torrefaction atmospheres. As discussed above, the rise in temperature increased the severity of torrefaction which led to extensive devolatilisation of lignocellulosic biomass resulting in increased carbon content and ultimately increased the product CV (Sabil *et al.*, 2013; Uemura *et al.*, 2017). Since flue gas enhances the severity of torrefaction, as seen in *Figure 1*, CV_{ratio} for torrefied OPFL and OPFS in flue gas are always higher than that in N_2 torrefaction at all the temperatures examined here and these findings appear to be consistent with the literature (Uemura *et al.*, 2017).

The major reason for this CV_{ratio} increase is found in the proximate and ultimate compositions of the product solids listed in *Table 3*. With increasing torrefaction severity (temperature and atmosphere), fixed carbon (FC) and total carbon (C) increased whereas volatile matter (VM) and oxygen (O) contents decreased, and so did the O/C ratio. Apparently, the CV increase found in *Figure 2* is brought about by the decrease of oxygen content, with concomitant relative increase of carbon content, due to the severer torrefaction conditions (temperature and atmosphere). It is stressed that the flue gas always enhanced these tendencies compared to inert gas, N_2, at similar torrefaction temperatures. This leads to the observation that the effect of flue gas atmosphere is to volatilise more of the oxygen containing entities in the feed biomass than N_2 atmosphere.

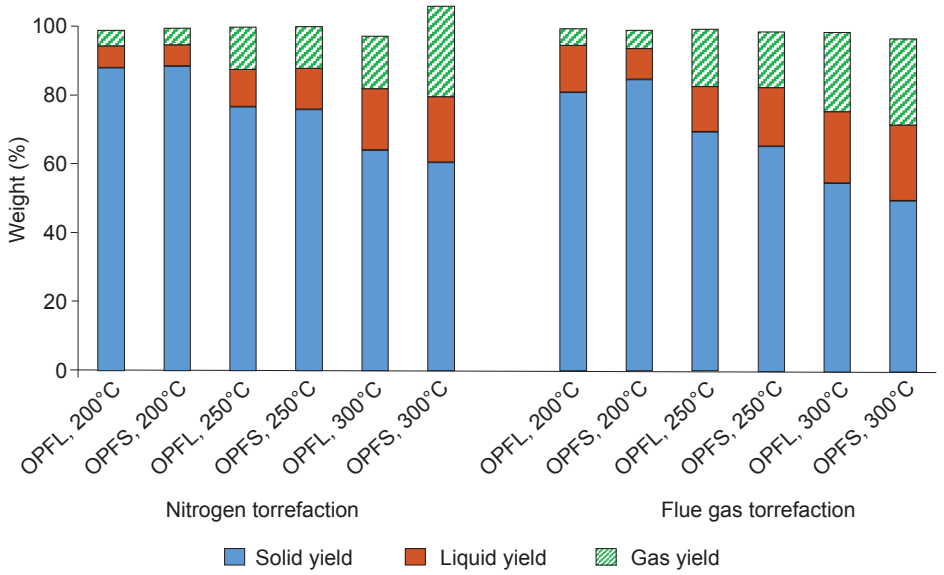


Figure 1. Yields (wt%) of solid, liquid and gas from the torrefaction of OPFL and OPFS under N_2 (left columns) and flue gas (right columns).

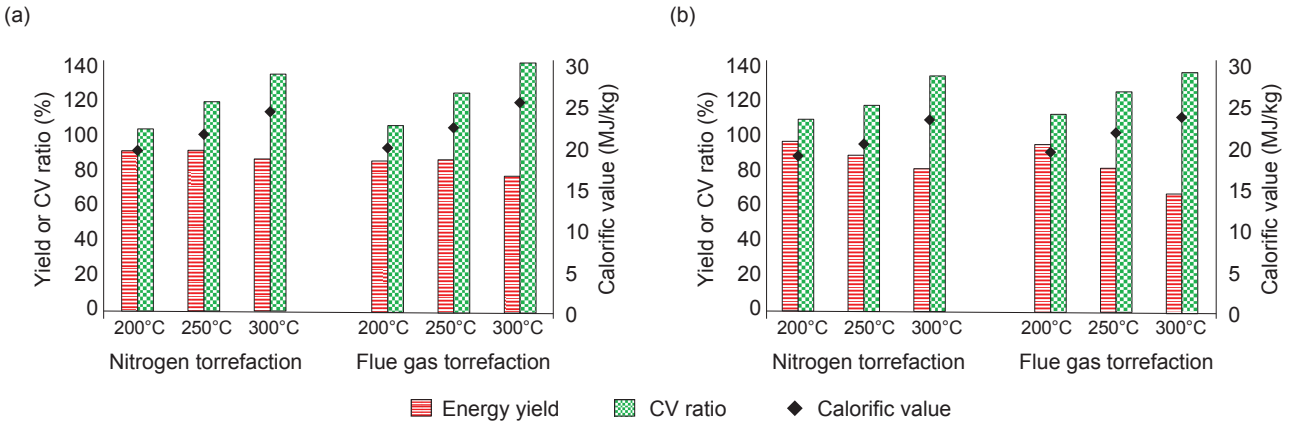


Figure 2. Calorific value, energy yield and CV ratio from the torrefaction of (a) OPFL and (b) OPFS.

TABLE 3. PROXIMATE AND ULTIMATE ANALYSES (wt%) OF RAW AND TORREFIED OPFL AND OPFS SOLIDS

			Proximate analysis				Ultimate analysis (db)					
			MC (wb)	VM (db)	Ash (db)	FC (db)	C	H	N	O	H/C	O/C
N_2 torrefaction	OPFL	200°C	1.03	77.93	5.18	16.89	50.64	5.90	1.45	36.83	0.117	0.727
		250°C	0.74	74.47	5.29	20.24	52.89	4.71	1.89	35.22	0.089	0.666
		300°C	0.64	68.28	6.82	24.90	56.87	3.41	1.95	30.95	0.060	0.544
	OPFS	200°C	0.72	80.02	3.46	16.52	45.67	4.58	0.35	45.93	0.100	1.006
		250°C	0.78	77.14	3.18	19.68	48.76	4.89	1.78	41.40	0.100	0.849
		300°C	0.77	69.60	4.27	26.13	52.51	3.86	1.71	37.64	0.074	0.717
Flue gas torrefaction	OPFL	200°C	0.72	75.75	5.31	18.94	51.74	5.87	1.78	35.30	0.113	0.682
		250°C	0.53	72.38	5.41	22.21	54.02	4.08	1.92	34.58	0.076	0.640
		300°C	0.59	66.36	7.96	25.68	59.68	3.06	1.98	27.32	0.051	0.458
	OPFS	200°C	0.64	78.41	4.38	17.21	47.59	3.74	0.22	44.06	0.079	0.926
		250°C	0.89	71.87	3.29	24.84	51.50	3.98	1.82	39.41	0.077	0.765
		300°C	0.70	67.94	4.61	27.45	55.26	3.34	1.85	34.94	0.060	0.632

Note: MC - moisture content; VM - volatile matter; FC - fixed carbon; wb - wet basis; db - dry basis.

Details of the volatilised matter, *viz.*, gas and liquid products, corroborate this observation. *Table 2* lists as-measured inlet and outlet torrefaction gas compositions. It is found in the table that the major gaseous products from torrefaction are CO_2 followed by CO (note that in this table inlet CO_2 and CO are not subtracted from the outlet CO_2 and CO). Therefore, in *Figure 3* net yields of CO_2 and CO from each torrefaction experiment is compared, along with the yields of water and organic matter collected as liquid products. Generally (with a few minor exceptions), higher temperature resulted in higher water, organic matter, CO_2, and CO yields and again, flue gas atmosphere enhanced this trend in terms of water, CO_2, and CO yields. Note that the yield of organic matter (calculated by subtracting the water weight percentage from bio-oil in total) did not change appreciably when torrefaction atmosphere is changed from inert N_2 to flue gas. Major organic matters in the bio-oil found by GC-MS analysis were acetic acid, followed by furfural, phenol and 1-hydroxy-2-propanone and these findings are consistent with previous research for the torrefaction of different biomass under inert and non-inert atmospheres (Chai *et al.*, 2021; Uemura *et al.*, 2017). Those data lead to the conclusion that flue gas atmosphere enhances the biomass volatilisation into simpler oxygen-bearing molecules such as water, CO_2, and CO but not into larger and more complex liquid organic molecules.

The Influence of O_2 and CO_2 in Flue Gas Torrefaction

Detailed product analysis in the previous section indicated that the present torrefaction eliminates oxygen from the feed, and the tendency is prominent with flue gas torrefaction compared to inert gas (N_2) torrefaction. In order to identify the components affected by flue gas torrefaction, FT-IR spectroscopy was performed on raw and torrefied solids and the obtained spectra are compared in *Figure 4a* and *4b* for OPFL and OPFS, respectively. The peak assignment was carried out following the

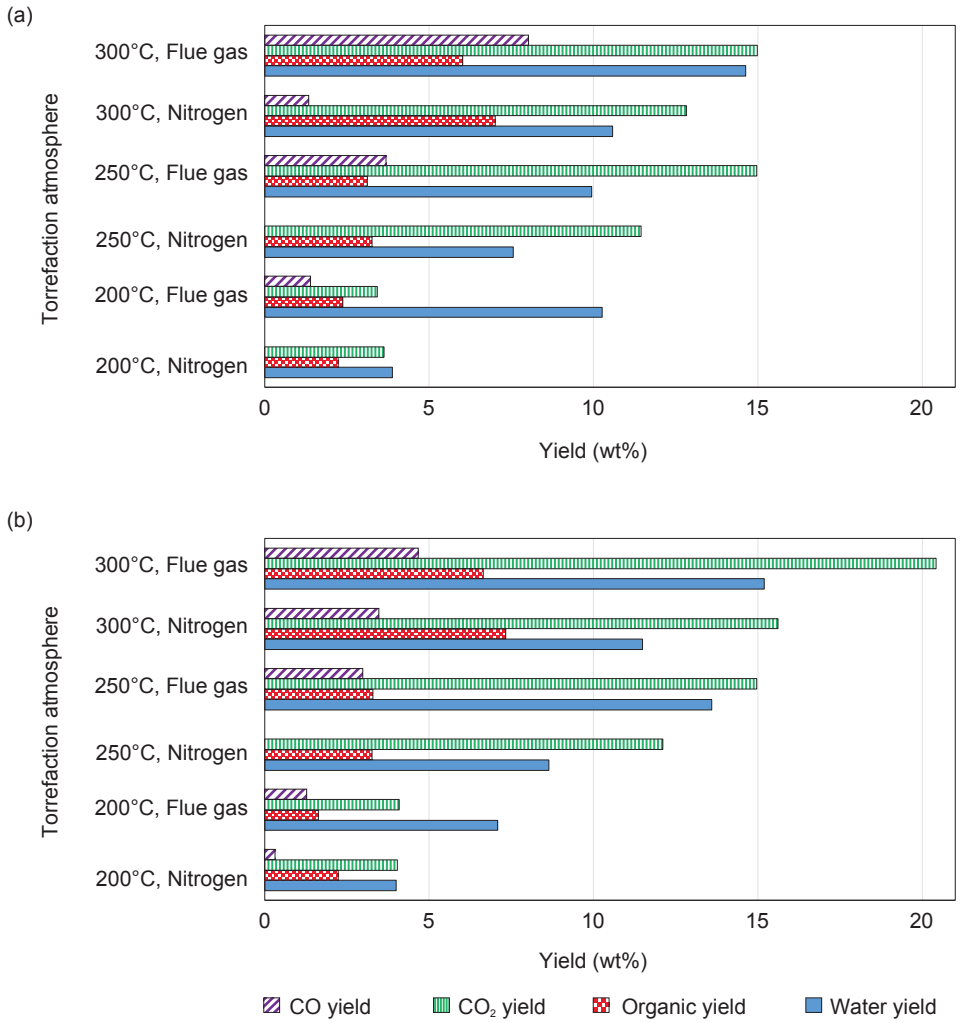


Figure 3. Yields (wt%) of water and organic compounds in bio-oil and CO_2 and CO in gaseous product from the torrefaction of (a) OPFL and (b) OPFS. Inlet CO and CO_2 have been subtracted for the respective yield calculations in the case of flue gas torrefaction.

references (Bilgic *et al.*, 2016; Hon and Shiraishi, 2001; Lv *et al.*, 2015; Matsunaga *et al.*, 1999) as listed in *Table 4*, along with their disappearance trends due to torrefaction process (last two columns).

The IR spectra of raw OPFL and OPFS (spectrum a in *Figure 4a* and *4b* consist of 13 peaks: 8 from hemicellulose/cellulose (α, β, χ, η, φ, κ, λ and μ) and five from lignin (δ, ε, ϕ, γ and ι). It is noted that many of the major peaks identified here (α, δ, ϕ, κ, λ and μ) are related to O-bearing functional groups. The most visible peak from the hemicellulose/cellulose group is C-OH in glucans or other unit sugars, which is the origin of the two major peaks α and μ as found in *Figure 4*. Their intensities decreased in torrefied samples because of dehydration, one of the major reactions in torrefaction. Similar decrease was reported by previous studies (Lv *et al.*, 2015). All other middle to low intensity peaks lost their intensities in comparison with the raw samples in a similar manner.

In addition to this major general trend, scrutiny of the IR spectra found the sub-trend of intensity losses between the two atmospheres (*Table 4*, last two columns) that can be classified into two types: Sub-trend A indicates peak intensity loss with temperature irrespective of the torrefaction atmosphere, and sub-trend B indicates peak intensity loss with temperature with apparent effect of flue gas.

Close examination of those two peaks intensity sub-trends in *Figure 4* and their breakdown listed in *Table 4* (last two columns) provides two observations: (1) all the IR peaks affected by the torrefaction atmosphere difference, *viz.*, sub-trend B, belong to hemicellulose/cellulose but not to lignin, and (2) OPFL shows very weak effect (if any) of torrefaction atmosphere compared to OPFS, as almost all of OPFL infrared peaks belong to sub-trend A. The first observation apparently indicates that flue gas as a torrefaction atmosphere enhances

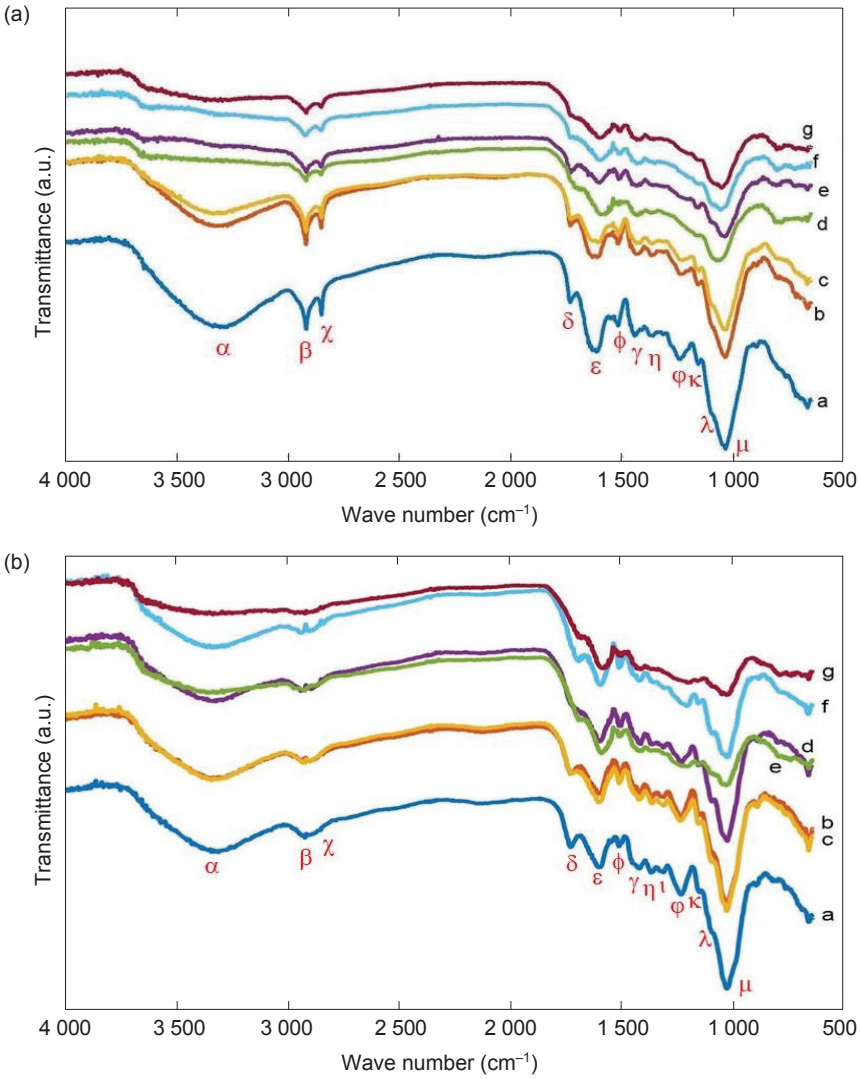


Figure 4. FT-IR spectra of OPFL (A) and OPFS (B): (a) raw, (b) torrefied under N_2 at 200°C, (c) torrefied under flue gas at 200°C, (d) torrefied under N_2 at 250°C, (e) torrefied under flue gas at 250°C, (f) torrefied under N_2 at 300°C and (g) torrefied under flue gas at 300°C. For peak assignments, see Table 4.

TABLE 4. FT-IR SPECTRA OF RAW AND TORREFIED OPFL AND OPFS

Code	Wave number (cm^{-1})		Assignment	Component*	Sub-trend**	
	OPFL	OPFS			OPFL	OPFS
α	3 316	3 316	OH stretching	HC and C	B	B
β	2 917	2 936	CH2 stretching	HC and C	A	B
χ	2 853	2 899	CH2 symmetric stretching	HC and C	A	B
δ	1 737	1 735	C=O stretch	L	A	A
ε	1 623	1 603	Aromatic skeletal	L	A	A
ϕ	1 529	1 518	Aromatic skeletal vibration	L	A	Not clear
γ	1 449	1 426	Aromatic skeletal *etc.*	L	A	A
η	1 375	1 371	CH bending	HC and C	A	B
ι	Not detected	1 320	S-ring plus G-ring condensed	L	Not detected	Not clear
φ	1 248	1 239	CH2 wagging, CH and OH deformation	HC	A	B
κ	1 167	1 162	Anti-symmetric stretching of C-O-C glycosidic linkages	HC and C	A	B
λ	1 101	1 110	CO (of COH) stretching	HC and C	A	B
μ	1 046	1 037	CO (of COH) stretching	HC and C	A	B

Note: * HC - hemicellulose; C - cellulose; L - lignin.

** Sub-trend A: peak intensity loss with temperature irrespective of the torrefaction atmosphere, sub-trend B: peak intensity loss with temperature with apparent effect of flue gas.

hemicellulose/cellulose degradation but not lignin. The second observation, then, may serve as supporting evidence of the first observation since OPFL composition is known to have much higher lignin content than OPFS (*Table 1*) (Abnisa *et al.*, 2013; Hashim *et al.*, 2011). A direct consequence of these observations is that, since lignin may play a role as a protector of hemicellulose and cellulose from thermal degradation and external chemical attack during torrefaction (Financie *et al.*, 2016; Wertz *et al.*, 2010), biomass with a higher amount of lignin content would be more tolerant to the combustion gas torrefaction. This conjecture would be natural if we recall that lignin is situated in a way to cover hemicellulose/cellulose, and if flue gas is to attack hemicellulose/cellulose it has to be done on the points where hemicellulose/cellulose is exposed or thinly covered by lignin through which flue gas penetrates to attack hemicellulose/cellulose.

The next question that may arise in the present study would be; which extra component in flue gas (mostly CO_2 and O_2, cf. *Table 2*) compared to inert atmosphere would be the cause of these flue gas torrefaction characteristics? There exist a few studies on the effect of pure CO_2 atmosphere torrefaction compared to pure N_2 atmosphere torrefaction, with mixed conclusions (Eseltine *et al.*, 2013; Howell *et al.*, 2019; Li *et al.*, 2018; Thanapal *et al.*, 2014). Eseltine *et al.* (2013) and Thanapal *et al.* (2014) compared the torrefaction of two different woody biomasses (Mesquite and Juniper) under pure N_2 and pure CO_2 atmospheres using TGA. By holding the samples at various torrefaction temperatures between 200°C and 300°C for 1 hr duration, they found that pure CO_2 atmosphere gives higher weight loss for both the samples above 240°C. Above 280°C, the weight loss difference between the two atmospheres was 3.8%-4.8% for both samples (Eseltine *et al.*, 2013). Energy retention values obtained from batch torrefaction experiments also followed similar trend. With a larger amount of batch torrefaction, however, the two atmospheres showed a difference only after 280°C for Mesquite and after 300°C for Juniper (Thanapal *et al.*, 2014). On the contrary, a study on the corncob torrefaction (Li *et al.*, 2018) reported that both pure N_2 and pure CO_2 torrefaction at 220°C resulted in the same solid yield, while at 260°C, CO_2 torrefaction showed 10.7% higher solid yield than N_2 torrefaction. Nevertheless, energy yield was better with pure CO_2 torrefaction above 260°C. This may point to the possibility that the CO_2 effect on torrefaction maybe feed dependent. More recently, Howell *et al.* (2019) reported Miscanthus torrefaction in pure N_2 and pure CO_2 using gas specific TGA calibration. They found mass yield to be independent of torrefaction atmosphere, and so is the heating value obtained from batch torrefied samples.

On the other hand, one of the present authors studied the effects of O_2 and CO_2 addition (up to 15 vol% each) in N_2 atmosphere on PKS torrefaction (Uemura *et al.*, 2013; 2015). It was found that the effects of O_2 and CO_2 addition (separately) to N_2 atmosphere became apparent at 300°C. The

increment of mass loss due to O_2 or CO_2 addition compared to pure N_2 torrefaction amounted to a few to 15% and O_2 addition removed more differential mass, 1.5 to 2.0 times as much, compared to CO_2 addition (Uemura *et al.*, 2015).

In order to examine the effect of CO_2 on the present torrefaction, TGA under pure N_2 and under simulated flue gas (20 vol% CO_2 + N_2) were compared for the present two samples. Due to the equipment limitation, no O_2 was able to be added in the simulated flue gas. The results are shown in *Figure 5*. Firstly, it is noted in the TGA profiles that OPFL experiences less weight loss compared to OPFS in the almost entire temperature range scanned here (up to 800°C), with a very minor exception in the temperature range between 100°C and 200°C. This lower weight loss of OPFL is the TGA manifestation of the torrefaction results in which OPFL produced higher solid yield (*Figure 1*) and higher CV_{ratio} compared to OPFS (*Figure 2*), as well as its lesser hemicellulose/cellulose IR peak intensity losses under flue gas torrefaction than OPFS.

When the two TGA atmospheres are compared, apparent differences are observed above 350°C for OPFS and above 500°C for OPFL. Below those temperature ranges, which includes the torrefaction temperature examined here (200°C-300°C), the addition of 20% CO_2 to pure N_2 does not seem to affect the weight loss of these biomass feeds. This could be interpreted in two ways: (1) for the present samples, the effect of CO_2 (20% in the torrefaction atmosphere) is very weak in the torrefaction temperature examined here (200°C-300°C). This interpretation is supported by the appearance of CO_2 effect at higher temperatures for both samples (*Figure 5*). (2) The weight losing process caused by the addition of CO_2 is very slow to appear in the TGA analysis with temperature ramping (not temperature holding), in other words, kinetically limited to be apparent within the TGA ramping time frame. On this point, it is noted that other TGA work is done at 100% of CO_2 concentration (Thanapal *et al.*, 2014) which would have accelerated the reaction compared to lower CO_2 concentration, and also that the CO_2-induced weight loss showing positive order on CO_2 concentration (1.7 in the case of PKS torrefaction) (Uemura *et al.*, 2015) which would indicate that higher concentration CO_2 accelerates the CO_2-related reactions. The above discussion seems to indicate that CO_2 participation with the present concentration in the flue gas (12.6%-16.5%) is weak or slow, and the present flue gas torrefaction of OPF on the enhanced solid yield decrease observed in *Figure 1* during the present flue gas torrefaction within the temperature range of 200°C-300°C would be attributed to the stronger participation of O_2. The effect of CO_2 would be more pronounced at the higher temperatures, as found in *Figure 5*, under the present conditions.

Possible Mechanism of Flue Gas Torrefaction

With all the collected data combined, it may be able to conjecture the following mechanism for the present flue gas torrefaction in the temperature range of 200°C-300°C. The O_2 in flue gas attacks O-bearing surface functional groups, extracting CO_2, CO and H_2O from terminal C=O, C-O-C, C-O and C-OH groups (*Figure 4*), resulting in lower H and O contents (*Table 3*) and thus, increasing C content (*Table 3*) and higher CV ratio (*Figure 2*) for the product solids than torrefaction under N_2. The flue gas attack appears to be mostly on hemicellulose/cellulose components of biomass (*Figure 4* and *Table 3*), indicating that lignin-rich biomass (OPFL in the present study) would be more tolerant toward flue gas as torrefaction atmosphere.

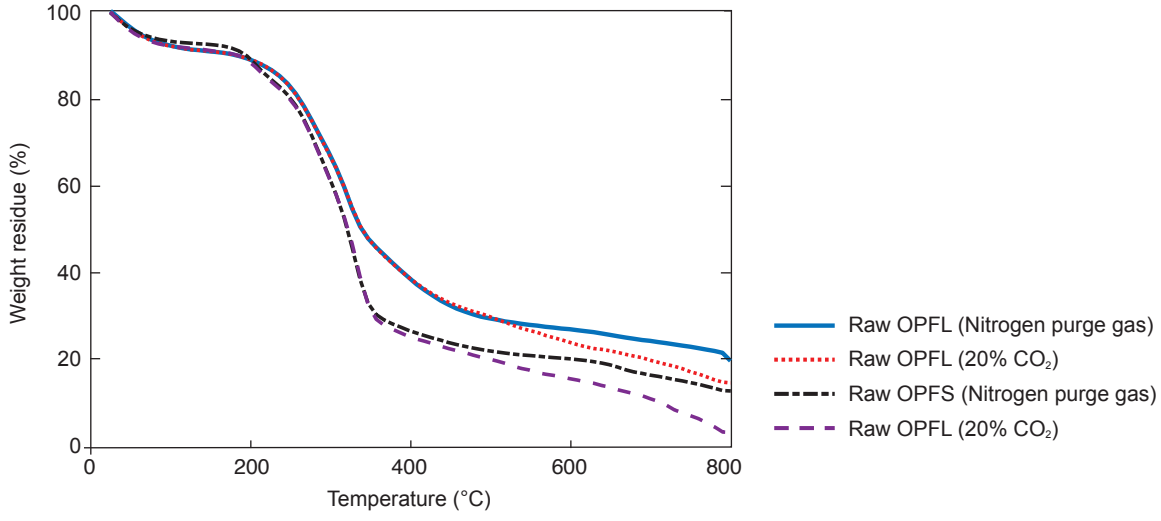


Figure 5. Weight loss profile (TGA curves) of raw OPFL and OPFS in the atmosphere of N_2 purge gas and 20% CO_2 mixed in N_2.

CONCLUSION

A comparative study of the torrefaction of OPF leaves and stems was performed under flue gas and inert N_2 atmospheres. Results indicated that flue gas atmosphere caused severer torrefaction than N_2 atmosphere, resulting in flue gas torrefied biomass producing solid products with higher calorific value ratio than N_2 torrefied ones in the temperature range of 200°C-300°C. The torrefaction severity of flue gas atmosphere is attributed to the presence of O_2 in the gas, causing increased removal of O from the feed compared to the torrefaction in the N_2 atmosphere. Lignin component appears to retard this flue gas attack on hemicellulose/cellulose components of biomass, as lignin-rich biomass (OPFL in the present study) would be more tolerant to the use of flue gas as torrefaction atmosphere.

ACKNOWLEDGEMENT

Support from the Ministry of Education Malaysia through HICoE award to CBBR is duly acknowledged. One of the authors (Premchand) would like to greatly acknowledge Universiti Teknologi PETRONAS for financial support under GA scheme to conduct this work.

REFERENCES

Abnisa, F; Arami-Niya, A; Daud, W M; Sahu, J N and Noor, I M (2013). Utilization of oil palm tree residues to produce bio-oil and bio-char via pyrolysis. *Energy Convers. Manag., 76*: 1073-1082.

Agar, D and Wihersaari, M (2012). Bio-coal, torrefied lignocellulosic resources - Key properties for its use in co-firing with fossil coal - Their status. *Biomass Bioenergy, 44*: 107-111.

Aljuboori, A H R (2013). Oil palm biomass residue in Malaysia: Availability and sustainability. *Int. J. Biomass Renew., 2*: 13-18.

Asadullah, M; Rasid, N S; Kadir, S A and Azdarpour, A (2013). Production and detailed characterization of bio-oil from fast pyrolysis of palm kernel shell. *Biomass Bioenergy, 59*: 316-324.

Bilgic, E; Yaman, S; Haykiri-Acma, H and Kucukbayrak, S (2016). Limits of variations on the structure and the fuel characteristics of sunflower seed shell through torrefaction. *Fuel Process. Technol., 144*: 197-202.

Brojolall, N and Surroop, D (2022). Improving fuel characteristics through torrefaction. *Energy, 246*: 123359.

Chai, M; Xie, L; Yu, X; Zhang, X; Yang, Y; Rahman, M M and Cai, J (2021). Poplar wood torrefaction: Kinetics, thermochemistry and implications. *Renew. Sust. Energ. Rev., 143*: 110962.

Chantanumat, Y; Phetwarotai, W; Sangthong, S; Palamanit, A; Abu Bakar, M S; Cheirsilp, B and Phusunti, N (2022). Characterization of bio-oil and biochar from slow pyrolysis of oil palm plantation and palm oil mill wastes. *Biomass Conv. Bioref*. DOI: 10.1007/s13399-021-02291-2.

Eseltine, D; Thanapal, S S; Annamalai, K and Ranjan, D (2013). Torrefaction of woody biomass (Juniper and Mesquite) using inert and non-inert gases. *Fuel, 113*: 379-388.

Financie, R; Moniruzzaman, M and Uemura, Y (2016). Enhanced enzymatic delignification of oil palm biomass with ionic liquid pretreatment. *Biochem. Eng. J., 110*: 1-7.

Hashim, R; Nadhari, W N; Sulaiman, O; Kawamura, F; Hiziroglu, S; Sato, M; Sugimoto, T; Seng, T G and Tanaka, R (2011). Characterization of raw materials and manufactured binderless particleboard from oil palm biomass. *Mater. Des., 32*: 246-254.

Hon, D N S and Shiraishi, N (2001). *Wood and Cellulosic Chemistry*. 2nd edition. Marcel Dekker, New York. p. 296-298, 331.

Howell, A; Stahlfeld, K; Mohammed, A B; Vijlee, S and Belmont, E (2019). Gas independence of *Miscanthus* x *giganteus* torrefied in nitrogen (N_2) and carbon dioxide (CO_2) using calibrated thermogravimetric analysis. *Bioresour. Technol. Rep., 7*: 100238.

Ibrahim, R H; Darvell, L I; Jones, J M and Williams, A (2013). Physicochemical characterisation of torrefied biomass. *J. Anal. Appl. Pyrolysis, 103*: 21-30.

Iovane, P; Donatelli, A and Molino, A (2013). Influence of feeding ratio on steam gasification of palm shells in a rotary kiln pilot plant. Experimental and numerical investigations. *Biomass Bioenergy, 56*: 423-431.

Kanaujia, P K; Sharma, Y; Garg, M; Tripathi, D and Singh, R (2014). Review of analytical strategies in the production and upgrading of bio-oils derived from lignocellulosic biomass. *J. Anal. Appl. Pyrolysis, 105*: 55-74.

Kaniapan, S; Hassan, S; Ya, H; Patma Nesan, K and Azeem, M (2021). The utilisation of palm oil and oil palm residues and the related challenges as a sustainable alternative in biofuel, bioenergy, and transportation sector: A review. *Sustainability, 13(6)*: 3110.

Li, M F; Chen, L X; Li, X; Chen, C Z; Lai, Y C; Xiao, X and Wu, Y Y (2016). Evaluation of the structure and fuel properties of lignocelluloses through carbon dioxide torrefaction. *Energy Conv. Manag., 119*: 463-472.

Li, S X; Chen, C Z; Li, M F and Xiao, X (2018). Torrefaction of corncob to produce charcoal under nitrogen and carbon dioxide atmospheres. *Bioresour. Technol., 249*: 348-353.

Li, X; Lu, Z; Chen, J; Chen, X; Jiang, Y; Jian, J and Yao, S (2021). Effect of oxidative torrefaction on high temperature combustion process of wood sphere. *Fuel, 286*: 119379.

Lv, P; Almeida, G and Perré, P (2015). TGA-FTIR analysis of torrefaction of lignocellulosic components (cellulose, xylan, lignin) in isothermal conditions over a wide range of time durations. *BioResources, 10*: 4239-4251.

Matsunaga, K; Nishi, K; Kamino, Y; Shinmura, T and Kokusho, T (1999). Study on characteristics of bamboo charcoal and bamboo vinegar. *Res. Report Kagoshima Pref. Inst. Indust. Technol., 13*: 23-30.

Na, B I; Kim, Y H; Lim, W S; Lee, S M; Lee, H W and Lee, J W (2013). Torrefaction of oil palm mesocarp fibre and their effect on pelletizing. *Biomass Bioenergy, 52*: 159-165.

Nyakuma, B B; Oladokun, O; Wong, S L and Abdullah, T A T (2021). Torrefaction of oil palm empty fruit bunch pellets: Product yield, distribution and fuel characterisation for enhanced energy recovery. *Biomass Conv. Bioref*. DOI: 10.1007/s13399-020-01185-z.

Onsree, T; Tippayawong, N; Williams, T; McCullough, K; Barrow, E; Pogaku, R and Lauterbach, J (2019). Torrefaction of pelletized corn residues with wet flue gas. *Bioresour. Technol., 285*: 121330.

Poh, P E; Wu, T Y; Lam, W H; Poon, W C and Lim, C S (2020). *Waste Management in the Palm Oil Industry*. Springer. 73 pp.

Premchand; Komiyama, M; Aqsha, A and Uemura, Y (2020). Effect of combustion and nitrogen gas atmospheres on the torrefaction performance of oil palm frond leaves and stems. *IOP Conf. Ser.: Mater. Sci. Eng., 736*: 022020.

Prins, M J; Ptasinski, K J and Janssen, F J (2006). More efficient biomass gasification via torrefaction. *Energy, 31*: 3458-3470.

Rousset, P; Macedo, L; Commandré, J M and Moreira, A (2012). Biomass torrefaction under different oxygen concentrations and its effect on the composition of the solid by-product. *J. Anal. Appl. Pyrolysis, 96*: 86-91.

Sabil, K M; Aziz, M A; Lal, B and Uemura, Y (2013). Effects of torrefaction on the physiochemical properties of oil palm empty fruit bunches, mesocarp fibre and kernel shell. *Biomass Bioenergy, 56*: 351-360.

Shuit, S H; Tan, K T; Lee, K T and Kamaruddin, A (2009). Oil palm biomass as a sustainable energy source: A Malaysian case study. *Energy, 34*: 1225-1235.

Tabakaev, R; Shanenkov, I; Kazakov, A and Zavorin, A (2017). Thermal processing of biomass into high-calorific solid composite fuel. *J. Anal. Appl. Pyrolysis, 124*: 94-102.

Tan, J P; Jahim, J M; Harun, S; Wu, T Y and Mumtaz, T (2016). Utilization of oil palm fronds as a sustainable carbon source in biorefineries. *Intl. J. Hydrog. Energy, 41*: 4896-4906.

Thanapal, S S; Chen, W; Annamalai, K; Carlin, N; Ansley, R J and Ranjan, D (2014). Carbon dioxide torrefaction of woody biomass. *Energy Fuels, 28*: 1147-1157.

Tran, K Q; Trinh, T N and Bach, Q V (2016). Development of a biomass torrefaction process integrated with oxy-fuel combustion. *Bioresour. Technol., 199*: 408-413.

Uemura, Y; Omar, W; Othman, N A; Yusup, S and Tsutsui, T (2013). Torrefaction of oil palm EFB in the presence of oxygen. *Fuel, 103*: 156-160.

Uemura, Y; Saadon, S; Osman, N; Mansor, N and Tanoue, K I (2015). Torrefaction of oil palm kernel shell in the presence of oxygen and carbon dioxide. *Fuel, 144*: 171-179.

Uemura, Y; Sellappah, V; Trinh, T H; Hassan, S and Tanoue, K I (2017). Torrefaction of empty fruit bunches under biomass combustion gas atmosphere. *Bioresour. Technol., 243*: 107-117.

Wertz, J L; Bédué, O and Mercier, J P (2010). *Cellulose Science and Technology*. EPFL Press.

Zhang, J and Zhang, X (2019). 15 - The thermochemical conversion of biomass into biofuels. *Biomass, Biopolymer-based Materials, and Bioenergy* (Verma, D; Fortunati, E; Jain, S; Zhang, X eds.). Woodhead Publishing. p. 327-368.

Journal of Oil Palm Research Vol. 35 (1) March 2023 p. 86-99
DOI: https://doi.org/10.21894/jopr.2022.0048

COMPARISON OF ARTIFICIAL INTELLIGENCE MODELS TO PREDICT OIL PALM BIOMASS PYROLYSIS AND KINETICS USING THERMOGRAVIMETRIC ANALYSIS

YASMIN MOHD ZAIFULLIZAN[1]; LIM MEI KUAN[2]; ARSHAD ADAM SALEMA[1,3]* and KASHIF ISHAQUE[4]

ABSTRACT

Kinetic modeling is a challenging aspect of biomass conversion due to its inherent complex reactions. Further, it is difficult to achieve the accuracy of predicting the biomass pyrolysis process at varying experimental conditions, particularly for more complex samples based on kinetic modeling alone. Therefore, this study aims to use artificial intelligence (AI) models [artificial neural network (ANN), support vector machine (SVM), and decision tree (DT)] to predict biomass thermogravimetric (TG) behaviour, derivative TG (DTG), product (volatile and char) yield, and kinetic triplets. Two oil palm biomass types-empty fruit bunches (EFB) and oil palm shells (OPS) - are used to generate a 72-experiment dataset from a thermogravimetric analyser (TGA) at different heating rates (5°C, 10°C, 15°C and 20°C min^{-1}). The results reveal that each AI model can accurately predict the DTG profile with high coefficients of determination (R^2) in the range of 0.94 and 0.99 and low mean square errors (MSE) between 0.09 and 5.12. The product yield prediction results are not as promising, as indicated by higher MSE values (4.27, 2.79, 6.67). However, the ANN models most capably predicted the activation energies of oil palm biomass pyrolysis (~260°C-360°C at 20°C min^{-1}) for both model-free and model-fitting methods, followed by the DT and SVM models.

Keywords: artificial intelligence, kinetics, oil palm biomass, pyrolysis, thermogravimetric.

Received: 1 January 2022; **Accepted:** 4 July 2022; **Published online:** 11 August 2022.

INTRODUCTION

Biomass pyrolysis is regarded as one of the most promising alternative methods for producing three different products; solid (char), liquid (bio-oil), and gas. It is a complex multi-scale process due to several interactive and parallel reactions that require further research work (Sharifzadeh *et al.*, 2019). One of the main challenges is that the pyrolysis process and product formation (yield and quality) performance depend strongly on process/operating conditions (Chen *et al.*, 2017; Guedes *et al.*, 2018; Mutsengerere *et al.*, 2019; Paenpong and Pattiya, 2016). It was found that pyrolysis temperature and heating rate play an essential role during pyrolysis and product formation (Guedes *et al.*, 2018; Sharifzadeh *et al.*, 2019). Moreover, feedstock properties and chemical complexity add to the difficulty of the problem. These factors make it difficult to understand the kinetic modeling of biomass pyrolysis (Cai *et al.*, 2018; Hameed *et al.*, 2019; Hu and Gholizadeh, 2019; Kaczor *et al.*, 2020; Wang *et al.*, 2017).

[1] Mechanical Engineering Discipline, School of Engineering, Monash University Malaysia, 47500 Bandar Sunway, Selangor, Malaysia.

[2] School of Information Technology, Monash University Malaysia, 47500 Bandar Sunway, Selangor, Malaysia.

[3] Monash Industry Palm Oil Research Platform (MIPO), School of Engineering, Monash University Malaysia, 47500 Bandar Sunway, Malaysia.

[4] Electrical and Computer Engineering, Mohammad Ali Jinnah University, 194823 Karachi, Sindh, Pakistan.

* *Corresponding author e-mail: arshad.salema@monash.edu*

The kinetic triplet, namely activation energy, pre-exponential factor and reaction model or mechanism helps to describe the complex thermal degradation process that can be beneficial for subsequent processes and applications (Mahmood *et al.*, 2019). The kinetic triplet of biomass pyrolysis is obtained by varying the heating rates during thermogravimetric analysis (TGA) and model-free methods such as the Flynn-Wall-Ozawa (FWO), Kissinger-Akihara-Sunose (KAS), and Friedman methods are employed (Zhang *et al.*, 2021). Model-fitting method such as the Coats-Redfern method is utilised as well with the added benefit of being able to hypothesize reaction mechanisms for the process. For example, Castells *et al.* (2021) presented a preliminary view that empty fruits bunch (EFB) samples showed a better fit for the diffusion reactions, while oil palm shell (OPS) and palm mesocarp fibre (PMF) could better fit n-order reactions under a combustion scheme. Surahmanto *et al.* (2020) applied the Coats-Redfern integral method for kinetic analysis of oil palm waste and found that they are best fitted to first-order reactions in the pyrolysis scheme.

Traditionally, biomass pyrolysis reaction is modelled using kinetic models (Hameed *et al.*, 2019). Kinetic models have been developed for decades and give useful insight into the reaction kinetics of biomass pyrolysis. Examples of kinetic models include the one-step global kinetic model (Papari and Hawboldt, 2015), parallel (Radmanesh *et al.*, 2006) and competitive (Várhegyi *et al.*, 1997) reactions, lumped kinetic models and the distributed activation energy model (DAEM) (Ahmad *et al.*, 2020) which mainly focus on primary reactions of pyrolysis. Although much effort has been put into investigating pyrolytic kinetic models, it is still difficult to capture the full complexity of the biomass structure and the interdependence of the individual components (Wang *et al.*, 2017). It is recommended that rather than modeling a singular biomass component *e.g.*, cellulose, it is better to model the whole biomass to observe the interactions between the different components and the possible effects of trace amounts of inorganic materials, as well as to include secondary reactions from the process (Hameed *et al.*, 2019).

Meanwhile, there has been an increasing interest in applying AI to the biomass conversion process in recent years. Several machine learning (ML) algorithms were recently applied to biomass pyrolysis (Alaba *et al.*, 2020; Aydinli *et al.*, 2017; Chen *et al.*, 2018; Ding *et al.*, 2020; Rezk *et al.*, 2019). Most of these studies have used artificial neural networks (ANN) and concluded that they could predict the pyrolysis process with high accuracy due to their ability to discover hidden patterns in complex data (Alaba *et al.*, 2020). Further, ANN was used to model TGA experimental datasets due to its capability to handle: (i) large datasets from TGA systems (>10 000 data samples per run); (ii) the complex non-linear nature of thermal conversion, and; (iii) fully automated modeling procedures (Teng *et al.*, 2019). Besides biomass, researchers have also applied ANN to sewage sludge (Naqvi *et al.*, 2018) and co-pyrolysis of sewage sludge with rice husk (Lakovic *et al.*, 2021; Naqvi *et al.*, 2019). Others have predicted the higher heating values of biomass using a hybrid adaptive neuro-fuzzy inference system (ANFIS) (Pattanayak *et al.*, 2020) and ANN (Çakman *et al.*, 2021).

Although AI models have been used to predict biomass pyrolysis behaviour (weight loss using TG curve), very few (Bhuyan *et al.*, 2020) have been applied to predict product yield (gas/volatile components and char). Furthermore, a few studies have used a support vector machine (SVM) involving biomass pyrolysis. For instance, Cao *et al.* (2016) and Ewees *et al.* (2017) applied SVM to predict the biochar yield from cattle manure. Another study by Chen *et al.* (2018) computed the product distribution and bio-oil heating value of different biomasses under fast pyrolysis using SVM. The studies on applying decision trees (DT) to biomass pyrolysis are even more scarce. For example, Zhang *et al.* (2019) applied random forest, a DT ensemble methwangod, to cattle manure pyrolysis, while Zhu *et al.* (2019) predicted biochar yields and carbon contents using random forest. Although some researchers have applied AI to biomass pyrolysis, few studies (Aghbashlo *et al.*, 2021) have provided a detailed investigation of kinetic parameter prediction such as activation energy using AI methods. To date, none have utilised and compared different AI models (ANN, SVM and DT) for biomass pyrolysis based on real-time data obtained from a TGA machine. It is hypothesised that AI would save significant time and effort by predicting the biomass pyrolysis behaviour as compared to time-consuming experimental procedures with TGA machines.

The objective of the present work is to develop, train, validate, and compare three AI models to predict the pyrolysis behaviour, kinetics, and product yield of two oil palm biomasses; EFB and OPS. The datasets were generated using a TGA machine at different heating rates and then used to develop and compare the performance of three AI models. The scope of this work also includes developing AI models based on individual biomass pyrolysis datasets and combining them. Another novelty of the present work is extracting the activation energy from the predicted values obtained by AI models. It should be noted that although the developed AI models are specific to oil palm biomass (OPS and EFB), it is expected that they would also work for other types of biomasses having a similar pyrolysis conversion trend.

MATERIALS AND METHODS

Materials

This study used OPS and EFB obtained from local palm oil mills in Malaysia. The biomasses were cleaned, dried in the open sun and then grounded to smaller-sized particles in the range of 75-250 µm to mitigate heat transfer effects (Wei *et al.*, 2006). Finally, the biomasses were stored in airtight Ziplock bags for further analysis. The proximate and ultimate analyses of the biomasses (*Table 1*) confirmed that EFB and OPS are different in chemical properties and exhibit different pyrolysis behaviours. The ultimate analyses were conducted with a Leco CHNS analyser model 932 (The Netherlands) according to ASTM D5373-14 and ISO 29541 method, and the analysis was repeated five times for each sample expressed as the dry basis of biomass.

TABLE 1. PROXIMATE AND ULTIMATE ANALYSIS OF OIL PALM BIOMASS

Proximate analysis (wt.%)		
	EFB	**OPS**
Moisture content (M)	6.10 ± 2.10	7.43 ± 1.98
Volatile matter (VM)	80.00 ± 1.00	73.5 ± 0.85
Ash (A)	5.80 ± 0.70	2.20 ± 0.80
Fixed carbon[#]	8.10 ± 0.75	16.87 ± 0.95
Ultimate analysis (%), dry basis		
C	47.26 ± 0.85	51.07 ± 1.18
H	5.83 ± 0.01	4.71 ± 0.25
N	0.82 ± 0.03	0.41 ± 0.02
S	<0.05	<0.05
O*	46.04	43.76

Note: [#]Fixed carbon is by difference = 100 - [M + VM + A] %.
*Oxygen is by difference, % = 100 – [C + H + N + S] %.

Thermogravimetric Analysis (TGA)

The experiments were conducted in a thermogravimetric analyser (TA Instrument Q50, USA). About 5-7 mg of biomass sample (EFB or OPS, respectively) was placed in a ceramic pan and loaded into the TGA in each experiment. The temperature was ramped from room temperature to maximum temperatures of 400°C, 450°C and 500°C, at different heating rates (β) of 5°C, 10°C, 15°C and 20°C min^{-1} in an inert (nitrogen) environment under a 60 mL min^{-1} constant gas flow rate. The maximum temperature of 400°C, 450°C and 500°C was selected as the biomass gets completely pyrolysed before 400°C. Lower heating rates are recommended (Vyazovkin *et al.*, 2011) to prevent thermal lag (by ensuring effective heat and mass transfer in the sample) so that the temperature error can be minimised or eliminated. Each experiment was conducted three times to guarantee data reproducibility.

Artificial Neural Network (ANN) Modeling

Six different ANN models (*e.g.,* OPS TG - Oil palm shell thermogravimetric; EFB DTG - Empty fruit bunch derivative thermogravimetric; OPS+EFB TG - Oil palm shell and EFB combined thermogravimetric) were trained and optimised for pyrolysis behaviour (TG and DTG curves). The first four models (OPS TG, OPS DTG, EFB TG, and EFB DTG) are based on individual biomass pyrolysis datasets with temperature and heating rate as the input, while the combined ANN models use OPS+EFB datasets that increase the complexity of the non-linear relationships.

The architecture was a typical multi-layer feed-forward backpropagation neural network consisting of an input layer, one hidden layer, and an output layer, known as a shallow neural network (*Figure 1a*). The input layer data consists of temperature and heating rate, while the output layer data were the TG curve, DTG curve, or product yield. The data from the TG machine performed under the heating rate of 20°C min^{-1} and temperature of 400°C was set aside for validation *i.e.*, 20%. The remaining data (80%) was used to train the model. The ANN parameters such as the training and transfer functions and the number of neurons in the hidden layer were optimised by trial and error to obtain the minimum mean square error (MSE). The performance of the ANN models is evaluated by calculating the MSE and coefficient of determination (R^2). Lower MSE values and higher R^2 values indicate better ANN model performance.

The product yield ANN models also used shallow neural networks (one input layer, one hidden layer, and one output layer). The only difference was that the output layer comprised the two different yields (volatiles and char) from the pyrolysis process. Two ANN models, one for each biomass (OPS and EFB), were developed to predict the yield.

Support Vector Machine (SVM) Modeling

The SVM algorithm is much faster and requires a smaller sample size than other machine learning algorithms (Russell and Norvig, 2016). Similar to ANN, six SVM regression models (*Figure 1b*) were created. The dataset was split into training and validation datasets in an 80:20 ratio. A kernel transforms the predictor variables to a higher-dimensional feature space. The Gaussian function was selected for this work due to its popularity and accuracy for regression (Arabloo *et al.*, 2015).

Decision Tree (DT) Modeling

DT has gained popularity due to its ease of interpretability and simplicity. DT follows a flowchart-like tree structure (*Figure 1c*), governed by decision rules similar to 'if-then' conditions, making it easily understandable (Myles *et al.*, 2004). DT has the advantage of requiring less training time than ANN and SVM. Like the ANN and SVM models, six DT models (or regression trees) were created for TG and DTG curves. The dataset for DT was split into an 80:20 ratio for training and validation. The optimised hyperparameters were branch nodes, leaf sizes, and tree depth, determined empirically to minimise the five-fold cross-validation loss (Myles *et al.*, 2004). All simulations were performed with MATLAB (R2018b, Version 9.5) on an Intel® Core™ i5-4570S, 16 GB RAM, 2.90 GHz processor, and Windows 10 64-bit operating system.

Kinetic and Reaction Mechanism Study

The kinetic triplets-activation energy (E_a), pre-exponential factor (A), and reaction model were evaluated in the main pyrolysis region based on the TG data. The activation energy is interpreted as the minimum energy threshold for a reaction to occur (Truhlar, 1978). The pre-exponential factor is the pre-exponential constant in the Arrhenius equation, an empirical relationship between temperature and rate coefficient (Jagannadham, 2010), which is used to study the reaction mechanism. Lastly, the reaction model or the reaction mechanism is the account of elementary reactions by which chemical change occurs in a compound (Smith and March, 2013). Model-free methods, such as the Flynn-Wall-Ozawa (FWO), Kissinger-Akihara-Sunose (KAS), and Friedman methods, were used to determine the kinetic parameters (Zhang *et al.*, 2021). In addition, the Coats-Redfern (CR) model-fitting method was adopted to determine the activation energy (E_a), pre-exponential factor (A) and reaction model by plotting versus (Chen *et al.*, 2019). If the value obtained by the CR model-fitting method based on a specific reaction model is comparable to the average obtained by the model-free methods (Friedman, FWO, and KAS), the reaction model is considered suitable for characterising the corresponding thermal degradation process (Chen *et al.*, 2019).

The trained ANN, SVM, and DT models were used to predict the TG data in the validation step. The activation energies and pre-exponential factors of the oil palm biomasses were then calculated from these predicted TG data using different kinetic methods (FWO, KAS, and Friedman). Finally, the predicted kinetic data were compared with those obtained from the experimental TG dataset.

RESULTS AND DISCUSSION

Thermogravimetric Analysis of OPS and EFB Biomass Samples

The TG and DTG profiles obtained at different heating rates and temperatures of OPS and EFB biomass pyrolysis showed some notable differences as shown in *Figure 2*. The first stage or peak from room temperature to 200°C corresponds to the removal of moisture and probably low volatile or

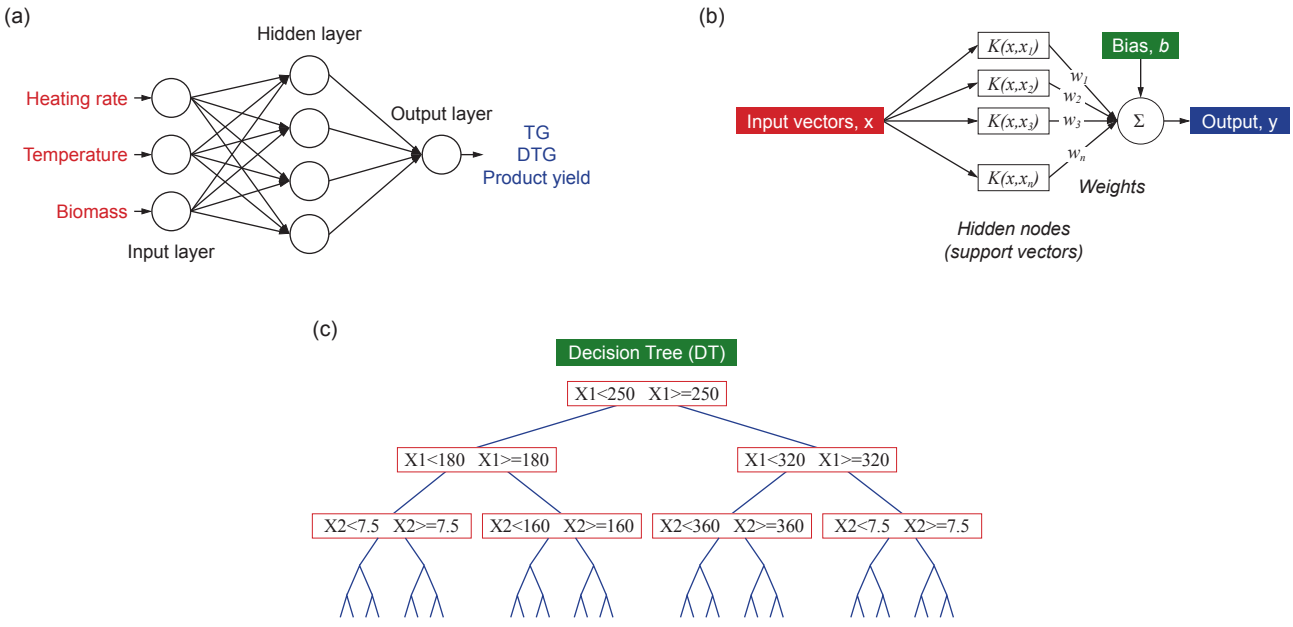


Figure 1. (a) ANN, (b) SVM, and (c) DT architecture to predict the oil palm biomass pyrolysis behaviour and product yield.

chemical compounds. The second stage between 200°C and 380°C is referred to as the main pyrolysis reaction stage in which cellulose and hemicellulose are decomposed to release volatile matter. A clear difference between hemicellulose (shoulder peak) and cellulose decomposition is identified in OPS biomass whereas it is almost absent in EFB biomass due to the lower content of hemicellulose (Abdullah and Gerhauser, 2008). The third stage is attributed to the char formation that occurs once all the volatile matter has been emitted (below 400°C) and denotes the completion of biomass pyrolysis. This can be observed by a gradual loss in weight after 380°C and usually, lignin decomposes in this region. Among the lignocellulosic materials, lignin is a stable component that has low reactivity. It decomposes slowly over a wide range of temperatures and can simultaneously decompose with hemicellulose and cellulose. A significant difference in pyrolysis behaviour (TG and DTG curves) was observed in the main decomposition region or second stage while the curves tend to merge in the char region or third stage. The derivative mass loss rate of EFB is higher than OPS due to the swift burning of volatile matter in form of cellulose (Asadieraghi and Daud, 2015).

As the heating rate increased, the DTG curves shifted to higher temperatures. This is in agreement with previous studies of non-isothermal heating (Yıldız *et al.*, 2016). The observed shift may be explained by the mathematical form of kinetic laws as explained by Janković *et al.* (2020). Typically, reaction intensity increases when the heating rate is increased thereby accelerating the devolatilisation process. However, the char formation stage gets delayed with the increase in heating rate. At lower heating rates, samples are heated more gradually with a low-temperature gradient, resulting in better

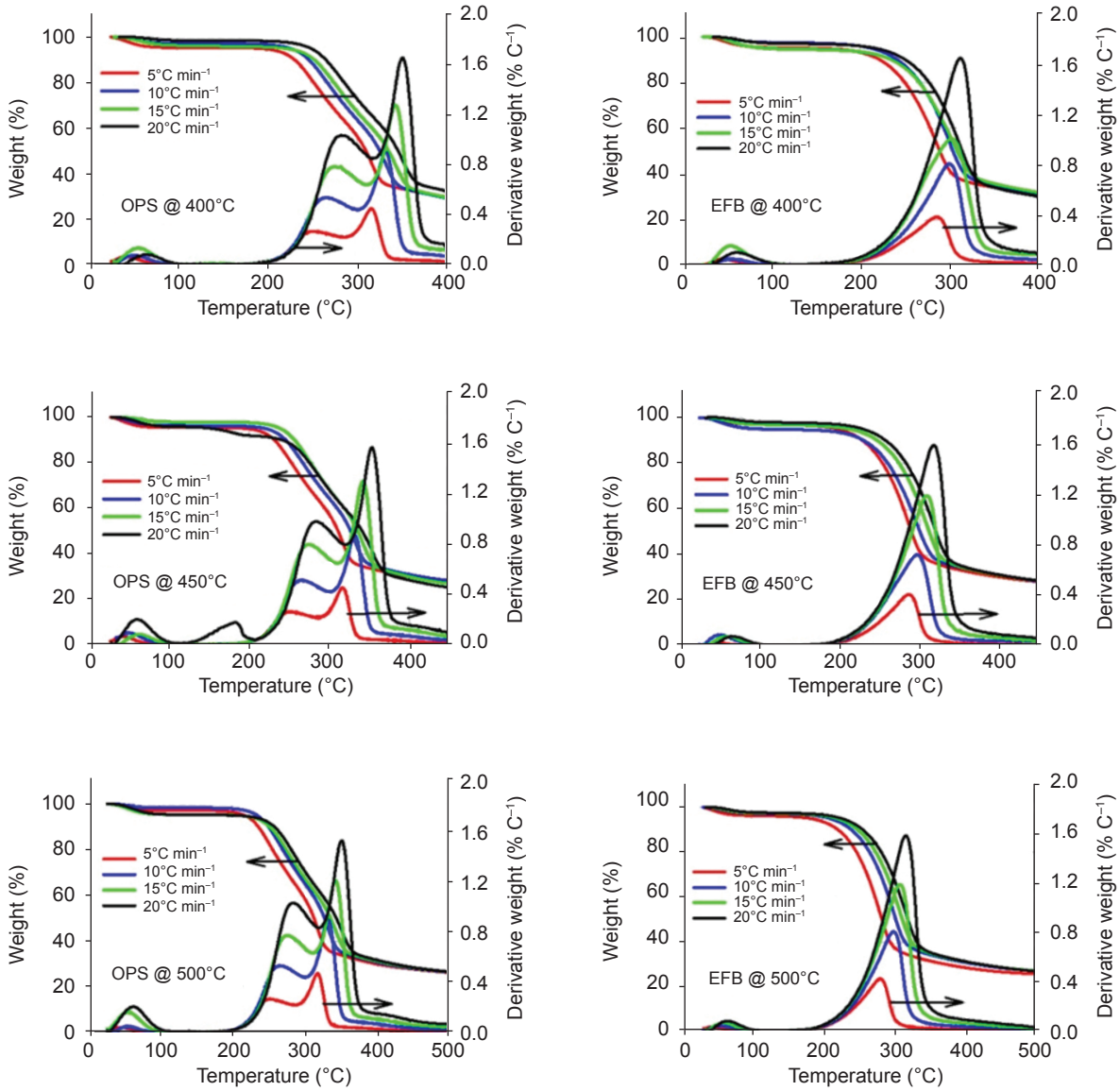


Figure 2. TG and DTG profiles of OPS and EFB biomass at different temperatures and heating rates.

heat transfer from the surface of the particles to the inner core. However, the high-temperature gradient is developed at higher heating rates resulting in reaction retardation. The TGA of OPS and EFB agrees with the previously published literature (Asadieraghi and Daud, 2015; Luangkiattikhun *et al.*, 2008), and hence, limited discussion is presented in this article.

Prediction of Biomass Pyrolysis Behaviour (TG-DTG) Using Different AI Models

Table 2 presents the performance of the AI model predictions of the pyrolysis behaviour (TG/DTG profiles) of oil palm biomass. The training columns represent the model performance after being trained, while the validation columns represent the model performance on the dataset not used in the training phase. *Figure 3* presents the predicted and the experimental TG and DTG profiles suggesting that the shape of the curves predicted by all the AI models followed the degradation curves from the experimental data. Overall, the accuracy of all the models was high. There was a strong agreement between the targeted and predicted output ($R^2 > 0.99$) for both the validation and training datasets.

The average R^2 values for both individual and combined ANN models training TG dataset was 0.999, indicating extremely high agreement between the measured and predicted results. For the validation TG dataset, the average R^2 values decreased slightly to 0.996. The average R^2 values for the DTG training and validation datasets were somewhat lower than for the TG dataset at 0.994 and 0.967, respectively.

On the other hand, the average MSE for both individual and combined ANN models were 0.77 for the training TG dataset and 3.94 for the validation dataset. In comparison, the average MSE values for the DTG training and validation dataset were 0.03 and 0.98, respectively. These MSE values show that the errors between the target and output values were minor for the training ANN models, indicating a well-trained model. However, there are significant differences between the ANN model training and validation MSE values for the TG and DTG predictions. The lower value of the MSE (below 1.0) for the DTG demonstrates the robustness of the ANN model. The difference in R^2 for the TG and DTG predictions is minor, which agrees with a previous study (Alaba *et al.*, 2020). The performance of the present ANN model was comparable to previous studies (*Table 2*). The performance of previous studies (Bi *et al.*, 2020; 2021; Naqvi *et al.*, 2019) were limited to TG data only. To the best of the author's knowledge, only one study (Zhang *et al.*, 2019) on DT was found whereby they obtained a DT model with R^2 of 0.9996 and RMSE of 0.501 for cattle manure. Meanwhile, no study was found on SVM, as SVM and DT were applied for the first time to predict the oil palm biomass pyrolysis behaviour.

However, the findings of the current study which suggest that ANN performs better than SVM and DT do not support some previous research. For instance, Cao *et al.* (2016) concluded that SVM predicted cattle manure pyrolysis better than the ANN model. Another study (Chen *et al.*, 2018) reported a similar SVM prediction outcome for biomass pyrolysis. This inconsistency may be due to the data used because cattle manure and oil palm biomass have different compositions and

TABLE 2. PERFORMANCE ANALYSIS OF ANN, SVM AND DT MODELS TO PREDICT PYROLYSIS BEHAVIOUR OF BIOMASS

Dataset	Parameters	AI models						
		ANN			SVM		DT	
		Training	Validation*	Comparison with literature	Training	Validation*	Training	Validation*
OPS TG	R^2	0.99	0.99	R^2 = 0.99992, RMSE = 0.3561 for sewage sludge and peanut shell TG (Bi *et al.*, 2021)	0.99	0.99	0.99	0.99
	MSE	0.51	2.79		3.10	3.28	0.53	2.97
OPS DTG	R^2	0.99	0.98		0.99	0.99	0.99	0.99
	MSE	0.02	0.43		0.03	0.09	0.02	0.39
EFB TG	R^2	0.99	0.99	R^2 = 0.99995, RMSE = 0.5194 for coal gangue and biomass TG (Bi *et al.*, 2020)	0.99	0.99	0.99	0.99
	MSE	1.02	5.04		1.25	5.09	1.05	5.11
EFB DTG	R^2	0.99	0.94		0.99	0.95	0.99	0.97
	MSE	0.04	1.56		0.06	1.34	0.04	1.58
OPS+EFB TG	R^2	0.99	0.99	R^2 = 0.9996, RMSE = 0.5142 for rice husk and sewage sludge TG (Naqvi *et al.*, 2019)	0.99	0.99	0.99	0.99
	MSE	0.77	3.99		0.96	4.90	0.81	4.21
OPS+EFB DTG	R^2	0.99	0.96		0.99	0.96	0.99	0.98
	MSE	0.03	0.93		0.04	0.97	0.03	0.98

Note: *Validation dataset for temperature 400°C and heating rate 20°C min^{-1}.

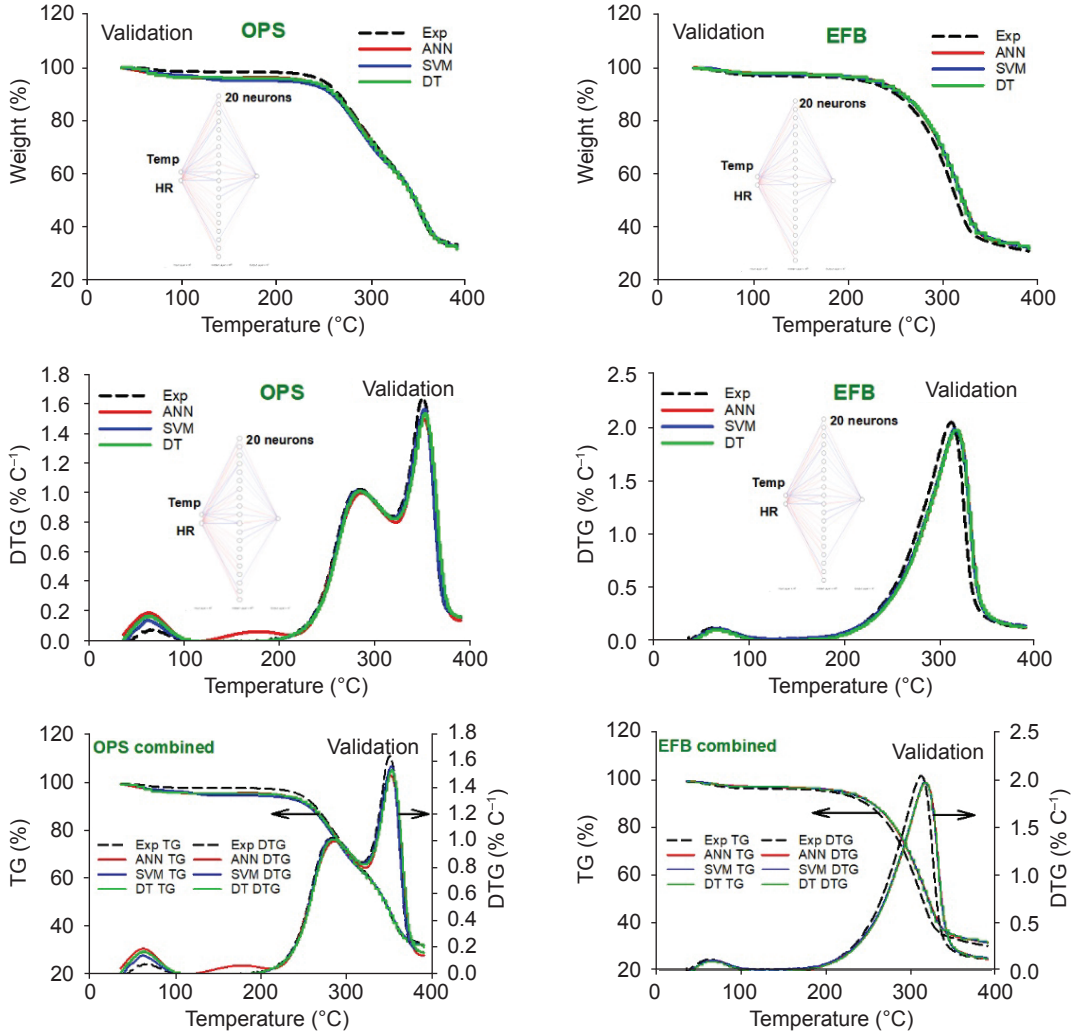


Figure 3. Comparison of ANN, SVM and DT validation models to predict the TG and DTG (derivative thermogravimetric) profiles of OPS and EFB biomass pyrolysis at a maximum temperature of 400°C and heating rate of 20°C min⁻¹.

thermal behaviour. Data collection and the size of the datasets also differ. For example, Chen *et al.* (2018) used data from previously published studies and collected 166 samples of various lignocellulosic biomass fast pyrolysis. Although the present results differ from some published studies (Cao *et al.*, 2016; Chen *et al.*, 2018), they are consistent with studies that have applied AI to biomass pyrolysis using TGA (Alaba *et al.*, 2020; Chen *et al.*, 2018; Yıldız *et al.*, 2016).

Another critical parameter to evaluate the performance of the AI models is training time. The average times to train the ANN, SVM, and DT models were 100, 319 and 87 s, respectively. The training time is highly dependent on the dataset size and computer hardware configuration. SVM took considerably more time for training, while DT trained the fastest. Although training the ANN network takes more time than DT, the TG and DTG predictions by the ANN are more accurate. Therefore, it can be concluded that ANN is the best performing algorithm for TG and DTG datasets since it provides a good trade-off between high accuracy (R^2), low error (MSE), and a reasonable training time (100 s). It is also worth noting that the AI system obtains validation results in approximately 2 s, which is faster than the time needed to perform real-time TGA experiments by a factor of 1000, which usually take hours to complete from laboratory preparation to clean up. Most studies in the field of AI application in biomass pyrolysis have failed to present the AI training time, which is one of the vital parameters in determining performance.

Application of ANN, SVM and DT Models to Predict Pyrolysis Product Yield

The yields of two major pyrolysis products (volatile and biochar) were obtained from the TG curves (*Figure 3*) by referring to the different stages of decomposition (Janković *et al.*, 2020). The product yield does not include the moisture content.

Pyrolysis product heating rate or temperature trends were not noticeable (*Figure 4*). Similar findings were reported in previous studies (Wang *et al.*, 2013; 2019). A possible reason for this could be the small sample size (5-7 mg) used in the TGA machine, ensuring efficient heat transfer. For the volatile and char yield training datasets, the ANN, SVM and DT models showed low MSE values of 0.17, 0.01 and 0.94, respectively. However, the MSE values for the ANN (4.27), SVM (2.79), and DT (6.67) models were higher for the validation set. This prediction (validation) result error is due to the small data sample size.

The MSE value of 5.171 for the ANN model testing datasets to predict the product yields of biomass pyrolysis was higher (Aydinli *et al.*, 2017) than the present ANN model product validation dataset. However, the present ANN (4.27) and SVM (2.79) model validation MSE values were almost similar to the root mean squared error (RMSE) of the ANN model (3.35-4.50) testing dataset and SVM model (2.53-3.34) testing dataset (Chen *et al.*, 2018). Therefore, the developed AI models in the present study are either slightly better or comparable to the previous studies.

Figure 4 compares the validation and measured product (volatile and char) yield using the ANN, SVM, and DT models. Contrary to the prediction results for pyrolysis (TG and DTG), the models moderately predicted the product yield percentage. The AI models either slightly over-predicted or under-predicted the product yield. The models' performance could be improved by increasing the dataset size.

Application of the ANN, SVM and DT Models to Predict Activation Energy and Pre-exponential Factor

The ANN predictions for in the main pyrolysis temperature range, (260°C-360°C) of OPS biomass was highly accurate for both model-free methods (KAS and FWO), as illustrated in *Figure 5*. The SVM prediction was accurate for OPS in the temperature range from 260°C to 305°C (from 10% to 40% conversion). Beyond 305°C, *i.e.*, after 40% conversion, the SVM over-predicted by an average factor of 1.17 for KAS and 1.16 for FWO. Surprisingly, all AI models predicted lower than the experimental data for the KAS and FWO methods for EFB biomass with an average factor of 0.91. This deviation in the prediction of could be due to the predicted TG profiles, since any deviation in the predicted TG profiles would change the values.

The value of from the KAS method first increased from ~100 kJ mol^{-1} (10% conversion) to 119 kJ mol^{-1} (60% conversion) for OPS biomass and then remained nearly constant (119 kJ mol^{-1}) until 90% conversion. The trend was similar for the FWO method but with a slightly higher values (~103 kJ mol^{-1} for 10% conversion to 122 kJ mol^{-1} for 60% conversion) for OPS biomass. The variation in in the main pyrolysis, the region is due to the decomposition of hemicellulose in the initial stage of the reaction, followed by degradation of cellulose with higher thermal stability starting in the later reaction (Wang *et al.*, 2019).

The DT model provided a much more accurate predictions, agreeing with the experimental values except for a small spike at 50% and 40% conversion for OPS and EFB biomass, respectively (*Figure 5*). These spikes could be due to a slight discrepancy in the DT model prediction of the TG profile (*Figure 3*) that may have caused the prediction to diverge. For the EFB biomass, the DT prediction of yielded a slightly higher error against experimental values compared to the ANN and SVM.

The average experimental and predicted activation energies for OPS and EFB biomass in the main pyrolysis region between 260°C and 330°C are presented in *Table 3*. It should be noted that the average activation energy and standard deviation refer to a value between 0.1 to 0.9 conversion degrees. Further, the average experimental value for OPS from the combined kinetic model-free methods (KAS, FWO, and Friedman) is 122 kJ

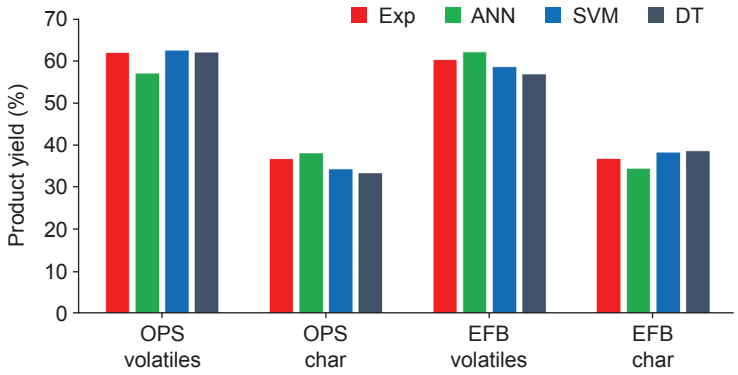


Figure 4. Performance of AI models in predicting the biomass pyrolysis product (volatiles and char) yield at 400°C and heating rate of 20°C min^{-1}.

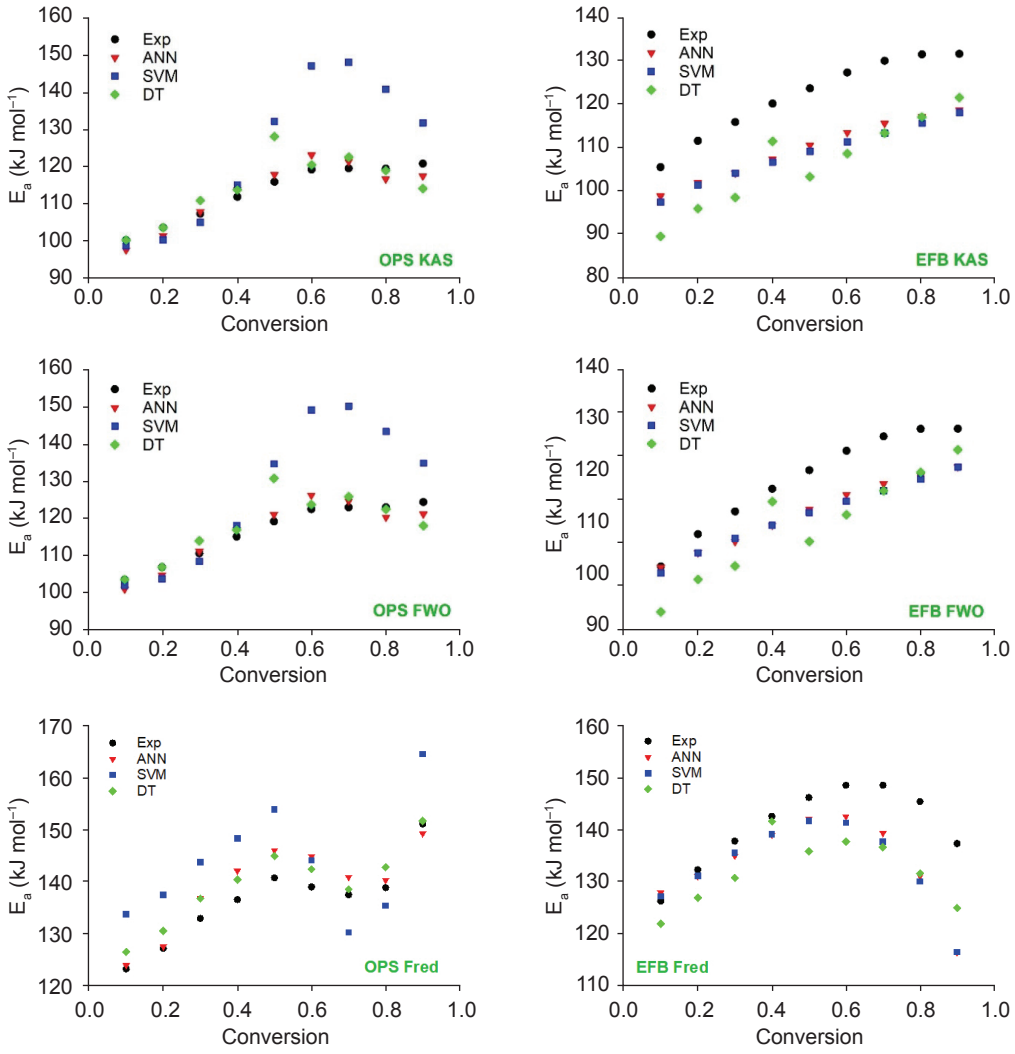


Figure 5. Comparison of extracted activation energy (E_a) using ANN, SVM and DT with experimental values.

mol^{-1} with a standard deviation of ±13, while the average for the ANN, SVM and DT are 122, 132, and 124 kJ mol^{-1} with standard deviations of ±14, ±10, and ±13, respectively. Whereas the average experimental for EFB from the combined kinetic model-free methods (KAS, FWO, and Friedman) is 127 kJ mol^{-1} with a standard deviation of 12. The average for the ANN, SVM and DT models are 119, 118, and 116 kJ mol^{-1} with standard deviations of 13, 14, and 14, respectively.

Therefore, for the OPS biomass, the error (%) between the average experimental and predicted activation energies for the ANN, DT, and SVM models were ~1%, ~2% and ~10%, respectively. For the EFB biomass, the corresponding errors were ~7%, ~10%, and ~8%, respectively. The change in activation energy with conversion degree was confirmed by previous studies (Huang *et al.*, 2019). They reported a 4% error between the predicted and experimental activation energy using a general regression neural network (GRNN) model. To conclude, among the AI models, ANN most accurately predicts the TG and DTG behaviour and biomass pyrolysis kinetics. The error between the experimental and predicted values from the FWO calculation method were lower, agreeing with very recently published work (Bong *et al.*, 2020).

Prediction of Reaction Mechanism Using the Model-fitting Method

In the present study, the values based on the CR method were compared with KAS and FWO model-free methods since the Friedman method provided higher values. The reaction mechanism was selected as the most suitable mechanism to characterise OPS and EFB pyrolysis when the values obtained from the CR method are closest to model-free methods. *Tables 4* and *5* show the comparison of values and pre-exponential factors from the experiment and AI models for OPS and EFB at a heating rate of 20°C min^{-1}, along with correlation coefficient and the average deviations between the results from the AI models and the experimental calculations.

On average, OPS AI models E_a and ln A deviated 6.48 kJ mol^{-1} and 1.38 from the calculated values obtained from the experiment. For EFB, the deviations were 7.01 kJ mol^{-1} and 1.57 for E_a and ln A, respectively. The biggest deviation for both OPS and EFB was for the decision tree model, while ANN showed the smallest deviation from the experimental values.

The experimental values of 102, 109, and 128 kJ mol^{-1} (*Table 4*) for OPS biomass corresponding to reaction model numbers 2 (chemical reaction), 6 (1st order reaction), and 7 (nucleation), respectively, is closest to KAS (113 kJ mol^{-1}) and FWO (116 kJ mol^{-1}). The values of the corresponding correlation coefficient were higher (0.8) for reaction models 2 and 6 but lower (0.7) for reaction model 7. For the EFB (*Table 5*), reaction models 1 (chemical reaction) and 9 (contracting disk) gave the closest experimental values of 137 and 131 kJ mol^{-1}, respectively, compared to KAS (119 kJ mol^{-1}) and FWO (122 kJ mol^{-1}). The values of the correlation coefficient were higher (0.8) in both cases. Zhang *et al.* (2021) pointed out that applying multiple model-free methods is more accurate than a single method for solid-state pyrolysis.

TABLE 3. COMPARISON OF PREDICTED AND EXPERIMENTAL AVERAGE ACTIVATION ENERGIES

Kinetic models	Experiment and AI models	Activation energies, kJ mol^{-1}			
		OPS		EFB	
		Average$^{\#}$	Stdev*	Average$^{\#}$	Stdev*
KAS	Experiment	113.01	7.75	118.77	9.51
	ANN	112.90	8.89	109.56	7.07
	SVM	124.26	19.97	108.38	6.78
	DT	114.64	8.96	106.40	10.50
FWO	Experiment	116.47	7.80	121.69	9.33
	ANN	116.37	8.84	112.32	6.87
	SVM	127.14	19.35	111.83	6.74
	DT	118.02	8.84	109.96	10.25
Friedman	Experiment	136.28	8.09	140.57	7.77
	ANN	139.02	8.50	133.8	8.40
	SVM	143.48	10.94	133.34	8.17
	DT	139.35	7.58	131.96	6.55

Note: $^{\#}$Average - average activation energy from 0.1-0.9 conversion degree.
*Stdev - standard deviation (±).

TABLE 4. COMPARISON OF ACTIVATION ENERGIES AND PRE-EXPONENTIAL FACTOR OBTAINED FROM EXPERIMENT AND AI MODELS USING COATS-REDFERN METHOD FOR OPS*

Reaction models	Experiment			ANN			SVM			DT			The average deviation from experimental values	
	R^2	E_a (kJ mol^{-1})	ln A	R^2	E_a (kJ mol^{-1})	ln A	R^2	E_a (kJ mol^{-1})	ln A	R^2	E_a (kJ mol^{-1})	ln A	E_a (kJ mol^{-1})	ln A
1	0.79	90.15	12.67	0.79	92.21	13.10	0.82	94.89	13.75	0.87	79.50	10.41	5.82	1.26
2	0.84	102.15	14.44	0.84	103.94	14.81	0.87	108.80	15.95	0.91	90.95	12.07	6.55	1.42
3	0.63	64.36	8.00	0.63	66.56	8.19	0.65	66.07	8.11	0.72	53.80	5.42	4.82	0.96
4	0.53	52.33	5.21	0.53	54.44	5.67	0.54	53.23	5.42	0.61	41.66	2.85	4.56	1.01
5	0.45	43.69	3.35	0.45	45.70	3.80	0.46	44.21	3.47	0.51	33.00	0.93	4.41	1.00
6	0.87	109.07	17.76	0.86	112.13	18.07	0.90	118.74	19.59	0.92	98.80	15.26	7.67	1.55
7	0.70	128.09	20.59	0.76	131.34	21.29	0.79	133.53	21.81	0.85	112.36	17.31	8.14	1.73
8	0.77	36.25	1.48	0.70	37.34	1.72	0.73	38.07	1.92	0.79	31.00	0.27	2.72	0.63
9	0.75	82.17	11.22	0.75	84.34	11.68	0.78	85.80	12.05	0.83	71.67	8.99	5.43	1.17
10	0.81	94.65	13.42	0.81	96.63	13.83	0.84	105.76	14.65	0.89	83.85	11.13	7.96	1.31
11	0.83	99.55	14.14	0.83	101.40	14.52	0.86	100.08	15.54	0.90	88.51	11.80	4.47	1.37
12	0.77	174.01	29.83	0.77	178.35	30.72	0.79	181.27	31.44	0.85	153.03	25.50	10.86	2.28
13	0.78	42.49	2.66	0.77	43.48	2.88	0.81	45.21	3.31	0.86	37.08	1.44	3.04	0.70
14	0.75	164.87	25.52	0.75	169.16	26.40	0.77	171.40	26.97	0.84	143.89	21.18	10.60	2.22
15	0.71	148.03	21.61	0.71	152.23	22.48	0.73	153.26	22.78	0.80	127.08	17.27	10.13	2.13

Note: *E_a and ln A calculations are based on temperature 400°C and heating rate 20°C min^{-1}.

TABLE 5. COMPARISON OF ACTIVATION ENERGIES AND PRE-EXPONENTIAL FACTOR OBTAINED FROM EXPERIMENT AND AI MODELS USING COATS-REDFERN METHOD FOR EFB*

Reaction models	Experiment			ANN			SVM			DT			Average deviation from experimental values	
	R^2	E_a (kJ mol^{-1})	ln A	R^2	E_a (kJ mol^{-1})	ln A	R^2	E_a (kJ mol^{-1})	ln A	R^2	E_a (kJ mol^{-1})	ln A	E_a (kJ mol^{-1})	ln A
1	0.88	136.86	23.53	0.75	141.19	24.43	0.89	136.80	23.43	0.96	124.22	20.69	5.68	1.28
2	0.92	153.42	26.36	0.92	151.22	25.77	0.92	151.33	25.79	0.97	137.48	22.76	6.74	1.59
3	0.76	102.67	16.67	0.77	104.50	17.02	0.77	105.18	17.17	0.88	93.09	14.53	4.64	1.00
4	0.68	87.03	13.36	0.70	89.32	13.84	0.70	90.04	13.99	0.82	77.51	11.24	4.94	1.08
5	0.61	75.65	10.92	0.63	78.35	11.49	0.64	78.80	11.59	0.76	65.88	8.723	5.21	1.15
6	0.93	165.37	30.48	0.93	161.37	29.48	0.93	161.54	29.51	0.98	146.41	26.20	8.93	2.08
7	0.86	193.84	35.67	0.86	194.80	35.77	0.86	195.32	35.88	0.94	177.12	31.97	6.39	1.34
8	0.83	61.03	7.51	0.84	58.70	6.92	0.84	58.88	6.96	0.93	52.80	5.58	4.24	1.02
9	0.85	131.37	22.64	0.86	126.75	21.52	0.86	127.10	21.59	0.94	114.96	18.95	8.43	1.95
10	0.90	143.02	24.66	0.77	146.80	25.43	0.90	142.26	24.40	0.96	129.29	21.57	6.09	1.37
11	0.91	149.79	25.81	0.78	152.96	26.44	0.91	148.19	25.35	0.97	134.67	22.41	6.63	1.50
12	0.86	272.07	52.10	0.87	262.85	49.89	0.87	263.55	50.03	0.95	239.28	44.86	16.84	3.84
13	0.88	66.84	8.56	0.88	66.32	8.40	0.89	66.46	8.43	0.92	59.97	6.96	2.59	0.63
14	0.84	249.47	44.78	0.85	251.22	45.02	0.85	251.94	45.17	0.94	227.52	39.96	8.72	1.82
15	0.81	227.14	39.62	0.82	229.69	40.05	0.82	230.46	40.21	0.92	205.73	34.93	9.09	1.90

Note: *E_a and ln A calculations are based on temperature 400°C and heating rate 20°C min^{-1}.

The lower R^2 value for the reaction models of OPS biomass (0.7) as compared to EFB (0.8) can be related to the DTG profile of OPS (*Figure 3*). It clearly shows two reaction peaks in the main devolatilisation region which indicates that the single-step approach may not be accurate in investigating the kinetic triplets, and a multi-step reaction model should be considered (Guo and Lua, 2001; Luangkiattikhun *et al.*, 2008). In contrast, the DTG profile of EFB (*Figure 3*) showed a single reaction peak.

Interestingly, among the AI models, the ANN model most accurately predicted values and pre-exponential factors compared to the experimental values using the CR kinetic method, followed by the SVM and DT models. Although the ANN and SVM models predicted values closer to the experimental dataset, the DT model predicted lower values. It was also observed that the predictions of the E_a and pre-exponential factor values also depend on the type of reaction mechanism. As discussed, the R^2 is lower for most of the reaction mechanisms, indicating that not all reaction mechanisms accurately represent the thermal degradation of oil palm biomass.

CONCLUSION

For the first time, three different AI models (ANN, SVM and DT) were used to predict pyrolysis behaviour, kinetic parameters, and the product yield of oil palm biomass using TGA. Interestingly, all three AI models accurately predicted the biomass pyrolysis behaviour with low MSE values between 0.09 and 5.11 and high R^2 values between 0.949 and 0.999. This study also permitted the extraction of kinetic parameters (activation energy, pre-exponential factor, and reaction model) from the predicted TG data and compared them to experimental data. The ability of the ANN model to predict pyrolysis behaviour, kinetic parameters, and biomass product yield demonstrates the robustness of the algorithm in obtaining the most promising results compared to the SVM and DT models. The ANN displayed high regression coefficients (R^2), low MSE values, and a reasonable training period (100 s). The performance of the developed AI models was slightly better or at least comparable in terms of MSE values to the existing AI models in the literature. AI models promise to become a powerful tool to predict biomass pyrolysis behaviour and kinetic parameters to avoid tedious and lengthy TGA experiments.

ACKNOWLEDGEMENT

This project was financially supported by the Ministry of Higher Education, Malaysia, under the Fundamental Research Grant Scheme (FRGS) No. FRGS/1/2018/TK10/MUSM/03/1. Author is also grateful to Monash University Malaysia campus for the graduate scholarship.

REFERENCES

Abdullah, N and Gerhauser, H (2008). Bio-oil derived from empty fruit bunches. *Fuel, 87(12)*: 2606-2613.

Aghbashlo, M; Almasi, F; Jafari, A; Nadian, M H; Soltanian, S; Lam, S S and Tabatabaei, M (2021). Describing biomass pyrolysis kinetics using a generic hybrid intelligent model: A critical stage in sustainable waste-oriented biorefineries. *Renew. Energy*, *170*: 81-91. DOI: 10.1016/j.renene.2021.01.111.

Ahmad, M S; Liu, H; Alhumade, H; Tahir, M H; Çakman, G; Yıldız, A; Ceylan, S; Elkamel, A and Shen, B (2020). A modified DAEM: To study the bioenergy potential of invasive Staghorn Sumac through pyrolysis, ANN, TGA, kinetic modeling, FTIR and GC–MS analysis. *Energy Convers. Manag., 221*: 113173.

Alaba, P A; Popoola, S I; Abnisal, F; Lee, C S; Ohunakin, O S; Adetiba, E; Akanle, M B; Abdul Patah, M F; Atayero, A A A and Wan Daud, W M A (2020). Thermal decomposition of rice husk: A comprehensive artificial intelligence predictive model. *J. Therm. Anal. Calorim., 140(4)*: 1811-1823. DOI: 10.1007/s10973-019-08915-0.

Arabloo, M; Ziaee, H; Lee, M and Bahadori, A (2015). Prediction of the properties of brines using least squares support vector machine (LS-SVM) computational strategy. *J. Taiwan Inst. Chem. Eng., 50*: 123-130. DOI: 10.1016/j.jtice.2014.12.005.

Asadieraghi, M and Daud, W M A W (2015). In-depth investigation on thermochemical characteristics of palm oil biomasses as potential biofuel sources. *J. Anal. Appl. Pyrolysis, 115*: 379-391.

Aydinli, B; Caglar, A; Pekol, S and Karaci, A (2017). The prediction of potential energy and matter production from biomass pyrolysis with artificial neural network. *Energ. Explor. Exploit., 35(6)*: 698-712. DOI: 10.1177/0144598717716282.

Bhuyan, N; Narzari, R; Bujar Baruah, S M and Kataki, R (2020). Comparative assessment of artificial neural network and response surface methodology for evaluation of the predictive capability on bio-oil yield of *Tithonia diversifolia* pyrolysis. *Biomass Convers. Biorefin.,*: 1-16. DOI: 10.1007/s13399-020-00806-x.

Bi, H; Wang, C; Jiang, X; Jiang, C; Bao, L and Lin, Q (2021). Thermodynamics, kinetics, gas emissions and artificial neural network modeling of co-pyrolysis of sewage sludge and peanut shell. *Fuel, 284:* 118988. DOI: 10.1016/j.fuel.2020.118988.

Bi, H; Wang, C; Lin, Q; Jiang, X; Jiang, C and Bao, L (2020). Combustion behavior, kinetics, gas emission characteristics and artificial neural network modeling of coal gangue and biomass via TG-FTIR. *Energy, 213*: 118790. DOI: 10.1016/j.energy.2020.118790.

Bong, J T; Loy, A C M; Chin, B L F; Lam, M K; Tang, D K H; Lim, H Y; Chai, Y H and Yusup, S (2020). Artificial neural network approach for co-pyrolysis of *Chlorella vulgaris* and peanut shell binary mixtures using microalgae ash catalyst. *Energy, 207*: 118289. DOI: 10.1016/j.energy.2020.118289.

Cai, J; Xu, D; Dong, Z; Yu, X; Yang, Y; Banks, S W and Bridgwater, A V (2018). Processing thermogravimetric analysis data for isoconversional kinetic analysis of lignocellulosic biomass pyrolysis: Case study of corn stalk. *Renew. Sustain. Energy Rev., 82*: 2705-2715. DOI: 10.1016/J.RSER.2017.09.113.

Çakman, G; Gheni, S and Ceylan, S (2021). Prediction of higher heating value of biochars using proximate analysis by artificial neural network. *Biomass Convers. Biorefin.,*: 1-9. DOI: 10.1007/s13399-021-01358-4.

Cao, H; Xin, Y and Yuan, Q (2016). Prediction of biochar yield from cattle manure pyrolysis via least squares support vector machine intelligent approach. *Bioresour. Technol., 202*: 158-164. DOI: 10.1016/j.biortech.2015.12.024.

Castells, B; Amez, I; Medic, L and García-Torrent, J (2021). Torrefaction influence on combustion kinetics of Malaysian oil palm wastes. *Fuel Process. Technol., 218*: 106843. DOI: 10.1016/j.fuproc.2021.106843.

Chen, H; Liu, J; Chang, X; Chen, D; Xue, Y; Liu, P; Lin, H and Han, S (2017). A review on the pretreatment of lignocellulose for high-value chemicals. *Fuel Process. Technol., 160*: 196-206. DOI: 10.1016/j.fuproc.2016.12.007.

Chen, R; Li, Q; Xu, X and Zhang, D (2019). Pyrolysis kinetics and reaction mechanism of representative non-charring polymer waste with micron particle size. *Energy Convers. Manag., 198*: 111923. DOI: 10.1016/J.ENCONMAN.2019.111923.

Chen, X; Zhang, H; Song, Y and Xiao, R (2018). Prediction of product distribution and bio-oil heating value of biomass fast pyrolysis. *Chem. Eng. Process.: Process Intensif., 130*: 36-42. DOI: 10.1016/j.cep.2018.05.018.

Ding, Y; Huang, B; Li, K; Du, W; Lu, K and Zhang, Y (2020). Thermal interaction analysis of isolated hemicellulose and cellulose by kinetic parameters during biomass pyrolysis. *Energy*, *195*: 117010. DOI: 10.1016/j.energy.2020.117010.

Ewees, A A; Aziz, M A E l and Elhoseny, M (2017). Social-spider optimization algorithm for improving ANFIS to predict biochar yield. *2017 8th International Conference on Computing, Communication and Networking Technologies (ICCCNT)*. Delhi, India. p. 1-6. DOI: 10.1109/ICCCNT.2017.8203950.

Guedes, R E; Luna, A S and Torres, A R (2018). Operating parameters for bio-oil production in biomass pyrolysis: A review. *J. Anal. Appl. Pyrolysis*, *129*: 134-149. DOI: 10.1016/J.JAAP.2017.11.019.

Guo, J and Lua, A C (2001). Kinetic study on pyrolytic process of oil-palm solid waste using two-step consecutive reaction model. *Biomass Bioenergy*, *20(3)*: 223-233. DOI: 10.1016/S0961-9534(00)00080-5.

Hameed, S; Sharma, A; Pareek, V; Wu, H and Yu, Y (2019). A review on biomass pyrolysis models: Kinetic, network and mechanistic models. *Biomass Bioenergy*, *123*: 104-122. DOI: 10.1016/j.biombioe.2019.02.008.

Hu, X and Gholizadeh, M (2019). Biomass pyrolysis: A review of the process development and challenges from initial researches up to the commercialisation stage. *J. Energy Chem.*, *39*: 109-143. DOI: 10.1016/j.jechem.2019.01.024.

Huang, Y W; Chen, M Q and Li, Q H (2019). Artificial neural network model for the evaluation of chemical kinetics in thermally induced solid-state reaction. *J. Therm. Anal. Calorim.*, *138(1)*: 451-460. DOI: 10.1007/s10973-019-08232-6.

Jagannadham, V (2010). How do we introduce the Arrhenius pre-exponential factor (A) to graduate students? *Creat.*, *1(2)*: 128. DOI: 10.4236/ce.2010.12019.

Janković, B; Manić, N and Stojiljković, D (2020). The gaseous products characterization of the pyrolysis process of various agricultural residues using TGA–DSC–MS techniques. *J. Therm. Anal. Calorim.*, *139(5)*: 3091-3106. DOI: 10.1007/s10973-019-08733-4.

Kaczor, Z; Buliński, Z and Werle, S (2020). modeling approaches to waste biomass pyrolysis: A review. *Renew. Energy*, *159*: 427-443. DOI: 10.1016/j.renene.2020.05.110.

Kan, T; Strezov, V and Evans, T J (2016). Lignocellulosic biomass pyrolysis: A review of product properties and effects of pyrolysis parameters. *Renew. Sustain. Energy Rev.*, *57*: 1126-1140. DOI: 10.1016/J.RSER.2015.12.185.

Lakovic, N; Khan, A; Petković, B; Petkovic, D; Kuzman, B; Resic, S; Jermsittiparsert, K and Azam, S (2021). Management of higher heating value sensitivity of biomass by hybrid learning technique. *Biomass Convers. Biorefin.* p. 1-8. DOI: 10.1007/s13399-020-01223-w.

Luangkiattikhun, P; Tangsathitkulchai, C and Tangsathitkulchai, M (2008). Non-isothermal thermogravimetric analysis of oil-palm solid wastes. *Bioresour. Technol.*, *99(5)*: 986-997. DOI: 10.1016/J.BIORTECH.2007.03.001.

Mahmood, H; Moniruzzaman, M; Iqbal, T; Yusup, S; Rashid, M and Raza, A (2019). Comparative effect of ionic liquids pretreatment on thermogravimetric kinetics of crude oil palm biomass for possible sustainable exploitation. *J. Mol. Liq.*, *282*: 88-96. DOI: 10.1016/j.molliq.2019.02.133.

Mutsengerere, S; Chihobo, C H; Musademba, D and Nhapi, I (2019). A review of operating parameters affecting bio-oil yield in microwave pyrolysis of lignocellulosic biomass. *Renew. Sustain. Energy Rev.*, *104*: 328-336. DOI: 10.1016/j.rser.2019.01.030.

Myles, A J; Feudale, R N; Liu, Y; Woody, N A and Brown, S D (2004). An introduction to decision tree modeling. *J. Chemom.*, *18(6)*: 275-285. DOI: 10.1002/cem.873.

Naqvi, S R; Hameed, Z; Tariq, R; Taqvi, S A; Ali, I; Niazi, M B K; Noor, T; Hussain, A; Iqbal, N and Shahbaz, M (2019). Synergistic effect on co-pyrolysis of rice husk and sewage sludge by thermal behavior, kinetics, thermodynamic parameters and artificial neural network. *Waste Manage.*, *85*: 131-140. DOI: 10.1016/j.wasman.2018.12.031.

Naqvi, S R; Tariq, R; Hameed, Z; Ali, I; Taqvi, S A; Naqvi, M; Niazi, M B K; Noor, T and Farooq, W (2018). Pyrolysis of high-ash sewage sludge: Thermo-kinetic study using TGA and artificial neural networks. *Fuel*, *233*: 529-538. DOI: 10.1016/j.fuel.2018.06.089.

Paenpong, C and Pattiya, A (2016). Effect of pyrolysis and moving-bed granular filter temperatures on the yield and properties of bio-oil from fast pyrolysis of biomass. *J. Anal. Appl. Pyrolysis*, *119*: 40-51. DOI: 10.1016/j.jaap.2016.03.019.

Papari, S and Hawboldt, K (2015). A review on the pyrolysis of woody biomass to bio-oil: Focus on kinetic models. *Renew. Sust. Energ. Rev., 52*: 1580-1595.

Pattanayak, S; Loha, C; Hauchhum, L and Sailo, L (2020). Application of MLP-ANN models for estimating the higher heating value of bamboo biomass. *Biomass Convers. Bioref., 11*: 2499-2508. DOI: 10.1007/s13399-020-00685-2.

Radmanesh, R; Courbariaux, Y; Chaouki, J and Guy, C (2006). A unified lumped approach in kinetic modeling of biomass pyrolysis. *Fuel, 85(9)*: 1211-1220.

Rezk, H; Nassef, A M; Inayat, A; Sayed, E T; Shahbaz, M and Olabi, A G (2019). Improving the environmental impact of palm kernel shell through maximizing its production of hydrogen and syngas using advanced artificial intelligence. *Sci. Total Environ., 658*: 1150-1160. DOI: 10.1016/j.scitotenv.2018.12.284.

Russell, S and Norvig, P (2016). *Artificial Intelligence: A Modern Approach.* 3rd edition. Pearson, London. p. 744-748.

Sharifzadeh, M; Sadeqzadeh, M; Guo, M; Borhani, T N; Murthy Konda, N V S N; Garcia, M C; Wang, L; Hallett, J and Shah, N (2019). The multi-scale challenges of biomass fast pyrolysis and bio-oil upgrading: Review of the state of art and future research directions. *Prog. Energy Combust. Sci., 71*: 1-80. DOI: 10.1016/J.PECS.2018.10.006.

Smith, M B and March, J (2013). *March's Advanced Organic Chemistry: Reactions, Mechanisms and Structure*. 7th edition. John Wiley and Sons, New Jersey. 2080 pp.

Surahmanto, F; Saptoadi, H; Sulistyo, H and Rohmat, T A (2020). Investigation of the pyrolysis characteristics and kinetics of oil-palm solid waste by using Coats-Redfern method. *Energy Explor. Exploit., 38(1)*: 298-309. DOI: 10.1177/0144598719877759.

Teng, S Y; Loy, A C M; Leong, W D; How, B S; Chin, B L F and Máša, V (2019). Catalytic thermal degradation of *Chlorella vulgaris*: Evolving deep neural networks for optimization. *Bioresour. Technol., 292*: 121971. DOI: 10.1016/j.biortech.2019.121971.

Truhlar, D G (1978). Interpretation of the activation energy. *J. Chem. Educ., 55(5)*: 309.

Várhegyi, G; Antal Jr, M J; Jakab, E and Szabó, P (1997). Kinetic modeling of biomass pyrolysis. *J. Anal. Appl. Pyrolysis, 42(1)*: 73-87.

Vyazovkin, S; Burnham, A K; Criado, J M; Pérez-Maqueda, L A; Popescu, C and Sbirrazzuoli, N (2011). ICTAC kinetics committee recommendations for performing kinetic computations on thermal analysis data. *Thermochim. Acta, 520(1-2)*: 1-19.

Wang, B; Xu, F; Zong, P; Zhang, J; Tian, Y and Qiao, Y (2019). Effects of heating rate on fast pyrolysis behavior and product distribution of Jerusalem artichoke stalk by using TG-FTIR and Py-GC/MS. *Renew. Energy*, *132*: 486-496. DOI: 10.1016/j.renene.2018.08.021.

Wang, S; Dai, G; Yang, H and Luo, Z (2017). Lignocellulosic biomass pyrolysis mechanism: A state-of-the-art review. *Prog. Energy Combust. Sci., 62*: 33-86. DOI: 10.1016/J.PECS.2017.05.004.

Wang, X; Li, D; Yang, B; Liu, Y and Li, W (2013). Pyrolysis characteristics and kinetics of bamboo. *J. Biobased Mater. Bioenergy, 7(6)*: 702-707.

Wei, L; Xu, S; Zhang, L; Zhang, H; Liu, C; Zhu, H and Liu, S (2006). Characteristics of fast pyrolysis of biomass in a free fall reactor. *Fuel Process. Technol., 87(10)*: 863-871.

Yıldız, Z; Uzun, H; Ceylan, S and Topcu, Y (2016). Application of artificial neural networks to co-combustion of hazelnut husk-lignite coal blends. *Bioresour. Technol., 200*: 42-47. DOI: 10.1016/j.biortech.2015.09.114.

Zhang, J; Liu, J; Evrendilek, F; Zhang, X and Buyukada, M (2019). TG-FTIR and Py-GC/MS analyses of pyrolysis behaviors and products of cattle manure in CO_2 and N_2 atmospheres: Kinetic, thermodynamic, and machine-learning models. *Energy Convers. Manag., 195*: 346-359. DOI: 10.1016/j.enconman.2019.05.019.

Zhang, W; Zhang, J; Ding, Y; He, Q; Lu, K and Chen, H (2021). Pyrolysis kinetics and reaction mechanism of expandable polystyrene by multiple kinetics methods. *J. Clean Prod., 285*: 125042. DOI: 10.1016/j.jclepro.2020.125042.

Zhu, X; Li, Y and Wang, X (2019). Machine learning prediction of biochar yield and carbon contents in biochar based on biomass characteristics and pyrolysis conditions. *Bioresour. Technol., 288*: 121527. DOI: 10.1016/j.biortech.2019.121527.

Journal of Oil Palm Research Vol. 35 (1) March 2023 p. 100-110
DOI: https://doi.org/10.21894/jopr.2022.0039

DEVELOPMENT AND FIELD EVALUATION OF A SEEDLING POLYBAG SOIL FILLING MACHINE FOR OIL PALM NURSERY

HASLINA HASSAN[1]; AZMI YAHYA[1,4,5]*; DARIUS EL PEBRIAN[2]* and AHMAD SUHAIZI MAT SU[3,4,5]

ABSTRACT

The need to produce high-quality seedlings with adequate quantity has placed a burden on nursery operators, who often require substantial capital and labour with limited daily production capability. The goal of this project was to develop a seedling polybag soil filling machine and evaluate its performance in a simulated oil palm nursery, emphasising small polybag production. The 51 kW diesel engine of a universal, multipurpose 4WD (four-wheel drive) prime mover was utilised to transmit the power to the mixer and auger of the machine system. The recorded average production capacity was 198 bags man hr^{-1}, which was 24.24% higher than the conventional practice of 150 bags man hr^{-1}. The final weight was within the limit (<5%) for both small and large polybags. The production capacity of the machine was moderately improved, despite an increase of approximately 53% in total costs per polybag over the conventional practice. Generally, the machine can be deployed in seedling production of the oil palm nursery stage to fill the polybags with suitable planting media selection.

Keywords: mechanisation, oil palm nursery, polybag machine, seedling polybag, soil filling.

Received: 28 October 2021; **Accepted:** 24 May 2022**; Published online:** 18 July 2022.

INTRODUCTION

Replanting the existing plantation areas is always given great attention by the Malaysian oil palm industry players as well as smallholders (Ishak *et al*., 2020) in an effort of sustaining its competitiveness as the second largest palm oil producing country in the world. This is consistent with Ismail and Mamat (2002), who stated that replanting should be conducted in estates having high costs of production but falling profit. Wahid and Simeh (2010) added that the replanting programme should enable changes to the palm supply chain, which catalyses the country's high-income strategy. Smallholders are involved in both the Replanting Subsidiary Scheme for Oil Palm Smallholders (TSSPK) and the Oil Palm Smallholders New Planting scheme (TBSPK) for Independent Smallholders (ISH) (Ishak *et al*., 2020) that has been established in 2011 as one of the eight Entry Point Projects (EPP) in National Key Economic Area of the 10th Malaysia Plan.

In 2020, there has been a steady supply of germinated oil palm seeds from the oil palm nurseries in the country, despite a decrease in demand by 4.9% from 2019, coupled with a reduction from 41 million to 39 million seeds due to the decrease in oil palm planted areas. Additionally, seedling losses owing to culling procedures account for around 25.0% to

[1] Department of Biological and Agricultural Engineering, Faculty of Engineering, Universiti Putra Malaysia, 43400 UPM Serdang, Selangor, Malaysia.

[2] Faculty of Plantation and Agrotechnology, Universiti Teknologi MARA, Melaka Branch, Jasin Campus, 77300 Merlimau, Melaka, Malaysia.

[3] Department of Agricultural Technology, Faculty of Agriculture, Universiti Putra Malaysia, 43400 UPM Serdang, Selangor, Malaysia.

[4] Institute of Plantation Studies, Universiti Putra Malaysia, 43400 UPM Serdang, Selangor, Malaysia.

[5] Smart Farming Technology Research Centre, Faculty of Engineering, Universiti Putra Malaysia, 43400 UPM Serdang, Selangor, Malaysia.

* *Corresponding author e-mail: azmiy@upm.edu.my, darius@uitm.edu.my*

30.0% and 20.0% to 25.0% of seedling losses in single-stage and double-stage nurseries, respectively, which averaged approximately 15.0% (Ab Rahman *et al*., 2008). As a result, an additional 15.0% of the annual demand must be added to the seedling preparation. This strategy is only conceivable with better nursery seedling variety selection, pest, and disease management (Rebitanim *et al*., 2020), and the addition of a new mechanism or machinery system that facilitates seedling planting.

In fulfilling the extensive demand for high-quality germinated seeds for the replanting and new planting areas throughout the country, two nursery techniques were commonly applied at the oil palm nursery, *i.e*., single-stage and double-stage nursery techniques (Turner and Gillbanks, 2003). In the single stage, the germinated seeds are planted directly into the large polybags (45 x 38 cm) at the main nursery without any pre-nursery activities. In the double-stage, the germinated seeds are first planted in small polybags (23 x 15 cm) and then arranged together in the special pre-nursery beds. These small polybags will be left on the beds for about 10 to 14 weeks before they are transplanted into large polybags (Duckett, 1989). Rankine and Fairhurst (1999) stated that the double-stage nurseries are generally preferred because the seeds can be given intensive care and attention during the critical early growth period.

The current practices in seedling production were tedious and laborious which contributed significantly to the worker's fatigue and stress. In addition, labour shortage in the oil palm plantation sector has now become a contributing factor in slowing down the seeds production for planting in new areas and replanting the present areas. The current labour usage in the oil palm plantations was only about 4 to 5 ha per worker. There have been very few studies attempted to build machinery for oil palm nursery operations, such as those conducted by Johari and Pebrian (2015) and Johari *et al*. (2020) for holing soil in large polybags at the nursery. However, their machinery was not specifically designed for soil filling in polybags.

This study presents the development and field evaluation processes of a newly developed seedling polybag soil filling machine, for use with a 23 x 15 cm size polybag in the oil palm nursery. This machine system is attached to a universal carrier 4WD prime mover with a 51 kW diesel engine size.

MATERIALS AND METHODS

Time and Motion Study on the Current Practice in Nursery

Before designing the proposed machine system, a time and motion study on the current operation of soil filling in polybags was carried out at an oil palm nursery in Tun Razak Agricultural Research Centre, Felda Jengka, Pahang, Malaysia (*Figure 1*). In this study, filling polybags with soil was divided into several tasks (*Table 1*). The duration to perform each task in the whole operation was also measured. Three workers were involved in the operation. This data was used as a benchmark to improve the processes and optimise the performance in the design of the proposed machine system.

Time for arranging the working area with wooden planks refers to the total time when the worker starts arranging the borders of the working area with available wooden planks. In the nursery, the working area for this operation has been already bordered by wooden planks. The workers are required to do a minor arrangement of the wooden planks before starting the actual work tasks. Time for breaking the soil clod and delivering the soils with a wheelbarrow refers to the total time when the worker starts breaking soil clods at the soil heap area and delivering the soils on the ground at the filling area. Filling polybags with soil refers to the total time when the worker starts filling a polybag with soil until it is filled. Planting germinated seeds refers to the total time when the worker starts planting a germinated seed in a polybag until it is completely planted.



(a) Breaking soil clods and delivering the soil to the filling area with a wheelbarrow.



(b) Filling polybags with soil.



(c) Planting germinated seeds.

Figure 1. Typical tasks involved in filling polybags with soil in current practice at oil palm nursery.

TABLE 1. TASK DURATION FOR FILLING POLYBAGS WITH SOIL IN THE CURRENT PRACTICE AT THE OIL PALM NURSERY

Tasks	Mean task duration, s man bag^{-1}	Proportion (%)
Arranging the working area with wooden planks	0.60	3.55
Breaking soil clods and delivering the soils with a wheelbarrow to the filling area	1.88	11.10
Filling polybags with soil	9.92	58.83
Planting germinated seeds	4.46	26.45
Total	16.86	100.00

The proportion of task duration was calculated by dividing a task duration by the total completion time of the operation. Filling polybags with soil was the most time-consuming task which took the largest share of about 58.83% of the total time in pre-nursery operation, followed by planting germinated seeds, breaking soil clods and delivering the soil to the filling area. Meanwhile, arranging the working area using wooden planks consumed about 3.55% of the total time, being the least time-consuming task in the operation (*Table 1*). The total completion time of the operation with the current practice was 16.86 s. Production capacity of the current practice (bags man hr^{-1}) was computed by dividing 1 hr or 3600 s by the mean total completion time of current practice (s man per bag) and multiplying the computed value by field efficiency (%). An average of 70% field efficiency was assumed to be sustained for 8 hr within the workday. This is taken into consideration as stated by Nybo *et al.* (2001), the consistency of humans' physical performance may decrease due to the increased working hours and other working environment factors. Thus, with a mean total completion time of 16.86 s man bag^{-1}, and assuming 70% field efficiency, the computed production capacity of current practice would be 150 bags man hr^{-1}.

Machine Design Criteria

The following criteria were considered in establishing the basic design of the seedling polybag soil filling machine system:

- Simple in construction, operation, and maintenance
- Fully integrated as a one-unit machine system with the universal, multipurpose 4WD prime mover
- Ergonomically constructed to reduce worker fatigue in conducting the operation
- Efficient in operation, with good working productivity with less manpower requirement
- Robust in construction, for high machine durability in rough working conditions

Machine Design Configuration

The design concept of the machine system as in *Figure 2,* consists of the hopper, mixing agitator, screw delivery auger, and operator and support platform. The overall dimension of the machine is 560 cm in length, 202 cm in width, and 259 cm in height. This machine is fully mounted on a universal, multipurpose 4WD prime mover with an engine size of 51 kW at the rated speed of 2600 rpm. This new machine (*Figure 3*) is used for filling planting media in 23 cm x 15 cm sized polybags or small-sized polybags.

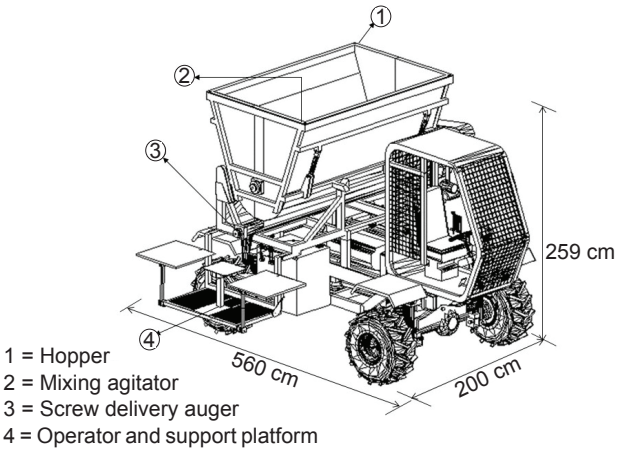


Figure 2. The 3D (three-dimensional) design concept of machine system fully mounted on a 4WD prime mover.



Figure 3. The prototype machine system is mounted on a 4WD prime mover.

Hopper. The hopper was designed to accommodate about 1.5 t of planting media. With a full capacity hopper, it can produce a total of about 1071 small sized polybags (23 x 15 cm), with each having an average weight of 1.4 kg. The hopper was constructed using a 4 mm thick mild steel (MS) sheet and has a trapezoidal shape with overall dimensions of 215 cm length x 145 cm width x 123 cm height. The front and rear walls of the hopper were hinged at the bottom to provide the possibility for the walls to be tilted towards the hopper's longitudinal centre by the action of the two small 4 cm bore x 20 cm stroke hydraulic cylinders on each side of the walls. This action is necessary to be done intermittently during the machine operation to overcome the clogging problems of the planting media in the hopper. This action, at the same time, could also help to push the planting media towards the hopper's longitudinal centre at the position where the screw deliver auger was positioned. The whole hopper was pivoted at its rear to support the frame structure, to allow the hopper to tip rearwards. These actions could be done hydraulically by the two 7 cm bore x 38 cm stroke hydraulic cylinders that were located on the sides of the hopper. Tipping of the hopper is necessary for clearing the planting media in the hopper before and after the polybag filling operation. This hopper was mounted to a common support frame that was made from 75 x 50 x 6 mm MS hollow sections. This same support frame was also used to provide the attachment facilities for other components that make up the complete polybag filling machine. All the earlier mentioned six hydraulic cylinders were powered by a Ronzio-11 tandem gear pump, with 11.3 cm^3 rev^{-1} displacement at 330 bar continuous pressure that was mounted in tandem with the Sauer Danfoss Series 40 main pump of the 4WD multipurpose prime mover.

Mixing agitator. A mixing agitator unit (*Figure 4*) was designed to break the clods and at the same time provide a homogenous planting media mixture in the hopper. The agitator had four MS blades with dimensions of 14 x 37 cm and was mounted on a rotating shaft located along with the centre longitudinal position of the hopper. This mixing agitator functions to turn and mix the planting media and prevents the occurrence of planting media blockage in the hopper which may hinder the easy flow of the mixture into the screw delivery auger at the bottom of the hopper. The rotating power for the mixing agitator in the hopper was provided by the Ronzio-20 tandem gear pump, with 20.1 cm^3 rev^{-1} displacement at 230 bar continuous pressure that was also connected in tandem to the Sauer Danfoss Series 40 main pump of the 4WD multipurpose prime mover. The power of the pump was used to run the Samhydraulik ARC 80 hydraulic with a 1:50 gear reduction (HU85A-WN, Watt Drive, Singapore) and finally a sprocket-chain drive system with a ratio of 1:2 and its driven pulley mounted on the mixing agitator shaft. With such speed reduction, the desired rotational speed of 9 rpm could be made possible for the mixing agitator.

Screw delivery auger. The screw delivery auger was designed to deliver the planting media out from the hopper at the required discharge rate into an awaiting polybag that is located at the outlet end of the screw deliver auger chute. The rotating power for this 6 cm diameter size and 7.5 cm pitch screw delivery auger is provided by the Ronzio-6 tandem gear pump with 6.28 cm^3 rev^{-1} displacement at 300 bar continuous pressure that was also connected in tandem to the Sauer Danfoss Series 40 main pump of the 4WD multipurpose prime mover. The rotating power from the hydraulic motor was then made to run a worm-type reduction gear with a 1:5 reduction ratio and a sprocket-chain drive system with a 1:2 reduction ratio to provide a final screw delivery auger rotational speed of 150 rpm. The screw delivery auger was operated by controlling the Ronzio-6 tandem gear pump through a foot pedal level located in the closed vicinity of the machine operator seat.



Figure 4. The mixing agitator is on top of the screw delivery auger in the hopper.

Operator and support platform. The operator and support platform where the major operation and control activities are being conducted by the machine operator. A comfortable seat is provided at the right side of the hopper and located close to the opening end of the screw delivery auger chute. Human-machine factors were considered in designing the seat to ensure comfort, easiness, and safety for the operator in carrying out his tasks. All hydraulic hand lever controls for the hopper cylinder hydraulics and mixing agitator motor was positioned at the operator's hand level position on the right side of the operator seat while the foot pedal level control for the screw delivery auger motor was positioned at the operator's foot level position at the right side of the operator seat. A support platform was provided at either side of the operator seat for the temporary placement of the filled polybag. A specially made wooden tray measuring 61 cm width x 61 cm length x 15 cm height, with eight equal space components was used to accommodate 8 filled polybags at one time. This wooden tray was used to transfer the filled polybags to the final seedling placement location in the nursery. About 10 sets of these wooden trays were used during the machine operation.

Machine Operation

This 4WD prime mover, with the mounted polybag filling machine system is operated by two operators; the prime mover driver, who conducts the filling of the polybags and drives the prime mover, while another operator carries and unloads the filled polybags from the wooden tray at the seedling placement area. Before starting the operation, the heaped planting media is loaded into the hopper of the machine. Prior to that, the planting media needs to be manually cleared from the presence of residual roots, woods, small stones and other debris. Lifting the planting media into the hopper of the machine system was done by a tractor with a front loader. Upon completion of filling the hopper to its full capacity, the operator would drive the 4WD prime mover with the mounted machine system to the place where the polybag filling operation is to be conducted within the available nursery area. This chosen working area shall also be the place where the filled polybags later were to be permanently kept in the nursery. The actual work starts with the running of the mixing agitator on the machine system while keeping the 4WD prime mower engine running ideal under a stationary mode position. The mixing agitator shall be left continuously running for at least 5 min to make sure that the planting media in the hopper was properly mixed and not clogged.

Field Performance Evaluation of the Developed Prototype Machine System

A field performance evaluation test on the developed prototype machine system was conducted for the polybag soil filling operation using a 23 x 15 cm sized polybag (small size) and 45 x 38 cm sized polybag (large size) under a simulated field environment at the laboratory (*Figures 5* and *6*). The test on the small-sized polybags was for the production of 400 units of the filled polybags while the test on the big-sized polybags was for the production of 100 units of the filled polybags. The same evaluation test on the machine system was repeated for three different days.

Generally, the completed work which involved filling the polybag with soil using this machine system for the seed planting operation in the nursery area involves the following five main tasks; 1. Filling polybags with soil, 2. Loading the filled polybags into a wooden tray/wheelbarrow, 3. Carrying or transporting filled polybags to seedling placement location in the nursery, 4. Unloading and arranging the filled polybags at the seedling placement location, 5. Carrying or transporting back the empty wooden tray/wheelbarrow to the machine. A millisecond digital stopwatch was used to measure the duration of time taken by the operator in completing each of the earlier five tasks for the preparation of 400 units of small and 100 units of largely filled polybags for the day. Polar S810 Heart Rate Monitor and Transmitter (Polar, 2013) were placed in direct contact with the upper body of the two operators for monitoring their heart rate while they were conducting the relevant tasks throughout the daily operation. This instrument had been proven to provide valid measurements of heart rate when compared with electrocardiograms (Karvonen *et al.*, 1984; Leger and Thivherge, 1988; Treiber *et al.*, 1989).

The definition of time durations measured in the time and motion study of the developed prototype machine system is tabulated in *Table 2*. The proportion of task duration was calculated by dividing a task duration by the total completion time of the operation.

Ten small-sized filled polybags and 10 large-sized filled polybags were randomly picked from the pool of the respective polybags after the third day of the soil filling operations with the machine system. The weight of these selected filled polybags was taken and recorded by using a Sartorius BCE8200-1S electronic weighing scale. Duncan's Multiple Range Test (DMRT) was applied to compare the mean task duration performed by the workers and the mean increase in heart rate of workers at a 0.05 probability level.

TABLE 2. THE DEFINITION OF TIME DURATIONS MEASURED IN THE TIME AND MOTION STUDY OF THE DEVELOPED PROTOTYPE MACHINE SYSTEM

Time duration	Definition
Time for filling a polybag with soil	Total time from when the machine operator starts placing an empty polybag to the outlet delivery auger chute until the time when the polybag was completely filled with soil
Time for loading eight filled small polybags on the wooden tray	Total time from when the operator starts loading the first filled small polybag into the wooden trays and repeating these steps until a total of eight filled small polybags were in the wooden tray
Time for loading four filled large polybags into the wheelbarrow	Total time from when the operator starts loading the first filled large polybag into the wheelbarrow and repeating these steps until a total of four filled large polybags were in the wheelbarrow
Time for carrying or transporting the fully loaded wooden tray	Total time from when the operator starts carrying the fully loaded wooden tray to the seedling placement location
Time for carrying or transporting fully loaded wheelbarrow	Total time from when the operator starts pushing the fully loaded wheelbarrow to the seedling placement location
Time for unloading and arranging the polybags (small size) at the seedling placement location	Total time from when the operator starts pulling the floor bottom of the wooden tray for the small filled polybags to be left on the ground at the seedling placement location
Time for unloading and arranging the polybags (large size) at the seedling placement location	Total time from when the operator starts unloading the first large filled polybag from the wheelbarrow and placing the polybag on the ground at the seedling placement location and repeats the task until a total of four filled polybags were on the ground at the seedling placement location
Time for carrying back the empty wooden tray to the machine system	Total time from when the operator starts carrying back the empty wooden tray from the seedling placement location to the machine system
Time for carrying back the empty wheelbarrow	Total time from when the operator starts pushing back the empty wheelbarrow from the seedling placement location to the machine system



(a) Filling polybag with soil.



(b) Loading the filled polybags in a wooden tray.



(c) Carrying the loaded wooden tray to the seedling placement location.



(d) Unloading and arranging the polybags at seedling placement location.



(e) Carrying the empty wooden tray back to the machine.

Figure 5. The tasks involved soil filling of small polybags with the machine system.



(a) Filling polybag with soil.



(b) Loading the filled polybags in a wheelbarrow.



(c) Transporting the loaded wheelbarrow to the seedbed.



(d) Unloading and arranging the polybags at the seedbed.



(e) Transporting the emptied wheelbarrow to the machine.

Figure 6. The tasks involved filling large polybags with the machine system.

RESULTS AND DISCUSSION

Overall Field Performance of Machine System

Tables 3 and *4* show the mean task duration and mean increase in the heart rate of the worker in completing the respective tasks with this new machine system. The task involved was interpreted either as time-consuming tasks or demanding tasks. Any task within the operation that showed the longest duration proportion would be regarded as the most time-consuming, while any task with the highest mean increase in heart rate would be regarded as the most demanding.

For small polybags as seen in *Table 3*, filling polybags with soil took about 48.02% of the mean total time and was the most time-consuming task among all other tasks that are involved with the machine system. Carrying a filled polybag in a wooden tray to the seedling placement location and carrying back an empty wooden tray to the machine system spent 5.23% and 5.01% of the mean total time and were the least time-consuming tasks. During filling the polybag with soil, the machine operator spent more time tapping and shaking the polybag to obtain the right firmness and content of the soil in the polybag. On the other hand, carrying the loaded wooden tray to the seedling placement location and carrying back the empty wooden tray to the machine system was the least time-consuming since the location of the seedling placement location with the machine system was quite close. Loading the filled polybags into the wooden tray and carrying the wooden tray to the seedling placement location where the two most demanding tasks since both showed the highest mean increase in heart rate of the operator.

For large polybags as in *Table 4*, filling polybags with soil took about 49.12% of the mean total time and was the most time-consuming task among the respective tasks. Transporting the loaded wheelbarrow and transporting the empty wheelbarrow back to the machine location spent about 3.72% and 4.33% of the mean total time. These two tasks were the least time-consuming tasks. As before, the operator spent a long time filling the polybag with soil since he had to frequently tap and shake the polybag to obtain the right firmness and content of the soil in the polybag. Nonetheless, with the large-sized polybag, the task was longer than the smaller sized polybags since a bigger volume and weight of soil mass was involved as compared with the earlier task with smaller sized polybags. Transporting the loaded wheelbarrow to the seedling placement location and transporting emptied wheelbarrow back to the machine system were the least time-consuming since the location between the seedbed and machine system was quite close. However, loading the filled polybags into the wheelbarrow, and unloading and arranging the filled polybags at the seedling placement location were the two most demanding tasks, as reflected by the highest mean increase in heart rate of the operator.

TABLE 3. TASK DURATION AND HEART RATE INCREASE OF WORKERS IN FILLING SMALL POLYBAGS WITH SOIL BY MACHINE SYSTEM

Task[1]	Number of replicates	Mean task duration (s man bag^{-1})	Proportion (%)	The mean increase in heart rate (beats min^{-1})
Filling polybag with soil	400	8.73^{a} ± 0.13	48.02	9.26^{d} ± 0.29
Loading the filled polybags into wooden tray	400	3.70^{b} ± 0.32	20.35	42.91^{a} ± 1.69
Carrying filled polybag in wooden tray to seedling placement location	400	0.95^{c} ± 0.06	5.23	41.84^{a} ± 1.42
Unloading and arranging the filled polybags at the seedling placement location	400	3.89^{b} ± 0.15	21.40	26.29^{c} ± 1.01
Carrying back empty wooden tray to machine system	400	0.91^{c} ± 0.06	5.010	28.58^{b} ± 1.24

Note: [1]Means in a given column having suffices with the same letters are treated not significantly different at 0.05 probability level by DMRT.

TABLE 4. TASK DURATION AND HEART RATE INCREASE OF WORKERS IN FILLING LARGE POLYBAGS WITH SOIL BY MACHINE SYSTEM

Task[1]	Number of replicates	Mean task duration (s man bag^{-1})	Proportion (%)	The mean increase in heart rate (beats min^{-1})
Filling polybag with soil	100	26.65^{a} ± 0.67	49.12	8.21^{c} ± 0.46
Loading filled polybags in wheel barrow	100	19.41^{b} ± 1.57	35.77	28.07^{a} ± 1.76
Transporting filled polybag in a wheelbarrow to the seedling placement location	100	2.02^{d} ± 0.19	3.72	24.39^{b} ± 1.61
Unloading and arranging the filled polybag at the seedling placement location	100	3.82^{c} ± 0.29	7.04	29.16^{a} ± 1.77
Transporting back empty wheel barrow to machine system	100	2.35^{d} ± 0.14	4.33	24.79^{b} ± 1.68

Note: [1]Means in a given column having suffices with the same letters are treated as not significantly different at 0.05 probability level by DMRT.

Generally, if further improvements can be made on this new machine system, the focus should be strategically made on the design improvement on the parts of the machine system, which were the most time consuming and demanding in completing the tasks within the whole operation.

Table 5 shows the production capacity comparison between using the new machine system and current practice in small polybag soil filling operations. Comparison with the large polybag was not possible here because there was no available data on the production capacity with large polybags using the current practising manual operation method at the nursery. The production capacity of this new machine system (bags man hr^{-1}) was computed by dividing 1 hr or 3600 s by the mean total completion time of this new machine system (s man per bag). With a mean total completion time of 18.18 s man bag^{-1} for all tasks in *Table 3*, thus, the computed production capacity of the new machine system was 198 bags man hr^{-1} or 24.24% higher than the output of 150 bags man hr^{-1} of the current practice at the nursery.

TABLE 5. PRODUCTION CAPACITY COMPARISON BETWEEN MACHINE SYSTEM AND CURRENT PRACTICE IN SMALL POLYBAG SOIL FILLING OPERATION

Parameter	Operational methods		Differences (%)
	Current practice	Machine system	
Production capacity (bags man hr^{-1})	150^{a}	198^{b}	24.24

Note: ^{a,b} Means in a given row having sufficed with the same letters are treated not significantly different at 0.05 probability level by DMRT.

Generally, the weight of polybags with soil was slightly higher than the recommended weight. The average weight of small polybags with soil was 2.44 kg or exceeded 38.00% of the recommended weight of 1.5 kg per polybag by Turner and Gilbanks (2003). The same situation also occurred when filling large polybags, where the average weight of large polybags with soil was 18.91 kg or exceeded 20.67% of the expected weight of 15.00 kg as suggested by Turner and Gilbanks (2003). The extra soil being filled in both the small and large polybags was due to the judgment error by the operator while conducting the soil filling task with the machine

system. Further design improvement by installing a weight sensor and control systems on the chute of the screw delivery auger would greatly help the machine system to consistently produce the recommended weight of soil-filled polybag.

Costs Analysis

An estimated total market price of RM101 975 for the machine system was derived from the sum of RM61 975 for the prime mover and RM40 000 for the soil bagging machine attachment. The estimated economic life of the prime mover with the machine attachment was computed based on the economic life of 16 000 hr for the 4WD tractors (ASABE, 2015b) divided by the total operating hours of the tractor in a year. The proposed estimated economic life was considered since the prime mover itself acts as a universal carrier for conducting other field operations such as field seedling transplanting, circle spraying, and in-field FFB collection-transportation. The total annual operating hours for the individual machine systems were estimated based on the listed parameters (Pebrian and Yahya, 2012; Roodi *et al*., 2011) as shown in *Table 6*.

The actual total annual operating hours of the prime mover with the polybag soil filling machine system were expected to be 2251 hr based on the operation frequency of one time a year (Ghani *et al*., 2001), average oil palm plantation estate size of 1005 ha (EPU, 2010) with a total of 1 336 680 million palm trees and a planting density of 136 palms ha^{-1}, and a machine output of 1584 bags man day^{-1}.

The machine system was assumed to have salvage values of 10% of its initial purchase price (Kepner *et al*., 1982). Tax, shelter, and insurance are 2% of the total initial costs of the machine systems (ASABE, 2015a). An interest rate on the higher extreme value of 10% was assumed under the present economic scenario in Malaysia. Repair and maintenance factors *RF1* of 0.003 and *RF2* of 2.0 were assumed for the new machine system based on the value of repair and maintenance factors for the 4WD tractors (ASABE, 2015b). Lubricant costs of the machine systems were estimated to be 15% of their fuel costs based on the study by Kepner *et al.* (1982). The daily standard wage for a tractor operator in an oil palm plantation is RM4.48 hr^{-1} based on personal communications with two oil palm plantation managers in Selangor and Pahang.

Thus, the estimated total cost of operation of the new machine system was RM25.65 hr^{-1} as in *Table 7*. With the machine production capacity of 198 bags man hr^{-1}, thus, the total cost of filling polybag operation would be RM0.13 bag^{-1} or slightly higher than that the costs of the current practice at RM0.06 bag^{-1}. An increment of about 53% in total costs per polybag was due to the high initial cost of the new machine. The depreciation cost was the highest among the cost components of the machine due to the estimated market price of the proposed machine system which was on the high side as the machine is in the prototype stage. Nonetheless, a small upgrade to the current machine system by the installation of a sensing and control circuit to the auger unit is highly recommended. Having such a system could help in speeding up the soil filling task and at the same time regulate the amount of soil going into the polybag, resulting in a significant increase in machine output capacity to justify the machine's high total cost.

CONCLUSION

A polybag soil filling machine system for the oil palm nursery had been successfully developed and evaluated. The machine has a mobility advantage

TABLE 6. REQUIRED NUMBER OF MACHINE SYSTEMS AND THEIR RESPECTIVE ANNUAL TOTAL OPERATING HOURS FOR AN AVERAGE-SIZED OIL PALM PLANTATION[1]

Machine system	Frequency of operation in a year	Machine field capacity, ha day^{-1} or bags man day^{-1}	Total required number of machine systems, dimensionless	Total annual operating hours for each machine system (hr)
Prime mover with a seedling polybag soil filling machine	1	1584	3	2 251
Prime mover with seedling transplanting	1	6.002	1	1 340
Prime mover with circle spraying	4	7.893	2	2 038
Prime mover with FFB infield collection transporting	26	14.163	6	2 460

Note: [1] Based on an average plantation size of 1005 ha and available total working days in the year of 312 days. (Pebrian and Yahya, 2012; Roodi *et al.*, 2011)

TABLE 7. ESTIMATED TOTAL COSTS OF THE DEVELOPED SOIL BAGGING MACHINE

Cost component	Cost (RM hr^{-1})	Proportion of total cost (%)	Rank based on the highest cost
Depreciation cost	5.82	22.69	1
Interest on investment cost	2.49	9.71	5
Tax, shelter and insurance cost	0.91	3.55	6
Repair and maintenance cost	4.82	18.79	4
Fuel consumption cost	5.65	22.03	2
Lubricants cost	0.85	3.31	7
Operator cost	5.11	19.92	3
Total costs	25.65	100.00	

since it is fully mounted onto a specially developed 4WD prime mover. Being mobile, this machine system could be transported to conduct the polybag soil filling operation at the seedling placement location in an open area of the oil palm nursery. The machine system performance could be further improved through proper refinement in its design and proper training for the person who is operating the machine system.

REFERENCES

ASABE (2015a). ASAE Standards EP 496.3 FEB 2006 (R2015). *Agricultural Machinery Management*. American Society of Agricultural and Biological Engineers (ASABE). https://elibrary.asabe.org/standards.asp, accessed on 1 May 2019.

ASABE (2015b). *ASAE Standards D 497.7 MAR 2011 (R2015). Agricultural Machinery Management Data*. American Society of Agricultural and Biological Engineers (ASABE). https://elibrary.asabe.org/standards.asp, accessed on 1 May 2019.

Ab Rahman, A K; Ramli, F; Shariff, S M and Simeh, M A (2008). The Malaysian palm oil supply chain: The role of the oil palm nursery operators. *Oil Palm Industry Economic J., 8(1)*: 24-33.

Duckett, J E (1989). *A Guide to Oil Palm Nurseries*. The Incorporated Society of Planters. Kuala Lumpur, Malaysia. p. 6-80.

EPU (2010). *Principle Statistics of Oil Palm Estates 2000-2008*. Economics Planning Unit Malaysia. http://www.epu.jpm.my., accessed on 1 February 2015.

Ghani, E A; Dolmat, M T and Wahid, M B (2001). *Manual Penanaman dan Penyelenggaraan Sawit untuk Sektor Pekebun Kecil*. MPOB, Bangi. p. 4-20.

Ishak, S M; Aman, Z and Taib, H M (2020). An evaluation on outcome of oil palm replanting scheme (TSSPK) and new planting scheme (TBSPK). *Int. J. Mod. Trends in Soc. Sci., 3(14)*: 129-148.

Ismail, A and Mamat, M N (2002). The optimal age of oil palm replanting. *Oil Palm Industry Economic J., 2(1)*: 11-18.

Johari, N A A B and Pebrian, D E (2015). Development of a self-propelled machine for holing soil in large polybags in oil palm nursery. *Proc. of the 10th Asian Control Conference (ASCC 2015)*. Kota Kinabalu, Malaysia. p. 1114-1118.

Johari, N A A; Pebrian, D E; Vaiappuri, S K N and Hayum, N A (2020). Preliminary field and costs evaluation of a new mechanised system for holing soil in large polybag in oil palm nursery. *J. Oil Palm Res., 32(2)*: 228-236.

Karvonen, J; Chwalbinska-Moneta, J and Saynajakangas, S (1984). Comparison of heart rates measured by ECG and microcomputer. *Phys. Sportsmed., 12(6)*: 65-69.

Kepner, R A; Bainer, R and Barger, E L (1982). *Principles of Farm Machinery.* 3rd edition. AVI Publishing Company, Inc. Westport, Connecticut. USA. p. 23-60.

Leger, L and Thivherge, M (1988). Heart rate monitors: Validity, stability and functionality. *Phys. Sportmed., 16(5)*: 143-151.

Nybo, L; Jensen, T; Nielsen, B and Gonzalez-Alonso, J (2001). Effects of marked hyperthermia with and without dehydration on VO_2 kinetics during intense exercise. *J. Appl. Psychol., 90(3)*: 1057-1064.

Pebrian, D E and Yahya, A (2012). New mechanized system for circle spraying of oil palms seedling emergence. *Sci. Agric., 69(2)*: 85-100.

Polar (2013). *Heart Rate Monitor*. http://www.polar.com., accessed on 17 October 2015.

Rankine, I R and Fairhurst, T H (1999). *Field Handbook Oil Palm Series: Nursery. Volume 1*. Oxford Graphic Printers Pte. Ltd, Singapore. p. 16-90.

Roodi, S M; Yahya, A and Aziz, S A (2011). Field performance of a single chassis integrated machine system in planting oil palm seedlings. *J. Agr. Machy. Sci*., *7(2)*: 185-190.

Rebitanim, N A; Hanafi, M M; Idris, A S; Abdullah, S N A; Mohidin, H and Rebitanim, N Z (2020). GanoCare® improves oil palm growth and resistance against *Ganoderma* basal stem rot disease in nursery and field trials. *BioMed Res. Internat., (2020)*: 1-16.

Treiber, F A; Musante, L; Hartdagan, S; Davis, H; Levy, M and Strong, W B (1989). Validation of a heart rate monitor with children in laboratory and field settings. *Med. Sci. Sport. Exerc., 21(3)*: 338-342.

Turner, P D and Gillbanks, R A (2003). *Oil Palm Cultivation and Management*. 2nd edition. The Incorporated Society of Planters. Kuala Lumpur, Malaysia. p. 173-254.

Wahid, M B and Simeh, M A (2010). Accelerated oil palm replanting: The way forward for a sustainable and competitive industry. *Oil Palm Industry Economic J., 10(2)*: 29-38.

Journal of Oil Palm Research Vol. 35 (1) March 2023 p. 111-120
DOI: https://doi.org/10.21894/jopr.2022.0029

COUNTING OF OIL PALM FRESH FRUIT BUNCHES USING COMPUTER VISION

MINARNI SHIDDIQ[1]*; DODI SOFYAN ARIEF[2]; DEFRIANTO[1]; VICKY VERNANDO DASTA[1]; DEBORAH MARGARETHA PANJAITAN[1] and DONI SAPUTRA[2]

ABSTRACT

Oil palm fresh fruit bunches (FFB) are the sources of crude palm oil (CPO). CPO is one of the largest export commodities for Indonesia and Malaysia. Automation or mechanisation in CPO processes is crucial to saving time, labour and cost. This study used the computer vision method to count moving oil palm FFB using video frames. It is possible to implement this counting method in the oil palm FFB sorting and grading stage to estimate the CPO mill capacity. Video recordings used an RGB camera with a frame rate of 20 FPS for 117 oil palm FFB of Tenera *varieties. The counting program consisted of two parts, a detector and a tracker. The detector algorithm was self-developed by adding a colour feature, converting the RGB images of oil palm FFB to HSV colour space. The counting results were validated using the confusion matrix method. The results showed that the counting accuracy could reach 100.00%. However, the counting accuracy depends on the colour of the FFB and room light intensity. The confusion matrix validation resulted in average counting accuracy of 79.35% for 10 videos. The results showed the potential use of computer vision in counting moving oil palm FFB.*

Keywords: computer vision, confusion matrix, fruit counting, oil palm FFB, video frame.

Received: 27 November 2021; **Accepted:** 29 March 2022; **Published online:** 27 May 2022.

INTRODUCTION

Nowadays, counting fruits on trees or in a postharvest sorting and grading stage is very important to save time and labour costs. Recently, fruit counting using imaging methods has been developed due to innovations in counting algorithms, computer, and camera technology (Syal *et al.*, 2013). Information on the number of fruits on trees is needed to estimate the total harvesting yield. Likewise, the total fruits sorted in a postharvest sorting process can be applied to calculate the sortation capacity in tonnes per hour (TPH) or the storage capacity. Fruit counting is usually carried out manually by human intervention or traditional mechatronic machines. Both methods possess some disadvantages. Fruit counting by human vision creates errors due to psychological states. Mechatronic counting using electronic sensors does not have spatial resolutions which contain the information on fruit shape, size and texture. The information is crucial for further evaluation (Bhargava and Bansal, 2018). Computer vision is the potential method to be implemented for a quick, non-destructive, reliable, in-line counting process because it offers speed and spatial resolution.

Crude palm oil (CPO) is one of the largest export commodities for Indonesia and Malaysia. Oil palm industries need remarkable breakthroughs for their sustainability. Maintaining CPO quality and increasing efficiency in time and labour costs need automation in some stages of the CPO processing. Labour shortage is another reason for automation in oil palm industries (Murphy, 2014). Oil palm fresh

[1] Department of Physics,
Faculty of Mathematics and Natural Sciences,
Universitas Riau Kampus Bina Widya,
Jalan HR. Soebrantas KM 12,5, Pekanbaru, 28293, Indonesia.

[2] Department of Mechanical Engineering,
Faculty of Engineering,
Universitas Riau Kampus Bina Widya,
Jalan HR. Soebrantas KM 12,5, Pekanbaru, 28293, Indonesia.

* *Corresponding author e-mail: minarni.shiddiq@lecturer.unri.ac.id*

fruit bunch (FFB) is the source of CPO. However, oil palm FFB harvesting, sorting and grading are still being carried out manually and traditionally using trained or experienced personnel (Utom *et al.*, 2018).

Oil palm FFB have to pass through sorting and grading before entering the CPO processing steps. The activities of sorting and grading at a palm oil mill start with a loaded FFB transporting truck entering the sorting site. After unloading the oil palm FFB, two experienced graders, equipped with axes and crowbars, begin sorting unwanted FFB such as empty, defective, long stalks and rotten bunches. Next, the graders pick randomly 100 FFB as grading samples and use ripeness levels and the variety of either *Tenera* or *Dura* as the grading criteria. The site location is usually next to a loading ramp. After the grading process, all the sorted FFBs that meet the grading requirements are pushed toward the loading ramp by a tractor. The ramp will load FFB into lorries which then bring the FFB to the steriliser to begin the process of CPO extraction (Akhbari *et al.*, 2020). At a later stage, CPO samples are collected to determine the CPO qualities such as moisture content and free fatty acid (FFA) level. The oil palm mills use the sorting and grading information results to calculate the grade and end prices of the sorted FFB.

Counting of oil palm FFB has two purposes, to estimate harvest yield and to count oil palm FFB leaving the plantations and arriving at the site of the oil palm mill. The benefits of oil palm FFB counting are to avoid embezzlement (Aripriharta *et al.*, 2020) and to estimate the daily palm oil process capacity. Oil palm mill capacity is the size of an oil palm mill that is usually in TPH. Throughput is the capacity target measured every day and collected yearly for oil palm plant capacity estimation. This capacity target is often obtained by estimating the number of FFB entering the loading ramp or before entering the transporting lorries to the FFB sterilisation stage in an hour (Raharja *et al.*, 2020).

The computer vision system embedded in a sorting machine with moving conveyors could be used to determine the total capacity where the weight and the number of the oil palm FFB are the parameters for the capacity estimation. Here, oil palm mills can introduce an automatic counting system using computer vision to count the number of FFB unloaded from a transporting truck or to count the number of FFB entering lorries after the sorting process. The counting system can also be designed to measure the mass of each FFB by adding a load cell-based scale below the conveyor floor.

Counting fruit on trees using computer vision has been adopted widely for many conditions and types of fruits. The innovations in machine vision technology such as higher frame rates, image processing algorithms, cloud computing and camera resolution make the implementations easier. The computer vision method and digital image analysis with RGB and YCbCr colour space are being employed to count the yield of fruits and flowers. The image processing used were noise removal, segmentation, size thresholding and shape analysis (Nisar *et al.*, 2015). The technique was also applied to locate and count green and red pepper fruits involving a tremendous amount of datasets in a greenhouse with controlled lighting (Song *et al.*, 2014). Estimating the individual size and mass and counting olive fruits have also used computer vision (Ponce *et al.*, 2019). The yield of agricultural products such as apples can be estimated automatically using two cameras carried on a vehicle that scans each tree from two sides and produce image sequences (Wang *et al.*, 2012).

Postharvest sorting and grading process can also implement fruit counting. This measurement is essential for agriculture industries in planning market needs and estimating necessary resources. Fruit counting can estimate harvested yield, the amount of materials for fruit storage, and then the capacity of a storage facility. Estimating harvest yields usually use manual fruit counting which needs labour. The manual counting has some issues such as insurance, salary and housing. In addition, the time used to count fruits is 10% of the whole sorting process time. The miscalculation of fruit quantity is also about 10% for the large agriculture industry (Syal *et al.*, 2013). Therefore, automatic, non-destructive counting methods for fruits and vegetables are needed.

Computer vision methods have been proposed and used in automatic sorting systems to count the number of agriculture products. Computer vision has a broader term than machine vision, including three-dimensional imaging and spectral imaging. Machine vision often refers to computer vision used along with a conveyor-based machine. Counting objects using image processing and machine vision becomes a trendsetter because it offers automatic, low cost, non-destructive measurement (Baygin *et al.*, 2018). However, counting fruit on a moving conveyor has not been explored intensively. Counting fruits on moving conveyors can be related to counting the number of objects from video frames, such as counting the number of people passing a gate or entrance in a train station (Velastin *et al.*, 2020) or the number of vehicles on a particular street in a busy highway (Song *et al.*, 2014).

Nowadays, artificial intelligence (AI) and machine learning (ML) have been used in the field of smart or precision agriculture, such as for counting harvest yield (Osman *et al.*, 2021) and for sorting and grading machine vision (Jacques *et al.*, 2021). The applications have many advantages,

such as real-time monitoring, measurement and efficient quality management and assessment. AI is the simulated intelligence used by a machine to do some tasks. It intends to imitate the work of the human brain in making a decision. ML is a tool that can be used to develop AI. ML gives the ability for a machine to do a task automatically. The other definition of ML is developing a computer program to do a task. Counting fruit using AI and ML is the latest research interest motivated for low cost, non-destructive, intelligent methods for precision agriculture. You only look once (YOLO) model and deep learning have been used in fruit counting (Yi *et al.*, 2021).

This study aimed to construct an automatic counting system that estimates the number of moving oil palm FFB on a conveyor. The computer vision method was used for the counting process by detecting and tracking FFB images in video frames. The counting algorithm was designed and written using Python language that consisted of two main components, a detector and a tracker. The detector algorithm detects the presence of oil palm FFB based on colour, while a tracker program will track the bounding box that assigned to the oil palm FFB image and count it. This study used 117 oil palm FFB. Ten videos were taken and then analysed to obtain how many FFB were counted in each video. A confusion matrix was used to measure the accuracy of the counting system.

MATERIALS AND METHODS

This study used a computer vision system that consisted of a moving conveyor, a Red-Green-Blue (RGB) camera, and a Python-based counting program with OpenCV library. Counting objects using an RGB camera in video mode and coding with the OpenCV library is more practical than using two moving cameras (Sturdevant *et al.*, 2018). The counting system is adopted from the similar counting process of vehicles or people crossing a highway or a gate (Liu and Na, 2017) and from GitHub (https://github.com) that discusses object detection intensively.

In this study, the ripeness levels of the FFB were not part of the evaluation. However, we developed the algorithm for the detection part that included the colour and fruit shape of the oil palm FFB to differentiate them from other fruits. Image processing in the counting system used Hue-Saturation-Value (HSV) colour space. An RGB camera has images in RGB colour space. Converting the images into HSV space has some advantages, such as removing the background image, saving detection time and improving efficiency.

Figure 1 shows the counting system with one oil palm FFB. The counting system consisted of an RGB camera, a moving conveyor, a laptop connected to the camera via a USB cable, and a counting program. The camera was placed 150 cm directly above the moving conveyor (Septiarini *et al.*, 2020). We used a webcam Havit HV-V662 with a 1/3" sensor size and an unadjustable lens. One can reduce the working distance by 150 cm using a wider camera sensor and a shorter lens focal length. A stand holder for the camera was fastened to the side of a conveyor to ease the video recording process of moving oil palm FFB. The conveyor consisted of a white surface to facilitate image processing of the oil palm FFB. We used 117 oil palm FFB of *Tenera* variety. The FFB samples came with variations in size and mass.

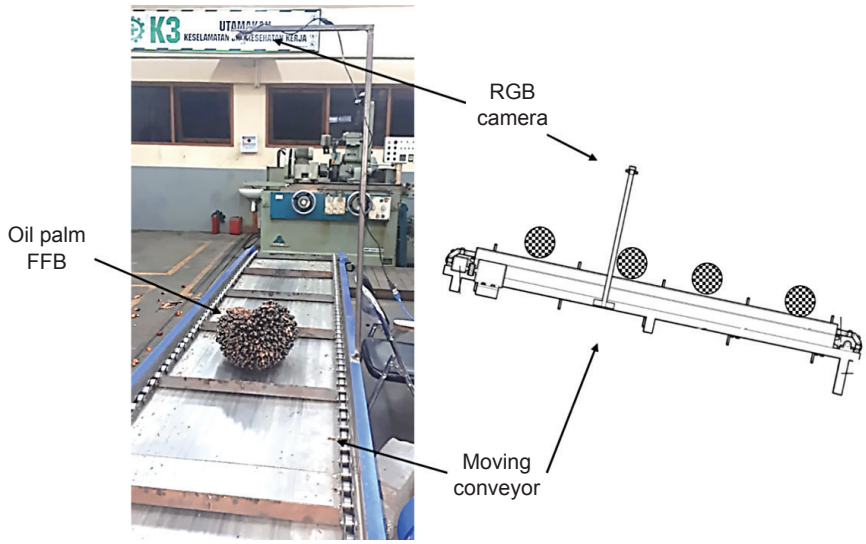


Figure 1. Counting system for oil palm fresh fruit bunches (FFB).

The conveyor unit is a vital part of this counting system. The conveyor type was a bucket conveyor as seen in *Figure 1*. The conveyor consisted of reducers as the speed controller of motor rotation, roller chains connected to a motor and sprockets. These roller chains used sprockets that function to change the rotation motion to the translation motion of buckets. The buckets pushed the oil palm FFB moving on the floor of the conveyor. All of the components positioned on the conveyor support frame. The white conveyor floor helped to increase background segmentation efficiency in image processing. Belt conveyors are not doable for moving oil palm FFB due to variations in FFB weights. This conveyor unit was made to be able to withstand the weight of an oil palm FFB of more than 40 kg.

Video Recording

The process of fruits or other objects counting using video frames has three stages, *i.e.*, detection, tracking and counting (Khude and Pawar, 2013). The counting program consisted of two main components, a detector and a tracker. The tracker had a counting step at the end of its algorithm. Video recording using an RGB camera was conducted in video mode live view. The camera utilised in video mode had a frame rate of 20 frames per second (FPS) and a video resolution of 640 x 480 pixels. We took 10 videos with different numbers of oil palm FFB in each video, numbers of FFB in a bucket and dates. The results of the video recording were RGB images. These images were later converted into HSV images. The counting algorithm allowed the counting process of moving FFB to be seen in real-time.

Detection Algorithm

The detection process consist of some stages. First, the OpenCV library read the image stream from the camera and converted the RGB matrix pixel into a grayscale pixel. Next, thresholding was applied to remove noise from the matrix pixel to obtain only the target pixels. After that, segmentation step used a background subtraction technique to extract the object from the background. The location of the extracted object was acquired using the contouring stage. The object location appeared as a bounding box of x, y, w and h in dimensions. The bounding box information was later sent to the tracker algorithm.

Figure 2 shows the algorithm of the detection process in detail. Pixels on the RGB channel were converted to HSV channels using cv2. cvtColor(frame, flag) command. The flag in the command script was the target channel, and the frame was the frame chosen to convert its colour channel to the colour of the target channel. The colour characteristics used were extracted from the histogram matrix of the saturation colour image or s channel. The conversion results of the RGB image to the s channel image were then thresholded to obtain a binary image. The purpose of this conversion and thresholding was to produce a still and stable background that is sensitive to foreground changes. The next step was to smooth pixel components in oil palm FFB images with dilation and erosion operations to anticipate the poor image quality of the resulting binary image.

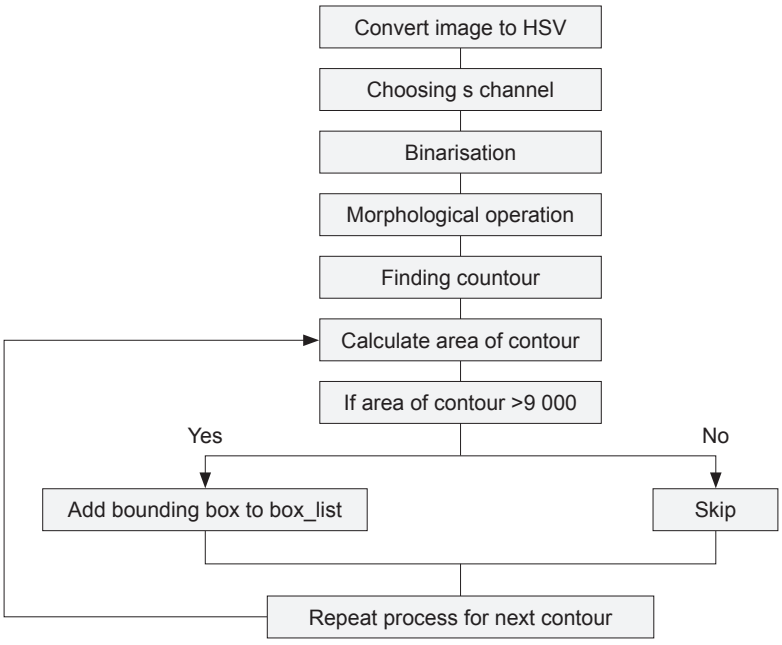


Figure 2. Object detection algorithm.

The next stage of the detection process was the morphological operation (Auroux *et al.*, 2011). The result of the morphological operation of the binary image would then be contoured. If the contour area was in the range above the value of 9000, then the object would be detected and added to the contour box list. The detection process would find the coordinates or region of interest (ROI). The output of the detection process was a centroid point needed for the tracking process.

Tracking and Counting Algorithms

The last part of the counting program was a tracker. *Figure 3* shows the tracker algorithm. The centroid-based tracker has three processes, register, update and deregister. The register step is a process to check whether the dictionary is empty. If the dictionary is found empty, it will assign an ID and a centroid to HashMap. All the bounding boxes will experience this process. Next, the update step is a process to check the centroid of each bounding box. If the distance of the centroid is close, then the centroid for the ID will be updated. However, if the centroid distance is too far, then the bounding box is assumed to be unrecognisable, so an ID will be reassigned. The last step is the deregister, which is deleting ID and centroid from the HashMap. An ID will be erased from the HashMap only if the ID is no longer detected in N consecutive frames.

This tracker algorithm also has a counting process. Centroid counting will be executed on each oil palm FFB on each frame. The final or overall centroid point information and object position will be saved as a benchmark by the tracker. If in the next frame a centroid value of the object is found and has a close distance to the previously detected centroid, then the object is assumed to be the previously detected object. The next process after updating the centroid tracker is implementing a loop of the resulted centroid tracker update in order to extract the ID and centroid of the oil palm FFB.

Confusion Matrix Analysis

The effectiveness and performance of the counting system were analysed using a confusion matrix or known as an error matrix (Novakovic *et al.*, 2017). The parameters used included Recall, F-Score, Accuracy, and Precision. The

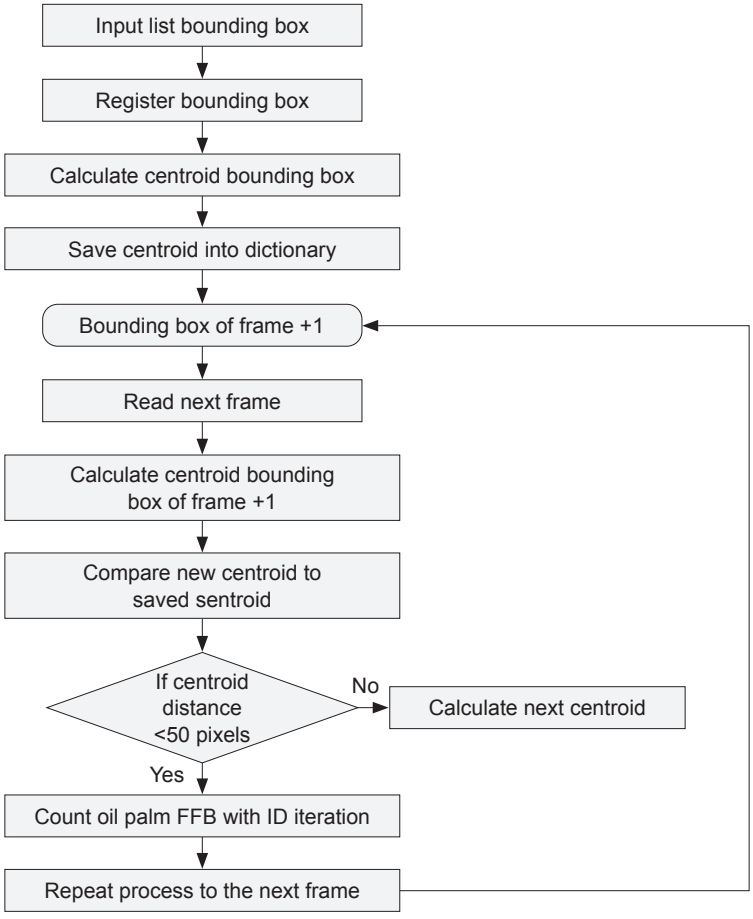


Figure 3. Object tracking and counting algorithm.

recall is a comparison or ratio of true positive (TP) predictions with the total number of data, consisting of TP and false negative (FN) data as in Equation (1).

$$\text{Recall} = \frac{TP}{TP + FN} \quad (1)$$

F-score is a measure or value that represents the performance level of the algorithm implemented on the system as measured using Equation (2).

$$\text{F-score} = \frac{2\ x\ (\ Precision\ x\ Recall)}{Precision + Recall} \quad (2)$$

The accuracy is the ratio value representing true-positive data to the overall data calculated using Equation (3).

$$\text{Accuracy} = \frac{TP}{TP + FN + FP} \times 100\% \quad (3)$$

Precision is a comparison between the true-positive predictions to the overall results that were predicted positive in Equation (4).

$$\text{Precision} = \frac{TP}{TP + FP} \quad (4)$$

RESULTS AND DISCUSSION

Counting of oil palm FFB was done using a counting system consisting of a RGB camera, a conveyor system, and a Python-based counting program. The program used video frames to detect and track oil palm FFB moving on a conveyor. Here, we presented the results and evaluated the performance of the counting process.

Segmentation Results

A colour feature was added to the counting algorithm to differentiate the oil palm FFB from other fruits. HSV colour space was used instead of RGB images such that the conversion of RGB to HSV images became essential. *Figure 4* shows the conversion results. The resulting HSV images have more contrast than the RGB images as seen in *Figure 4a*. The object and the background could be differentiated easily, therefore improving the quality of the segmentation result.

Figure 5 shows the signature of an oil palm FFB as a white blob after the thresholding step implemented on the HSV image. The image represented by white is the resulting detected oil palm FFB, while the black image shows the object's background. *Figure 5a* shows the resulting binary image. It shows that the image has thickened. The morphological operations have improved the contrast. It shows that the thresholding step has differentiated more between the object and the background.

In this study, contouring was executed using a minimum threshold to an area aiming to detect oil palm FFB successfully. The minimum threshold value for the contour area used in this study is 9000. If the contour area is >9000, then the contour is considered as a signature blob of the oil palm FFB.

The Counting Performances

Testing the performance of the counting system can be done by adding more oil palm FFB in one bucket. *Figure 6* shows some cases of the resulting images of the detection and tracking from the video frames. As seen in *Figure 6a*, the counting system will respond to every oil palm FFB movement in real-time detection. In the resulting image, the green bounding box is a marker that the oil palm FFB is detected. The bounding box will automatically follow the movement of the oil palm FFB in the ID iteration process.

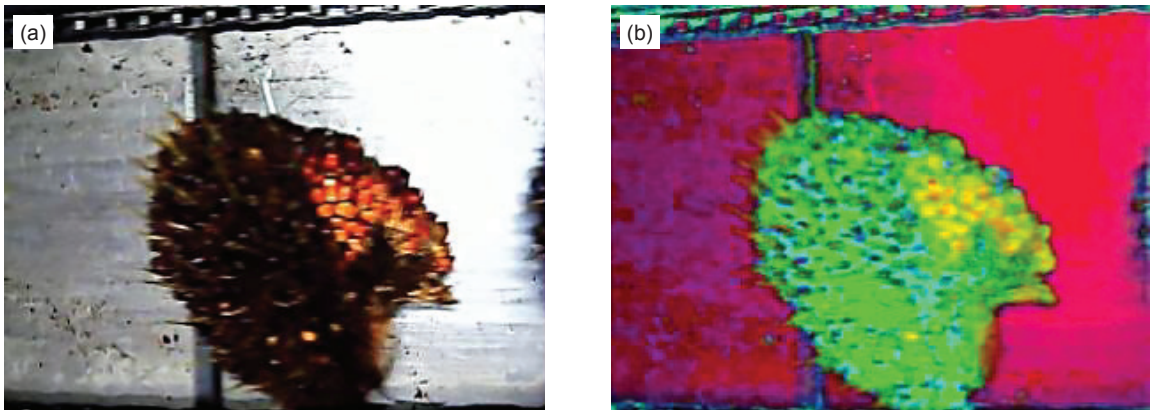


Figure 4. Converting (a) RGB image to (b) HSV image.

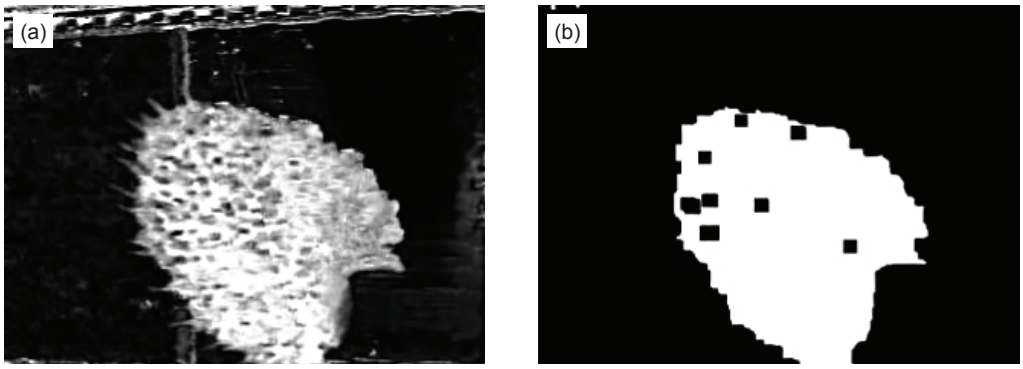


Figure 5. Result of binarisation and thresholding process. (a) Binary image and (b) thresholding result

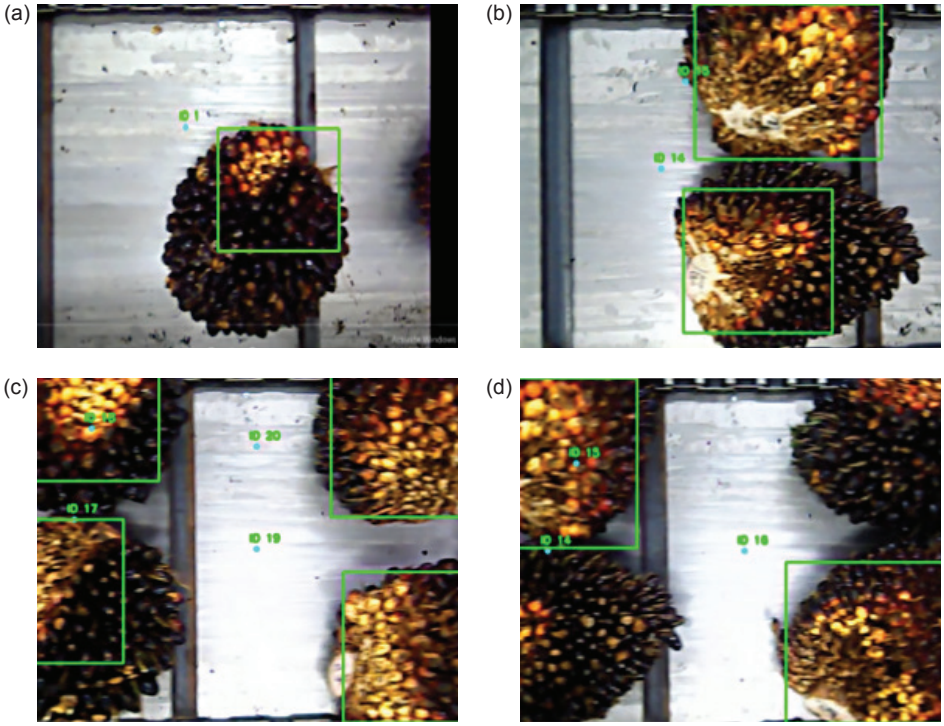


Figure 6. Detection, tracking and counting performance. (a) Detect and count correctly; (b) detect and count correctly; (c) detect and count correctly and (d) detect incorrectly

Figure 6 shows the counting performance. *Figure 6a* shows the algorithm has counted correctly. The same is true in *Figure 6b* where the counting system has detected two oil palm FFBs correctly. *Figure 6c* shows the counting system was capable of detecting and tracking accurately four oil palm FFB at once with ID and bounding box. However, counting four oil palm FFB in a bucket can lead to a failure shown in *Figure 6d*, where only three oil palm FFB were detected. This case was due to the distance between two adjacent oil palms affecting the system. Oil palm FFB with close centroid points were detected as the same object by the system, therefore failing to count four oil palm FFB correctly.

There were some other errors found in detecting and tracking oil palm FFB. One error was an error in assigning an ID, where sometimes an oil palm FFB has two ID numbers. This error could arise because of too high room light intensity during image acquisition that one oil palm FFB has a contour area above 9000 (Septiarini *et al.*, 2020). It also could be caused by the physical characteristics of the oil palm FFB especially colours, masses and shapes (Razali *et al.*, 2012).

Confusion Matrix evaluated the accuracy of the counting performance. This matrix is in the form of a table that describes the performance information of a classification model on a series of testing data to the actual classification results. *Table 1* shows the Confusion Matrix results for 10 videos and the values of TP, false positive (FP), and FN. In *Table 1*, the 5th video recording had the highest TP because all the oil palm FFB were counted right by the program, the same as the actual number. Therefore,

the recall, precision and F-score have values of 1 as shown in *Table 2*. The accuracy is 100%. The 10th video recording has the highest FP, which means the program has counted far more than the actual number of oil palm FFB. The 9th video recording also has a higher FP. FN tells that the program has made mistakes in counting the oil palm FFB and that the number of oil palm FFB counts was less than it should be. This happened to the 1st and 2nd video recordings.

Table 2 shows the summary of the accuracies of the counting system. The recall and precision values in *Table 2* are the ratio of the TP, FN and FP of each video recording. The accumulation of the recall and precision results defines the algorithm's performance, represented by F-Score values. In *Table 2*, The highest F-scores values were found at the 5th and 8th video recordings. Here, the values were influenced by the room light intensities and the physical characteristics of the oil palm FFB. Due to the additional colour feature added to the detection algorithms, the room light intensities can affect the accuracies. In addition, the oil palm FFB came in different shapes, masses and ripeness. Each video has oil palm FFB with different shapes, mass and ripeness. But we observed that most of the miscalculation was due to the orientation of the FFB surface on the bucket. Oil palm FFBs have ellipsoidal shapes and can be divided into three parts: basal, middle and top. The FFB top part has a darker colour than the basal part. The basal part has a lighter colour, unfertile fruitlets. It also can be divided into two faces, front and back. The back face or surface has a lighter colour than the front (Owolarafe *et al.*, 2007; Razali *et al.*, 2012). The miscalculation happened when the FFB part and surface seen by the camera is dark. This is due to the detection algorithm of HSV conversion that has a certain limit and causes ID and centroid unidentified. These errors can be avoided by using the YOLO algorithm in the detection program (Yi *et al.*, 2021).

Ambient light is one of the factors that can affect counting performance (Sengupta and Lee, 2014). Therefore some studies on counting fruits have used a controlled artificial light or worked nighttime (Song *et al.*, 2014; Wang *et al.*, 2012). The counting system in this study was conducted in a laboratory

TABLE 1. CONFUSION MATRIX RESULTS

Video label	Actual count	Count by the system	True positive (TP)	False positive (FP)	False negative (FN)
Video 1	14	13	12	1	2
Video 2	15	13	13	-	2
Video 3	15	16	15	1	-
Video 4	3	6	3	3	-
Video 5	15	15	15	-	-
Video 6	11	13	11	2	-
Video 7	3	4	3	1	-
Video 8	11	11	11	-	-
Video 9	15	24	15	9	-
Video 10	15	25	15	10	-

TABLE 2. COUNTING ACCURACY OF EACH VIDEO

Video samples	Duration (min)	Light intensity (lux)	Recall	Precision	F-Score	Accuracy (%)
Video 1	1′11″	120	0.86	0.92	0.89	80.00
Video 2	1′02″	160	0.87	1.00	0.93	86.67
Video 3	0′52″	235	1.00	0.94	0.97	93.75
Video 4	0′11″	40	1.00	0.50	0.67	50.00
Video 5	0′57″	190	1.00	1.00	1.00	100.00
Video 6	0′37″	140	1.00	0.85	0.92	84.61
Video 7	0′36″	100	1.00	0.75	0.86	75.00
Video 8	0′47″	200	1.00	1.00	1.00	100.00
Video 9	1′05″	80	1.00	0.63	0.77	62.50
Video 10	1′05″	60	1.00	0.60	0.75	60.00

where its room light was not adjustable. The samples of oil palm FFB used came from a plantation in the vicinity that sometimes arrived late in the evening. Therefore, the room light intensity varied each time in each video recording. The RGB camera has auto exposure or white balance hence creating a colour difference in the camera during video recordings (Lumenera, 2017).

In *Table 2*, the highest level of accuracy of 100% resulted in the light intensity of 190 and 200 Lux. Low light conditions gave an accuracy of about 50%, such as in video 4 with an intensity level of 40 Lux. Too bright room light conditions also resulted in low accuracies, such as in Video 3, which had less than 95% accuracy with the intensity of 235 Lux. The room light intensity affects the counting system of recognising and detecting oil palm FFB. This system can work well at light intensity levels of around 180-210 Lux.

Table 2 also shows the duration of each video recording that varies for the same amount of oil palm FFB. We believe the problems with the intensity variations were due to the room light conditions and the characteristics of the webcam. The camera position and the distance from the camera to the conveyor base were unchanged during each video recording. However, due to the long working distance and no controlled lighting around the oil palm FFB, the room lighting in the laboratory caused the intensity to vary. The camera specifications also affect the computer vision system performance. At the time of video recording, the conveyor speed and the frame rate were not matched. We used a low-cost webcam with a resolution of 640 × 480 pixels and a maximum frame rate of 30 FPS. The sensor size is the smallest which is 1/3". The unmatched conveyor speed and the frame rate values could cause the program's accuracy. The sensor will detect an object if the light reflected by the object enters the sensor area. The sensor has difficulty receiving light due to faster moving objects (Lumenera, 2017).

CONCLUSION

This study has investigated the possibility of using a computer vision method for counting moving oil palm FFB on a conveyor. There is a potential to use the counting system in sorting and grading machine vision where masses of the oil palm FFB are also measured. The capacity of the oil palm mill then can be estimated non-destructively and faster using mass measurement and counting. The built counting system has reached the accuracy of 100% depending on the oil palm FFB surface colours and the intensity of the room light and a lighter surface can be calculated accurately. The orientation of an oil palm FFB in a conveyor bucket sometimes caused the darker part of the oil palm FFB to face the camera, hence it led to misdetection due to HSV colour conversion in the detecting algorithm. A suitable lighting condition and the higher camera specifications are the key factors to overcome the light intensity effects for the counting system. For future works, the counting system could add more features in addition to the colour and a deep learning algorithm. Nonetheless, it has shown the potential of using the computer vision-based counter for oil palm FFB.

ACKNOWLEDGEMENT

The authors would like to acknowledge the Indonesia Endowment Fund for Education (LPDP), the Ministry of Finance, and the Universitas Riau Institution of Research and Community Services for supporting this study through research grant of PRJ/57/2020.

REFERENCES

Akhbari, A; Kutty, P K; Chuen, O C and Ibrahim, S (2020). A study of palm oil mill processing and environmental assessment of palm oil mill effluent treatment. *Environ. Eng. Res.*, *25(2)*: 212-221. DOI: 10.4491/eer.2018.452.

Aripriharta, A; Firmansah, A; Mufti, N; Horng, G J and Rosmin, N (2020). Smartphone for palm oil fruit counting to reduce embezzlement in harvesting season. *Bulletin of Social Informatics Theory and Application*, *4(2)*: 76-82. DOI: 10.31763/businta.v4i2.283.

Auroux, D; Cohen, L D and Masmoudi, M (2011). Contour detection and completion for inpainting and segmentation based on topological gradient and fast marching algorithms. *Int. J. Biomed Imaging*, *2011*: 592924. DOI: 10.1155/2011/592924.

Baygin, M; Karakose, M; Sarimaden, A and Akin, E (2018). An image processing based object counting approach for machine vision application. https://arxiv.org/abs/1802.05911, accessed on 9 March 2021.

Bhargava, A and Bansal, A (2018). Fruits and vegetables quality evaluation using computer vision: A review. *J. King Saud Univ. - Comput. Inf. Sci. 33(3)*: 243-257. DOI: 10.1016/j.jksuci.2018.06.002.

Boatswain Jacques, A A; Adamchuk, V I; Park, J; Cloutier, G; Clark, J J and Miller, C (2021). Towards a machine vision-based yield monitor for the counting and quality mapping of shallots. *Front. Robot. AI*, *8*: 627067. DOI: 10.3389/frobt.2021.627067.

Khude, P S and Pawar, S S (2013). Object detection, tracking and counting using enhanced BMA on static background videos. *Proc. of International Conference on Computational Intelligence and Computing Research*. p. 1-4. 978-1-4799-1597-2. DOI:10.1109/ICCIC.2013.6724236.

Liu, J and Na, W (2017). Fast moving object counting from video. *Proc. of International Symposium on Intelligent Signal Processing and Communication Systems*. p. 337-340. DOI: 10.1109/ISPACS.2017.8266499.

Lumenera.Co. (2017). Introduction: Designing a vision system. Lumenera White Paper Series. https://www.lumenera.com/media/wysiwyg/documents/casestudies/designing-a-vision-system-white-paper.pdf, accessed on 20 December 2021.

Murphy, D J (2014). The future of oil palm as a major global crop: Opportunities and challenges. *J. Oil Palm Res.*, *26(1)*: 1-24.

Nisar, H; Yang, H Z and Ho, Y K (2015). Predicting yield of fruits and flowers using image analysis techniques. *Indian J. Sci. Technol.*, *8(32)*: 1-6. DOI: 10.17485/ijst/2015/v8i32/93730.

Novakovic, J D J; Veljovic, A; Ilic, S S; Pavic, Z and Tomovic, M (2017). Evaluation of classification models in machine learning. *Theory Appl. Math. Comput. Sci.*, *7(1)*: 39-46.

Osman, Y; Dennis, R and Elgazzar, K (2021). Yield estimation using deep learning for precision agriculture. *7th IEEE World Forum on Internet of Things, WF-IoT 2021*. p. 542-550. DOI: 10.1109/WF-IoT51360.2021.9595143.

Owolarafe, O K; Olabige, M T and Faborode, M O (2007). Physical and mechanical properties of two varieties of fresh oil palm fruit. *J. Food Eng.*, *78(4)*: 1228-1232. DOI: 10.1016/j.jfoodeng.2005.12.049.

Ponce, J; Aquino, A; Milan, B and Andujar, J (2019). Automatic counting and individual size and mass estimation of olive-fruits through computer vision techniques. *IEEE*, *7*: 2169-3536. DOI: 10.1109/access.2019.2915169.

Raharja, I B; Sulistiono and Ramadhan, A I (2020). Identification of palm oil mill throughput capacity of 60 t/hr (case study at xyz palm oil mill). *J. Appl. Sci. Adv. Technol.*, *2(3)*: 83-86. DOI: 10.24853/jasat.2.3.83-86.

Razali, M H; Somad, A S; Halim, M A and Roslan, S A (2012). Review on crop plant production and ripeness forecasting. *Int. J. Agric. Crop Sci.*, *14*: 54-63.

Sengupta, S and Lee, W S (2014). Identification and determination of the number of immature green citrus fruit in a canopy under different ambient light conditions. *Biosyst. Eng.*, *117*: 51-61. DOI: 10.1016/j.biosystemseng.2013.07.007.

Septiarini, A; Hamdani, H; Hatta, H R and Anwar, K (2020). Automatic image segmentation of oil palm fruits by applying the contour-based approach. *Scientia Horticulturae*, *261*: 108939. DOI: 10.1016/j.scienta.2019.108939.

Song, H; Liang, H; Li, H; Dai, Z and Yu, X (2019). Vision-based vehicle detection and counting system using deep learning in highway scenes. *Eur. Trans. Res. Rev.*, *11*: 51. DOI: 10.1186/s12544-019-0390-4.

Song, Y; Glasbey, C A; Horgan, G W; Polder, G; Dieleman, J A and Van der Heijden, G W A M (2014). Automatic fruit recognition and counting from multiple images. *Biosyst. Eng.*, *118(1)*: 203-215. DOI: 10.1016/j.biosystemseng.2013.12.008.

Sturdevant, M; Hollinger, M and Chitiveli, S (2018). Object tracking in video with OpenCV and Deep Learning. https://developer.ibm.com/technologies/artificial intelligence/patterns/detect-track-and-count-cars-in-a-video/, accessed on 9 March 2021.

Syal, A; Garg, D and Sharma, S (2013). A survey of computer vision methods for counting fruits and yield prediction. *Int. J. Computer Sci. Engineering*, *2(6)*: 346-350.

Utom, S L; Mohamad, E J; Mohmad Ameran, H L; Abdul Kadir, H; Mohd Muji, S Z; Abdul Rahim, R and Pusppanathan, J (2018). Non-destructive oil palm fresh fruit bunch (FFB) grading technique using optical sensor. *Int. J. Integr. Eng.*, *10(1)*: 35-39. DOI: 10.30880/ijie.2018.10.01.006.

Velastin, S; Fernandez, R; Oviedo, J E E and Bay, A (2020). Detecting, tracking and counting people getting on/off a metropolitan train using a standard video camera. *Sensors*, *20(21)*: 6251. DOI: 10.3390/s20216251.

Yi, S; Li, J; Zhang, P and Wang, D (2021). Detecting and counting of spring-see citrus using YOLOv4 network model and recursive fusion of features. *Transactions of the CSAE*, *37(18)*: 161-169. DOI: 10.11975/j.issn.1002-6819.2021.18.019.

Wang, Q; Nuske, S; Bergerman, M and Singh, S (2012). Automated crop yield estimation for apple orchards (Desai, J; Dudek, G; Khatib, O; Kumar, V eds.). *Experimental Robotics. Springer Tracts in Advanced Robotics, Vol 88*. Springer, Heidelberg. DOI: 10.1007/978-3-319-00065-7_50.

Journal of Oil Palm Research Vol. 35 (1) March 2023 p. 121-132
DOI: https://doi.org/10.21894/jopr.2022.0030

COMPARISON OF REAL-TIME PCR, CONVENTIONAL PCR AND RT-LAMP FOR THE DETECTION OF *COCONUT CADANG-CADANG VIROID* VARIANT IN OIL PALM

NUR DIYANA ROSLAN[1]; GANESAN VADAMALAI[2]; ABU SEMAN IDRIS[1]; KONG LIH LING[3] and SHAMALA SUNDRAM[1]*

ABSTRACT

Real-time quantitative polymerase chain reaction (real-time PCR) was designed for the detection of oil palm Coconut Cadang-cadang Viroid *(CCCVd) 246 nt variant. The primers and probe specifically designed for the real-time PCR were optimised with 300 nM of probe against a primer concentration of 400 nM for the detection of oil palm CCCVd variants. Oil palm CCCVd 246 nt variant was successfully detected using real-time PCR in leaf samples collected from 14 symptomatic oil palm from various regions. The sensitivity of real-time PCR was compared with reverse transcription loop-mediated isothermal amplification (RT-LAMP) and conventional PCR. The latter two techniques were reported earlier to be able to detect CCCVd variants in oil palm. Conventional PCR analysis using CCCVd full-length primers detected the presence of CCCVd 246 nt variant in 10 while RT-LAMP detected only seven positive samples from the total 14 field samples. The real-time PCR was highly sensitive and reliable compared to the two detection techniques. The primers designed for the real-time PCR were specific as only the oil palm CCCVd variant plasmid was detected with high fluorescence and lowest quantification cycle (Cq value) compared to the other tested viroids (ASSVd, CTiVd, ELVd, HLVd and PLMVd). The present study has proven the reliability of the technique, thus, highly recommending the next step of developing the high-throughput diagnostic procedure for the eventual use in epidemiological monitoring programmes.*

Keywords: CCCVd detection, conventional PCR, oil palm, real-time PCR, RT-LAMP.

Received: 19 January 2022**; Accepted:** 25 April 2022**; Published online:** 2 June 2022.

INTRODUCTION

Coconut Cadang-cadang Viroid (CCCVd) is a single-stranded, circular, and non-coding ribonucleic acid (RNA) molecule with a small genome (246-297 nt), causing cadang-cadang disease in coconut. More than 40 million coconut palms have been affected and destroyed due to the viroid in the Philippines (Randles and Rodriguez, 2003). Although initial studies on the viroid were reported in coconut palms, the occurrence of its variants has also been reported in African oil palm (*Elaeis guineensis* Jacq.) as it is associated with orange spotting (OS) disorder in commercial oil palm plantations (Vadamalai *et al.*, 2006; Wu *et al.*, 2013).

Due to the devastation experienced by the coconut industry in the Philippines, there is an immediate need to monitor the presence of the variant in oil palm as part of the biosecurity

[1] Malaysian Palm Oil Board, 6 Persiaran Institusi, Bandar Baru Bangi, 43000 Kajang, Selangor, Malaysia.

[2] Department of Plant Protection, Faculty of Agriculture, Universiti Putra Malaysia, 43400 UPM Serdang, Selangor, Malaysia.

[3] Institute of Plantation Studies, Universiti Putra Malaysia, 43400 UPM Serdang, Selangor, Malaysia.

* *Corresponding author e-mail: shamala@mpob.gov.my*

mitigation approach. Hence, it is absolutely crucial to develop a reliable detection tool to detect the variant in oil palm to avoid and mitigate its impact on the oil palm industry. The development of a quick, reliable and sensitive method to detect CCCVd variants would be the ideal solution. However, the viroid lacks of protein coding (Lee and Koonin, 2022), consequently rendering any detection tools using serological techniques unfeasible. Nevertheless, detection via molecular technique would be the most practical approach in developing the viroid detection tool in oil palm. Additionally, the technique requires high sensitivity to detect the viroid in lower titre within the tested samples. A wide range of diagnostic techniques have been employed for the identification of orange spotting CCCVd (OS-CCCVd) in oil palm: Polyacrylamide gel electrophoresis (PAGE) (Randles *et al.*, 1980); northern blot hybridisation, two dimensional polyacrylamide gel electrophoresis (2D-PAGE), conventional polymerase chain reaction (PCR) and ribonucleic protection assay (RPA) (Vadamalai *et al.*, 2006) and reverse transcription loop-mediated isothermal amplification (RT-LAMP) (Madihah *et al.*, 2020; Thanarajoo, 2014). The techniques mentioned above for detecting OS-CCCVd variants are mainly to detect the presence of the viroid in the palm through the application of radioactive label and colourimetric changes or turbidity. Apart from the safety hazards due to the use of radioactive labelling, these methods increase the risk of contamination because the dyes are added during the post RT-LAMP reaction, and the changes in hydroxy naphthol blue colour can be perceived variably by different observers (Scott *et al.*, 2020; Wastling *et al.*, 2010). Meanwhile, a weak hybridisation signal through 2D-PAGE and northern blot has been reported by Vadamalai (2005), showing that the CCCVd-like RNA in the oil palm samples was present at low concentration. Although the viroid concentration in oil palm is low, this weakness can potentially be solved by using a real-time PCR as reported by previous studies on other viroids (Botermans *et al.*, 2020; Leichtfried *et al.*, 2021; Seigner *et al.*, 2020; Tsushima and Fuji, 2022).

In this study, the hydrolysis probe PCR or often known as TaqMan probe has been adopted whereby two fluorescent dyes are added at the 5′ end as reporter and 3′ end as quencher of the hydrolysis probe. Together with the new specific primer target, the probe specifically binds to the target and the Taq polymerase extends the primer until the probe cleaves at the 3′ reporter to eventually emit the fluorescence. Recently, real-time PCR has been used successfully to detect some viroids, such as *Potato spindle tuber viroid* (PSTVd), *Citrus exocortis viroid* (CeVd) and *Grapevine latent viroid* (GLVd) (Ghobakhloo *et al.*, 2019; Osman *et al.*, 2017; Tsushima and Fuji, 2022; Zhang *et al.*, 2018). For this study, dual-labelled probe hydrolysis was selected due to the ease of designing this probe and their typically higher sensitivity in detecting and quantifying low concentration of viroid in oil palm. Although previous studies have demonstrated better amplification efficiency of RT-LAMP as compared to PCR, there is yet a comprehensive report to evaluate the sensitivity of CCCVd detection among RT-LAMP, conventional PCR, and real-time PCR. Therefore, the aim of this study was to compare the currently developed real-time PCR with two other available detection methods and concurrently determine the performance of detection. The two earlier reported techniques namely RT-LAMP (Madihah *et al.*, 2020; Thanarajoo, 2014) and conventional PCR (Vadamalai *et al.*, 2006) were compared with real-time PCR technique. Therefore, we reported the development of a detection tool using real-time PCR by incorporating hydrolysis Taqman probe to gauge the sensitivity of CCCVd detection in oil palm leaves. To the best of our knowledge, this is the first report of using TaqMan probe based on real-time PCR to detect the OS-CCCVd in commercial oil palm plantations.

MATERIALS AND METHODS

Field Samples

Leaf samples with OS from 14 oil palms of *Dura* x *Pisifera* (DxP) based on the OS symptoms were collected from local oil palm plantations in different states of Malaysia, including Sabah and Sarawak (*Table 1*). The samples were collected from symptomatic palms with isolated cases (*Figure 1a*) in the field that expressed typical OS with irregular shapes (*Figure 1b*) as described by Sundram *et al.* (2017). The leaves were harvested from frond 20 (middle portion of the crown), wrapped in paper and transported to the lab within 24 hr. Approximately 500 g of leaflets from the sampled frond 20 were cut to 30 cm in length and rinsed with tap water before being soaked in 5% bleach (sodium hypochlorite) in distilled water for 2 min. The leaflets were wiped with tissue paper and sealed in plastic bags before being kept at -80°C. Viroid-related samples from other countries could not be used in this study because of the quarantine regulations in Malaysia that strictly prohibit the entry of any invasive alien species.

Total Nucleic Acid Extraction, Purification by Polyacrylamide Gel Electrophoram (PAGE) and Complimentary Deoxyribonucleic Acid (cDNA) Synthesis

Natrium-EDTA-Tris-Mercaptoethanol extraction (NETME) was adopted from Thanarajoo (2014).

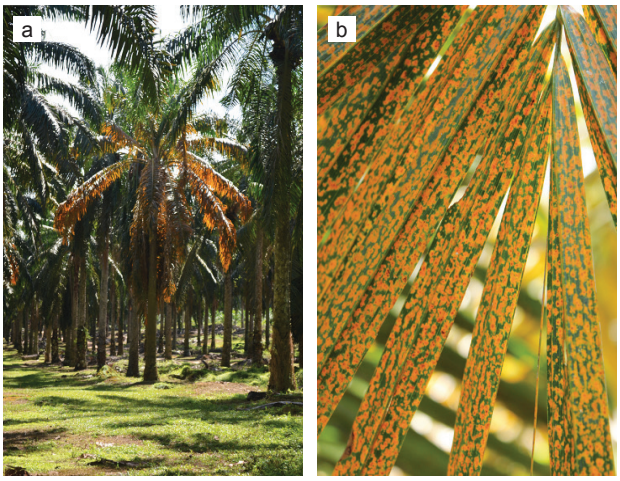


Figure 1. (a) Oil palm deemed as an isolated case in the field with typical symptoms of orange spotting (OS). (b) A closer view of the affected leaflets with OS symptoms.

TABLE 1. OIL PALM SAMPLES USED FOR CCCVd DETECTION WITH THE LOCATIONS AND THE YEAR OF PLANTING

Sample No.	Sample ID	Location	Year
1.	KLJ 3	Johor	2000
2.	KLJ 1	Johor	2000
3.	KLJ 5	Johor	2000
4.	KLJ 7	Johor	2000
5.	KLJ 6	Johor	2000
6.	KLJ 2	Johor	2000
7.	KLJ 4	Johor	2000
8.	S 1	Sarawak	2003
9.	S 2	Sarawak	2003
10.	DSR 1	Selangor	2003
11.	DSR 2	Selangor	2003
12.	AP 1	Perak	2008
13.	AP 2	Perak	2008
14.	AP3	Perak	2008

Approximately 2.5 g of oil palm leaves were ground using liquid nitrogen and mixed with 8 mL of NETME buffer (2 M NaCl; 0.1 M NaOAc; 0.05 M Tris-HCl, pH 7.5; 0.05 M EDTA, pH 8 and 20% ethanol) in which 4 mL SDS and 20 µL β-mercaptoethanol were added. The mixture was shaken at 151 rpm (Daihan, Japan) using an incubator shaker for 30 min at room temperature and then centrifuged at 11 000 rpm (Eppendorf, Germany) for 15 min. The supernatant was reextracted with Phenol: Chloroform: Isoamyl alcohol (25:24:1) and Chloroform: Isoamyl alcohol (24:1). Isopropanol (1 volume) was added to the supernatant and incubated overnight at -20°C. The mixture was centrifuged at 11 000 rpm (Eppendorf, Germany) for 15 min. The pellet was washed with 1 mL 70% ethanol and centrifuged at 11 000 rpm (Eppendorf, Germany) for 10 min. The resulting pellet was air dried, eluted in 30 µL of distilled water and stored at -80°C.

Due to the low level of CCCVd in oil palm and the specific aim to separate and enrich the viroid circular RNA of 246 nt in size from all other linear RNAs of various host or viral origins, the nucleic acid was fractionated using 5% non-denaturing PAGE buffered with 1× Tris-Borate EDTA (TBE) at 20 mA for 150 min (Vadamalai, 2005). Briefly, 20 µL of nucleic acid sample was mixed with loading dye (1:1 ratio) (Ambion, USA) and the region of the gel where CCCVd RNA was expected to migrate was cut for elution. The excised gel was crushed until homogenous and soaked in 3 volumes of elution buffer (0.5 M ammonium acetate, 0.1% SDS and 1 mM EDTA pH 8.0) for 16 hr at 37°C with shaking at 121 rpm (Daihan, Japan) using incubator shaker. The eluted samples were centrifuged at 12 000 rpm (Eppendorf, Germany) for 2 min at room temperature. The supernatant was collected, mixed with 3 volumes of absolute ethanol and incubated at -20°C for 6 hr followed by centrifugation at 12 000 rpm (Eppendorf, Germany) for 20 min. The resulting pellet was air-dried for 30 min, dissolved in 20 µL of distilled water and stored at -80°C until further use.

Complementary deoxyribonucleic acid (cDNA) was synthesised using GoScript™ Reverse Transcription Systems kit (Promega, USA) according to the manufacturer's protocol. Briefly, 5 µL RNA eluted from PAGE was added with 1 µL of reverse primer of CCCVd Vir R, mixed, heated at 80°C for 12 min and then chilled in ice. Subsequently, 15 U of AMV reaction mix, 1 mM dNTP, 1× RT-Buffer, 5 mM $MgCl_2$ and 20 U RNasin were mixed and incubated at 25°C for 5 min and 55°C for 30 min. The reaction was inactivated by incubation at 70°C for 15 min.

Primers and Probe Designing

In this study, the primer for conventional PCR was retrieved from Vadamalai *et al.* (2006) and RT-LAMP from Madihah *et al.* (2020). The sequences are listed in *Table 2*. The primers and probes in this study were designed from the sequences of CCCVd oil palm variants 270, 297, 293 and 246 nt (GenBank Accession: HQ608513, DQ097183, DQ097184 and DQ097183) retrieved from NCBI. A multiple sequence alignment was generated using MEGA X software (Kumar *et al.*, 2018). A single probe was designed using the sequences of the central conserved region (CCR) with partial coverage of the variable domain. The forward primer was designed from the pathogenic

TABLE 2. SEQUENCE AND POSITION OF THE PRIMERS AND PROBE

Name	Sequence	Position	References
Vir probe	CCTCAAGCGAATCTGGGAAGGGAGCGT	69-95	This study
Vir F	GCAGGAGAGGCCGCTTGA	35-52	This study
Vir R	GATCGTGCGCGTTGGAG	105-121	This study
GV4 F	ACTCACGCGGCTCTTACC	191-172	Vadamalai *et al.* (2006)
GV4 R	TGTATCCACCGGGTAGTCTC	192-209	Vadamalai *et al.* (2006)
CCCVdF3	PSQIRL-N-N-N-N-N-N-KPLQER	PI 2017702332	Madihah *et al.* (2020)
CCCVdB3	VRVGGDSP-N-N-N-N-N-SPK	PI 2017702332	Madihah *et al.* (2020)
CCCVdFIP	GKS-N-N-N- N-GT	PI 2017702332	Madihah *et al.* (2020)
CCCVdBIP	AA- N-N-N-N-N-N-VS	PI 2017702332	Madihah *et al.* (2020)

region (P) and CCR while the reverse primer was designed from the terminal right region. The probe and both primers were designed (*Table 2*) using Beacon Designer Software Bio-Rad by considering the melting temperatures, secondary structure, base composition and amplicon lengths. The specificity of the probe and primers for CCCVd was confirmed through a homology search. Highly purified salt-free primers and hydrolysis probes were obtained commercially from Integrated DNA Technologies (IDT).

Preparation of *in vitro* Oil Palm CCCVd 246 nt Variant Plasmid

Plasmid with CCCVd 246 nt cloned between *EcoR1* and *SalI* in pBlueScript II KS (+) vector with T7 promoter was used for the *in vitro* transcription. The plasmid was linearised by digestion using *KpnI* restriction enzyme during the incubation at 37°C for overnight and the *in vitro* transcription was performed using HiScribe™ T7 Quick High Yield RNA Synthesis kit (New England Biolabs, USA) according to the manufacturer's protocol. The DNA was removed with DNaseI (Promega, USA) and the RNA was recovered by extraction using a Phenol: Chloroform (1:1), followed by ethanol precipitation.

Testing Primer and Probe Combination

The primer and probes were tested using a fixed template (10^{-4}) cDNA prepared from *in vitro* oil palm CCCVd 246 nt variant plasmid. The cDNA was prepared using GoScript™ Reverse Transcription Systems kit (Promega, USA) according to the manufacturer's protocol. A combination of five concentrations (300 nM, 350 nM, 400 nM, 450 nM and 500 nM) of both forward and reverse primers with a constant probe concentration was determined. The combination showing the highest fluorescence was subsequently tested at four different probe concentrations (50-300 nM). Real-time PCR was performed using CFX96 (Bio-Rad, USA), following thermal cycling conditions: 95°C for 1 min, initial denaturation at 9°C for 15 s followed by 40 cycles of 65°C for 60 s for annealing. The combination of primer and probe concentration that yielded the optimal assay performance was selected for further experiments.

Real-time PCR

The final optimised real-time PCR reaction mixture used contained 5 µL of 5× Luna® Universal Probe PCR Master Mix (New England Biolabs USA), 0.45 µL (0.45 mM) of Vir F primer and Vir R primer, 0.3 µL Vir Probe, and 1 µL template in final reaction volume of 10 µL. The following thermal cycling conditions were used: 95°C for 1 min, initial denaturation at 95°C for 15 s followed by 40 cycles of 65°C for 60 s for annealing. All tests were run on a CFX96 real-time thermocycler (Bio-Rad, USA) by two steps of PCR reaction in three replicates for each sample. Data were analysed with Bio-Rad CFX manager 2.0 software (Bio-Rad, USA), applying a default threshold (relative fluorescent units) for BHQ and FAM.

Standard Curve

Data collected were analysed using Bio-Rad CFX manager 2.0 software (Bio-Rad, USA) by applying a default threshold (relative fluorescent units) for BHQ and FAM. In this study, the cDNA prepared from *in vitro* oil palm CCCVd 246 nt variant transcript was serially diluted from 15.4 ng/µL; 1.54 ng/µL; 0.154 ng/µL; 0.0154 ng/µL and 0.00154 ng/µL. The result was analysed by plotting the log of the template concentration against the number of cycle/cycle threshold (Cq value) using the formula $E = [10^{(-1/slope)} - 1] \times 100$ where E is the amplification efficiency. The reaction mixture for

the real-time PCR and the amplification conditions were as above.

Determination of Specificity

Specificity of primers and probe was verified using artificially synthesised plasmid of *Apple scar skin viroid* (ASSVd), *Coconut tinangaja viroid* (CTiVd), *Egg latent viroid* (ELVd), *Hop latent viroid* (HLVd) and *Potato Mosaic Latent Viroid* (PLMVd).

Sensitivity Comparison of Real-time PCR with Conventional PCR

Comparison between the sensitivity of real-time PCR and the conventional PCR was carried out using 10-fold dilution (10^{-1} to 10^{-6}) of *in vitro* oil palm CCCVd 246 nt variant transcripts as templates. Samples with cycle (Cq value) greater than 35 were ignored as these were unreliable on weak positive samples (Khan *et al.*, 2015).

Comparison of Detection Methods

Conventional PCR. The real-time PCR was compared with conventional PCR using full-length primer CCCVd 246 bp, GV4 primer. The synthesised cDNA was amplified by PCR using GoTaq® Green Master Mix (Promega, USA) containing 12.5 µL of 2× GoTaq® Green Buffer and 0.4 µM of GV4 forward and reverse primers (*Table 2*), nuclease-free water and approximately 5 µL of cDNA was added to a final volume of 25 µL reaction volume. The conventional PCR reaction described by Vadamalai (2005) was followed. The initial denaturation was set at 96°C for 3 min and amplification was done under the following conditions: 93°C for 45 s; 55°C for 45 s and 72°C for 3 min for 40 cycles; and 72°C for 15 min. All the PCR products were analysed on a 1% agarose gel in 1× TBE buffer and stained with ethidium bromide for UV visualisation. The PCR products were purified and sent for direct sequencing to confirm.

Loop-mediated Isothermal Amplification (RT-LAMP). RT-LAMP reaction was performed in an 8-strip tube in a 20 µL total reaction, each containing 12.5 µL Isothermal Master Mix (Optigene Ltd., United Kingdom) and 5 µL of cDNA. RT-LAMP primers for CCCVd specific amplification, as optimised by Madihah *et al.* (2020), were added to the reaction mixture at the following final concentrations: External F3 and B3 primers at 0.2 µM, inner FIP and BIP primers at 1 µM, respectively. The RT-LAMP reactions in the 8-strip tube were conducted at 65°C for 70 min and deactivation at 100°C for 5 min. The reactions were carried out using Genie® III (Optigene Ltd., United Kingdom).

RESULTS AND DISCUSSION

Optimisation of Real-time PCR using Hydrolysis Probe Dually Labelled Fluorescent

In order to develop a reliable real-time PCR, various technical parameters should be considered. The reaction and sample volume, primer and probe concentration and melting temperature are among the parameters that should be well designed and optimised (Bharucha *et al.*, 2018; Faggioli *et al.*, 2017). The best combination of concentration primers and probe was optimised based on the number of cycles (Cq value) of real-time PCR assays as described in *Table 3*. It was observed that for Vir F and Vir R

TABLE 3. QUANTIFICATION CYCLE (Cq) AMPLIFICATION PLOT WITH VARIOUS PRIMER AND PROBE CONCENTRATIONS

Optimisation of primer concentrations		
Primer/Probe	**Concentration (nM)**	**Quantification cycle (Cq)**
Vir F	300	
Vir R	300	18.60
Vir probe	300	
Vir F	350	
Vir R	350	18.42
Vir probe	300	
Vir F	400	
Vir R	400	19.13
Vir probe	300	
Vir F	450	
Vir R	450	18.08
Vir probe	300	
Vir F	500	
Vir R	500	37.21
Vir probe	300	
Optimisation of probe concentrations		
Vir F	450	
Vir R	450	21.81
Vir probe	50	
Vir F	450	
Vir R	450	19.52
Vir probe	100	
Vir F	450	
Vir R	450	18.53
Vir probe	200	
Vir F	450	
Vir R	450	17.87
Vir probe	300	

Note: The optimisation was done with constant primer concentration followed by constant probe concentration.

primers, the concentration of 300 nM showed the Cq value of 18.60, 350 nM showed the Cq value of 18.42, 400 nM showed the Cq value of 19.13, 450 nM showed the Cq value of 18.08 and 500 nM showed the Cq value of 37.21. Meanwhile, for the optimisation of Vir probe with constant 450 nM of Vir F and Vir R primers, the probe concentration of 50 nM, 100 nM, 200 nM and 300 nM showed the Cq value of 21.81, 19.52, 18.53 and 17.87, respectively.

Conventional PCR can be used to detect CCCVd 246 nt but it possesses several inherent drawbacks, such as primer dimer formation, low viroid titre in samples and the unequal distribution of CCCVd throughout the plant. These drawbacks have later paved the way for the emergence of several innovated PCR, such as real-time PCR. The usage of primers that yield long fragments of PCR product leads to possible risk of saturated levels of fluorescence or depletion of PCR reagents rapidly (Jansson and Hedman, 2019). The short viroid genome sequence limits the choice of probe and primers selection. Therefore, the probe and primers designed in this study yielded specific and efficient amplification of an 80 nt fragment. The primers and probe were suitable for real-time PCR, required shorter polymerisation time for replication and reduced the amplification of contaminating genomic DNA. A range of primer and probe concentration is essential for an optimal reaction as if it is too low, no fluorescent signal is observed. If it is too high, the result can lead to a high fluorescent background, which can mislead the detection and quantification (Kralik and Ricchi, 2017). Prior to performing a real-time PCR reaction, optimisation of primers and probe was done. In this study, primer concentration of 450 nM and probe concentration of 300 nM were observed with the lowest Cq value and high fluorescent signal, and therefore, was selected as the suitable conditions for the technique.

Preparation of Standard Curve

A standard curve was constructed using cDNA constructed from *in vitro* transcript with 450 nM of primer and 300 nM of probe to determine the PCR efficiency and linearity of template amplification. The standard curve showed slope close to -3.3 with strong linear relationship along with a correlation coefficient of 0.98 and amplification efficiencies at 100.2%, indicating maximum PCR efficiency (*Figure 2a*). The ability to detect low concentrations indicated the effectiveness of optimised probes and primers to develop precise and reliable markers in detecting CCCVd in oil palm.

Specificity and Sensitivity Assessment of Real-time PCR

The primers designed for this assay detected the oil palm CCCVd variant with high fluorescence and lowest Cq value as compared to other tested viroids, such as ASSVd, CTiVd, ELVd, HLVd and PLMVd with Cq value of 36.61, 36.99, 37.05 and 36.64, respectively (*Figure 2b*). The specificity of other viroids of different genus and closely related viroids in the same genus revealed that the primer and probe design did not specifically match the sequences. It was only the CCCVd variants 246 nt plasmids that was detected by the real-time PCR while other viroids had low Cq values, suggesting the specificity of the real-time PCR assay developed to detect CCCVd variants in oil palm. In addition, compared to RT-LAMP's specificity, the real-time PCR was more specific since the reported RT-LAMP primers also detected the HLVd and ELVd apart from the CCCVd (Madihah *et al.*, 2020). This is another major drawback of the RT-LAMP technique which may contribute to false positive presence of CCCVd.

The real-time PCR sensitivity was assessed with a series of dilutions of cDNA from the *in vitro* transcript. The real-time assay was able to detect the lowest concentration of 10^{-5} of the *in vitro* oil palm CCCVd 246 nt variant transcript with Cq value of 34.02 (*Figure 2c*). Meanwhile, the evaluation of sensitivity using conventional PCR showed that it only detected with no multiple bands up to 10^{-4} of *in vitro* oil palm CCCVd 246 nt variant transcript (*Figure 2d*). However, the developed real-time PCR in this study had around 10-fold higher sensitivity as compared to the conventional PCR.

Application of Real-time PCR and Comparison with Conventional PCR and RT-LAMP

A total of 14 oil palm leaves with typical symptoms of OS were subjected to the testing using real-time PCR in comparison to conventional PCR and RT-LAMP for the detection of CCCVd. The real-time PCR successfully detected the presence of CCCVd in all 14 samples with Cq values ranging from 25.12 to 30.64 cycles, suggesting higher sensitivity (*Table 4*). On the contrary, the conventional PCR analysis showed detection in only 10 samples. All the positive samples produced an amplicon of 246 bp in size, but primer dimer formation was shown in *Figure 3*. Meanwhile, the RT-LAMP only managed to detect seven samples. *Figure 4* illustrates the annealing curve which shows that the RT-LAMP primer is CCCVd specific.

To enhance the reliability of the assay, a complete control system was introduced including cDNA from *in vitro* transcript as positive control followed by healthy oil palm leaves, spiked in with cDNA from the *in vitro* transcript as reaction control and non-template control (NTC). Our observations suggested that the real-time PCR performed more efficiently in detection when compared to the conventional PCR and RT-

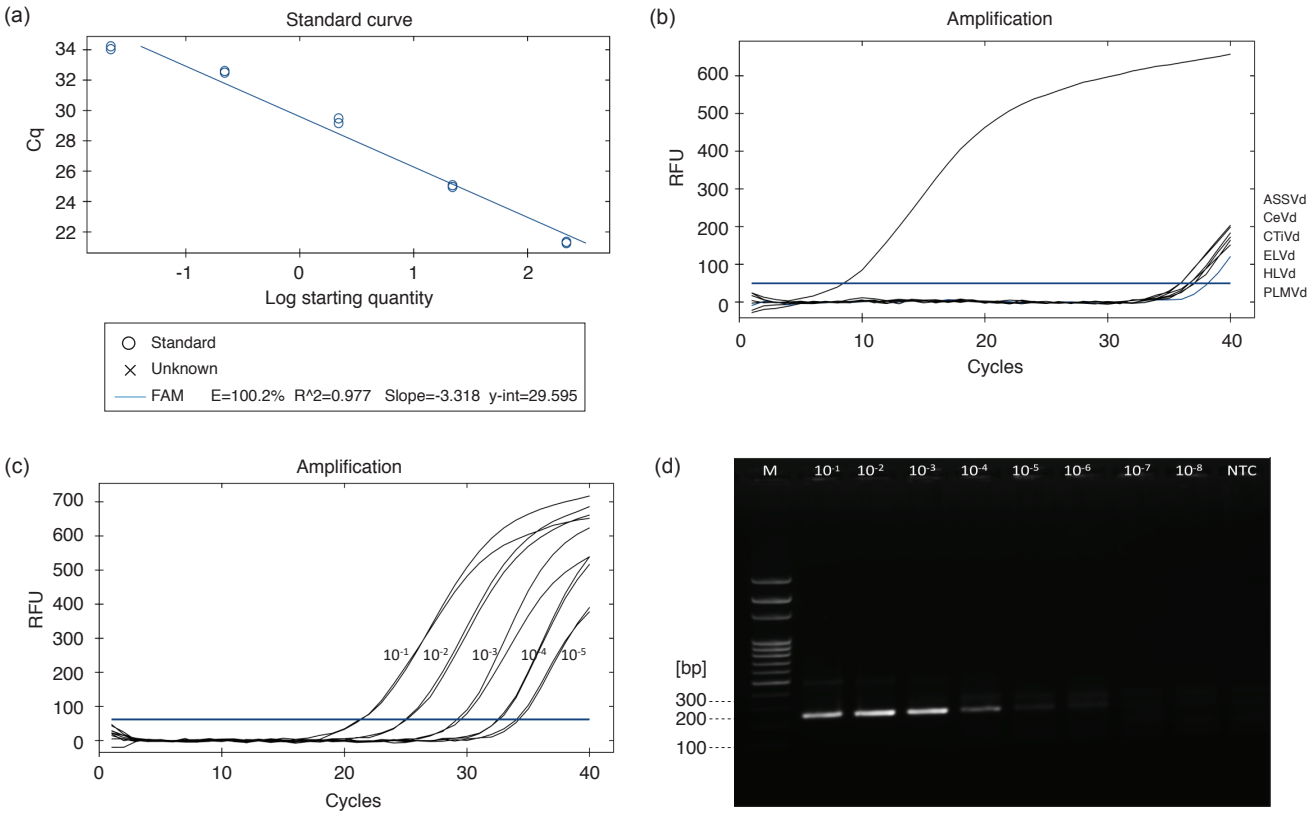


Figure 2. (a) Standard curve obtained from oil palm CCCVd 246 nt variant quantification for the efficiency of the real-time PCR. The horizontal axis represents a series of 10-fold dilutions of in vitro *oil palm CCCVd 246 nt variant plasmid while the vertical axis represents the Cq value obtained from the reaction with three replications. The E-value represents the efficiency of the assay and the R^2 is used to evaluate the accuracy between replicates; (b) Evaluation of specificity of real-time PCR on ASSVd, CTiVd, ELVd, HLVd and PLMVd; (c) Evaluation of sensitivity of 10-fold dilutions of* in vitro *transcript of CCCVd using real-time PCR; (d) Evaluation of sensitivity of 10-fold dilutions of* in vitro *transcript of CCCVd using conventional PCR.*

LAMP. In addition, the conventional PCR may be unsuitable in detecting the lower concentration of viroid in oil palm because the result showed that four samples of the 14 palms were observed with negative detection when subjected to conventional PCR, affecting the detection assessment. In some instances, multiple non-specific products in the conventional PCR were obtained, further reducing the reliability of the technique (Khan *et al.*, 2015). This highlights the practicality of real-time PCR in detecting CCCVd 246 nt. The optimised CCCVd real-time PCR was able to detect the viroid at a lower concentration. Its high sensitivity proves its potential as an ideal diagnostic tool for the use of epidemiological monitoring programmes.

The presence of CCCVd was detected with the amplification of conventional PCR using adjacent specific CCCVd primer GV4 and templates concentration optimised by Vadamalai (2005) while with the RT-LAMP using optimised RT-LAMP primers and templates concentration by Madihah *et al.* (2020) using Genie® III (Optigene Ltd). Based on the result, the conventional PCR amplified the CCCVd but it showed multiple bands which may affect the detection assessment. RT-LAMP only managed to detect seven out of 14 palms as positive with CCCVd presence (*Table 4*). The inconsistency of detecting CCCVd circular form and high detection limits in the reaction suggests the possibility of the less sensitive RT-LAMP results in this study. Although RT-LAMP has been demonstrated to be practical for pathogen detection in the field, it may not be sensitive enough to detect low concentrations of the pathogen. This is demonstrated by a study comparing the detection of *Alternaria solani* and *Xylella fastidiosa* using RT-LAMP, conventional PCR, and real-time qPCR, showing that real-time qPCR was more sensitive than RT-LAMP (Harper *et al.*, 2010; Khan *et al.*, 2018), implying the necessity for comparative detection.

To the best of our knowledge, this study is the first validation report on comparison and evaluation of different PCR-based and RT-LAMP techniques using similar nucleic acid sources for the detection of CCCVd circular form, targeting variant 246 nt. Although RT-LAMP was reported as a convenient method for rapid pathogen detection, there is a high potential risk of false negative and false positive. As an example, RT-LAMP is prone to contamination due to the carryover of the LAMP product from one assay to another assay as the product increases three-fold every half cycle (Panno *et al.*, 2020). As a consequence, it is usually

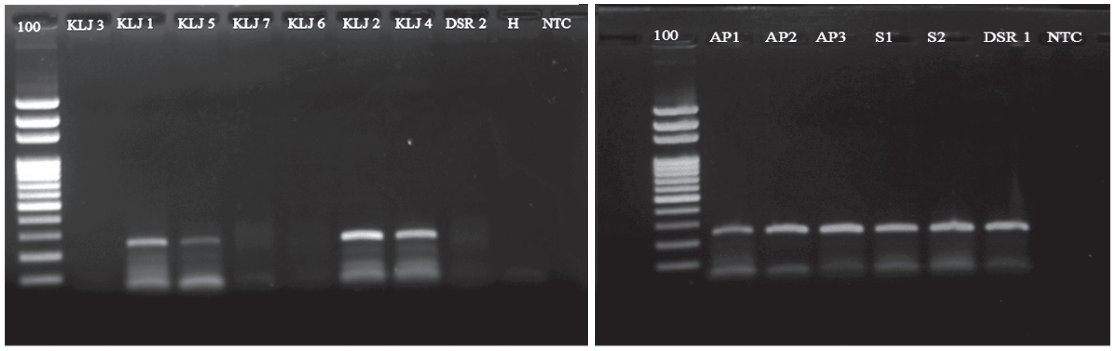


Figure 3. Detection of 14 oil palm samples from field by conventional PCR. The 100 bp ladder was labelled as 100 (Solis Biodyne, Estonia). The 246 bp amplicon corresponds to oil palm CCCVd 246 nt RNA.

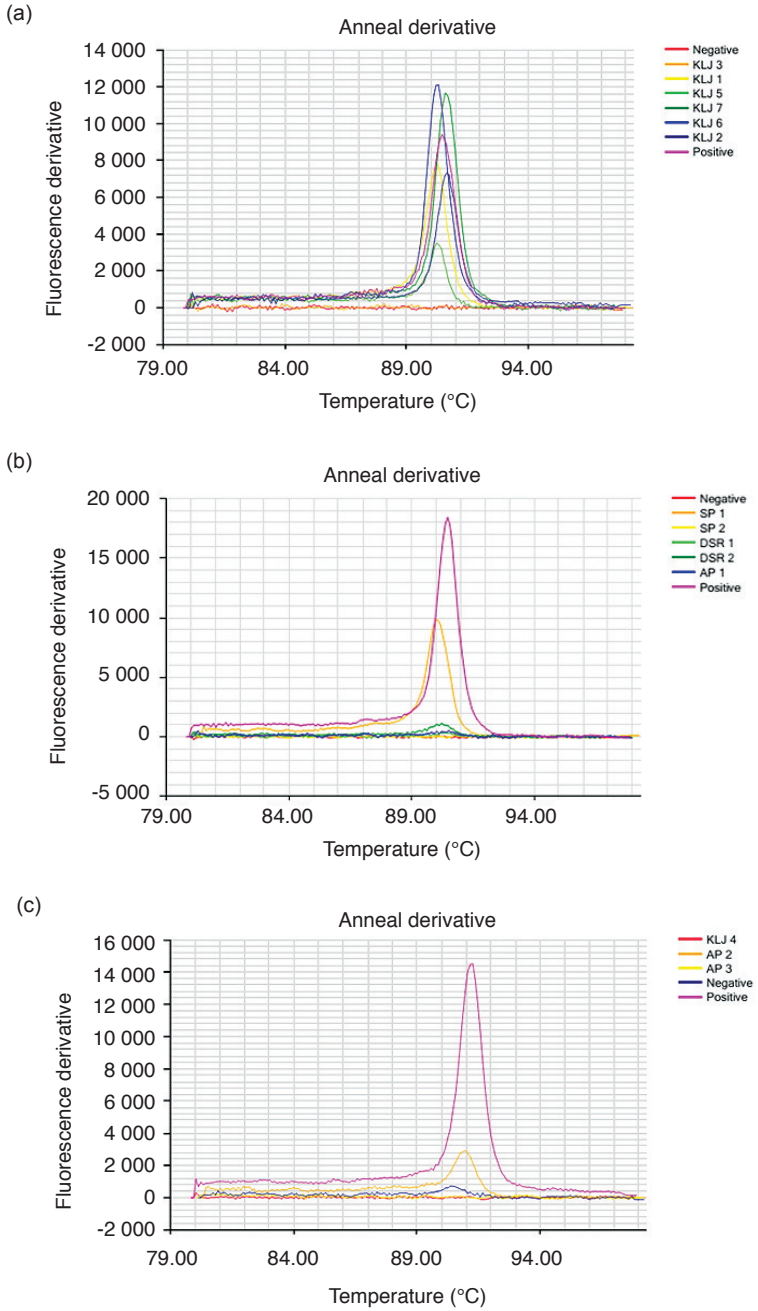


Figure 4. Reverse transcription loop-mediated isothermal amplification (RT-LAMP) annealing derivative curve detected for oil palm from field with threshold value of 2000 after 65 min incubation time in 63°C. Any peak below the threshold was considered as negative, (a) KLJ 1, 2, 5, 6, 7 and 2 = positive, whereas KLJ 3 and KLJ 4 = negative; (b) only SP 2 = positive; (c) KLJ 4, and AP3 = negative whereas AP2 = positive.

TABLE 4. COMPARATIVE ANALYSIS OF REAL-TIME PCR ASSAY IN OS-CCCVd SAMPLES WITH RT-PCR AND RT-LAMP

Samples	**Real-time PCR Mean Cq value**		
Std-1	7.2 ± 0.65		
Std-2	10.8 ± 0.46		
Std-3	13.8 ± 0.03		
Std-4	17.3 ± 0.34		
Std-5	21.6 ± 0.79		
Healthy oil palm leaves	37.0 ± 0.19		
Healthy oil palm leaves + spiked in cDNA from *in vitro* transcript	15.1 ± 0.49		
cDNA from *in vitro* transcript	14.9 ± 0.48		
NTC	Undertermined		
OS-CCCVd samples	**Real-time PCR Mean Cq value**	**Conventional PCR**	**RT-LAMP**
KLJ 3	+ (30.06 ± 0.31)	–	–
KLJ 1	+ (26.80 ± 0.34)	+	+
KLJ 5	+ (28.74 ± 0.48)	+	+
KLJ 7	+ (29.45 ± 0.80)	–	+
KLJ 6	+ (28.06 ± 2.89)	–	+
KLJ 2	+ (28.88 ± 1.28)	+	+
KLJ 4	+ (28.98 ± 0.73)	+	–
S 1	+ (28.98 ± 0.73)	+	+
S 2	+ (23.24 ± 2.02)	+	–
DSR 1	+ (25.83 ± 0.33)	+	–
DSR 2	+ (30.64 ± 0.49)	–	–
AP 1	+ (25.55 ± 1.45)	+	–
AP 2	+ (25.77 ± 1.39)	+	+
AP3	+ (23.12 ± 2.01)	+	–

Note: The assays included five points of dilution for standard curve, healthy oil palm leaves, healthy oil palm leaves spiked in with cDNA from *in vitro* oil palm CCCVd 246 nt variant and cDNA from *in vitro* oil palm CCCVd 246 nt variant for control reactions.
NTC - non–template control; – - Negative; + - Positive; Cq - quantitative cycle.

recommended that at least two diagnostic methods are compared for viroid detection purposes (Murcia *et al*., 2009).

A previous study employed RT-PCR with NETME extracted nucleic acids to detect CCCVd and recognised partial CCCVd sequence. This resulted in fewer positive samples with CCCVd presence (Roslan *et al*., 2016). In addition, according to the International Committee on Taxonomy of Viruses (Owens R A *et al*., 2012), the identification of viroids should be based on the analysis of their complete genome. However, complete sequences are still difficult or impossible to be obtained from samples with low viroid levels because traditional RT-PCR techniques lack the required sensitivity to generate full-length amplicons. Furthermore, conventional RT-PCR is generally more prone to inhibition by matrix components (Botermans *et al*., 2020). Therefore, to address the weakness in the detection methods reported earlier, the viroid was enriched by PAGE following the NETME extraction, allowing the complete length sequence / copies of CCCVd to be effectively amplified, and more samples to be evaluated. Using a full-length primer in RT-PCR detection allowed further sequence characterisation to identify sequence variants that may occur in field samples and accumulation analysis. This finding also addressed a gap in a previous study (Thanarajoo, 2014), which claimed that RT-LAMP could only identify the CCCVd variants in six oil palm samples out of 15 oil palm samples collected randomly from the field. However, the technique has yet to be verified for CCCVd detection sensitivity.

The ever-evolving real-time PCR may be the answer and future strategy in mitigating continuous spread of plant diseases by screening and culling contaminated materials. The early detection of CCCVd variants in oil palm allows planters to carefully select and breed only CCCVd-free materials. The detection using real-time PCR typically takes an hour as compared to using conventional PCR with GV4 primers which take approximately 3 hr. Meanwhile, in this study, the amplification of CCCVd 246 nt in the RT-LAMP was observed within 60-65 min, similar to studies by Thanarajoo *et al.* (2014) and Madihah *et al.* (2020). The runtime required to perform a real-time PCR is almost equal to RT-LAMP for maximum production of amplified product for CCCVd detection. The detection of other viroids using RT-LAMP was reported to be distinctly rapid where the turbidity was observed within 20-40 min for *Pepper chat fruit viroid* (PCFVd) (Boubourakas and Kyriakopoulou, 2022; Tangkanchanapas *et al.*, 2018). However, some observations could detect in 50 min for PSTVd (Verma *et al.*, 2020) and 60 min for *Peach latent mosaic viroid* (PLMVd) (Lee and Jeong, 2020). Hence, the duration depends on the viroid species and their genome sequence (Bhuvitarkorn *et al.*, 2019). Higher consideration in developing modern detection methodology is encouraged for reliable detection as it is critical for the quarantine and certification of oil palm planting materials. In Japan, real-time PCR detection was used for inspecting dahlia's seedlings to prevent the invasion of PSTVd at the border, leading to the quick eradication of the viroid (Tsushima and Fuji, 2022). Similar approach will be applicable in Malaysia especially in allowing exotic materials entering into the country as part of the biosecurity plan of the commodity crop.

CONCLUSION

In conclusion, an optimised and validated real-time PCR for CCCVd with higher sensitivity was successfully developed with the reaction specific to CCCVd. The real-time PCR was the only technique that managed to detect CCCVd presence in all 14 oil palm samples with a range of Cq value from 25.12 to 30.64 compared to RT-LAMP, which only detected seven samples while the RT-PCR detected 10 samples. The real-time PCR enables rapid detection with higher sensitivity. A complementary method such as the real-time PCR increases the confidence of detection level assessment by comparing the Cq value. In the past, epidemiology research on CCCVd variants in affected oil palms, particularly the OS, has been hampered by the lack of reliable detection of the viroid. Therefore, this improved real-time PCR technique provides a valuable tool to enhance the knowledge of the viroid in oil palms. This is essential for future strategies involving the control and mitigation of any outbreaks in oil palm to ensure a sustainable crop production.

ACKNOWLEDGEMENT

The authors would like to thank the Director-General of the MPOB for the permission to publish this article. We thank all members who were involved in this study for their technical assistance. The work was supported by a research grant provided to the Plant Pathology and Biosecurity Unit, MPOB.

REFERENCES

Bharucha, T; Sengvilaipaseuth, O; Vongsouvath, M; Vongsouvath, M; Davong, V; Panyanouvong, P; Piorkowski, G; Garson, J A; Newton, P N and De Lamballerie, X (2018). Development of an improved RT-qPCR assay for detection of *Japanese encephalitis virus* (JEV) RNA including a systematic review and comprehensive comparison with published methods. *PLoS ONE, 13(3)*: e0194412.

Bhuvitarkorn, S; Klinkong, S and Reanwarakorn, K (2019). Enhancing *Columnea latent viroid* detection using reverse transcription loop-mediated isothermal amplification (RT-LAMP). *Int. J. Agric. Technol., 15*: 215-228.

Botermans, M; Roenhorst, J W; Hooftman, M; Verhoeven, J T J; Metz, E; Van Veen, E J; Geraats, B P; Kemper, M; Beugelsdijk, D C and Koenraadt, H (2020). Development and validation of a real-time RT-PCR test for screening pepper and tomato seed lots for the presence of pospiviroids. *PLoS ONE, 15(9)*: e0232502.

Boubourakas, I N and Kyriakopoulou, P E (2022). *Reverse Transcription Loop-Mediated Isothermal Amplification (RT-LAMP) at the Service of Viroid Detection. Viroids*. Springer. p. 195-210.

Faggioli, F; Luigi, M and Boubourakas, I N (2017). Viroid amplification methods: RT-PCR, Real-Time RT-PCR and RT-LAMP. *Viroids and Satellites.* 1st edition. Elsevier. p. 381-391.

Ghobakhloo, M; Dizadji, A and Yamchi, A (2019). A real-time PCR assay for detection and absolute quantitation of *Citrus exocortis viroid* in two sensitive and tolerant rootstocks. *Crop Prot., 115*: 27-30.

Harper, S; Ward, L and Clover, G (2010). Development of LAMP and real-time PCR methods for the rapid detection of *Xylella fastidiosa* for quarantine and field

applications. *Phytopathology, 100(12)*: 1282-1288.

Jansson, L and Hedman, J (2019). Challenging the proposed causes of the PCR plateau phase. *Biomol. Detect. Quant., 17*: 100082.

Khan, M; Wang, R; Li, B; Liu, P; Weng, Q and Chen, Q (2018). Comparative evaluation of the LAMP assay and PCR-based assays for the rapid detection of *Alternaria solani*. *Front. Microbiol., 9*: 2089.

Khan, S; Mackay, J; Liefting, L and Ward, L (2015). Development of a duplex one-step RT-qPCR assay for the simultaneous detection of *Apple scar skin viroid* and plant RNA internal control. *J. Virol. Methods, 221*: 100-105.

Kralik, P and Ricchi, M (2017). A basic guide to real time PCR in microbial diagnostics: Definitions, parameters and everything. *Front. Microbiol., 8*: 108.

Kumar, S; Stecher, G; Li, M; Knyaz, C and Tamura, K (2018). MEGA X: Molecular evolutionary genetics analysis across computing platforms. *Mol. Biol. Evol., 35(6)*: 1547.

Lee, B D and Koonin, E V (2022). Viroids and viroid-like circular RNAs: Do they descend from primordial replicators? *Life, 12(1)*: 103.

Lee, H-J and Jeong, R-D (2020). Reverse transcription loop-mediated isothermal amplification assay for detecting peach latent mosaic viroid in peach pollen. *Hortic. Sci. Technol., 38(6)*: 830-839.

Leichtfried, T; Reisenzein, H; Steinkellner, S and Gottsberger, R A (2021). Improvement in the sensitivity of viroid detection by adapting the reverse transcription step in one-step RT-qPCR assays. *J. Virol. Methods, 292*: 114123.

Madihah, A; Maizatul-Suriza, M and Idris, A (2020). Reverse transcription loop-mediated isothermal amplification (RT-LAMP) for detection of *Coconut Cadang-cadang Viroid* (CCCVd) variants in oil palm. *J. Oil Palm Res., 32*: 453-463.

Murcia, N; Serra, P; Olmos, A and Durán-Vila, N (2009). A novel hybridization approach for detection of citrus viroids. *Mol. Cell. Probes, 23(2)*: 95-102.

Osman, F; Dang, T; Bodaghi, S and Vidalakis, G (2017). One-step multiplex RT-qPCR detects three citrus viroids from different genera in a wide range of hosts. *J. Virol. Methods, 245*: 40-52.

Owens, R A; Flores, R; Di Serio, F; Li, S-F; Pallás, V; Randles, J W; Sano, T and Vidalakis, G (2012). Viroids. *Virus Taxonomy: Ninth Report of the International Committee on Taxonomy of Viruses* (Kining Amq, A M; Carstens, E B and Lefkowitz, E J eds.). Elsevier/ Academic Press. London, United Kingdom. p. 1221-1234.

Panno, S; Matić, S; Tiberini, A; Caruso, A G; Bella, P; Torta, L; Stassi, R and Davino, S (2020). Loop mediated isothermal amplification: Principles and applications in plant virology. *Plants, 9(4)*: 461.

Randles, J; Boccardo, G and Imperial, J S (1980). Detection of the *Cadang-cadang* associated RNA in African oil palm. *Phytopathology, 70*: 185-189.

Randles, J W and Rodriguez, M J (2003). *Coconut Cadang-cadang Viroid. Viroids* (Hadidi, A; Flores, R; Randles, J W and Semancik, J S eds.). Australia; CSIRO. p. 233-241.

Roslan, N D; Meilina, O A; Mohamed-Azni, I-N A; Seman, I A and Sundram, S (2016). Comparison of RNA extraction methods for RT-PCR detection of *Coconut cadang-cadang viroid* variant in orange spotting oil palm leaves. *Canadian J. Plant Pathol., 38(3)*: 382-388.

Scott, A T; Layne, T R; O'connell, K C; Tanner, N A and Landers, J P (2020). Comparative evaluation and quantitative analysis of loop-mediated isothermal amplification indicators. *Anal. Chem., 92(19)*: 13343-13353.

Seigner, L; Liebrecht, M; Keckel, L; Einberger, K and Absmeier, C (2020). Real-time RT-PCR detection of *Citrus bark cracking viroid* (CBCVd) in hops including an mRNA-based internal positive control. *J. Plant Dis. Prot., 127(6)*: 763-767.

Sundram, S; Norman, K; Roslan, N; Vasagi, R; Seman, I and Kushairi, A (2017). *Orange Spotting on Oil Palm in Malaysia: A Pictorial Guide to Identify Symptoms of Orange Spotting in Oil Palms*. MPOB, Bangi.

Tangkanchanapas, P; Höfte, M and De Jonghe, K (2018). Reverse transcription loop-mediated isothermal amplification (RT-LAMP) designed for fast and sensitive on-site detection of *Pepper chat fruit viroid* (PCFVd). *J. Virol. Methods, 259*: 81-91.

Thanarajoo, S S (2014). Rapid detection, accumulation and translocation of *Coconut cadang-cadang viroid* variants in oil palm. PhD thesis, Universiti Putra Malaysia.

Tsushima, D and Fuji, S I (2022). Comparison of two highly sensitive methods to detect *Potato spindle tuber viroid* in Dahlia using quantitative-reverse transcription-polymerase chain reaction assays. *J. Virol. Methods, 300*: 114401.

Vadamalai, G (2005). An investigation of orange spotting disorder in oil palm. PhD thesis, Universiti Putra Malaysia.

Vadamalai, G; Hanold, D; Rezaian, M and Randles, J (2006). Variants of *Coconut cadang-cadang viroid* isolated from an African oil palm (*Elaies guineensis* Jacq.) in Malaysia. *Arch. Virol., 151(7)*: 1447-1456.

Verma, G; Raigond, B; Pathania, S; Kochhar, T and Naga, K (2020). Development and comparison of reverse transcription-loop-mediated isothermal amplification assay (RT-LAMP), RT-PCR and real time PCR for detection of *Potato spindle tuber viroid* in potato. *Eur. J. Plant Pathol., 158(4)*: 951-964.

Wastling, S L; Picozzi, K; Kakembo, A S and Welburn, S C (2010). LAMP for human African trypanosomiasis: A comparative study of detection formats. *PLOS Negl. Trop. Dis., 4(11)*: e865.

Wu, Y H; Cheong, L C; Meon, S; Lau, W H; Kong, L L; Joseph, H and Vadamalai, G (2013). Characterization of *Coconut cadang-cadang viroid* variants from oil palm affected by orange spotting disease in Malaysia. *Arch. Virol., 158(6)*: 1407-1410.

Zhang, Z; Cui, X; Jiang, J; Xiao, H; Wang, H; Wu, Q; Habili, N and Li, S (2018). Improved detection of *grapevine latent viroid* by RT-qPCR, its bioassay analysis, and its rare occurrence worldwide. *J. Virol. Methods, 254*: 13-17.

Journal of Oil Palm Research Vol. 35 (1) March 2023 p. 122-146
DOI: https://doi.org/10.21894/jopr.2022.0032

DESIGNING gRNAs TARGETING OIL PALM PHYTOENE DESATURASE (*EgPDS*) GENE AND CONSTRUCTION OF VECTORS FOR OIL PALM CRISPR/CAS9 STUDY

NORFAEZAH JAMALUDIN[1]; BOHARI BAHARIAH[1]; NOOR AZMI SHAHARUDDIN[2]; CHAI LING HO[3]; OMAR ABDUL RASID[1]; GHULAM KADIR AHMAD PARVEEZ[1] and MAT YUNUS ABDUL MASANI[1]*

ABSTRACT

*The CRISPR/Cas9 system is a precise and versatile genetic tool used to induce site-specific manipulation in the targeted gene. This study elaborates on the strategy to select the gRNAs targeting the oil palm phytoene desaturase (*EgPDS*) gene, which complements CRISPR-GE and sequence analysis. Sixty-one gRNAs were selected from 167 gRNA candidates generated by the CRISPR-GE tool. These gRNA candidates were further analysed to meet the specific criteria, including the guanine (G) and cytosine (C) content of 35%-60% and the presence of preferable gRNA features. From 61 gRNAs, seven gRNAs were selected, which represent three different parts of the* EgPDS *gene in the genome. The efficiency of each gRNA candidate to cause cleavage on the target gene was confirmed by* in vitro *cleavage analysis. All seven gRNA candidates were then cloned into the pYLsgRNA-OsU6 cassette before being incorporated seamlessly into the final transformation vector, pYLCRISPR/Cas9P35S-H, via Gibson assembly. Three CRISPR/Cas9 transformation vectors targeting the* EgPDS *gene, namely pYLEgPDS1-35S-H, pYLEgPDS2-35S-H and pYLEgPDS3-35S-H, were successfully constructed. These constructs will be transformed into oil palm protoplasts via polyethylene glycol (PEG)-mediated transformation and subsequently into oil palm embryogenic calli via biolistic and* Agrobacterium*-mediated transformation to determine the efficacy of the multiplex CRISPR/Cas9 system in oil palm genome.*

Keywords: CRISPR/Cas9, gRNA, *in vitro* cleavage assay, oil palm, phytoene desaturase.

Received: 28 December 2021**; Accepted:** 25 April 2022**; Published online:** 10 June 2022.

INTRODUCTION

Oil palm (*Elaeis guineensis*) is a monocot perennial oil-producing fruit tree with a significant socio-economic prospect in Africa and Asia. Currently, the demand for crude palm oil in various industries is increasing (Parveez *et al.*, 2021). Thus, it is urgent to improve the yield and quality of palm oil better than what conventional techniques have achieved. Previously, significant achievements in oil palm biotechnology have been reported in biochemical research, including identification, isolation of promoters and functional genes from oil palm (Masani *et al.*, 2018). Numerous transformation constructs using the previously isolated promoters and genes for various target products have been extensively developed (Masani *et al.*, 2018). The development of oil palm transformation methods and molecular analyses of oil palm putative transformants was actively carried out (Rahman *et al.*, 2020). In 2013, Malaysian Palm Oil Board

[1] Malaysian Palm Oil Board,
6 Persiaran Institusi, Bandar Baru Bangi,
43000 Kajang, Selangor, Malaysia.

[2] Department of Biochemistry,
Faculty of Biotechnology and Biomolecular Sciences,
Universiti Putra Malaysia,
43400 UPM Serdang, Selangor, Malaysia.

[3] Department of Cell and Molecular Biology,
Faculty of Biotechnology and Biomolecular Sciences,
Universiti Putra Malaysia,
43400 UPM Serdang, Selangor, Malaysia.

* *Corresponding author e-mail: masani@mpob.gov.my*

(MPOB) released the whole genome sequence of African oil palm species (Singh *et al.*, 2013), which has opened an opportunity to shift into oil palm genome editing.

Clustered Regularly Interspaced Short Palindromic Repeats (CRISPR) with CRISPR-associated protein 9 (Cas9) was first introduced in 2013 (Charpentier and Doudna, 2013). It has been successfully applied in various plant species, including recalcitrant crop species (Ma *et al.*, 2015). Therefore, this system offers a promising solution for oil palm genome editing. Evaluation studies of CRISPR/Cas9 in oil palm are essential to mitigate certain restrictions such as inefficient guide RNA (gRNA) design, off-target activity, and selection of vector system that can affect the CRISPR/Cas9 efficiency. CRISPR/Cas9 utilises the Cas9 protein and gRNA, which interact to form a complex that can identify target sequences with high selectivity (Charpentier and Doudna, 2013). The gRNA is responsible for locating, and the Cas9 will cleave the target DNA, producing double-strand breaks (DSBs). The DSBs can induce various types of mutations (*e.g.*, base insertion, deletion and substitution) through the error-prone non-homologous end-joining pathway and specific modification through the homology-directed repair pathway. Predictably, when the induced mutations are located in the genes coding region, the corresponding genes may entirely or partially lose their functions (Ma and Liu, 2016).

The binding of Cas9 nuclease to the target sequence occurs only with the presence of the protospacer adjacent motif (PAM) sequence. In CRISPR/Cas9 system, the *Streptococcus pyogenes* Cas9 (*Sp*Cas9) nuclease cleaves at 3-4 nucleotides upstream of the PAM sequence 5'-NGG-3' ("N" confers any nucleotide base). In addition, the 20-nucleotide sequence of gRNA is also crucial in determining the efficiency of designed gRNA (Doench *et al.*, 2014). For example, guanine is favoured directly after the PAM sequence (nucleotide position 20), whereas cytosine is unpreferable. This is because guanine has a better affinity for Cas9 binding over cytosine (Wang *et al.*, 2014a). The efficacy of each gRNAs, accessibility at a specific position for Cas9 binding and presence of stem-loops were also predicted based on their secondary structure (Bruegmann *et al.*, 2019). Furthermore, off-target activity also should be avoided. Few mismatches between gRNA and the target sequence are intolerable as Cas9 still cuts the off-target region. Thus, various gRNA design tools using a computerised prediction method have been developed (Wang *et al.*, 2020).

Analyses of successfully targeted mutations have revealed that the expression levels, expression timing, and variants of gRNA and Cas9 need to be highly regulated (Ma *et al.*, 2015). Therefore, the promoters of these genes and the target site are the critical factors for genome-editing efficiency in oil palm. Various modified CRISPR/Cas9 editing vector systems that can carry multiple gRNAs in a single construct are available. This technology is known as a multiplex CRISPR/Cas9 system. A multiplex genome editing can be achieved by simultaneous insertion and expression of multiple gRNAs. The generation of multiple DSBs followed by the deletion of large fragments between these multiple gRNA-targeted sites on the same chromosome has been achieved in many species (Wang *et al.*, 2014b). Hence, using a multiplex CRISPR/Cas9 genome editing system may foretell the successful genome editing in oil palm.

This study highlights the preliminary work of the CRISPR/Cas9 study in oil palm, including the gRNAs selection strategy, targeting the oil palm phytoene desaturase (*EgPDS*) gene and *in vitro* cleavage assay to determine the functionality of designed gRNAs. We also elaborated on the construction of CRISPR/Cas9 transformation vectors carrying multiple gRNAs to kickstart the CRISPR/Cas9 study in oil palm.

MATERIALS AND METHODS

Selection of gRNA Candidates Targeting *EgPDS* Gene

The identification of possible CRISPR/Cas9 target sites in the 1.7 kb coding sequence of *EgPDS* was performed using the CRISPR-GE online tool (Ma *et al.*, 2015). The generated targets were gRNA sequences that are 20 bases in length, followed by the PAM sequence (20n-NGG). gRNA candidates were identified based on the CRISPR-GE targetDesign tool. The off-target analysis was carried out using NCBI BLAST. The gRNA candidates' sequence was BLAST with a 'somewhat similar sequence' option to omit candidates with high similarity with other possible off-target sequences in the genome.

Secondary Structure Analysis of *EgPDS* gRNA Candidates

The secondary structure prediction was carried out using RNA Folding Form v2.3 (http://mfold.rna.albany.edu/?q=mfold/RNA-Folding-Form2.3). The gRNA sequence without its PAM linked to the nucleotides of the scaffold sequence (GTTTTAGAGCTAGAAATAGCAAGTTAAAATAAGGCTAGTCCGTTATCAACTTGAAAAAGTGGCACCGAGTCGGTGCTTTTTTT) was submitted for analysis. gRNA candidates having at least stem-loop 2 and stem-loop 3 were selected for further experiments.

In vitro Transcription of gRNA Targeting *EgPDS* Gene

The gRNA candidates were PCR amplified using Guide-it™ sgRNA *In vitro* Transcription and Screening Systems (Takara Bio, USA) following the manufacturer's protocol. The PCR reaction contained the designed forward primers (0.5 μM), the Guide it Scaffold template (1.0 μM), 1× PrimeSTAR Max Premix (12.5 μL) and RNase free water to bring the total of 20 μL. The PCR amplification of the gRNA template was carried out using the following program: 33 cycles of 98°C for 10 s, 68°C for 10 s. Subsequently, the PCR product was incubated at 37°C for 4 hr for *in vitro* transcription of gRNAs. The transcribed gRNAs were purified using Guide-it IVT RNA Clean-Up Kit (Takara Bio, USA) according to the manufacturer's protocol. RNase-free water, 20 μL was used in the final elution.

In vitro Cleavage Assay

The components required for the *in vitro* cleavage reaction are the oil palm control PCR fragment containing the target sites (wild type), the previously transcribed gRNAs and the Cas9 enzyme (Guide-it Recombinant Cas9 Nuclease, Takara Bio, USA). The amplification of the control target fragments was carried out using specific primers for each gRNA (*Table 1*). The PCR products were then purified by NucleoSpin® Gel and PCR Clean-up (Macherey Nagel, Germany). *In vitro* cleavage assay was carried out for a single gRNA and multiple gRNA (two to three gRNAs targeting one PCR fragment) according to the manufacturer's protocol (Guide-it™ sgRNA *In vitro* Transcription and Screening Systems, Takara Bio, USA). The gRNAs were first incubated with the recombinant Cas9 nuclease for 5 min at 37°C. Then, the Cas9-gRNAs were mixed with Cas9 reaction buffer, BSA, RNase free water and the control PCR fragment (250 ng) containing the target sequence, incubated at 37°C for 1 hr, then 80°C for 5 min. The cleavage reaction was observed on 2% agarose gel.

Preparation of Target Adapters and Ligation into pYLsgRNA-OsU6 Cassettes

The design of target adapter primers (*Table 1*) for cloning gRNA sequences into pYLsgRNA-OsU6a and pYLsgRNA-OsU6b cassettes was carried out using primerDesign in CRISPR-GE (Ma *et al.*, 2015). The target adapter primers were designed such that the 5'end of the adapters contained a compatible *Bsa*I digested end site of the corresponding U6 promoters. The corresponding U6 promoters were either OsU6a for gRNA1, gRNA3, gRNA5 and gRNA7 or OsU6b for gRNA2, gRNA4 and gRNA6. The OsU6a and OsU6b promoters were derived from pYLsgRNA-OsU6a and pYLsgRNA-OsU6b cassettes, respectively, which were obtained from Prof. Liu YG Lab (South China Agricultural University). The target adapters were prepared by dissolving 5 μL of 100 μM forward primer (FP) and 5 μL of 100 μM of reverse primer (RP) for each gRNA cassette in one tube. The tubes were heated in 100°C boiled water for 1 min, and cooled to room temperature for 2 hr. Then, the double-stranded target adapters were ligated into either pYLsgRNA-OsU6a or pYLsgRNA-OsU6b, which were previously linearised with the *Bsa*I enzyme according to the standard protocol (New England Biolabs). The ligation reaction was carried out at 37°C for 10 min using T4 DNA ligase (Promega, USA).

Construction of pYLEgPDS1-35S-H, pYLEgPDS2-35S-H and pYLEgPDS3-35S-H

The integrated gRNA expression cassettes carrying the target adapters were then amplified by overlapping PCR in two sets of reactions with different primer combinations (*Table 2*). In the first PCR (PCR GXL), the previous ligation products were used as the template in a 15 μL PCR reaction containing 1x PRIMESTAR GXL buffer, 2.5 mM dNTP mix, 0.2 μM of each FP and RP primers (*Tables 1* and *2*) and 0.75 U PRIMESTAR GXL DNA Polymerase (PrimeSTAR® GXL DNA Polymerase, Takara Bio USA). The PCR cycling condition was 98°C for 1 min, 25 cycles of 98°C for 15 s; 63°C for 30 s; 68°C for 45 s, final extension at 68°C for 2 min. The PCR GXL products were then electrophoresed on 2% agarose gel and purified using NucleoSpin® Gel and PCR Clean-up (Macherey Nagel, Germany). The purified DNA fragments were used as the template for the subsequent PCR amplification.

In the second PCR, PCR GXL1, the combination of PCR products from PCR GXL (reaction 1 and reaction 2; *Table 2*) was used as a template for PCR amplification using U-F and gR-R primers (*Table 1*), using the same cycling program. The PCR product was purified and used as the template for PCR GXL2. In PCR GXL2, the position-specific primers (*Table 2*) were used to create the overlapping ends that allow multiple gRNA expression cassettes to be ligated into a final vector. The sequence of the primers used is shown in *Table 1*. The PCR cycle was, 95°C for 30 s; 36 cycles of 95°C for 10 s, 58°C for 15 s and 68°C for 30 s; the final extension at 68°C for 2 min. Three μL of PCR product were gel electrophoresed and visualised under the UV gel imager to confirm the amplification of a correct fragment. The remaining PCR product was then purified using ethanol precipitation

TABLE 1. LIST OF PRIMERS

Primer name	Sequence (5'->3')	Purpose
EgPDSgRNA1FP	CCTCTAATACGACTCACTATAGG**CCATAAAGTTAGCCCTCTTC** GTTTAAGAGCTATGC	Forward primer contains a T7 promoter (underlined), additional guanine (red) and gRNA sequence (bold) used to PCR transcribed the gRNA template for *in vitro* assay
EgPDSgRNA2FP	CCTCTAATACGACTCACTATAGG**CATTCTTTCGTAATTGTGCA** GTTTAAGAGCTATGC	
EgPDSgRNA3FP	CCTCTAATACGACTCACTATAGG**CAATGAGATGCTGACATGGC** GTTTAAGAGCTATGC	
EgPDSgRNA4FP	CCTCTAATACGACTCACTATAGG**CAAGCTTATGTGGAGGCCC** GTTTAAGAGCTATGC	
EgPDSgRNA5FP	CCTCTAATACGACTCACTATAGG**CTTGAGATCCATTCCTCTGC** GTTTAAGAGCTATGC	
EgPDSgRNA6FP	CCTCTAATACGACTCACTATAGG**TTGGGGACCTCTGTAGAGGG** GTTTAAGAGCTATGC	
EgPDSgRNA7FP	CCTCTAATACGACTCACTATAGG**AGAAATACTTGGCTTCAATG** GTTTAAGAGCTATGC	
EgPDSF1	AAGTGGAACGGTGCAGAGA	Amplification of *EgPDS* gene for gRNA1/gRNA2
EgPDSR1	GAGGGAGCAAAACTAAGACAAAATC	
EgPDSF2	CGGTTCGTGATATTAAAGGTGCAGTGCC	Amplification of *EgPDS* gene for gRNA3/gRNA4
EgPDSR2	GGTAAGCTGAGAGCATCCATTAAC	
EgPDSF3	GGGATGGCGAAGTATCCTCTTAC	Amplification of *EgPDS* gene for gRNA5/gRNA6/gRNA7
EgPDSR3	GCATTTCGACAATCAGCCCATCCATC	
AdFP1	gccgCCATAAAGTTAGCCCTCTTC	Target adapter forward and RP for cloning of the guide sequence into the pYLsgRNAOsU6 cassette. The lowercase sequences are the overhangs complementary to the overhangs of the cloning vector digested by *Bsa*I Also used in colony PCR to screen for positive clones in vector construction of pYLEgPDS1-35S-H, pYLEgPDS2-35S-H and pYLEgPDS3-35S-H
AdRP1	GGTATTTCAATCGGGAGAAGcaaa	
AdFP2	gttgCATTCTTTCGTAATTGTGCA	
AdRP2	GTAAGAAAGCATTAACACGTcaaa	
AdFP3	gccgCAATGAGATGCTGACATGGC	
AdRP3	GTTACTCTAGACTGTACCGcaaa	
AdFP4	gttgCAAGCTTATGTGGAGGCCC	
AdRP4	GTTCGAATACACCTCCGGGcaaa	
AdFP5	gccgCTTGAGATCCATTCCTCTGC	
AdRP5	GAACTCTAGGTAAGGAGACGcaaa	
AdFP6	gttgTTGGGGACCTCTGTAGAGG	
AdRP6	AACCCCTGGAGACATCTGGGcaaa	
AdFP7	gccgAGAAATACTTGGCTTCAATG	
AdRP7	TCTTTATGAACCGAAGTTACcaaa	
U-F	CTCCGTTTTACCTGTGGAATCG	Universal position-specific primers used for the vector construction of CRISPR/Cas9 vectors
gR-R	CGGAGGAAAATTCCATCCAC	
U-GAL	ACCGGTAAGGCGCGCCGTAGTGCTCGACTAGTATGGAATCGGCAGCAAAGG	
Pgs-GA2	CAGGGAGCGGATAACAATTTCACACAGGCACATCCACTCCAAGCTCTTG	
U-GA2	GTGCCTGTGTGAAATTGTTATCCGCTCCCTGGAATCGGCAGCAAAGG	
Pgs-GA3	CCACGCATACGATTTAGGTGACACTATAGCGCATCCACTCCAAGCTCTTG	
U-GA3	CGCTATAGTGTCACCTAAATCGTATGCGTGGTGGAATCGGCAGCAAAGG	
Pgs-GA4	GTCGCTAGTTATTGCTCAGCGGCCAAGCTCATCCACTCCAAGCTCTTG	
U-GA4	GAGCTTGGCCGCTGAGCAATAACTAGCGACTGGAATCGGCAGCAAAGG	
Pgs-GAR	TAGCTCGAGAGGCGCGCCAATGATACCGACGCGTATCCATCCACT CCAAGCTCTTG	

TABLE 2. PRIMERS USED IN THE CONSTRUCTION OF *EgPDS* CRISPR/CAS9 VECTORS

Target	Target adapter	Template	PCR GXL		PCR GXL1	PCR GXL2		Construct
			Reaction 1	Reaction 2		Sites	Primer	
gRNA1	AdFP1+AdRP1	Osu6a-gRNA1	gR-R/AdFP1	U-F/AdRP1	U-F/gR-R	Site B-L Site 2	U-GAL+ Pgs-GA2	pYLEgPDS1-35S-H
gRNA2	AdFP2+AdRP2	Osu6b-gRNA2	gR-R/AdFP2	U-F/AdRP2	U-F/gR-R	Site 2 Site B-R	U-GA2+ Pgs-GAR	
gRNA3	AdFP3+AdRP3	Osu6a-gRNA3	gR-R/AdFP3	U-F/AdRP3	U-F/gR-R	Site B-L Site 2	U-GAL+ Pgs-GA2	pYLEgPDS2-35S-H
gRNA4	AdFP4+AdRP4	Osu6b-gRNA4	gR-R/AdFP4	U-F/AdRP4	U-F/gR-R	Site 2 Site B-R	U-GA2+ Pgs-GAR	
gRNA5	AdFP5+AdRP5	Osu6a-gRNA5	gR-R/AdFP5	U-F/AdRP5	U-F/gR-R	Site B-L Site 2	U-GAL+ Pgs-GA2	pYLEgPDS3-35S-H
gRNA6	AdFP6+AdRP6	Osu6b-gRNA6	gR-R/AdFP6	U-F/AdRP6	U-F/gR-R	Site 2 Site 3	U-GA2+ Pgs-GA3	
gRNA7	AdFP7+AdRP7	Osu6a-gRNA7	gR-R/AdFP7	U-F/AdRP7	U-F/gR-R	Site 3 Site B-R	U-GA3+ Pgs-GAR	

and the concentration was determined using a spectrophotometer. These purified PCR products containing gRNA cassettes were ligated into the linearised pYLCRISPR/Cas9P35S-H (Ma *et al.*, 2015) that was previously digested with *Bsa*I. The recombination reaction was carried out using ClonExpress MultiS One Step Cloning Kit (Vazyme Biotech Co., Ltd, China) following the manufacturer's protocol.

RESULTS AND DISCUSSION

Identification of gRNA Candidates for *EgPDS* Gene

Since the *PDS* gene was broadly used to verify the feasibility of the CRISPR/Cas9 system in many plant species (Ma *et al.*, 2015; Zhang *et al.*, 2016), including oil palm (Yeap *et al.*, 2021), we selected *EgPDS* gene to study the efficiency of CRISPR/Cas9 system in oil palm. The *EgPDS* gene sequence was obtained from the oil palm EG5 database. The *EgPDS* genomic sequence is located in chromosome 13 and consists of 14 exons and 13 introns (*Figure 1a*). Out of 167 listed gRNA candidates, 61 gRNAs with GC content more than 35% or less than 60% range, no poly-T and less than seven gRNA-pairing targets were selected for further analysis. Then, the gRNA candidates with the presence of guanine (G) at nucleotide 20, cytosine (C) at position 16 and purine residues (A/G) at the last four nucleotide sequences, and also the absence of C at nucleotide 3, were selected for off-target analysis (data not shown). The GC percentage of gRNAs was positively correlated with CRISPR/Cas9 on-target efficiency. The guanine-rich sequences can fold into stable noncanonical structures called G-quadruplexes *in vivo*, contributing to the DNA and RNA stability (Zhang *et al.*, 2015).

Sequence Verification of gRNA Candidates for *EgPDS* Gene

Analysis to detect the presence of preferable features in the 61 gRNA candidates was carried out based on previous studies (Wang *et al.*, 2014a; Wong *et al.*, 2015), and seven sgRNAs were chosen for further experiments. The selected gRNA1-gRNA7 are targeting exon 1, exon 2, exon 6, exon 12 and exon 13 of *EgPDS* (*Figure 1a*). The selected motifs of seven gRNAs were summarised in *Table 3*. Doench *et al.* (2014) reported that, within the gRNA sequence, cytosine was disfavoured at nucleotide 3, whilst guanine, cytosine and adenine were most favoured at nucleotide 20, 16 and in the middle of the gRNA, respectively. Therefore, all gRNA1-gRNA7 do not have cytosine at position 3 in the gRNA sequence. In addition, gRNA6 and gRNA7 are the gRNAs that contain guanine at position 20. gRNA7 also has cytosine at position 16, which was reported to be a favourable motif for gRNA sequence (Wu *et al.*, 2014). Furthermore, gRNA1, gRNA2, gRNA4 and gRNA5 have adenine in the middle of the gRNA sequence. In addition, purine residues in the last four nucleotides of the gRNA sequence were also preferable because it can promote the strong binding between gRNA and Cas9 (Bruegmann *et al.*, 2019; Wang *et al.*, 2014b). Thus, all gRNA selected contains purine residue except gRNA1. Repetitive TTTT, UUU and GGGG were also avoided in selecting gRNA candidates except for gRNA6 (having GGGG) because it may significantly lead to insufficient CRISPR/Cas9

activity (Wong *et al.*, 2015). In addition, the GGGG sequence is also prone to form a guanine tetrad that causes the gRNA sequence to be less accessible for target sequence recognition and binding. However, since 4.9% of functional gRNAs contain repetitive Gs (Wong *et al.*, 2015), gRNA6 was selected for further analysis. We also selected gRNAs targeting both strands, with gRNA5 and gRNA6 targeting the antisense strand. Both strands have been reported to have no significant influence on the CRISPR/Cas9 activity (Doench *et al.*, 2014).

Secondary Structure Analysis of gRNA Candidates

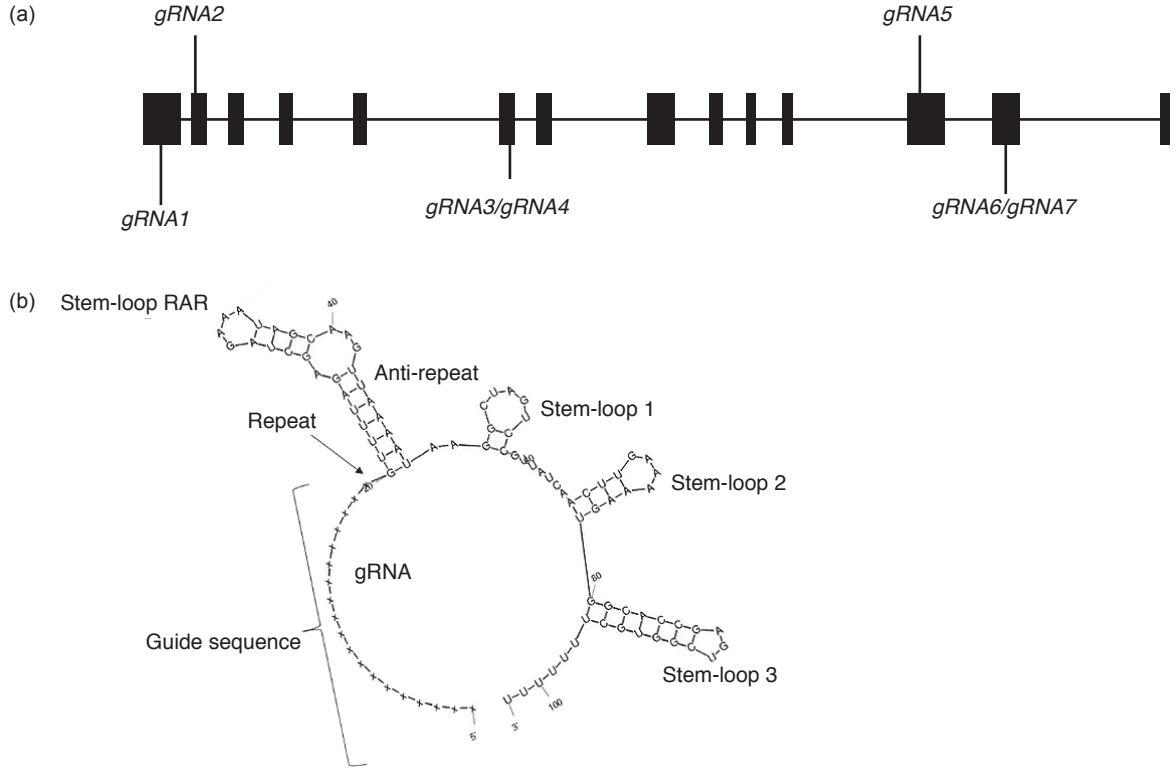
The secondary structure of gRNA has also been reported to interfere with the gene-editing mechanism (Wong *et al.*, 2015). Generally, a gRNA secondary structure consists of a CRISPR RNA (crRNA) sequence that comprises 20 nucleotides of gRNA and 12 nucleotides repeat region, and *trans*-activating RNA (tracrRNA) sequence derived from a combination of anti-repeat region and three stem-loop structures. These structures, so-called artificial tetraloop, are linked together to form a single RNA transcript structure (*Figure 1b*). The tetraloop is the repeat and anti-repeat region or also known as RAR stem-loop (GAAA), stem-loop 1 (CUAG), stem-loop 2 (GAAA) and stem-loop 3 (AGU). As shown in *Figures 1c-1i*, all seven gRNAs contain at least stem-loop 2 and stem-loop 3 structures, with gRNA2 and gRNA5 having all the required structures. The RAR stem-loop stimulates the precursor CRISPR RNA (pre-crRNA) processing by the RNase III enzyme and activates the crRNA-guided DNA cleavage by Cas9, whilst stem-loops 2 and 3 aid in the formation of a stable Cas9-gRNA-DNA complex (Liang *et al.*, 2016). Although stem-loop 1 has been shown as a beneficial structure for the functionality of the Cas9-gRNA-DNA complex, 82% of functional gRNA absent stem-loop 1, indicating that it may not be linked to editing efficiency (Liang *et al.*, 2016).

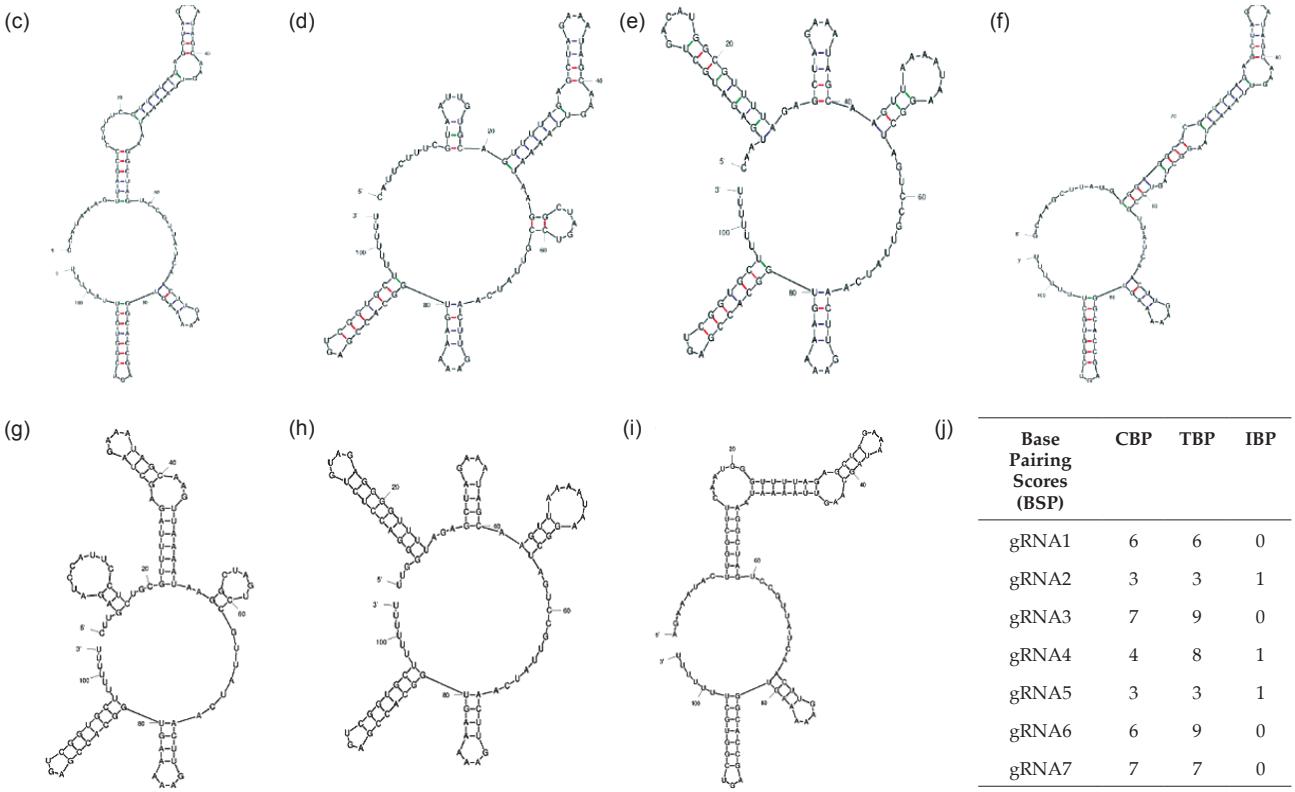
We also assessed the gRNA accessibility at the seed region (10-12 nucleotide proximal to PAM sequence) at positions 18-20 and 51-53 of the gRNA secondary structure (*Figure 1*; *Table 3*). The accessibility of nucleotides 18-20 and 51-53 is crucial in the target recognition process to allow the binding of Cas9-gRNA to the gRNA complementary site (Doench *et al.*, 2014). Therefore, the 18-20 and 51-53 nucleotides should be unpaired for the binding to occur. However, Bruegmann *et al.* (2019) reported successful mutation using gRNA with partially accessible nucleotides 18-20 and 51-53. As shown in *Figures 1c-1i*, only gRNA5 has accessible nucleotide 18-20, whilst the other gRNA candidates were only partially accessible. For positions 51-53, we found that gRNA1, gRNA4 and gRNA7 (*Figures 1c, 1f* and *1i*, respectively) are partly paired to the seed region and formed an extended stem-loop secondary structure. Furthermore, gRNA4 was shown to have 'C' as the last nucleotide of the seed region which has a solid propensity to pair with AAG at positions 51-53 of the gRNA, forming an extended stem-loop secondary structure (Wong *et al.*, 2015). This extended stem-loop structure will restrict the base accessibility at 51-53 and reduce the chance of proper binding of Cas9-gRNA to the target site. However, CRISPR/Cas9 editing in poplar showed that successful editing was still achieved with 'C' paired with AAG at positions 51-53 of the gRNA (Bruegmann *et al.*, 2019).

Next, we evaluated the gRNAs based on the base-pairing scores of the gRNA secondary structure. A stable complex between the gRNA sequence and the other nucleotide bases can affect the base pairing of the guide sequence with its target DNA (Liang *et al.*, 2016). The base pairing scores are the total base-pairing scores (TBP), consecutive base-pairing scores (CBP) and internal base-pairing scores (IBP). The TBP score is the total base pair in the guide sequence with other sequences of the gRNA, while the CBP score is the number of bases in the guide sequence with other sequences. Meanwhile, the IBP score is the internal base pair in the gRNA. Based on Liang *et al.* (2016), gRNA sequences with no more than 12 TBP scores, a maximum of seven CBP and six IBP, were preferred as efficient parameters for selecting gRNA. Therefore, in this study, gRNA candidates were selected with a maximum of nine TBP for gRNA3 and gRNA6, a maximum of seven CBP for gRNA7, and a maximum of one IBP for gRNA2, gRNA4 and gRNA5. The overall base-pairing scores are shown in *Figure 1j*.

Off-target Analysis of gRNA Candidates

Within the genome, the presence of off-target sites that share sequence similarities with the actual target sites may lead to the possibility of off-target editing. However, if the off-target sequences contain mismatches in the seed region of the gRNA, it will destroy the chance of target DNA binding and the Cas9 cleavage activity (Charpentier and Doudna, 2013). In this work, each gRNA candidate sequence was aligned and compared with all known sequences in the oil palm genome using NCBI BLAST (data not shown). As a result, the seed sequences of gRNA3, gRNA4, gRNA6 and gRNA7 were unique in the oil palm genome, thus, minimising off-target activity. Furthermore, the overall similarity percentage for each gRNA candidate with possible off-target sequences in the genome was not more than 43%, and even though single and double mismatches were found in gRNA1, gRNA2 and gRNA5 (data not shown), the capability to trigger the off-target activity could





(j)

Base Pairing Scores (BSP)	CBP	TBP	IBP
gRNA1	6	6	0
gRNA2	3	3	1
gRNA3	7	9	0
gRNA4	4	8	1
gRNA5	3	3	1
gRNA6	6	9	0
gRNA7	7	7	0

Figure 1. (a) Structural organisation of the EgPDS *gene. Exons and introns are shown as black boxes and lines, respectively. The location of each gRNA candidate in the exon is shown in the diagram. (b) Schematic representation of the general secondary structure of gRNA. (c)-(i) The predicted secondary structures of gRNA candidates (gRNA1-gRNA7) targeting* EgPDS *gene. (j) Base pairing scores (BSP) for gRNA1-gRNA7.*

be low since the off-target sequence is tolerated to certain degrees depending on their position along with the gRNA-DNA interface (Jiang *et al.*, 2013). A recent study has also reported that CRISPR/Cas9 off-target activity is not as boundless as speculated before, and random targeting of non-coding regions in the genome usually has no functional consequences (Wu *et al.*, 2014).

TABLE 3. SELECTED FEATURES OF SEVEN *EgPDS* gRNA CANDIDATES

EgPDS gRNA	GC content	Guanine at position 20	Cytosine at position 16	Adenine at position 9 to 11	No cytosine at position 3	Purine residues in the last 4 nucleotides	Target strand	RAR stem-loop (GAAA)	Stem-loop 1 (CUAG)	Stem-loop 2 (GAAA)	Stem-loop 3 (AGU)	Unpaired seed region	Unpaired 18-20 nt	Unpaired 51-53 nt
gRNA1 CCATAAAGTTAGCCCTCTTCAGG	45%	No (C)	No	Yes	Yes (A)	No	Sense	Present	Absent	Present	Present	Partly paired	Unpaired	Partly paired to seed region
gRNA2 CATTCTTTCGTAATTGTGCACGG	35%	No (A)	No	Yes	Yes (T)	2 (tgca)	Sense	Present	Present	Present	Present	Partly paired	No (Partly paired)	Partly paired (51-53)
gRNA3 CAATGAGATGCTGACATGGCCGG	50%	No (C)	No	No	Yes (A)	2 (tggc)	Sense	Absent	Absent	Present	Present	Partly paired	No (Fully paired)	Partly paired (51-53)
gRNA4 GCAAGCTTATGTGGAGGCCCAGG	60%	No (C)	No	Yes	Yes (A)	1 (gccc)	Sense	Present	Absent	Present	Present	Partly paired	No (Partly paired)	Partly paired to seed region
gRNA5 CTTGAGATCCATTCCTCTGCAGG	50%	No (C)	No	Yes	Yes (T)	1 (ctgc)	Antisense	Present	Present	Present	Present	Partly paired	Unpaired	Partly paired (51-53)
gRNA6 TTGGGGACCTCTGTAGAGGGCGG	60%	Yes (G)	No	No	Yes (G)	4 (aggg)	Antisense	Absent	Absent	Present	Present	Partly paired	No (Fully paired)	Partly paired (51-53)
gRNA7 AGAAATACTTGGCTTCAATGAGG	40%	Yes (G)	Yes	No	Yes (A)	3 (aatg)	Sense	Present	Absent	Present	Present	Partly paired	Unpaired	Partly paired to seed region

In vitro Cleavage Analysis of gRNA Candidates

In vitro cleavage assay is important to select the most efficient gRNA *in vitro* before deploying the gRNA into the plant (Bente *et al.*, 2020). In this study, approximately 694-1600 bp of PCR products were amplified to have the target sites (gRNAs) located asymmetrically within the target region to produce cleavage products with unequal sizes. This allows easy visualisation of subsequent cleavage of genomic *EgPDS* gene fragments. As shown in *Figures 2a, 2b* and *2c*, we tested seven gRNAs that were complementary to three target regions of 736 bp, 694 bp and 1600 bp fragments of *EgPDS* loci. The forward primer that composted the T7 promoter, target gRNA sequence and the scaffold template was used to amplify 130 bp of gRNA (*Figures 2d* and *2e*). These DNA fragments were transcribed to RNAs and combined with Cas9 to cleave the three target *EgPDS* regions. The determination of cleavage efficiency was performed by comparing the intensity of the uncut fragment with the control fragment. Based on *Figure 2f*, the cleavage efficiency of individual gRNAs was varied, with gRNA5 showing 100% cleavage efficiency. For multiplex gRNAs, a combination of three gRNAs (gRNA5, gRNA6, and gRNA7) has resulted in 100% cleavage efficiency. The results also showed that all gRNAs were able to cleavage target DNA sequences of the *EgPDS* gene into two to three fragments, with the expected sizes visible on the gel. A single (gRNA1 or gRNA2) and multiple (gRNA1 and gRNA2) *in vitro* cleavage assays were carried out for gRNA1 and gRNA2, producing DNA fragments with sizes of 551 bp, 395 bp, 341 bp and 185 bp (*Figure 2f*). For gRNA3 and gRNA4, *in vitro* cleavage analysis of 694 bp fragment produced four DNA fragments as 407 bp, 356 bp, 338 bp and 287 bp (*Figure 2f*). Meanwhile, multiple *in vitro* cleavage assays for gRNA5, gRNA6 and gRNA7 produced six bands with expected sizes of 1196 bp, 1419 bp, 850 bp, 750 bp, 431 bp and 181 bp (*Figure 2f*). Taken together, all the seven gRNAs were able to cleavage the corresponding target regions into the expected DNA fragments.

Construction of Multiplex gRNA-CRISPR/Cas9 Vectors Targeting *EgPDS* Gene

A schematic representation for the simplified construction procedure of CRISPR/Cas9 vectors carrying multiple gRNAs targeting the *EgPDS* gene is shown in *Figure 3*. In order to integrate the gRNA sequence into pYLsgRNA-OsU6a and pYLsgRNA-OsU6b, the target-gRNAs must contain guanine nucleotide as a definite transcription initiation site (Ma *et al.*, 2015). The selection of target-gRNAs in the genome is usually 5′-GN(19)NGG, so-called regular target gRNAs (Ma and Liu, 2016). However, the number of possible regular target gRNAs was found to be limited in the coding region of the *EgPDS* gene. As shown in *Figure 3*, six out of seven gRNAs were irregular targets with starting adenine (gRNA7), thymine (gRNA6) and cytosine (gRNA1, gRNA2, gRNA3, gRNA5). It was previously reported that the target-gRNAs with additional 'G' nucleotide at the 5' end (derived from the vector ligation site) could also lead to CRISPR/Cas9 editing in plants and produce similar editing efficiency (Ma *et al.*, 2015).

CRISPR/Cas9 multiplex genome editing system was proven to be highly effective in producing high frequencies of targeted mutation in many plant species, including those with very low transformation efficiency (Ma *et al.*, 2015). Previous CRISPR/Cas9 study in oil palm reported successful mutations of the oil palm PDS gene by using a single vector cassette for Cas9 or individual gRNA in oil palm immature embryos (Yeap *et al.*, 2021). However, in this study, we employed the multiplex CRISPR/Cas9 vector system consisting of gRNA expression cassettes, namely pYLsgRNA-OsU6a and pYLsgRNA-OsU6b and a binary vector pYLCRISPR/Cas9P35S-H. As shown in *Figures 4a* and *4b*, the assembly of gRNA expression cassettes in the pYLCRISPR/Cas9P35S-H vector was based on the position of gRNAs in the PDS sequence. The OsU6a and OsU6b promoters were originated from an indica rice cultivar 93-11 and a japonica rice cultivar *Nipponbare* (Ma *et al.*, 2015), monocotyledon plant species. Thus, the promoters were expected to work in oil palm. Furthermore, the activity of OsU6 promoters has been tested in rice and proven to be highly expressive and could also be possibly efficient for genome editing in oil palm (Bahariah *et al.*, 2021).

Gibson assembly method was used to assemble the gRNA expression cassettes into the pYLCRISPR/Cas9P35S-H vector. Sequentially, a series of PCR amplification (*Table 2*) denoted as PCR GXL, PCR GXL1 and PCR GXL2 were carried out to create overlapping ends that allow the cloning of multiple gRNA expression cassettes into the final vector, pYLCRISPR/Cas9P35S-H. The construction of the CRISPR/Cas9 vector was initiated with the ligation of double-stranded gRNA into the gRNA expression cassettes. The pYLsgRNA-OsU6a and pYLsgRNA-OsU6b were previously linearised using *Bsa*I and purified before being ligated with the double-stranded target-gRNAs. During the linearisation of the gRNA expression cassette, over-digestion with excess *Bsa*I and prolonged reaction time were avoided because it could produce abnormal constructs and reduce the cloning efficiency (Ma *et al.*, 2015). The ligated target-gRNA-cassettes were

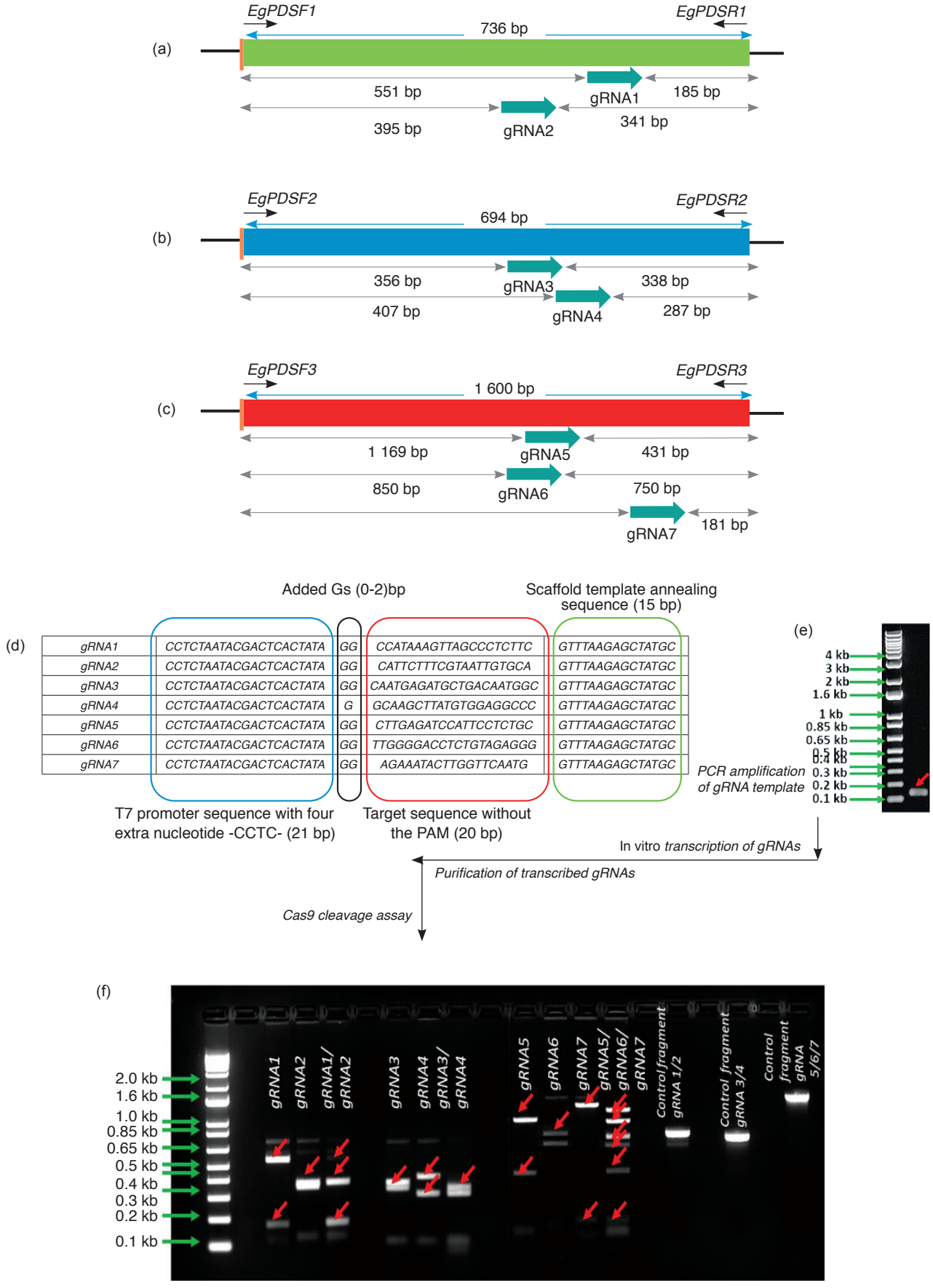


Figure 2. In vitro *cleavage assay reaction of seven gRNA candidates. (a)-(c) Schematic representation of three regions of* EgPDS *gene loci targeted by gRNA1-gRNA7. (d) The designed forward primers (56-58) nucleotide were used to transcribe the gRNA template carrying the target sequence and its scaffold. (e) The amplified gRNA template was observed on the gel as 130 bp amplification for each gRNA. (f)* In vitro *cleavage assay was carried out using the transcribed gRNAs coupled with Cas9 enzyme against the control template in single and multiple gRNA reactions.*

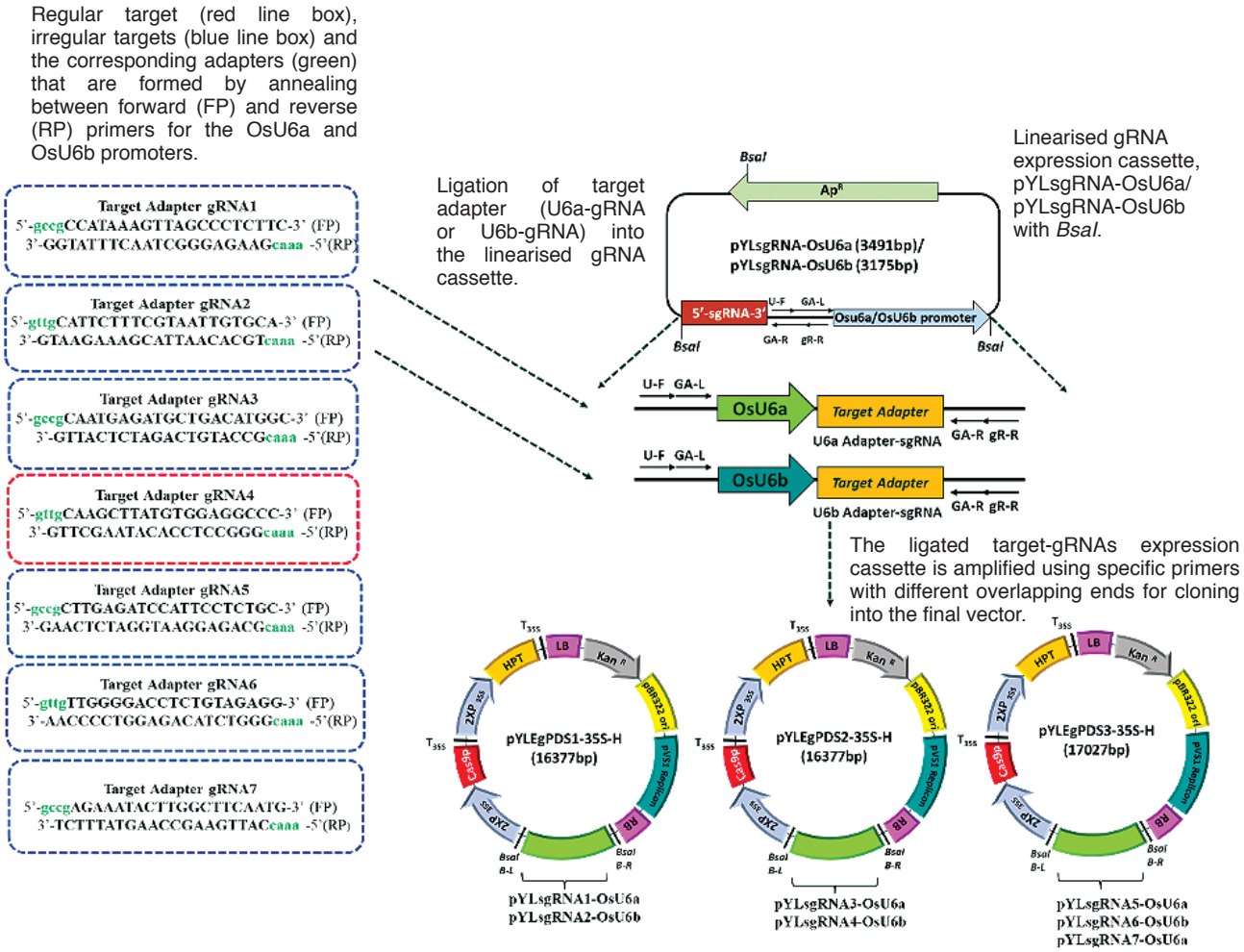


Figure 3. Schematic representation of a step-by-step procedure for constructing CRISPR/Cas9 vectors carrying multiple gRNAs (gRNA1-gRNA7) targeting the EgPDS *gene. The blue and red line boxes show the regular and irregular target adapters sequence for each gRNA candidate. These target adapters were ligated into the* BsaI *site of their corresponding gRNA expression cassettes; pYLsgRNA-OsU6a or pYLsgRNA-OsU6b. Then, the ligated target-gRNA expression cassette was amplified using nested PCR primers U-F/gR-R and position-specific primers (GA-L/GA-R) to create different overlapping ends for cloning into the final transformation vector pYLCRISPR/Cas9P35S-H via Gibson assembly reaction. The gRNA expression cassettes were arranged into the final vector as follows; pYLEgPDS1-35S-H carry two gRNA expression cassettes (gRNA1/gRNA2), pYLEgPDS2-35S-H have two gRNA expression cassettes (gRNA3/gRNA4), and pYLEgPDS3-35S-H carry three gRNA expression cassettes (gRNA5/gRNA6/gRNA7).*

PCR amplified using nested PCR primers U-F/gR-R and target adapter primers in PCR GXL. PCR GXL produced approximately 500 bp OsU6a-gRNA (OsU6a-gRNA1, OsU6a-gRNA3, OsU6a-gRNA5 and OsU6a-gRNA7) and 400 bp OsU6b-gRNA (OsU6b-gRNA2, OsU6b-gRNA4 and OsU6a-gRNA6) for reaction 1 and 150 bp gRNA-scaffold for reaction 2 (*Figure 4c*). The amplified PCR products from PCR GXL were used in the second amplification (PCR GXL1) to yield the 650 bp fragment for OsU6a-gRNA-scaffold and 550 bp fragment for OsU6b-gRNA-scaffold (*Figure 4d*). The PCR products were then used as templates in PCR GXL2. In PCR GXL2, position-specific primers (*Tables 1* and *2*) were used to amplify the overlapping ends of PCR products (*Figure 4e*) for assembling multiple gRNA expression cassettes in the respective positions of the vector backbone pYLCRISPR/Cas9P35S-H. PCR fragment of each target-gRNA cassette was purified and ligated into the linearised pYLCRISPR/Cas9P35S-H/*BsaI* (*Figure 4f*), and successfully cloned DNA plasmids were confirmed by restriction analysis with *AscI* (*Figure 4g*). A fragment of 1150 bp was observed for plasmids carrying two gRNA cassettes designated as pYLEgPDS1-35S-H and pYLEgPDS2-35S-H. Meanwhile, *Asc*I digested plasmid produced approximately 1800 bp fragment was designated as pYLEgPDS3-35S-H, which carries three gRNA expression cassettes.

Three CRISPR/Cas9 transformation vectors, pYLEgPDS1-35S-H, pYLEgPDS2-35S-H and pYLEgPDS3-35S-H, were successfully constructed for transformation into oil palm. For pYLEgPDS1-

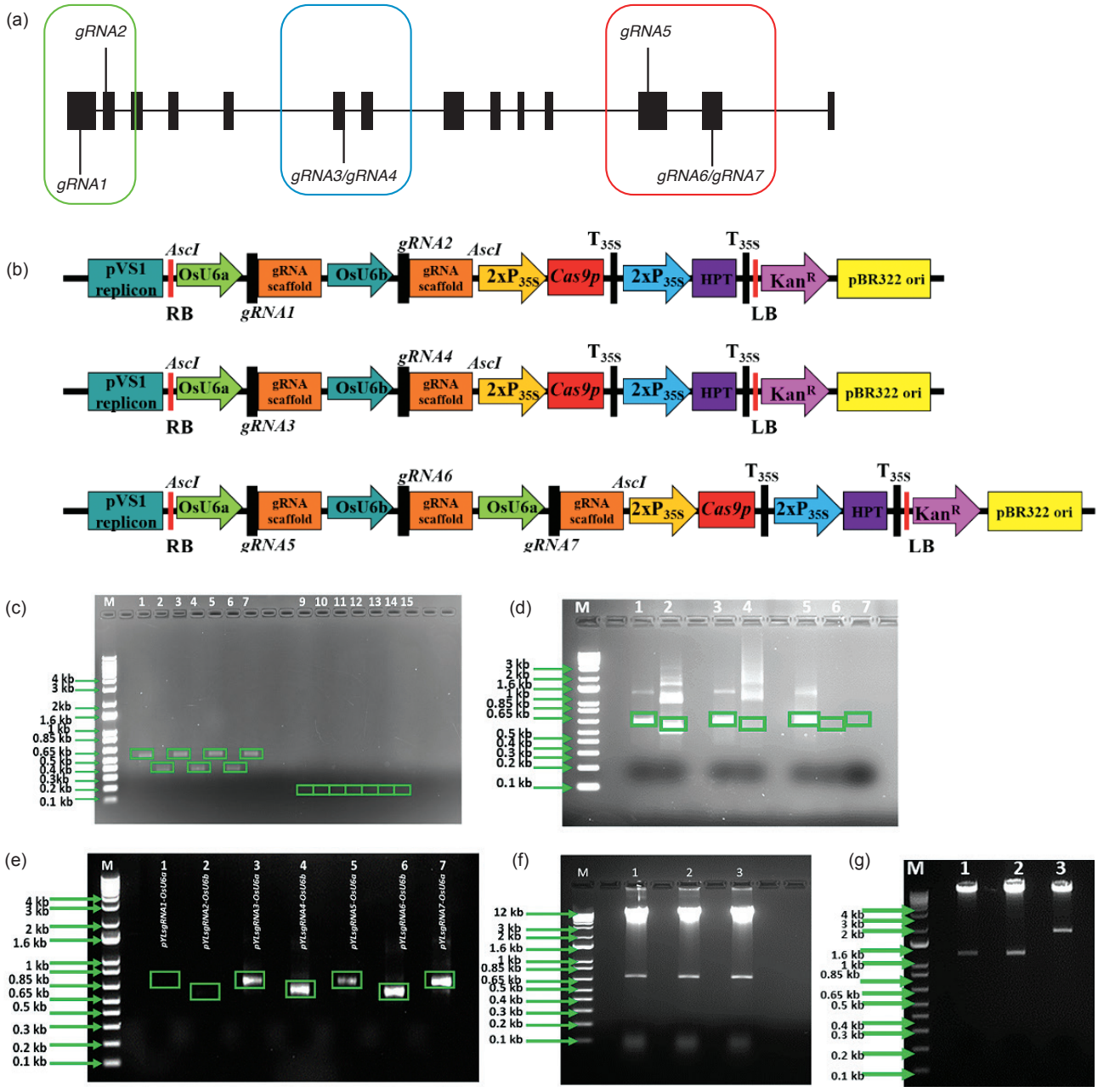


Figure 4. Construction of CRISPR/Cas9 vectors using multiplex genome editing system. (a) Structural organisation of the EgPDS *gene, exons and introns are shown as black boxes and lines, respectively. The green line box indicates the target gRNAs in pYLEgPDS1-35S-H vector, the blue line box indicates the target gRNAs in pYLEgPDS2-35S-H and the red line box indicates the target gRNAs in pYLEgPDS3-35S-H. (b) Schematic arrangement of OsU6 promoters driving-sgRNA cassettes, pYLsgRNAOsU6a and pYLsgRNAOsU6b for each gRNA candidate (gRNA1-gRNA7) in the final vector (pVS1 replicon: pVS1 for replication, RB: Right border of T-DNA, 2XP35S: Double cauliflower mosaic virus 35S promoter, Cas9p: CRISPR associated protein 9, HPT: hygromycin phosphotransferase, Kan^R: Kanamycin resistance gene, pBR322: pB322 vector, T_{35S}: Cauliflower mosaic virus 35S terminator, LB: Left border). (c) PCR GXL of gRNA expression cassettes; pYLsgRNA-OsU6a and pYLsgRNA-OsU6b amplified using primers gR-R/gRNA target adapter forward primer for reaction 1, U-F/gRNA target adapter RP in reaction 2. (d) PCR GXL1 of gRNA expression cassettes; pYLsgRNA-OsU6a and pYLsgRNA-OsU6b on amplified using primers U-F/gR-R. (e) PCR GXL2 of gRNA expression cassettes on amplified using position-specific primers (f) Restriction analysis of pYLCRISPR/Cas9P35S-H with* BsaI. *(g) Verification of the final CRISPR/Cas9 vectors using restriction analysis with* AscI.

35S-H, two gRNAs cassettes carrying gRNA1 (pYLsgRNA-OsU6a) and gRNA2 (pYLsgRNA-OsU6b) were arranged alternately in the pYLCRISPR/Cas9P35S-H. These two gRNAs were located in the first part of the *EgPDS* gene targeting exon 1 and exon 2. The second vector, pYLEgPDS2-35S-H, carries gRNA3 and gRNA4, both targeting exon 6 and the third vector, pYLEgPDS3-35S-H, carries gRNA5, gRNA6 and gRNA7, targeting the terminal region of the *EgPDS* gene on exon 12 and 13. These CRISPR/Cas9 vectors were designed to possibly increase the editing efficiency of the oil palm genome targeting the *EgPDS* gene. The use of multiple gRNAs targeting a single gene has been proven to increase the mutation frequency in tomato (Brooks *et al.*, 2014).

CONCLUSION

Seven gRNAs located at exon 1, exon 2, exon 6, exon 12 and exon 13 of chromosome 13 targeting the *EgPDS* gene in the oil palm genome were successfully designed and validated. These gRNAs have several preferable features, including the GC content of 35%-60%, preferable gRNA sequence motifs, secondary structure with at least stem-loop 2 and stem-loop 3, and minimum off-target effects. Furthermore, *in vitro* cleavage assay confirmed the cleavage ability of these gRNAs on the corresponding target regions of the *EgPDS* genomic sequence. Inserting gRNAs into pYLsgRNA-OsU6 cassettes and then assembling the gRNA cassettes into pYLCRISPR/Cas9P35S-H have successfully produced three CRISPR/Cas9 expression vectors. Thus, the CRISPR/Cas9 vectors carrying seven gRNAs targeting the oil palm *EgPDS* gene are now available for CRISPR/Cas9 studies in oil palm.

ACKNOWLEDGEMENT

The authors would like to thank the MPOB management for permission to publish this article. The authors would also like to acknowledge all the Transgenic Technology Group (TTG) members of MPOB for their assistance. Special thanks to Prof. Yao Guang Liu (South China Agricultural University, China) for providing us with the CRISPR/Cas9 vectors, pYLsgRNAOsU6 and pYLCRISPR/Cas935S-H.

REFERENCES

Bahariah, B; Masani, M Y A; Rasid, O A and Parveez, G K A (2021). Multiplex CRISPR/Cas9-mediated genome editing of the FAD2 gene in rice: A model genome editing system for oil palm. *J. Genet. Eng. Biotechnol., 19*: 86.

Bente, H; Mittelsten Scheid, O and Donà, M (2020). Versatile *in vitro* assay to recognize Cas9-induced mutations. *Plant Direct, 4(9)*: e00269.

Brooks, C; Nekrasov, V; Lippman, Z B and Van Eck, J (2014). Efficient gene editing in tomato in the first generation using the clustered regularly interspaced short palindromic repeats/CRISPR-associated 9 system. *Plant Physiol., 166(3)*: 1292-1297.

Bruegmann, T; Deecke, K and Fladung, M (2019). Evaluating the efficiency of gRNAs in CRISPR/Cas9 mediated genome editing in poplars. *Int. J. Mol. Sci., 20(15)*: 3623.

Charpentier, E and Doudna, J A (2013). Rewriting a genome. *Nature, 495(7439)*: 50-51.

Doench, J G; Hartenian, E; Graham, D B; Tothova, Z; Hegde, M; Smith, I; Sullender, M; Ebert, B L; Xavier, R J and Root, D E (2014). Rational design of highly active sgRNAs for CRISPR-Cas9–mediated gene inactivation. *Nat. Biotechnol., 32(12)*: 1262-1267.

Jiang, W; Zhou, H; Bi, H; Fromm, M; Yang, B and Weeks, D P (2013). Demonstration of CRISPR/Cas9/sgRNA-mediated targeted gene modification in Arabidopsis, tobacco, sorghum and rice. *Nucleic Acids Res., 41(20)*: e188-e188.

Liang, G; Zhang, H; Lou, D and Yu, D (2016). Selection of highly efficient sgRNAs for CRISPR/Cas9-based plant genome editing. *Sci. Rep., 6(1)*: 1-8.

Ma, X and Liu, Y G (2016). CRISPR/Cas9-based multiplex genome editing in monocot and dicot plants. *Curr. Protoc. Mol. Biol., 115(1)*: 31-36

Ma, X; Zhang, Q; Zhu, Q; Liu, W; Chen, Y; Qiu, R; Wang, B; Yang, Z; Li, H; Xie, Y; Shen, R; Wang, Z; Chen, Y; Guo, J; Chen, L; Zhao, X and Liu, Y G (2015). A robust CRISPR/Cas9 system for convenient, high-efficiency multiplex genome editing in monocot and dicot plants. *Mol. Plant, 8(8)*: 1274-1284.

Masani, M Y A; Izawati, A M D; Rasid, O A and Parveez, G K A (2018). Biotechnology of oil palm: Current status of oil palm genetic transformation. *Biocatal. Agric. Biotechnol., 15*: 335-347.

Parveez, G K A; Tarmizi, A H A; Sundram, S; Loh, S K; Ong-Abdullah, M; Palam, K D P; Salleh, K M; Ishak, S M and Idris, Z (2021). Oil palm economic performance in Malaysia and R&D progress in 2020. *J. Oil Palm Res., 33(2)*: 181-214.

Rahman N A; Parveez, G K A; Rasid, O A and Masani, M Y A (2020). Optimisation of the bombardment parameters for transformation and regeneration of stable oil palm transformants. *J. Oil Palm Res., 32(4)*: 696-704.

Singh, R; Ong-Abdullah, M; Low, E T L; Manaf, M A A; Rosli, R; Nookiah, R; Ooi, L C L; Ooi, S E; Chan, K L; Halim, M A; Azizi, N; Nagappan, J; Bacher, B; Lakey, N; Smith, S W; He, D; Hogan, M; Budiman, M A; Lee, E K; DeSalle, R; Kudrna, D; Goicoechea, J L; Wing, R A; Wilson, R K; Fulton, R S; Ordway, J M; Martienssen, R A and Sambanthamurthi, R (2013). Oil palm genome sequence reveals divergence of interfertile species in old and new worlds. *Nature, 500(7462)*: 335-339.

Wang, T; Wei, J J; Sabatini, D M and Lander, E S (2014a). Genetic screens in human cells using the CRISPR-Cas9 system. *Science, 343(6166)*: 80-84.

Wang, Y; Cheng, X; Shan, Q; Zhang, Y; Liu, J; Gao, C and Qiu, J L (2014b). Simultaneous editing of three homoeoalleles in hexaploid bread wheat confers heritable resistance to powdery mildew. *Nat. Biotechnol., 32(9)*: 947-951.

Wang, J; Zhang, X; Cheng, L and Luo, Y (2020). An overview and metanalysis of machine and deep learning-based CRISPR gRNA design tools. *RNA Biol., 17(1)*: 13-22.

Wong, N; Liu, W and Wang, X (2015). WU-CRISPR: Characteristics of functional guide RNAs for the CRISPR/Cas9 system. *Genome Biol., 16(1)*: 1-8.

Wu, X; Kriz, A J and Sharp, P A (2014). Target specificity of the CRISPR-Cas9 system. *Quant. Biol., 2(2)*: 59-70.

Yeap, W C; Norkhairunnisa, K C M; Norfadzilah, J; Muad, M R; Appleton, D R and Harikrishna, K (2021). An efficient clustered regularly interspaced short palindromic repeat (CRISPR)/CRISPR-associated protein 9 mutagenesis system for oil palm (*Elaeis guineensis*). *Front. Plant Sci., 12*: 773656-773656.

Zhang, X H; Tee, L Y; Wang, X G; Huang, Q S and Yang, S H (2015). Off-target effects in CRISPR/Cas9-mediated genome engineering. *Mol. Ther. Nucleic Acids*, 4, e264.

Zhang, Y; Liang, Z; Zong, Y; Wang, Y; Liu, J; Chen, K; Qiu, J L and Gao, C (2016). Efficient and transgene-free genome editing in wheat through transient expression of CRISPR/Cas9 DNA or RNA. *Nat. Commun., 7(1)*: 1-8.

Journal of Oil Palm Research Vol. 35 (1) March 2023 p. 147-156
DOI: https://doi.org/10.21894/jopr.2022.0033

IMPROVING THE GROWTH PERFORMANCE OF OIL PALM SEEDLINGS BY MIXTURES OF ORGANIC AND CHEMICAL FERTILISERS

MOHD FAHMI KENI[1]*; NURHAFIZHOH ZAINUDDIN[1] and MOHAMED MAZMIRA MOHD MASRI[1]

ABSTRACT

The application of biofertilisers can be the best alternative to reduce the dependency on chemicals in oil palm nurseries. The impact of oil palm-based compost with a microbial-based organic fertiliser in reducing chemical use on young oil palm seedlings was investigated at the nursery stage. A total of six treatments and five controls were used in a completely randomised design (CRD). The objective of this study was to evaluate the growth of young seedlings using mixtures of chemicals with microbial-based organic fertiliser. Treatment T6 (a consortium of microbes 2 + 30% chemical) recorded the highest mean of meristem diameter (5.38 cm), and palm height (149.28 cm), and was significantly different compared to control on 10 months old seedlings. The combination of consortium microbe with 30% chemical fertiliser was optimal for the oil palm seedling growth as seen in the vegetative measurement and its nutrient contents higher compared to control. The application of biofertiliser assisted in the increase of essential nutrient content; nitrogen (N), phosphorus (P), potassium (K) and carbon (C). Our studies showed that biofertilisers performed better when chemical nutrients were added to the microbial consortium, providing a significant increase in growth performance and nutrient content.

Keywords: biofertiliser, growth performance, microorganism, nutrients content, oil palm.

Received: 20 April 2021; **Accepted:** 25 April 2022; **Published online:** 14 June 2022.

INTRODUCTION

The palm oil industry should increase oil palm yields in order to fulfil the global market demand (Iskandar *et al.*, 2018). Oil palm requires an optimum and balanced supply of nutrients to support an optimised growth and yield production (Chen, 2006; Miransari, 2013). Fertilisers are an essential component of modern agriculture because they provide plant nutrients (Adesemoye *et al.*, 2009). Chemical fertilisers have been routinely applied in oil palm plantations to maintain soil fertility and also as nutrient supply to the plants (Chen, 2006; Miransari, 2013). Nutrient requirements for oil palm can vary according to the target yield, type of planting material used, palm spacing, palm age, soil type, groundcover conditions, climate and other environmental factors (Anuar *et al.*, 2015). However, the excessive usage of chemical fertilisers has caused decline in productivity and can contribute to adverse environmental impacts such as soil acidification, greenhouse gas emission and depletion of soil micro-organisms (Anuar *et al.*, 2015; Savci, 2012; Zhao *et al.*, 2016). Besides that, excessive usage of fertilisers can cause negative effects on soil quality and soil microbial community structure with reduced soil organic matter (OM) and soil fertility, thus, increasing soil acidification which in turn reduces the crop yield (Li *et al.*, 2017; Qiao *et al.*, 2018; Wang *et al.*, 2020).

Excessive usage of synthetic fertilisers has also created a damaging impact on the global environment such as water pollution (Tang *et al.*, 2003), imbalance atmospheric gasses (Kim and Dale, 2008), groundwater pollution and soil acidification. All the factors actively contribute to reduced soil fertility for agricultural activity (Barak

[1] Malaysian Palm Oil Board,
6 Persiaran Institusi, Bandar Baru Bangi,
43000 Kajang, Selangor, Malaysia.

* *Corresponding author e-mail: fahmikeni@mpob.gov.my*

et al., 1997; Li *et al.*, 2017; Qiao *et al.*, 2018; Zhao *et al.*, 2016). The chemical fertiliser usage will also cause air and ground water pollution, resulting from eutrophication and this practice affects the roots of the crops which causes the crop to be less efficient in acquiring nutrients (Voon Kheong *et al.*, 2012; Wang *et al.*, 2009). The usage of biofertiliser in the agricultural industry is deemed as a potential solution to mitigate the harmful effects caused by chemical fertilisers (Khan *et al.*, 2012; Mohamed and Babiker, 2012). Hence, the development of organic and other microbial products in biofertilisers can therefore gradually reduce the dependence on the chemical fertiliser in oil palm plantations (Bhardwaj *et al.*, 2014; Munda *et al.*, 2015; Taryo-Adiwiganda *et al.*, 2006). Biofertiliser that is comprised of microbial inoculants or assemblages of beneficial microorganisms would benefit crop yield, and also the plant growth (Itelima *et al.*, 2018; Zainuddin *et al.*, 2019).

Biofertiliser is usually prepared by using microbial inoculant that consists of live microorganisms and commonly used for the application of seed, soil or composting areas to increase the numbers of beneficial microorganisms. This would also accelerate the microbial processes to augment the extent of the nutrient's availability in a form which can be assimilated by the plant (Khosro and Yousef, 2012; Rokhzadi *et al.*, 2008). The usage of biofertiliser accelerates the decomposition of organic residues and agricultural by-products through various processes which contribute to the healthy growth of crops (Abdul Halim, 2009). Ajeng *et al.* (2020) stated that some of the microbes contained in the biofertiliser produced by local Malaysian manufacturers include *Bacillus cereus* JCM 2152, *Bacillus amyloliquefaciens* strain MPA 1034 and *Bacillus tequilensis* strain 10b; *Lactobacillus* spp.; *Azospirillum* spp. and *Rhizobium* spp. Meanwhile, some biofertiliser products consist of a very diverse group of microbes: Actinomycetes such as *Kocuria rhizophila*, *Arthrobacter methylotrophus*, *Bacillus* spp. such as *B. pumilus*, *B. subtilis* (subspecies spizizenii), *B. vallismortis, B. thuringiensis, B. mycoides, B. mucilaginosus, Brevibacillus reuszeri, Paenibacillus polymax*, *Paenibacillus azoreducens* and *Azospirillum brasilense.* Additionally, fungi such as *Aspergillus niger* and *Aspergillus awamori*, and yeast such as *Saccharomyces cerevisiae* are also used as inoculants.

Biofertilisers are the most important component of integrated nutrient management and play an important role in the sustainability of soil and yield of chickpea (*Cicer arietinum* L.). It is eco-friendly and cost-effective for farmers (Rokhzadi *et al.*, 2008). The roles of beneficial soil microorganisms in the sustainable development of agriculture could accelerate and improve plant growth as well as protect plants from pests and diseases (Lee and Pankhurst, 1992; Wani *et al.*, 1995). Khosro and Yousef (2012) reported that organisms that are commonly used as components of biofertilisers are mainly nitrogen fixers (N-fixer), potassium solubilisers (K-solubiliser) and phosphorus solubiliser (P-solubiliser), or with the combination of fungi. Most of the bacteria included in the biofertiliser formulation have close relationships with plant roots. Rhizobium has symbiotic interaction with legume roots, and Rhizobacteria commonly inhabits the root surface or in rhizosphere soil. The phospho-microorganisms, mainly bacteria and fungi make insoluble phosphorus available to the plants. Several soil bacteria and several species of fungi possess the ability to convert insoluble phosphates in soil into soluble forms by secreting organic acids. However, the use of biofertiliser for commercial agricultural production, especially in oil palm, is still not widely practised by most of the plantations. Therefore, the objective of this study was to evaluate the growth of young seedlings in combination with a microbial-based organic fertiliser in the pursuit of reducing chemical usage in oil palm production.

MATERIALS AND METHODS

Oil Palm Seedling

The trial was carried out in a nursery at the Malaysian Palm Oil Board (MPOB), Kluang, Johor, Malaysia. Uniform oil palm seedlings of three months old were selected and transplanted in 15 x 18 inch polybags. Commercial *Dura* x *Pisifera* (DxP) oil palm seedlings were provided by MPOB and used in these trials.

Treatments

A total of 11 different treatments, including one control treatment (blank) were tested, as shown in *Table 1*. Six treatments with two different consortia of microbes with three levels of chemical fertilisers were carried out, as shown in *Table 2*. A completely randomised design (CRD) was used in this experiment with eight replicates for each treatment.

Preparation of Inoculum and Biofertiliser Formulation

Twelve different species of microorganisms from several classes of bacteria and fungi were utilised in the production of the biofertiliser. The microbes were chosen based on their capability to promote plant growth. The consortium of microbes consisted of five microbes from prokaryotes of the group Proteobacteria; two bacteria were from the genus *Bacillus* while the other three bacteria were from the genera of *Providencia, Phyllobacterium* and

TABLE 1. TREATMENTS OF THE EXPERIMENT

Treatment code	Treatment	Rate
T1	Treatment 1	Consortium 1 + 0% chemical
T2	Treatment 2	Consortium 1 + 15% chemical
T3	Treatment 3	Consortium 1 + 30% chemical
T4	Treatment 4	Consortium 2 + 0% chemical
T5	Treatment 5	Consortium 2 + 15% chemical
T6	Treatment 6	Consortium 2 + 30% chemical
C1	Organic fertiliser	Nursery rate
C2	Control - Blank	Nil
C3	Chemical fertiliser	Nursery rate
C4	Organic Compost A	Nursery rate
C5	Organic Compost B	Nursery rate

Note: 100% chemical fertiliser rate is 280 g/seedling in nursery stage (40.00 g/seedling/application); 100% organic fertiliser rate is 200 g/seedling in nursery stage (28.57 g/seedling/application).

TABLE 2. DIFFERENT CONSORTIUM OF MICROBES

Consortium	Microbes
Consortium 1	*Tricho* 5 N, P, K Microbe
Consortium 2	*Trichoderma harzianum* N, P, K Microbe

Sphingobacterium. Fungi consisted of three species of *Trichoderma* and one species each of *Antrodia, Pichia, Pycnoporus* and *Phanerochaete*. The microbes are capable to promote the growth of oil palm and are protected under the Malaysian Patent No: PI 2017703375.

In order to prepare the microbial consortium formulation for fungi, a malt extract broth was prepared by dissolving 19.0 g of malt extract broth powder in 400 mL of distilled water. For bacteria, 400 mL nutrient broth was prepared by dissolving 3.2 g of nutrient broth powder in 400 mL distilled water. The fermentation media were sterilised by autoclaving at 121°C for 20 min and allowed to cool down before inoculating with the individual microbes. After inoculation, the broths containing inoculum were incubated in an INNOVA44 incubator shaker at a speed of 170 rpm at 30°C for three days, to produce the fermented products. The different individual fermented microbes were pooled together based on synergistic behaviour. This microbial preparation protocol followed the optimisation method previously reported by Zainuddin *et al*. (2019).

Application of Fertiliser

The fertiliser application followed the protocol from Rankine and Fairhurst (1999) with some modifications. The commercial chemical fertiliser with a ratio of 12:12:17:2 (N: P: K: Mg), and commercial organic fertiliser, organic compost A and organic compost B were used in this study. Three-month-old oil palm seedling were treated with 11 treatments during seven months intervals. The application of fertilisers was conducted every month and their performances were monitored within seven months. The application rates for the fertilisation are as shown in *Table 1*.

Harvesting, Data Recording and Destructive Sampling

Vegetative measurements of the seedlings were recorded monthly from three to seven months after treatment (MAT). Different growth parameters such as the height, meristem diameter and dry weight of the palm were recorded during each harvest. The dried leaflets were analysed for foliar nutrients analysis. Parameters for data recording followed that of Zainuddin *et al*. (2019) with some modifications.

Leaf Analysis

Total nitrogen (TN) and total carbon (TC) analyses were carried out using PRIMACS^{SNC} (Skalar, Netherlands). Analyses of phosphorus, potassium, micronutrients and trace elements were carried out using ElanDRCe ICP-MS (Perkin Elmer, USA). For ICP-MS analysis, leaf samples were acid digested using Microwave Oven (Memmert, Germany) according to the US EPA test method 3050B (US EPA, 1996). The digested samples were filtered using filter paper and diluted with MilliQ water before analysis. Primac^{SNC} was used for the analysis of carbon and nitrogen content in oil palm leaflets. Initially, 50 mg of dried leaf samples were weighed into each crucible. The samples were then subjected to TC and TN analyses with Primac^{SNC}.

Statistical Analysis

The analyses were carried out using IBM SPSS 22.0 software. Analysis of variance (ANOVA), at $p<0.05$ was used to determine the significant difference between the treatments. The mean for each treatment for the respective analysis was separated statistically using Tukey Pairwise comparison to test the differences among mean values of every treatment.

RESULTS AND DISCUSSION

The combination of beneficial microbes with chemical fertilisers has received a considerable amount of attention in the last decades as the microbes are effective in promoting plant growth. The beneficial microbes contained in the biofertiliser had improved the plant quality, helped in nutrients intake by the plants, and enhanced the populations of bacteria (Zainuddin *et al.*, 2019). In this study, the effects of fertiliser treatments on meristem diameter, dry upper mass and palm height of oil palm seedlings are presented in *Tables 3-5*. Analysis for nitrogen, phosphorous, potassium and carbon content are presented in *Tables 6-9*.

An increase of meristem diameter in oil palm seedlings for all the treatments were observed when the seedlings reached six to 10 months old (*Table 3*). Nevertheless, the rate of increment of the meristem diameter seemed to be different between each treatment. Slight increments were observed in treatment T5 and T6 as compared to control when the seedlings reached eight to 10 months old. There was no significant difference ($p>0.05$) between all treatments and controls for oil palm seedlings aged six months. However, treatment T6 (consortium 2 + 30% chemical) showed a significant difference ($p<0.05$) as compared to C3 (chemical fertiliser) at the ages of nine and 10 months. The result recorded for treatment T6 was comparable to C3 at seven and eight months old seedlings. Compared to organic fertiliser (Organic Fertiliser and Organic Compost B), treatment T6 recorded a significant difference to control at eight months until 10 months old seedlings. Biofertilisers application has been reported to increase the trunk diameter of other trees such as grapes as compared to a non-treated tree (El-Sabagh *et al.*, 2011). In this study, treatment T6 recorded the highest mean for meristem diameter with 5.38 cm on 10 months old seedlings. The meristem diameter showed a significant difference between treatments and control after longer exposure to biofertiliser treatments. Zainuddin *et al.* (2019) reported that the oil palm seedlings treated with biofertiliser + 50% chemical fertiliser were taller than those treated with 100% chemical and standard organic at the age of eight months. The increase in meristem diameter is likely due to the microbes in the biofertiliser which are attached to the roots and hence colonised the root surfaces efficiently for the development and health of the plants (Hayat *et al.*, 2010; Vacheron *et al.*, 2013).

The dried upper mass for oil palm seedling had increased every month for all treatments and controls (*Table 4*). Treatment T1 and T4 (Consortium 1 and 2 + 0% chemical) recorded a two fold increase in the dry upper mass of oil palm seedlings between eight to 10 months. Means of the dry upper mass of oil palm seedlings recorded a significant difference (ANOVA, $p<0.05$) between the treatments. The results showed that there was no significant difference between all treatments and controls at the age of six months. However, treatment T6 (consortium 2 + 30% chemical) was significantly different ($p<0.05$) from chemical fertiliser (C3) at 10 months old. Mohamed and Babiker (2012) reported all inoculation treatments on faba beans in a semi-desert zone showed significant ($p\leq0.05$) increments

TABLE 3. MERISTEM DIAMETER FOR SIX, SEVEN, EIGHT, NINE AND 10 MONTHS OLD OIL PALM SEEDLINGS TREATED WITH DIFFERENT TREATMENT

Treatments	Meristem diameter (cm)				
	6 months	7 months	8 months	9 months	10 months
Consortium 1 + 0% chemical (T1)	1.22 a	1.70 ab	2.44 abc	3.00 bc	3.48 abc
Consortium 1 + 15% chemical (T2)	1.21 a	1.77 ab	2.94 bcd	3.16 c	4.90 de
Consortium 1 + 30% chemical (T3)	1.20 a	1.88 ab	3.08 cd	3.33 cd	4.15 bcd
Consortium 2 + 0% chemical (T4)	1.35 a	1.75 ab	2.60 bcd	3.35 cd	3.47 abc
Consortium 2 + 15% chemical (T5)	1.27 a	1.96 b	3.28 d	3.98 de	5.08 de
Consortium 2 + 30% chemical (T6)	1.27 a	1.92 ab	3.02 cd	4.34 e	5.38 e
Organic Fertiliser (C1)	1.30 a	2.01 b	2.27 ab	2.71 abc	3.13 ab
Blank (C2)	1.19 a	1.41 a	1.76 a	2.20 a	2.77 a
Chemical (C3)	1.31 a	1.54 ab	2.55 bc	3.08 c	4.27 cd
Organic Compost A (C4)	1.02 a	1.58 ab	2.61 bcd	3.18 c	3.36 abc
Organic Compost B (C5)	1.13 a	1.52 ab	2.27 ab	2.40 ab	3.17 ab

Note: Values in each column with different letter(s) are significantly different at $p=0.05$.

in shoot dry weights between eight and 10 weeks after sowing, compared to control. Treatment T6 also showed a significant difference compared to organic fertilisers (Organic Fertiliser and Organic Compost B), between nine and 10 months. Treatment T6 recorded the highest means of dry upper mass with 31 g at the age of nine months (*Table 4*).

The increased height of the oil palm seedlings was recorded between six to 10 months (*Table 5*). The increase in dried upper mass for the oil palm seedlings was recorded every month for all treatments and controls. The seedlings' height had increased gradually from six to 10 months for all treatments. No significant differences (p>0.05) were found between all treatments and controls at the age of six to eight months. However, T6 (treatment consortium 2 + 30% chemical) was comparable to C3 (chemical fertiliser) at the age of 10 months. Treatment T6 showed a significant difference from organic fertilisers (Organic Fertiliser and Organic Compost B) between nine to 10 months. Similar findings were reported by other researchers (Azimzadeh and Azimzadeh, 2013; Namvar and Khandan, 2014; Negawer and Mahfouz, 2010). They found that inoculation with biofertilisers had increased the plants' height as compared to the non-inoculated plants. Treatment T6 recorded the highest means of palm height at 149.28 cm at 10 months. Mahfouz and Sharaf-Eldin (2007) also found that the application of biofertiliser combined with chemical fertilisers increased the vegetative growth of fennel (plant height, number of branches and herb fresh and dry weight per plant) as compared to chemical fertilisers only. Harman and Uphoff (2019) reported that some microorganisms have the opportunity to inhabit plant roots thus, becoming root symbionts which can raise crop yields by promoting the growth of both shoots and roots, enhancing, nutrient uptake, fixation and by improving plants resistance to pests and diseases.

Nitrogen content was recorded to be fluctuating between six to 10 months (*Table 6*). The nitrogen content for chemical control and Organic Compost A showed an increase between six to 10 months

TABLE 4. DRY UPPER MASS FOR SIX, SEVEN, EIGHT, NINE AND 10 MONTHS OLD OIL PALM SEEDLINGS TREATED WITH DIFFERENT TREATMENT

Treatments	Dry upper mass (g)				
	6 months	7 months	8 months	9 months	10 months
Consortium 1 + 0% chemical (T1)	2.77 a	6.39 ab	12.10 ab	15.61 ab	27.70 b
Consortium 1 + 15% chemical (T2)	2.29 a	6.44 ab	20.12 bc	28.24 c	33.15 c
Consortium 1 + 30% chemical (T3)	2.47 a	8.98 ab	20.58 bc	27.05 c	33.40 c
Consortium 2 + 0% chemical (T4)	2.68 a	7.51 ab	15.40 abc	28.70 c	34.05 cd
Consortium 2 + 15% chemical (T5)	2.85 a	8.58 ab	24.87 c	30.23 c	36.71 d
Consortium 2 + 30% chemical (T6)	3.26 a	10.72 b	20.44 bc	31.00 c	36.48 d
Organic Fertiliser (C1)	2.85 a	10.38 b	14.15 abc	16.75 ab	26.67 b
Blank (C2)	2.58 a	4.98 a	7.22 a	8.78 a	18.71 a
Chemical (C3)	3.17 a	5.60 ab	17.20 abc	27.61 c	33.40 c
Organic Compost A (C4)	1.83 a	6.59 ab	17.82 abc	22.42 bc	32.26 c
Organic Compost B (C5)	2.51 a	4.80 a	12.51 ab	12.82 a	20.65 a

Note: Values in each column with different letter(s) are significantly different at p=0.05.

TABLE 5. PALMS' HEIGHT FOR SIX, SEVEN, EIGHT, NINE AND 10 MONTHS OLD OIL PALM SEEDLINGS TREATED WITH DIFFERENT TREATMENT

Treatments	Palm height (cm)				
	6 months	7 months	8 months	9 months	10 months
Consortium 1 + 0% chemical (T1)	60.25 a	80.00 a	107.14 a	115.00 abc	133.66 cd
Consortium 1 + 15% chemical (T2)	56.81 a	85.12 a	112.28 a	121.00 abcd	143.20 ef
Consortium 1 + 30% chemical (T3)	59.37 a	88.62 a	116.66 a	130.83 cd	143.14 ef
Consortium 2 + 0% chemical (T4)	64.00 a	93.00 a	115.71 a	128.00 cd	143.85 ef
Consortium 2 + 15% chemical (T5)	54.87 a	88.00 a	113.14 a	131.33 cd	147.00 ef
Consortium 2 + 30% chemical (T6)	63.37 a	100.73 a	109.14 a	137.71 d	149.28 f
Organic Fertiliser (C1)	63.37 a	97.00 a	101.14 a	115.71 abc	127.00 bc
Blank (C2)	60.75 a	85.62 a	99.12 a	107.62 a	117.25 a
Chemical (C3)	62.87 a	86.42 a	100.87 a	126.57 bcd	143.42 ef
Organic Compost A (C4)	53.50 a	83.87 a	116.14 a	121.87 abcd	138.00 ab
Organic Compost B (C5)	60.00 a	84.37 a	101.62 a	108.42 ab	119.85 de

Note: Values in each column with different letter(s) are significantly different at p=0.05.

old oil palm seedlings. The findings showed that there were no significant differences between all treatments and controls between six and eight months. Treatment T6 showed significant differences compared to organic fertilisers (Organic Fertiliser, Organic Compost A and Organic Compost B) at seven and 10 months. Treatment T6 recorded the highest means of nitrogen content at 3.54% in oil palm leaves, at seven months. The beneficial effect of biofertiliser application is the improvement in nitrogen content (Shehata and El-Khawas, 2003) due to the increase of nutrient uptake by the plant (Hirel *et al*., 2011; Sharma and Namdeo, 1999).

The phosphorus content was recorded to increase uniformly from six months until 10 months for all treatments (*Table 7*). The phosphorus content decreased at nine months but later increased by two folds at 10 months, for most of the treatments and controls due to the growth process. The results showed that treatment T6 (consortium 2 + 30% chemical) was comparable to C3 (chemical fertiliser) at all ages of oil palm seedlings. Meanwhile, treatment T6 was significantly different from organic fertiliser (Organic Compost B) between seven and 10 months. The findings of Mohammadi *et al*. (2011) showed that the application of biofertilisers (combined with the application of phosphate solubilising bacteria and *Trichoderma harzianum*) had significant effects on nutrient uptake of chickpea, with the highest leaf P content of 0.33%. This may be due to the increase in the solubility of soluble phosphorus in the plants. The treatment T3 recorded higher means of phosphorus content with 6099.72 ppm in oil palm leaves at 10 months.

The potassium content was recorded to decrease at 10 months old for all treatments and controls (*Table 8*). The potassium content was higher at 9-month-old seedlings for most of the treatments and controls. This may be due to the planting of the oil palm seedlings in polybags and the full utilisation of potassium in the soil. The finding showed that there were no significant differences between all treatments and controls at the ages of six months. However, treatment T6 (consortium 2 + 30% chemical) was comparable to C3 (chemical fertiliser) at the age of eight months. Treatment T6

TABLE 6. NITROGEN CONTENT FOR SIX, SEVEN, EIGHT, NINE AND 10 MONTHS OLD OIL PALM SEEDLINGS TREATED WITH DIFFERENT TREATMENT

Treatments	Nitrogen (%)				
	6 months	7 months	8 months	9 months	10 months
Consortium 1 + 0% chemical (T1)	2.44 a	2.24 abc	2.07 a	1.74 a	1.84 ab
Consortium 1 + 15% chemical (T2)	2.60 a	2.39 bc	2.45 a	1.89 a	2.97 c
Consortium 1 + 30% chemical (T3)	2.54 a	2.76 cd	2.83 a	2.26 ab	3.04 c
Consortium 2 + 0% chemical (T4)	2.44 a	2.34 abc	2.09 a	2.43 ab	1.95 ab
Consortium 2 + 15% chemical (T5)	2.70 a	2.75 cd	2.69 a	2.28 ab	2.95 c
Consortium 2 + 30% chemical (T6)	2.71 a	3.54 e	2.92 a	2.68 c	3.05 c
Organic Fertiliser (C1)	2.93 a	2.52 bc	2.85 a	2.23 c	1.77 a
Blank (C2)	2.94 a	1.79 a	2.02 a	2.11 cd	2.17 ab
Chemical (C3)	2.36 a	3.29 de	2.88 a	2.66 d	2.99 c
Organic Compost A (C4)	2.29 a	2.49 bc	2.44 a	2.75 b	2.22 b
Organic Compost B (C5)	2.48 a	2.12 ab	1.75 a	2.24 ab	1.86 ab

Note: Values in each column with different letter(s) are significantly different at p=0.05.

TABLE 7. PHOSPHOROUS CONTENT FOR SIX, SEVEN, EIGHT, NINE AND 10 MONTHS OLD OIL PALM SEEDLINGS TREATED WITH DIFFERENT TREATMENT

Treatments	Phosphorous (ppm)				
	6 months	7 months	8 months	9 months	10 months
Consortium 1 + 0% chemical (T1)	939.94 abc	1993.34 d	3302.93 d	2319.08 ab	3335.87 ab
Consortium 1 + 15% chemical (T2)	932.49 abc	1464.97 abc	2497.31 cd	2174.88 ab	5071.87 bcd
Consortium 1 + 30% chemical (T3)	1048.78 abc	1437.57 ab	2717.77 cd	1844.83 ab	6099.73 d
Consortium 2 + 0% chemical (T4)	1194.54 c	1964.11 cd	3135.40 d	2032.49 ab	4360.63 abcd
Consortium 2 + 15% chemical (T5)	1106.80 bc	1388.27 ab	2255.19 bcd	2246.18 ab	5008.72 bcd
Consortium 2 + 30% chemical (T6)	950.74 abc	2159.30 d	1991.02 bc	2157.42 ab	5496.62 cd
Organic Fertiliser (C1)	1189.14 c	1865.58 bcd	2678.35 cd	2348.97 ab	4906.56 bcd
Blank (C2)	832.22 a	1064.20 a	921.056 a	2096.15 ab	4171.86 abc
Chemical (C3)	1178.71 c	1866.86 bcd	2051.89 bc	1624.84 a	4408.47 abcd
Organic Compost A (C4)	1035.82 abc	1435.29 ab	2674.98 cd	2129.69 ab	2832.46 a
Organic Compost B (C5)	871.68 ab	1298.40 a	1214.35 ab	2493.41 b	3465.44 ab

Note: Values in each column with different letter(s) are significantly different at p=0.05.

was significantly different from organic fertiliser (Organic Compost B) at the age of seven months. Treatment T6 recorded higher means of potassium content with 2.14% in the leaves of oil palm seedlings at the age of nine months. However, the highest potassium content was found in C3 at 2.73%. This result is similar to the finding reported by Shehata and El-Khawas (2003) on sunflowers and Sharma and Namdeo (1999) on soybean. They stated that the potassium content increased significantly in response to the biofertiliser application.

Carbon content was maintained at 40.00% to 45.00% from six months until 10 months for all treatments (*Table 9*). Statistical analysis also showed that there were no significant differences between all treatments and controls at the ages of six months. However, Treatment T6 (consortium 2 + 30% chemical) was comparable to C3 (chemical fertiliser) at the age of seven months. Treatment T6 showed significant differences with organic fertiliser (Organic Compost B) at the age of eight months. Treatment T6 also recorded the highest means of carbon content, with 44.85% in the leaves of oil palm seedlings at the age of seven months. The results showed that the application of biofertilisers is one of the best management practices that could help to maintain or increase the content of OM, improve soil fertility and increase soil carbon sequestration (Bożena *et al*., 2016).

Biofertilisers amended with chemical fertilisers are used to increase nutrient availability to the plant and can also affect the soil microbial biodiversity (Javoreková *et al*., 2015). The uptake of N from the soil as the nutrient is responsible for chlorophyll content and is also vital for the synthesis of food materials in plants which increase the vegetative measurement of the young oil palm (Fraile *et al*., 2015). It was revealed that the integration of microbial inoculants in biofertilisers was significant for plant height, diameter and yield (El-Naggar, 2010). In addition, biofertilisers alongside chemical fertilisers also improves the nutrient uptake of the seedlings and enhanced their growth in terms of height, girth size, chlorophyll content and soil nutrient status at a reduced rate to chemical fertilisers (Ajeng *et al*., 2020).

TABLE 8. POTASSIUM CONTENT FOR SIX, SEVEN, EIGHT, NINE AND 10 MONTHS OLD OIL PALM SEEDLINGS TREATED WITH DIFFERENT TREATMENT

Treatments	Potassium (%)				
	6 months	7 months	8 months	9 months	10 months
Consortium 1 + 0% chemical (T1)	0.43 a	0.45 a	1.08 abc	2.10 ab	1.47 ab
Consortium 1 + 15% chemical (T2)	0.34 a	0.48 a	1.16 abc	1.98 ab	1.32 ab
Consortium 1 + 30% chemical (T3)	0.28 a	0.50 a	2.21 d	2.08 ab	1.59 ab
Consortium 2 + 0% chemical (T4)	0.37 a	1.85 b	1.75 bcd	2.14 ab	1.57 ab
Consortium 2 + 15% chemical (T5)	0.39 a	1.79 b	1.79 bcd	2.03 ab	1.50 ab
Consortium 2 + 30% chemical (T6)	0.39 a	1.94 bc	1.81 cd	2.14 ab	1.49 ab
Fascal Embio (C1)	0.32 a	2.20 c	2.32 d	2.26 b	1.30 ab
Organic Fertiliser (C1)	0.17 a	2.18 c	0.71 a	2.22 b	1.00 a
Blank (C2)	0.29 a	2.22 c	1.64 bcd	2.73 c	1.85 b
Chemical (C3)	0.34 a	0.44 a	1.12 abc	1.86 a	1.01 a
Organic Compost A (C4)	0.37 a	0.40 a	0.90 ab	2.12 ab	1.16 a
Organic Compost B (C5)					

Note: Values in each column with different letter(s) are significantly different at p=0.05.

TABLE 9. CARBON CONTENT FOR SIX, SEVEN, EIGHT, NINE AND 10 MONTHS OLD OIL PALM SEEDLINGS TREATED WITH DIFFERENT TREATMENT

Treatments	Carbon (%)				
	6 months	7 months	8 months	9 months	10 months
Consortium 1 + 0% chemical (T1)	42.46 a	43.95 ab	42.79 ab	43.56 bc	39.46 a
Consortium 1 + 15% chemical (T2)	42.23 a	43.43 ab	41.77 a	42.99 b	42.99 bc
Consortium 1 + 30% chemical (T3)	42.02 a	43.36 ab	42.21 ab	43.65 bc	42.30 bc
Consortium 2 + 0% chemical (T4)	42.08 a	43.47 ab	42.87 ab	43.38 bc	43.91 bc
Consortium 2 + 15% chemical (T5)	41.17 a	43.12 a	43.34 b	43.11 b	43.37 bc
Consortium 2 + 30% chemical (T6)	41.97 a	44.85 b	43.14 b	43.12 a	41.72 ab
Organic fertiliser (C1)	38.89 a	43.93 ab	42.14 ab	43.05 a	42.24 bc
Blank (C2)	42.39 a	43.79 ab	43.00 ab	43.55 a	44.56 c
Chemical (C3)	42.00 a	43.88 ab	43.11 b	43.98 a	44.60 c
Organic Compost A (C4)	42.68 a	43.10 a	43.28 b	43.11 b	42.88 bc
Organic Compost B (C5)	42.89 a	43.72 ab	41.78 a	44.16 c	42.01 abc

Note: Values in each column with different letter(s) are significantly different at p=0.05.

CONCLUSION

The combined usage of chemical fertilisers with consortium microbes helped to regulate the availability of nutrients in the soil which resulted in the healthy growth of oil palm seedlings. Besides that, the consortium microbes contained in the biofertiliser had improved the plant quality, helped in nutrient intake by the plants, and enhanced the populations of phosphate-solubilising and proteolytic bacteria. Based on this study, Treatment T6 (consortium microbe 2 combines with 30% chemical fertiliser) showed higher growth performance and nutrient content in the oil palm seedlings compared to control treatments. Therefore, the use of consortium microbes as biofertiliser should be recommended as an alternative approach to reduce chemical fertiliser application, hence less harmful to the environment. Biofertilisers can now be suggested as a potential substitute for chemical fertilisers in oil palm nurseries, which could provide a positive impact on oil palm growth and sustainability.

ACKNOWLEDGEMENT

The authors would like to thank the Director-General of MPOB and the Director of Biology and Sustainability Research (BSR) Division of MPOB for supporting the project. We would also like to thank Dr. Siti Ramlah Ali (retired from MPOB in 2016) for her guidance, knowledge and support throughout the project. Last but not least, we would like to extend our appreciation to the staff of the Entomology and Integrated Pest Management (EIPM) Unit who were involved in assisting and conducting the experiments.

REFERENCES

Abdul Halim, N B (2009). *Effects of using enhanced biofertiliser containing N-fixer bacteria on patchouli growth.* B.E. Thesis, Universiti Malaysia Pahang.

Adesemoye, A O; Torbert, H A and Kloepper, J W (2009). Plant growth-promoting Rhizobacteria allow reduced application rates of chemical fertilisers. *Microb. Ecol., 58*: 921-929. DOI: 10.1007/s00248-009-9531-y.

Ajeng, A A; Abdullah, R; Malek, M A; Chew, K W; Ho, Y C; Ling, T C; Lau, B F and Show, P L (2020). The effects of biofertilisers on growth, soil fertility, and nutrients uptake of oil palm (*Elaeis guineensis*) under greenhouse conditions. *Processes, 8(12)*: 1681. DOI: 10.3390/pr8121681.

Anuar, E N; Nulit, R and Idris, A S (2015). Growth promoting effects of endophytic fungus *Phlebia* GanoEF3 on oil palm (*Elaeis guineensis*) seedlings. *Int. J. Agric. Biol., 17(1)*: 135-141. DOI: 13–1307/2015/17–1–135–141.

Azimzadeh, S M and Azimzadeh, S J (2013). Effect of nitroxin biofertiliser and nitrogen chemical fertiliser on yield and yield components of rapeseed (*Brassica napus* L.). *Int. J. Agric.Crop Sci., 6(18)*: 1284-1291. DOI: 10.2298/JAS1503361K.

Barak, P; Jobe, B O; Krueger, A R; Peterson, L A and Laird, D A (1997). Effects of long-term soil acidification due to nitrogen fertiliser inputs in Wisconsin. *Plant Soil, 197*: 61-69. DOI: 10.1023/A:1004297607070.

Bhardwaj, D; Ansari, M W; Sahoo, R K and Tuteja, N (2014). Biofertilisers function as key player in sustainable agriculture by improving soil fertility, plant tolerance and crop productivity. *Microb. Cell Factories, 13*: 66. DOI: 10.1186/1475-2859-13-66.

Bożena, D; Jacek, D; Anna, P D and Magdalena, B S (2016). The impact of a bio-fertiliser on the soil organic matter status and carbon sequestration - Results from a field-scale study. *J. Soils Sediments, 16*: 2335-2343. DOI: 10.1007/s11368-016-1430-5.

Chen, J H (2006). The combined use of chemical and organic fertiliser and or biofertiliser for crop growth and soil fertility. Paper presented at the International Workshop on Sustained Management of the Soil-Rhizosphere System for Efficient Crop Production and Fertiliser Use. Land Development Department, Bangkok, Thailand. 16-20 October 2006.

El-Naggar, A H (2010). Effect of biofertiliser, organic compost and mineral fertilisers on the growth, flowering and bulbs production of *Narcissus Tazetta*, L. *J. Agric. Env. Sci. Alex. Univ. Egypt, 9(1)*: 24-52. DOI: 10.21608/alexja.2017.5788.

El-Sabagh, A S; El-Morsy, F M and Farag, A R (2011). Effect of biofertilisers as a partial substitute for nitrogen on vegetative growth, yield, fruit quality and leaf mineral content of two seedless grape Cultivars I: Vegetative growth and yield. *J. Horticultural Science and Ornamental Plants, 3(2)*: 166-175.

Fraile, G P; Menendez, E and Rivas, R (2015). Role of bacterial biofertilisers in agriculture and forestry. *AIMS Bioeng., 2(3)*: 183-205. DOI: 10.3934/BIOENG.2015.3.183.

Harman, G E and Uphof, N (2019). Symbiotic root-endophytic soil microbes improve crop productivity

and provide environmental benefits. *Scientifica, 2019*: 1-25. DOI: 10.1155/2019/9106395.

Hayat, R; Ali, S; Amira, U; Khalid, R and Ahmed, I (2010). Soil beneficial bacteria and their role in plant growth promotion: A review. *Ann. of Microbiol., 60(4)*: 579-598.

Hirel, B; Tetu, T; Lea, P J and Dubois, F (2011). Improving nitrogen use efficiency in crops for sustainable agriculture. *Sustainability, 3(9)*: 1452-1485.

Iskandar, M J; Azizah, B; Farah, H A and Rizafizah, O (2018). Palm oil industry in Southeast Asia and the effluent treatment technology - A review. *Environ. Technol. and Innov., 9*: 169-185.

Itelima, J U; Bang, W J; Onyimba, I A; Sila, M D and Egbere, O J (2018). Bio-fertiliser as key player in enhancing soil fertility and crop productivity: A Review. *Direct Res. J. Agric. and Food Sci., 6*: 73-83.

Javoreková, S; Maková, J; Medo, J and Kovácsová, S (2015). Effect of bio-fertilisers application on microbial diversity and physiological profiling of microorganisms in arable soil. *Eurasian J. Soil Sci., 4*: 54-61.

Khan, Z; Tiyagi, S A; Mahmood, I and Rizvi, R (2012). Effects of N fertilisation, organic matter and biofertilisers on the growth and yield of chilli in relation to management of plant-parasitic nematodes. *Turk. J. Bot., 36*: 73-81.

Khosro, M and Yousef, S (2012). Bacterial biofertilisers for sustainable crop production: A Review. *J. Agric. Biol. Sci., 7(5)*: 307-316.

Kim, S and Dale, B E (2008). Effects of nitrogen fertiliser application on greenhouse gas emissions and economics of corn production. *Environ. Sci. Technol., 42*: 6028-6033.

Lee, K E and Pankhurst, C E (1992). Soil organisms and sustainable productivity. *Aust. J. Soil Res., 30*: 855-892. DOI: 10.1071/SR9920855.

Li, X G; Jia, B; Lv, J; Ma, Q; Kuzyakov, Y and Li, F (2017). Nitrogen fertilization decreases the decomposition of soil organic matter and plant residues in planted soils. *Soil Biol. Biochem., 112*: 47-55.

Mahfouz, S A and Sharaf-Eldin, M A (2007). Effect of mineral *vs*. biofertiliser on growth, yield and essential oil content of fennel *(Foeniculum vulgare* Mill.). *Int. Agrophys. 21*: 361-366.

Miransari, M (2013). Soil microbes and the availability of soil nutrients. *Acta Physiol. Plant, 35(11)*: 3075-3984.

Mohamed, S S E and Babiker, H M (2012). Effects of *Rhizobium* inoculation and urea fertilization on faba bean (*Vicia faba* L.) production in a semi-desert zone. *Adv. Environ. Biol., 6*: 824-830.

Mohammadi, K; Ghalavand, A; Aghaalikhani, M; Heidari, G R and Sohrabi, Y (2011). Introducing the sustainable soil fertility system for chickpea (*Cicer arietinum* L.). *Afr. J. Biotechnol., 10(32)*: 6011-6020.

Munda, S; Shivakumar, B G; Gangaiah, B; Manjaiah, K M; Rana, D S; Layek, J and Koneru, L (2015). Influence of direct and residual phosphorus fertilisation on growth and yield of potato in a soybean-potato cropping system. *Aust. J. Crop Sci., 9(3)*: 191-202.

Namvar, A and Khandan, T (2014). Biopriming and mineral fertilisers effects on agronomical performance of rapeseed (*Brassica napus* L.). *Ekologija, 60(3)*: 54-63.

Negawer, E A and Mahfouz, S A (2010). Response of canola (*Brassica napus* L.) to biofertilisers under Egyptian conditions in newly reclaimed soil. *Int. J. Agric. Sci.,* 2(1): 12-17.

Qiao, C; Xu, B; Han, Y; Wang, J; Wang, X; Liu, L; Liu, W; Wang, S; Tan, H; Liu, Y and Zhao, X (2018). Synthetic nitrogen fertilisers alter the soil chemistry, production and quality of tea. A meta-analysis. *Agron. Sustain. Dev., 38(1)*: 1-10.

Rankine, I R and Fairhurst, T H (1999). Pocket Guide: Oil Palm Series, Volume 4: Nursery. IPNI Southeast Asia Program (IPNI SEAP). Penang. 82 pp.

Rokhzadi, A; Asgharzadeh, A; Darvish, F; Nour-Mohammadi, G and Majidi, E (2008). Influence of plant growth-promoting rhizobacteria on dry matter accumulation and yield of chickpea (*Cicer arietinum* L.) under field condition. *Am-Euras. J. Agric. Environ. Sci., 3(2)*: 253-257.

Savci, S (2012). An agricultural pollutant: Chemical fertiliser. *Int. J. Environ. Sci. Dev., 3(1)*: 11-14.

Shehata, M M and El-Khawas, S A (2003). Effect of two biofertilisers on growth parameters, yield characters, nitrogenous components, nucleic acids content, minerals, oil content, protein profiles and DNA banding pattern of sunflower (*Helianthus annus* L. cv. Vedock) yield. *Pak. J. Biol. Sci., 6(14)*: 1257-1268.

Sharma, K N and Namdeo, K N (1999). Effect of biofertiliser and phosphorous on NPK contents, uptake and grain quality of soybean (*Glycine max* L. Merrill) and nutrient status of soil. *Crop Res. (Hisar) 17*: 164-169.

Tang, D; Kester, D R; Ni, I; Qi, Y and Kawamura, H (2003). *In situ* and satellite observations of a harmful algal bloom and water condition at the Pearl River estuary in late autumn 1998. *Harmful Algae, 2:* 89-99.

Taryo-Adiwiganda, Y; Balaman, T and Berani, P (2006). Effect of bio fertiliser on mature oil palm in North Sumatra and Riau. *Indones. J. Agric. Sci., 7(1)*: 20-26.

US EPA (1996) *Method 3050B: Acid Digestion of Sediments, Sludges, and Soils*. Second Revision. Washington, DC.

Vacheron, J; Desbrosses, G; Bouffaud, M L; Touraine, B; Loccoz, Y M; Muller, D; Legendre, L;Dye, F W and Prigent-Combaret, C (2013). Plant growth promoting rhizobacteria and root system functioning. *Front. in Plant Sci., 4:* 356.

Voon Kheong, L; Rahman, Z A; Musa, M H and Hussein, A (2012). Effects of severing oil palm roots on leaf nutrient levels and P uptake. *J. Oil Palm Res., 24:* 1343-1348.

Wang, J; Li, R; Zhang, H; Wei, G and Li, Z (2020). Beneficial bacteria activate nutrients and promote wheat growth under conditions of reduced fertiliser application. *BMC Microbiol., 20(38*): 1-12.

Wang, B; Lai, T; Huang, Q W; Yang, X M and Shen, Q R (2009). Effect of N fertilisers on root growth and endogenous hormones in strawberry. *Pedosphere, 19*: 86-95.

Wani, S P; Rego, T G; Rajeshwari, S and Lee, K K (1995). Effect of legume-based cropping systems on nitrogen mineralization potential of Vertisol. *Plant Soil., 175(2)*: 265-274.

Zainuddin, N; Keni, M F and Ibrahim, S A S (2019). Effect of biofertiliser containing different percentage rates of chemical fertiliser on oil palm seedlings. *J. Oil Palm Res., 31(4)*: 582-591.

Zhao, J; Ni, T; Li, J;Lu, Q; Fang, Z; Huang, Q; Zhang, R; Li, R; Shen, B and Shen, Q (2016). Effect of organic-inorganic compound fertiliser with reduced chemical fertiliser application on crop yields, soil biologcalactivity and bacterial community structure in a rice-wheat cropping system. *Appl. Soil Ecol., 99*: 1-12.

Journal of Oil Palm Research Vol. 35 (1) March 2023 p. 157-167
DOI: https://doi.org/10.21894/jopr.2022.0034

PATHOGENESIS-RELATED PROTEIN INDUCTION IN *Streptomyces* GanoSA1-TREATED OIL PALM SEEDLINGS DURING EARLY INFECTION BY *Ganoderma boninense*

SHARIFFAH-MUZAIMAH SYED ARIPIN[1]*; IDRIS ABU SEMAN[1]; MOHD HEFNI RUSLI[1] and SHAMALA SUNDRAM[1]

ABSTRACT

Basal stem rot (BSR) disease in oil palm is caused by a fungal pathogen identified as Ganoderma boninense. *In our previous study,* Streptomyces nigrogriseolus *GanoSA1 showed strong antagonistic activity against* G. boninense *PER71 in laboratory, nurseries, and field studies. This study aimed to identify the role of* Streptomyces *GanoSA1 in inducing pathogenesis-related proteins in oil palm seedlings during the early infection by the pathogen. Three-month-old commercial oil palm seedlings (D×P) were inoculated with* Streptomyces *GanoSA1 and artificially infected with* G. boninense *PER71 through the rubberwood block sitting technique. The seedlings were harvested at 0, 3, 7, 14, 28 and 60 days after inoculation (DAI) with* G. boninense *PER71. The seedlings were tested for the production of β-glucanase, peroxidase (POX), polyphenol oxidase (PPO), and phenylalanine lyase (PAL). The* Streptomyces *GanoSA1 significantly induced the production of β-glucanase (3.04-fold), POX (1.68-fold), PPO (1.88-fold), and PAL (1.127-fold) in oil palm roots compared to control seedlings. The biological control activity by* Streptomyces *GanoSA1 might be contributed by the induction of pathogenesis-related proteins.*

Keywords: actinomycetes, artificial inoculation, defence-enzyme, *Ganoderma*.

Received: 23 December 2021; **Accepted:** 25 April 2022; **Published online:** 17 June 2022.

INTRODUCTION

Oil palm (*Elaeis guineensis* Jacq.) is an important crop in Malaysia, with nearly 5.84 million hectares of cultivation areas throughout the country (Parveez *et al.*, 2021). The crop, however, is susceptible to some pests and diseases. One of the severe threats is the basal stem rot (BSR) disease caused by *Ganoderma* spp. (Idris, 2012), with a potential yield loss of 68.73% (Assis *et al.*, 2020). According to Idris (2019), the incidence of BSR in 2016-2017 was 7.40%, affecting approximately 221 000 ha of oil palm cultivated areas. Cultural practices, application of chemical fungicides, and biological control were among the strategies recommended to control the disease and sustain the infected oil palm (Idris *et al.*, 2016; Naidu *et al.*, 2015; Siddiqui *et al.*, 2021; Surendran *et al.*, 2018).

Biological control is an appealing environmentally friendly option for controlling fungal plant pathogens. The introduction of antagonistic actinomycetes into the rhizosphere has the potential to alter the soil's native microorganism ecosystems. This exposure leads to the suppression of soilborne pathogens and interference of survivability or disease-producing activities by the phytopathogen. Several studies have shown that many beneficial microorganisms, such as actinomycetes, bacteria and fungi, can effectively lower plant disease incidence (Amaresan *et al.*, 2018; Gowdar *et al.*, 2018; Meena *et al.*, 2017). Many species of actinomycetes, especially those belonging to the *Streptomyces* group, are well known to produce antibiotics

[1] Malaysian Palm Oil Board,
6 Persiaran Institusi, Bandar Baru Bangi,
43000 Kajang, Selangor, Malaysia.

* *Corresponding author e-mail*: *muzaripin@mpob.gov.my*

and cell-wall degrading enzymes (Amaresan *et al*., 2018; Tamreihao *et al*., 2016) and remain as major contributors to secondary metabolites (Matsumoto and Takahashi, 2017). They have been proven to potentially inhibit or affect the growth of phytopathogenic fungi (Al-Dhabi *et al*., 2019; Bettache *et al*., 2018; Dias *et al*., 2017), including *Ganoderma* sp. (Lim *et al*., 2018; Nur Azura *et al*., 2016; Pithakkit *et al*., 2015; Queendy and Roza, 2019; Shariffah-Muzaimah *et al*., 2015; Sujarit *et al*., 2020; Tan *et al*., 2002; Ting *et al*., 2014). Apart from that, a reduction in disease incidence was also observed in an *in Plantae* experiment (Dias *et al*., 2017; Idris and Shariffah-Muzaimah, 2021; Ramamoorthy *et al*., 2002; Salla *et al*., 2016; Zhang *et al*., 2016), indicating their potential to be utilised as a biocontrol agent. The biocontrol of phytopathogen may be related to mechanisms such as the production of antibiotics (Lim *et al*., 2017; Wonglom *et al*., 2019), secretion of hydrolytic enzymes (Jog *et al*., 2012; Mun *et al*., 2020; Wonglom *et al*., 2019), production of siderophores or competition for nutrient (Zeng *et al*., 2018) and induced systemic resistance in plants (Dias *et al*., 2017; Kurth *et al*., 2014; Zhang *et al*., 2016; 2020; Zhao *et al*., 2012).

In previous studies, *Streptomyces nigrogriseolus* GanoSA1 have shown a significant suppressive effect on *Ganoderma* disease (Idris and Shariffah-Muzaimah, 2021; Shariffah-Muzaimah *et al*., 2020). The present report describes the biochemical responses with defence enzymes, such as polyphenol oxidase (PPO), peroxidase (POX), and phenylalanine ammonia-lyase (PAL), that are involved in phytoalexins and phenolic synthesis in *Streptomyces* sp. GanoSA1 treated oil palm (*Elaeis guineensis* Jacq.) seedlings infected with *G. boninense* PER71.

MATERIALS AND METHODS

Planting Materials

A total of 100 three-month-old *Dura* x *Pisifera* (D×P) oil palm seedlings used in this study were obtained from the Malaysian Palm Oil Board (MPOB). The seedlings were grown in polypropylene bags (15 × 23 cm) containing approximately 15 kg of soil mixture of commercial topsoil and sand (3:1) and maintained in a nursery (temperature variation of 30°C to 35°C) one month before treatment.

Streptomyces GanoSA1, *Ganoderma boninense* PER71 and Culture Condition

Streptomyces nigrogriseolus GanoSA1 (MT150593) was previously isolated from the rhizosphere of a healthy oil palm located in an area with severe BSR incidence in Peninsular Malaysia (1°57′10.7″N 103°22′16.6″E). This strain showed strong antagonistic activity against *G. boninense* PER71 in both *in vitro* and *in vivo* experiments (Idris and Shariffah-Muzaimah, 2021; Shariffah-Muzaimah *et al*., 2020). *Streptomyces* GanoSA1 and a virulent stock culture of *G. boninense* PER71 were obtained from the Plant Pathology and Biosecurity Unit Laboratory, Biology and Sustainability Research Division, MPOB, Malaysia. The working culture of *Streptomyces* GanoSA1 was prepared by streaking out one loopful of the glycerol stock on yeast malt extract (YME) agar. The *G. boninense* PER71 working culture was prepared by sub-culturing a stock culture onto potato dextrose agar (PDA). Plates were sealed individually and incubated at 28°C for seven days.

Powder formulation of *Streptomyces* GanoSA1 for the nursery experiment was prepared as described by Idris and Shariffah-Muzaimah (2021). The strain was cultivated in YME broth and incubated with agitation at 180 rpm for seven days. Commercial vermiculite (2-4 mm) and bio-charcoal (2-4 mm) were mixed at the ratio of 1:1 and autoclaved twice on two consecutive days for sterilisation. A total of 50 g of the vermiculite-bio charcoal powder was then inoculated with 20% of the *Streptomyces* GanoSA1 culture to achieve the concentration of 10^8 colony forming units (CFU) per gram. The inoculum of *G. boninense* PER71 for artificial inoculation in oil palm seedlings was prepared using 6 × 6 × 6 cm rubber woodblock (RWB) according to the method described by Sundram *et al.* (2015).

Experimental Design, Inoculation of *Streptomyces* GanoSA1 and Artificial Inoculation of *Ganoderma boninense* PER71 to Oil Palm Seedlings

The experiment was laid down in a complete randomised design (CRD) with four treatments, and each treatment consisted of 24 seedlings with four replicates per harvest. For each treatment, four seedlings were sampled from each replication separately on days 0, 3, 7, 14, 28 and 60 post-inoculation with *G. boninense* PER71. The four treatments were seedlings without *Streptomyces* GanoSA1 or *G. boninense* PER71, as control (T1); seedlings without *Streptomyces* GanoSA1 and with *G. boninense* PER71 (T2); seedlings with *Streptomyces* sp. GanoSA1 without *G. boninense* PER71 (T3); and seedlings with *Streptomyces* sp. GanoSA1 and with *G. boninense* PER71 (T4) (*Table 1*). Seedlings in treatments T3 and T4 were pre-treated with 50 g of *Streptomyces* GanoSA1 vermiculite bio-charcoal powder by soil mixing. Fourteen days after the pre-treatment activity, each seedling in treatments T2 and T4 were artificially inoculated with *G. boninense* PER71 using the RWB sitting technique (Idris and

Shariffah-Muzaimah, 2021; Shariffah-Muzaimah *et al.*, 2020). All of the seedlings used in this study were maintained in a nursery with standard practices as described by Esnan *et al.* (2001).

The confirmation of *Ganoderma* infection was done by referring to Rees *et al.* (2009) with modification where surface-sterilised root tissue was placed on *Ganoderma* Selective Media (GSM). The sterilisation of the root was carried out using 1% v/v sodium hypochlorite (commercial household, Clorox®).

TABLE 1. DESCRIPTION OF TREATMENT USED IN THE EXPERIMENT

Treatment	Description	
	Streptomyces GanoSA1 treatment	*Ganoderma* artificial inoculation
T1	-	-
T2	-	+
T3	+	-
T4	+	+

Determination of Pathogenesis-related Protein Activity

Pathogenesis-related proteins were determined at days 0, 3, 7, 14, 28 and 60 after the seedlings were infected with *G. boninense* PER71. For each treatment, four seedlings were sampled from each replication separately. Root samples were prepared according to Salla *et al.* (2016) and Xue *et al.* (2016). The roots were washed in running tap water to remove the soil particles, dried, and ground in liquid nitrogen using a mixer mill (MM400, Retsch, Germany) and homogenised with 1 mL (1:2, w/v) of 100 mM pH 6.5 sodium phosphate buffer. The homogenate was then centrifuged at 16 000 xg for 20 min at 4°C. The supernatant obtained represents the crude enzyme used in all enzymatic activity tested in this study except for PAL. Assay for the estimation of β-1,3-glucanase, chitinase, POX, and PAL was done by referring to Ramamoorthy *et al.* (2002), while estimation of PPO was done as described in Tuncay and Yagar (2011). The spectrophotometric readings were done by using a UV–VIS Spectrophotometer (Genesys 10S UV-VIS, USA).

β-1,3-Glucanase activity. The laminarin-dinitrosalicylic acid method was used to estimate the activity of β-1,3-glucanase in this study. The reaction mixture consisted of a 1:1 ratio of 4% laminarin and crude enzyme with a total volume of 125 µL. After 10 min of incubation at 40°C, the reaction was stopped by adding 375 µL of dinitrosalicylic acid, followed by a 5 min heating on boiling water. The reaction solution was then vortexed before transferring into a plastic cuvette. The absorbance was measured at 500 nm and enzyme activity was expressed as µg glucose min^{-1} mg^{-1} of fresh weight.

Polyphenol oxidase (PPO). The PPO activity was estimated by referring to Tuncay and Yagar (2011). A total of 1.15 mL of phosphate buffer (50 mM, pH 7) was mixed with 0.30 mL of 10 mM pyrogallol and maintained in a water bath at 25°C. The reaction was initiated by adding 0.05 mL of the crude enzyme. Enzyme activity was measured by observing changes in absorbance at 420 nm for 3 min. The enzyme activity was expressed as changes in the absorbance min^{-1} mg^{-1} of fresh weight.

Peroxidase (POX). The method for POX activity includes the addition of 0.25 mL of the crude enzyme into a substrate solution containing 0.75 mL of 0.05 M pyrogallol and 0.25 mL of 1% hydrogen peroxide (H_2O_2) and incubated at room temperature for 2 min. The absorbance was determined at 470 nm for three min at a 30 s interval and POX activity was expressed as changes in the absorbance min^{-1} mg^{-1} of fresh weight.

Phenylalanine lyase (PAL) activity. A mixture of ice-cold 0.1 M sodium borate buffer, pH 7, 1.4 mM of 2-mercaptoethanol and 0.1 g of insoluble polyvinylpyrrolidone was added to 1.0 g of the root sample and homogenised evenly by using a mixer mill (MM400, Retsch, Germany). The homogenate was filtered through a cheesecloth, and the filtrate obtained was centrifuged at 16 000 xg for 15 min. A 0.4 mL of the supernatant was then mixed with 0.5 mL of 0.1 M borate buffer, pH 8.8 and 0.5 mL of 12 mM of L-phenylalanine and incubated for 30 min at 30°C. The absorbance of the solution was measured at 290 nm. The amount of trans-cinnamic acid formed from the conversion of L-phenylalanine was calculated using the Beer-Lambert formula (molar absorptivity of 9630/M/cm). The enzyme activity was expressed as µmol of trans-cinnamic acid min^{-1} mg^{-1} of fresh weight.

Statistical Analysis

All experiments were carried out in triplicate. The results are presented as mean ± standard deviation (SD). The data were analysed by analysis of variance (ANOVA) using SAS® software version 15 for Windows. Analysis of the differences was conducted using the least significant difference (LSD) test, and a $p<0.05$ was considered to demonstrate a significant difference.

RESULTS AND DISCUSSION

Confirmation of *Ganoderma boninense* PER71 on Roots Sample

The ability of *Streptomyces* spp. to promote plant growth had previously been reported in several plants such as chilli pepper, chickpea, banana, rice, cucumber, tomato and sunflower (El-Tarabily, 2008; El-Tarabily *et al.*, 2009; Gopalakrishnan *et al.*, 2011; Goudjal *et al.*, 2014; Patil *et al.*, 2011; Pornsuriya and Sunpapao, 2014; Thakker *et al.*, 2013). The results on the effect of *Streptomyces* GanoSA1 on oil palm growth have been reported and elaborated by Idris and Shariffah-Muzaimah (2021) and Shariffah-Muzaimah *et al.* (2020). Based on our observation during sampling, lesions on the root tissues can be seen on the roots of seedlings inoculated with *G. boninense* (*Figure 1a*), especially in the area near the inoculum source. The presence of *Ganoderma* was confirmed on GSM (*Figure 1b*). A white fluffy colony with a brown pigmented halo was observed on GSM, indicating the appearance of the basidiomycete. The same observable colony was also reported by Naidu *et al*. (2018) from the cross-sections of the infected tissues indicating the possible appearance of the pathogenic *G. boninense*. Based on the observations during harvest, seedling height, and root number on T3 treatment were higher compared to other treatments (*Figure 1c*).

Effect of *Streptomyces* GanoSA1 on Pathogenesis-related Proteins of Oil Palm with or without *Ganoderma boninense* PER71

In our previous study, *Streptomyces* GanoSA1 demonstrated its potential to lower the disease incidence caused by *G. boninense* in oil palms under greenhouse and field conditions (Idris and Shariffah-Muzaimah, 2021; Shariffah-Muzaimah *et al.*, 2020). Previous works on *Streptomyces* GanoSA1 have focused more on the strain's effectiveness under laboratory, nursery, and field studies with limited work focusing on the mechanism. Therefore, this current study explored the role of the strain in triggering induced systemic resistance in oil palm. To assess the induction of resistance in oil palm seedlings, we examined the production of plant defence-related enzymes in seedlings treated with different treatments at different time intervals. The results demonstrated that *Streptomyces* sp. GanoSA1 enhanced the production of these enzyme activities in oil palm roots with or without *G. boninense* PER71.

The results showed a significant difference in the activities of β-1,3-glucanase between all the treatments used in this study (*Figure* 2). On days 3, 7 and 14 days after treatment, glucanase activities were higher in seedlings treated with *Streptomyces* (T3 and T4) compared to the untreated (T1). The independent presence of *Ganoderma* enhanced the production of glucanase at the highest point up to 1.94-3.20 folds higher than the other treatments at seven days after inoculation (DAI). However, the activity was observed as a short-lasting response as the production tended to decline at 14, 28 and 60 DAI and reflected a downward trend toward the end of the experiment. Meanwhile, the presence of *G. boninense* PER71 in *Streptomyces*-treated seedlings (T4) had the highest activity of glucanase. In the treatment, the optimum activity reached 3.800 ± 0.01 μmol min^{-1} mg^{-1} fresh weight at 60 DAI, which was significantly higher compared to *Streptomyces* GanoSA1, *G. boninense* PER71 and control treatment with 2.758 ± 0.96, 0.5648 ± 1.15 and 1.252 ± 0.46 μmol min^{-1} mg^{-1} fresh weight, respectively. An increased amount of glucanase was reported as one of the main responses by the plant due to infection and pathogenesis by pathogens, which frequently occur before the visible symptoms are observable (Sahebi *et al.*, 2018). Treatment with biological control agents not only induced higher glucanase production in plants but also contributes to the production of the enzymes itself as one of the

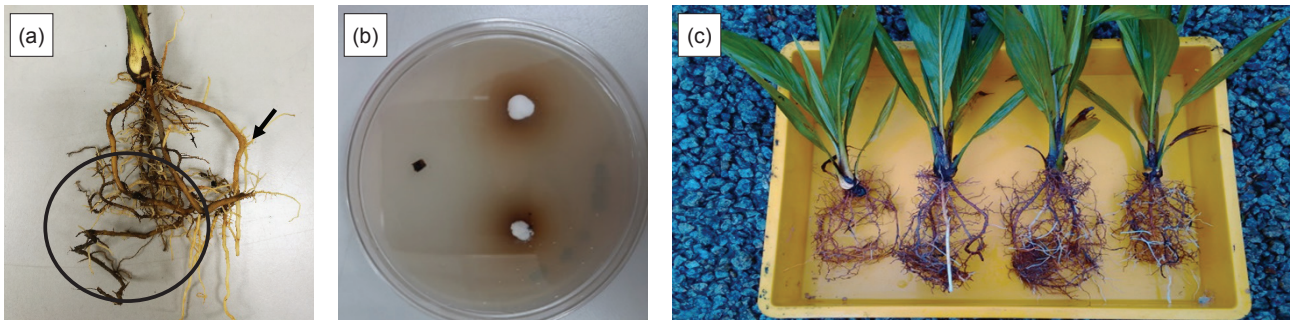


Figure 1. Effect of Streptomyces nigrogriseolus *GanoSA1 treatment and* Ganoderma boninense *PER71 inoculation on oil palm seedlings, (a) Oil palm seedlings root showing lesion (circle) and healthy (arrow) symptoms, and (b)* Ganoderma *Selective Medium (GSM) added with root pieces from T2 and T4 treatment, and (c) seedlings observed during harvesting at 14 DAI (From left to right, T1, T2, T3 and T4 where, T1 = untreated and uninoculated seedling (control), T2 = seedling inoculated with* G. boninense *PER71, T3 = seedling treated with* S. nigrogriseolus *GanoSA1 and T4 =seedling inoculated with* G. boninense *PER71 and treated with* S. nigrogriseolus *GanoSA1).*

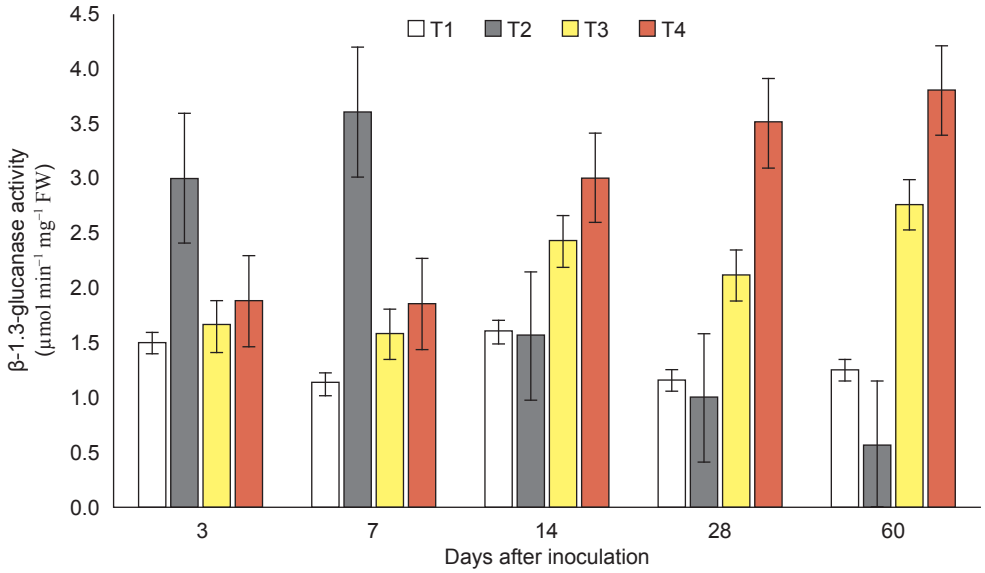


Figure 2. Induction of β-1,3-glucanase activity by Streptomyces nigrogriseolus *GanoSA1 in oil palm roots challenged with or without the* G. boninense *PER71. [T1 = untreated and uninoculated seedling (control), T2 = seedling inoculated with* G. boninense *PER71, T3 = seedling treated with* S. nigrogriseolus *GanoSA1 and T4 = seedling inoculated with* G. boninense *PER71 and treated with* S. nigrogriseolus *GanoSA1]. Vertical bars indicate standard deviations of four replications.*

important mechanisms during the pathogen control activities (Meena *et al.*, 2017). The POX activity in seedlings inoculated with *G. boninense* PER71 either treated with or without *Streptomyces* GanoSA1 was higher compared to seedlings with *Streptomyces* GanoSA1 only and control treatment. Significance differences in POX activity in all treatments were observed from day 14 onwards (*Figure 3a*). Based on the observation, the activities were enhanced when the pathogen was present. The POX activity reached a maximum level of 1.955 ± 2.15 and 2.143 ± 1.56 μmol min^{-1} mg^{-1} of fresh weight, in T3 and T4 treatments, respectively at 60 DAI, which was 3.6-4.0 folds higher compared to those acquired in the seedlings untreated with *Streptomyces* GanoSA1 and seedlings uninoculated with *G. boninense* PER71.

Based on the present study, PPO activity in all seedlings showed higher activity compared to PPO activity at control seedlings showing the lowest activity of all tested time points ranging from 0.02-0.08 μmol min^{-1} mg^{-1} of fresh weight (*Figure 3b*). At 3, 7 and 14 DAI, seedlings inoculated with *G. boninense* PER71 with or without *Streptomyces* GanoSA1 exhibited increased PPO activity in comparison to other treatments. PPO activity in seedlings treated with *Streptomyces* GanoSA1 with the inoculation of the pathogen continues to be expressed higher in 7, 14, 28 and 60 DAI than in the other three treatments (*Figure 3b*). Dias *et al.* (2017) reported a similar response on tomato plants inoculated with *Streptomyces* sp. The increase of both enzymes at early and later points in time, respectively in the evaluation period is related to the defence response. The PPO response in a plant may be associated with the production of toxic phenol molecules; meanwhile, the POX activity might be responsible for the oxidation of phenols for strengthening the cell walls to act as a barrier in constraining the spread of the pathogen (Dias *et al.*, 2017). Remarkably, *Streptomyces* GanoSA1 induced stronger POX and PPO production, especially with the presence of the *G. boninense* PER71. PPO activity in our study demonstrated little variation in the *Streptomyces* GanoSA1-treated seedlings, especially in the early DAI. This phenomenon may be related to the recognition of non-harmful plant-microbe interaction by oil palm seedlings which leads to low expression, as observed in our results. *Ganoderma boninense* PER71 inoculation caused an obvious rise in PAL activity 7 DAI compared with the other treatments; however, the activity was reduced thereafter (*Figure 3c*). Pre-treatment with *Streptomyces* GanoSA1 modulated the response of PAL. Seedlings treated with *Streptomyces* GanoSA1 alone showed higher PAL activity compared to treatments of control and *G. boninense* alone at 14 DAI onwards, but activity was not as much as in *G. boninense* PER71-inoculated seedlings. The amount of PAL in seedlings with the presence of the pathogen was 3.09-fold and 1.60-fold higher than those obtained in the control group, *G. boninense* PER71 only, and *Streptomyces* GanoSA1 only, respectively (*Figure 3c*).

Plants have a wide range of defence responses that can be activated in response to attacks by a pathogen (Agrios, 2005). The usage of beneficial microbes has been reported as one of the efficient biotechnological tools to stimulate plant metabolism and reduce the risk of phytopathogen infection

(Bonanomi *et al.*, 2018; Cappellari *et al.*, 2017; Meena *et al.*, 2017; Russo *et al.*, 2012; Siddiqui *et al.*, 2015). It is known from the literature that the bacterial genera of *Pseudomonas*, *Bacillus*, *Azospirillum* and *Streptomyces* are some of the common genera which have been reported with promising PGPR activity. Additionally, a countless number of actinomycetes from the genus of *Streptomyces* have been reported to contribute to plant resistance against various phytopathogens (Alekhya and Gopalakrishnan, 2014; Gopalakrishnan *et al.*, 2015; Hata *et al.*, 2015; Jacob *et al.*, 2016; Kamal and Sharma, 2014; Lyu *et al.*, 2017; Manhas and Talwinder, 2016; Sangdee *et al.*, 2016; Srividya *et al.*, 2012), which possibly occur through a plant growth promotion activity (Lehr *et al.*, 2008; Schrey and Tarkka, 2008; Viaene *et al.*, 2016) and/or induction of defence-related enzymes (Dias *et al.*, 2017; Salla *et al.*, 2014; 2016; Shao *et al.*, 2018; Singh and Gaur, 2017; Xue *et al.*, 2016; Zhang *et al.*, 2016). This gram-positive filamentous genus is well-known for its potential in producing various secondary metabolites with diversified biological activities and functions (Olanrewaju and Babalola, 2019; Pacios-Michelena *et al.*, 2021).

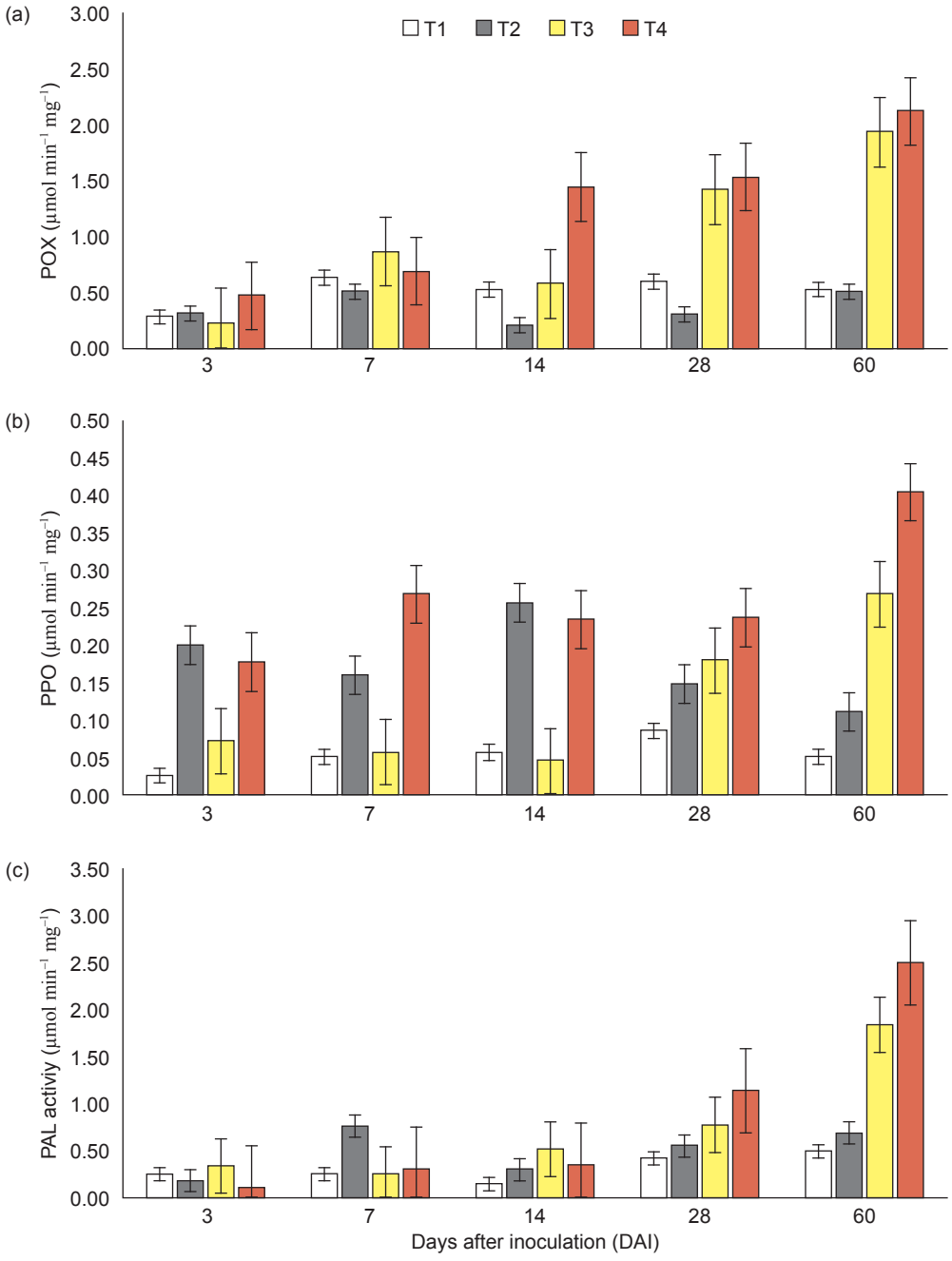


Figure 3. Changes in (a) peroxidase (POX), (b) polyphenol oxidase (PPO), and (c) phenylalanine lyase (PAL) activity induced by Streptomyces nigrogriseolus *GanoSA1 in oil palm roots challenged with or without the pathogen* G. boninense *PER71. Vertical bars indicate standard deviations of four replications.*

This report concurs with earlier works on the induced systemic resistance that usually results from the rhizosphere colonisation by PGPR, such as *Pseudomonas* spp., *Bacillus* spp., *Trichoderma* spp., and *Streptomyces* spp. (Pieterse *et al.*, 2014; Zhang *et al.*, 2020). This study showcased the ability of *Streptomyces* GanoSA1 in enhancing the production of pathogenesis-related enzymes related to inducing systemic resistance in oil palm. These findings are supported by the observation of other researchers, who reported on increased activity of glucanase, POX, PPO and PAL when plants were treated with *Streptomyces* sp. (Dias *et al.*, 2017; Salla *et al.*, 2016; Singh and Gaur, 2017; Zhang *et al.*, 2016), *Streptomyces* bioactive compounds (Zhang *et al.*, 2020), *Trichoderma* strain (Musa, 2017; Paudzai *et al.*, 2019) and *Pseudomonas fluorescens* (Ramamoorthy *et al.*, 2002; Saikia *et al.*, 2004).

CONCLUSION

This study demonstrated the potential role of plant defence enzymes in developing systemic disease resistance through *Streptomyces* GanoSA1 against BSR disease in oil palm. The potential *in vivo* antagonism of the strain, along with reducing the incidence of the *Ganoderma* disease and the modulation of defence-related enzymes, PPO, POX and PAL, highlighted the biological control traits of the strain. It indicates a possible rapid induction of enzymes involved in phenylpropanoid metabolism and PR proteins in response to treatment with biocontrol agents. To the best of our knowledge, this is the first report which demonstrate the effect of *Streptomyces* spp. to enhance the production of pathogenesis-related proteins in oil palm with or without *Ganoderma* infection. Further studies on a gene related to protein expression would strengthen the finding. Field evaluation on a large scale with a longer timeframe and impact on the productivity of oil palm would provide a novice finding on the strain's effectiveness under a natural environment for sustainable oil palm planting.

ACKNOWLEDGEMENT

The authors would like to thank the Director-General of the Malaysian Palm Oil Board (MPOB) for being very supportive and permission to publish this article and the staff of MPOB for their assistance in conducting this study.

REFERENCES

Agrios, G (2005). How plants defend themselves against pathogens. *Plant Pathology*. 5th edition. Elsevier Academic Press. p. 208-248.

Al-Dhabi, N A; Esmail, G A; Duraipandiyan, V and Arasu, M V (2019). Chemical profiling of *Streptomyces* sp. Al-Dhabi-2 recovered from an extreme environment in Saudi Arabia as a novel drug source for medical and industrial applications. *Saudi J. Biol. Sci.*, *26(4)*: 758-766.

Alekhya, G and Gopalakrishnan, S (2014). Characterisation of antagonistic *Streptomyces* as a potential biocontrol agent against fungal pathogens of chickpea and sorghum. *Philipp. Agric. Sci.*, *97(2)*: 191-198.

Amaresan, N; Kumar, K; Naik, J H; Bapatla, K G and Mishra, R K (2018). *Streptomyces* in plant growth promotion: Mechanism and Role. *New and Future Developments in Microbial Biotechnology and Bioengineering* (Singh, B P; Gupta, V K; Passari, A K eds). Elsevier. p. 125-135.

Assis, K; Chong, K P; Idris, A S and Ho, C M (2020). Estimating the yield loss of oil palm due to *Ganoderma* basal stem rot disease by using Bayesian Model Averaging. *J. Oil Palm Res.*, *33(1)*: 46-55.

Bettache, A; Azzouz, Z; Boucherba, N; Bouiche, C and Hamma, S (2018). Lignocellulosic biomass and cellulolytic enzymes of actinobacteria. *SAJ Biotechnol.*, *5(2)*: 106.

Bonanomi, G; Lorito, M; Vinale, F and Woo, S L (2018). Organic amendments, beneficial microbes, and soil microbiota: Toward a unified framework for disease suppression. *Annu. Rev. Phytopathol.*, *56*: 1-20.

Cappellari, L del R; Chiappero, J; Santoro, M V; Giordano, W and Banchio, E (2017). Inducing phenolic production and volatile organic compounds emission by inoculating *Mentha piperita* with plant growth-promoting rhizobacteria. *Sci. Hortic.*, *220*: 193-198.

Dias, M P; Bastos, M S; Xavier, V B; Cassel, E; Astarita, L V and Santarém, E R (2017). Plant growth and resistance promoted by *Streptomyces* spp. in tomato. *Plant Physiol. Biochem.*, *118*: 479-493.

El-Tarabily, K A (2008). Promotion of tomato (*Lycopersicon esculentum* Mill.) plant growth by rhizosphere competent 1-aminocyclopropane-1-carboxylic acid deaminase-producing S*treptomycete actinomycetes. Plant Soil., 308(1)*: 161-174.

El-Tarabily, K A; Nassar, A H; Hardy, G E S J and Sivasithamparam, K (2009). Plant growth promotion and biological control of *Pythium aphanidermatum*, a pathogen of cucumber, by endophytic actinomycetes. *J. Appl. Microbiol.*, *106(1)*: 13-26.

Esnan, A G; Mohd Basri, W and Mohd Tayeb, D (2001). Manual penanaman dan penyelengaraan sawit untuk sektor pekebun kecil. MPOB, Bangi. 134 pp.

Gopalakrishnan, S; Pande, S; Sharma, M; Humayun, P; Kiran, B K; Sandeep, D; Vidya, M S; Deepthi, K and Rupela, O (2011). Evaluation of actinomycete isolates obtained from herbal vermicompost for the biological control of *Fusarium* wilt of chickpea. *Crop Protection. 30(8)*: 1070-1078.

Gopalakrishnan, S; Srinivas, V; Alekhya, G; Prakash, B; Kudapa, H; Rathore, A and Varshney, R K (2015). The extent of grain yield and plant growth enhancement by plant growth-promoting broad-spectrum *Streptomyces* sp. in chickpea. *SpringerPlus*, *4(1)*: 1-10.

Goudjal, Y; Toumatia, O; Yekkour, A and Sabaou, N (2014). Biocontrol of *Rhizoctonia solani* damping-off and promotion of tomato plant growth by endophytic actinomycetes isolated from native plants of Algerian Sahara. *Microbiol. Res.*, *169*: 59-65.

Gowdar, S B; Deepa, H and Amaresh, Y S (2018). A brief review on biocontrol potential and PGPR traits of *Streptomyces* sp. for the management of plant diseases. *J. Pharmacogn. Phytochem.*, *7(5)*: 3-7.

Hata, E M; Sijam, K; Ahmad, Z A M; Yusof, M T and Azman, N A (2015). *In vitro* antimicrobial assay of actinomycetes in rice against *Xanthomonas oryzae* pv. *oryzicola* and as potential plant growth promoter. *Brazilian Arch. Biol. Technol.*, *58(6)*: 821-832.

Idris, A S (2012). Latest research and management of *Ganoderma* disease in oil palm. *Proc. of the Fourth IOPRI-MPOB International Seminar: Existing and Emerging Pests and Diseases of Oil Palm Advances in Research and Management*. Bandung, Indonesia. p. 1-23.

Idris, A S; Nur Rashyeda, R; Rusli, M H; Sundram S and Norman, K (2016). *Standard Operating Procedures (SOP) Guidelines for Managing* Ganoderma *Disease in Oil Palm*. MPOB, Bangi. 44 pp.

Idris, A S (2019). Integrated *Ganoderma* management in oil palm plantations. *The Planter*, *95(1117)*: 255-262.

Idris, A S and Shariffah-Muzaimah, S A (2021). Nursery and field evaluation of *Streptomyces nigrogriseolus* GanoSA1 to control basal stem rot in oil palm seedlings. *The Planter*, 97(*1141)*: 219-236.

Jacob, S; Sajjalaguddam, R R; Kumar, K V K; Varshney, R and Sudini, H K (2016). Assessing the prospects of *Streptomyces* sp. RP1A-12 in managing groundnut stem rot disease caused by *Sclerotium rolfsii* Sacc. *J. Gen. Plant Pathol.*, *82(2)*: 96-104.

Jog, R; Nareshkumar, G and Rajkumar, S (2012). Plant growth promoting potential and soil enzyme production of the most abundant *Streptomyces* spp. from wheat rhizosphere. *J. Appl. Microbiol.*, *113(5)*: 1154-1164.

Kamal, R and Sharma, A K (2014). Control of *Fusarium* wilt using biological agent *Streptomyces* sp. CPP-53 isolated from compost with plant growth promoting effect on tomato under greenhouse condition. *J. Microbiol. Antimicrob.*, *6(6)*: 97-103.

Kurth, F; Mailänder, S; Bönn, M; Feldhahn, L; Herrmann, S; Groβe, I; Buscot, F; Schrey, S D and Tarkka, M T (2014). *Streptomyces*-induced resistance against oak powdery mildew involves host plant responses in defense, photosynthesis and secondary metabolism pathways. *Mol. Plant. Microbe. Interact.*, *27(9)*: 891-900.

Lehr, N A; Schrey, S D; Hampp, R and Tarkka, M T (2008). Root inoculation with a forest soil streptomycete leads to locally and systemically increased resistance against phytopathogens in Norway spruce. *New Phytol.*, *177(4)*: 965-976.

Lim, P H; Gansau, J A and Chong, K P (2018). *Streptomyces* spp. A potential biocontrol agent against *Ganoderma boninense* of basal stem rot. *J. Oil Palm Res.*, *30*: 265-275.

Lim, S M; Yoon, M Y; Choi, G J; Choi, Y H; Jang, K S; Shin, T S; Park, H W; Yu, N H; Kim, Y H and Kim, J C (2017). Diffusible and volatile antifungal compounds produced by an antagonistic *Bacillus velezensis* G341 against various phytopathogenic fungi. *Plant Pathol. J.*, *33(5)*: 488-498.

Lyu, A; Liu, H; Che, H; Yang, L; Zhang, J; Wu, M; Chen, W and Li, G (2017). Reveromycins A and B from *Streptomyces* sp. 3-10: Antifungal activity against plant pathogenic fungi *in vitro* and in a strawberry food model system. *Front. Microbiol.*, *8(Apr)*. DOI: 10.3389/fmicb.2017.00550.

Manhas, R K and Talwinder, K (2016). Biocontrol potential of *Streptomyces hydrogenans* strain DH16 toward *Alternaria brassicicola* to control damping-off and black leaf spot of *Raphanus sativus*. *Front. Plant Sci.*, *7*: 1-13.

Matsumoto, A and Takahashi, Y (2017). Endophytic actinomycetes: Promising source of novel bioactive compounds. *J. Antibiot.*, *70(5)*: 514-519.

Meena, M; Swapnil, P; Zehra, A; Aamir, M; Dubey, M K; Goutam, J and Upadhyay, R S (2017). Beneficial microbes for disease suppression and plant growth promotion. *Plant-Microbe Interactions in Agro-Ecological Perspectives,* (Singh, D P; Singh, H B and Prabha, R eds.). Springer, Singapore. p. 395-432.

Mun, B G; Lee, W H; Kang, S M; Lee, S U; Lee, S M; Lee, D Y; Muhammad Shahid; B W Yun and Lee, I J (2020). *Streptomyces* sp. LH 4 promotes plant growth and resistance against *Sclerotinia sclerotiorum* in cucumber via modulation of enzymatic and defense pathways. *Plant Soil*, *448*: 87-103.

Musa, H (2017). *Efficacy of* Trichoderma *spp. consortium as potential biocontrol agents of* Ganoderma *disease of oil palm, and involvement of antioxidant enzymes and total phenolic content*. Ph.D thesis, Universiti Putra Malaysia.

Naidu, Y; Idris, A S; Nusaibah, S A; Norman, K and Siddiqui, Y (2015). *In vitro* screening of biocontrol and biodegradation potential of selected hymenomycetes against *Ganoderma boninense* and infected oil palm waste. *For. Path.*, *45(6)*: 474-483.

Naidu, Y; Siddiqui, Y; Rafii, M Y; Saud, H M and Idris, A S (2018). Inoculation of oil palm seedlings in Malaysia with white-rot hymenomycetes: Assessment of pathogenicity and vegetative growth. *Crop Prot.*, *110*: 146-154.

Nur Azura, A B; Yusoff, M; Tan, G Y A; Jegadeesh, R; Appleton, D R and Vikineswary, S (2016). *Streptomyces sanglieri* which colonised and enhanced the growth of *Elaeis guineensis* Jacq. seedlings was antagonistic to *Ganoderma boninense* in *in vitro* studies. *J. Ind. Microbiol. Biotechnol.*, *43(4)*: 485-493.

Olanrewaju, O S and Babalola, O O (2019). Streptomyces: Implications and interactions in plant growth promotion. *Appl. Microbiol. Biotechnol.*, *103(3)*: 1179-1188.

Pacios-Michelena, S; Aguilar González, C N; Alvarez-Perez, O B; Rodriguez-Herrera, R; Chávez-González, M; Arredondo Valdés, R; Ascacio Valdés, J A; Govea Salas, M and Ilyina, A (2021). Application of *Streptomyces* antimicrobial compounds for the control of Phytopathogens. *Front. Sustain. Food Syst.*, *5(September)*: 1-13.

Parveez, G K A; Tarmizi, A H A; Sundram, S; Loh, S K; Ong-Abdullah, M; Palam, K D P; Salleh, K M; Ishak, S M and Idris, Z (2021). Oil palm economic performance in Malaysia and R&D progress in 2020. *J. Oil Palm Res.*, *33(2)*: 181-214.

Patil, H J; Srivastava, A K; Singh, D P; Chaudhari, B L and Arora, D K (2011). Actinomycetes mediated biochemical responses in tomato (*Solanum lycopersicum)* enhances bioprotection against *Rhizoctonia solani*. *Crop Prot.*, *30(10)*: 1269-1273.

Paudzai, F A M; Sundram, S; Yusof, M T; Angel, L P L; Hashim, A M and Abdullah, S N A (2019). Induced systemic resistance and promotion of plant growth in oil palm seedlings by endophytic *Trichoderma virens*. *J. Oil Palm Res.*, *31(4)*: 572-581.

Pieterse, C M J; Zamioudis, C; Berendsen, R L; Weller, D M; Van Wees, S C M and Bakker, P A H M (2014). Induced systemic resistance by beneficial microbes. *Annu. Rev. Phytopathol.*, *52*: 347-375.

Pithakkit, S; Petcharat, V; Chuenchit, S; Pornsuriya, C and Sunpapao, A (2015). Isolation of antagonistic actinomycetes species from rhizosphere as effective biocontrol against oil palm fungal diseases. *Walailak J. Sci. Technol.*, *12(5)*: 481.

Pornsuriya, C and Sunpapao, A (2014). Formulations of *Streptomyces philanthi* RL-1-178 biocontrol agent against sclerotium root and stem rot of chilli pepper (*Capsicum annuum* L.). *Philipp. Agric. Sci.*, *97(3)*: 273-279.

Queendy, V and Roza, R M (2019). Aktivitas antifungi isolat aktinomisetes arboretum Universitas Riau terhadap jamur *Fusarium oxysporum* f. sp *lycopersici* dan *Ganoderma boninense*. *Al-Kauniyah J. Biol.*, *12(1)*: 73-88.

Ramamoorthy, V; Raguchander, T and Samiyappan, R (2002). Induction of defense-related proteins in tomato roots treated with *Pseudomonas fluorescens* Pf1 and *Fusarium oxysporum* f. sp. *lycopersici*. *Plant Soil*, *239(1)*: 55-68.

Rees, R W; Flood, J; Hasan, Y; Potter, U and Cooper, R M (2009). Basal stem rot of oil palm (*Elaeis guineensis*); Mode of root infection and lower stem invasion by *Ganoderma boninense*. *Plant Pathol.*, *58(5)*: 982-989.

Russo, A; Pietro, G; Vettori, L; Felici, C; Cinelli, F and Toffani, A (2012). Plant beneficial microbes and their application in plant biotechnology. *Innovations in Biotechnology* (Aybo, E C ed.). Intech Open, London. p. 57-72.

Sahebi, M; Hanafi, M M; Mohidin, H; Rafii, M Y; Azizi, P; Idris, A S; Fariz, A; Abiri, R; Taheri, S and Moradpoor, M (2018). Antioxidant enzyme activities and secondary metabolite profiling of

oil palm seedlings treated with combination of NPK fertilisers infected with *Ganoderma boninense*. *Biomed Res. Int.*, *2018*. DOI: 10.1155/2018/1494157.

Saikia, R; Kumar, R; Singh, T; Srivastava, A K; Arora, D K and Lee, M W (2004). Induction of defence-related enzymes and pathogenesis-related proteins in *Pseudomonas fluorescens*-treated Chickpea in response to infection by *Fusarium oxysporum* f. sp. *ciceri*. *Mycobiology*, *32(1)*: 47.

Salla, T D; Ramos da Silva, T; Astarita, L V and Santarém, E R (2014). *Streptomyces* rhizobacteria modulate the secondary metabolism of *Eucalyptus* plants. *Plant Physiol. Biochem.*, *85*: 14-20.

Salla, T D; Astarita, L V and Santarém, E R (2016). Defence responses in plants of *Eucalyptus* elicited by *Streptomyces* and challenged with *Botrytis cinerea*. *Planta*, *243(4)*: 1055-1070.

Sangdee, A; Kornphachara, S and Srisawat, N (2016). *In vitro* screening of antagonistic activity of soil *Streptomyces* against plant pathogenic fungi and assessment of its characters. *J. Agric. Technol.*, *12(1)*: 173-185.

Schrey, S D and Tarkka, M T (2008). Friends and foes: *Streptomycetes* as modulators of plant disease and symbiosis. *Antonie van Leeuwenhoek*, *94(1)*: 11-19.

Shao, Z; Li, Z; Fu, Y; Wen, Y and Wei, S (2018). Induction of defence responses against *Magnaporthe oryzae* in rice seedling by a new potential biocontrol agent *streptomyces* JD211. *J. Basic Microbiol.*, *58(8)*: 686-697.

Shariffah-Muzaimah, S A; Idris, A S; Madihah, A Z; Dzolkhifli, O; Kamaruzzaman, S and Cheong, P C H (2015). Isolation of actinomycetes from the rhizosphere of oil palm (*Elaeis guineensis* Jacq.) for antagonism against *Ganoderma boninense*. *J. Oil Palm Res.*, *27(1)*: 19-29.

Shariffah-Muzaimah, S A; Idris, A S; Nur-Rashyeda, R; Naidu, Y; ZainolHilmi, N H and Norman, K (2020). Impact of pre-inoculating soil with *Streptomyces* sp. GanoSA1 on oil palm growth and *Ganoderma* disease development. *Biocatal. Agric. Biotechnol.*, *29*: 101814.

Siddiqui, Y; Naidu, Y and Ali, A (2015). Bio-intensive management of fungal diseases of fruits and vegetables utilizing compost and compost teas. *Organic amendments and soil suppressiveness in plant disease management*. (Meghvansi, M K and Varma, A eds). Springer, Cham. p. 307-329.

Siddiqui, Y; Surendran, A; Paterson, R R M; Ali, A and Ahmad, K (2021). Current strategies and perspectives in detection and control of basal stem rot of oil palm. *Saudi J. Biol. Sci.*, *28(5)*: 2840-2849.

Singh, S P and Gaur, R (2017). Endophytic *Streptomyces* spp. underscore induction of defense regulatory genes and confers resistance against *Sclerotium rolfsii* in chickpea. *Biol. Control*, *104*: 44-56.

Srividya, S; Thapa, A; Bhat, D V; Golmei, K and Dey, N (2012). *Streptomyces* sp. 9p as effective biocontrol against chilli soilborne fungal phytopathogens. *Eur. J. Exp. Biol.*, *2(1)*: 163-173.

Sujarit, K; Mori, M; Dobashi, K; Shiomi, K and Wasu Pathom-aree S L (2020). New antimicrobial phenyl alkenoic acids isolated from an oil palm rhizosphere-associated. *Microorganism*, *8(3)*: 350.

Sundram, S; Palm, M; Board, O; Meon, S; Putra, U; Othman, R and Putra, U (2015). Application of arbuscular mycorrhizal fungi with *Pseudomonas aeruginosa* UPMP3 reduces the development of *Ganoderma* basal stem rot disease in oil palm seedlings. *Mycorrhiza*, *25*: 387-397.

Surendran, A; Siddiqui, Y; Manickam, S and Ali, A (2018). Role of benzoic and salicylic acids in the immunization of oil palm seedlings-challenged by *Ganoderma boninense*. *Ind. Crops Prod*, *122*: 358-365.

Tamreihao, K; Ningthoujam, D S; Nimaichand, S; Singh, E S; Reena, P; Singh, S H and Nongthomba, U (2016). Biocontrol and plant growth promoting activities of a *Streptomyces corchorusii* strain UCR3-16 and preparation of powder formulation for application as bio fertiliser agents for rice plant. *Microbiol. Res.*, *192*: 260-270.

Tan, C J; How, K C; Loh-Mia, P P; Ismet, A; Getha, K; Seki, T and Vikineswary, S (2002). Bioactivity of selected actinomycetes against *Ganoderma boninense*. *Asia-Pacific J. Mol. Biol. Biotechnol.*, *10(2)*: 119-125.

Thakker, J N; Patel, S and Dhandhukia, P C (2013). Induction of defense-related enzymes in banana plants: Effect of live and dead pathogenic strain of *Fusarium oxysporum* f. sp. *cubense*. *ISRN Biotechnol.*, *2013*: 1-6.

Ting, A S Y; Hermantoa, A and Lin, P K (2014). Indigenous actinomycetes from empty fruit bunch compost of oil palm: Evaluation on enzymatic and antagonistic properties. *Biocatal. Agric. Biotechnol.*, *3(4)*: 310-315.

Tuncay, D and Yagar, H (2011). Comparison of polyphenol oxidases prepared from different parts of artichoke (*Cynara scolymus* L.). *Int. J. Food Prop.*, *14(4)*: 809-821.

Viaene, T; Langendries, S; Beirinckx, S; Maes, M and Goormachtig, S (2016). *Streptomyces* as a plant's best friend? *FEMS Microbiol. Ecol.*, *92(8)*: 1-10.

Wonglom, P; Suwannarach, N; Lumyong, S; Ito, S; Matsui, K and Sunpapao, A (2019). *Streptomyces angustmyceticus* NR8-2 as a potential microorganism for the biological control of leaf spots of *Brassica rapa* subsp. *pekinensis* caused by *Colletotrichum* sp. and *Curvularia lunata*. *Biol. Control*, *138*: 104046.

Xue, L; Gu, M Y; Xu, W L; Lu, J J and Xue, Q H (2016). Antagonistic *Streptomyces* enhances defence-related responses in cotton for biocontrol of wilt caused by phytotoxin of *Verticillium dahliae*. *Phytoparasitica*, *44(2)*: 225-237.

Zeng, J; Xu, T; Cao, L; Tong, C; Zhang, X; Luo, D; Han, S; Pang, P; Fu, W; Yan, J; Liu, X and Zhu, Y (2018). The role of iron competition in the antagonistic action of the rice endophyte *Streptomyces sporocinereus* OsiSh-2 against the pathogen *Magnaporthe oryzae*. *Microb. Ecol.*, *76*: 1021-1029.

Zhang, Q; Yong, D; Zhang, Y; Shi, X; Li, B; Li, G; Liang, W and Wang, C (2016). *Streptomyces rochei* A-1 induces resistance and defense-related responses against *Botryosphaeria dothidea* in apple fruit during storage. *Postharvest Biol. Technol.*, *115*: 30-37.

Zhang, S W; Yang, Y; Wu, Z ming and Li, K T (2020). Induced defense responses against *Rhizoctonia solani* in rice seedling by a novel antifungalmycin N2 from *Streptomyces* sp. N2. *Australasian Plant Pathol.*, *49(3)*: 267-276.

Zhao, S; Du, C M and Tian, C Y (2012). Suppression of *Fusarium oxysporum* and induced resistance of plants involved in the biocontrol of *Cucumber fusarium* Wilt by *Streptomyces bikiniensis* HD-087. *World J. Microbiol. Biotechnol.*, *28(9)*: 2919-2927.

Journal of Oil Palm Research Vol. 35 (1) March 2023 p. 168-184
DOI: https://doi.org/10.21894/jopr.2022.0035

TRANSPIRATION OF OIL PALM (*Elaeis guineensis* Jacq.) BASED ON SAP FLOW MEASUREMENT: THE RELATION TO SOIL AND CLIMATE VARIABLES

IPUT PRADIKO[1]*; SUROSO RAHUTOMO[1]; RANA FARRASATI[1]; EKO NOVIANDI GINTING[1]; FANDI HIDAYAT[1] and MUHDAN SYAROVY[1]

ABSTRACT

This study measured sap flow (SF) using Heat Ratio Method (HRM) to estimate the transpiration of two 14 years old oil palms for 29 days. Plant water potential (Ψ_{frond}) was also observed with a psychrometer. Environmental factors such as solar radiation (Qs), vapour pressure deficit (VPD), rainfall (RF), and soil moisture (SM) were also gauged to quantify their contribution to oil palm water flux. Results showed that SF increased after sunrise, peaked after midday, reached a maximum of 386.77-457.79 cm^3 hr^{-1}, and declined thereafter. Environmental factors and Ψ_{frond} explained 76.59%-80.02% variation in quarter-hourly sap flux. The contribution of environment variables on SF followed the order of Qs > VPD > SM > RF. The Ψ_{frond} was opposite with SF and at the lowest point after SF reached the peak for 30-45 min. Minimum values of Ψ_{frond} on palms No. 1 and 2 were -0.84 and -0.78 MPa, respectively. The contribution of environment variables on Ψ_{frond} was less than 24%, with the highest coming from Qs and VPD. Daily stand transpiration of oil palm was at 0.82-1.66 mm day^{-1} which comprised about 30% of stand evapotranspiration. Hence, Qs and VPD showed a significant role in affecting oil palm transpiration in this study.

Keywords: oil palm, plant water potential, sap flow, transpiration, water requirement.

Received: 23 December 2021; **Accepted:** 10 May 2022; **Published online:** 29 June 2022.

INTRODUCTION

Water is the basic requirement for crop growth and development. Water promotes seed germination, mediates nutrition uptake from the soil, circulates minerals and organic nutrients throughout the plant, controls turgor pressure, generates plant cell expansion, supports plant form and function, and controls stomatal movements (Blatt *et al.*, 2014). Hence, adequate water is needed to support plant development and maximise the crop's yield (Nascimento *et al*, 2018).

Amounts of water required by a specific crop vary from one site to another due to the crop growth stages, environmental conditions, and agricultural practices (Pereira and Alves, 2005). There are various methods to estimate crop water requirements, *i.e.*, evapotranspiration based-methods (Doorenbos and Pruitt, 1977), lysimeter method (Ruiz-Penalver *et al.*, 2015), and transpiration based-methods. The transpiration based-methods consist of the Penman-Monteith combination equation (Milne *et al.*, 1985), energy balance method (Milne *et al.*, 1985), water potential based-method (Garnier *et al.*, 1988), gravimetric (Ferrara and Flore, 2003), allometric based-method (Legros *et al.*, 2009) and gas exchange measurements (Ferrara and Flore, 2003; Suresh *et al.*, 2012a). Bayona-Rodríguez and Romero (2016) stated that all methods generally provided information

[1] Indonesian Oil Palm Research Institute (IOPRI), Brigjen Katamso No. 51, 20158, North Sumatra, Indonesia.

* *Corresponding author e-mail: iputpradiko@gmail.com*

about the actual water demand of a specific crop under partially controlled conditions. Thus, direct measurement is needed to determine water use under field conditions.

Not all of the methods stated can be used to estimate water use on perennial crops under field conditions, particularly for oil palm. Unfortunately, measurement of actual water requirements on oil palm is not easy due to the unique vegetative structures, long duration of generative stages (almost three years) (Carr, 2011), monocot vascular tissue (Madurapperuma *et al*., 2009), and morphological structures of oil palm. Heat Ratio Method (HRM) is one of the methods that has been successfully used to measure sap flow (SF) on monocots plants, *i.e*., oil palm (Madurapperuma *et al*., 2009). The HRM is a heat pulse method that can do direct measurements of SF *in situ*, it is relatively cheap and easily automated for continuous, high-resolution monitoring of plant water demand (Smith and Allen, 1996). HRM gauges SF rates and volumetric flow of water in xylem tissue uses a short heat pulse principle (Bleby *et al*., 2004; Burgess *et al*., 2001).

SF is defined as the flow of water in the xylem tissue. SF is also described as a flow of water or assimilates generated by soil water resistance and hydraulic conductance of the plant (Kirkham, 2014). The SF maintains the hydraulic connection between soil and atmosphere (Steppe *et al*., 2015), therefore investigations of SF characteristics can be used to estimate actual water transpiration as well as crop water requirements (Haijun *et al*., 2015; Ismanov *et al*., 2019). Several studies have shown that transpiration response to environmental variables is specific to the climate and ecosystem where plants grow (Xu and Yu, 2020). This information is crucial because it can be used to determine transpiration heterogeneity between stands (Oteino *et al*., 2017) and calculate the ecosystem water budget (Zhao *et al*., 2016).

Moreover, Zhang *et al.* (1999) stated that the effects of the environment on plant water relations could be examined by measurements of SF in conjunction with the component of water potentials (Ψ). Water potentials are fundamental for the movement of water to the leaves in the process of photosynthesis. The gradient between Ψ_{soil} and Ψ_{plant} is the driving force for soil water uptake by the plant, while the gradient between Ψ_{plant} and $\Psi_{atmosphere}$ drives the water movement from the plant to the atmosphere (Fricke, 2017; Zhang *et al*., 2017). On oil palm, water potential can be measured using a psychrometer (Yono *et al*., 2019).

Recent studies on oil palm SF using HRM to estimate transpiration have been carried out by Bayona-Rodríguez and Romero (2016); Brum *et al.* (2020); Ellsäßer *et al.* (2020); Hardanto *et al.* (2017); Merten *et al.* (2016); Niu *et al.* (2015); Röll *et al.* (2015); Santi *et al.* (2021). On the contrary, not many have observed the Ψ_{plant} of oil palm under field conditions, one of which was Suresh *et al.* (2012b). Moreover, measurement of SF and oil palm water potential was still partially done. Hence, the characteristics of oil palm water flux as a response to environment factors are still unclear.

This research employed direct-integrated measurements of SF, Ψ_{plant}, climate, and soil variables in oil palm under field conditions. In addition, this study estimated the actual daily stand transpiration and quantified environmental variables' contribution to oil palm water flux dynamics. Thus, this study was expected to provide more detailed information about primary ecological factors that control oil palm water flux.

MATERIALS AND METHODS

Study Site

The study was conducted from 21 August to 18 September 2018 in Medan, North Sumatera. The study site had a flat topography (slope of 0%-3%) and a dominant soil type of Typic Dystrudepts. Two oil palm trees (*Elaeis guineensis* Jacq.) arranged in a 9 m wide triangle were selected. Both palms were 14 years old and well maintained. The trunk height of palm No. 1 was 6.87 m, while palm No. 2 was 7.35 m. Soil texture around oil palm sample No. 1 was sandy loam with sand, silt, and clay portions of 60%, 32% and 8%, respectively. Oil palm sample No. 2 also had a similar soil texture with the proportion of sand, silt, and clay at 55%, 36% and 9%, respectively. The rainfall (RF) pattern in the study site was equatorially marked by two peaks of the rainy season in May and September (Pradiko *et al*., 2016a). The average annual RF during the period of 2013-2018 was 2164 mm yr^{-1}. Mean air temperature ranged between 27°C to 28°C, while maximum and minimum air temperatures were 38°C and 22°C, respectively. Average relative air humidity was 80%, where lower humidity was in the middle of the year (June-August). Average solar radiation (Qs) fluctuated from 13.69 to 20.07 MJ m^{-2}.

Oil palm is a monocot, and it has a non-wood lignocellulosic material (Hashim *et al*., 2011). In contrast to dicot plants, the xylem and phloem vessels of oil palm are located within a complex structure known as vascular bundle. In the trunk, vascular bundles are scattered with various densities depending on the depth and height (Darwis *et al*., 2013). Niu *et al.* (2015) stated that the vascular bundle density in palm leaf petioles was higher compared with the trunk. It is confirmed in this study (*Figure 5*). Thus, SF and water potential can be measured at the petiole.

Sap flow (SF) measurement. SF velocity measurement was calculated using the following Equations (1) and (2):

$$V_s = \frac{V_c \rho_b (c_w + m_c c_s)}{\rho_s c_s} \quad (1)$$

where,

$$V_c = bV_h + cV_h^2 + dV_h^3 \quad (2)$$

where V_s is sap velocity (cm hr^{-1}), V_c is corrected heat pulse velocity (cm hr^{-1}), V_h is heat pulse velocity (cm hr^{-1}), ρ_b is the basic density of wood (dry weight/fresh volume), ρ_s is density of water, c_w is the specific heat capacity of wood at an average air temperature of 30°C, 1260 J kg^{-1} °C^{-1} (Becker and Edwards, 1999), c_s is the specific heat capacity of the water, 4182 J kg^{-1} °C^{-1} (Lide, 1992), then m_c is the water content of sapwood. Sapwood properties with installed Sap Flow Meter (SFM1) were taken to estimate ρ_b and m_c. Fresh and dry weights of sapwood were gauged before and after oven drying at 60°C for 72 hr. Fresh volume was estimated by immersing the samples in distilled water following Archimedes' principle [modified from Madurapperuma *et al.* (2009)]. V_c was estimated from V_h by using b-d as the correction coefficient (Burgess *et al.*, 2001). In this study, it was assumed that $V_c = V_h$ because the wound diameter was very small [<0.17 cm; minimum wound width listed in Burgess *et al.* (2001)].

V_h was measured using SFM1 produced by ICT International Australia. SFM1 employed the HRM, which gauged the ratio of temperature increment, following the release of a pulse of heat, at points equidistant downstream and upstream from a line heater (Bayona-Rodríguez and Romero, 2016). SFM1 sensors consisted of three probes where one probe located in the middle generated a heat pulse, and the other two were positioned above and below the heater probe equipped with thermocouples. SFM sensors were installed according to standard practice provided by ICT International, including the use of a steel drill guide to ensure that holes were drilled parallel and correctly. Also, including the use of aluminium foil and plastic shield to avoid external disturbances such as Qs, air temperature, *etc.*, SFM1 was attached in the petiole where higher vessel density and homogeneity were located (Madurapperuma *et al.*, 2009). One sensor was installed at frond No. 17 of each palm (*Figure 1*). Frond No. 17 was selected to represent the intermediate value between the upper (frond No. 9) and lower frond (frond No. 25) (Bayona-Rodríguez and Romero, 2016). Frond addition of sampled palms was just at only one frond per month (data not shown); thus, it was assumed that there was no change in fronds number. The heat pulse used was 30 J. The selection of heat pulse levels depends on environmental conditions and the plant's transpiration rate. If during the measurement there is a diagnostic comment, such as 'temperature rises insufficient' then the heat pulse must be increased. But it should be noted that plant tissue could be damaged when the heat pulse level is too high. As a comparison, Bayona-Rodríguez and Romero (2016) used 35 J in similar research conducted previously.

Volumetric SF (Q) was calculated by multiplying V_s with the total area that actively transpires (A) the sap of each petiole near SFM1 attached. 'A' was estimated by multiplying the area and the total number of active vascular bundles. The images of the petiole were processed using ArcGIS 10 to measure the total petiole area, as well as the number and total area of the active vascular bundles. The calculation of the active vascular bundles only addressed the vascular bundles that transpired a safranin solution (*Figure 5*).

Measurement of Frond Water Potential

The frond water potential of the sample palms was measured using a psychrometer (PSY1) produced by ICT International Australia. PSY1 can log changes in plant water status/potential continuously; thus, the data logged by PSY1 directly reflect the energy required to access water (Dixon and Downey, 2013). PSY1 was attached to the petiole of frond No. 17 and maintained using the procedures by Tran *et al.* (2015). PSY1 was placed in the front part of the petiole, while the SFM1 was installed in the back part of the petiole. PSY1 was installed 20 cm away from SFM1, as illustrated in *Figure 1*. Heat pulse velocity (cm hr^{-1}) and frond water potential/ Ψ_{frond} (MPa) data were logged every 15 min during 29 days of observation.

Measurement of soil and climate variables. Observation of soil physical properties included bulk density (g cm^{-3}), porosity (%), permeability (cm hr^{-1}), and soil moisture (SM) (%). For these properties, undisturbed soil samples were collected using a core/ring sampler at the radius of 50 cm, 100 cm, 150 cm and 200 cm from the basal stem. Bulk density was calculated based on the dry weight of the soil and the volume of the ring sampler. Then, porosity was determined from the bulk and particle densities. The particle density was obtained from the ratio of the soil dry weight to soil volume. A pycnometer was employed to calculate soil volume. Meanwhile, the permeameter calculated the permeability. Furthermore, Soil Moisture Meter (SMM) MP 306 was installed at the same radius of soil sampling (*Figure 1*).

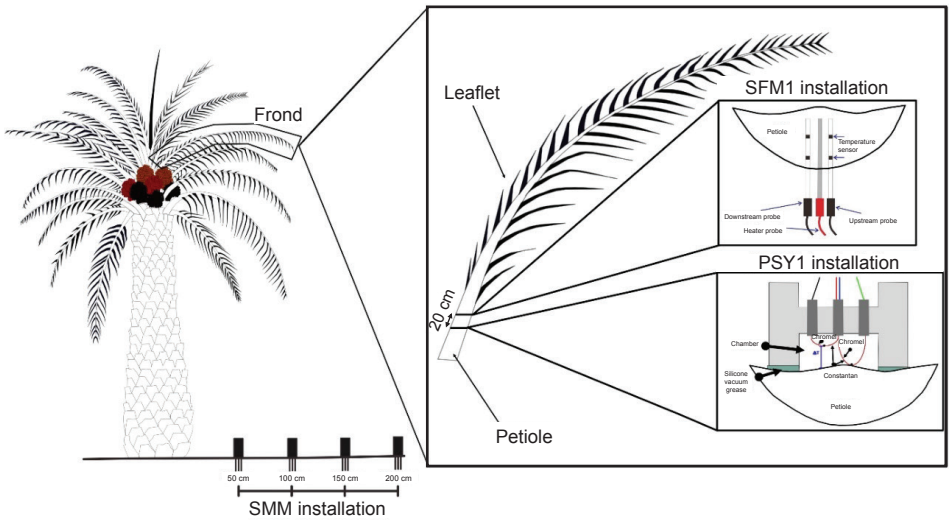


Figure 1. Installation of SFM1, PSY1 and SMM on the plotted palms.

RF (mm), air temperature (°C), relative humidity (%), and Qs (W m^{-2}) were gauged by AWS Davis Vantage Pro-II Plus. The data logging interval of AWS was formatted every 15 min and the same for SFM1, PSY1, and SMM. Vapour pressure deficit (VPD) was estimated from air temperature and relative humidity using an equation postulated by Murray (1967). Daily Qs (MJ m^{-2} d^{-1}) was calculated from the quarter-hourly of Qs (W m^{-2}) based on the following Equation (3):

$$Qs.d = \frac{\Sigma\,(G_{15} \times \text{logging periods})}{1\,000\,000} \qquad (3)$$

where, $Qs._d$ is daily Qs (MJ m^{-2}), $Qs._{15}$ is Qs per 15 min (W m^{-2}), logging periods is 15 min or 900 s.

Data analysis. The daily volumetric SF was cumulated to estimate the total daily transpiration. The multiple linear regression method was employed to determine the effects of Ψ_{frond}, SM, RF, Qs, and VPD on SF dynamic. A similar method was also used to quantify the effects of climate (RF, Qs, and VPD) and SM on Ψ_{frond}. According to Ismanov *et al.* (2019) and Cai *et al.* (2020), gradients of water potential on the soil-plant-atmosphere continuum (SPAC) are a driving force for SF and transpiration.

Data analysis also included quantification of the contribution of Ψ_{frond}, SM, RF, Qs and VPD to the dynamic of SF. Furthermore, the contribution of SM, RF, Qs, and VPD to Ψ_{frond} fluctuations was also quantified. Quantification of the contribution of each variable to SF and Ψ_{frond} was estimated using a computer-intensive relative importance metric developed by Lindemann, Merenda, and Gold (known as metric LMG) (Grömping, 2006; 2015; Lindemann *et al.*, 1980). The metric LMG was calculated using R-software version 4.0.4 and RStudio version 1.4.1106, where its calculation package or the package relaimpo was obtained from the following website: http://prof.beuth-hochschule.de/groemping/software/relaimpo/.

Moreover, the effects of environment variables that have a major contribution to the SF rate (cm^3 hr^{-1}) and Ψ_{frond} were analysed diurnally using a hysteresis curve. The hysteresis curve is commonly used to identify the responses of SF and Ψ_{frond} to environment variables. Analysis using the hysteresis curve was employed in this study because, in a diurnal pattern, changes in environment variables in the morning will result in a different pattern compared to that in the mid-day (Roddy *et al.*, 2013). In this study, plot points in the hysteresis curve were divided into three time zones, they were before dusk (24.00-06.15), daytime (06.30-18.45), and after dawn (19.00-23.45). In this study, the hysteresis of SF and frond was expressed by the area inside the curve or loops.

RESULTS AND DISCUSSION

Soil and Climate Variables Condition

Soil physical properties around sampled palms are shown in *Table 1*. It indicates that soil bulk density increased from the most outer radius to the most inner radius. On the contrary, soil porosity and soil permeability decreased from the most outer radius to the most inner radius.

TABLE 1. SOIL'S PHYSICAL PROPERTIES AT DIFFERENT RADIUS OF 50, 100, 150 AND 200 CM FROM THE BASAL STEM

Radius (cm)	Bulk density (g cm^{-3})	Porosity (%)	Permeability (cm hr^{-1})
50	1.53 ± 0.02	44.05 ± 0.73	0.22 ± 0.09
100	1.40 ± 0.04	49.05 ± 1.75	0.27 ± 0.03
150	1.32 ± 0.04	52.04 ± 1.98	0.52 ± 0.07
200	1.25 ± 0.07	55.04 ± 1.30	0.55 ± 0.03

Note: Soil samples were collected twice in weeding circle of each palm. SE is the standard error.

Figure 2 shows SM (%vwc), RF (mm), Qs (W m^{-2}), and VPD (kPa) during the study. SM at a radius of 200 cm is the highest compared to another radius. The SM pattern followed the pattern of other soil physical properties. The highest SM is found in the soil with lower bulk density, higher porosity, and higher permeability. A previous study showed that soil physical properties in the weeding circle affected SM, where the highest value of average SM was found in the radius of 200 cm (Pradiko *et al.*, 2020).

Furthermore, it has been raining more for the last 15 days of the study. Most of the RF occurred in the afternoon to evening. Therefore, it implied a lower VPD value while Qs was relatively unaffected.

SF Characteristics

SF measurement during the study is shown in *Figure 2*. Overall, SF in both sample plants did not exceed 800 cm^3 hr^{-1}. The SF is similar to Qs and VPD, which is low at night and then peaks during the day. Meanwhile, there is no clear pattern between SF and other environmental variables.

Based on the multiple linear regression analysis, Ψ_{frond} and environmental factors (RF, Qs, VPD, and SM) explained 80.02% and 76.59% of the SF on plant samples No. 1 and 2, respectively. The results are similar to the research conducted by Xu and Yu (2020) on arid and semi-arid ecosystems showing that Qs and VPD are two of three climatic factors besides air temperature that can explain 77.00% to 84.00% of variations in plant SF. Qs and VPD had a major contribution to the SF, which can be seen from the higher value of contribution (%) and correlation coefficient (r) in *Table 2*. VPD explains 33.73% and 25.72% palm 1 and 2 SF dynamics, respectively. The correlation between Qs and SF, as well as VPD and SF, is more than 0.60. Therefore according to Obilor and Amadi (2018), it is classified as significantly strong. Moreover, Qs explain SF dynamic is higher than VPD. Qs also has a considerably stronger correlation to SF than VPD. It means Qs is more dominant in affecting the SF than VPD. Therefore, Qs is more prevalent in affecting the transpiration of oil palm. It is related to research conducted by Xu and Yu (2020) which shows Qs is an environmental factor that acts as the primary driving force for SF.

The findings in this study were different from the research by Bayona-Rodríguez and Romero (2016), which stated that the daily fluctuation of SF depended on weather variations, especially VPD. Brum *et al.* (2020) also noted that VPD assigned more influences on transpiration than PAR (Photosynthetic Active Qsiation). Meanwhile, in another study, Röll *et al.* (2015) stated that transpiration was related to VPD and Qs, though it was unclear which one was more dominant in affecting SF.

Figure 3a shows that the SF rate started to increase at 06:30 am and reached the peak at 00:45-1:00 pm. Average SF at the peak was 386.77 cm^3 hr^{-1} and 457.79 cm^3 hr^{-1} on palm samples No. 1 and 2, respectively. Furthermore, SF tended to plateau and then started to decrease after 3:00 pm. Results of this study were different from the other studies, which described that daily transpiration of oil palm reached the peak at 10:00-11:00 am, it was before maximum Qs (12:00 am-1:00 pm), and when VPD reached the peak (2:00-3:00 pm) (Röll *et al.*, 2015).

Meanwhile, a previous study reported a relatively similar pattern of SF fluctuation using a five-year-old oil palm in Colombia. In that study, the SF rate on oil palm started to increase at 07:30 am, peaked by mid-day, and decreased after 3:50 pm (Bayona-Rodríguez and Romero, 2016). However, the pattern of SF in this study was relatively similar to those in other studies using different plants, *i.e.*, poplar (Zhang *et al.*, 1999), banana (Haijun *et al.*, 2015), and black locust (Zhang *et al.*, 2018).

The plot between quarter-hourly stand SF against Qs and VPD shows clockwise hysteresis loops (*Figure 3b*). The same pattern was observed in hardwood forests (Matheny *et al.*, 2014) and plants in arid and semi-arid ecosystems (Xu and Yu, 2020). The difference in response of SF to the environment before dusk, during the daytime, and after dawn can be seen in the hysteresis loops. During the daytime, the SF rate tended to increase along with the increment of VPD. However, when VPD was higher than 1 kPa, there was no further dramatic increase in transpiration rate; even the SF decreased when VPD was 2.1 kPa. These findings were similar to the previous studies that described a decrease in transpiration of oil palm when VPD was 1.7-2.0 kPa (Carr, 2011; Meijide *et al.*, 2017; Waite *et al.*, 2019). A decrease in transpiration rate is closely associated with stomatal conductance (g_s), where the high value of VPD (Hernandez *et al.*, 2016; Ocheltree *et al.*, 2014; Su *et al.*, 2019) or Qs (Francesconi *et al.*, 1997; Massonnet *et al.*, 2007) cause a depression in the stomatal conductance. Li *et al.* (2019a) added that the concentration of phytohormones, *i.e.*, abscisic acid (ABA), in leaf was correlated positively with the sensitivity of stomata conductances to VPD. It

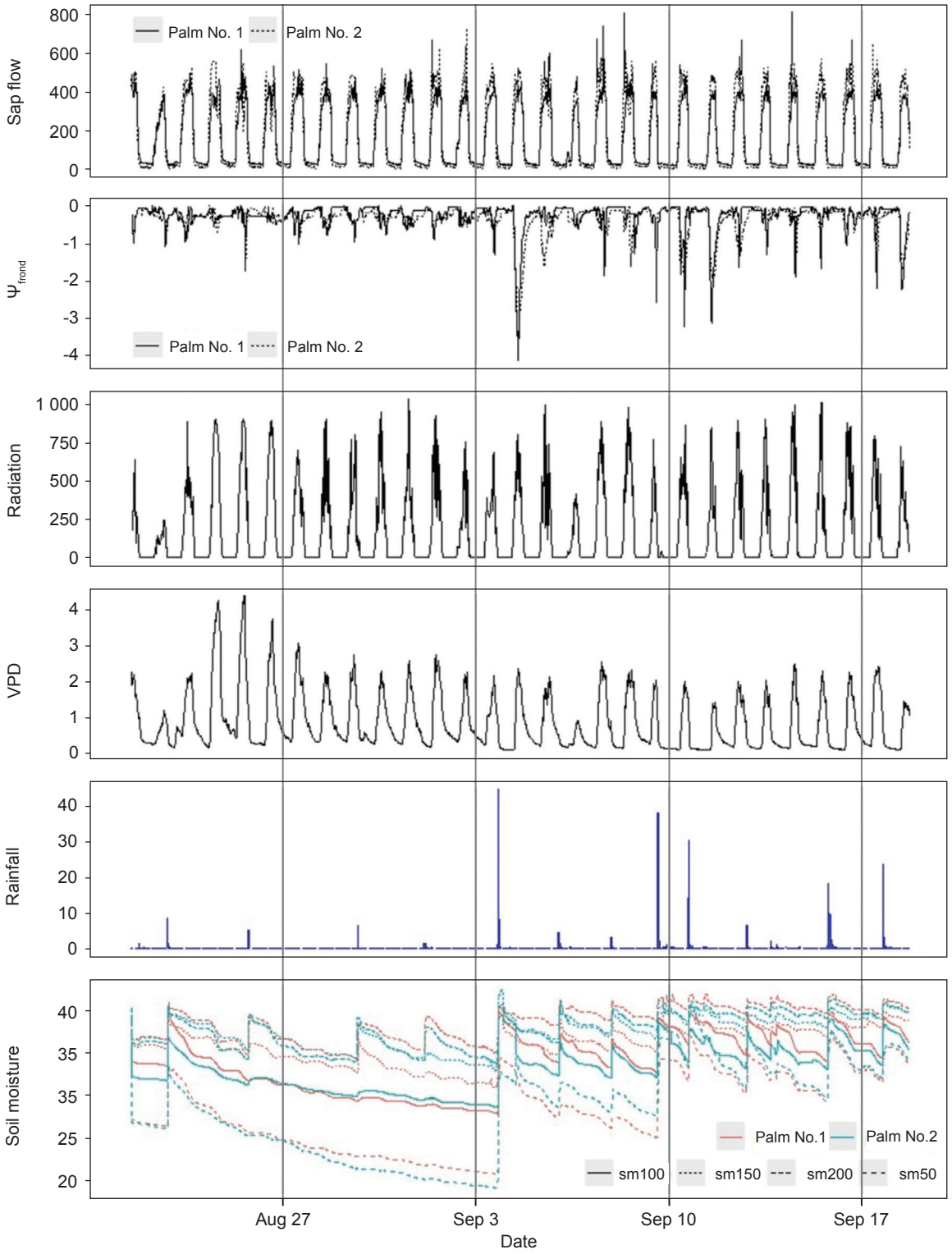


Figure 2. Qs (W m^{-2}), VPD (kPa), RF (mm), SM (%), daily Ψ_{frond} (MPa) and SF (cm^3 hr^{-1}) of frond No. 17 during the observation. SM_{50}, SM_{100}, SM_{150}, and SM_{200} are SM at a radius of 50 cm, 100 cm, 150 cm and 200 cm from the basal stem, respectively.

is unclear whether stomata conductance is a direct response of oil palm to environmental stress or is mediated by a chemical reaction or another signal stress (Waite *et al.*, 2019). In another study, it stated that the stomatal aperture could be regulated by sugars and sugar-derived molecules (Figueroa and Lunn, 2016); water status, turgor, and ABA concentration (Brodribb and McAdam, 2017); CO_2 concentration in ambient air and intercellular air spaces (Engineer *et al.*, 2016).

The SF-hysteresis curve as a function of Qs showed a similar clockwise pattern (*Figure 3c*) to that in *Figure 3b*. An identical pattern was obtained in hysteresis loops between sap flux

TABLE 2. THE CONTRIBUTION AND PARTIAL PEARSON CORRELATION OF VARIABLES TO SAP FLOW (SF)

Variables	Palm 1		Palm 2	
	Contribution (%)	r	Contribution (%)	R
Ψ_{frond}	7.90	-0.46**	8.05	-0.45**
VPD	33.73	0.83**	25.72	0.75**
RF	0.17	-0.08**	0.22	-0.08**
Qs	35.63	0.84**	40.43	0.85**
SM_{50}	0.49	-0.12**	0.37	-0.10**
SM_{100}	0.58	-0.15**	0.55	-0.15**
SM_{150}	0.56	-0.16**	0.63	-0.15**
SM_{200}	0.96	-0.18**	0.60	-0.14**
Total	80.02		76.59	

Note: The contribution (%) was calculated using the metrics LMG (Grömping 2006; 2015).
The total contribution is equal with R^2 of variables to SF.
Ψ_{frond} - frond water potential; VPD - vapour pressure deficit; RF - rainfall; Qs - solar radiation; SM_{50-200} - soil moisture at radius 50 cm, 100, 150 and 200 from basal stem.
**correlation is significant at the 0.01 level (1-tailed).

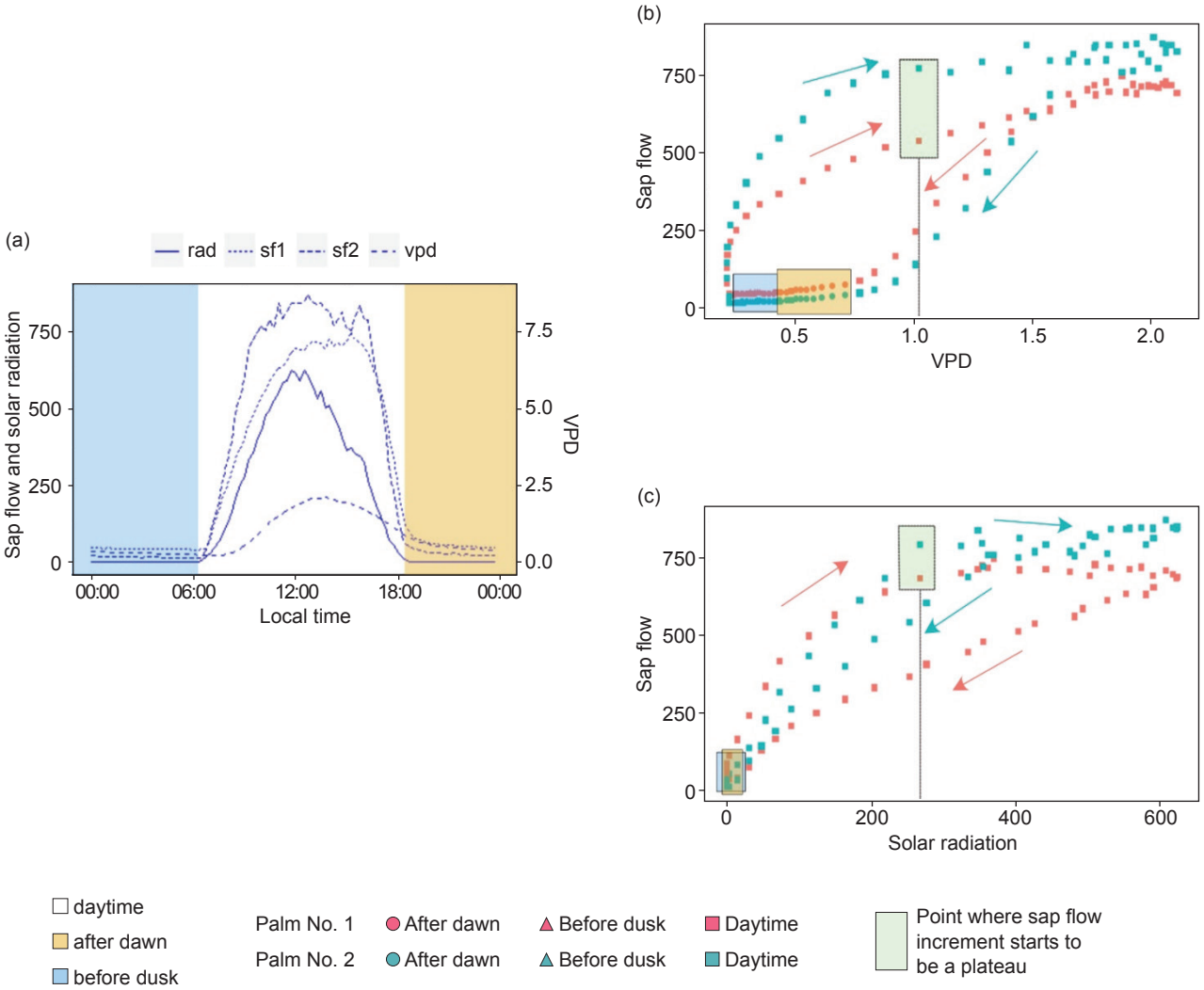


Figure 3. Fluctuation of SF, Qs, and VPD in every 15 min (a) Hysteresis curve of SF as a function of VPD and Qs [(b) and (c)]. SF ($cm^3\ hr^{-1}$), Qs ($W\ m^{-2}$), VPD- vapour pressure deficit (kPa). Arrows in Figures 3b *and* 3c *indicated the progression of the diurnal cycle from sunrise to sunset. The data in the yellow box shows the conditions after dawn, while the data in the blue box shows the conditions before dusk. Box in the black dashed vertical line is a point where the increment of SF rate starts to be a plateau. The detail of average and standard deviation SF, Qs, and VPD data from* Figure 3a *came from the average of all-day data.*

and Qs by Xu and Yu (2020). The data of sap flux response to Qs at night, where there is no light, are low and concentrated in the bottom-left of the curve. During the daytime, the SF rate drastically increased until solar was 267 W m^{-2}; then the SF tended to be stagnant. SF then decreased after Qs was 622 W m^{-2}. These findings were different from the study by Brum *et al.* (2020), which described that decrease in the rate of sap flux density on oil palm occurred when the value of PAR was 600 µmol m^{-2} s^{-1} or 130 W m^{-2} (assumed 1 W m^{-2} = 4,6 µmol m^{-2} s^{-1}) and VPD was more than 1 kPa. Meijide *et al.* (2017) also stated that mature oil palm reached maximum transpiration when PAR was 600 µmol m^{-2} s^{-1}.

Figures 3b and *3c* show that the SF rate is lower in the period after sunset to the time before sunrise. Another interesting fact from the hysteresis curves is that the SF after dawn is slightly higher than before dusk. These conditions indicate that plants are trying to replenish water loss in plants during daytime transpiration (Xu and Yu, 2020). The SF at night reveals the presence of night-time transpiration. The respiration causes night-time transpirational water loss at night. This process can provide more efficiency in using water for leaf expansion (Fricke, 2019). A gradual decrease of the hysteresis curve between SF and VPD before dusk and after dawn indicates that the VPD is involved in regulating night-time transpiration. A previous study on eucalyptus plants showed that VPD and wind speed were factors that drive nocturnal transpiration (Phillips *et al.*, 2010).

Based on the response of the SF rate to VPD and Qs conditions, this study concludes that the SF rate reached the plateau point at VPD of 1 kPa and Qs of 267 W m^{-2}. Dufrene and Saugier (1993) explained that there was no significant change in stomatal conductance and net rate of CO_2 uptake after PAR exceeded 1100 µmol m^{-2} s^{-1} (equal to 239 W m^{-2}) at VPD of 1 kPa. Cheah and Teh (2020) obtained the light saturation for stomatal conductance at about 1500 µmol m^{-2} s^{-1} (equal to 326 W m^{-2}). The plateau point here was defined as a point where the increment in VPD and Qs did not drastically increase the SF rate.

Although this research shows that Qs affect SF more, different combinations of Qs and VPD conditions will affect the SF differently. There is a complex relationship between Qs and VPD in influencing SF dynamics. Qs and VPD had a significant combined effect on SF (Matheny *et al.*, 2014). Thus, further study is needed to understand how these factors affect SF of oil palm. According to Apichatmeta *et al.* (2017), a mature oil palm would reach optimum photosynthesis at a PAR value of 600 µmol m^{-2} s^{-1} without describing its association with VPD. Meanwhile, Meijide *et al.* (2017) reported that transpiration of oil palm started decreasing when the PAR had not reached the maximum point. At this point, stomata had partially closed due to leaf-level water stress initiated by VPD and PAR (Waite *et al.*, 2019). Brum *et al.* (2020) described sap flux which reached the highest point before the maximum value of PAR, showing that the physiological condition of oil palm was more affected by atmospheric water stress than light availability.

Factors Affecting Frond Water Potential

The frond was negatively correlated to the SF (*Figure 2*), with the value of partial Pearson correlation being negatively moderate (*Table 2*). Ψ_{frond} reached the minimum at mid-day (*Figure 5a*), it agreed with the previous study by Suresh *et al.* (2012b). In detail, Ψ_{frond} has the minimum values at about 30-45 min after SF reached the maximum value. The minimum value of Ψ_{frond} on palm samples No. 1 and 2 was -0.84 and -0.78 MPa, respectively. The leaf water potential decreased in the mid-day while the SF increased (Beyer *et al.*, 2018; Zhang *et al.*, 1999). Thus, when the Ψ_{frond} was more negative, the potential gradient between plant and environment would be more significant, and then the SF rate would be higher (Cai *et al.*, 2020).

Analysis of the determination coefficient showed that Ψ_{frond} fluctuation was only able to explain 7.90% of SF fluctuation on palm No. 1 and 8.05% on palm No. 2. It indicates that measurement of Ψ_{frond} solely is insufficient to explain SF dynamic because SF movement is a function of water potential gradients between the SPAC, as stated in the previous study by Steppe *et al.* (2015). A more complete water potential observation (not only in the frond) will determine the relationship between water potential and transpiration. For example, Wang *et al.* (2013) research showed that the potential difference between root and leaf showed a significant relation with transpiration. Furthermore, a study conducted by Zhang *et al.* (2014) showed that the condition of the leaf-root-soil water potential would significantly affect the plant's evapotranspiration.

Plant water potential (represented by Ψ_{frond}) was affected by variables of climate, soil, and condition of the plant (Wang *et al.*, 2013). Quantification of Ψ_{frond} response to climate and soil variables is listed in *Table 3*. The analysis using the LMG Method showed that the effects of climate and soil variables on Ψ_{frond} were not higher than 24%. Climate variables consistently had more impacts on Ψ_{frond} than SM. A similar condition was found in *Robinia pseudoacacia*, where leaf water potential values were more affected by air temperature, air humidity, and Qs than soil temperature (Wang *et al.*, 2013).

Qs and VPD are two variables with the highest values of partial Pearson correlation to Ψ_{frond}. Coolong *et al.* (2012) stated that Ψ_{frond} was well correlated with air temperature, humidity, dew point, and Qs. Nevertheless, VPD only represented 8.53% and 8.39% of Ψ_{frond} fluctuation on palms No. 1 and 2, respectively. Meanwhile, Qs only explained 9.21% and 7.57% of Ψ_{frond} flux on palm samples No. 1 and 2, respectively. There was no consistent contribution of Qs and VPD to the dynamics of Ψ_{frond} on the two plant samples. Therefore the contribution pattern of the two variables on Ψ_{frond} remained unclear.

The less contribution of the environment to the Ψ_{frond} dynamics in this study is related to the complexity of SPAC. Changes in environmental conditions will affect the plant, soil and atmospheric water potential. Therefore, to improve understanding of the water potential dynamic, it is better to simultaneously measure the soil-plant-atmosphere water potential. In addition, the oil palm stem plays a significant role in diurnal water flux by storing water (Waite *et al.*, 2019) and large amounts of carbohydrates to buffer environmental influences (Legros *et al.*, 2009; Suresh *et al.*, 2012b). Therefore, not all ecological changes will immediately affect the dynamics of Ψ_{frond}.

Figures 4a and *4b* reveal that Ψ_{frond} were more negative as Qs and VPD increased. Then, Ψ_{frond} tended to increase drastically to about -0.1 MPa after dawn until dusk. *Figures 4c* and *4d* show the clockwise hysteresis loops. Both figures show that Ψ_{frond} after dawn is lower (more negative) than before dusk. This condition is in line with the pattern of SF response to Qs and VPD. Moreover, Ψ_{frond} reached the minimum value at the mid-day when the VPD value was 2.1 kPa and Qs reached the value of 622 W m^{-2}.

Oil palm is an isohydric plant. It can maintain a more or less constant midday leaf water potential regardless of variations in atmospheric conditions and predawn soil water potential (Hochberg *et al.*, 2018; Martínez-Vilalta and Garcia-Forner, 2017). Isohydric plants are characterised by flatter slopes between predawn and midday water potential (Charrier, 2020; Villalobos-González *et al.*, 2019). The slope between predawn and midday water potential in this study is 0.915 (less than 1 - data not shown), indicating that oil palm is an isohydric species. Consequently, to avoid hydraulic failure, oil palm plants develop considerable plasticity in the hydraulic system, develop embolic resistance from environmental conditions, and take advantage of the large stem capacitance (Waite *et al.*, 2019).

Effects of RF and SM on SF and Ψ_{frond}

In comparison to other variables, RF and SM were not dominant in affecting SF and Ψ_{frond}. A similar result was found in the previous research on black locusts by Zhang *et al.* (2018), where RF and SM were not correlated to the daily stand transpiration. The less contribution of RF was because it did not directly affect SF and Ψ_{frond}. However, it affected Qs, VPD, and SM. RF might decrease Qs and VPD as well as increase SM (Li *et al.*, 2019b). More detailed studies on the effects of RF and SM at several radius in an oil palm weeding circle had been reported by Pradiko *et al.* (2020), where there was a strong and positive correlation between RF and SM.

The results are different from previous studies, which showed a significant SF response to SM as in the study of Ismanov *et al.* (2019); Sitková *et al.* (2014); Zha *et al.* (2017). SM also did not contribute much to Ψ_{frond}. In contrast, other studies explain that SM also plays a vital role in the dynamics of leaf water potential (Rivera-Méndez *et al.*, 2012). *Figure 3* shows that SF and Ψ_{frond} fluctuations do not follow SM changes. For example, SF and Ψ_{frond} tend to be constant even though there was a decrease in SM from 27 August to 4 September. The day after, midday Ψ_{frond} was observed to reach its lowest value on palm samples No. 1 and 2,

TABLE 3. THE CONTRIBUTION AND PARTIAL PEARSON CORRELATION OF VARIABLES TO Ψ_{frond}

Variables	Palm No. 1		Palm No. 2	
	Contribution (%)	r	Contribution (%)	r
VPD	8.53	-0.37**	8.39	-0.37**
RF	0.03	-0.03	0.05	-0.10
Qs	9.21	-0.40**	7.57	-0.37**
SM_{50}	1.37	-0.10**	5.02	-0.12**
SM_{100}	0.86	-0.07**	1.03	-0.04**
SM_{150}	1.35	-0.03	1.12	-0.03
SM_{200}	0.29	-0.02	0.65	-0.05
Total	21.65		23.83	

Note: The contribution (%) was calculated using the metrics LMG (Grömping 2006; 2015). The total contribution is equal with R^2 of variables to Ψ_{frond}. VPD - vapour pressure deficit; RF - rainfall; Qs - solar radiation; SM_{50-200} - soil moisture at radius 50 cm, 100, 150, and 200 from basal stem. **correlation is significant at the 0.01 level (1-tailed).

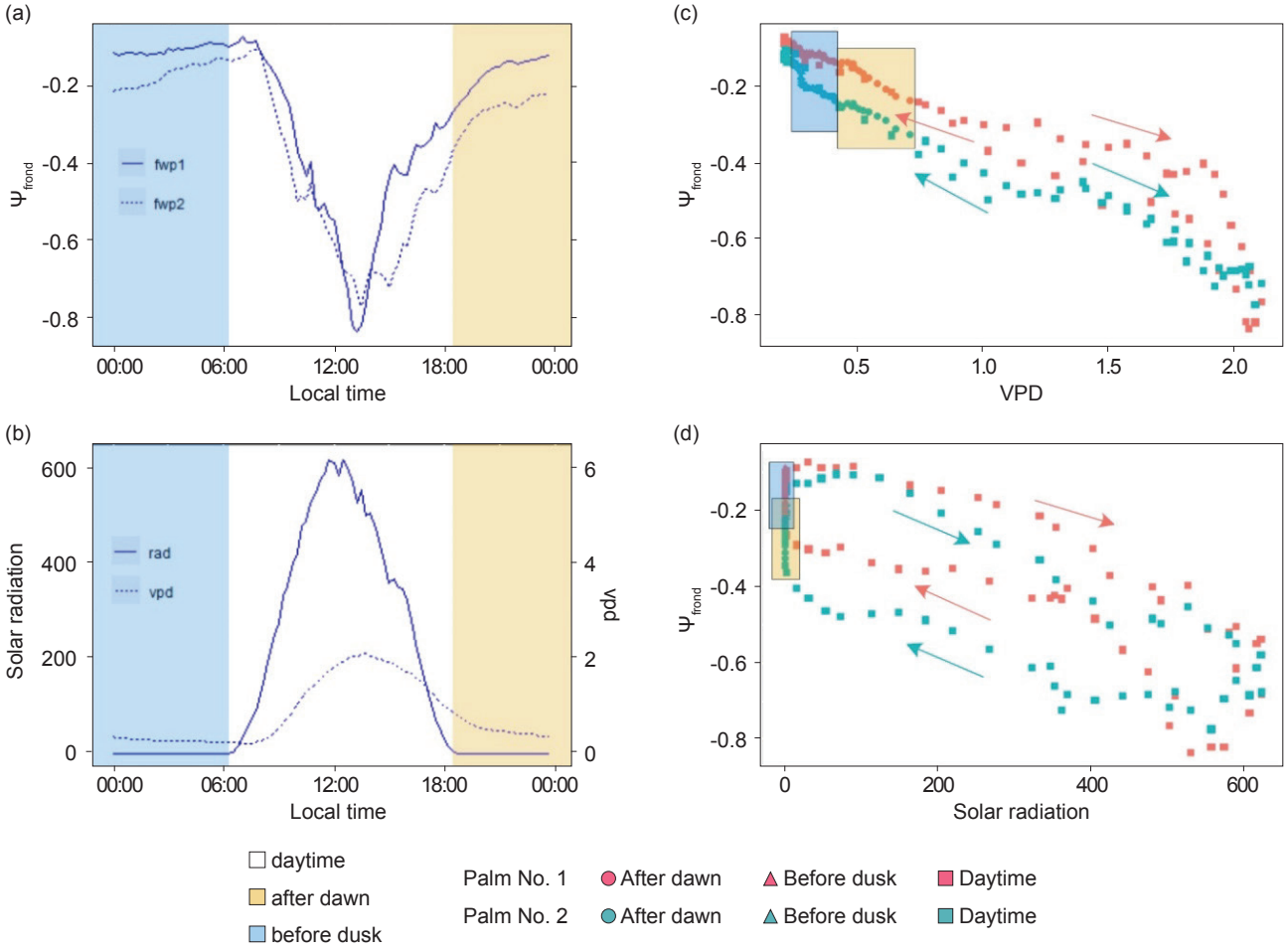


Figure 4. The quarter-hourly data of frond water potential (Ψ_{frond}) (a). VPD and Qs (b). Hysteresis curve for average values of frond water potential as a function of the VPD and Qs [(c) and (d)]. fwp1: frond water potential of palm No. 1 (MPa), fwp2: frond water potential of palm No. 2 (MPa), rad: Qs (W/m²), vpd: vapour pressure deficit (kPa). The arrows in Figures 4c *and* 4d *indicated the progression of the diurnal cycle from sunrise to sunset. The data in the yellow box shows the conditions after dawn, while the data in the blue box shows the conditions before dusk. The details of average and standard deviation frond water potential, Qs as well as VPD data from* Figure 4a *came from the average of all-day data.*

i.e., -3.58 MPa and -4.13 MPa, respectively. The SF value during the plateau phase also tends to be lower than the previous days. The same thing also happened in the period 5-9 September, where Ψ_{frond} did not immediately respond to the decline in SM. Instead, the Ψ_{frond} reduction was observed on 10-11 September. The lag, especially between the decrease in SM and Ψ_{frond}, ensures that oil palm has a specific capacitance in buffering environmental changes.

SM contribution to SF fluctuation was different when compared to Ψ_{frond}. The contribution of SM to SF followed the order of $SM_{200} > SM_{100} > SM_{150} > SM_{50}$ (*Table 2*), and the order was $SM_{50} > SM_{150} > SM_{100} > SM_{200}$ for the contribution of SM to Ψ_{frond} (*Table 3*). This study indicated that SM at the edge of the weeding circle tended to have more influence on SF than those at the other radius. The pattern of SF response to SM was regulated by roots distribution because tertiary and quaternary roots, which have a significant role in water and nutrient uptake, were dominantly found at >150 cm from the basal stem (Pradiko *et al.*, 2016b). However, the contribution pattern of SM to the Ψ_{frond} is difficult to explain. Aside from buffer effects, the absence of drought and drastic changes in SM during the study allegedly caused the contribution of SM to water flux (especially Ψ_{frond}) to be minimal. Waite *et al.* (2019) stated that oil palm growing in riparian areas has lower xylem water potential than in well-drained areas. Therefore, it is necessary to conduct further research in drier areas to ascertain the role of SM in Ψ_{frond}.

Oil Palm Transpiration

As explained before, the SF needs to be multiplied by the area of the active vascular bundles to obtain the oil palm stand transpiration. The density of vascular bundles in the petiole of the two palms is shown in *Figure 5*. It shows that the vascular bundles spread across the entire

cross-section, where more vascular bundles are located near the bark of the petiole. The total area of active vascular bundles for palm samples No. 1 and 2 are 31.890 cm^2 (78.49% of total petiole area) and 34.350 cm^2 (83.36% of total petiole area), respectively. It should be understood that the calculation of vascular bundles is critical so that the estimation of oil palm stand transpiration is not overestimated.

Stand transpiration of the oil palm in this study is shown in *Figure 6*. The daily stand transpiration ranged between 0.83-1.53 mm day^{-1} and 0.82-1.66 mm day^{-1} on the oil palm samples No. 1 and 2, respectively. Furthermore, average transpiration was 1.28 dan 1.39 mm day^{-1} on palm trees No. 1 and 2, respectively. The pattern of daily transpiration of the two palms nearly followed the daily fluctuation of Qs and VPD. The low daily transpiration occurred when the daily Qs were less than 10 MJ m^{-2} day^{-1} and the average VPD was less than 0.5 kPa. Though the daily transpiration increased along with the increment of Qs and VPD, it tended to be stagnant when the Qs were higher than 15 MJ m^{-2} day^{-1}, and the average VPD was higher than 1.0 kPa.

At least for four days, stand daily transpiration was lower than on any other day (*Figure 6*). The combination of Qs and VPD is a significant contributor to this situation. However, there is also an indication that decreasing Ψ_{frond} due to the drop in SM at 1-2 days earlier has a role in lowering stand daily water loss (*Figure* 3). SM may have a more significant contribution in determining daily transpiration in drier areas, such as the southern part of Indonesia (Darlan *et al.*, 2016). Research conducted by Sitková *et al.* (2014) on European beech showed that sap flux would decrease by up to 30% compared to well-irrigated areas under drought stress conditions.

Compared to other previous studies, the transpiration of the 14 years old oil palm in this study was higher than the younger palm. Bayona-Rodríguez and Romero (2016) estimated that transpiration of five years old oil palm was 1.15 mm day^{-1}. Moreover, transpiration of 12 years old oil palm was 1.1 mm day^{-1} by Niu *et al.* (2015) and 2.5 mm day^{-1} by Röll *et al.* (2015). In this study, the stand transpiration of oil palm was relatively similar to the other crops. In comparison, transpiration of rubber was 2.44 mm day^{-1} (Kobayashi *et al.*, 2014), cacao under different shade tree shelters was about 0.5-2.2 mm day^{-1} (Kohler *et al.*, 2014), reforestation and agroforestry stands were about 0.6-2.5 mm day^{-1} (Dierick *et al.*, 2010), and the tropical forest was about 1.0-1.7 mm day^{-1} (McJannet *et al.*, 2007).

Assumed that evapotranspiration of oil palm was about 4.7 mm day^{-1}, it was estimated that transpiration of oil palm in this study comprised about 30% of the stand evapotranspiration. A previous study stated that the transpiration of oil palm included about 8%-53% of total evapotranspiration. The remaining 70% component of the evapotranspiration was the evaporation of the soils and other vegetations on the soil surface. In addition, the trapped water on the leaves petioles might have contributed to the evapotranspiration of oil palm (Röll *et al.*, 2015).

Information about the daily stand transpiration supports oil palm agricultural practices, especially water management. The results can be used for model development to estimate oil palm water requirements and apply water conservation in oil palm plantations. Water conservation is essential to conserve excess water in the rainy season and improve SM in the dry season. High SM in the dry season, where Qs and VPD are pretty high, can increase oil palm productivity (Brum *et al.*, 2020). Several techniques to conserve water in an oil palm plantation, such as silt pit, ridge terrace, or cover crops (Ariyanti *et al.*, 2016). Bare soil should be avoided on the plantation's floor because it can elevate water losses from the ground due to the evaporation process and make the soil vulnerable to erosion and nutrient leaching (Satriawan *et al.*, 2021).

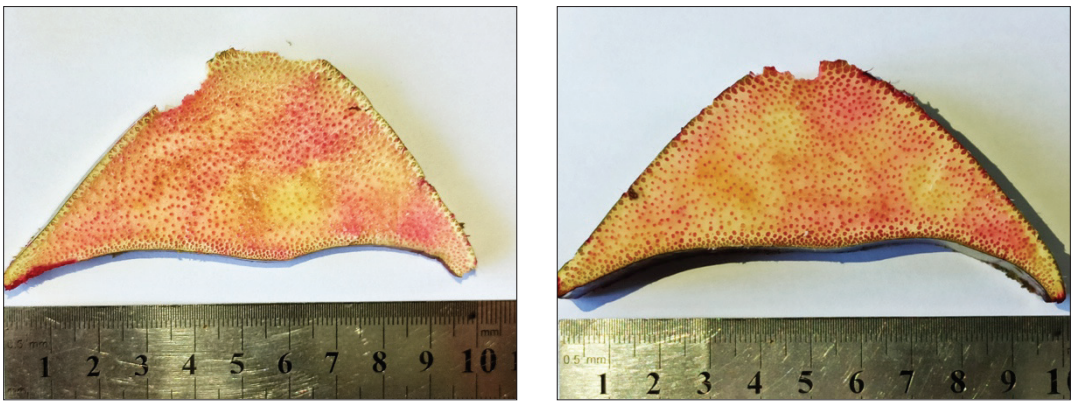


Figure 5. A bottom-up view of the petiole segment from sample palm No. 1 (left) and palm No. 2 (right) after soaking in a container of 1% safranin solution and left to transpire for 72 hr. Some parts were damaged during the preparation of the sample.

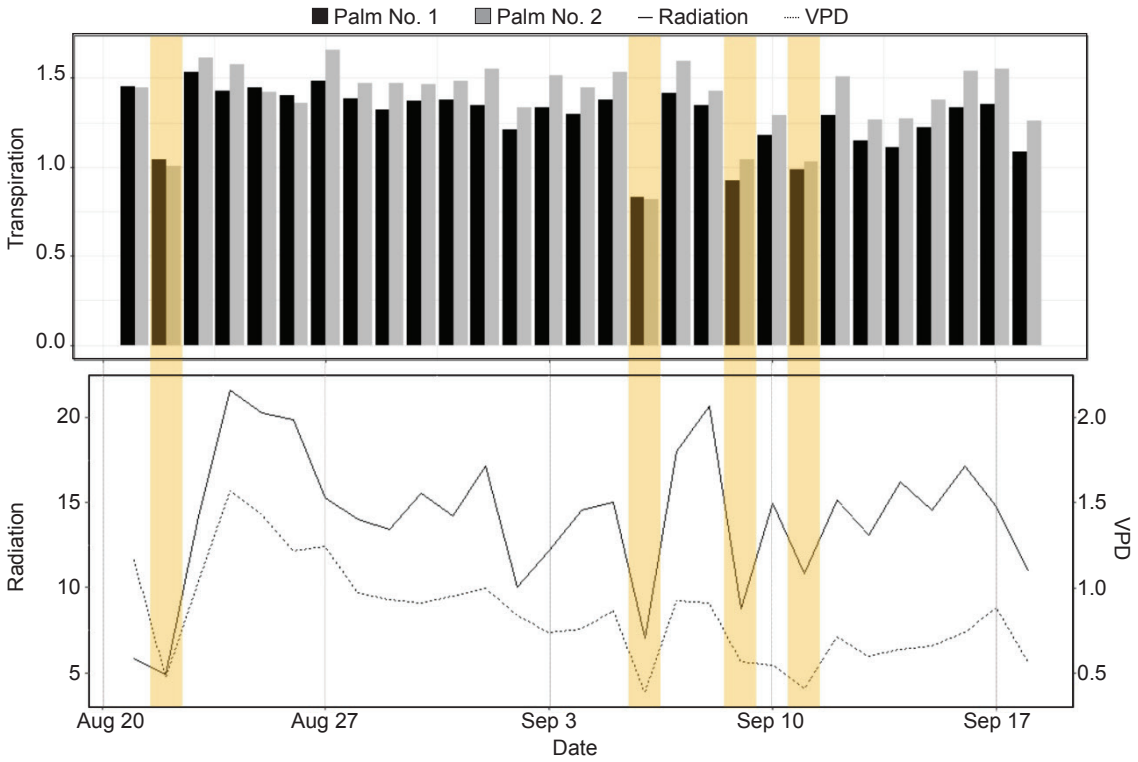


Figure 6. Stand transpiration of the oil palm during the study. The low values of Qs (Qs) and VPD at the beginning of the study were caused by the process of data recording that started at 00:30 pm local time. Transpiration was calculated using SF rate that was measured using HRM. Assumed that the oil palm had 40 fronds and the radius of the canopy was 2.5 m. Unit of the transpiration, Qs, and VPD was mm day^{-1}, MJ m^{-2} day^{-1}, and kPa, respectively. The area highlighted in yellow was the low stand transpiration when the Qs was <10 MJ m^{-2} day^{-1} and or VPD was <0.5 kPa.

CONCLUSION

This study showed that SF on oil palm increased after 06:30 am, reached the peak by mid-day, tended to be a plateau until 03:00 pm, and then decreased thereafter. Environment variables that had a major contribution in affecting SF were Qs > VPD > SM > RF. Frond water potential (Ψ_{frond}) was negatively correlated to the SF. However, the measurement of only Ψ_{frond} may not be sufficient to understand the SF movement in oil palm, it needs to be accomplished with the data of gradient of water potential in the continuum of soil-plant-atmosphere.

Frond water potential decreased as the SF increased, it reach the minimum value when the SF reached the maximum value. Environment variables that had a major contribution to the Ψ_{frond} were Qs and VPD. However, the contribution of environmental variables to the Ψ_{frond} fluctuation was not as high as their contribution to the dynamics of SF. This indicated that changes in environmental conditions might cause more impacts on atmospheric water potential ($\Psi_{atmosphere}$), so there would be changes in gradient potential between $\Psi_{atmosphere}$ and Ψ_{frond} that decrease or increase the SF rate.

This study also revealed that daily stand transpiration of the 14 years old oil palm estimated by SF measurement was about 0.82-1.66 mm day^{-1}. The stand transpiration comprised about 30% of the stand evapotranspiration. Data of stand transpiration are useful for improving agronomic practices, especially in water management.

ACKNOWLEDGEMENT

The authors are grateful for all the support from the Indonesian Oil Palm Research Institute (IOPRI), colleagues, technicians, and reviewers in preparing this article. Moreover, we would also like to thank PT Labodia Prima as the sensors provider.

REFERENCES

Apichatmeta, K; Sudsiri, C J and Ritchie, R J (2017). Photosynthesis of oil palm (*Elaeis guineensis*). *Sci. Hortic.*, *214*: 34-40. DOI: 10.1016/j.scienta.2016.11.013.

Ariyanti, M; Yahya, S; Murtilaksono, K; Suwarto and Siregar, H H (2016). Water balance in oil palm plantation with ridge terrace and *Nephrolepis biserrata* as cover crop. *J. Tropical Crop Sci.*, *3(2)*: 35-41.

Bayona-Rodríguez, C J and Romero, H M (2016). Estimation of transpiration in oil palm (*Elaeis*

guineensis Jacq.) with the heat ratio method. *Agron. Colomb.*, *34(2)*: 172-178. DOI: 10.15446/agron.colomb.v34n2.55649.

Becker, P and Edwards, W R N (1999). Corrected heat capacity of wood for sap flow calculations. *Tree Physiol.*, *19*: 767-768.

Beyer, R; Pretzsch, H and Cournède, P H (2018). The co-regulatory interaction of transpiration and water potential, and implications for stomatal conductance models. *bioRxiv*. p. 1-10. DOI: 10.1101/237826.

Blatt, M R; Chaumont, F and Farquhar, G (2014). Focus on water. *Plant Physiol.*, *164*: 1553-1555. DOI: 10.1104/pp.114.900484.

Bleby, T M; Burgess, S S O and Adams, M A (2004). A validation, comparison and error analysis of two heat-pulse methods for measuring sap flow in *Eucalyptus marginata* saplings. *Funct. Plant Biol.*, *31*: 645-658. DOI: 10.1071/FP04013.

Brodribb, T J and McAdam, S A M (2017). Evolution of the stomatal regulation of plant water content. *Plant Physiol.*, *174*: 639-649. DOI: 10.1104/pp.17.00078.

Brum, M; Oliveira, R S; López, J G; Licata, J; Pypker, T; Chia, GS; Tinôco, R S and Asbjornsen, H (2020). Effects of irrigation on oil palm transpiration during ENSO-induced drought in the Brazilian Eastern Amazon. *Agric. Water Manag.*, *245(4)*: 1-11. DOI: 10.1016/j.agwat.2020.106569.

Burgess, S S O; Adams, M A; Turner, N C; Beverly, C R; Ong, C K; Khan, A A H and Bleby, T M (2001). An improved heat pulse method to measure low and reverse rates of sap flow in woody plants. *Tree Physiol.*, *21*: 589-598.

Cai, G; Ahmed, M A; Dippold, M A and Zarebanadkouki, M (2020). Linear relation between leaf xylem water potential and transpiration in pearl millet during soil drying. *Plant Soil*, *447*: 565-578.

Carr, M K V (2011). The water relations and irrigation requirements of oil palm (*Elaeis guineensis* Jacq.): A review. *Exp. Agric.*, *47(4)*: 629-652. DOI: 10.1017/S0014479711000494.

Charrier, G (2020). Extrapolating physiological response to drought through step-by-step analysis of water potential. *Plant Physiol.*, *184(2)*: 560-561. DOI: 10.1104/pp.20.01110.

Cheah, S S and Teh, C B S (2020). Parameterization of the farquhar-von caemmerer-berry C3 photosynthesis model for oil palm. *Photosynthetica*, *58(3)*: 769-779. DOI: 10.32615/ps.2020.020.

Coolong, T; Snyder, J; Warner, R; Strang, J and Surendran, S (2012). The relationship between soil water potential, environmental factors, and plant moisture status for Poblano Pepper Grown using tensiometer-scheduled irrigation. *Int. J. Vegetable Sci.*, *18(2)*: 137-152. DOI: 10.1080/19315260.2011.591483.

Darlan, N H; Pradiko, I; Winarna and Siregar, H H (2016). Effect of *El Niño* 2015 on oil palm performance in central and southern Sumatera. *Jurnal Tanah dan Iklim*, *40(2)*: 113-120. DOI: 10.21082/jti.v40n2.2016.113-120.

Darwis, A; Nurrochmat, D R; Massijaya, M Y; Nugroho N; Alamsyah, E M; Bahtiar, E T and Safe'I, R (2013). Vascular bundle distribution effect on density and mechanical properties of oil palm trunk. *Asian J. Plant. Sci.*, *12(5)*: 208-2013. DOI: 10.3923/ajps.2013.208.213.

Dierick, D; Kunert, N; Köhler, M; Schwendenmann, L and Hölscher, D (2010). Comparison of tree water use characteristics in reforestation and agroforestry stands across the tropics. *Tropical Rainforests and Agroforests under Global Change: Ecological and Socio-economic Valuations* (Tscharntke, T; Leuschner, C; Veldkamp, E; Faust, H; Guhardja, E and Bidin, A eds.). Springer, Berlin. p. 293-308.

Dixon, M and Downey, A (2013). *PSY1 Stem Psychometer Manual Ver. 4.7*. ICT International, Armidale. 162 pp.

Doorenbos, J and Pruitt, W O (1977). Guidelines for predicting crop water requirements. *FAO Irrigantion and Drainage Paper*. p. 1-144.

Dufrene, E and Saugier, B (1993). Gas exchange of oil palm in relation to light, vapour pressure deficit, temperature and leaf age. *Funct. Ecol.*, *7(1)*: 97-104. DOI: 10.2307/2389872.

Ellsäßer, F; Röll, A; Ahongshangbam, J; Waite, P A; Hendrayanto; Schuldt, B and Hölscher, D (2020). Predicting tree sap flux and stomatal conductance from drone-recorded surface temperatures in a mixed agroforestry system - A machine learning approach. *Remote Sens.*, *12(24)*: 1-20. DOI: 10.3390/rs12244070.

Engineer, C; Hashimoto-Sugimoto, M; Negi, J; Israelsson-Nordstrom, M; Azoulay-Shemer, T; Rappel, W J; Iba, K and Schroeder, J (2016). CO_2 sensing and CO_2 regulation of stomatal conductance: Advances and open questions. *Trends Plant Sci.*, *21(1)*: 16-30. DOI: 10.1016/j.tplants.2015.08.014.

Ferrara, G and Flore, J A (2003). Comparison between different methods for measuring transpiration in potted apple trees. *Biol. Plantarium*, *46(1)*: 41-47. DOI: 10.1023/A:1022301931508.

Figueroa, C M and Lunn, J E (2016). Topical review on sugars a tale of two sugars: Trehalose 6-phosphate and sucrose. *Plant Physiol.*, *172:* 7-27. DOI: 10.1104/pp.16.00417.

Francesconi, A; Lakso, A and Denning, S (1997). Light and temperature effects on whole-canopy net carbon dioxide exchange rates of apple trees. *Acta Hortic.*, *451*: 287-294.

Fricke, W (2017). Water transport and energy. *Plant Cell Environ.*, *40(6)*: 977-994. DOI: 10.1111/pce.12848.

Fricke, W (2019). Night-time transpiration – favouring growth? *Trends Plant Sci.*, *24(4)*: 311-317. DOI: 10.1016/j.tplants.2019.01.007.

Garnier, E; Berger, A and Martin, M (1988). How to estimate leaf transpiration from water potential measurements? *Flora*, *181*: 131-135. DOI: 10.1016/S0367-2530(17)30358-4.

Grömping, U (2006). Relative importance for linear regression in R: The package relaimpo. *J Stat. Softw.*, *17(1)*: 1-27. DOI: 10.18637/jss.v017.i01.

Grömping, U (2015). Variable importance in regression models. *WIREs Comput. Stat.*, *7(2)*: 137-152. DOI: 10.1002/wics.1346.

Haijun, L; Cohen, S; Lemcoff, J H; Israeli, Y and Tanny, J (2015). Sap flow, canopy conductance and microclimate in a banana screenhouse. *Agric. For Meteorol.*, *201*: 165-175. DOI: 10.1016/j.agrformet.2014.11.009.

Hardanto, A; Röll, A; Niu, F and Meijide, A (2017). Oil palm and rubber tree water use patterns: Effects of topography and flooding. *Front. Plant Sci.*, *8*: 1-12. DOI: 10.3389/fpls.2017.00452.

Hashim, R; Nadhari, W N A W; Sulaiman, O; Kawamura, F; Hiziroglu, S; Sato, M; Sugimoto, T; Seng, T G and Tanaka, R (2011). Characterization of raw materials and manufactured binderless particleboard from oil palm biomass. *Mater. Des.*, *32*: 246-254. DOI: 10.1016/j.matdes.2010.05.059.

Hernandez, M J; Montes, F; Ruiz, F; Lopez, G and Pita, P (2016). The effect of vapour pressure deficit on stomatal conductance, sap pH and leaf-specific hydraulic conductance in *Eucalyptus globulus* clones grown under two watering regimes. *Ann. Bot.*, *117*: 1063-1071. DOI: 10.1093/aob/mcw031.

Hochberg, U; Rockwell, F E; Holbrook, N M and Cochard, H (2018). Iso/anisohydry: A plant – environment interaction rather than a simple hydraulic trait. *Trends Plant Sci.*, *23(2)*: 112-120. DOI: 10.1016/j.tplants.2017.11.002.

Ismanov, M; Francis, P; Henry, C and Espinoza, L (2019). Relations among sap flow, soil moisture, weather, and soybean plant parameters in high water demand and final growth stages. *Agric. Sci.*, *10*: 371-385. DOI: 10.4236/as.2019.103030.

Kirkham, M B (2014). Sap flow. *Principles of Soil Plant Water Relations*. Academic Press, Oxford. p. 375-390.

Kobayashi, N; Kumagai, T; Miyazawa, Y; Matsumoto, K; Tateishi, M; Lim T K; Mudd, R G; Ziegler, A D; Giambelluca, T W and Yin, S (2014). Transpiration characteristics of a rubber plantation in Central Cambodia. *Tree Physiol.*, *34*: 285-301. DOI: 10.1093/treephys/tpu009.

Kohler, M; Hanf, A; Barus, H; Hendrayanto and Holscher, D (2014). Cacao trees under different shade tree shelter: Effects on water use. *Agroforest Syst.*, *88*: 63-73. DOI: 10.1007/s10457-013-9656-3.

Legros, S; Mialet-Serra, I; Caliman, J P; Siregar, F A; Clément-Vidal, A and Dingkuhn, M (2009). Phenology and growth adjustments of oil palm (*Elaeis guineensis*) to photoperiod and climate variability. *Ann. Bot.*, *104(6)*: 1171-1182. DOI: 10.1093/aob/mcp214.

Li, J; Zhang, G Z; Xia, L; Wang, Y; Wang, F Z and Li, X M (2019a). Seasonal change in response of stomatal conductance to vapor pressure deficit and three phytohormones in three tree species. *Plant Signal. Behav.*, *14(12)*: 1-11. DOI: 10.1080/15592324.2019.1682341.

Li, J; Mamtimin, A; Zhaogou, L; Jiang, C and Minzhong, W (2019b). Effects of summer rainfall on the soil thermal properties and surface energy balances in the badain jaran desert. *Adv. Meteorol.*, *2019*: 1-13. DOI: 10.1155/2019/4960624.

Lide, D R (1992). *CRC Handbook of Chemistry and Physics: A Ready Reference Book of Chemical and Phyical Data*. CRC Press, Boca Raton. 658 pp.

Lindeman, R H; Merenda, P F and Gold, R Z (1980). *Introduction to Bivariate and Multivariate Analysis.* Scott, Foresman and Company, Glenview. 444 pp.

Madurapperuma, W S; Bleby, T M and Burgess, S S O (2009). Evaluation of sap flow methods to determine water use by cultivated palms. *Environ. Exp. Bot.*, *66*: 372-380. DOI: 10.1016/j.envexpbot.2009.04.002.

Martínez-Vilalta, J and Garcia-Forner, N (2017). Water potential regulation, stomatal behaviour and hydraulic transport under drought: Deconstructing the iso/anisohydric concept. *Plant Cell Environ.*, *40(6)*: 962-976). DOI: 10.1111/pce.12846.

Massonnet, C; Costes, E; Rambal, S; Dreyer, E and Regnard, J L (2007). Stomatal regulation of photosynthesis in apple leaves: Evidence for different water-use strategies between two cultivars. *Ann. Bot.*, *100*: 1347-1356. DOI: 10.1093/aob/mcm222.

Matheny, A M; Bohrer, G; Vogel, C S; Morin, T H; He, L; Prata De Moraes Frasson, R; Mirfenderesgi, G; Schäfer, K V R; Gough, C M; Ivanov, V Y and Curtis, P S (2014). Species-specific transpiration responses to intermediate disturbance in a northern hardwood forest. *J. Geophys. Res.: Biogeosci.*, *119*: 2292-2311. DOI: 10.1002/2014JG002804.

McJannet, D; Fitch, P; Disher, M and Wallace, J (2007). Measurements of transpiration in four tropical rainforest types of North Queensland, Australia. *Hydrol. Process*, *21*: 3549-3564. DOI: 10.1002/hyp.6576.

Meijide, A; Röll, A; Fan, Y; Herbst, M; Niu, F; Tiedemann, F; June, T; Rauf, A; Hölscher, D and Knohl, A (2017). Controls of water and energy fluxes in oil palm plantations: Environmental variables and oil palm age. *Agric. For Meteorol.*, *239*: 71-85. DOI: 10.1016/j.agrformet.2017.02.034.

Merten, J; Röll, A; Guillaume, T; Meijide, A; Tarigan, S; Agusta, H; Dislich, C; Dittrich, C; Faust, H; Gunawan, D; Hein, J; Hendrayanto, A; Knohl, A; Kuzyakov, Y; Wiegand, K and Hölscher, D (2016). Water scarcity and oil palm expansion: Social views and environmental processes. *Ecol. Soc.*, *21(2)*: 5. DOI: 10.5751/ES-08214-210205.

Milne, R; Deans, J D; Ford, E D; Jarvis, P G; Leverenz, J and Whitehead, D (1985). A comparison of two methods of estimating transpiration rates from a sitka spruce plantation. *Boundary-Layer Meteorol.*, *32(1)*: 155-175.

Murray, F (1967). On the computation of saturation vapor pressure. *J. Appl. Meteorol.*, *6*: 203-204.

Nascimento, P T; Castro, G F de and Júnior, J C F B (2018). Water requirement of irrigated and rainfed crops. *Int. J. Hydrol.*, *2(3)*: 338-341. DOI: 10.15406/ijh.2018.02.00093.

Niu, F; Röll, A; Hardanto, A; Meijide, A; Köhler, M and Hölscher, D (2015). Oil palm water use: Calibration of a sap flux method and a field measurement scheme. *Tree Physiol.*, *35*: 563-573. DOI: 10.1093/treephys/tpv013.

Obilor, E I and Amadi, E C (2018). Test for significance of Pearson's Correlation Coefficient (r). *Int. J. Innov. Math. Stat. Energy Policies*, *6(1)*: 11-23.

Ocheltree, T W; Nippert, J B and Prasad, P V V (2014). Stomatal responses to changes in vapor pressure deficit reflect tissue-specific differences in hydraulic conductance. *Plant Cell Environ.*, *37:* 132-139. DOI: 10.1111/pce.12137.

Otieno, D; Li, Y; Liu, X; Zhou, G; Cheng, J; Ou, Y; Liu, S; Chen, X; Zhang, Q; Tang, X; Zhang, D; Jung, E Y and Tenhunen, J (2017). Spatial heterogeneity in stand characteristics alters water use patterns of mountain forests. *Agric. For. Meteorol.*, *236*: 78-86. DOI: 10.1016/j.agrformet.2017.01.007.

Pereira, L S and Alves, I (2005). Crop water requirements. *Encyclopedia of Soils in the Environment*. Elsevier, New York. p. 322-334.

Phillips, N G; Lewis, J D; Logan, B A and Tissue, D T (2010). Inter-and intra-specific variation in nocturnal water transport in Eucalyptus. *Tree Physiol.*, *30*: 586-596. DOI: 10.1093/treephys/tpq009.

Pradiko, I; Farrasati, R; Rahutomo, S; Ginting, E N; Candra, D A A; Krissetya, Y A and Mahendra, Y S (2020). Pengaruh iklim terhadap dinamika kelembaban tanah di piringan pohon tanaman kelapa sawit. *Warta PPKS*, *25(1)*: 39-51.

Pradiko, I; Ginting, E N; Darlan, N H; Winarna and Siregar, H H (2016a). *Hubungan pola curah hujan dan performa tanaman kelapa sawit di Pulau Sumatra dan Kalimantan selama* El Nino *2015. Jurnal Penelitian Kelapa Sawit, 24(2)*: 87-96. DOI: 10.22302/iopri.jur.jpks.v24i2.11.

Pradiko, I; Hidayat, F; Darlan, N H; Santoso, H; Rahutomo, S and Sutarta, E S (2016b). Ukuran lubang tanam dan aplikasi tandan kosong sawit yang berbeda. *Jurnal Penelitian Kelapa Sawit*, *24(1)*: 23-36. DOI: 10.22302/iopri.jur.jpks.v24i1.4.

Rivera-Méndez, Y D; Chacón, L M; Bayona, C J and Romero, H M (2012). Physiological response of oil palm interspecific hybrids (*Elaeis oleifera* H.B.K. Cortes versus *Elaeis guineensis* Jacq.) to water deficit. *Braz. J. Plant Physiol.*, *24(4)*: 273-280. DOI: 10.1590/S1677-04202012000400006.

Roddy, A B; Winter, K and Dawson, T E (2013). Sap flow through petioles and petiolules reveals leaf-level responses to light and vapor pressure deficit

in the tropical tree *Tabebuia rosea* (*Bignoniaceae*). *bioRxiv*. p. 30-34. DOI: 10.1101/000711.

Röll, A; Niu, F; Meijide, A; Hardanto, A; Hendrayanto; Knohl, A and Hölscher, D (2015). Transpiration in an oil palm landscape: Effects of palm age. *Biogeosciences*, *12(19)*: 5619-5633. DOI: 10.5194/bg-12-5619-2015.

Ruiz-Penalver, L; Vera-repullo, J A; Jiménez-buendía, M; Guzman, I and Molina-Martinez, J M (2015). Development of an innovative low cost weighing lysimeter for potted. *Agric. Water Manag*., *151*: 103-113. DOI: 10.1016/j.agwat.2014.09.020.

Santi, L P; Ardiyanto, A; Kurniawan, A; Prabowo, L A and Sebastian, I (2021). Improvement of water and nutrient efficiencies oil palm through bio-silicic acid application. *Menara Perkebunan*, *89(1)*: 26-36. DOI: 10.22302/iribb.jur.mp.v89i1.409.

Satriawan, H; Fuady, Z and Fitri, R (2021). Soil erosion control in immature oil palm plantation. *J. Water Land Dev.*, *49*: 47-54. DOI: 10.24425/jwld.2021.137095.

Sitková, Z; Nalevanková, P; Střelcová, K; Fleischer, P; Ježík, M; Sitko, R; Pavlenda, P and Hlásny, T (2014). How does soil water potential limit the seasonal dynamics of sap flow and circumference changes in European beech? *Forestry Journal*, *60(1)*: 19-31. DOI: 10.2478/forj-2014-0002.

Smith, D M and Allen, S J (1996). Measurement of sap flow in plant stems. *J. Exp. Bot*., *47(305)*: 1833-1844. DOI: 10.1093/jxb/47.12.1833.

Steppe, K; Vandegehuchte, M W; Tognetti, R and Mencuccini, M (2015). Sap flow as a key trait in the understanding of plant hydraulic functioning. *Tree Physiol*., *35(4)*: 341-345. DOI: 10.1093/treephys/tpv033.

Su, Y; Shao, W; Vlcek, L and Langhammer, J (2019). Ecohydrological behaviour of Mountain Beech Forest: Quantification of stomatal conductance using sap flow measurements. *Geoscience*, *9(243)*: 1-16. DOI: 10.3390/geosciences9050243.

Suresh, K; Nagamani, C; Kantha, D L and Kumar, M K (2012a). Changes in photosynthetic activity in five common hybrids of oil palm (*Elaeis guineensis* Jacq.) seedlings under water deficit. *Photosynthetica*, *50(4)*: 549-556. DOI: 10.1007/s11099-012-0062-2.

Suresh, K; Kiran, K M; Lakshmi, K D; Prasanna, L R and Sunil, K K (2012b). Variations in photosynthetic parameters and leaf water potential in oil palm grown under two different moisture regimes. *Indian J. Plant Physiol*., *17(3-4)*: 233-240.

Tran, N; Bam, P; Black, K; Graham, T; Zhang, P; Dixon, M; Reeves, B and Downey, A (2015). Improving irrigation scheduling protocols for nursery trees by relating cumulative water potential to concurrent vapour pressure. *Acta Hortic*., *1085*: 129-134. DOI: 10.17660/ActaHortic.2015.1085.22.

Villalobos-González, L; Muñoz-Araya, M; Franck, N and Pastenes, C (2019). Controversies in midday water potential regulation and stomatal behavior might result from the environment, genotype, and/or rootstock: Evidence from Carménère and Syrah grapevine varieties. *Front. Plant Sci*., *10*: 1-15. DOI: 10.3389/fpls.2019.01522.

Waite, P; Schuldt, B; Link, R M; Breidenbach, N; Triadiati, T; Hennings, N; Saad, A and Leuschner, C (2019). Soil moisture regime and palm height influence embolism resistance in oil palm. *Tree Physiol*., *39(10)*: 1696-1712. DOI: 10.1093/treephys/tpz061.

Wang, X; Zhang, W and Liu, X (2013). Daily variations in transpiration rate and water potential of *Robinia pseudoacacia*. *J. Food Agric. Environ*., *11(1)*: 999-1005.

Xu, S and Yu, Z (2020). Environmental control on transpiration: A case study of a desert ecosystem in Northwest China. *Water*, *12:* 1-16. DOI: 10.3390/W12041211.

Yono, D; Purwanti, E; Sahara, A; Nugroho, Y A; Tanjung, Z A; Aditama, R; Dewi, C; Sihotang, A E; Utomo, C and Liwang, T (2019). Physiology and genotyping of adaptive and sensitive oil palm progenies under unwatered stress condition physiology and genotyping of adaptive and sensitive oil palm progenies under unwatered stress condition. *Proc. of the 2nd International Conference on Natural Resources and Life Sciences*. *IOP Conf. Ser.: Earth Environ. Sci.* Surabaya, Indonesia. p. 1-11.

Zha, T; Qian, D; Jia, X; Bai, Y; Tian, Y; Bourque, C P A; Ma, J; Feng, W; Wu, B and Peltola, H (2017). Soil moisture control of sap-flow response to biophysical factors in a desert-shrub species, *Artemisia ordosica*. *Biogeosciences*, *14(19):* 4533-4544. DOI: 10.5194/bg-14-4533-2017.

Zhang, H; Morison, J I L and Simmonds, L P (1999). Transpiration and water relations of poplar trees

growing close to the water table. *Tree Physiol.*, *19(9)*: 563-573. DOI: 10.1093/treephys/19.9.563.

Zhang, D; Du, Q; Zhang, Z; Ji, X; Song, X and Li, J (2017). Vapour pressure deficit control in relation to water transport and water productivity in greenhouse tomato production during summer. *Sci. Rep.*, *4:* 1-11. DOI: 10.1038/srep43461.

Zhang, Q; Manzoni, S; Katul, G; Porporato, A and Yang, D (2014). The hysteretic evapotranspiration-vapor pressure deficit relation. *J. Geophys. Res. Biogeosci.*, *119:* 125-140. DOI: 10.1002/2013JG002484.

Zhang, Q; Jia, X; Shao, M; Zhang, C; Li, X and Ma, C (2018). Sap flow of black locust in response to short-term drought in southern Loess Plateau of China. *Sci Rep.*, *8:* 1-10. DOI: 10.1038/s41598-018-24669-5.

Zhao, W; Liu, B; Chang, X; Yang, Q; Yang, Y; Liu, Z; Cleverly, J and Eamus, D (2016). Evapotranspiration partitioning, stomatal conductance, and components of the water balance: A special case of a desert ecosystem in China. *J. Hydrol.*, *538*: 374-386. DOI: 10.1016/j.jhydrol.2016.04.042.

SHORT COMMUNICATION

Journal of Oil Palm Research Vol. 35 (1) March 2023 p. 185-192
DOI: https://doi.org/10.21894/jopr.2022.0003

SHORT COMMUNICATION: CULTURABLE BACTERIA POPULATION IN DIFFERENT OIL PALM PEAT SOIL OPERATIONAL ZONES

MOHD SHAWAL THAKIB MAIDIN[1]*; GOGULA SELVI ASANG[2]; MOHD FAHMI KENI[1] and MOHAMED MAZMIRA MOHD MASRI[1]

ABSTRACT

The bacterial community in an ecosystem can contribute to crucial soil ecosystem functions. Different soil variations in a single oil palm tree may lead to the diversity of bacterial populations. Hence, this study aimed to isolate the culturable bacteria from different operational zones in oil palm peat soil. A total of four operational zones, namely Frond Pile (FP), Harvesting Path (HP), Weeded Circle (WC), and Inter Palm Row (IPR) at Sungai Miang, Pekan, Pahang, Malaysia were selected as the sampling plots. The soil samples were cultivated in selective mineral media. The bacterial isolates were obtained by three times repeated series of plating on solid media and grown at 30°C for four days. Results of the 16S ribosomal ribonucleic acid (16S rRNA) discovery revealed a diverse group of bacteria in groups of Proteobacteria, which were detected in a higher percentage relative to other classes of bacteria. The γ-proteobacteria was the prevalent class of Proteobacteria followed by α-proteobacteria and β-proteobacteria. The highest γ-proteobacteria population was obtained in IPR followed by HP, WC and FP. These diverse Proteobacteria communities at the aforementioned operational zones harboured significant roles in the peat soil ecosystems, which need to be further analysed in future research.

Keywords: culturable bacteria, oil palm, operational zones, peat soil.

Received: 31 December 2020**; Accepted:** 14 November 2021**; Published online:** 17 January 2022.

INTRODUCTION

Oil palm (*Elaeis guineensis* Jacq.) is planted in an equilateral triangular design with a spacing of 8.50-10.25 m (Corley and Tinker, 2003). There is significant variability in soil properties on the scale of individual palms, caused by plant features and management practices (Anamulai *et al*., 2019; Tinker, 1960). Oil palm is becoming an increasingly important crop in the tropics (Cramb and Curry, 2012), and accurate evaluation of soil properties under oil palm is crucial to the industry's productivity and sustainability. Consideration of tree-scale variability is needed for soil condition monitoring, fertiliser application recommendations, and calculations of water, carbon, and nutrient stock (Nelson *et al*., 2014; 2019).

Soil biodiversity plays a major role in the functioning of the ecosystem, which helps to maintain soil sustainability (Delgado-Baquerizo *et al*., 2020). However, information on the ecosystem function in different oil palm operational zones is still lacking. According to Carron *et al*. (2015), the zones around the palms contain varying amounts of soil fauna and nutrients. The samples collected

[1] Malaysian Palm Oil Board,
6 Persiaran Institusi, Bandar Baru Bangi,
43000 Kajang, Selangor, Malaysia.

[2] School of Agriculture Sciences and Biotechnology,
Faculty of Bioresources and Food Industry,
Universiti Sultan Zainal Abidin, Besut Campus,
22200 Besut, Terengganu, Malaysia.

* *Corresponding author e-mail: shawal@mpob.gov.my*

in any particular management zone do not describe anything about processes in other zones, which may be important for the palm. As a result of typical management regimes, direct linkage of the operational zones with the soil microbes in an oil palm plantation, which is crucial for many critical ecosystem functions, including nutrient cycling, carbon sequestration and plant nutrient uptake (Schröder *et al*., 2016), requires further investigation.

This study involves the cultivation and comparison of the bacterial diversity in the peat soil of an oil palm plantation in Pekan, Pahang, Malaysia. The studied area was the four operational zones, which consists of the frond pile (FP), harvesting path (HP), weeding circle (WC), and inter palm row (IPR).

METHODOLOGY

Soil Sampling

A sampling of soil for methanotrophic bacteria diversity study at fertilised oil palm plantation, Pekan, Pahang, Malaysia, was conducted from four operational zones consisting of FP, HP, WC and IPR (*Figure 1*) in August 2017. Sampling was done at the respective GPS coordinates of 3°26'09.748" N, 103°23'23.555" E, 3°26'10.794" N, 103°23'17.438" E, 3°26'18.062" N, 103°23'19.458" E and 3°26'17.328" N, 103°23'28.560" E at a depth of 0-30 cm. Soil sampling was done in triplicates using a 5 cm internal diameter auger, carefully kept in the ice box, and stored at -80°C for further analysis.

Enrichment Culture

The basal medium, nitrate mineral salts (Whittenbury *et al*., 1970), was used for bacterial consortium enrichment. 1 L of the basal medium was sterilised by autoclaving at 121°C for 15 min. Then, a total of 1 g of the soil sample was inoculated into a serum flask filled with a 20% capacity of the basal medium. Methane gas was continuously supplied at 10% (v/v). The culture was stirred at 150 rpm in a shaker incubator and incubated at 30°C for three days.

Isolation of Soil Bacteria

Nitrate mineral salt agar, nutrient agar, soil enriched medium, nitrogen-deficient medium, Pikovskaya medium, Aleksandrov medium, anaerobic medium and actinomycetes medium were used for bacterial isolation using the spread plate method. Isolated colonies were subcultured repeatedly to obtain a single type of isolated bacterial colony. The culture was incubated at 30°C for three days.

Polymerase Chain Reaction (PCR) Amplification of 16S Ribosomal Ribonucleic Acid (16S rRNA) and Purification

Isolates from plate cultures were added into 100 µL of sterilised distilled water and boiled for 10 min at 100°C to lyse the cells and subsequently amplified using PCR. The primer set used was forward (f) primer, 341f (5'-cct-acg-gga-ggc-agc-ag-3') and reverse (r) primer 907r (5'-ccc-cgt-caa-

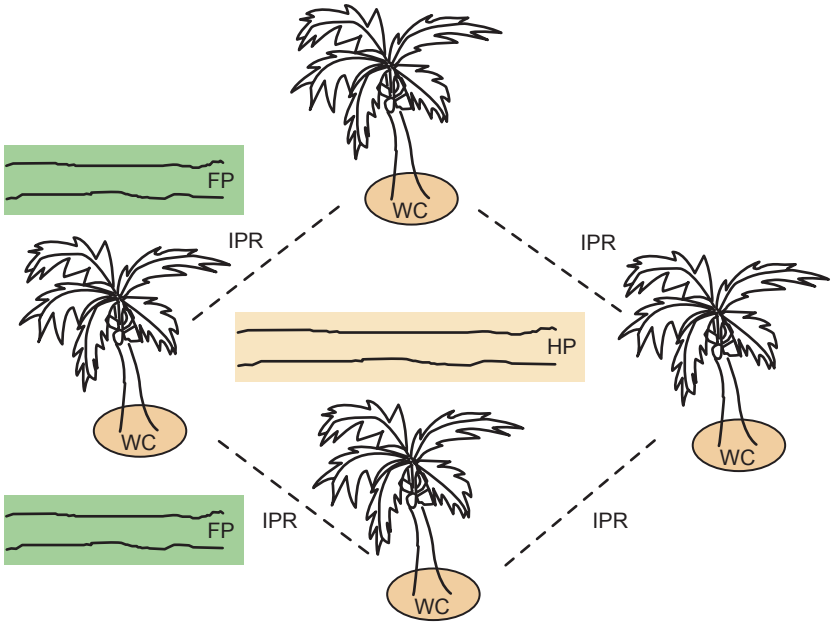


Figure 1. Typical operational zones of a mature oil palm plantation. The pattern is repeated throughout the plantation. Operational zones are the frond pile (FP), where pruned fronds are placed, the weeded circle (WC), which is kept bare to facilitate harvesting, the harvest path (HP), upon which fruit is removed from the plantation and workers access for other management practices, and the inter palm row (IPR), is the space between palms.

ttc-att-tga-gtt-t-3′) using the PCR program (Muyzer *et al*., 1993). The PCR was performed in 25 µL of reaction volume with a thermocycler (gradient) containing a succession of 10 pmol of each primer, 100 mM dNTPs, 1X PCR buffer, 50 mM Mg_2Cl, 0.3% BSA, and 2.5 units of Taq polymerase. The PCR started with initial denaturation at 94°C for 2 min, 35 cycles of 94°C for 30 s, 52°C for 30 s and 72°C for 30 s, final extension at 72°C for 2 min, and held at 10°C. Eluted DNA from excised agarose gel was purified using QIAquick gel extraction kits (QIAGEN, Inc., Valencia, CA, USA) according to the kit's protocol.

Sequencing Analysis

The purified PCR products were sent to First Base Laboratories for sequencing. The nucleotide sequences were read using the software ChromasPro (www.technelysium.com.au/ChromasPro.html) and analysed using an online sequence database available at the National Center for Biotechnology Information (NCBI). A sequence similarity search was conducted using the nucleotide-nucleotide basic logic alignment search tool (BLASTn) in the NCBI GenBank database to identify the nearest relatives of the partially sequenced 16S rRNA genes of excised bands.

Statistical and Phylogenetic Analysis

Alpha diversity and principal component analysis (PCA) matrices scatter biplot were performed based on the identified isolated bacteria to compare the bacterial diversity in the soil samples among the four aforementioned operational zones using the PAST software program (Hammer *et al*., 2001).

The nucleotide sequences determined in this study were aligned, and neighbour-joining trees were constructed using Molecular Evolutionary Genetics Analysis (MEGA) version 7.0 (Kumar *et al*., 2016). Neighbour-joining phylogenetic trees were constructed based on the 16S rRNA gene by using the Kimura two-parameter substitution model evaluated by 1000 bootstrap samplings of the data, and nodes with bootstrap values were indicated.

RESULTS AND DISCUSSION

Based on the data of total microbes, the Dominance (D) and Berger Parker indices data in *Table 1* showed that the Proteobacteria dominated the soil community. This is due to the highest value of Proteobacteria classes compared to other bacterial classes. Among them, β-proteobacteria was the most dominant, followed by α-proteobacteria and γ-proteobacteria. In comparison, the Shannon (H) index (*Table 1*) shows that bacilli was the most diverse among other bacterial classes.

The relative abundance of the identified bacterial classes was plotted in *Figure 2* and the accession number is included in *Table 2*. The Proteobacteria was the most prevalent phylum amongst the prokaryotic population. Firmicutes was the second most frequent, followed by Actinobacteria. The phylum Bacteroidetes for class Sphingobacteria could only be found in the HP area and was also the only site, which did not harbour the ß-proteobacteria. The γ-proteobacteria was found in the highest percentage and could be found within all sites with the highest occurrence in IPR (52%), followed by HP (32%), WC (29%), and FP (10%). The second prevalent class was α-proteobacteria, which mostly appeared in FP (43%), followed by HP (32%), WC (10%), and IPR (5%). ß-proteobacteria could be found mostly in WC (14%), IPR (10%), and FP (5%). Bacterial class of bacilli can also be found in peat soil with the percentage occurrence of FP (38%), WC, and IPR both (24%), and HP (21%). Whilst, the percentage of occurrences in class Actinobacteria were WC (24%), HP (11%), IPR (10%), and FP (5%).

PCA was used to correlate the bacterial classes with the operational zones (*Figure 3*). The differences between the bacterial communities can be seen clearly in the distribution of the bacterial classes. The α-proteobacteria and bacilli were generally clustered together in the FP. Both classes are essential in FP, mainly involved in decomposition and as an additional carbon source (Hirano *et al*., 2009). The α-proteobacteria was also clustered in HP along with γ-proteobacteria. Most of the known methanotrophs belong to α-proteobacteria and γ-proteobacteria (Semrau *et al*., 2010). This is an

TABLE 1. BACTERIAL BIODIVERSITY INDICES FOR 16S rRNA GENE LIBRARIES REPRESENTING PEAT SOIL SAMPLE PEKAN, PAHANG, MALAYSIA

Diversity indices	Bacterial class				
	Actinobacteria	Bacilli	Proteobacteria		
			Alpha	Beta	Gamma
Dominance_D	0.3288	0.2653	0.3701	0.3817	0.3086
Berger-Parker	0.4800	0.3551	0.4778	0.4828	0.4228
Shannon_H	1.238	1.358	1.125	1.022	1.259

TABLE 2. SUBMITTED NCBI BLASTn BACTERIAL NAME AND ACCESSION NUMBER

Description	Accession
Sphingomonas zeae	KX682019.1
Sphingomonas paucimobilis	LN867216.1
Sphingomonas zeae strain	KX682019.1
Methylobacterium radiotolerans	KT592238.1
Stenotrophomonas sp.	KY084474.1
Methylobacterium radiotolerans	KT923692.1
Pseudarthrobacter defluvii	KY882049.1
Stenotrophomonas sp.	KY084474.1
Sphingomonas zeae	KX682019.1
Methylobacterium radiotolerans	KF777382.1
Luteibacter jiangsuensis	KY029044.0
Stenotrophomonas maltophilia	JN592614.1
Methylobacterium radiotolerans	KF777382.1
Paenibacillus barengoltzii	KP704353.1
Arthrobacter defluvii	FN908791.1
Stenotrophomonas maltophilia	JN592614.1
Stenotrophomonas sp.	KY084474.1
Luteibacter jiangsuensis	KY029044.1
Luteibacter jiangsuensis	KY029044.1
Staphylococcus sp.	KF777547.1
Bacillus koreensis	KT986105.1
Staphylococcus epidermidis	KR809425.1
Bacillus subtilis	JQ246902.1
Bacillus subtilis	KX453903.1
Staphylococcus sp.	KY865751.1
Bacillus subtilis	KX453903.1
Arthrobacter chlorophenolicus	GU326384.1
Moraxellaceae bacterium	KF777626.1
Micrococcus luteus	LN884071.1
Arthrobacter sp.	KY476117.1
Pseudarthrobacter defluvii	KY882049.1
Pandoraea thiooxydans	CP014839.1
Moraxellaceae bacterium	KF777626.1
Moraxella osloensis	LT718623.1
Arthrobacter sp.	KY476117.1
Brevibacillus fluminis	KF958491.1
Bacillus altitudinis	KY820045.1
Brevibacillus fluminis	NR_116293.1
Staphylococcus hominis	KP780178.1
Spirometra erinaceieuropaei	LN020105.1
Bacillus altitudinis	KY820045.1
Brevibacillus sp.	KU578096.1

Description	Accession
Brevibacillus fluminis	NR_116293.1
Serratia sp.	KY848325.1
Bacillus thuringiensis	KU180424.1
Bacillus cereus	KY029074.1
Pseudarthrobacter equi	LT629779.1
Bacillus sp.	JX532715.1
Pseudomonas stutzeri	KF318832.1
Bacillus megaterium	FJ944677.1
Brevibacillus panacihumi	KU921113.1
Bacillus flexus	KX853169.1
Mesorhizobium soli	NR_145552.1
Luteibacter jiangsuensis	KY029044.1
Burkholderia sp.	JQ316420.1
Dyella yeojuensis	FN796854.1
Bacillus amyloliquefaciens	AB735985.1
Serratia marcescens	KU522248.1
Serratia sp.	KY848325.1
Rhizobium sp.	KU097063.1
Methylobacterium radiotolerans	KY882119.
Sphingomonas sp.	FR872453.1
Ochrobactrum sp.	HQ652578.1
Luteibacter jiangsuensis	KY029044.1
Luteibacter jiangsuensis	KY029044.1
Dyella yeojuensis	FN796854.1
Methylobacterium oryzae	AY683046.1
Methylobacterium radiotolerans	KF777382.1
Ralstonia sp.	KF777622.1
Dyella japonica	AM268334.1
Methylobacterium radiotolerans	KF777382.1
Luteibacter jiangsuensis	KY029044.1
Amycolatopsis sp.	KP232907.1
Streptomyces diastaticus	KY458979.1
Burkholderia soli	KP687356.1
Luteibacter jiangsuensis	KY029044.1
Brevundimonas aurantiaca	KC429645.1
Methylobacterium oryzae	AY683046.1
Pedobacter cryoconitis	KC788066.1
Massilia aurea	LT718650.1
Oxalobacteraceae bacterium	KM274103.1
Pseudomonas luteola	KX301304.1
Dyella japonica	AM268334.1

exciting discovery since both bacterial classes were also reported to co-dominate the active methane-oxidising communities in an acidic boreal peat bog (Esson *et al*., 2016). The soil structure in HP usually has a higher bulk density to facilitate the movement of labour and equipment on the plantation (Melling and Henson, 2011). Actinobacteria and ß-proteobacteria were both clustered together in WC, whereas γ-proteobacteria was only clustered in IPR. WC-clustered actinobacteria can play critical roles in various plant growth-promoting attributes, such as phosphorus solubilisation, potassium and zinc, and biological nitrogen fixation (Yadav and Yadav, 2019). Both HP and IPR showed the prevalent cluster of γ-proteobacteria. Further research needs to be conducted to unravel the role of γ-proteobacteria in methane mitigation in these two operational zones and oil palm plantations subsequently.

Phylogenetic tree indicated the presence of 56 bacterial species isolated from peat soil is shown in *Figure 4*. This phylogenetic tree was constructed based on similar nucleotide sequences using BLASTn, Kimura two-parameter algorithm, and the neighbour-joining method. The major phyla of Firmicutes, Actinobacteria, Proteobacteria, and Bacteroidetes are shown and clustered. The abundance presence of bacterial genus under the class of α-proteobacteria and γ-proteobacteria would be related to previous studies on their contribution to the global nutrient cycle. According to Aislabie and Deslippe (2013), the important genus isolated for α-proteobacteria was among the heterotroph and methanotrophs. The genera include *Methylobacterium*, *Mesorhizobium*, *Rhizobium*, and *Sphingomonas*. *Methylobacterium* plays a major role as a soil methane oxidiser. Both *Mesorhizobium* and *Rhizobium* have dual functions as nitrogen fixers and form a symbiotic relationship with legumes. In contrast, *Sphingomonas* can degrade toxic compounds like pentachlorophenol and polyaromatic hydrocarbons. The *Pseudomonas* genus in γ-proteobacteria was implicated in oil degradation studies. Under aerobic conditions, isolated *Pseudomonas* genes and enzymes can degrade alkanes, monoaromatics, naphthalene, and phenanthrene as a sole carbon source (Martirani-Von Abercron *et al*., 2017).

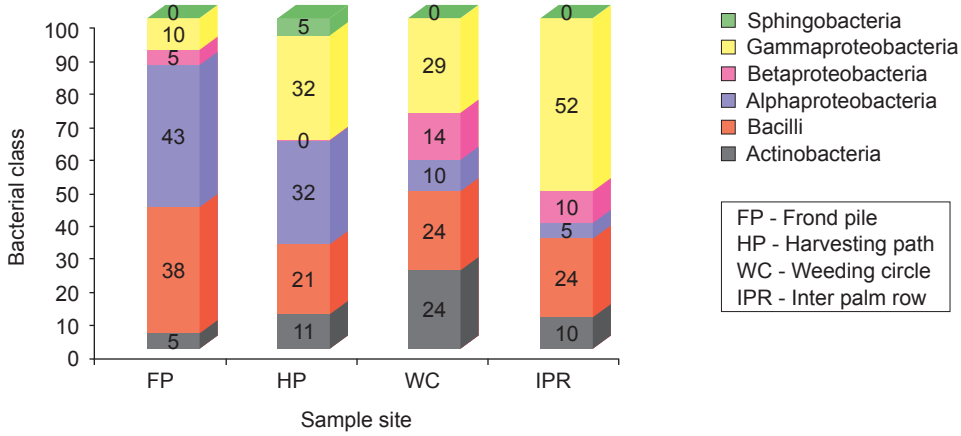


Figure 2. Percentage of bacterial class via 16S rRNA gene identification.

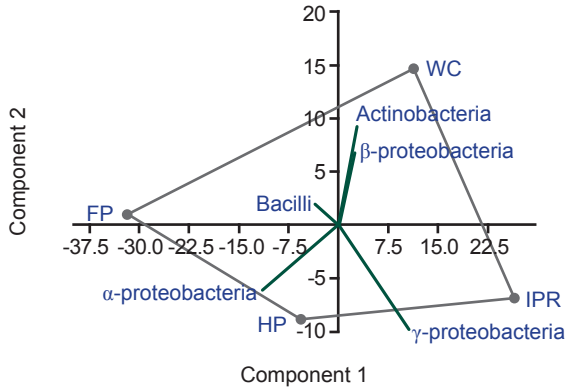


Figure 3. Principal Component Analysis (PCA) of bacterial classes isolated from oil palm peat soil at Pekan, Pahang, Malaysia.

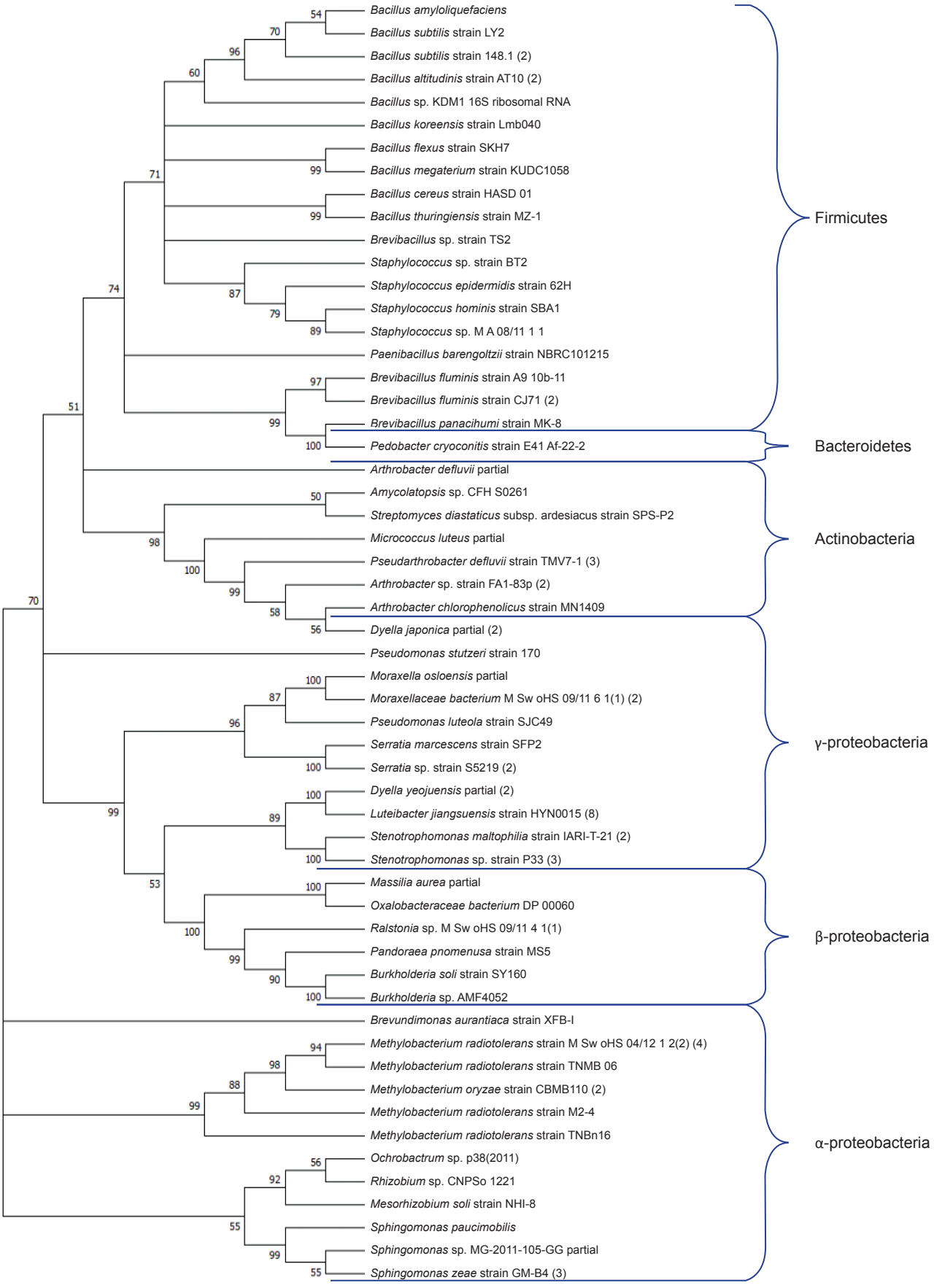


Figure 4. Phylogenetic tree derived from microbes isolated from peat soil at Pekan, Pahang, Malaysia. The tree was constructed based on similar nucleotide sequences using BLASTn, Kimura two-parameter algorithm and the neighbour-joining method. Bootstrap values (expressed as percentage of 1000 replications) are reported at each node. The scale bar indicates 0.1 substitutions per nucleotide positions.

CONCLUSION

Phylum Proteobacteria dominated the peat soil in Pekan, Pahang, Malaysia. Proteobacteria, comprised of α-proteobacteria, ß-proteobacteria, and γ-proteobacteria, were the most dominant bacterial class in the FP, HP, WC, and IPR. The Proteobacteria community that inhabits the aforementioned operational zones is the crucial indicator of nutrient cycling, carbon sequestration and plant nutrient uptake for sustainable soil in oil palm plantations.

ACKNOWLEDGEMENT

The authors would like to give the utmost gratitude to the Director-General of MPOB and the Director of Biology and Sustainability Research Division for permission to publish this article. Special thanks also go to the Entomology and Integrated Pest Management Group for their assistance and commitment in completing this study.

REFERENCES

Aislabie, J and Deslippe, J R (2013). Soil microbes and their contribution to soil services. *Manaaki Whenua Press*. Lincoln, New Zealand. p. 148-156.

Anamulai, S; Sanusi, R; Zubaid, A; Lechner, A M; Ashton-Butt, A and Azhar, B (2019). Land use conversion from peat swamp forest to oil palm agriculture greatly modifies microclimate and soil conditions. *PeerJ*., *7*: e7656.

Carron, M P; Auriac, Q; Snoeck, D; Villenave, C; Blanchart, E; Ribeyre, F; Marichal, R; Darminto, M and Caliman, J P (2015). Spatial heterogeneity of soil quality around mature oil palms receiving mineral fertilization. *Eur. J. Soil Biol*., *66*: 24-31.

Corley, R H V and Tinker, P B (2003). *The Oil Palm*. 4th edition. Blackwell Science. Oxford. p 284.

Cramb, R and Curry, G N (2012). Oil palm and rural livelihoods in the Asia-pacific region: An overview. *Asia Pac. Viewp*., *53*: 223-239.

Delgado-Baquerizo, M; Reich, P B; Trivedi, C; Eldridge, D J; Abades, S; Alfaro, F D; Bastida, F; Berhe, A A; Cutler, N A; Gallardo, A; García-Velázquez, L; Hart, S C; Hayes, P E; He, J Z; Hseu, Z Y; Hu, H W; Kirchmair, M; Neuhauser, S; Pérez, C A; Reed, S C; Santos, F; Sullivan, B W; Trivedi, P; Wang, J T; Weber-Grullon, L; Williams, M A and Singh, B K (2020). Multiple elements of soil biodiversity drive ecosystem functions across biomes. *Nat. Ecol. Evol., 4(2)*: 210-220.

Esson, K C; Lin, X; Kumaresan, D; Chanton, J P; Murrell, J C and Kostka, J E (2016). Alpha-and gammaproteobacterial methanotrophs codominate the active methane-oxidizing communities in an acidic boreal peat bog. *Appl. Environ. Microbiol*., *82(8)*: 2363-2371.

Hammer, Ø; Harper, D A T and Ryan, P D (2001). PAST: Paleontological statistics software package for education and data analysis. *Palaeontol Electron*, *4*: 9.

Hirano, T; Jauhiainen, J; Inoue, T and Takahashi, H (2009). Controls on the carbon balance of tropical peat lands. *Ecosystems*, *12*: 873-887.

Kumar, S; Stecher, G and Tamura, K (2016). MEGA7: Molecular evolutionary genetics analysis version 7.0 for bigger datasets. *Mol. Biol. Evol*., *33(7)*: 1870-1874.

Martirani-Von Abercron, S M; Marín, P; Solsona-Ferraz, M; Castañeda-Cataña, M A and Marqués, S (2017). Naphthalene biodegradation under oxygen-limiting conditions: Community dynamics and the relevance of biofilm-forming capacity. *Microb. Biotechnol*., *10(6)*: 1781-1796.

Melling, L and Henson, I E (2011). Greenhouse gas exchange of tropical peatlands - A review. *J. Oil Palm Res*., *23*: 1087-1095.

Muyzer, G; de Waal, E C and Uitterlinden, A G (1993). Profiling of complex microbial populations by denaturing gradient gel electrophoresis analysis of polymerase chain reaction-amplified genes coding for 16S rRNA. *Appl. Environ. Microbiol*., *59(3)*: 695-700.

Nelson, P N; Webb, M J; Banabas, M; Nake, S; Goodrick, I; Gordon, J; O'grady, D and Dubos, B (2014). Methods to account for tree-scale variability in soil-and plant-related parameters in oil palm plantations. *Plant Soil, 374*: 459-471.

Nelson, P; Webb, M; Huth, N; Banabas, M; Sheaves, M; Johnston, R; Mcneill, A; Nake, S; Pipai, R; Koczberski, G and Davies, K (2019). Project sustainable management of soil and water resources for oil palm production systems in PNG. *ACIAR Final Reports*. FR2019/101.

Schröder, J J; Schulte, R P O; Creamer, R E; Delgado, A; van Leeuwen, J; Lehtinen, T; Rutgers, M; Spiegel, H; Staes, J; Tóth, G and Wall, D P (2016). The elusive role of soil quality in nutrient cycling: A review. *Soil Use Manage*., *32(4)*: 476-486.

Semrau, J D; Dispirito, A A and Yoon, S (2010). Methanotrophs and Copper. *FEMS Microbiol. Rev.*, *34*: 496-531.

Tinker, P B H (1960). Soil heterogeneity and sampling procedure under oil palms. *J. West Afr. Inst. Oil Palm Res.*, *4*: 7-15.

Whittenbury, R; Phillips, K C and Wilkinson, J F (1970). Enrichment, isolation and some properties of methane-utilizing bacteria. *Microbiology*, *61*: 205-218.

Yadav, N and Yadav, A N (2019). Actinobacteria for sustainable agriculture. *J. Appl. Biotechnol.*, *6(1)*: 38-41.



Contents of the Coming Issue
Journal of Oil Palm Research
Vol. 35 (2) June 2023*

- Oil Palm Economic Performance in Malaysia and R&D Progress in 2022.
  Ghulam Kadir Ahmad Parveez; Kalsom Zakaria; Mohd Najib Ahmad; Humaira Mat Taib; Mohd Azwan Mohd Bakri; Sitti Rahma Abdul Hafid; Tn. Noor Maznee Tn. Ismail; Loh Soh Kheang; Meilina Ong-Abdullah; Omar Abd. Rasid and Zainab Idris

- Membrane Technologies in the Oil Industry and the Potential Application for Their Recovery of Phytonutrients from Palm Oil
  Adriana Isabel Rada-Bula; Jesus Alberto Garcia-Nunez; Carlos Jesus Muvdi-Nova and Consuelo Diaz-Moreno

- Effect of Storage Temperature and Duration on Rheological and Thermal Characteristics of Superolein Oleogels
  Mei Huey Saw; Wen Huei Lim; Chee Beng Yeoh and Chin Ping Tan

- Esterification of Free Fatty Acid from Sludge Palm Oil using Zeolite Sulfonated Carbon from Sugar Cane Catalysts
  Hasanudin; Wan Ryan Asri; Tri Eltiyah Muthiarani; David Bahrain and Fitri Hadiah

- Mixed Planting with Rhizomatous Plants Interfered with *Ganoderma* Disease in Oil Palm
  Suwandi Suwandi; Rudi Putra Munandar; Suparman Suparman; Chandra Irsan and A. Muslim

- Field Efficacy of Anticoagulant Rodenticides against Rat Infestation in Oil Palm Plantation
  Ariff Ateed Mohd Noh; Muhammad Syafiq Mohd Zaludin; Wan Mohd Hafezul Wan Abdul Ghani; Abu Hassan Ahmad and Hasber Salim

Note: * Subject to change.



PIPOC 2023

MPOB International Palm Oil Congress and Exhibition

Navigating Uncertainties Building Resilience

7-9 NOVEMBER 2023
Kuala Lumpur Convention Centre

MINISTRY OF PLANTATION AND COMMODITIES

MPOB

Organised by
Malaysian Palm Oil Board
Ministry of Plantation and Commodities, Malaysia

pipoc@mpob.gov.my

pipoc.mpob.gov.my | www.mpob.gov.my